JAEA-Review
2006-042



JP0750162

JAEA-Review

JAEA Takasaki Annual Report 2005

(Ed.) Yoshihiro OHARA

Takasaki Advanced Radiation Research Institute

February 2007

Japan Atomic Energy Agency

日本原子力研究開発機構

本レポートは日本原子力研究開発機構が不定期に発行する成果報告書です。
本レポートの入手並びに著作権利用に関するお問い合わせは、下記あてにお問い合わせ下さい。
なお、本レポートの全文は日本原子力研究開発機構ホームページ（http://www.jaea.go.jp/index.shtml）より発信されています。このほか財団法人原子力弘済会資料センター*では実費による複写頒布を行っております。

〒319-1195　茨城県那珂郡東海村白方白根2番地4
日本原子力研究開発機構　研究技術情報部　研究技術情報課
電話 029-282-6387, Fax 029-282-5920

*〒319-1195　茨城県那珂郡東海村白方白根2番地4　日本原子力研究開発機構内

This report is issued irregularly by Japan Atomic Energy Agency
Inquiries about availability and/or copyright of this report should be addressed to
Intellectual Resources Section, Intellectual Resources Department,
Japan Atomic Energy Agency
2-4 Shirakata Shirane, Tokai-mura, Naka-gun, Ibaraki-ken 319-1195 Japan
Tel +81-29-282-6387, Fax +81-29-282-5920

© Japan Atomic Energy Agency, 2007

JAEA-Review 2006-042

JAEA Takasaki Annual Report 2005

(Ed.) Yoshihiro OHARA

Takasaki Advanced Radiation Research Institute

Japan Atomic Energy Agency

Watanuki-machi, Takasaki-shi, Gunma-ken

(Received December 14, 2006)

JAEA Takasaki annual report 2005 describes research and development activities performed from April 1, 2005 to March 31, 2006 with Takasaki Ion Accelerators for Advanced Radiation Application (TIARA, four ion accelerators), and those in a recent few years with electron/gamma-ray irradiation facilities (an electron accelerator and three ^{60}Co gamma-ray irradiation facilities) at Takasaki Advanced Radiation Research Institute, Japan Atomic Energy Agency (JAEA Takasaki). These activities are classified into four research fields: 1) nuclear and energy engineering, 2) environmental conservation and resource security, 3) biotechnology and medical application, 4) advanced materials, analysis and novel technology. This annual report contains 182 reports consisting of 174 research papers and 8 status reports on operation/maintenance of above irradiation facilities, and a list of publications, related press-releases, TV programs, patents, and the type of research collaborations as Appendices.

Keywords: TIARA, Ion Accelerators, Electron Accelerator, Gamma-ray Facilities, Nuclear and Energy Engineering, Environment Conservation, Resource Security, Biotechnology, Medical Application, Advanced materials, Analysis, Novel Technology, Materials for Space, Semiconductors, Inorganic Materials, Organic Materials, Functional Materials, Radiation Chemistry, Radiation Biology, Radioisotope Production, Nuclear Chemistry, Material Analyses, Solid State Physics, Microbeam Technology, Accelerator Technology, Accelerator Operation, Safety Control

---

(Editorial committee) Yoshihiro OHARA, Hisayoshi ITOH, Atsushi TANAKA, Kazuo ARAKAWA, Shigeru TANAKA, Fumio YOSHII, Kazumasa NARUMI, Takuji KOJIMA, Michiro OTSUBO, Yoshiteru NAKAMURA and Hiroyuki TACHIBANA

高崎量子応用研究所研究年報 2005

日本原子力研究開発機構 高崎量子応用研究所
（編） 小原 祥裕

（2006 年 12 月 14 日受理）

高崎量子応用研究所研究年報 2005 は、同研究所にある TIARA 施設（イオン加速器 4 基）を利用して 2005 年 4 月 1 日から 2006 年 3 月 31 日までの間に行われた研究・技術開発成果、及び電子・ガンマ線照射施設（電子加速器 1 基、^{60}Co ガンマ線照射施設 3 棟）を利用して最近数年間で行われた研究・技術開発成果をまとめたものである。この研究年報には、1）宇宙・原子力・エネルギー、2）環境・資源、3）バイオ技術・医学応用、4）先端材料・計測・基盤技術の 4 分野に分類した 174 編の論文及び 8 編の施設の運転・管理状況報告からなる合計 182 編が収録されている。また、論文リスト、新聞発表、テレビ放映、出願特許、及び研究実施形態・利用施設の一覧表が付録として含まれている。

高崎量子応用研究所：〒370-1292 群馬県高崎市綿貫町 1233
編集委員：（著者代表）小原 祥裕、伊藤 久義、田中 淳、荒川 和夫、田中 茂、吉井 文男、鳴海 一雅、小嶋 拓治、大坪 道朗、中村 義輝、橘 宏行

PREFACE

Takasaki Advanced Radiation Research Institute was established on October 1st in 2005 accompanying with the foundation of Japan Atomic Energy Agency, and took over the research activities of Takasaki Radiation Research Establishment, JAERI.

This report covers research and development activities in Takasaki Advanced Radiation Research Institute, JAEA, during the period from October 2005 to March 2006, and Takasaki Radiation Research Institute, JAERI, during the period from April to September 2005, which was conducted with TIARA (Takasaki Ion Accelerators for Advanced Radiation Application), electron beam and Co-60 gamma-ray irradiation facilities.

The research fields of papers appeared in this annual report are 1)Space, Nuclear and Energy Engineering, 2)Environmental Conservation and Resource Security, 3)Biotechnology and Medical Application, 4)Advanced Materials, Analysis and Novel Technology, and 5)Status of Irradiation Facilities.

In the field of Space, Nuclear and Energy Engineering, radiation response of solar cells newly developed for space application, single-event phenomena in highly sophisticated integrated-circuits having SOI (silicon on insulator) structures, and development of radiation resistant devices based on silicon carbide (SiC) semiconductors, have been investigated using TIARA, electron accelerator, and gamma-ray irradiation facilities. In recent years, computer simulation technique has been widely applied for analyzing radiation effects. Radiation resistance of organic and inorganic materials used in nuclear and fusion reactors and accelerators has also been examined to predict the durability of such materials in severe environments. In addition, high quality polymer electrolyte membranes have been fabricated using ion beams for their application to fuel cells.

In the field of Environmental Conservation and Resource Security, metal ion adsorbents have been developed by using electron beams and gamma-rays to realize the recovery of rare metals from hot spring water as well as the removal of toxic materials from industrial waste water. Biodegradable hydro-gels and polymers have also been investigated using radiation cross-linking for their industrial, agricultural, and medical applications. Fundamental and applied studies on the decomposition and removal of trace amount of pollutants such as toxic organic compounds in flue gas or wastewater have been performed to develop new process technologies for environmental conservation.

In the field of Biotechnology and Medical Application, a new biotech reagent has been developed during the study on DNA repair mechanisms of the radioresistant bacterium. Ion beam breeding technique has been applied not only for flowers and crops but also for yeasts, algae and fungi. Heavy-ion induced bystander effects were investigated at many biological endpoints such as γH2AX foci formation, micronucleus formation, clonogenic survival, *etc.*,

in human normal and cancer cells. A mathematical modeling method was installed to positron emitting tracer imaging system (PETIS) and the average flow speeds and distribution ratios of photoassimilates in a plant stem were accurately estimated.

In the field of Advanced Materials, Analysis and Novel Technology, the energy spread $\Delta E/E$ of 260-MeV $^{20}Ne^{7+}$ beam was reduced to about 5×10^{-4} using the flat-top acceleration system of the AVF-cyclotron. And a beam spot of less than 1.2μm in diameter was successfully formed in a focusing high-energy heavy ion microbeam system. Micro-machining by the proton beam writing (PBW) technique has successfully progressed for thick resists with several tens of micrometers on silicon. To clarify the mechanism of acute cadmium (Cd) toxicity in testis, the intercellular distribution of metal elements were analyzed using in-air micro-PIXE, and the comformation of Fe in Cd-induced testis was found. The charge states were measured for the constituent of 1MeV/atom C_3^+ passing through a carbon thin foil; the average charge of each ion dissociation from C_3^+ ions in linear-chain structure is larger than that of triangle structure. In the development of monitor and dosimeter for radiation, DARWIN (Dose monitoring system Applicable to various Radiation with WIde energy raNges) has been developed for real-time monitoring doses of neutron with a energy ranging from thermal to 1GeV. And a handy measurement technique of two dimensional particle fluence distribution was developed by using GAF film and the PC scanner.

All the accelerators in TIARA, namely the AVF cyclotron, the 3MV tandem accelerator, the 3MV single-ended accelerator and the 400kV ion implanter, have been operated steadily as well as an electron accelerator and irradiation systems in Co-60 gamma-ray irradiation facilities.



Hideki Namba,
Director General
Takasaki Advanced Radiation Research Institute
Japan Atomic Energy Agency

Contents

1 Space, Nuclear and Energy Engineering ····· 1

1-01 Radiation Response and Recovery Characteristics of Amorphous Silicon Solar Cells ····· 5
1-02 Recovery of the Electrical Performance of Proton-Irradiated 3J Solar Cells by Current Injection ····· 6
1-03 Electron Radiation Induced Defects in Lattice-Mismatched Solar Cells ····· 7
1-04 Development of Radiation Hardened High-Speed Logic Circuits by Using 0.15μ m SOI Technology ····· 8
1-05 Bias Dependence of the Single Event Transient Currents due to Nuclear Products in Semiconductors ····· 9
1-06 Influence of Carrier Recombination Process on Single Event Transient Current in Si Diodes under High Injection by Heavy Ions ····· 10
1-07 Heavy-Ion Induced Current through an Oxide Layer ····· 11
1-08 Single Event and Total Dose Synergy Effects in SOI Devices ····· 12
1-09 Decrease in Charge Collection Efficiency Obtained for 6H-SiC n^+p Diodes by Ni Ion Incidence ····· 13
1-10 Relationship between Defects Induced by Irradiation and Reduction of Hole Concentration in Al-Doped 4H-SiC ····· 14
1-11 EPR Study of Electron-Irradiated SiC: Structure Determination of Intrinsic Defects in *4H-SiC* ····· 15
1-12 EPR Study of High Energy Phosphorus Ion Implanted SiC: Phosphorus Donors Substituting for Carbon Atoms ····· 16
1-13 Development of Optoelectronic Devices for Radiation Environments - Improvement of Luminescence Capability of Tb Using AlGaN - ····· 17
1-14 Mechanical Properties of Austenitic Stainless Steel Ion-Irradiated under External Stress ····· 18
1-15 Influences of Multi Ion Beam Irradiation on Radiation Hardening and Microstructure in Low Activation Ferritic/Martensitic Steels ····· 19
1-16 Study on Irradiation Defect Generation Process and Radiation Induced Segregation in Fe-Based Model Alloys ····· 20
1-17 Effect of Ion-Irradiation on Microstructure of Zirconium ····· 21
1-18 Effect of Al and Be as Transmutation Atoms on Formation and Growth of Helium Bubbles in SiC/SiC Composites ····· 22
1-19 Evaluation on Irradiation Effects for Surface Modified Material ····· 23
1-20 Evaluation of Property Change in Advanced Fuel Cladding Material under Ultra High Burn-up Condition Simulated by Triple Ion Irradiation ····· 24
1-21 Irradiation-Induced Changes in Surface Topology of Cerium Dioxide Investigated with Scanning Electron Microscopy and X-Ray Spectroscopy ····· 25
1-22 Observation of Microstructural Changes and Irradiation Damages in Li_2TiO_3 Caused by Multi Ion Beam Irradiation ····· 26
1-23 Change in Electrical Resistance in Titanium Dioxide Irradiated with Energetic Particles ····· 27
1-24 Threshold Energy for Defect Production in Fe-50 at.%Rh Alloy ····· 28

1-25 Irradiation Effects on Utility Materials in J-PARC Facilities ····· 29
1-26 65 MeV Neutron Irradiation of NdFeB Permanent Magnets ····· 30
1-27 Radiation Resistance of Organic Materials in Superconducting Magnets at 77 K
-Mechanical Properties- ····· 31
1-28 Radiation Resistance of Organic Materials in Superconducting Magnets at 77K
-Gas Evolution- ····· 32
1-29 Gamma-Ray Irradiation Effects on Thermal Decomposition Behavior of Cable Materials ····· 33
1-30 Operation Test Result of a Radio-Proof Cryogenic Valve under Cobalt 60 Irradiation ····· 34
1-31 Nano-Structure Controlled Polymer Electrolyte Membranes for Fuel Cell Applications
Prepared by Ion Beam Irradiation ····· 35

2 Environment Conservation and Resource Security ····· 37

2-01 Preparation of Ion Exchange Fibres by Emulsion Graft Polymerization ····· 39
2-02 Development of Radiation Induced Graft Polumerization in Aqueaous Medium;
Approach for Styrene Based Monomers ····· 40
2-03 Development of Boron Adsorbent for Environmental Drainage ····· 41
2-04 Mercury Adsorbent Synthesized by Graft Polymerization onto Cellulose
Nonwoven Materials ····· 42
2-05 Development of Bifunctional Chelating Fibers with High Performance in Metal Ion
Adsorption Kinetics ····· 43
2-06 Development and Application of Fiberous Bifunctional Phosphonate-Sulfonate
Cation Exchanger ····· 44
2-07 Cost Estimation of Uranium Collection from Seawater with Braid Type Adsorbent ····· 45
2-08 The Recovery Method of Scandium from Hot Spring Water ····· 46
2-09 Development of Equipment to Remove Cadmium from Waste of Scallop Processing by
Graft Adsorbent ····· 47
2-10 Development of Grafting Adsorbent for Ultra Pure Water Production ····· 48
2-11 Preparation of Amidoxime-Type Chelating Fabric and Its Removal Performance of
Toxic Heavy Metals ····· 49
2-12 Removal of Ferric and Manganese Ions with Fibrous Iminodiacetic Acid Adsorbent
Synthesized by Graft Polymerization ····· 50
2-13 Off-On Biodegradability of Poly(3-hydroxybutyrate) Film Modified by
Graft Polymerization ····· 51
2-14 Metal Adsorption of Chitin / Chitosan Derivatives Hydrogels Crosslinked with
Irradiation ····· 52
2-15 Modification of Poly(lactic acid) by Radiation-Induced Crosslinking ····· 53
2-16 Development of DNA-Derived Environmental Material by Gamma-Ray Irradiation ····· 54
2-17 Enhancement of Plant Growth Activity of Irradiated Alginate ····· 55
2-18 Cooperative Research on Radiation Processing of Natural Polysaccharides
between VAEC and JAEA ····· 56
2-19 Radiation Effects on PTFE Moulding Powder ····· 57

2-20 Hexyl Methacrylate-Based Monolithic Columns Prepared by Radiation-Induced Polymerization ····· 58
2-21 Development of Electron Beam Technology for the Treatment of PCDD/Fs in Municipal Waste Incinerator Gases ····· 59
2-22 Electron Beam Treatment of Formalin Sterilization Gas ····· 60
2-23 Decomposition of Endocrine Disrupting Chemicals in Real Wastewater by ^{60}Co γ-Ray Irradiations ····· 61
2-24 Dependence of Differential Yields of Heavy Ion Induced OH Radicals in Water on Mass and Specific Energy of Heavy Ions, and Elapsed Time ····· 62

3 Biotechnology and Medical Application ····· 63

3-01 *Deinococcus radiodurans* DNA Repair-Promoting Protein: Applications to Biotech Industry ····· 69
3-02 The Radiation Responsive Promoter of the *Deinococcus radiodurans pprA* Gene ····· 70
3-03 Detection Method for Irradiated Foods Using ESR ····· 71
3-04 Detection of Oxidative DNA Damage Using Anti-8-OHdG Antibody –A Useful Method to Distinguish Irradiated Foods– ····· 72
3-05 Application of Hydrogel on Wound Dressing and Future View of Hydrogel ····· 73
3-06 Development of an Efficient Method for Mutation Induction in Plants ····· 74
3-07 DNA Damage Yields in Hydrated DNA after He Ion Irradiation ····· 75
3-08 Study of Molecular Mechanism of Ion Beam Induced Mutations in the *Saccharomyces cerevisiae* ····· 76
3-09 Quantitative Analysis of DNA Double-Strand Breaks in Tobacco Protoplasts Irradiated with Helium, Carbon and Neon Ion Beam ····· 77
3-10 Comparison of the Mutation Inducing Effect between Ion Beams and Gamma Ray ····· 78
3-11 Molecular Analysis of Ion Beam-Irradiated Orchids ····· 79
3-12 Selection of Rootstock Eggplant Resistant to Bacterial Wilt from Regenerants Derived from Ion Beam-Irradiated Microspores ····· 80
3-13 Mutation Induction from Osteospermum Leaf Cultures with Ion Beam Irradiation ····· 81
3-14 Breeding of Stress-Tolerant Variety Series in Ornamentals by Ion Beam Irradiation ····· 82
3-15 The Optimum Dose of Ion Beam Irradiation to Tissue Cultured of Leaf Explants for Breeding Sugarcane ····· 83
3-16 Mutation Induction in Sugi Cedar and Hinoki Cypress by Ion Beam Irradiation ····· 84
3-17 Mutation Induction in Garlic with Ion Beam Irradiation ····· 85
3-18 Mutagenesis in Gynomonoecious Spinach (*Spinacia oleracea* L.) Plants and Selection of Low Oxalate Variants ····· 86
3-19 Effect of Ion Beam Irradiation on Coloration of Fruit Skin of Eggplant (*Solanum melongena* L.) ····· 87
3-20 Studies on Flower Color and Morphological Mutations from Chrysanthemum In Vitro Explants Irradiated with Ion Beams ····· 88
3-21 Induction of Mutation by the Ion Beam Irradiation to the Calluses of *Lilium* × *formolongi* Hort (*cv. White Aga*.) ····· 89

3-22 Mutation Induction on Hybrid Limonium 'Moon Light' Using Ion Beams ····· 90
3-23 Effects of Ion Beam Irradiation on Spore Germination, Mycelial Growth and Fruit Body Formation of *Pleurotus ostreatus* ····· 91
3-24 Mutation Induction of Asiatic Hybrid Lily Using Ion Beam Irradiation ····· 92
3-25 Screening of Cadmium Resistant Rice Mutants Induced by Carbon Ion Irradiation ····· 93
3-26 Ion Beam Breeding of Rice Variety Suitable for Low Nitrogen Input ····· 94
3-27 Flower Color and Cluster Modification by Ion Beams in Chrysanthemum ····· 95
3-28 Mutation Induction in Azalea Using Ion Beam Irradiation and Its Gene Analysis ····· 96
3-29 Deletion of Minor Enzyme Activities of *Rhizomucor miehei* by Irradiation of Heavy-Ion Beam ····· 97
3-30 Mutation Breeding of Koji Mold Induced by Ion Beams ····· 98
3-31 Analysis of Cellular Effects and Local Damage Induced by High LET Heavy Ions ····· 99
3-32 Recent Improvements of Heavy-Ion Microbeam System for Bystander Study ····· 100
3-33 Late-Arising Loss of Clonogenicity in the Progeny of Cells Surviving High- and Low-LET Ionizing Radiations ····· 101
3-34 Bystander Killing of Human Lung Cancer Cells by Heavy Charged Particle Irradiation ····· 102
3-35 Analysis of Radiation-Induced Apoptosis in Early *Drosophila* Embryos ····· 103
3-36 Bystander Effect of High Linear Energy Transfer Charged Particle Radiation on Human Glioblastoma Cells ····· 104
3-37 Effects of Heavy-Ion, UV-C, and X-Ray Irradiation on the Susceptibilities of Human Cells to HIV-1 Infection ····· 105
3-38 Effects of Heavy Ion Microbeam Irradiation on Isolated Single Fibers of Skeletal Muscle ····· 106
3-39 Research into the Radiosensitivity of Normal Brain Tissue ····· 107
3-40 Response of Associative Learning and Nervous System of *Caenorhabditis elegans* to Heavy Ion Beam Irradiation ····· 108
3-41 Heavy Ion Microbeam Irradiation to the Central Nervous System of *Caenorhabditis elegans* and Development of Effect Prediction Simulator. Why is Associative Learning of *Caenorhabditis elegans* Promoted by Ionizing Irradiation? ····· 109
3-42 Particle Number- and LET- Dependency of Bystander Effect through the Gap Junction Signalling in Human Normal Fibroblast Cells Exposed to Heavy-Ion Beams ····· 110
3-43 Analysis of Molecular Mechanisms for Radiation-Induced Bystander Effects Using Heavy Ion Microbeams ····· 111
3-44 Chromosomal Aberrations by Medium-Mediated Bystander Effects Induced by High-LET Radiations ····· 112
3-45 Construction of Monitoring System for Biological Effects of Local Ionizing Radiation Using the Nematode *C. elegans* ····· 113
3-46 Ion Beam Irradiation has Different Influences on Glutathione Peroxidase of Cultured Human Retinal Vascular Endothelial Cells among ^{20}Ne, ^{12}C, and ^{4}He ····· 114
3-47 The Characteristics of Radiation-Induced Cell Responses in the Canine Spontaneous Tumor Cells ····· 115
3-48 Effects of Heavy Ions and Gamma-Ray on the Tardigrade *Milnesium tardigradum* ····· 116

3-49 Regeneration Mechanism of Hemopoietic Organs in the Silkworm, *Bombyx mori*, after Heavy-Ion Irradiation : Analysis by Transplantation of the Irradiated Organs Using a Transgenic Silkworm Strain ····· 117
3-50 Analysis of Local Irradiation of Heavy-Ion Microbeam Influence on Embryo or Yolk in the Silkworm, *Bombyx mori*, Egg by the Incidence of Somatic Mutation Appearing in the Larvae ····· 118
3-51 Identification of the Functional Tissues for Hydrotropism in Comparison with Those for Gravitropism ····· 119
3-52 Circadian Rhythms in Resistance to γ Irradiation and Heavy Ion Beam in *Euglena* ····· 120
3-53 Analysis of the Maturation Process of Photosynthetic Activities in a Leaf Using Positron Emitting Tracer Imaging System (PETIS) ····· 121
3-54 Interaction between Nitrogen Nutrients Acquisition Function and Distribution of Photosynthetic Products ····· 122
3-55 Determination of Photosynthesis and Partitioning Rate Using by PETIS ····· 123
3-56 ^{52}Fe Tranlocation from the Roots to the Ear of Rice Using a Positron Emitting Tracer Imaging System (PETIS). ····· 124
3-57 Evaluation of Effect of Root Parasite on Nitrogen Translocation and Distribution in the Host Plant by Positron Emitting Tracer Imaging System (PETIS) ····· 125
3-58 Imaging of Parallel Routes of Photoassimilate Transport in an Intact Plant Body ····· 126
3-59 Non-Invasive Imaging of Cadmium Transport in Crop Plants ····· 127
3-60 Positron Related Analysis of ^{13}N-Nitrate in Transgenic Rice Plant Over-Expressing Nitrate Transporter ····· 128
3-61 Effect of Cadmium on Translocation of Photoassimilates in Rice (*Oryza sativa* L.) ····· 129
3-62 Impacts of Aluminum Ion for the Translocation of Signaling Molecule in Higher Plants ····· 130
3-63 Kinetic Analysis for Studying Photosynthesis in a Leaf Using $^{11}CO_2$ and Positron Emitting Tracer Imaging System ····· 131
3-64 Production of Radioisotopes for Nuclear Medical Application ····· 132
3-65 The Sensitivity Evaluation of Anticancer Drug Using In-Air Micro PIXE, The 21st Century COE Program 'Biomedical Research Using Accelerator Technology' ····· 133
3-66 The Targeting of the Chemotherapeutic Agents or Radiosensitizer by Radiation, Using the Liquid Core Microcapsules ····· 134
3-67 Fluorine Uptake into the Human Tooth from the Thin Layer of F-Releasing Material ····· 135

4 Advanced Materials, Analysis and Novel Technology ····· 137

4-01 Development of the Heavy Ion Beam Pulse Radiolysis ····· 141
4-02 LET Effect on Irradiation of Hydroxy Imide Compounds in Alcohol Solution ····· 142
4-03 Preparation of Submicron Copper Wires in Ion Track-Etched Membranes of Thermally Stable Polyimide: Effect of Electrodeposition Temperature on Their Morphology ····· 143
4-04 Gas Separation SiC Membrane Developed from Precursor Polymers by Radiation Curing ····· 144
4-05 1-D Crosslinked Polymer Nanowires Prepared by Single Particle Nanofabrication Techniques ····· 145

4-06 Characterization of Carbonizing Processes of Titanium Thin Films by Carbon-Implantation ····· 146
4-07 Ion-Induced Luminescence of Cr-Doped Alumina ····· 147
4-08 Effects of Hydrogen and Hydroxyl on Ion Beam Induced Luminescence of Ceramics ····· 148
4-09 Spectroscopic Analysis of Si Bombarded with C_{60} Ions ····· 149
4-10 Raman Analysis of Damage of C_{60} Thin Films by Fast Ion Bombardment ····· 150
4-11 Chemical State Analysis of Vacancy-Impurity Complexes by Positron Annihilation Spectroscopy ····· 151
4-12 Characterization of Ion Beam-Induced Quantum Structures Using a Slow Positron Beam ····· 152
4-13 Analysis of Light Elements in Carbon Materials ····· 153
4-14 Radiation-Induced Luminescence from TiO_2 by Ion Irradiations ····· 154
4-15 Disorder Analysis of Laser Crystal Surfaces Irradiated by a Neutral Argon Beam ····· 155
4-16 Application of X-Ray Photoelectron Spectroscopy to Characterization of Metallic Nanoclusters Formed by Ion Implantation-III ····· 156
4-17 Cr Ion Irradiation Effects on Hydrogen Storage Characteristics of Pd ····· 157
4-18 Visible Photoluminescence of ZnO Rods Grown on Cu Implanted Substrate ····· 158
4-19 Blister Formation in Rutile TiO_2 (100) Films by Helium Irradiation ····· 159
4-20 Improvement of Gasochromic Properties in Tungsten Oxide by Ion Irradiation ····· 160
4-21 Hydrogen Sensing Characteristics of Ag Implanted WO_3 ····· 161
4-22 Improved Separation of Cadmium-107 from Silver Cyclotron Targets by Precipitaion Method ····· 162
4-23 Synthesis of Hydrophilic Endohedral ^{133}Xe-Fullerenol by Using Higher Fullerene ····· 163
4-24 Deuteron-Induced Activation Cross Section Measurement of Fe, Cr, Mn, Ni and Au for IFMIF Accelerator ····· 164
4-25 Production of Radioisotopes for Nuclear Medicine Using Ion Beam Technology and Its Utilization for Both Therapeutic and Diagnostic Application in Cancer ····· 165
4-26 Nuclear Reaction Micro-Analysis of Boron Doped Steel ····· 166
4-27 Measurement of Three-Dimensional Structure of Biological Samples by STIM for PIXE Analysis ····· 167
4-28 Analysis of Radiation-Induced Cell Death In Vivo by Micro Particle-Induced X-Ray Emission (Micro PIXE) ····· 168
4-29 Studies on the Cadmium Distribution of Acute Cd Toxicity in Testis Using In-Air Micro Particle Induced X-Ray Emission (PIXE) ····· 169
4-30 Analysis of Boron Distribution in 9L Gliosarcoma Cells Using Particle Induced γ-Ray Emission (PIGE) ····· 170
4-31 Standard Reference Material for Determination of Platinum in Biological Materials by Micro Beam PIXE ····· 171
4-32 Development of In-Air On/Off -Axis STIM ····· 172
4-33 Fundamental Research of Highly Sensitive PIXE by Grazing Exit X-Ray Measurement ····· 173
4-34 Micro-Machining of Resists on Silicon by Proton Beam Writing ····· 174
4-35 Thermal Stability of Deformation and Refractive Index Change in Silica Glass Induced by Ion Microbeam ····· 175

4-36 Measurement of Structure and Charge States of Swift Carbon Cluster Passing Through a Thin Foil ····· 176
4-37 TOF Mass Spectrometry of Secondary Ions from HOPG Target Bombarded by Fast C and Au Cluster Ion Beams ····· 177
4-38 Effect of 1.66 MeV/atom Au Cluster Ion Irradiation in Si Single Crystals ····· 178
4-39 Highly Sensitive Surface Contaminant Analysis Using Pulsed Cluster Ion Beams ····· 179
4-40 Aerosol Formation Induced by Proton Irradiation to Air ····· 180
4-41 Measurement of Double Differential Fragment Production Cross-Section Induced by Ten's MeV Nucleons ····· 181
4-42 Development of Monitor and Dosimeter Applicable to High-Energy Neutrons ····· 182
4-43 Easy Measurement Technique for 2D Distribution of Fluence Using GAF-Film and PC-Scanner ····· 183
4-44 Preliminary Study on Applicability of B3 Film Dosimeter for Two Dimensional Dose Distribution Using a PC-Scanner ····· 184
4-45 Focused Microbeam Formation for Heavy Ion Beam from AVF Cyclotron (II) ····· 185
4-46 Design of Age-Related Macular Degeneration (AMD) Treatment System Using a Carbon Ion Beam ····· 186
4-47 Development of Ion-Induced Fluorescence Measurement Technology at the External Light Ion Microbeam System ····· 187
4-48 Formation of a Large-Area Uniform Ion Beam Using Multipole Magnets ····· 188
4-49 The Effect of Support Gas in Fullerene (C_{60}) Ion Production ····· 189
4-50 Development of All-Permanent-Magnet ECR Ion Source for the JAEA Cyclotron ····· 190
4-51 Improvement of the Cyclotron System for Microbeam Formation ····· 191
4-52 Development of Beam Generation and Irradiation Technology for Electrostatic Accelerator ····· 192

5 Status of Irradiation Facilities 2005 ····· 193

5-01 Safety Measures, Utilization Condition and Introduction of New Utilization System in TIARA Facility ····· 195
5-02 Operation of JAEA AVF Cyclotron System ····· 196
5-03 Operation of the Electrostatic Accelerators ····· 197
5-04 Radiation Control in TIARA ····· 198
5-05 Radioactive Waste Management in TIARA ····· 199
5-06 Utilization of the Electron Accelerator and Gamma-Ray Irradiation Facilities ····· 200
5-07 Operation of the Electron Accelerators ····· 201
5-08 Operation of the Co-60 Gamma-Ray Irradiation Facilities ····· 202

Appendix ····· 203
Appendix 1 List of Publication ····· 205
Appendix 2 List of Related Patents ····· 234
Appendix 3 List of Related Press-Release and TV Programs ····· 237
Appendix 4 Type of Research Collaboration ····· 238

This is a blank page.

1 Space, Nuclear and Energy Engineering

1-01 Radiation Response and Recovery Characteristics of Amorphous Silicon Solar Cells ····· 5
K. Shimazaki, M. Imaizumi, S. Kawakita, C. Morioka, T. Ohshima, H. Itoh and K. Kibe
1-02 Recovery of the Electrical Performance of Proton-Irradiated 3J Solar Cells by Current Injection ····· 6
T. Ohshima, H. Miyamoto, M. Imaizumi, C. Morioka, S. Kawakita, K. Shimazaki, K. Kibe, K. Kawano and H. Itoh
1-03 Electron Radiation Induced Defects in Lattice-Mismatched Solar Cells ····· 7
T. Sasaki, N.J. Ekins-Daukes, H.S. Lee, T. Takamoto, M. Imaizumi, T. Ohshima, H. Itoh and M. Yamaguchi
1-04 Development of Radiation Hardened High-Speed Logic Circuits by Using 0.15μ m SOI Technology ····· 8
H.Shindou, M.Midorikawa, Y.Satoh, N.Ikeda, S.Kuboyama, A.Makihara, T.Hirao, T.Ohshima and H.Itoh
1-05 Bias Dependence of the Single Event Transient Currents due to Nuclear Products in Semiconductors ····· 9
S. Onoda, T. Hirao, H. Abe, T. Sanami and H. Itoh
1-06 Influence of Carrier Recombination Process on Single Event Transient Current in Si Diodes under High Injection by Heavy Ions ····· 10
K. Mishima, T. Hirao, S. Onoda, H. Abe, H. Itoh and K. Kawano
1-07 Heavy-Ion Induced Current through an Oxide Layer ····· 11
K. Ohnishi, Y. Takahashi, Y. Nakajima, T. Nagasawa, T. Hirao, S. Onoda, K. Mishima and H. Itoh
1-08 Single Event and Total Dose Synergy Effects in SOI Devices ····· 12
H. Mori, S. Satoh, T. Hirao, S. Onoda, H. Abe and H. Itoh
1-09 Decrease in Charge Collection Efficiency Obtained for 6H-SiC n^+p Diodes by Ni Ion Incidence ····· 13
T. Ohshima, S. Onoda, M. Oikawa, T. Satoh, T. Hirao, T. Kamiya and H. Itoh
1-10 Relationship between Defects Induced by Irradiation and Reduction of Hole Concentration in Al-Doped 4H-SiC ····· 14
H. Matsuura, S. Kagamihara, Y. Itoh, T. Ohshima and H. Itoh
1-11 EPR Study of Electron-Irradiated SiC: Structure Determination of Intrinsic Defects in *4H-SiC* ····· 15
J. Isoya, T. Umeda, N. Mizuochi, M. Katagiri, T. Ohshima, N. Morishita and H. Itoh
1-12 EPR Study of High Energy Phosphorus Ion Implanted SiC: Phosphorus Donors Substituting for Carbon Atoms ····· 16
J. Isoya, T. Umeda, N. Mizuochi, M. Katagiri, T. Ohshima, N. Morishita and H. Itoh
1-13 Development of Optoelectronic Devices for Radiation Environments - Improvement of Luminescence Capability of Tb Using AlGaN - ····· 17
A. Wakahara, H.Okada, F.Oikawa, K.Takemoto, T.Ohshima and H.Itoh

1-14 Mechanical Properties of Austenitic Stainless Steel Ion-Irradiated under External Stress ····· 18
I.Ioka, Y. Ishijima, M.Futakawa, T.Suzuki, K.Kiuchi and T.Naoe
1-15 Influences of Multi Ion Beam Irradiation on Radiation Hardening and Microstructure in
Low Activation Ferritic/Martensitic Steels ····· 19
N. Okubo, T. Sawai, E. Wakai, D. Yamaki, S. Kitazawa, S. Jitsukawa, H. Tanigawa, K. Oka
and S. Ohnuki
1-16 Study on Irradiation Defect Generation Process and Radiation Induced Segregation in
Fe-Based Model Alloys ····· 20
T. Tobita, Y. Chimi, N. Ishikawa, S. Nakagawa and A. Iwase
1-17 Effect of Ion-Irradiation on Microstructure of Zirconium ····· 21
S. Yamada, M. Kinoshita, T. Taguchi and T. Sawai
1-18 Effect of Al and Be as Transmutation Atoms on Formation and Growth of Helium Bubbles in
SiC/SiC Composites ····· 22
T. Taguchi, N. Igawa, E. Wakai, S. Jitsukawa and A. Hasegawa
1-19 Evaluation on Irradiation Effects for Surface Modified Material ····· 23
T. Naoe, H. Kogawa, M. Futakawa, H. Takeuchi, Y. Ishijima, Y. Nakahara and I. Ioka
1-20 Evaluation of Property Change in Advanced Fuel Cladding Material under Ultra High Burn-up
Condition Simulated by Triple Ion Irradiation ····· 24
Y. Ishijima, I. Ioka, Y. Nanjyo, K. Kiuchi, K. Fujimura and H. Obata
1-21 Irradiation-Induced Changes in Surface Topology of Cerium Dioxide Investigated with
Scanning Electron Microscopy and X-Ray Spectroscopy ····· 25
T. Mihara, H. Abe, T. Sonoda, T. Sawai and E. Wakai
1-22 Observation of Microstructural Changes and Irradiation Damages in Li_2TiO_3 Caused by
Multi Ion Beam Irradiation ····· 26
D. Yamaki, T. Tanifuji, T. Aruga and S. Jitsukawa
1-23 Change in Electrical Resistance in Titanium Dioxide Irradiated with Energetic Particles ····· 27
N. Ishikawa, Y. Chimi and S. Yamamoto
1-24 Threshold Energy for Defect Production in Fe-50 at.%Rh Alloy ····· 28
A. Iwase, M. Fukuzumi, Y. Zushi, N. Ishikawa and Y. Chimi
1-25 Irradiation Effects on Utility Materials in J-PARC Facilities ····· 29
J. Kusano and members of J-PARC project team
1-26 65 MeV Neutron Irradiation of NdFeB Permanent Magnets ····· 30
X-M. Marechal, Y. Asano, T. Bizen and T. Hara
1-27 Radiation Resistance of Organic Materials in Superconducting Magnets at 77 K
-Mechanical Properties- ····· 31
T. Nakamoto, H. Ohhata, T. Ogitsu, N. Kimura, Y. Makida, A. Yamamoto, A. Idesaki,
M. Gokan, N. Morishita and H. Itoh
1-28 Radiation Resistance of Organic Materials in Superconducting Magnets at 77K
-Gas Evolution- ····· 32
A. Idesaki, M. Gokan, N. Morishita, H. Itoh, T. Nakamoto, T. Ogitsu, H. Ohhata, N. Kimura,
Y. Makida and A. Yamamoto

1-29 Gamma-Ray Irradiation Effects on Thermal Decomposition Behavior of Cable Materials ····· 33
A. Idesaki, M. Gokan, N. Morishita, O. Takeda, H. Itoh and J. Kusano
1-30 Operation Test Result of a Radio-Proof Cryogenic Valve under Cobalt 60 Irradiation ····· 34
Y. Makida, H. Ohhata, T. Okamura, T. Ogitsu, T. Nakamoto, N. Kimura, A. Idesaki, M. Gokan and N. Morishita
1-31 Nano-Structure Controlled Polymer Electrolyte Membranes for Fuel Cell Applications Prepared by Ion Beam Irradiation ····· 35
T. Yamaki, A. Hiroki, M. Asano, Y. Maekawa, K.-O. Voss, R. Neumann and M. Yoshida

This is a blank page.

1-01 Radiation Response and Recovery Characteristics of Amorphous Silicon Solar Cells

K. Shimazaki [a], M. Imaizumi [a], S. Kawakita [a], C. Morioka [a], T. Ohshima [b], H. Itoh [b] and K. Kibe [a]

[a]Institute of Aerospace Technology, Japan Aerospace Exploration Agency,
[b]Environment and Industrial Materials Research Division, QuBS, JAEA

Thin-film amorphous silicon (a-Si) solar cells are attractive for space applications because they offer the advantages of high specific power density, low cost, light weight, flexibility and high end-of-life (EOL) performance. The radiation response and recovery characteristics of a-Si solar cells have been studied in recent decades, and the obtained data proved the superior radiation tolerance. However, little is known about the basic mechanisms of the radiation degradation and recovery characteristics of a-Si solar cells. To address this, we have been investigating such characteristics of a-Si thin film solar cells.

Two kinds of dual-junction a-Si solar cells, a-Si/a-Si and a-Si/a-SiGe, developed commercially were used for this study. The initial efficiencies of these devices were, on average, 4% and 7% under AM0 illumination at 25°C. The cells were irradiated under open-circuit condition in a vacuum and in dark at ambient temperature (~ 28°C) with monoenergetic protons from 0.05 to 10MeV. Irradiation tests were performed at TIARA. The proton energies used were chosen to completely penetrate the device or maximize the amount of damage produced in the device active layer. The output parameters of irradiated cells were measured at JAXA Tsukuba Space Center a few days after irradiation tests except for the 10MeV-proton irradiation.

Figure 1 plots remaining factors of the short-circuit current (Isc) versus displacement damage dose (Dd)[1] for the proton-irradiated a-Si/a-SiGe solar cells. Dd is the product of particle fluence and the rate of non-ionizing energy loss (NIEL) in active region of the cells. If the damage had been due to displacement damage effects, the data would be expected to fall on a single curve. As can be seen in Fig. 1, the change in Isc can express a single characteristic curve as a function of Dd even if the proton energy is low enough to create local damage in the active layers. The results indicate that the energy dependence of the a-Si solar cell damage correlates with the displacement damage effects.

It has been reported that light illumination during proton irradiation tests reduced the degradation rate of a-Si solar cells.[2] However, the illumination experiments may include the possibility of thermal annealing effects which cannot be completely eliminated without special attention. The illumination tests were therefore performed for a-Si/a-SiGe solar cell irradiated with 200keV protons at a fluence of 3.0×10^{13}cm^{-2}. Figure 2 illustrates the recovery characteristics of the degraded cell as a function of elapsed time from the end of the irradiation test. The tests were carried out five months after the irradiation so that self-healing effect at room temperature could have been negligible (see Fig. 2 left). The cell was illuminated with an AM0 solar simulator at 25°C under open-circuit conditions for three hours. The cell did not exhibit recovery but actually exhibited slight degradation. We performed a thermal annealing test after the illumination test at 130°C. As a result, the cell performance quickly and significantly recovered. From these findings, we deduced that the light illumination except for the temperature rise resulting from the illumination does not contribute to the recovery of degraded a-Si/a-SiGe solar cells.

References

1) For example, G. P. Summers et al., IEEE Trans. Nucl. Sci. 40, 1993, pp.1372-1379.
2) J. E. Granata et al., Proc 3rd Int. Energy Conversion Engineering Conf., 2005, AIAA 2005-5650.

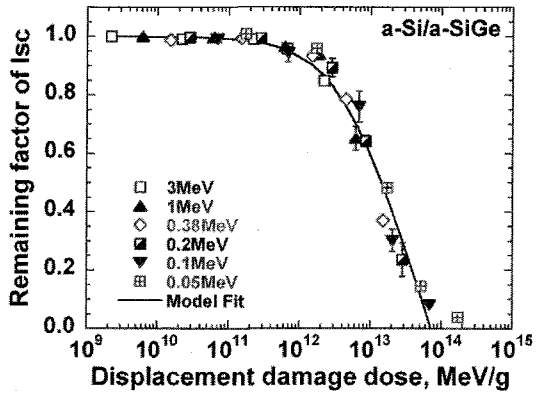


Fig. 1 Remaining factor of short-circuit current versus displacement damage dose for a proton-irradiated a-Si/a-SiGe solar cell.

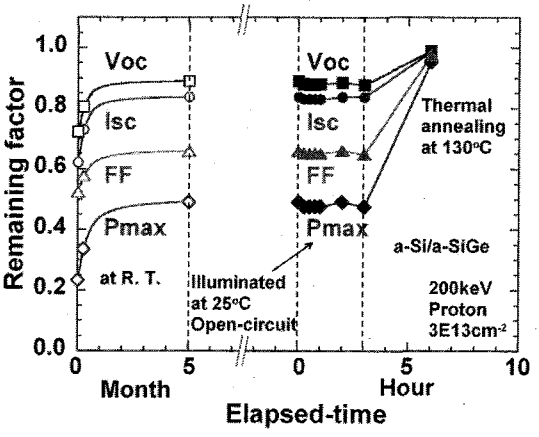


Fig. 2 Recovery characteristics of electrical outputs (Voc: open-circuit voltage, Isc: short-circuit current, Pmax: maximum power, FF: filling factor) for 200keV proton-irradiated a-Si/a-SiGe solar cell. The cell was stored in an open-circuit condition.

1-02 Recovery of the Electrical Performance of Proton-Irradiated 3J Solar Cells by Current Injection

T. Ohshima[a)], H. Miyamoto[a,b)], M. Imaizumi[c)], C. Morioka[c)], S. Kawakita[c)], K. Shimazaki[c)], K. Kibe[c)], K. Kawano[b)] and H. Itoh[a)]

[a)] Environment and Industrial Materials Research Division, QuBS, JAEA, [b)] The University of Electro-Communication, [c)] Institute of Space Technology and Aeronautics, JAXA

Triple junction (3J) solar cells are regarded as a promising candidate for space solar cells[1)]. For the prediction of their lifetime in space, it is important to understand their radiation response. In general, the electrical performance of solar cells monotonically degrades with increasing particle fluence. On the other hand, it was reported that the electrical performance of electron-irradiated InP-related solar cells was recovered by current injection[2)]. Since 3J solar cells contain InGaP as a top cell, their lifetime might be affected by the recovery effect. Therefore, it is necessary to reveal the recovery behaviors of 3J solar cells. In previous studies[2,3)], the recovery of InGaP solar cells irradiated with electrons or protons at high energies was mostly reported. For 3J solar cells irradiated with low energy protons such as several tens keV, sufficient information on their recovery has not been obtained yet. In this study, we compared low energy proton irradiation effects on electrical performance of 3J solar cells to the high energy proton's ones.

The samples used in this study were 3J solar cells grown on Ge substrates (InGaP/GaAs/Ge) by metal organic chemical vapor deposition. The solar cells were irradiated with protons at 50 keV or 10 MeV at room temperature (RT). In 50 keV-proton irradiation, damage is created in the InGaP top cell only because the projection range is shorter than the thickness of the InGaP cell. Damage is created in the whole 3J solar cells by 10 MeV-protons irradiation. After irradiation, current (minority carriers) injection into 3J solar cells was performed at RT using an external current source. The electrical characteristics of solar cells were *in situ* measured under AM0 illumination.

The values of short-circuit current (J_{SC}), open-circuit voltage (V_{OC}) and maximum power (P_{MAX}) decreased with increasing 50keV- and 10MeV-proton fluences. For 50 keV-proton irradiation, the remaining factors of J_{SC}, V_{OC} and P_{MAX} became 81, 81 and 56 % respectively at a fluence of 1.2×10^{12} /cm^2. For 10 MeV-proton irradiation, these values were 83, 69 and 47 % at a fluence of 3×10^{13}/cm^2. This indicates that the degradation of the electrical performance of 3J solar cells irradiated with 50 keV-protons is approximately one order of magnitude larger than that of 3J solar cells irradiated with 10 MeV-protons. Since low energy protons can create high dense defective layer near the surface, the obtained result can be interpreted in terms that the InGaP top cell is heavily damaged by 50 keV-protons as compared to 10 MeV-protons at the same fluence.

After irradiation, current injection into solar cells was performed at current densities between 0.03 and 0.25 A/cm. Figure 1 shows the remaining factor of J_{SC} as a function of injected charge. The values of J_{SC} are normalized by the value of J_{SC} after proton irradiation. Open and closed circles represent the results obtained for 3J solar cells irradiated with 50 keV- and 10 MeV-protons, respectively. The values of J_{SC} increased with increasing injected charge, and no significant difference in the increase of J_{SC} was observed between 3J solar cells irradiated with 50 keV- and 10 MeV-protons. Since defects act as carrier traps and/or scattering centers, the obtained result suggests that J_{SC} recovered by annealing of defects due to the current injection. In order to obtain the information on defect-annealing, the normalized defect density was estimated as follows. The diffusion length (L) of minority carriers decreases with increasing defect density, and J_{SC} decreases with decreasing L. These relationships are expressed as

$$1/J^2_{SC\Phi} - 1/J^2_{SC0} \propto 1/L^2_{\Phi} - 1/L^2_0 = BN_{T0}, \quad (1)$$

$$1/J^2_{SCA} - 1/J^2_{SC0} \propto 1/L^2_{A} - 1/L^2_0 = BN_{TA}, \quad (2)$$

where suffix 0, Φ and A mean before proton irradiation, after irradiation and after annealing. N_{T0} and N_{TA} are defect densities after irradiation and annealing, respectively. B is a constant. From eqs. (1) and (2), the normalized defect density (N_{TA}/N_{T0}) is obtained as

$$N_{TA}/N_{T0} = (1/J^2_{SCA} - J^2_{SC0}) / (1/J^2_{SC\Phi} - 1/J^2_{SC0}). \quad (3)$$

As the result of the analysis, N_{TA}/N_{T0} decreased with increasing injected charge, and the behavior for 50 keV-proton irradiated 3J solar cells is the same as that for 10 MeV-irradiated ones.

References

1) M. Imaizumi, *et al.*, Proc. of 3rd World Conference on Photovoltaic Energy Conversion, 3O-D6-02.
2) M. Yamaguchi, *et al.*, Appl. Phys. Lett. **44** (1984) 432.
3) A Khan, *et al.*, Jpn. J. Appl. Phys. **41** (2002) 1241.

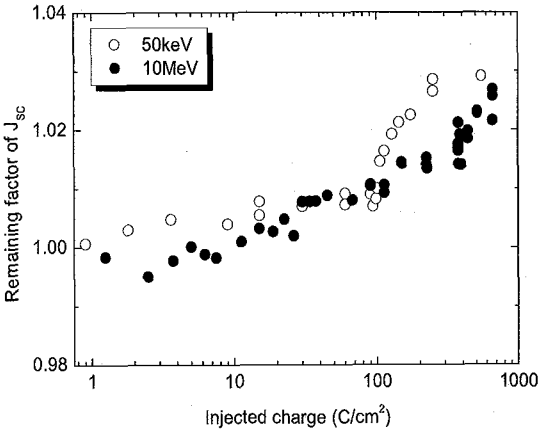


Fig. 1. Remaining factor of J_{SC} as a function of injected charge for 3J solar cells irradiated with 50keV or 10 MeV protons.

1-03 Electron Radiation Induced Defects in Lattice-Mismatched Solar Cells

T. Sasaki[a)], N.J. Ekins-Daukes[a)*], H.S. Lee[a) **], T. Takamoto[b)], M. Imaizumi[c)], T. Ohshima[d)], H. Itoh[d)] ana M. Yamaguchi[a)]

[a)] Toyota Technological Institute, [b)] Sharp Corporation, [c)] Japan Aerospace Exploration Agency (JAXA), [d)] Environment and Industrial Materials Research Division, QuBS, JAEA

Abstract

DLTS studies of lattice mismatched InGaAs and InGaP solar cells irradiated with 1MeV electrons have been presented. In both cases a complex evolution of the defect spectrum was observed under 1MeV electron irradiation. In the case of lattice mismatched InGaAs, it was found that whereas the TCA treatment was beneficial for improving BOL performance, it enhanced radiation degradation.

変換効率 31.5%を達成している格子整合系 InGaP/GaAs/Ge 3接合太陽電池のさらなる高効率化のためには，積層させるセルのバンドギャップ(Eg)を最適化し，太陽光スペクトルの吸収損失を低減させるアプローチがある．最適な Eg の組み合わせを考えると，ミドルセルである GaAs (Eg=1.4eV) の代わりに In を 16%添加させた $In_{0.16}Ga_{0.84}As$ (Eg=1.2eV)を用いることで熱損失が低減され，変換効率が 39%まで向上すると期待されている．しかし，Eg を最適化することでヘテロ界面は格子不整合となり，界面付近には多くの転位等の欠陥が生じてしまう．我々は基板上に製膜したバッファ層に TCA (Thermal Cycle Annealing) を施すことで，その上に形成する太陽電池層の転位密度が減少し (Fig.1)，さらに太陽電池の重要な特性パラメータである開放電圧 Voc の増加を見出している．そこで，TCA の回数が異なる，つまり太陽電池層の転位密度の異なるサンプルにおいて電子線照射効果を調べ，格子不整合系太陽電池の耐放射線性について検討を行った．

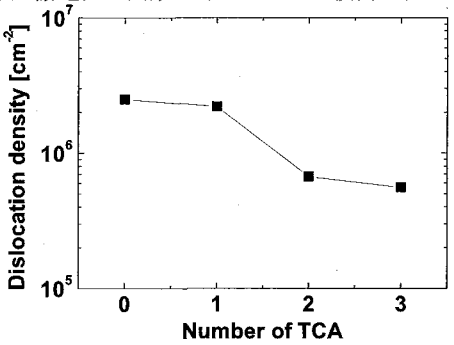


Fig.1 Dislocation density for lattice- mismatched InGaAs.

サンプルは MOCVD 法によって(001)GaAs 基板上に作製された n^+-i-p 構造 $In_{0.16}Ga_{0.84}As$ 単接合太陽電池である．基板と太陽電池層の間に In の組成比が連続的に変化する傾斜組成バッファ層 $In_xGa_{1-x}As(0<x<0.16)$を導入し，その成長後 300℃と 800℃の TCA を 0～3 回施した(TCA0～TCA3)．1MeV 電子線照射は室温で $1\times10^{16}cm^{-2}$ の照射量で行った．格子不整合系 InGaAs の放射線耐性を調べるため DLTS(Deep Level Transient Spectroscopy)法により照射前のネイティブな欠陥と 1MeV 電子線照射後に生成される欠陥を TCA の回数が異なるサンプルで測定した．

電子線照射前において，サンプルに TCA を施すことで多数キャリア（正孔）トラップ，少数キャリア（電子）トラップともに減少することが分かった．しかし，その減少は Fig.1 で示す転位密度の減少と明確な相関がなかったため，照射前に観測されたネイティブな欠陥は転位等の格子欠陥ではなく，材料の不純物起因の欠陥であると考えられる．1 MeV 電子線照射後では，Fig.2 に示すように正孔トラップ H0(E_v+0.26eV)と 2 つの電子トラップ E1(E_v+0.34eV)，E2(E_v+0.45eV)が新たに観測された．また，TCA を施したサンプル（TCA1-3）の方が DLTS 信号の増加が見られた．これより，格子不整合系太陽電池への TCA 処理は転位等のネイティブな欠陥を低減するには有効であるが，放射線照射による劣化の影響を受けやすいと考えられる．この結果は太陽電池の BOL(Beginning of Life)と EOL(End of Life)にとって重要な意味を持つと思われる。

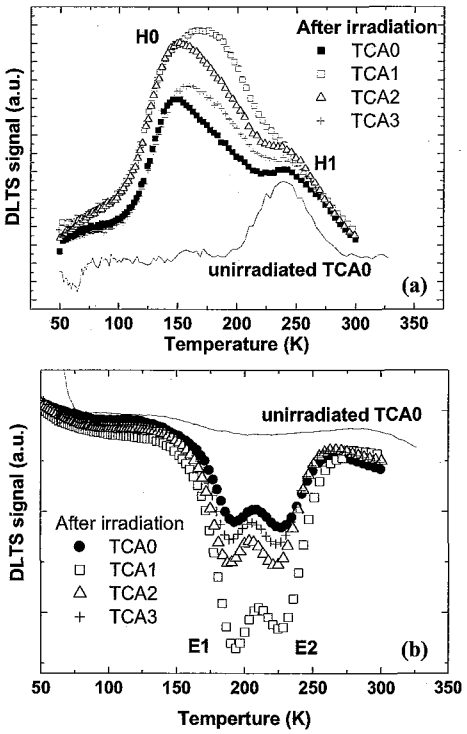


Fig.2 Majority- (a) and minority-carrier (b) DLTS spectra in *p*-InGaAs before (TCA0) and after 1 MeV electron irradiation (TCA0-3) with a fluence of $1\times10^{16}cm^{-2}$.

格子不整合 InGaP 太陽電池についても同様に 1MeV 電子線照射効果を DLTS 法により調べた．InGaP においても転位起因のトラップは観測されなかったが，材料に元来存在する欠陥の照射による振る舞いについて新たな知見が得られた．

* Present Affiliation: University of Sydney, Australia.

** Present Affiliation: LG Electronics, Korea.

1-04 Development of Radiation Hardened High-Speed Logic Circuits by Using 0.15μm SOI Technology

H.Shindou [a], M.Midorikawa [a], Y.Satoh [a], N.Ikeda [a], S.Kuboyama [a], A.Makihara [b], T.Hirao [c], T.Ohshima [c] and H.Itoh [c]

[a] Institute of Aerospace Technology, Japan Aerospace Exploration Agency (JAXA),
[b] High-Reliability Components Corporation (HIREC),
[c] Environment and Industrial Materials Research Division, QuBS, JAEA

Silicon On Insulator (SOI) devices are utilized for high-performance and low-power systems such as computer servers for high-end commercial markets. SOI is a layered structure consisting of a thin layer of silicon mounted on an insulating substrate. The typical cross section image is shown in Fig.1. Compared with bulk Si devices, the amount of electrical charge necessary to operate transistors is very low in SOI devices. SOI is also very attractive as semiconductor devices for space application. Because the sensitive volume for Single-Event Upsets (SEUs) and Single-Event Transients (SETs) in SOI devices is much smaller than in bulk devices, SOI devices are expected to have an advantage over equivalent bulk devices for Single-Event Effects (SEEs) caused by heavy ions and high-energy protons.

The objective of this study is to design SET-free logic cells using SOI technology and evaluate their SEU/SET immunities. Here, the SET is the current spike of short time duration generated by the ion strike to the semiconductor devices. This noise signal leads to other effects such as SEU. In general, there are two ways to eliminate errors caused by SET signals: (a) use SET signal discriminators that ignore unexpected short pulses at input terminals, or (b) use SET-free logic circuits that never generate SET signals at their output. Figure 2 shows the equivalent circuits of inverter logics with redundant transistors in bulk and SOI. The SET signal generation is unavoidable in bulk technologies because all the transistors are isolated by reverse biased p-n junctions. Therefore, the adoption of SET signal discriminator circuits, including temporal redundancy is the only effective mitigation approach for bulk technologies. However, it was reported that the duration of the SET signal in 0.18 μm bulk Si technologies exceeded 1.0 ns at an LET of 50 MeV/(mg/cm^2) [1]. This fact means that the maximum operating frequency of LSIs with complete SET mitigation technique is limited to 500 MHz. In contrast, in SOI technologies, all transistors are electrically isolated by dielectric material. This feature results in a significant advantage over bulk Si technologies in terms of SET mitigation. It is possible, for SOI technologies, to eliminate SET signal generation using circuit techniques.

Test chips of SET-free logic cells were designed and fabricated with a 0.15 μm fully depleted SOI commercial process at OKI (Tokyo, Japan). Figure 3 shows the irradiation test results of latch circuits installed in test chips. It was demonstrated that SET-free latch circuits have excellent SEU/SET immunity[2]. We are planning to use SOI technologies to develop the next generation semiconductor devices for space application.

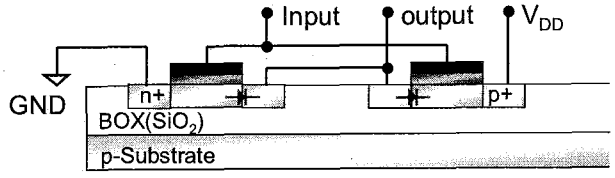
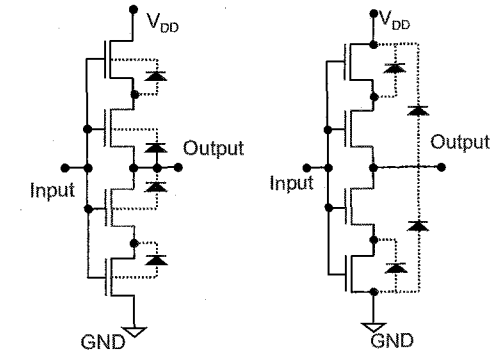


Fig. 1 Cross section image of SOI device (Inverter logic circuit)



(a) bulk (not SET-free) (b) SOI (SET-free)

Fig. 2 Inverter logic circuits with redundant transistors

References

1) P. Eaton et al., IEEE Trans. Nucl. Sci., Vol.51, 3365 (2004).
2) A. Makihara et al., IEEE Trans. Nucl. Sci., Vol. 52, 2524 (2005)

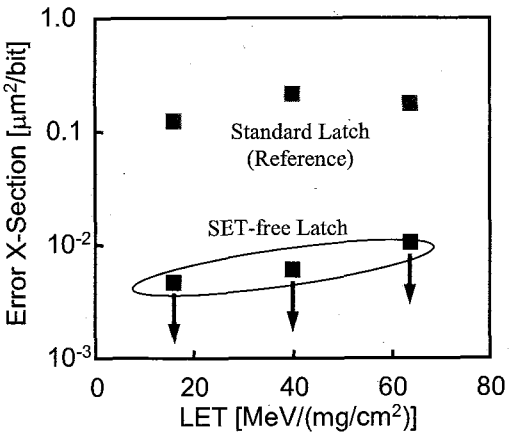


Fig. 3 Error cross section as a function of LET (Standard and SET-free Latch logic circuits)

1-05 Bias Dependence of the Single Event Transient Currents due to Nuclear Products in Semiconductors

S. Onoda[a)], T. Hirao [a)], H. Abe [a)], T. Sanami [b)] and H. Itoh [a)]

[a)]Environment and Industrial Materials Research Division, QuBS, JAEA,
[b)]Radiation Science Center, KEK

High energy neutrons and protons can trigger Bit Error Rate (BER) degradation in optical data links used in radiation environments. It is known that the photodetectors, which are the principle component of optical receivers, are more prone to BER degradation than external encoding electronics. Although the direct ionization results in BER degradation in the photodetectors operated under low optical power level, it is also possible for the secondaries generated by nuclear reactions to induce BER degradation. In silicon based materials, the inelastic as well as elastic reactions generate high-energy secondaries such as He, C, N, O, F, Ne, Na, Mg, Al, Si, P, and recoiling Si atoms with energies up to several tens of MeV. The ionizing energy loss of these secondaries induces a current on the terminal of the photodetector resulting in a Single Event Transient (SET) current that contributes to BER degradation.

In order to clarify the carrier dynamics resulting in the SET currents in Si pin photodiodes due to neutrons, we have evaluated the distributions of collected charge using quasi-monoenergetic neutrons[1]. From the comparison of its distribution and the nuclear cross sections from Evaluated Nuclear Data Format (ENDF-VI), the shape of the experimentally obtained distribution was quite similar to the sum of the cross sections of the secondary nuclides. Then we have concluded that the SET currents were characterized by the spectrum of secondary nuclei. Here, the distributions of the SET characteristics such as collected charge, peak current, risetime and fall time are evaluated by using secondary products due to 65MeV protons being almost equivalent to 65MeV neutrons.

The device examined in this work was a commercial 1.5GHz (at -3dB) Si pin photodiode with a diameter of 450μm. The p-layer width was about 0.2μm, the depletion width was about 15μm at -10V as estimated by the capacitance-Voltage (C-V) and cross-sectional Transient Ion Beam Induced Current (TIBIC) methods. All proton induced SET currents were measured at various biases from -5 to -20V.

Some variation in the SET pulse shape was observed due to variation in the mass, energy and projected range of possible secondary nuclei, as shown in Fig. 1. Although not shown here, the SET currents having multi-peak were obtained when plural nuclei were emitted at the same time i.e., nucleus and alpha. To examine these statistical variations, the collected charge distribution was simply calculated by integrating each SET current and forming a histogram as displayed in Fig. 2 (a). In addition to collected charge, the distributions of other SET parameters represented in Figs. 2 (b), 2 (c) and 2 (d). As shown in Fig. 2 (a) the charge was collected up to approximately 1pC, which is corresponding to the maximum energy of secondaries (about 22MeV). In this estimation, the energy

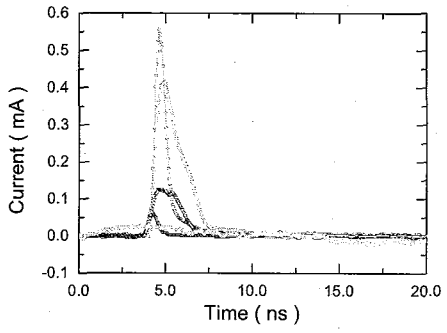


Fig.1 Typical SET currents induced by 65MeV protons.

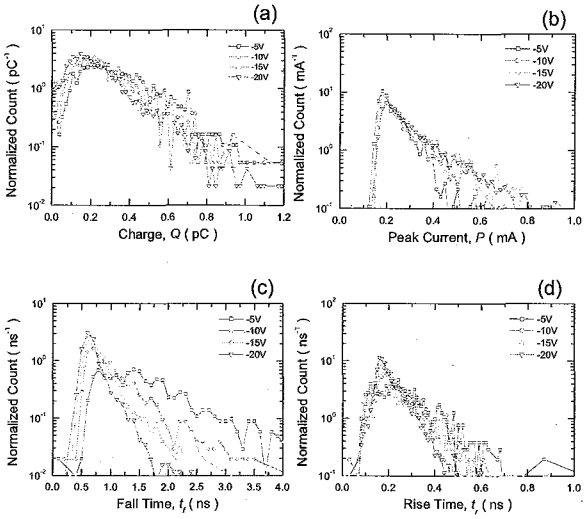


Fig.2 Distributions of SET current characteristics: (a) collected charge, (b) peak current, (c) fall time, and (d) rise time.

for the generation of an e-h pair in Si was assumed to be 3.62eV. Slight differences in the charge distributions among biases were observed. The most likely reason for the differences is the bias dependence of peak current distribution as shown in Fig. 2 (b). The higher bias leads to the faster drift velocity of carriers, which results in the higher peak current. As a result, the SET currents due to a secondary ion with low energy cannot exceed the trigger level especially for the case of low bias, i.e. -5V. As shown in Figs. 2(c) and 2(d), both the fall time and the rise time decreased with increasing bias, which is caused by the faster drift velocity. The experimentally obtained distributions indicate that the knowledge of the carrier dynamics is one of the most important issues to understand the SET currents induced by neutrons and protons.

References

1) T. Wakasa et al., TIARA annual report 2003 (2004), 21.

1-06 Influence of Carrier Recombination Process on Single Event Transient Current in Si Diodes under High Injection by Heavy Ions

K. Mishima[a,b], T. Hirao [a], S. Onoda [a], H. Abe [a], H. Itoh [a] and K. Kawano [b]

[a] Environment and Industrial Materials Research Division, QuBS, JAEA,
[b]The University of Electro-Communication

Artificial satellites are exposed to a lot of high energy heavy ions in space. When an ion penetrates into semiconductors, dense carriers are generated and lead to Single Event Effects (SEEs) in LSI circuits[1]. Therefore, understanding of the carrier dynamics is required for the development of semiconductors with high radiation resistance. In this study, to clarify the carrier dynamics in SEE processes, Single Event Transient Currents (SETCs) generated by an oxygen (O) ion in Si p-i-n diodes were measured and calculated. Comparing these results, the influence of carrier recombination processes on total collected charge is discussed.

The devices used in this work were commercial Si p-i-n photodiodes with a diameter of 450μm. The p-i-n diode consisted of highly doped p^+ ($\sim 8\times10^{18}cm^{-3}$), the semi-intrinsic ($\sim 1\times10^{14}cm^{-3}$), and highly doped n^+ ($\sim 2\times10^{18}cm^{-3}$) region. A constant reverse bias of 10V was applied to the device during irradiation. Under this bias setting the depletion width was about 15μm, which was evaluated by C-V mesurements. The SETCs were measured by using Transient Ion Beam Induced Current (TIBIC) system[2].

Figure1 shows the SETCs induced by a 15MeV O ion. The closed squares indicate the experimental results. The amount of collected charge is estimated to be 596±56fC from the integration of the SETC. On the other hand, the total charge is theoretically calculated to be 689fC by using SRIM[3]. In this calculation the energy for the generation of an electron-hole (e-h) pair in Si is assumed to be 3.6eV. We evaluate the difference between experimental and analytical charges by considering the carrier recombination processes which are potentially a source of this difference. For this aim, we have simulated the SETCs using the Synopsis TCAD version 10. The DESSIS package is used to simultaneously solve the Poisson and e-h continuity equations under cylindrical symmetry (quasi-three-dimensional). Physical models used in the simulations are Fermi-Dirac statistics, Shockley-Read-Hall (SRH) statistics, the band gap narrowing (Bennett-Wilson model), the high field saturation (Canali model), the doping dependence and the carrier-carrier scattering (Brooks-Herring model)[2]. In addition, we evaluate the influence of the recombination processes on the total collected charge by considering following processes: SRH, Auger and radiative recombination. Both SRH and Auger recombination depend on the carrier density. Especially, Auger recombination is dominant process under high injection condition[2]. Radiative recombination is relatively unimportant in Si, because its radiative lifetime is extremely long[4]. Therefore, radiative recombination can be neglected in this study.

All of the calculated results are represented in Fig.1. The open circles, open diamonds, and closed triangles describe the simulated SETCs assuming no recombination, SRH recombination, and both SRH and Auger recombination, respectively. Comparing the calculated results, there was almost no difference. In addition, comparing the calculated SETCs with the experimental one, the calculated charge is 1.1 times higher than the experimental one. This fact suggests that the recombination process dose not affect the total charge. These facts mean that almost all carriers are swept by drift and diffusion processes before recombination.

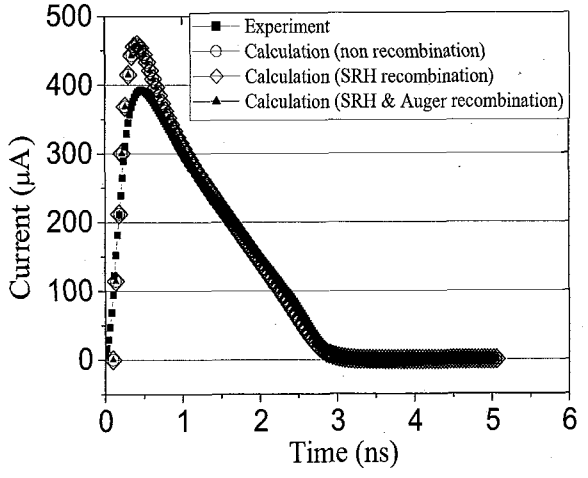


Fig.1 Experimentally and theoretically obtained SETCs for the Si p-i-n diode sample with a 15MeV O ion.

References

1) T. Weatherford, IEEE NSREC short course, sec. IV (2002).
2) J. S. Laird, T. Hirao, S. Onoda and H. Itoh, J. Appl. Phys., vol. 98, 013530-14 (2005).
3) http://www.srim.org
4) R. Hacker and A. Hangleiter, J. Appl. Phys. vol. 75, pp. 7570-7572 (1994).

1-07 Heavy-Ion Induced Current through an Oxide Layer

K. Ohnishi[a)], Y. Takahashi[a)], Y. Nakajima[a)], T. Nagasawa[a)], T. Hirao[b)], S. Onoda[b)], K. Mishima[b)] and H. Itoh[b)]

[a)] NIHON University, [b)] Environment and Industrial Materials Research Division, QuBS, JAEA

Abstract

The heavy-ion induced transient gate current in MOSFETs has been investigated. When the drain and source electrodes were connected to the substrate (back) electrode, it was found that the transient current with both positive and negative peaks was observed by ion irradiation to the gate area and that the amount of collected charge converged to almost zero within 100-200ns after irradiation. These phenomena show that the radiation-induced current through an oxide layer is dominated by a displacement current.

宇宙空間など放射線環境下で半導体デバイスを使用すると，重イオンなど高速粒子線照射により半導体中で生じた電荷に起因した過渡電流が発生し，メモリ内容の反転など誤動作が引き起こされる．一方，埋め込み酸化膜を有するSOI基板を用いた場合，能動領域を薄くできるため誘起電流を抑制でき，放射線耐性向上が期待される．ただしSOI素子に高エネルギー重イオンを照射した場合，予想を大きく上回る誘起電流が観測されるとの報告もあり[1),2)]，酸化膜（絶縁膜）を介した重イオン誘起電流発生メカニズムの解明が非常に重要である．本研究では，MOS構造の重イオン誘起電流について検討を行っている．これまでに，MOSダイオードを用いた実験およびシミュレーション結果との比較により，変位電流により説明可能であることを示した[3)]が，伝導電流を否定する実験的確証は得られていない．そこで今回，MOSFETを用いた重イオン照射誘起電流測定を行い，電流発生機構について更なる検討を行った．

Alゲートp-MOSFET（d_{ox}=42nm，L=100μm，W=300μm）を作製し，日本原子力研究開発機構のタンデム加速器およびサイクロトロンに接続されたマイクロビームシステムを用いて各種重イオン照射試験を行い，高速オシロスコープにより照射誘起過渡電流の測定を行った[4)]．Fig. 1 に，ソース・ドレイン電極を接地（基板と同電位）した状態で，ゲート領域に酸素イオン（15MeV）を照射した場合の，ゲート電極における照射誘起過渡電流および収集電荷（電流積分値）の測定結果を示す．なお図中のパラメータは照射中のゲート電圧である．結果より照射中，負のゲート電圧を印加した場合には，ピーク値の異なる正・負の電流が観測され，またその積分値は照射後100ns程度でほぼ0となることがわかった．なお，正のゲート電圧を印加して照射を行った際には，過渡電流は測定できなかった（ノイズレベル）．一方，ソース・ドレイン電極を開放状態として照射を行った場合には，正方向の電流ピークのみしか観測されなかった(MOSダイオードにおける照射誘起電流と同様)．

酸化膜を介した照射誘起電流の発生メカニズムとしては，伝導電流（酸化膜リーク電流）および変位電流が考えられる．ここで本誘起電流が伝導電流によるものであれば，正方向の電流のみが観測される．一方，変位電流のみによる場合には電流の時間積分値が0になるはずである．よって本測定結果より，酸化膜を介した照射誘起電流が，ほぼ変位電流であることを実験的に確認した．またシミュレーション結果との比較より，拡散層電位が開放の場合，照射により発生し界面付近に蓄積された正孔が，基板電子との再結合により徐々に消滅するため，非常に小さな負方向電流しか発生しないのに対し，拡散層電位を0Vとすることにより，内蔵電位により過剰正孔が急速にソース・ドレイン電極に収集されることにより，大きな負方向電流が生成されることが明らかになった．

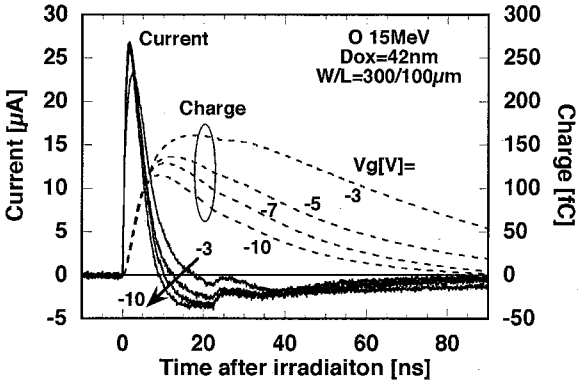


Fig.1 Transient gate current and collected charge induced by 15MeV O ions in a MOSFET, in which V_g= -3~-10V and V_s= V_d= 0V.

References

1) P.E. Dodd, et al., "SEU-sensitive volumes in bulk and SOI SRAMs from first-principles calculations and experiments," IEEE Trans. Nucl. Sci., NS-48, 6, 1893 (2001).
2) T. Hirao, et al., "Study of single-event current pulses induced in SOI diodes by collimated swift heavy-ions micro-beams," Nuclear Instruments and Methods in Physics Research B 206, 457 (2003).
3) Y. Takahashi, et al., "MOS構造における重イオン照射誘起電流," 電子情報通信学会論文誌, J89-C, 3, 104 (2006).
4) J.S. Laird, et al., "Development of a new data collection system and chamber for microbeam and laser investigations of single event phenomena," Nuclear Instruments and Methods in Physics Research B 181, 87 (2001).

1-08 Single Event and Total Dose Synergy Effects in SOI Devices

H. Mori[a)], S. Satoh[a)], T. Hirao[b)], S. Onoda[b)], H. Abe[b)] and H. Itoh[b)]

[a)]Graduate School of Engineering, University of Hyogo,
[b)]Environment and Industrial Material Research Division, QuBS, JAEA

Semiconductor devices installed in artificial satellites are exposed to space radiations. They cause two kinds of radiation effects, which are called a single event effect and a total dose effect. In the space environments, it is most probable that these effects simultaneously occur in semiconductor devices. However, very little is known about the single event and total dose synergy effect. In this study, we aim at clarifying the synergy effect in SOI (silicon on insulator) devices, which have received considerable interest recently because of their excellent performance, e.g., high speed and low power operation, required for space application. In this paper, we report the synergy effect in SOI devices from C-V measurements before and after proton irradiation and single event transient current measurements using single oxygen ion irradiation.

For test samples, MOS capacitors and Schottcy diodes were fabricated on the same SOI wafer, which has an SOI layer with the thickness of 3.5 μm and the resistivity of 5-20 Ω, and a BOX layer with the thickness of 0.5 μm. Proton and oxygen ion irradiations were performed at TIARA facility. The proton energy was chosen to be 370 keV to form the damage profiles at the center of the BOX layer and the oxygen energy to be 15 MeV to pass through the BOX layer. The fluence of protons ranged from $1x10^9$ to $2x10^{10}$ cm^{-2}. High-frequency back gate C-V measurements were performed to obtain the electrical characteristics before and after proton irradiation for three regions of the SOI samples, i.e., (1) the interface between the SOI layer and the BOX one, (2) the interface between the BOX layer and the Si substrate, and (3) the BOX layer. Figure 1 shows the flat band voltage derived from the back gate C-V curves for the samples irradiated with 370 keV-protons. It was found that the flat band voltage shifted toward the negative voltage side by the irradiation. This result indicates that positive fixed charges are produced in the BOX layer by proton irradiation. After proton irradiation, single event transient currents were measured for the Schottcy diode sample to evaluate electron hole pairs generated in the SOI layer. Figure 2 shows the waveforms of transient currents induced by an oxygen ion in the sample before and after proton irradiation. As shown in Fig. 2, the peak value of transient current changed with proton fluence. However, the amount of collected charge, which is obtained by integrating the transient current, is almost the same in all conditions. This result suggests strongly that the amount of collected charge is not influenced by positive charge in the BOX layer and the interface traps between the SOI layer and BOX one. These facts also indicate that SOI devices are useful for space applications.

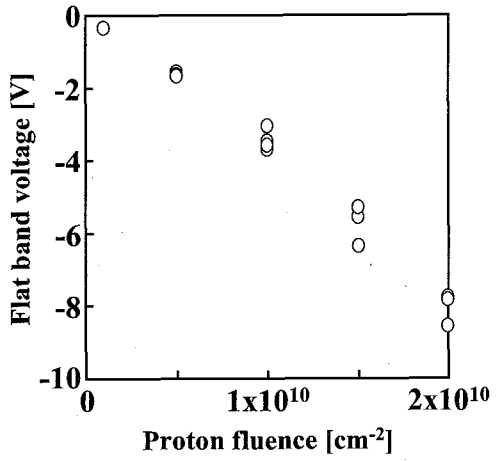


Fig 1. Change in the flat band voltage in the SOI samples due to proton irradiation.

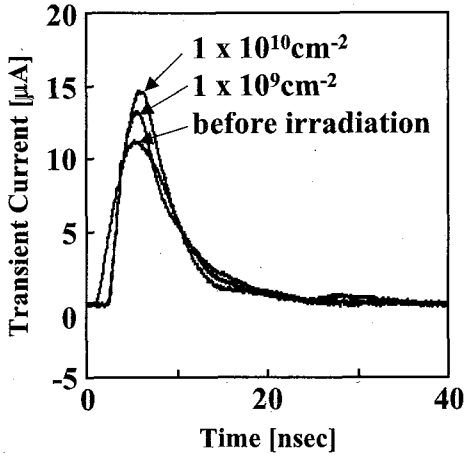


Fig 2. Waveforms of the transient currents induced by an oxygen ion in the SOI samples irradiated with protons and in the unirradiated one.

1-09 Decrease in Charge Collection Efficiency Obtained for 6H-SiC n^+p Diodes by Ni Ion Incidence

T. Ohshima[a)], S. Onoda[a)], M. Oikawa[b)], T. Satoh[b)], T. Hirao[a)], T. Kamiya[b)] and H. Itoh[a)],

[a)]Environment and Industrial Materials Research Division, QuBS, JAEA
[b)]Department of Advanced Radiation Technology, TARRI, JAEA

One of the applications expected for silicon carbide (SiC) is particle detectors used in radiation environments since SiC shows superior radiation tolerance[1]. For this purpose, it is important to understand the behavior of charge generated in SiC by ion incidence. In a previous study[2], Nava et al. reported that Charge Collection Efficiency (CCE) obtained from 4H-SiC diodes irradiated with alpha particles was 100 %. The CCE of 100 % was also reported for 6H-SiC diodes irradiated with oxygen (O) ions[3]. These results suggest that SiC is suitable for particle detectors. However, for the development of particle detectors, CCE of SiC diodes should be evaluated using a wide variety of ions since charge generated by ion incidence depends on ion species. Heavy ions generate dense electron-hole (e-h) pairs in diodes, and this leads to a transient change in electric field (space-charge effect)[4]. Because carrier transport properties are disturbed by the space-charge effect, it is important to reveal the behavior of charge generated in SiC by heavy ion irradiation. In this study, we evaluate charge generated in 6H-SiC diodes by nickel (Ni) ions at 18 MeV.

Samples used in this study were 6H-SiC n^+p diodes fabricated on 30 μm thick p-type epitaxial layer with an aluminum concentration of $1x10^{15}$ /cm^3. The n^+ region with a thickness of 100 nm was formed using phosphorus (P) ion implantation (a mean P concentration of $5x10^{19}$ /cm^3) at 800 °C followed by annealing at 1650 °C for 5 min in argon. Before Ni irradiation, the current – voltage characteristics for the 6H-SiC n^+p diodes were measured in a shielded probe box to minimize external noises. The current in order of 10^{-8} A/cm^2, which is the detection limit of the measurement system, was observed at the reverse bias of 40 V. The diodes were irradiated with 18 MeV-Ni microbeams under applied reverse biases up to 150V, and transient current generated by irradiation of Ni ions was measured using the Transient Ion Beam Induced Current (TIBIC) system[5].

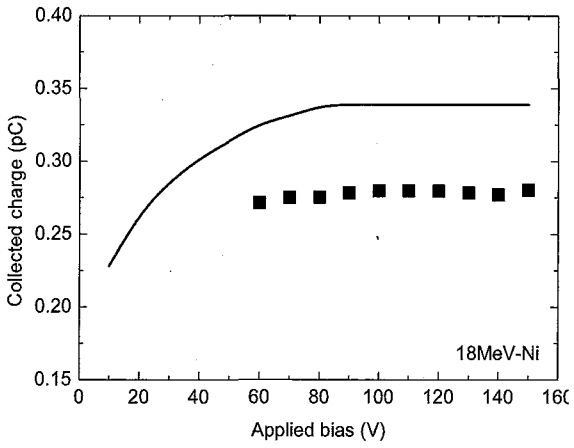


Fig. 1. Value of collected charge as a function of applied reverse bias. The estimated value of charge generated in the depletion layer (ideal value) is also represented as a solid line.

Charge collected from 6H-SiC diodes was estimated from the integration of the TIBIC signals. Figure 1 shows the value of collected charge as a function of applied reverse bias. The estimated value of charge generated in the depletion layer (ideal value) is also represented as a solid line. In the estimation, ionizing energies deposited from 18 MeV Ni ions into SiC were calculated by Monte Carlo simulation code SRIM2003[6]. The energy for the generation of an e-h pair ($E_{e\text{-}h}$) in 6H-SiC is assumed to be 7.8 eV (= $2.8E_g$) on the analogy of $E_{e\text{-}h}$ in Si because the value of the energy for 6H-SiC has not yet been determined. As shown in Fig. 1, the collected charge does not depend on applied bias above 60 V and the value is 0.275 pC. On the other hand, the ideal value is estimated to be 0.339 pC. Since the depletion layer is estimated to be 5 μm at an applied bias of 20V and the range of 18 MeV-Ni is 5 μm, the obtained result indicates that approximately 20 % of charge generated in the depletion layer are not collected at reverse biases between 60 and 150 V. In the case of O and Si ions, the CCE obtained for this diode is approximately 100 %. Since high dense e-h pairs are generated by heavy ion incidence, and the recombination of generated carriers might occur in such high dense plasma[7], the result obtained in this study can be interpreted in terms of the recombination of carriers generated in depletion layer.

References

1) T. Ohshima et al.: J. Appl. Phys. **96** (2001) 3038.
2) F. Nava et al.: Nucl. Instr. & Meth. A **505** (2003) 645.
3) T. Ohshima et al.: Nucl. Instr. & Meth. A **541** (2005) 236.
4) J. S. Laird et al.: J. Appl. Phys. **98** (2005) 13530.
5) J. S. Laird et al.: Nucl. Instr. and Meth. B **181** (2001) 87.
6) J. F. Ziegler, *Handbook of Ion Implantation Technology*, Elssevier Science Publishers B.V., The Netherland (1992) pp.1-68.
7) V. Zajic, P. Thieberger, IEEE Trans. Nucl. Sci. **46** (1999) 59.

1-10 Relationship between Defects Induced by Irradiation and Reduction of Hole Concentration in Al-Doped 4H-SiC

H. Matsuura[a)], S. Kagamihara[a)], Y. Itoh[a)], T. Ohshima[b)] and H. Itoh[b)]

[a)]Electronic Engineering and Computer Science, Osaka Electro-Communication University,
[b)]Environment and Industrial Materials Research Division, QuBS, JAEA

From the temperature dependence of the hole concentration p(T) for lightly Al-doped 4H-SiC epilayers, one acceptor species with ~200 meV and another acceptor species with ~350 meV were observed [1,2], where all the energy levels were measured from the valence band maximum (E_V). From photoluminescence (PL), the shallow acceptor species was ascribed to an Al atom (Al_{Si}) at a Si sublattice site. The origin of the deep acceptor (i.e., defect) has so far not been determined. The density (N_{Defect}) of this defect was a little lower than the density (N_{Al}) of the Al acceptor, with the N_{Defect} proportional to the Al-doping density [1]. This indicated that the deep defect might be related to Al.

Irradiation with 4.6 MeV electrons at 2.6×10^{14} cm^{-2} fluence reduced N_{Al} by ~10, while reducing N_{Defect} only slightly [2]. Therefore, the reduction in p(T) with this irradiation results from a decrease in N_{Al}. The decrease in N_{Al} is due to either the displacement of Al_{Si} or the bond breaking between the Al_{Si} and its nearest neighbor C.

Since the atomic mass of C is smaller than that of Si, the minimum electron energy necessary for displacing one substitutional C atom (C_s) should be lower than that for one substitutional Si atom (Si_s). According to literature [3], an electron with 0.19~0.36 MeV can displace only C_s.

Free carrier concentration spectroscopy (FCCS) is applied to determine the densities and energy levels from p(T) without any assumptions regarding the acceptor species and the defects [1,2].

A 10 μm-thick Al-doped p-type 4H-SiC epilayer (Al-doping density: ~5×10^{14} cm^{-3}) on n-type 4H-SiC (thickness: 376 μm, resistivity: 0.02 Ωcm) was cut to a 1x1 cm^2 size. The p(T) was measured by van der Pauw configuration in the temperature range from 120 to 600 K at a magnetic field of 1.4 T. The sample was irradiated with 1.0×10^{16} cm^{-2} fluence of 0.2 MeV electrons at room temperature.

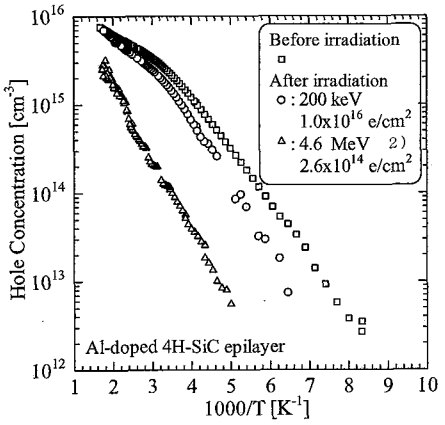


Fig. 1 Temperature dependence of hole concentration in 4H-SiC before and after electron irradiation.

Figure 1 shows the experimental p(T) for the unirradiated sample (□) and the sample (○) irradiated with the 1.0×10^{16} cm^{-2} fluence of 0.2 MeV electrons. The p(T) for the sample irradiated with the 2.6×10^{14} cm^{-2} fluence of 4.6 MeV electrons is also shown by (△) [2]. The reduction in p(T) by irradiation with 0.2 MeV electrons is less than that due to irradiation with 4.6 MeV electrons, although the larger amount of electrons was delivered to the sample in the case of the 0.2 MeV electron irradiation.

In the samples before and after irradiation, an Al acceptor level (ΔE_{Al}), N_{Al}, a defect level (ΔE_{Defect}), and N_{Defect} were determined by FCCS, and are listed in Table 1.

With irradiation by 0.2 MeV electrons at 1.0×10^{16} cm^{-2} fluence, the decrement of N_{Al} is nearly equal to the increment of N_{Defect}, as shown in Table 1. If the bond between the Al_{Si} and its nearest neighbor C_s is broken due to the displacement of C_s by this electron irradiation, the Al acceptor density is decreased and the density of the Al_{Si}-V_C complex is increased, which is consistent with the experimental finding. Therefore, the origin of the deep acceptor is most likely Al_{Si}-V_C.

With irradiation by electrons at $\geq$0.5 MeV, the N_{Al} should decrease due to the displacement of both C_s and Al_{Si}. If the deep acceptor is Al_{Si}-V_C, N_{Defect} should decrease due to the displacement of Al_{Si}, and should increase due to the displacement of Al's nearest neighbor C_s. Therefore, N_{Al} is reduced significantly, whereas N_{Defect} is decreased slightly, which is in good agreement with the experimental results [2].

REFERENCES

1) H. Matsuura, M. Komeda, S. Kagamihara, H. Iwata, R. Ishihara, T. Hatakeyama, T. Watanabe, K. Kojima, T. Shinohe, and K. Arai, J. Appl. Phys. **96** (2004) 2708.
2) H. Matsuura, K. Aso, S. Kagamihara, H. Iwata, T. Ishida, and K. Nishikawa, Appl. Phys. Lett. **83** (2003) 4981.
3) H. Matsuura, S. Kagamihara, Y. Itoh, T. Ohshima, and H. Itoh, Physica B **376-377** (2006) 342.

Table 1 Results from p(T).

	unirradiated	0.2 MeV	4.6 MeV [2]
ΔE_{Al} [meV]	203	217	206
N_{Al} [x10^{15} cm^{-3}]	5.2	4.3	0.82
ΔE_{Defect} [meV]	357	363	383
N_{Defect} [x10^{15} cm^{-3}]	3.5	5.2	3.5

1-11 EPR Study of Electron-Irradiated SiC: Structure Determination of Intrinsic Defects in *4H*-SiC

J. Isoya[a], T. Umeda[a], N. Mizuochi[a], M. Katagiri[a], T. Ohshima[b], N. Morishita[b] and H. Itoh[b]

[a]Graduate School of Library, Information and Media Studies, University of Tsukuba,
[b]Environment and Industrial Materials Research Division, QuBS, JAEA

Silicon Carbide (SiC) is promising material for electronic devices for high power applications and of high radiation resistance. Electron paramagnetic resonance (EPR) is utilized both for identifying impurity and defects and estimating each concentration of them. An EPR spectrum from an intrinsic defect in SiC consists of strong primary line(s) and weak ^{29}Si (I=1.2, 4.7%) and ^{13}C (I=1/2, 1.1%) hyperfine lines. Although intrinsic defects are distinguishable by the line position(s), i.e. g-values of primary line(s), unambiguous identification of an intrinsic defect requires a full set of ^{29}Si and ^{13}C hyperfine interactions of major atoms constituting the defect. Once the assignment of the EPR spectrum to an intrinsic defect is established, the primary line(s) are sufficiently utilized in characterization for improving the quality of substrates and epilayers, for improving the efficiency of ion-implantation doping and for understanding the mechanism of radiation-induced degradation. We have been identifying the intrinsic defects in *4H*-SiC by detailed analysis of the angular dependence of the EPR line positions including weak ^{29}Si and ^{13}C satellite lines. Pulsed ENDOR to resolve the hyperfine lines and photo-EPR to determine the energy positions in the gap are also used. By selecting conditions of electron irradiation such as total dose and irradiation temperature (RT to 800°C) and by proper choice of the conductivity of the unirradiated substrates, we increased the signal intensity of a particular defect while minimizing the disturbance from other signals.

For negatively charged silicon vacancy (V_{Si}^-) in *4H*-SiC, we have revealed a small distortion from T_d symmetry and distinguished hexagonal (h) and quasicubic (k) sites from the ^{13}C hyperfine interactions[1]. We have identified that the TV_{2a} center is an analog of V_{Si}^- from the ^{13}C hyperfine interactions and from the effective spin of S=3/2 determined by nutation method and by pulsed ENDOR[2, 3]. It has been clarified that the lattice relaxation is significantly different between $V_C^+(h)$ (the EI6 spectrum) and $V_C^+(k)$ (the EI5 spectrum)[4,5]. The HEI1 center has been identified to be $V_C^-(k)$[6]. The P6/P7 spectra (S=1) are identified to be arising from divacancy, $(V_CV_{Si})^0$, in which the unpaired electron is localized predominantly on three carbon atoms of the V_{Si} side[7]. If a carbon atom neighbor of V_{Si}^- moves into the vacancy, carbon antisite is formed with accompanying carbon vacancy. The EI5 center is identified to be carbon antisite-vacancy pair in the negative charge state, $(C_{Si}V_C)^-$ [8].

References

1) N. Mizuochi, S. Yamasaki, H. Takizawa, N. Morishita, T. Ohshima, H. Itoh, J. Isoya, Phys. Rev. B 68, 165206 (2003)
2) N. Mizuochi, S. Yamasaki, H. Takizawa, N. Morishita, T. Ohshima, H. Itoh, J. Isoya, Phys. Rev. B66, 235202 (2002)
3) N. Mizuochi, S. Yamasaki, H. Takizawa, N. Morishita, T. Ohshima, H. Itoh, T. Umeda, J. Isoya, Phys. Rev. B 72, 235208 (2005)
4)T. Umeda, J. Isoya, N. Morishita, T. Ohshima, and T. Kamiya, Phys. Rev. B 69, 121201(R), (2004)
5) T. Umeda, J. Isoya, N. Morishita, T. Ohshima, T. Kamiya, A. Gali, P. Deak, N. T. Son, E. Janzen, Phys. Rev. B 70, 235212 (2004)
6) T. Umeda, Y. Ishitsuka, J. Isoya, N. T. Son, E. Janzen, N. Morishita, T. Ohshima, H. Itoh, A. Gali, Phys. Rev. B 71 193202 (2005)
7) N. T. Son, P. Carlsson, J. ul Hassan, E. Janzen, T. Umeda, J. Isoya, A. Gali, M. Bockstedte, N. Morishita, T. Ohshima, H. Itoh, Phys. Rev. Lett. 96, 055501 (2006)
8) T. Umeda, N. T. Son, J. Isoya, E. Janzen, T. Ohshima, N. Morishita, H. Itoh, A. Gali, M. Bockstedte, Phys. Rev. Lett. 96, 145501 (2006)

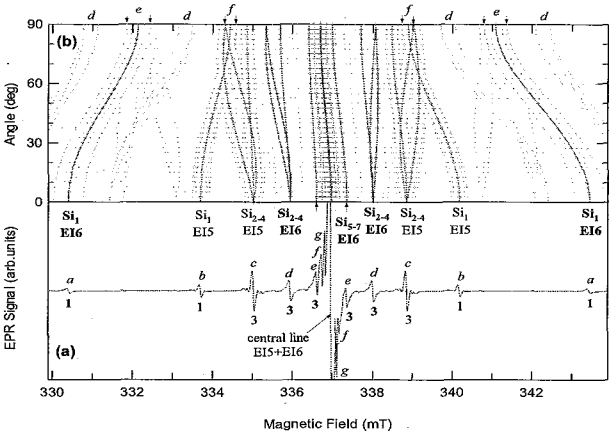


Fig.1 EPR spectra of EI5 and EI6 (150K)

1-12 EPR Study of High Energy Phosphorus Ion Implanted SiC: Phosphorus Donors Substituting for Carbon Atoms

J. Isoya[a)], T. Umeda [a)], N. Mizuochi [a)], M. Katagiri [a)], T. Ohshima [b)], N. Morishita [b)] and H. Itoh [b)]

[a)]Graduate School of Library, Information and Media Studies, University of Tsukuba,
[b)]Environment and Industrial Materials Research Division, QuBS, JAEA

Silicon Carbide (SiC) is promising material for electronic devices for high temperature, high frequency, high power applications and of high radiation resistance. For fabrication of semiconductor devices, controlling of conductivity by doping shallow donors or acceptors is essential. In SiC, nitrogen (N) shallow donors, which are easily incorporated during the growth, encounter a saturation of free carrier concentration at high doping level (~10^{19}cm^{-3}). Phosphorus (P) is an alternative shallow donor to N, especially in the high concentration range.

In hexagonal polytypes of SiC, each silicon and carbon has inequivalent sites, two (*h* and *k*) in *4H*-SiC and three (*h*, k_1, and k_2) in *6H*-SiC. By applying electron paramagnetic resonance (EPR) technique, not only phosphorus donors are picked out among those phosphorus introduced into the lattice, but also phosphorus donors occupying different inequivalent sites are distinguished.

In SiC, doping of P by diffusion is difficult. The first report of EPR spectra (P_a, P_b) arising from P donors in *6H*-SiC used neutron transmutation doping.[1)] The P_a/P_b spectra were also observed in *6H*-SiC implanted with P-ions of 9-21MeV/340keV.[2)] Detailed studies of P-related centers other than P_a/P_b were severely hampered by the disturbing, strong signals of shallow N donors in the substrates obtainable at those times.

With P-ion implantation of *4H*-SiC of normally available substrates, EPR spectrum corresponding to P_a/P_b was hardly separated from strong signals of N. As shown in Fig.1, by using high-purity semi-insulating (HPSI) or low-N substrates, we have found the P_c spectrum arising from P donors in *4H*-SiC implanted with P-ions (5×10^{13}cm^{-2} at 9 steps of 9-21 MeV, 800°C) with the subsequent annealing (1650°C, 30min.).

The P_a/P_b spectra were assumed to be arising from P donors at silicon sites.[1,2)] However, it was pointed out that a considerable fraction of P might end up in occupying the carbon site after high-temperature annealing required for electrical activation in both neutron-transmutation and ion-implantation doping.[3)] Theoretical study suggested P_a, P_b are arising from P at C (k_1, k_2).[3)] Thus, it is likely that P at C(k) gives rise to the P_c spectrum in *4H*-SiC.

By using CVD grown epitaxial film of successful *in-situ* P-doping, we have observed EPR spectra of P donors at Si (k_1,k_2) instead of P_a/P_b in *6H*-SiC and that of P donors at Si(*k*) instead of P_c in *4H*-SiC.[4)] The site assignment is based on both the observation of the ^{13}C hyperfine lines of the nearest-neighbor atoms and the results of *ab initio* supercell calculations.

As shown in Fig.2, by using HPSI-*6H*-SiC, both P donors at Si(k_1, k_2) sites and P donors at C(k_1, k_2) sites (i.e. P_a/P_b) have been observed in *6H*-SiC implanted with P-ions (5×10^{13}cm^{-2} at 9 steps of 9-21 MeV, 800°C) with the subsequent annealing (1650°C, 30min.). In P-implanted *4H*-SiC (Fig.1), EPR signals of P donors at Si sites were not resolved due to the presence of the residual defects (HPSI substrate) or of N donors (low-N substrate).

Our present work demonstrates that EPR technique should be utilized as a powerful characterization method for studying the electrical activation process in P ion-implantation doping, especially for controlling the ratio between P at Si and P at C sites.

Reference

1) A. I. Veinger *et al*, Fiz. Tverd. Tela 28, 1659 (1986) [Sov.Phys. Solid State 28, 917 (1986)]

2) J. Isoya *et al*, Nucl. Instrum. Methods Phys. Res. B 206, 965 (2003)

3)E. Raulset *et al*, Phys. Rev. B 70, 85202 (2004)

4) N. T. Son, A. Henry, J. Isoya, M. Katagiri, T. Umeda, A. Gali, E. Janzen, Phys. Rev. B 73, 075201 (2006)

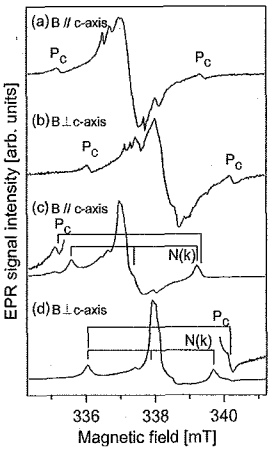


Fig.1 EPR spectra of P-ion implanted and annealed *4H*-SiC (a)(b) HPSI (5K), (c)(d) Low-N (5K).

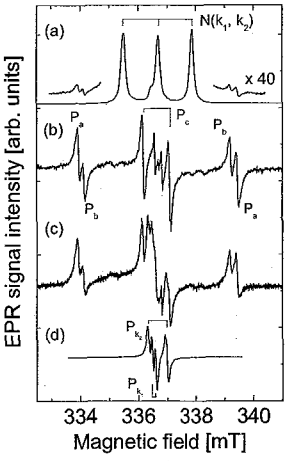


Fig.2 EPR spectra (B//c-axis) of P-ion implanted and annealed *6H*-SiC (a) n-type (60K), (b) HPSI (60K), (c) HPSI (6K), and (d) CVD-grown P-doped *6H*-SiC (8K).

1-13 Development of Optoelectronic Devices for Radiation Environments - Improvement of Luminescence Capability of Tb Using AlGaN -

A. Wakahara[a)], H.Okada [a)], F.Oikawa [a)], K.Takemoto [a)], T.Ohshima [b)] and H.Itoh [b)]

[a)]Department of Electrical and Electronic Engineering, Toyohashi University of Technology,
[b)] Environment and Industrial Materials Research Division, QuBS, JAEA

We have been investigating optoelectronic devices based on rare-earth doped group-III nitrides which can be utilized in high temperature and/or radiation environments. Our previous study shows that luminescence capability can be dramatically improved by using AlGaN as the host material for rare-earth impurity which acts as an efficient luminescence center[1]. We have recently reported that the luminescence caused by the inner shell transition of rare-earth impurities doped in III-nitrides showed high radiation tolerance and that no degradation in luminescence properties could be observed with 3MeV electron irradiation up to a total dose of $10^{17}cm^{-2}$ [2]. In order to realize optoelectronic devices based on rare-earth doped III-Nitrides, the mechanizums of the improvement have to be clarified. In this report, we investigate the energy transfer process in Tb-doped AlGaN, which shows large improvement of luminescence capability by the use of AlGaN, by means of time-resolved photoluminescence (TRPL).

Tb was introduced by ion implantation with the acceleration energy of 200keV and the dose was fixed at $5 \times 10^{14}cm^{-2}$. Single crystalline $Al_xGa_{1-x}N$ thin films with the AlN molar fraction x=0.2 and 0.8 were used as the host materials, where improvement of the luminescence capability is larger for higher AlN molar fraction. The Tb-implanted samples were annealed in N_2 and NH_3 mixture at 1100°C for 120s to eliminate the implantation damage. TRPL measurements were carried out by using ArF excimer laser as the excitation light source with the pulse duration of 25ns and the power density of $8.3mJ/cm^2$.

Figure 1 shows the transient decay of $^5D_4$—$^7F_6$ transition at room temperature. In case of AlN molar fraction of x=0.2, both raise and decay times seem to be shorter than those observed in x=0.8. We used rate equation analysis to know the energy transfer/back-transfer process. In order to explain thermal quenching, both inter band radiative and non-radiative transitions in AlGaN were taken into account in addition to the conventional model (Fig.2).

The results of rate equation analysis reproduce the experimental results, including thermal quenching. From the results, it can be concluded that the improvement of the luminescence intensity by increasing the AlN molar fraction is due to the improvement of the energy transfer efficiency with increasing the AlN fraction. The reduction of thermal quenching is due to the reduction of the energy back-transfer rate by increasing the AlN fraction, which would be due to an increase of the energy separation between the back-transfer and Tb inner levels via increased energy gap of the host. Based on the results, further investigations of effects of high energy particles on TRPL of Tb-related luminescence are necessary to clarify the improvement effects of AlGaN and for realizing radiation hard optoelectronic devices.

References

1) A. Wakahara, Optical Mater. **28**, 731 (2006).
2) Y.Nakanishi, A.Wakahara, H.Okada, A.Yoshida, T.Ohshima, and T.Itoh, Appl. Phys. Lett. 81, 1943 (2002)

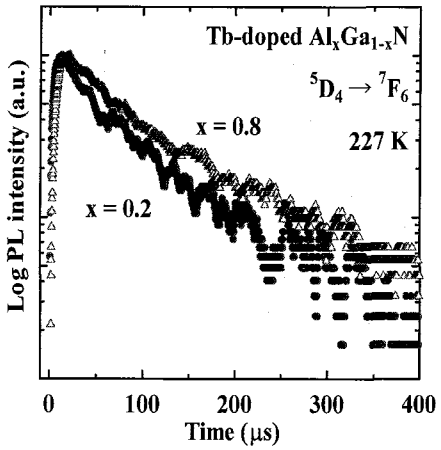


Fig.1 Typical transient decay of luminescence corresponding to $^5D_4$—$^7F_6$ transition in Tb. Higher AlN contained sample shows longer decay time.

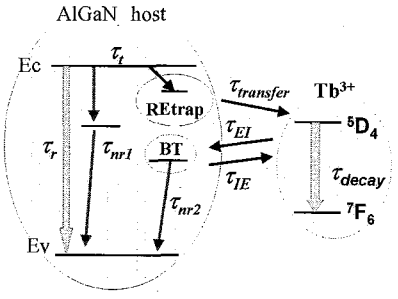


Fig.2 Analysis model used in the present work. In addition to the conventional energy-transfer and/or back-transfer model for rare-earth doped semiconductors, radiative and non-radiative transitions in the host are considered.

1-14 Mechanical Properties of Austenitic Stainless Steel Ion-Irradiated under External Stress

I.Ioka[a], Y. Ishijima[a], M.Futakawa[b], T.Suzuki[a], K.Kiuchi[a] and T.Naoe[c]

[a] Division of Fuels and Materials Engineering, NSED, JAEA
[b] Proton Accelerator Facility Development Center, QuBS, JAEA
[c] Graduate School of Ibaraki University

1. Introduction

Irradiation creep has been studied extensively to provide data that can be used for component analysis of fusion, fast breeder and light water reactors. It is now generally recognized that the irradiation creep data were in agreement with an empirical equation[1]. Moreover, there have been many irradiation experiments done under applied stress to investigate stress effects on microstructural evolution. It is reported that the total nucleation rate of Frank loops was increased with increasing external stress[2]. However, there are few studies on the effect of external stress on mechanical properties of the material under irradiation. The purpose of this study is to evaluate the mechanical properties of the irradiated material under external stress.

2. Experimental procedure

The material tested is SUS304 in the solution-annealed condition. Chemical composition of specimen is shown in Table 1. The thickness of specimen is about 0.5mm. The surface of specimen was polished with #2400 paper. The spring was used in order to apply the required stress in the specimen during irradiation. The strain gauge was attached the specimen to measure the tensile strain before ion-irradiation. The tensile strain was about 0.2%. The applied stress, about 228MPa, was estimated from the stress-strain curve of SUS304SS. The strain gauge was removed before irradiation.

The specimens were irradiated in triple (12MeV Ni^{3+}, 1.1MeV He^{+} and 380keV H^{+}) ion beam mode at a temperature of 300°C using the triple ion beam facility (TIARA). The temperature of the specimen was measured by an infrared thermometer (THERMAL VISION, Nikon Co.). The displacement damage in the specimen was mainly attributed to Ni^{3+} ion irradiation. The peak dose was about 10dpa around 2μm. The He^{+} and H^{+} ions were implanted in depth ranges from 1.0 to 1.5μm using aluminum foil energy degraders. The concentrations of He^{+} and H^{+} ions in the implanted range were 11 appmHe and 91 appmH, respectively, which correspond to LWR condition. The dose was about 5dpa in the implanted range of He^{+} and H^{+} ions. Two specimens were irradiated. One was a stressed specimen. The other was a stressed-free specimen which was prestressed at the same stress level of the stressed specimen.

Table 1 Chemical composition of the material in wt%

Materials	Fe	C	Si	Mn	Cr	Ni
SUS304	bal.	0.063	0.49	1.45	18.72	10.27

The nanoindentation test was carried out on the surfaces of the irradiated and unirradiated specimens at room temperature. A conical indenter that had a hemispherical apex with radius of 1.2μm was used. A DUH-200 (Shimadzu Co.) testing machine was used for the nanoindentation test. The load was applied with a loading speed of 2.6×10^{-3} N/s, held 1 second and then removed. During loading and unloading, the load was continuously monitored along with the displacement with a resolution of 19.6mN and 0.01μm, respectively.

3. Results

Figure 1 shows the universal hardness of the irradiated and the unirradiated specimens. The irradiated specimen was irradiated under external stress. The universal hardness of the irradiated specimen was about 2 times higher than those of the unirradiated specimen. The irradiated specimen was hardened by irradiation and external stress. The universal hardness of the prestressed specimen after irradiation will be measured in order to separate the effect of irradiation and external stress. And also, the microstructure of the irradiated specimens will be observed.

References

1)F.A.Garner, M.B.Toloczko, J. Nucl. Mater. 251 (1997) 252.
2) H.Tanigawa. Y.Katoh, A.Kohyama, Nucl. Instru. and Methods in Phy. Resea. B 102(1995)151.

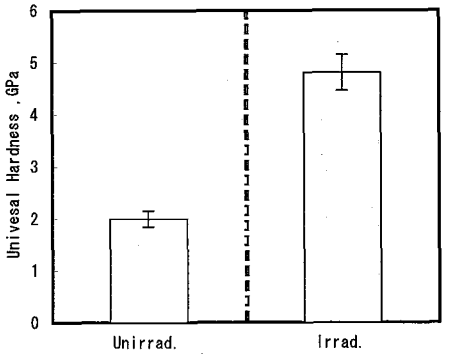


Fig.1 Universal hardness of unirradiated and irradiated specimens

1-15 Influences of Multi Ion Beam Irradiation on Radiation Hardening and Microstructure in Low Activation Ferritic/Martensitic Steels

N. Okubo[a)], T. Sawai [a)], E. Wakai [a)], D. Yamaki [a)], S. Kitazawa [a)], S. Jitsukawa [a)], H. Tanigawa [a)], K. Oka [b)] and S. Ohnuki [b)]

[a)] Division of Fuels and Materials Engineering, NSED, JAEA
[b)] Hokkaido Univ.

Abstract

Influences of multi ion beam irradiation on radiation hardening and microstructure have been studied for ferritic steel F82H, doped with 60 ppm B and 200 ppm N, to evaluate fundamental irradiation response before irradiation at fission reactors. The doping with B and N for the F82H and the appropriate heat treatments provided permissible mechanical properties. Single ion irradiations of 10.5 MeV Fe^{3+} and dual ion irradiations of 10.5 MeV Fe^{3+} and simultaneous 1.05 MeV He^{+} of 10 appmHe/dpa rate were performed at 633 k to 20 dpa. Micro hardness was measured before and after the irradiation. The change of radiation hardening of F82H doped with B and N was nearly equal to that of F82H non-doped.

低放射化フェライト鋼は、核融合炉用構造材料の候補の一つであるが [1,2]、高速中性子照射によるはじき出し損傷と同時に核変換生成物である He の影響を評価することが重要である。He の影響を調べるために、核分裂炉を利用した B 添加鋼の照射がしばしば用いられるが [3]、B 単独添加鋼の強度特性は、B 添加によりその強度特性や照射挙動が未添加鋼に比べて、変化することが知られている [4,5]。本研究では、低放射化フェライト鋼（F82H）に B と N を同時に添加した F82H 鋼を作製し、強度特性に与える熱処理の効果を調べた。また、トリプルイオン照射装置を用いて多重ビーム照射を行い、核分裂炉での中性子照射による挙動変化との比較に資するための強度特性評価を行った。

供試材として、F82H鋼、F82Hに10B、11B及びNをそれぞれ60及び200 ppm同時添加した鋼（F82H+10B+N及びF82H+11B+N）を作製し、さらに比較材としてF82H（IEAヒート）を用いた。熱処理は、まず、1150℃で30分間焼きならし、700℃で120分間焼き戻した。次に、1000℃で10分間焼きならし、780℃で30分間焼き戻した。2回目の焼き戻し温度を700、750、780℃と変えた試料に対して、引張試験及びシャルピー試験を行った。微細組織は、電解研磨後、TEMにより観察した。イオン照射は、10.5 MeV Fe^{3+} のシングル照射及び10.5 MeV Fe^{3+} と1.05 MeV He^{+}（10 appmHe/dpa）のデュアル照射を、線量及び温度を変化させて行い、照射後に微小硬さ試験により硬さ変化を測定した。

焼き戻し温度を 700 から 780℃に変化させた場合、F82H+10B+N の降伏応力は約 240 MPa 減少し、F82H 及び F82H+11B+N と同様の焼き戻し温度依存性を示した。延性-脆性遷移温度（DBTT）は、焼き戻し温度が、700、750 及び 780℃の時、それぞれ、-55、-90 及び-90℃であった。焼き戻し温度が 750 及び 780℃の場合を比較すると、降伏応力は、焼き戻し温度の増加による転位密度の減少に依存して減少しているのに対して、DBTT の変化はほとんどなかった。微細組織観察の結果、780℃の場合、転位密度は減少しているが、炭化物の数密度が上昇しており、この炭化物の増加により DBTT が上昇したものと考えられる。

次に、イオン照射による微小硬さの変化を調べた。シングルイオン及びデュアルイオン照射を633Kにて20dpaまで行ったF82H+B+Nの硬さ変化の損傷量依存性は、それぞれF82Hと同様の傾向を示した。Fig.1に、F82H+10B+N、F82H+11B+N、F82H、及びF82H（IEA）に対して、デュアルイオン照射を633Kにて10dpaまで照射した前後の微小硬さ及び硬さ変化を示す。F82H+10B+N及びF82H+11B+NともにF82Hと同様の照射硬化挙動を示し、本研究では、鋼種によらず、ほぼ同様の硬さ変化であった。

以上のように、B及びNを同時添加したF82Hは、F82HにBを単独で添加した場合のような靭性低下は示さず、未添加のF82Hと同等の強度及び靭性を有することが明らかになった。また、照射硬化挙動もF82Hと同等であったことから、核分裂炉を用いてF82HにおけるHe効果を評価するために、B及びN同時添加材は有用であると考えられる。

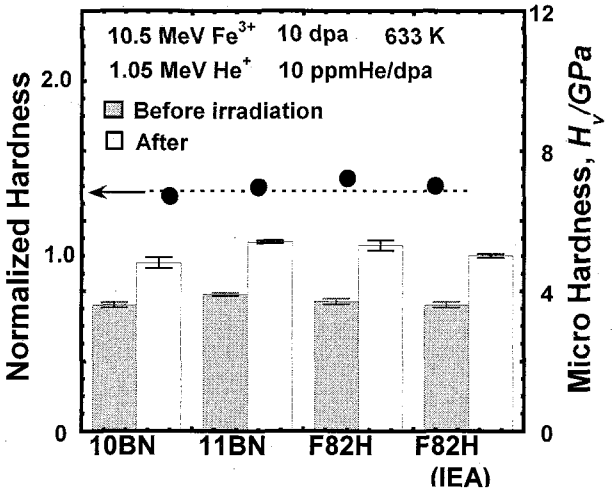


Fig. 1 Micro-hardness before and after irradiation and radiation hardening of F82H+10B+N, F82H+11B+N, F82H and F82H IEA Heat

References

1) R. L. Klueh, D. S. Gelles, S. Jitsukawa, A. Kimura, G. R. Odette, B. van der Schaaf and M. Victoria, J. Nucl. Mater. 307-311 (2002) 455.
2) A. Hishinuma, A. Kohyama, R.L. Klueh, D.S. Gelles, W. Dietz and K. Ehrlich, J. Nucl. Mater. 258-263 (1998) 193.
3) N. Hashimoto, R.L. Klueh and K. Shiba, J. Nucl. Mater. 307–311 (2002) 222.
4) E. Wakai, S. Matsukawa, T. Yamamoto, Y. Kato, F. Takada, M. Sugimoto and S. Jitsukawa, Mat. Trans. 45, 8 (2004) 2642.
5) E. Wakai, M. Sato, T. Sawai, K Shiba and S. Jitsukawa, Mat. Trans. 45, 2 (2004) 407.

1-16 Study on Irradiation Defect Generation Process and Radiation Induced Segregation in Fe-Based Model Alloys

T. Tobita[a)], Y. Chimi[a)], N. Ishikawa[a)], S. Nakagawa[b)] and A. Iwase[b)]

[a)]Reactor Safety Research Unit, NSRC, JAEA, [b)]Department of Materials Science, Osaka Prefecture University

Abstract

To investigate the fundamentals of irradiation embrittlement mechanisms of RPV steel, we have performed electron irradiation experiments using Fe-Cu model alloys. We measured the changes of electrical resistivity on several types of Fe-Cu model alloys induced by 2MeV electron irradiations at high temperature (523K) to evaluate the irradiation damage mechanisms, such as the behaviours of irradiation defect and Cu clustering in the materials. We obtained the dose dependence and Cu content dependence of the electrical resistivity change. To estimate the irradiation temperature effect, thermal aging experiments at same temperature was performed. The electrical resistivity decreasing was observed both in the electron irradiation and in thermal aging except for low-Cu content alloy, however, the change in the thermal aging was small. These results suggest the followings. The Cu clustering was clearly enhanced by electron irradiation. There was no accumulation of the irradiation defect in this irradiation temperature.

原子炉供用期間の長期化に伴い照射脆化予測手法の高精度化が求められている。本研究は、原子炉圧力容器の照射脆化予測の精度向上に寄与するため、照射により生じた欠陥の挙動、それに伴うCu、P等の不純物の析出・偏析過程を調査しモデル化することを目標としている。試料として原子炉圧力容器鋼の不純物に着目したモデル合金、照射場として最もシンプルな照射欠陥を生成する電子線照射を用い、照射損傷等の指標として材料の変化に敏感な電気抵抗の変化を測定することにより基本的な照射欠陥及び不純物の挙動を観測し、反応速度論に基づく計算モデルの検証を行うものである。前報[1)]では室温におけるFe-0.6%Cu合金の電子線照射試験を行い、電気抵抗率変化の照射量及び照射速度依存性を調査するとともに、欠陥挙動の反応速度論に基づいたモデル計算との比較を試みた。モデル計算の検証データを拡充するため、本報では原子炉の運転温度に近い高温での電子線照射及び熱時効試験を行った結果について報告する。

Cuの濃度を変えた3種類のモデル合金Fe-0.02wt%Cu、Fe-0.6wt%Cu及びFe-1.2wt%Cuについて、30μm厚の薄膜リボン状に圧延したのち850°C-10分間保持後に急冷する固溶化熱処理を施した。試料の化学成分をTable 1に示す。この試料をヒーター付き銅板に乗せ、電子線が貫通する薄い銅板で挟むことで照射中の温度を250℃に精度良くコントロールした。照射条件は電子線エネルギー2MeV、照射速度約1.6×10^{-9}dpa/s、照射量約4×10^{-5}dpaである。電気抵抗の測定の際には、照射を中断して試料を取り出し、液体窒素中で測定を行った。また同様の方法で電子線照射と同じ温度での熱時効試験を行い電気抵抗率の変化を調べた。

Fig.1に照射及び熱時効による電気抵抗率の変化を示す。Fe-0.02%Cuを除き、電子線照射、熱時効試験両方において時間(および照射量)と共に抵抗率の低下が生じた。しかしながら熱時効での抵抗率低下は電子線照射に比して明らかに小さく、電子線照射によりCuの析出が促進されることを示している。また、Cu濃度増加に伴い抵抗率の低下が大きくなる傾向にあり、明確にCu濃度依存性が確認できる。純鉄に近いFe-0.02%Cuの抵抗率に変化が無いことから、照射による格子欠陥の生成-対消滅が活発であり格子欠陥の蓄積がないことが示唆される。初期に大きく抵抗率が低下する原因としては、試料の急冷熱処理により初期に過剰に存在している熱空孔の影響が考えられる。以上、計算モデルの検証に必要とされる重要なデータを得ることができた。

Table 1 Chemical composition of materials.

Specimen	Fe	Cu	C	Si	O	N
Fe-0.02wt%Cu	Bal.	0.022	0.003	0.003	0.015	0.0006
Fe-0.6wt%Cu	Bal.	0.61	0.002	0.002	0.015	0.0006
Fe-1.2wt%Cu	Bal.	1.19	0.002	0.002	0.013	0.0006

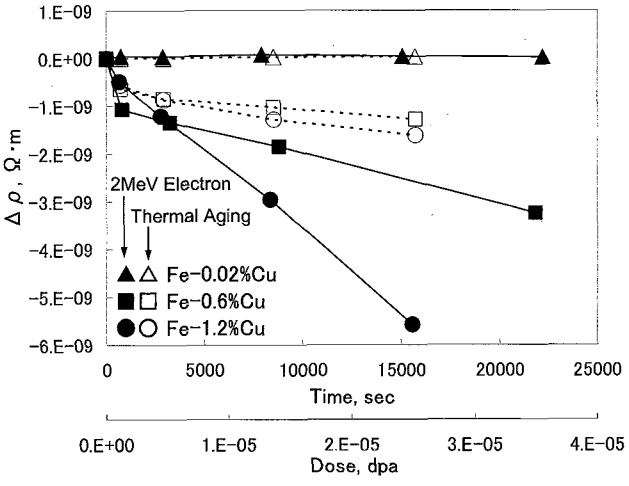


Fig.1 Electrical resistivity change (@77K) induced by electron irradiation and thermal aging at 523K.

References

1) T. Tobita et al., TIARA annual report 2004 (2005) 245.

1-17 Effect of Ion-Irradiation on Microstructure of Zirconium

S. Yamada[a)], M. Kinoshita[b)], T. Taguchi[c)] and T. Sawai[d)]

[a)]Materials Science Research Laboratory, Central Research Institute of Electric Power Industry (CRIEPI),
[b)]Nuclear Technology Research Laboratory, CRIEPI, [c)]Neutron Materials Research Center, QuBS, JAEA,
[d)]Policy Planning and Administration Department, JAEA

Abstract

We report the microstructure of polycrystalline zirconium after ion irradiation. The specimen was irradiated up to 20 dpa with 12 MeV Zr^{4+} ions at 673 K. Thin foils were prepared using the focused ion beam method and were characterized by transmission electron microscopy. It is shown that the characteristic damage structure of <c> component dislocations produced on {0002} planes in Zircaloy-2 by neutron irradiation can be simulated in pure Zr by Zr ion irradiation.

軽水炉発電のコストダウンには、高燃焼度化に代表される技術開発や新技術の導入が必要不可欠である。しかし、現行のジルコニウム合金製燃料被覆管は、高燃焼時に延性が低下し、脆化することが報告されている[1)]。その原因として、中性子による照射損傷、腐食によって発生する水素の蓄積および水素化物の形成、機械的応力による塑性変形などが考えられている。脆化に対する各要因の影響を把握することは、燃料被覆管の健全性維持には重要と考えられる。われわれは、加速器照射、水素注入を利用して、要因別に段階的に脆化機構を解明する研究を進めている。これまで、実炉照射によってジルコニウム合金(Zircaloy-2)中に形成される損傷組織(c成分転位)をジルコニウムイオン照射によって模擬できることを報告した[2)]。本研究では、ジルコニウム母材への照射効果のみを分離して調べるため、純ジルコニウムにジルコニウムイオンを照射し、そのミクロ組織を透過型電子顕微鏡(TEM)で観察した。

照射用試料には純ジルコニウムを用い、照射面は電解研磨した。イオン照射には、原子力機構高崎研イオン照射研究施設(TIARA)の3MVタンデム加速器を利用した。イオン種はZr^{4+}、加速エネルギーは12MeV、照射温度は673K、照射欠陥量は20dpaである。TEM用薄膜試料の作製には集束イオンビーム(FIB)装置を用い、300kV電界放出型透過電子顕微鏡(FE-TEM)を用いて組織を調べた。

Fig.1(a)に照射試料のTEM明視野像を示す。TEM試料は照射面を基準に深さ~3.0μmの位置から採取した。TRIMコードによると、ダメージピーク位置は深さ~2.5μmと推測される。組織中に六方晶底面(0001)に平行な、間隔約40nmの直線状コントラストが観察された。この特徴的な組織は、高照射領域で中性子照射されたZircaloy-2の組織と良く似ている。Fig.1(b)に0004反射による同視野の暗視野像を示す。直線コントラストは消失せず、これよりこのコントラストは[0001]方向成分のバーガースベクトルを有する転位であることが分かる。他の反射による暗視野像についても調べた結果、この転位はc成分転位であることが明らかになった。以上の結果から、純ジルコニウムへの加速器を用いたジルコニウムイオン照射により、高照射領域で実炉照射されたZircaloy-2中に形成される典型的な損傷組織(c成分転位)を模擬できることが分かった。今後、これらの照射模擬材に水素を追加注入することにより、水素の蓄積過程と損傷組織との相関を調べる予定である。

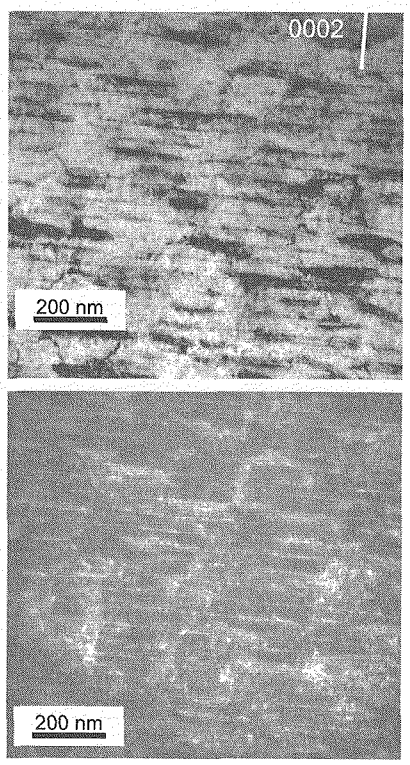


Fig.1 TEM images of Zr irradiated up to 20 dpa with 12 MeV Zr^{4+} ions at 673 K; (a) bright-field image; (b) dark-field image (g=0004).

References

1) 平成13年度高燃焼度等燃料安全試験に関する報告書, (財) 原子力発電機構, 平成14年3月.
2) S. Yamada, J. Ohta, T. Sonoda, M. Kinoshita, T. Sawai and S. Jitsukawa, JAERI-Review 2003-033 (2003) 186.

1-18 Effect of Al and Be as Transmutation Atoms on Formation and Growth of Helium Bubbles in SiC/SiC Composites

T. Taguchi[a)], N. Igawa [a)], E. Wakai [b)], S. Jitsukawa [b)] and A. Hasegawa [c)]

[a)]Neutron Materials Research Center, QuBS, JAEA, [b)]Division of Fuels and Materials Engineering, NSED, JAEA, [c)]Department of Quantum Science and Energy Engineering, Tohoku University

SiC/SiC composites are considered for use as functional and structural materials in first wall components in fusion reactors due to their high temperature strength and low-residual radioactivity following neutron irradiation[1]. In the fusion environment, helium (He) and hydrogen (H) are produced as transmutation products and He bubbles can be formed in the SiC by irradiation with 14-MeV neutrons[1]. These He bubbles may reduce the tensile strength and thermal conductivity of SiC/SiC composites. Several elements are also produced by 14-MeV neutron irradiation as transmutation products: aluminum (Al), magnesium (Mg), beryllium (Be), etc.[2]. Wakai et al. reported that the formation and growth of He bubbles in ferritic/martensitic steel was suppressed by pre-implantation of carbon ions[3]. It is, therefore, important to understand the effect of transmutation products and impurities on microstructural change and, the formation and growth of He bubbles in SiC/SiC composites. In this study, the effect of Al and Be ions pre-implantation on microstructural change and, the formation and growth of He bubbles in SiC/SiC composite was investigated.

The SiC/SiC composites were fabricated using the forced thermal gradient chemical vapor infiltration process. Simultaneous ion-beams irradiation was carried out at the TIARA facility of JAEA. Aluminum (Al) or beryllium (Be) ions were pre-implanted uniformly into the SiC by changing the implantation energies at 1000 °C. Four kinds of ion implanted specimens were prepared with 100 appm Al, 1000 appm Al, 100 appm Be and 1000 appm Be implanted. And then un-implanted and pre-implanted SiC/SiC composites were simultaneously irradiated at 1000 °C with triple ion-beams of Si^{2+}, He^{+} and H^{+} ions as a simulation of fusion reactor conditions.

No microstructural change was observed in the matrices and fibers of SiC/SiC composites implanted with Al or Be ions up to 1000 appm. Helium bubbles were formed in every matrix and fiber of un-implanted and pre-implanted SiC/SiC composites irradiated by triple ion-beams. The average size of He bubbles in the in-implanted matrix was smaller than those in the Al or Be ions pre-implanted matrices. The size distribution of He bubbles diameter in the matrix of Al and Be ions pre-implanted SiC/SiC composite was shown in Fig. 1. The He bubbles exhibited a bimodal size distribution for both the Al and Be ions pre-implanted matrices. The effect of the concentration of pre-implanted Al or Be ions on the average size of He bubbles larger than 4 nm was given in Fig. 2. The average size of He bubbles in the matrix was increased by implanting Al or Be ions and increased with increasing amount of implanted Al or Be ions. The average size of He bubbles smaller than 4 nm in the matrices implanted with Al or Be ions was consistent with that in un-implanted matrix (3.4 nm). The size of He bubbles in the fiber was slightly increased by implanting Al or Be ions. These results suggest that Al or Be as transmutation products and impurities may accelerate the growth of He bubbles in SiC/SiC composites under fusion reactor conditions.

References

1) B. Riccardi et al., J. Nucl. Mater. 329-333 (2004) 56.
2) R. H. Jones et al., J. Nucl. Mater. 307-311 (2002) 1057
3) E. Wakai et al., J. Nucl. Mater. 318 (2003) 267.

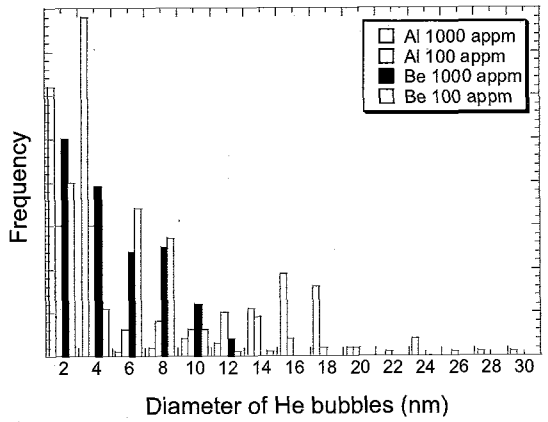


Fig.1 Size distribution of He bubbles diameter in the matrix of specimens implanted with Al or Be ions and then irradiated by triple ion-beams at 1000 °C.

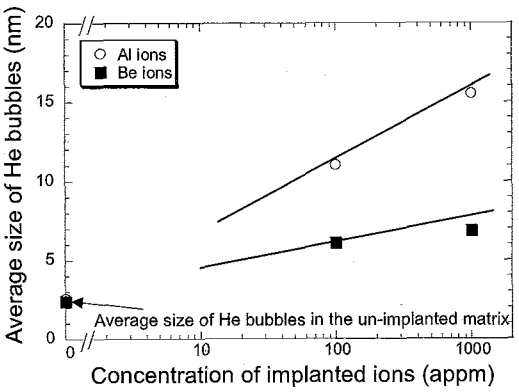


Fig.2 Effect of the concentration of implanted Al or Be ions on the average size of He bubbles larger than 4 nm.

1-19 Evaluation on Irradiation Effects for Surface Modified Material

T. Naoe[a], H. Kogawa[b], M. Futakawa[b], H. Takeuchi[c], Y. Ishijima[d], Y. Nakahara[d] and I. Ioka[d]

[a]Graduate School of Ibaraki University, [b]Proton Accelerator Facility Division, QuBS, JAEA,
[c]NDK Incorporated, [d]Division of Fuels and Materials Engineering, NSED, JAEA

Abstract

Liquid mercury target system will be installed in spallation neutron source of J-PARC (Japan Proton Accelerator Research Complex). In the mercury target, pressure waves will be generated by thermal shock induced by proton beam injection. Repeated stress is loaded to the target vessel by pressure waves propagation. At the same time, negative pressure will be generated in the interface between the mercury and the target vessel and form cavitation bubble. Pitting damage, which is induced by cavitation bubble collapse, is important factor to evaluate lifetime of target vessel. The authors developed a novel surface hardening treatment, combination of plasma nitriding and carburizing treatments, to reduce the pitting damage. In this paper, from the view point of irradiation effect, the change in mechanical properties by ion-irradiation is examined. They are hardly affected by ion-irradiation.

現在、J-PARC(Japan Proton Research Complex)の中核施設として建設が進められている核破砕中性子源では、液体水銀ターゲットが用いられる。液体水銀にパルス陽子線が入射すると、核破砕反応による中性子の発生と共に、水銀中には、熱膨張による圧力波が生じる。この圧力波は、水銀を充填しているターゲット容器へと伝播し、ターゲット容器に繰り返し衝撃荷重を負荷する。また、圧力波の伝播過程で、水銀と容器の界面では負圧の発生に伴いキャビテーション気泡が発生する。このキャビテーション気泡の崩壊によりターゲット容器内壁には、ピッティング損傷が形成される[1]。ピッティング損傷による壊食は、照射損傷、及び繰り返し応力負荷と共に、ターゲット容器の健全性を低下させる因子である。ターゲット容器の健全性向上、及び中性子源の高出力化のために、ピッティング損傷抑制及び疲労強度向上を目的としてターゲット容器内壁に表面改質処理を施すことが検討されている。

これまでに、種々の表面改質処理材における水銀キャビテーション壊食試験[2]及びキャビテーションによる衝撃を模擬した固／液界面衝突解析[3]により、表面改質によるピッティング損傷抑制効果について検討を行い、損傷抑制に最適な表面改質条件を見いだした。本照射試験では、新たに考案し、ターゲット容器内壁に適用が検討されている階層型表面改質処理材に対して、核破砕条件を模擬したイオン照射を行い、照射による力学特性の変化を評価した。

階層型処理は、キャビテーション気泡崩壊に伴い局所的に負荷される衝撃荷重に対して、割れや剥離を抑制するために、改質層から基材部にかけてなだらかな傾斜力学特性分布を与えることを目的とし、プラズマ浸炭とプラズマ窒化の複合処理とした。また、本改質処理は、水銀ターゲット容器構造材であるオーステナイトステンレス鋼に対して行うため、耐食性が低下しないように低温で十分な改質層厚さが得られるように処理条件の最適化を行った。

試料は、プラズマ浸炭(450℃ 20h)及びプラズマ窒化(400℃ 190h)の階層処理を施した3x2.5x6mm^{3}のSA316ssである。 改質層断面を鏡面研磨後、核破砕条件を考慮して、Ni^{3+}:10dpa、H^+:2000appm/dap、He^+:200appm/dpaでトリプルビーム同時照射を行った。10dpaは、1MW運転時における容器寿命とされる2500時間に受ける2倍の照射量である。照射温度は、容器内壁の温度である200℃とした。

イオン照射による力学特性変化を調べるために、照射領域、及び銅板によりマスキングした非照射領域に対して、ベルコビッチ圧子を用いた微小押し込み試験により荷重−深さ曲線を計測し、最大深さより硬度を算出した。試験荷重は、29.4mN、負荷速度は3mN/sであり、改質層における最大押込み深さは約0.3μmである。Fig.1に改質層表面からの距離を変化させて計測した硬度分布を示す。非照射領域では，表面から基材にかけてなだらかな硬度分布を有していることが確認できる。改質層厚さは約40μmである。照射領域は、基材部であるSA316ssでは、最大50%の硬度の上昇が見られたが、改質層表面に近づくにつれて硬度の上昇は隠微になる。改質表層付近では、照射による硬度変化は殆ど見られない。これは、浸炭及び窒化処理により転位が形成され、はじき出しによる新たな転位の形成が顕在化しないためと考えられる[4]。従って、階層型表面改質における照射による力学特性変化は殆ど無く、ターゲット容器材料として適用可能であると考えられる。

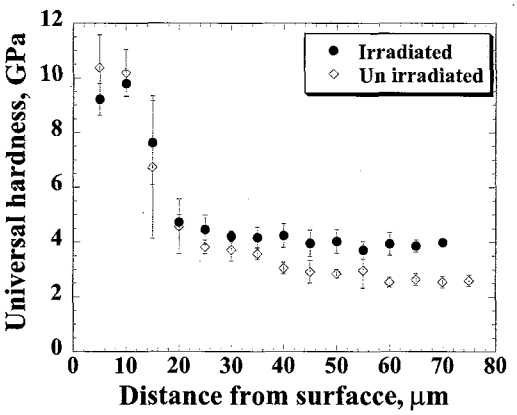


Fig.1 Hardness change due to the irradiation along the distance from modified surface

References

1) M. Futakawa, et al., "Measurement of dynamic response of liquid metal subjected to uniaxial strain wave", J. Phys. IV, 10, p.237-242 (2000)
2) M. Futakawa, et al., "Pitting damage by pressure waves in a mercury target", J. Nucl. Mater., 343, p.70-80 (2005)
3) M. Futakawa, et al., "Micro-impact damage caused by mercury bubble collapse", JSME Int. J., A, 48-4, p.234-239 (2005)
4) T. Naoe, et al., "Evaluation of mechanical properties and microstructures in ion-irradiated surface layer", JSME Int. J., A, 48-4, p.280-285 (2005)

1-20 Evaluation of Property Change in Advanced Fuel Cladding Material under Ultra High Burn-up Condition Simulated by Triple Ion Irradiation

Y. Ishijima[a)], I. Ioka[a)], Y. Nanjyo[a)], K. Kiuchi[a)], K. Fujimura[b)] and H. Obata[b)]

[a)] Division of Fuels and Materials Engineering, NSED, JAEA
[b)] The Japan Atomic Power Company

Abstract

Dose dependence of mechanical properties was evaluated for the candidate (Fe-25Cr-35Ni-0.2Ti) and SUS304 tubes. Specimens were irradiated by ions from TIARA facility up to 50dpa at the irradiation temperature of 537K. Measured values of universal hardness of the candidate and 304SS were quasi-saturated at over 10 dpa in the range of 40-60wt%. An increase in universal hardness of the candidate was less than that of SUS304. The similar tendency was observed in neutron irradiation. It is considered that the candidate has higher ductility than that of SUS304 after the ultra high burn-up.

発電炉における廃棄物低減、Pu 有効利用及び経済性向上を目的として、平均燃焼度 100GWd/t 級の超高燃焼度化を目指した MOX 燃料に使用する被覆管材料の開発を行っている。候補材には、粒界近傍の Cr 濃度低下の抑制やγ相安定化のための成分調整、結晶粒微細化と析出物の粒内均一分散・固定化を狙った加工熱処理(歪時効-中高温再結晶)、及び超高純度溶製法を用いた改良ステンレス鋼（25Cr-35Ni-0.2Ti UHP）を採用した[1)]。本報告では、開発した候補材の延性に及ぼす照射の影響を評価するため、トリプルイオンビーム照射した候補材のミクロ組織及び硬さの変化を調べた。

Table 1 に候補材及び比較材の組成を示す。イオン照射は、原子力機構 高崎量子応用研究所の TIARA にて実施した。照射条件は超高燃焼度 BWR で想定されるはじき出し損傷、及び(n, α)、(n, p)核反応を模擬するため、イオン種を 12MeV Ni^{3+}、0.38MeV H^+、1.1MeV He^+のトリプルイオンビーム、照射温度を 573K、注入量を 3 He appm/dpa、30 Happm/dpa とした。照射量は 5-50 dpa とした。注入した H^+及び He^+は局在化するため、アルミ薄膜ディグレータを使用して注入領域を広げて照射を行った。照射による延性低下の度合いは、硬さの変化より評価した。硬さ試験機は測定は三角錐型圧子を用い、照射面から押し込んだ。押し込み荷重 5gf、押し込み速度 0.45 gf/sec とした。得られた「荷重-押し込み深さ」曲線は、「荷重/押し込み深さ-押し込み深さ」曲線に再プロットし、押し込み開始から傾斜に変化が現れるまでの間（押し込み深さ約 0.4μm）の傾斜を硬さ($g/\mu m^2$)として算出した。

候補材及び比較材のイオン照射後の微小硬さ増加量の照射量依存性を Fig.1 に示す。JRR-3 で約 1dpa 中性子照射した両試験片の硬さの増加量も追記した。照射量は少ないが、イオン照射と中性子照射の結果は比較的よく一致した。イオン照射においては、いずれも約 10dpa 以降で硬さの増加量が 4ー6 割に収斂する。これは、照射欠陥密度の照射量依存性[2)]とほぼ同じ傾向を示している事から、本照射条件下における照射硬化はフランクループ生成に支配されていると考えられる。また、候補材の硬さの増加は、SUS304 に比べ若干少ない傾向を示した。

100GWd/t 級の超高燃焼度相当の弾き出し損傷に対応したトリプルイオン模擬照射により、候補材の照射硬化度の評価を実施した。オーステナイト相安定性を高めた超高純度候補材の照射硬化は、10ー20dpa で飽和傾向にあり、SUS304 に比べその程度は少ないものと予想される。

References

1) 木内他，“高性能燃料被覆管材質の研究”，JAERI-Tech 2002-008.
2) Y.Nanjo et al., “Microstructural Evolution of the Advanced Fuel Cladding Materials by Triple Ion Irradiation(II)“, JAERI-Review 2003-033(2003).

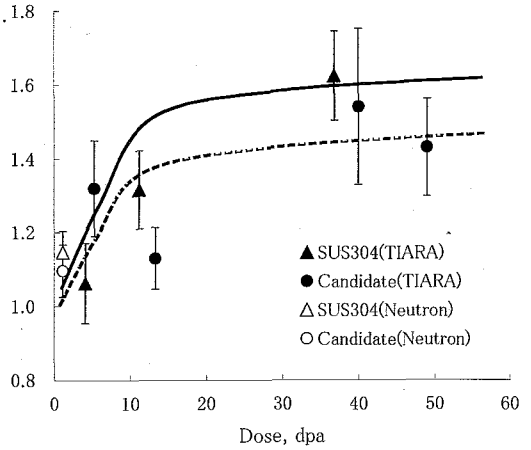


Fig.1 Dose dependence of universal hardness of the candidate and SUS304

Table 1 Chemical composition of the candidate and SUS304 (wt %)

Materials	Fe	Cr	Ni	Ti	C	N	O	S	Si	Mn	P
Candidate	bal.	24.55	34.99	0.18	0.0013	0.0014	0.0011	0.0009	<0.005	0.001	0.001
SUS304	bal.	18.72	10.27	-	0.063	-	-	0.012	0.49	1.45	0.016

1-21 Irradiation-Induced Changes in Surface Topology of Cerium Dioxide Investigated with Scanning Electron Microscopy and X-Ray Spectroscopy

T. Mihara [a], H. Abe [a], T. Sonoda [b], T. Sawai [c] and E. Wakai [d]

[a] The University of Tokyo, [b] Central Research Institute of Electric Power Industry, [c] Policy Planning and Administration Department, JAEA, [d] Division of Fuels and Materials Engineering, NSED, JAEA

Introduction

Nuclear fuels, such as UO_2, are subjected with intense irradiations by neutrons and fission products (FP) leading formation of the high burn-up structure. It is characterized as coarsened FP bubbles and sub-divided grains[1], being release sources of FP gases resulting deterioration of thermal conductivity. Therefore, it is important to clarify formation mechanism of the high burn-up structure.

In this study, cerium dioxide was selected so as to simulate the microstructual behaviors of uranium dioxide. Especially we focused changes in surface morphology and in chemical composition by scanning electron microscopy (SEM) and energy dispersive x-ray spectroscopy (EDS) and Raman spectroscopy.

Experimental

High purity (99.99 %) CeO_2 powder was pressed and sintered at 1670 K for 8 hours in air. The bulk materials were cut into disks of 9mm $\Phi \times$ 1mmt followed by optical polish on both surfaces. They were, then, irradiated with 300 keV Xe^+ ion beam up to the fluence of 3×10^{17} i/cm^2 at the surface temperatures of 630K, 890K and 1000K using the Ion Implanter at TIARA. The irradiated samples were investigated with SEM/EDS observation and micro Raman spectroscopic analysis at ambient temperature.

Result and Discussion

Irradiation at the elevated temperatures enhanced intergranular etching and in-grain surface reconstruction as shown in Fig.1. At the higher temperature, the etching layer became eroded and the in-grain surface became ragged both presumably due to surface, grain boundary diffusion and sputtering. The intra- and inter- granular cracking was observed at lower temperature probably because of cracking during cooling pried after irradiation.

According to TRIM (SRIM) calculation[2], the range of 300keV Xe in CeO_2 is about 60 nm which is out of region of contrast formation in SEM. However as shown in Fig.2, both of secondary electrons and scattering electrons were eligible for the Xe-bubble image. This result indicates that the bubbles of several tens of nm in size were located beneath surface especially in the pits.

The main Raman peak (F_{2g}), equivalent to vibration of oxygen sublattice, shifted toward lower wavenumbers. Heavy irradiation induces dense oxygen vacancies and introduces surface composition change, which is probably attributable to the Raman shift variation.

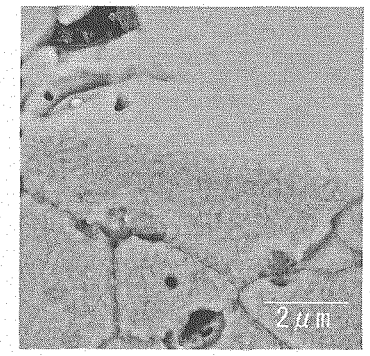


Fig.1 SEM image of the sample irradiated at 730℃. The lower region is irradiated.

Summary

300keV-Xe irradiation was performed in CeO_2 at elevated temperatures and investigated with SEM/EDS and Raman spectroscopy. Irradiation at elevated temperatures enhanced intergranular etching and in-grain surface reconstruction. Xe bubbles were located beneath surface. The main Raman peak (F_{2g}) shifted toward lower wavenumbers. Temperature dependence of intergranular etching and surface reconstruction as well as Xe bubbles formation was observed. The variation of surface morphology was interpreted with irradiation-enhanced diffusion and sputtering associated with preferential formation of oxygen vacancies.

References

1) Hj. Matzke, J. Nucl. Mater., 189 (1992) 141-148
2) J. F. Ziegler, J. P. Biersack and U. Littmark, Pergamon Press, New York, 1985

Acknowledgement

A part of this study was financially supported by the Budget for Nuclear Research of the Ministry of Education, Culture, Sports, Science and Technology, based on the screening and counseling by the Atomic Energy Commission.

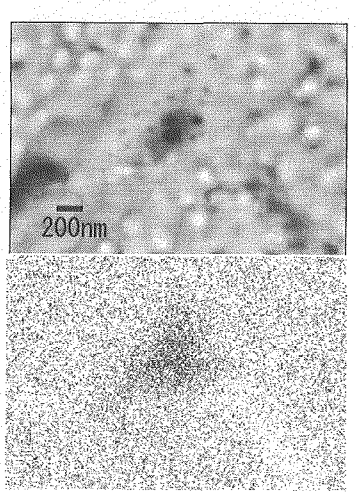


Fig.2 (a) Magnified SEM image of the sample irradiated at 730℃ (b) the corresponding EDS spectroscopic image taking Xe-L lines

1-22 Observation of Microstructural Changes and Irradiation Damages in Li_2TiO_3 Caused by Multi Ion Beam Irradiation

D. Yamaki, T. Tanifuji, T. Aruga and S. Jitsukawa

Division of Fuels and Materials Engineering, NSED, JAEA

Li_2TiO_3 is regarded as one of the most suitable candidates for the solid tritium breeder material of D-T fusion reactors. Simulation of the fusion reactor environment and hence the study of a synergistic effect of atomic displacement damage in Li_2TiO_3 are presumed to be approached by a simultaneous irradiation with "triple" ion beams which consist of O^{2+}, He^+ and H^+ ion beams. In this study, the results of the FT-IR photoacoustic spectroscopy (PAS) with Li_2TiO_3 samples irradiated with the single beams, with the triple ion beams simultaneously and with the triple ion beams sequentially were analyzed for investigation of microstructral changes.

The characteristics of the Li_2TiO_3 samples and the experimental parameters used in this experiment were described in ref.1. The characteristic peaks in FT-IR PAS spectra for non-irradiated Li_2TiO_3 sample were observed around 680, 780, 880, 1090, 1430, 1480, 1570, 3150 and 3450 cm^{-1}. In comparison to the reported spectra of TiO_2 and Li_2TiO_3, 680 and 780 cm^{-1} peaks are identified from Ti-O bond, 1570, 3150 and 3450 cm^{-1} peaks are from the O-H bond in hydroxyls adsorbed on or near the surface, and others are from C=O bond in Li_2CO_3 formed by reaction with CO_2 in the atmosphere on or near the surface.

Among the observed peaks, irradiation effect is clearly found for 780, 1090 and 3450 cm^{-1} peaks. In the previous study, the dependence of the 780 and 3450 cm^{-1} peak area on the radiation dose indicates that TiO_2 and hydroxyl are formed near the surface by irradiation, and the amount of them were found to be strongly affected by displacement per atom (dpa). Particularly, the amount of formed hydroxyl is affected not only by dpa but also by the method of irradiation, that is, the single, the simultaneous triple or the sequential triple irradiation.

Figure 1 shows the relation between dpa and the 1090 cm^{-1} peak area from the C=O bond, for each irradiation. It is shown that the peak area increases in proportional to the dpa, and any difference is not observed in the dependence of the peak area on dpa among the single, the simultaneous triple and the sequential triple ion beams irradiation. The results suggest that the amount of Li_2CO_3 formed is proportional to the dpa and that the method of irradiation does not affect the dependence of formation of Li_2CO_3.

These microstructural changes may strongly affect the tritium release behavior from Li_2TiO_3, and durability of Li_2TiO_3 and compatibility of Li_2TiO_3 with other components of the breeder blanket such as structural materials in the fusion reactor system under operation. Further study of the irradiation effects on these microstructural changes is needed to enhance the reliability of the related materials.

References

1) D.Yamaki, T.Nakazawa, T.Tanifuji, T.Aruga, S.Jitsukawa and K.Hojou, J.Nucl.Mater. 329-333 (2004)1279-1282.

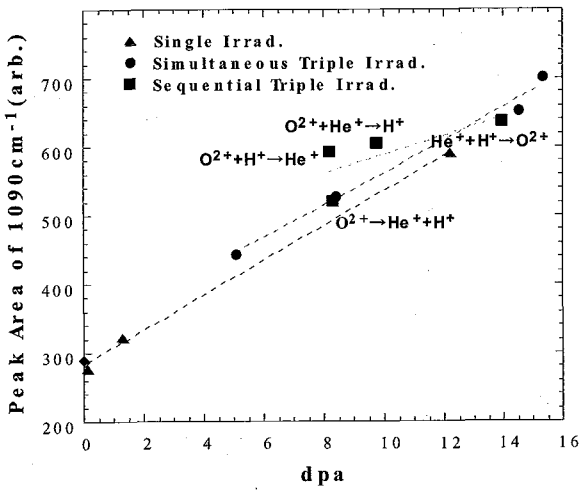


Fig. 1. Dependence of the 1090 cm^{-1} peak area on dpa. Notation for the sequential irradiation as " A→B" means that irradiation of beam B was performed after closing of irradiation of beam A.

1-23 Change in Electrical Resistance in Titanium Dioxide Irradiated with Energetic Particles

N. Ishikawa [a], Y. Chimi [b] and S. Yamamoto [c]

[a] Division of Fuels and Materials Engineering, NSED, JAEA,
[b] LWR Long-term Reliability Research Unit, NSRC, JAEA,
[c] Environment and Industrial Materials Research Division, QuBS, JAEA

Abstract

Titanium dioxide thin films were irradiated with 2.5MeV electrons and 120MeV Au ions, and the electrical resistance was measured in-situ at low temperature and at room temperature. The electrical resistance decreases and tends to saturate for the specimen irradiated with 2.5MeV electrons, while it increases in an exponential manner for the specimen irradiated with 120MeV Au ions. The morphology of the irradiation induced defects is probably the origin of the different behaviour of the resistance change. The radius of the columnar defect created by 120MeV Au ion irradiation is estimated to be 13nm.

keV-MeVオーダーの粒子照射による固体内照射損傷の評価法は、いわゆるdpa(displacement per atom)ベースの評価法が良く知られている。金属材料が照射対象である場合に限っては、この損傷評価法が汎用的に使用され、同じ共通単位で相互の材料の損傷量を比較論的に議論することが出来るというコンセンサスができている。しかし、この照射損傷評価法をさらに拡張しようとすると、以下の例のように深刻な問題が生じる可能性が大きい。

例えば、粒子エネルギーが100MeV以上では、弾性的はじき出しとは異なるプロセスで損傷が生じることが知られている。その代表的なものが、いわゆる電子励起効果であり、酸化物においては特に顕著な損傷を引き起こす事例が多い。また、酸化物は、純金属とは違い、損傷量を実験的に評価する測定法が確立していない。

そこで、本課題では、電気物性的アプローチにより損傷評価を行えるようにすることを目的として、電気抵抗測定による照射損傷データを取得した。具体的には、弾性的はじき出しを支配的に起こすことが分かっている2.5MeV電子線、電子励起効果が支配的であることが分かっている120MeV Auイオンをチタン酸化物に照射し、それぞれの電気抵抗変化の振る舞いを評価した。

試料として、$SrTiO_3$(100)単結晶基板上に蒸着したas-depositedのTiO_{2-x}薄膜を用いた。格子欠陥生成に対して電気物性変化が比較的顕著であることが期待されるからである。試料厚さは、電子線が試料を通過するのに十分薄い約0.3μmとした。シングルエンド加速器で加速された2.5MeV電子線、東海研究開発センタータンデム加速器で加速された120MeV Auイオンを真空中で試料に照射した。冷凍機を用いて低温・室温で照射し、電気抵抗を通常の四端子法によりその場測定を行った。

Fig. 1に電子線照射の場合の電気抵抗変化の照射量依存性を示す。照射量に対して単調に電気抵抗が減少する傾向が観測された。この減少は、酸素原子のはじき出しを介したキャリア濃度の上昇が主な理由として考えられる。特に、照射前のキャリア濃度が低い場合、照射前の電気抵抗で規格化された電気抵抗増加は相対的に大きくなることが予想される。この電気抵抗の照射量依存性は飽和挙動を示し、照射温度（＝測定温度）によって漸近先が異なることも分かった。

Fig. 2に高エネルギーイオン照射の場合の電気抵抗変化の照射量依存性を示す。電子線の場合と対照的に電気抵抗の増加が観測され、それがきれいに指数関数的に振舞うことが分かる。この電気抵抗の増加は、イオン軌跡に沿った柱状欠陥形成を仮定して$R=R_0\exp(r^2\pi\Phi)$ (r：柱状欠陥の半径、Φ: 照射量)に従うとすると説明できる。データフィッティングの結果、柱状欠陥の半径を13nmと推定することが出来た。低温(10K)でイオン照射を行うと電気抵抗が反対に減少した。今後は、電気抵抗変化の振る舞いの温度依存性を詳細に調べ、欠陥形態と電気抵抗変化との相関を体系化する予定である。

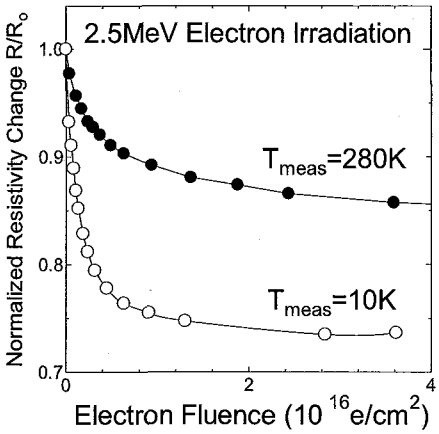


Fig.1 Resistance normalized by that of unirradiated specimen as a function of electron fluence in TiO_{2-x} irradiated with 2.5MeV electrons.

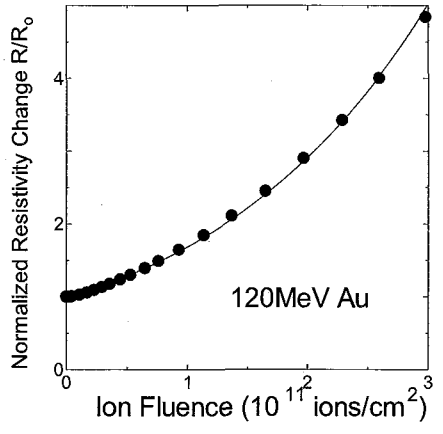


Fig.2 Resistance normalized by that of unirradiated specimen as a function of ion fluence in TiO_{2-x} irradiated with 120MeV Au ions. Solid curve represents an exponential function assuming formation of columnar defects.

1-24 Threshold Energy for Defect Production in Fe-50 at.%Rh Alloy

A. Iwase[a)], M. Fukuzumi[a)], Y. Zushi[a)], N. Ishikawa[b)] and Y. Chimi[c)]

[a)]Department of Materials Science, Osaka Prefecture University
[b)]Division of Fuels and Materials Engineerring, NSED, JAEA,
[c)]LWR Long-term Reliability Research Unit, NSRC, JAEA

1. Introduction

Recently, we have found that energetic electron irradiation induces the change in the ferromagnetic-antiferromagnetic transition temperature of Fe-50at.%Rh. To discuss this phenomenon quantitatively, we have to know the concentration of defects produced by electron irradiation. In this report, we show the values of threshold energy for defect production in this alloy, which are indispensable for the calculation of the concentration of irradiation-produced defects.

2. Experimental Procedure

A sheet of Fe-50at.%Rh alloy was irradiated with 0.5-2.0 MeV electrons near 20 K. The change in resistivity was measured *in-situ* as a function of fluence for each electron energy.

Results and Discussion

Figure. 1 shows the resistivity change as a function of electron-fluence. For clarity, data only for the electron energies below 1.1 MeV are shown. As can be seen in the figure, the electrical resistivity increases linearly with increasing electron fluence. The resistivity change rate, $d(\Delta\rho)/d\Phi$, which can be calculated from the slope of each straight line in Fig.1, is plotted as a function of electron energy in Fig.2. Here $\Delta\rho$ is the resistivity change by the irradiation and Φ is the electron fluence. As the resistivity change, $\Delta\rho$, is proportional to the concentration of irradiation-produced defects, the value of $d(\Delta\rho)/d\Phi$ corresponds to the defect production cross section. Theoretically, the defect production cross section for the relativistic electrons is given by the formula of McKnley and Feshbach. By fitting the experimental data with theoretically calculated cross section, the values of threshold energy for the defect production have been determined as 30 eV for Fe atom and 45 eV for Rh atom. In Fig. 2, the curves calculated by McKnley-Feshbach formula are also shown.

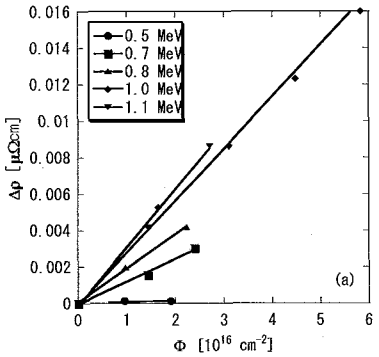


Fig.1 Change in electrical resistivity as a Function of electron fluence.

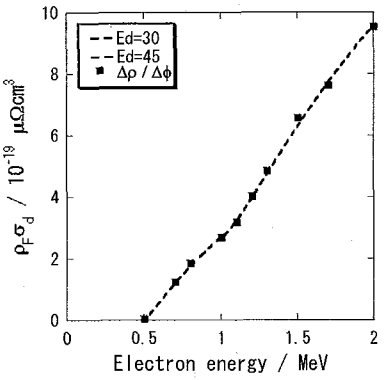


Fig.2 Resistivity change rate as a function of electron energy.

1-25 Irradiation Effects on Utility Materials in J-PARC Facilities

J. Kusano and members of J-PARC project team

J-PARC Center, JAEA/KEK

Abstract

The J-PARC, a research facility complex with high-intensity proton accelerators, produces high radiation area along the proton beam line and close the target region caused by undesirable beam loss of the accelerators. Various evaluation works of irradiation effect on utility materials were carried out these years to obtain the guideline of the maintenance procedure and also to study the reliable life of the each function for the instruments.

はじめに

J-PARC加速器のビーム出力強度は1MWを予定しており、リニアック・3 GeVシンクロトロン・50GeVシンクロトロンの連続する3つの加速器それぞれのビーム入出射領域のビームロスポイントに於けるロスビームパワーは5 kW超に至ることが想定されている。保守作業時の被ばく量の制限から、作業者が放射化した機器に近づいて作業が可能なレベルは、ロスビームが0.5 kW程度までであることを考慮すると、如何に機器・材料の不測の故障を抑え、必要な作業を短時間に且つ確実な方法で行うかが極めて重要となる。また、施設の安定稼働の観点からは、ビーム加速系、真空系、電磁石系、冷却系、制御系、ビームモニタ系の加速器主要系統の安定性はもとより、電源接地系安定度、建家空調制御の信頼性および建家構造材の耐放射線安定度も求められる。このため、J-PARC共同建設者である原子力機構および高エネルギー加速器研究機構のメンバーが高放射線環境に於けるJ-PARC用の汎用器材について、γ線照射による耐放射線特性評価試験を過去3年間行って来た。結果はそれぞれの機器の設計に反映している。

ケーブル関係の照射試験

J-PARCの汎用ケーブルは政府通達による「大型公共工事に於けるエコケーブルの使用」が義務づけられており、更に加速器トンネル等に於いては地元消防との協議により防火対策として高難燃ケーブルの使用を大原則としている。しかし、建設開始当初はエコケーブル(EM)及びエコマテリアルの高難燃ケーブル(NH)の耐放射線特性データは非常に乏しかったことから、架橋ポリエチレンをシース材とする汎用ケーブル(EM)(NH)の照射試験を行ってきた(Table 1)。

Table1 Gamma-ray Irradiation Examination for Ordinary Cables

1	Permissible dose range for ordinary EM and NH cables : - Electrical property, mechanical property, fire retardancy etc.
2	Radiation durability for ordinary coaxial cables : - Electrical insulation, RF transmission, impedance etc.
3	Dynamic RF transmission performance for ordinary coaxial cables at high radiation field :
4	Radiation dose effect for fire retardancy of NH cables :
5	Radiation durability of peripheral parts for cable handling : - Connector, cable tie band, cable tag etc.

汎用ケーブルの耐放射線特性としては、電気的諸特性の変化はもとより、保守作業を考慮した場合の機械的強度変化および難燃特性の変化のそれぞれ異なる要素について使用限界となる放射線吸収線量の調査を行った。絶縁抵抗等の電気的特性については、3ー5MGyまでは実用の範囲であることを確認した。しかし、機械的特性と難燃特性は1MGy前後で実用の範囲から外れるものが多かったが、ケーブルメーカーの最近の新規開発品の中には実用範囲が2.5MGyに至るものが現れてきている。また、制御用およびビームモニタ用に用いる同軸ケーブルについては、積算線量が2 MGyを超えると高周波伝送特性に約10%の特性劣化が認められた。短時間に高線量照射が発生するビームロスを想定した動特性試験では、同軸ケーブルの特性インピーダンスは変化しないが、時間依存性のある絶縁抵抗低下とケーブル全体の帯電現象が観測され、J-PARC高ビームロス部のビームモニタ系に使用する場合の重要な注意事項であることが判明した。

冷却水関係の照射試験

冷却水系についても使用する部品の種類は多くないが点数は極めて多い。電磁石、真空ポンプ等の保守・交換時には電源・制御ケーブル、冷却水配管等を分離した上で作業を行うこととなるが、分離・再接続の際の動作安定性を高放射線環境の中で確保しなければならない。このため、リモート操作で容易に脱着が可能となる冷却水配管接続用カプラの開発を進めている。シールはリップシール方式EPDM材のクイックジョイントカプラ(QJカプラ)を候補として、改良EPDM材の選定とカプラ形状の改良によるモデルカプラを試作し、冷却水の連続通水状態でのγ線照射試験を行ってきた。従来型のカプラでは、積算線量が0.5MGy程度でシール材の放射線硬化劣化により水漏れが生じていた。今回のモデルカプラでは連続通水の照射試験において9MGyを超える積算線量レベルまで安定なシール性能を実証した(Fig.1)。シール材は9MGyを超えた照射の後にもエラストマーとしての弾性を残し、金属接触面のベタつきも無く実用上は再利用可能な状態であった。尚、ここで用いた改良型EPDMは建設資材のEXPANSION-JOINT用止水板材料として耐放射線特性を改良したEPDMを、カプラ装着時の操作性向上のために初期硬度を下げたものである。

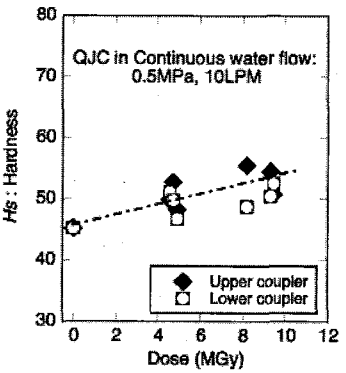


Fig.1 Hardness of seal elastomer in QJ coupler

塗料その他の照射試験と試験結果のデータベース化

J-PARCの高放射線環境に曝される機器の表面塗料についても多数の照射試験が実施されている。使用上で注意すべき点としては、塗装色を変えるための顔料の違いが同手法の塗装でも劣化進行を大きく左右する結果が得られている。一般的には10MGy程度までは内部被ばくの原因となり得る微粉末の発生は見られないが、20MGyを超えると塗装法・塗料の差が顕著になり、付着力が弱いものは剥離が発生する。

以上、ここに紹介したケーブル系、冷却水系のデータを含め多数の汎用器材の試験結果が得られており、これらを項目毎にとりまとめ、データベース集として刊行する予定である。

1-26 65 MeV Neutron Irradiation of NdFeB Permanent Magnets

X-M. Marechal [a)], Y. Asano [a,b,c)], T. Bizen [a)] and T. Hara[c)]

[a)]SPring-8, JASRI [b)]SPring-8, JAEA [c)] SPring-8 Center/RIKEN

Rare-earth permanent magnets (REPMs) are playing a major role in accelerators where their high intrinsic qualities allow for compact and flexible designs at no operating cost of beam transport systems[1)] and light sources[2)]. Unfortunately, REPMs are highly sensitive to direct and scattered radiation which cause demagnetization: the lifetime of these magnetic components is therefore a major issue. Numerous studies have been carried out to clarify the demagnetization mechanism or to test magnetic materials for a particular application under specific conditions of irradiation[3)]. Yet, neutron irradiation experiments have been mainly carried out so far, at reactors, where neutrons have a wide, but mainly low, energy spectrum. The objective was thus to study the effect of mono and highly energetic neutrons. The experiments were carried out at the AVF cyclotron in TIARA of the Japan Atomic Energy Agency.

Four different types of NdFeB permanent magnets representing a wide range of characteristics[4)] have been studied: Neomax^{TM} 27VH (remanent field B_r = 1.02~1.10T; coercivity H_{cJ}= 2864 KA/m; maximum energy product $(BH)_{max}$ = 199~231 kJ/m^3), 32AH (1.12~1.2 T; 2626 kA/m; 246~279 kJ/m^3), 35EH (used in the SPring-8 in-vacuum undulators: 1.17~1.25T; 1989 kA/m; 262~295kJ/m^3) and 44H (1.3~1.36T; 1273 kA/m; 326~358 kJ/m^3). Magnets with a high coercivity are known to be more radiation resistant. The samples were 8x8x8 mm^3 in size (corresponding to a permeance P_c[5)] of 3.1 (2.2 when averaged over the magnet, the effect of the neighboring magnets being negligible[6)]), and coated with 5 μ m TiN to protect them from corrosion and oxidation. The five samples were mounted on two water cooled aluminium frames to keep the temperature constant during irradiation. The magnetization was parallel to the direction of irradiation for the four samples closest to the neutron source (27VH, 32AH, 35EH and 44H) and was perpendicular for the far off one (35EH). The 65 MeV neutrons came from TIARA LC beamline, with a typical flux of 2.5 10^4 n/cm^2/s. After each irradiation, the magnet samples were left to "cool down", then taken to a separate room, where their magnetic field was measured. The hall probe was placed in a copper holder with a thermistor and a resistance heater to keep the probe temperature constant. The repeatability error of the measurement system was less than 0.1%.

The total irradiation time was a little over 25h. No demagnetization was observed within the realm of experimental errors up to a fluence of 2.4 10^9 n/cm^2 for the foremost magnet, and up to 2.2 10^9 n/cm^2 for the far off one, as shown in Fig.2. Previous results in the same fluence range were obtained with the lower neutron energy of a ^{252}Cf source (1 MeV average)[7)]. The NdFeB samples (N38H : B_r ~ 1.2 T, H_{cJ} =1353 kA/m, $(BH)_{max}$ ~ 290kJ/m^3) at 50x47.5x7 mm^3 in size (P_c ~ 0.3, therefore more susceptible to irradiation) showed no effects up to a fluence of ~ 4.0 10^{13} n/cm^2. We were therefore able to confirm that neutrons with an energy up to 65 MeV do not affect NdFeB magnets with a coercivity > 1273 kA/m for fluences up to 2.4 10^9 n/cm^2 and P_c >2.2.

We would like to thank Dr. A. Endo of the JAEA for his help during the experiment, as well as the staff of the TIARA AVF cyclotron facility.

References

1) R. H. Kraus, IEEE Trans. Mag. 30 **4** (1994) 1547.
2) H. Onuki and P. Elleaume Eds., Taylor & Francis Pub. (2002), ISBN: 0415280400.
3) X.-M. Marechal et al. AIP Conf. Proc. **705** (2004) 282.
4) http://www.neomaxamerica.com
5) Parker, Rollin J.; John Wiley & Sons, Inc., New York (1990), ISBN: 0471822930.
6) using RADIA: P. Elleaume et al., Proc. of the PAC97 Conference (1997) 3509.
7) J. Alderman, et al., Nucl. Instr. Meth. A **481** (2002) 98.

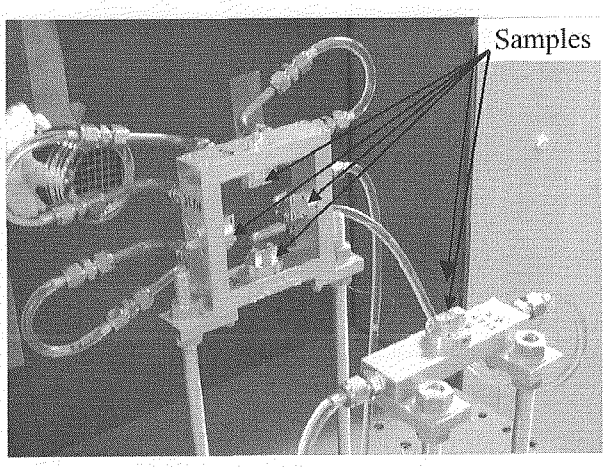


Fig.1 The sample set-up with the water-cooling circuit.

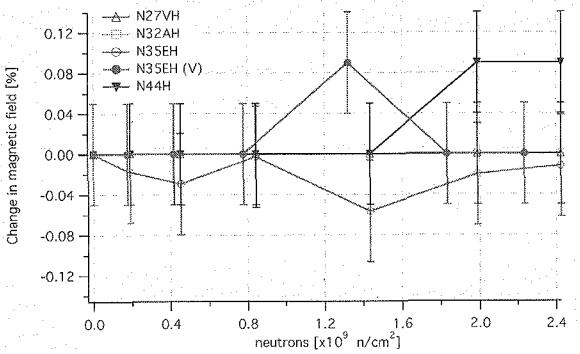


Fig.2 Change in magnetic field as a function of neutron fluence.

1-27 Radiation Resistance of Organic Materials in Superconducting Magnets at 77 K -Mechanical Properties-

T. Nakamoto[a)], H. Ohhata[a)], T. Ogitsu[a)], N. Kimura[a)], Y. Makida[a)], A. Yamamoto[a)], A. Idesaki[b)], M. Gokan[b)], N. Morishita[b)] and H. Itoh[b)]

[a)]KEK, [b)] Environment and Industrial Materials Research Division, QuBS, JAEA

Abstract

Radiation resistance of organic materials used in superconducting magnets for a 50 GeV-750 kW proton beam line for the J-PARC neutrino experiment was studied with respect to mechanical properties. Specimens cooled at a liquid nitrogen temperature of 77 K were irradiated by gamma rays. The flexural strength of glass-fiber reinforced plastics (GFRPs), the tear strength of polyimide films and the tensile lap-shear strength of adhesive films were evaluated. It was verified that the organic materials used in the superconducting magnets have the sufficient radiation resistance, and the degradation of their mechanical properties after the 10 years operation was estimated to be negligible.

高エネルギー加速器研究機構と日本原子力研究開発機構が共同で建設している大強度陽子加速器J-PARCでは、50 GeV-750 kW陽子ビームを利用したニュートリノ振動実験が計画されており、本ビームラインには超伝導磁石システムが採用される[1)]。超伝導磁石に用いられるフェノール樹脂(PM9640)、エポキシ樹脂(G10, G11)等のガラス繊維強化プラスチック(GFRP)やポリイミドフィルム(Upilex-RN)等は、高放射線環境下に曝されるため耐放射線性が非常に重要となる。本研究ではこれらの高分子材料にγ線を照射した場合の機械特性の変化について実験的研究を行い、耐放射線性を検証した。

接着用絶縁シートGUGを除く各試料は、ガラスアンプルに真空封入された後、原子力機構の^{60}Coγ線照射施設において、常温または液体窒素温度(77 K)で、最大25 MGy程度まで照射された。GUGに関しては2枚のステンレス板と接着した状態で、液体窒素に直接浸ったまま照射された。照射後は、試料を室温まで昇温し、各試料の機械特性評価を行った。

Fig. 1及び2にフェノール樹脂(PM9640)及びエポキシ樹脂(G11)それぞれの曲げ強度のγ線照射量依存性を示す。PM9640及びG11の曲げ強度は、77 K照射の場合、15 MGyまで殆ど変化が見られないことが判る。しかしながら、G11の常温照射では明白な吸収線量依存性が現れており、10 MGyでは未照射の約半分にまで曲げ強度が低下していた。Fig. 3にUpilex-RNフィルム引き裂き強度のγ線照射量依存性を示す。吸収線量の増加に伴いフィルム引き裂き強度が低下しているが、その減少率は1 MGy当たり約1 %であり、非常に小さい。なおロール方向の異方性は判別できなかった。Fig. 4にビームチューブ絶縁材料として用いるGUGの接着強度の線量依存性を示す。77 Kでのγ線照射では、10 MGyまで性能の劣化が殆ど見られない。

実際の運転では10年間の積分吸収線量が約0.3 MGyと見積もられている。したがって、J-PARCニュートリノビームライン超伝導磁石で使用される高分子材料が十分な耐放射線性を有することを、実験的に確認できた。

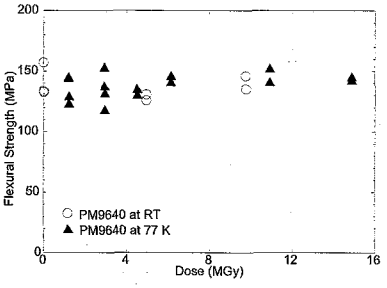


Fig. 1 Irradiation effects on the flexural strength of PM9640.

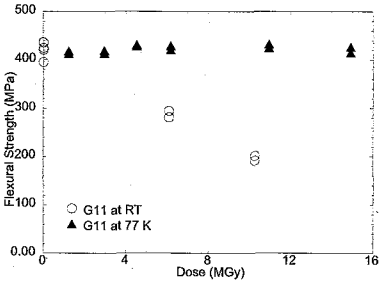


Fig. 2 Irradiation effects on the flexural strength of G11.

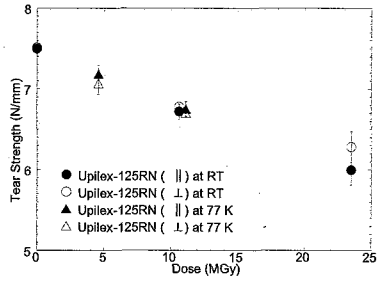


Fig. 3 Irradiation effects on the tear strength of Upilex-125RN.

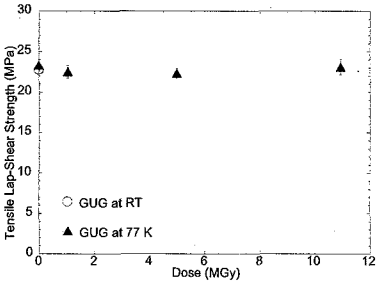


Fig. 4 Irradiation effects on the tensile lap-shear strength of GUG.

References

1)T. Ogitsu et al., "Superconducting Combined Function Magnet System for J-PARC Neutrino Experiment", *IEEE Trans. Appl. Superconduct*, Vol. 15, No. 2, 1175-1180, 2005.

1-28 Radiation Resistance of Organic Materials in Superconducting Magnets at 77K -Gas Evolution-

A. Idesaki[a)], M. Gokan[a)], N. Morishita[a)], H. Itoh[a)],
T. Nakamoto[b)], T. Ogitsu[b)], H. Ohhata[b)], N. Kimura[b)], Y. Makida[b)] and A. Yamamoto[b)]

[a)] Environment and Industrial Materials Research Division, QuBS, JAEA,
[b)] High Energy Accelerator Research Organization (KEK)

Abstract

Radiation resistance of polymeric materials used in the superconducting magnets installed for the J-PARC neutrino beam line was studied with respect to gas evolution. The polymeric materials were irradiated by γ-ray at 77K. It was found that hydrogen gas evolved mainly from the polymeric materials, and the amount of hydrogen from whole superconducting magnet system per 1 year was estimated to be 0.37mol. This amount of hydrogen is low enough to be removed by a hydrogen absorbing apparatus. Therefore, the influence of hydrogen evolved from the magnet system on the operation of the helium purifying system can be negligible.

日本原子力研究開発機構と高エネルギー加速器研究機構が共同で建設を進めている大強度陽子加速器施設(Japan Proton Accelerator Research Complex; J-PARC)では、50GeV-750kW陽子ビームを利用したニュートリノ振動実験が計画されている。本施設では、陽子ビームをニュートリノ生成ターゲットに導くために超伝導磁石システムが採用される。このシステムにおいては電気絶縁材や構造材料の一部としてポリイミドやガラス繊維強化プラスチック(GFRP)の高分子材料が用いられるが(Fig. 1参照)、これらの材料は低温(超臨界ヘリウム：5K以下)、およびビームロスにより発生する中性子・γ線の放射線場(1年間で約30kGyの積算吸収線量)に曝される。超伝導磁石システムの安定な運転、メンテナンスの観点から、これら高分子材料の耐放射線性を評価することが不可欠であり、本研究では、ポリイミドフィルムやGFRPに液体窒素温度(77K)でγ線を照射し、ガス発生挙動を調べた。試料には、ポリイミドとしてUpilex-RN Film、Upilex-RN Tape(Upilex-RN Filmにエポキシ系粘着剤を塗布したもの)、GFRPとしてG11(母材：エポキシ樹脂)、PM9640(母材：フェノール樹脂)を用いた。また、ビームチューブ絶縁材として使用されるGUG(ポリイミド/ガラスクロス+エポキシ樹脂の積層テープ材)も実験に供した。本研究では、極低温環境模擬の観点から、液体窒素温度での照射を行った。ガラスアンプルに真空封入した試料に77Kにおいて^{60}Coγ線を最大15MGyまで照射した後、ガラスアンプルを室温で約16h保持後、アンプル内に蓄したガスを圧力計およびガスクロマトグラフによって分析した。

Fig. 2に本磁石システムで使用される高分子材料からγ線照射によって発生したガスを示す。Upilex-RN Filmの場合、照射によってほとんどガスが発生しなかった。これに対して、Upilex-RN Tape、G11、PM9640、およびGUGでは全体で10^{-6}～10^{-5}mol/gオーダーのガスが発生し、その主成分は水素であった。

水素は超伝導磁石システムに流通させる超臨界ヘリウムにとって不純物であり、除去しなければならない。ヘリウム精製機には水素吸着装置が装備されるが、除去可能な量に限界がある。そこで、ガス分析の結果を基に超伝導磁石システム全体で発生する水素量を算出した。

先述のように、実際の運転では、本磁石システムで使用される高分子材料は1年当たり約30kGyの放射線照射を受けると想定されている。Fig. 2の低線量域における直線部分の傾きから30kGy照射時のガス発生量を計算すると、超伝導磁石1基について発生する水素の総量は1.33×10^{-2}mol/yearとなる。J-PARCニュートリノビームラインでは28基の超伝導磁石が使用されるため、全体の発生量は0.37mol/year(液体水素の体積として0.01L/year)となる。この量は、現在ヘリウム精製機に装備されている水素吸着装置で十分除去できる量であり、このことから、照射によって発生する水素がヘリウム精製機の運転へ及ぼす影響はほとんど無視することができると考えられる。

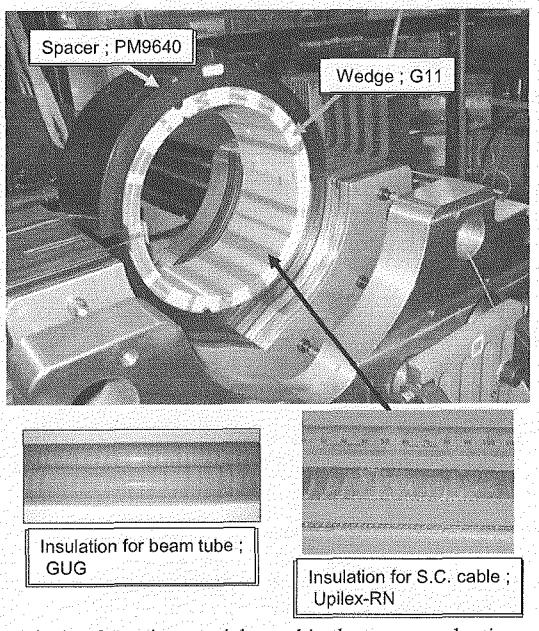


Fig.1 Organic materials used in the superconducting magnet for the J-PARC neutrino beam line.

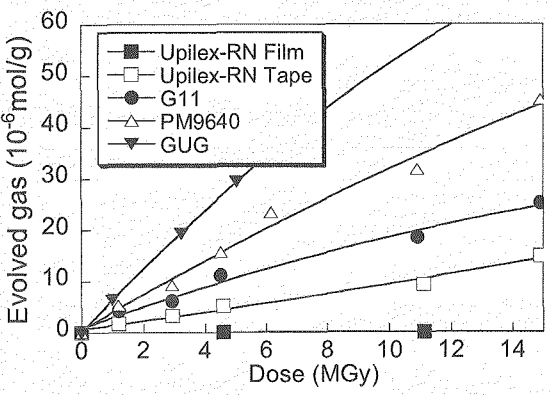


Fig.2 Evolved gas from polymeric materials used in superconducting magnets by γ-ray irradiation at 77K.

1-29 Gamma-Ray Irradiation Effects on Thermal Decomposition Behavior of Cable Materials

A. Idesaki [a)], M. Gokan [a)], N. Morishita [a)], O. Takeda [b)], H. Itoh [a)] and J. Kusano [c)]

[a)]Environment and Industrial Materials Research Division, QuBS, JAEA,

[b)]Proton Accelerator Facility Development Center, QuBS, JAEA, [c)]J-PARC Center, JAEA

Abstract

It is required for various apparatus used in the tunnel of J-PARC accelerators to possess radiation resistance. Whereas halogen-free and flame retardant cables will be adopted for power cables, there are few reports about their radiation resistance. In this work, the gamma-ray irradiation effects on thermal degradation behavior of the cable materials have been investigated. It was found that the starting temperature of thermal degradation of sheath material shifted to lower temperature and that the temperature range of water evolution from flame retardant agent shifted to higher temperature by irradiation.

現在、日本原子力研究開発機構　東海サイトにおいて建設が進められている大強度陽子加速器施設(Japan Proton Accelerator Research Complex; J-PARC)の加速器トンネル内に設置される装置・機器はビームロスによる中性子・γ線の放射線場に曝されるため、耐放射線性を要求される。特に電力ケーブルは3MGy以上の耐放射線性を有していることが望ましいとされている。J-PARC加速器トンネル内は通常の防火区画の設定が困難であるため、電力ケーブルにはノンハロゲン高難燃ケーブルが使用される予定であるが、これまで高難燃ケーブルの耐放射線性について報告された例はほとんどない。そこで我々は、ケーブルの燃焼特性面からの耐放射線性に着目した。

ケーブル材料の燃焼特性と熱分解挙動の間には密接な関係があることから、本研究では、高難燃ケーブル材料の熱分解挙動に及ぼす放射線照射の影響について調べた。

供試材として、配合の異なる3種類のノンハロゲン高難燃ケーブルを使用した。ケーブルの絶縁材はポリエチレン、シース材はポリエチレン/難燃剤(水酸化金属)が主成分である。各ケーブルをレーストラック状に固定し、高崎量子応用研究所^{60}Coγ線照射施設において室温、空気中、線量率1.2～5.6kGy/hの条件で最大3MGyまで照射した。照射後、ケーブルの任意の部分から試料を切り出し、窒素中、室温から500℃までの熱重量-示差熱分析(TG-DTA)、およびヘリウム中、室温から450℃までの熱重量-質量分光分析(TG-MS)を行った。

熱分析の結果、3種類のケーブル材料はほぼ同様の傾向を示したので、ここでは代表的な結果について示す。Fig. 1にシース材のTG-DTA曲線、およびFig. 2に低温域のTG曲線拡大図を示す。Fig. 1より、未照射試料について、熱分解過程は(1)300℃以下、(2)300～420℃、および(3)420℃以上、の3つの領域に分けることができる。領域(1)では、シース材は緩やかな重量減少を示した。領域(2)では、400～420℃にかけて大きな重量減少を示すとともに、405℃に吸熱ピークが見られた。領域(3)では480℃まで急激な重量減少を示すとともに、465℃に吸熱ピークが見られた。TG-MSの結果から、領域(2)ではH_2O(分子量18)が、領域(3)ではポリエチレンの典型的な熱分解生成物(分子量43)が主に検出された。このことから、領域(2)では難燃剤からの脱水、領域(3)ではポリエチレンの熱分解が起こっていると考えられる。

一方、照射試料の場合、熱分解過程は未照射の場合とほぼ同様であるが、領域(1)において、重量減少が未照射よりも大きくなること(Fig. 2)、領域(2)では大きな重量減少を示す温度域が高温側にシフトするとともに吸熱ピークが420℃まで上昇すること、領域(3)では未照射よりも低温側で重量減少が大きくなるとともに吸熱ピークが455℃まで下降することが明らかになった。

すなわち、ノンハロゲン高難燃ケーブルのシース材に放射線を照射すると、低温で熱分解が開始するとともに、難燃剤からの脱水が高温まで起こらない傾向を示した。このような放射線照射による熱分解挙動の変化について、低温での熱分解開始は材料表面での放射線酸化劣化に起因すると考えている。脱水挙動の変化については、照射により難燃剤周辺の環境が変化することが原因であると推測しているが、まだ不明な点があり、今後さらに検討する予定である。

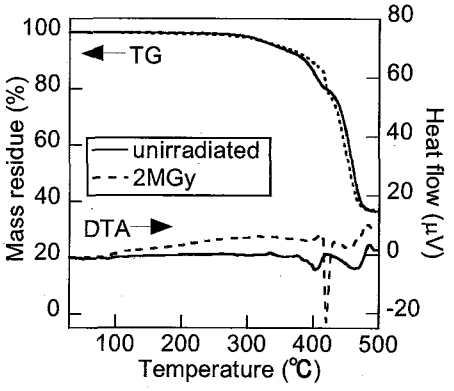


Fig. 1　TG-DTA curves of 2MGy-irradiated and unirradiated sheath materials in N_2.

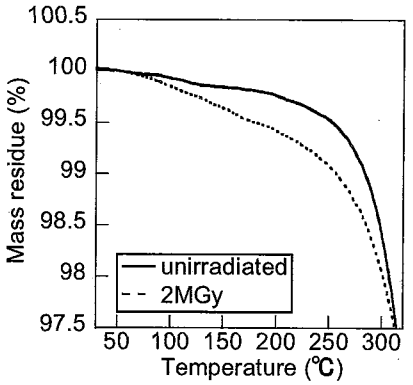


Fig. 2　Enlargement of TG curves (Fig. 1) in low temperature range (<300℃).

1-30 Operation Test Result of a Radio-Proof Cryogenic Valve under Cobalt 60 Irradiation

Y. Makida [a)], H. Ohhata [a)], T. Okamura [a)], T. Ogitsu [a)], T. Nakamoto [a)], N. Kimura [a)], A. Idesaki [b)], M. Gokan [b)] and N. Morishita [b)]
[a)]KEK, [b)] Environment and Industrial Materials Research Division, QuBS, JAEA

Abstract

A string of superconducting magnets is to be set at an arc section of the J-PARC neutrino beam line. To keep the magnets at superconducting condition, a helium cryogenic facility is to be constructed. Parts of cryogenic devices are located beside the magnets, so their resistance to radiation with predicted dose of 1 MGray in maximum must be assured. A cryogenic control valve is one of the active devices used in the radio-active area, and its radio-proof characteristics is improved by (1) exchanging intolerant materials(ex. PTFE or Neoprene) by proof ones (ex. PEEK , EPT, or mineral), (2) moving the feed back control circuit unit including electronics from the valve body to a low radio-active area.

Two prototype valves, a tuning valve and a Gauzky relief valve, have been prepared and have been tested by using the Cobalt 60 irradiation facility in JAEA. Actual operations of the both prototypes have been checked at the irradiation test bench, and they were successfully operated after irradiation of 1 MGray.

1. はじめに

J-PARCニュートリノビームライン(JNU)では、超伝導マグネットが採用され、ヘリウム冷凍機が付設される。圧縮機、冷凍機など主要な冷凍機器は地上の一般環境下に設置されるが、マグネット及びクライオスタットはビームラインとトンネル内にて50 GeV陽子ビームによる高放射線環境下に曝される。このため耐放射線性を有するクライオスタット部品の調査・開発を行っており、開発機器の動作確認として原子力機構高崎のコバルト照射（γ線）試験施設を利用した照射試験を実施している。今回、①低温用制御弁、②ガウツキー安全弁を対象とした照射試験を行い、目標値1MGy以上の動作を確認したのでその報告をする。

2. バルブ設計

低温用制御弁やガウツキー安全弁は耐放射線性を持たせるために、以下のような方針で設計を進めた。(1)有機材料（ゴム、プラスチック）は避け、金属材料を使用する。(2)パッキン、弁座やガイドなど有機材使用が避けられない箇所も、耐放射線性を有する材料(ポリイミド、peek材など)を使用する一方、テフロンやブチルゴムなどは使用してはならない。(3)電子回路部は誤動作するのでバルブ本体から分離する。放射線管理区域外までポジショナーなど電子回路部を分離するとJNU設備の場合最大150mの距離となる。

2.1 制御弁　　制御弁は2回照射試験を行った。1回目の照射試験では、クロロプレンゴムを用いたダイヤフラム式アクチュエーターが0.5MGyに至る前に破断する一方、通常仕様のACリバーシブルモーター駆動の電動弁は試験終了1.23MGyまで駆動した[1)]。この結果を踏まえて開閉速度と安定度、分解能を上げた2号機を製作し、Fig.1のような構成で２回目の照射試験を行った。

2.2 ガウツキー安全弁　　ガウツキー安全弁は、ベローズで仕切られた参照圧力側とプロセス圧力側のバランスで開閉動作を行うバルブで、参照圧力調整で吹き出し圧力を変えることができる。励磁中は設定0.4MPaでクエンチ時緊急放出に備える。長軸弁構造で、オッシレーション防止リング及び弁座の一部にpeek材を使用している以外、全て金属材料を使用した。Fig.2のような構成で照射試験を実施した。

3. 試験結果

制御弁は連続的に開度指令値を変化させ、ポテンショメーターで実開度を測定した。ガウツキー安全弁は、約1時間おきにプロセス圧力を上げて吹始め、吹止まり圧力及び閉止時のシート漏れを測定した。3ヶ月にわたって照射を行い、コバルト線源側正面で2.5MGy以上の積算照射量に達したが、量バルブとも異常は観測されなかった。

Reference

1) 大畠洋克他：2004年度秋季低温工学・超伝導学会講演概要集　p.44

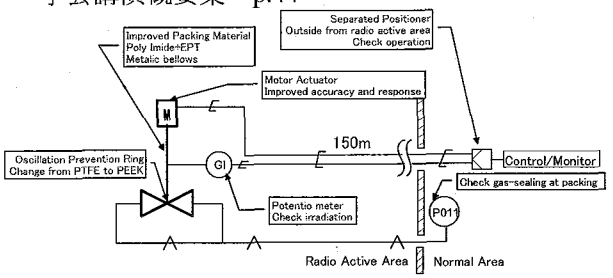


Fig. 1 Setup of the motor-operated valve test.

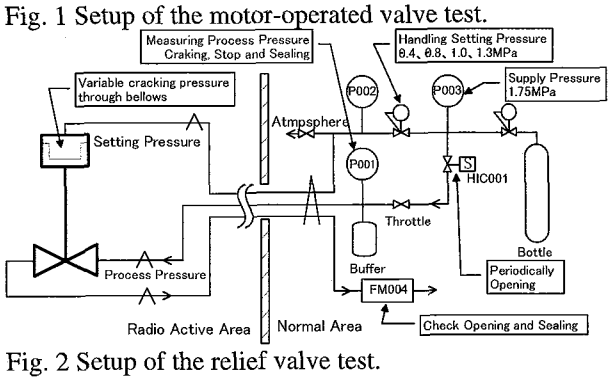


Fig. 2 Setup of the relief valve test.

1-31 Nano-Structure Controlled Polymer Electrolyte Membranes for Fuel Cell Applications Prepared by Ion Beam Irradiation

T. Yamaki[a)], A. Hiroki[a)], M. Asano[a)], Y. Maekawa[a)], K.-O. Voss[b)], R. Neumann[b)] and M. Yoshida[a)]

[a)]Environment and Industrial Materials Research Division, QuBS, JAEA, [b)]Material Research Department, GSI

For recent several years, our group has been developing the proton exchange membranes (PEMs) for polymer electrolyte fuel cells (PEFCs) based on the techniques of polymer crosslinking and graft polymerization induced by ionizing radiation such as a γ-ray or electron beam[1]. On the other hand, this study concerns the use of swift heavy ions, instead of the γ and electron radiations, for the preparation of the PEMs[2,3]. A cylindrical damage area produced by bombardment of high-energy ions, i.e., a latent track, is preferentially dissolved during chemical etching to give uniform pores in the nanometer range. We report here a novel method of membrane preparation that involves the filling of proton-conductive sulfonic acid groups into the etched-track pores. In this case, the base material without any graft electrolyte chains is expected to prevent the excess swelling during the PEFC operation.

A 25-μm-thick poly(vinylidene fluoride) (PVDF) film was bombarded by 3.5 MeV/n ^{129}Xe and 11.4 MeV/n ^{238}U ions from the TIARA cyclotron (JAEA) and the UNILAC linear accelerator (GSI), respectively. The track etching was then done in a 9 M KOH aqueous solution at 80°C. The pore density ranged between 3.0×10^6 and 3.0×10^9 /cm^2, which agreed with the number of actually irradiated ions per 1 cm^2. The sulfonic acid groups were introduced into the track-etched cylindrical pores via the γ-ray-induced styrene grafting and the subsequent sulfonation[1].

Figure 1 plots the surface pore diameter determined by the scanning electron microscope (SEM) observation as a function of the etching time. The time variation of the diameter was best fitted by two straight lines with different slopes. The steep line during the initial stage corresponds to the radial etching rate in the latent track. In contrast, the later gentle slope roughly agreed with the dissolution speed in non-irradiated part, which was independent of the irradiation conditions. Thus, the diameter at the intersection of the lines is assumed to represent the size of the track for each irradiated ion. The track diameter is estimated to be 235 and 280 nm for 3.5 MeV/n ^{129}Xe and 11.4 MeV/n ^{238}U, respectively. Most importantly, the pore size was arbitrarily controlled by the etching time in the range of 50-400 nm in diameter.

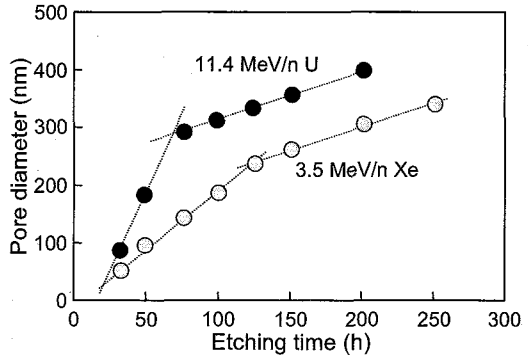


Fig. 1. Change in the pore diameter obtained from the SEM observation as a function of the etching time for PVDF films irradiated with the swift Xe and U ions.

The track-etched PVDF membranes with 100-nm diameter pores (area density: 3.0×10^9 /cm^2) were obtained by the 50-hour alkaline treatment after the ^{129}Xe irradiation. In the styrene grafting by a γ-ray pre-irradiation procedure, it is noted that the graft chains must grow only on or near the internal wall of the pore, and also both sides of the membrane surface without homogeneous distribution over the film together with monomer diffusion. Accordingly, the reaction was stopped in a very short time within one hour from the beginning.

Figure 2 shows the proton conductivity, σ, in the in-plane and thickness directions for the sulfonated electrolyte membranes whose ion exchange capacity was controlled up to 2.2 mmol/g by the grafting time. The proton transport *only* in the thickness direction, increasing with the ion exchange capacity, was observed at < 1.6 mmol/g. This indicates the formation of one-dimensional straight proton conductive pathways parallel to the ion-beam incident axis. It was found from the results of transmittance electron microscopic observation that the electrolyte membranes with such anisotropic conductivity had a cylindrical electrolyte part with a diameter of about 100 nm, comparable to the size of the etched pore.

Our materials undoubtedly become interesting because of their specific nano-controlled structure, especially in the proton conductive regions. Further studies are now in progress to examine other membrane properties and to optimize the preparation conditions.

References

1) T. Yamaki et al., Polymer 45 (2004) 6569.
2) T. Yamaki et al., GSI Scientific Report 2004 (2005) 260.
3) T. Yamaki et al., ECS Transactions, in press.

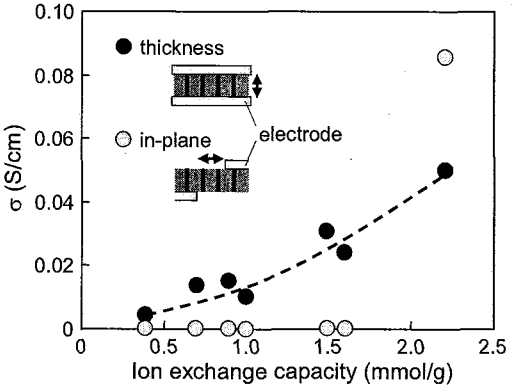


Fig. 2. Proton conductivity in the in-plane and thickness directions for the PVDF-based electrolyte membranes with different ion exchange capacities.

This is a blank page.

2 Environment Conservation and Resource Security

2-01 Preparation of Ion Exchange Fibres by Emulsion Graft Polymerization ····· 39
N. Seko, N. Thi Yen Ninh and M. Tamada
2-02 Development of Radiation Induced Graft Polymerization in Aqueaous Medium ; Approach for Styrene Based Monomers ····· 40
K. Okada, N.Seko and M.Tamada
2-03 Development of Boron Adsorbent for Environmental Drainage ····· 41
H. Hoshina, N. Seko and M. Tamada
2-04 Mercury Adsorbent Synthesized by Graft Polymerization onto Cellulose Nonwoven Materials ····· 42
A. Sekine, Y. Suzuki, N. Seko and M. Tamada
2-05 Development of Bifunctional Chelating Fibers with High Performance in Metal Ion Adsorption Kinetics ····· 43
A. Jyo, Y. Shibata, M. Tamada, N. Seko and A. Katakai
2-06 Development and Application of Fiberous Bifunctional Phosphonate-Sulfonate Cation Exchanger ····· 44
K. Okada, N. Seko, T. Masao and A. Jyo
2-07 Cost Estimation of Uranium Collection from Seawater with Braid Type Adsorbent ····· 45
M. Tamada, N. Seko, N. Kasai and T. Shimizu
2-08 The Recovery Method of Scandium from Hot Spring Water ····· 46
N. Kasai, N.Seko, M.Tamada and E.Ichikawa
2-09 Development of Equipment to Remove Cadmium from Waste of Scallop Processing by Graft Adsorbent ····· 47
H. Nakai, T. Temma, M. Tamada, T. Sawamura,T. Saito, T. Honma and K. Sato
2-10 Development of Grafting Adsorbent for Ultra Pure Water Production ····· 48
T. Takeda and M. Tamada
2-11 Preparation of Amidoxime-Type Chelating Fabric and Its Removal Performance of Toxic Heavy Metals ····· 49
A.Katakai, M.Tamada, H.Nagamoto, S.Ono and H.Miyagawa
2-12 Removal of Ferric and Manganese Ions with Fibrous Iminodiacetic Acid Adsorbent Synthesized by Graft Polymerization ····· 50
K. Tanaka, N. Anzai, N. Seko and M. Tamada
2-13 Off-On Biodegradability of Poly(3-hydroxybutyrate) Film Modified by Graft Polymerization ····· 51
Y. Wada, H. Mitomo, N. Seko and M. Tamada
2-14 Metal Adsorption of Chitin / Chitosan Derivatives Hydrogels Crosslinked with Irradiation ····· 52
N. Nagasawa, Jarosław M. Wasikiewicz, N. Seko, T. Yagi, L. Zhao, H. Mitomo, F. Yoshiia and M. Tamada
2-15 Modification of Poly(lactic acid) by Radiation-Induced Crosslinking ····· 53
N. Nagasawa, A. Kaneda, T. Matsuzaki, S. Kanazawa, T. Yagi, Tran Minh Quynh, H. Mitomo, F. Yoshii and M. Tamada
2-16 Development of DNA-Derived Environmental Material by Gamma-Ray Irradiation ····· 54
K. Furusawa, E. Kita, T. Dobashi, N. Nagasawa and M. Tamada

2-17 Enhancement of Plant Growth Activity of Irradiated Alginate ····· 55
N. Nagasawa, Le Q. Luan, T. Yagi, F. Yoshii, T. Kume, T. M. Nakanishi and M. Tamada
2-18 Cooperative Research on Radiation Processing of Natural Polysaccharides between VAEC and JAEA ····· 56
A. Hiroki, N. Nagasawa, T. Yagi , T. Kume, F. Yoshii and M. Tamada
2-19 Radiation Effects on PTFE Moulding Powder ····· 57
T. Yagi, M. Tamada, A. Udagawa
2-20 Hexyl Methacrylate-Based Monolithic Columns Prepared by Radiation-Induced Polymerization ····· 58
Y. Ueki, T. Umemura, Y. Iwashita, H. Hotta, T. Odake, K. Tsunoda, A. Katakai and M. Tamada
2-21 Development of Electron Beam Technology for the Treatment of PCDD/Fs in Municipal Waste Incinerator Gases ····· 59
K. Hirota, M. Taguchi , T. Hakoda and T. Kojima
2-22 Electron Beam Treatment of Formalin Sterilization Gas ····· 60
A. Shimada, T. Hakoda, T. Kojima, T. Takubo, T. Iwasaki and S. Kinoshita
2-23 Decomposition of Endocrine Disrupting Chemicals in Real Wastewater by ^{60}Co γ-Ray Irradiations ····· 61
A. Kimura, M. Taguchi, Y. Ohtani, H. Hiratsuka and T. Kojima
2-24 Dependence of Differential Yields of Heavy Ion Induced OH Radicals in Water on Mass and Specific Energy of Heavy Ions, and Elapsed Time ····· 62
M. Taguchi and T. Kojima

2-01 Preparation of Ion Exchange Fibres by Emulsion Graft Polymerization

N. Seko[a], N. Thi Yen Ninh[b] and M. Tamada[a]
[a] Environment and Industrial Materials Research Division, QuBS, JAEA
[b] Institute for Technology of Radioactive and Rare Elements, VAEC

Abstract

Radiation induced graft polymerization is powerful technique for modification of polymeric materials such as membrane, film and fiber. An epoxy-group-containing polymer chain was grafted onto the polyethylene (PE) fiber by the immersion of the electron beam-irradiated PE fiber in emulsion solution of glycidyl methacrylate (GMA) that mixed water and sodium n-dodecyl sulfate as a surfactant. Degree of grafting (Dg) which was estimated by the weight gain after grafting increased with the increment of GMA concentration in the range of 2-8%. Dg depends on the size of GMA/SDS micelles in emulsion graft polymerization.

放射線グラフト重合技術[1] を用いて作製したイオン交換繊維は、水中の金属イオンや大気中の有害ガスを効率的に除去できる。これらイオン交換繊維はターゲット因子を高速で高容量に捕捉することが可能[2]であるが、合成する際には反応活性点を生成するために電子線を用いているため、市販の樹脂と比較してコスト高が否めない。本研究では、イオン交換繊維の製造コストの低減化および製造時の環境負荷の低減化を図るため、イオン交換繊維の前駆体であるメタクリル酸グリシジル（GMA）をグラフト重合で導入する方法として、これまで反応溶媒に用いていた有機溶剤に変わり、水系のエマルション状態で重合するための条件探索を行った。

GMAを水と相溶させるためにドデシル硫酸ナトリウム（SDS）を界面活性剤として用いた。相溶性試験は、GMA濃度を固定し、SDS濃度を変化させて行った。GMA/SDSの各組成において粒度分布を測定し、エマルションの粒径とグラフト率の相関関係を検討した。

イオン交換繊維の作製は基材のポリエチレン繊維に電子線を照射後、GMAのエマルション溶液中でグラフト重合することによって得た。比較の有機溶媒の系としてジメチルスルホキシド（DMSO）とメタノール（MeOH）を用いた。

GMAとSDSの相溶性試験は、GMA濃度5%でSDS濃度を0.2%から12%に変化させて行ったところ、SDS濃度が0.5%以上で混合溶液は透明になり可溶化した。従来、GMAをグラフト反応では、電子線を200kGy照射した後、反応溶媒にDMSOなどの有機溶媒を用いて行っていたが、Fig. 1に示すように、エマルション系では反応が促進され、3時間の反応でグラフト率（Dg: 反応前後の重量増加により算出）は150%に達し、DMSOと比較すると、約10倍の速さで進行することがわかった。これにより照射線量をこれまでの200kGyから50kGyに下げて、エマルショングラフト重合を行っても、3時間の反応でグラフト率が130%程度に達し、イオン交換繊維に必要なグラフト率を得ることが可能になった（Fig. 2）。グラフト反応速度はエマルションの粒径に依存し、GMA/SDSの系ではSDSの濃度増加に伴い、粒径は増大しGMAの吸収量も増加するが、グラフト率が低下するという傾向が見られた。SDS濃度が8%（GMA濃度8%）以上では、反応の効率が悪くなり、逆に反応速度を低下する要因になることがわかった。

得られたGMAのグラフト重合体にジエチレントリアミンを転化させアミン型のイオン交換繊維を作製し、白金に対する吸着性能を検討したところ、広いpH範囲で吸着性能は良好で、pH2において100万倍に濃縮できることがわかった。

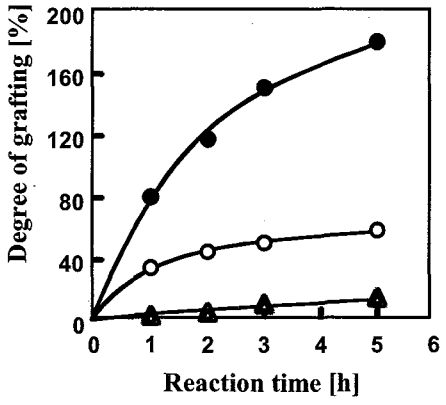


Fig.1 Comparison of Dg between emulsion and organic solution at 5% GMA :
(●) emulsion,(○) MeOH, (△) DMSO
(0.5% of SDS conc., 40℃ of reaction temp.)

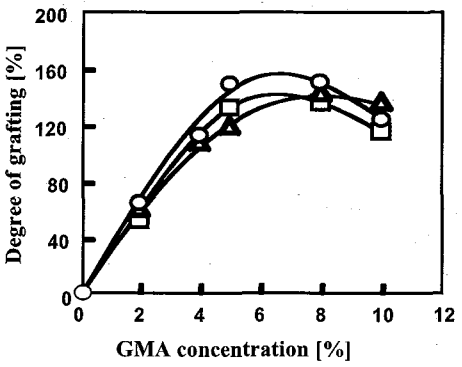


Fig. 2 Effect of GMA concentration on Dg at 313K for 3 h at 5% GMA with 4% SDS; (○)200kGy, (△) 100kGy, (□) 50kGy

References
1) K. Saito, et al., "High-performance polymeric materials for separation and reaction, prepared by radiation-induced graft polymerization", Radiation Chemistry, (2001) 671.
2) N. Seko, et al., "Rapid removal of arsenic(V) by zirconium(IV) loaded phosphoric chelate adsorbent synthesized by radiation induced graft polymerization", React. Funct. Polym., 59 (2004) 235.
3) K. Saito, et al., "High-performance polymeric materials for separation and reaction, prepared by radiation-induced graft polymerization", Radiation Chemistry, (2001) 671.
4) N. Seko, et al., "Rapid removal of arsenic(V) by zirconium(IV) loaded phosphoric chelate adsorbent synthesized by radiation induced graft polymerization", React. Funct. Polym., 59 (2004) 235.

2-02 Development of Radiation Induced Graft Polumerization in Aqueaous Medium; Approach for Styrene Based Monomers

K. Okada, N.Seko and M. Tamada

Environment and Industrial Materials Research Division, QuBS, JAEA

Abstract

Techniques of radiation induced graft polymerization by electron beam are convenient methods for the preparation of ion exchange fibers. In this study, a new method of radiation induced graft polymerization that can be applied in aqueous medium was developed by means of two kinds of monomers; styrene and chroromethyl styeren . Graft polymerization was carried out onto 50 kGy irradiated fiber with the concentrations of 1% monomer and 3% Sodium dodecylebenzoate(SDBS) in water for 1 hr at, to obtain 100 % degree of grafting. Under optimized conditions, total radiation dose, concentration of monomer were significantly lower than those of non-aqueous mediums such as methanol and DMSO etc..

放射線グラフト重合技術を用いて作製した繊維状捕集材は繊維径が10-20μmであるため、従来の金属吸着樹脂(粒子径0.5mm)に比較して、10～100倍の処理速度が実現可能となり、水中の金属イオンや大気中の有害ガスを効率的に除去することが可能であり[1]、イオン交換樹脂と比較して、吸着容量や吸着速度が著しく向上することが知られている[2,3]。これまで繊維状金属捕集材の合成は、基材への電子線照射後、ジメチルスルホキシド(DMSO)、ジメチルホルムアミド(DMA)、メタノールなどの有機溶媒中でグラフト重合を行なっている。

本研究では製造コストおよび環境負荷の低減化を目的として、スチレン(St)またはクロロメチルスチレン(CMS)を水系においてグラフト重合し、その最適条件を検討した。モノマーを水に相溶させるために界面活性剤としてドデシルベンゼンスルホン酸ナトリウム(SDBS)、ツィーン20、脂肪族ホスホン酸エステルであるアデカコールPS-440Eを用いて最適条件を検討した。実験は基材であるポリエチレン被覆ポリプロピレン繊維に50～200kGy電子線を照射した後、反応温度40℃としてモノマー溶液と接触させてエマルショングラフト重合実験を行った。

ポリエチレン被覆ポリプロピレン繊維を基材として、スチレン(St)またはクロロメチルスチレン(CMS)を効率的にグラフト重合する手法として、従来の方法である反応溶媒を有機溶媒であるジメチルスルホキシド(DMSO)とした場合、グラフト率100 %の金属捕集材を得るためには、電子線を200kGy照射した後に、St 20%で1時間、10%では6時間、CMS 30%では6時間の反応時間を要する(Fig.1)。これに対して、水を溶媒として電子線を50～100kGy照射した後、界面活性剤濃度 5%、モノマー濃度10%（CMSのみ重合禁止剤を除去）の溶液を用いてグラフト重合を行った結果、重合速度が極めて速く、グラフト率の制御が困難であったため、モノマー濃度1%におけるグラフト重合を検討した。その結果、界面活性剤の濃度を0.1～5%(St,CMSともに重合禁止剤を除去)としてグラフト重合を行った結果、3～5%において界面活性剤の種類によらず1時間で100%程度のグラフト率(dg)が得られた。Fig.2にSDBS濃度3%におけるグラフト重合の結果を示した。その結果、有機溶媒中におけるグラフト重合実験と比較して、照射線量、モノマー濃度を削減したにもかかわらず、重合速度、反応効率が大きく向上した。また、これらの重合反応に用いたエマルションについて粒径アナライザーFPAR-1000Hを用いて動的光散乱法により粒径測定を行った。その結果、界面活性剤濃度が高いものほど平均粒径が小さく、重合速度が速いことがわかった。

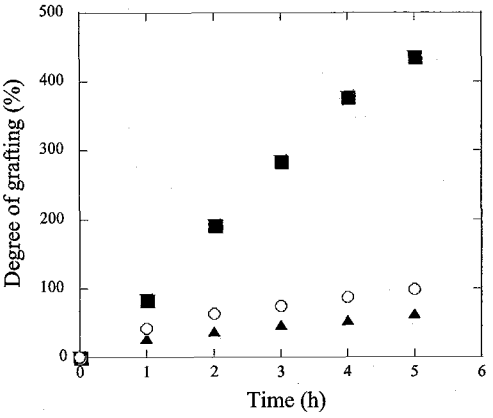


Fig.1 Degree of grafting for St and CMS in DMSO.
St-20%; (■), St-10%; (▲), CMA-30%; (○)
Degree of grafting = $100\{(W-W_0)/W_0\}$
W0; Weight of the fiber before grafting
W; Weight of the fiber after grafting

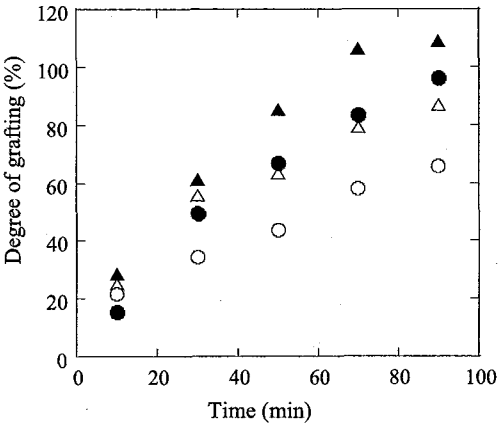


Fig.2 Degree of grafting for St and CMS in emulsion state.
St;(▲), 100kGy, (●) 50kGy,
CMS;(△) 100kGy, (○) 50kGy.

References

1)玉田正男、放射線と産業、No.93（2003）
2)A. Jyo, S. Aoki, T. Kishita, K. Yamabe, M.Tamada,and T. Sugo, *Analytival Science*, **17**, 201-204(2001).
3)S. Aoki, K. Saito, A. Jyo, A. Katakai, and T. Sugo, *Analytival Science*, **17**, 205-208(2001).

2-03 Development of Boron Adsorbent for Environmental Drainage

H. Hoshina, N. Seko and M. Tamada

Environment and Industrial Materials Research Division, QuBS, JAEA

Abstract

It is well known that ion exchangers having N-methylglucamine units preferentially take up boron. Fiber developed in this study has promising properties of rapid removal and recovery of boron in the streaming water. The precursory fiber was prepared by radiation induced graft polymerization of glycidyl methacrylate onto polyethylene fiber in aqueous medium, and following chemical modification with N-methylglucamine. The resulting fiber was evaluated by its adsorption ability toward boron of 0.1ppm concentration at the temperature range from 25℃ to 85 ℃ at pH 6. It was found that the adsorption performance was enhanced with the increase of the adsorption temperature.

環境排水中には人体に有害なヒ素やホウ素などの陰イオンが溶存しており、近年水質汚濁防止法での規制が厳しくなってきている。ホウ素の排出基準は10ppmに規制されており、環境基準としては、さらに1/10の1ppmまで規制される。しかしながらホウ素は消毒液の原料ともなっていることから、除去後のホウ素については資源としての活用も可能である。一方、ホウ素を吸着除去する研究はこれまでも行われており、グルカミン基がホウ素に対して吸着性能が良好であることが知られている。しかし、これまでのグルカミン型の吸着材は、吸着速度が遅いため処理に時間がかかるという問題があった[1]。

本研究では、放射線グラフト重合法を用いて繊維状の不織布にグルカミン基を導入することで高速に処理ができる吸着材の創製を試みた。また、これまで反応溶媒に使用していたメタノールなどの有機溶媒に代えて水を溶媒に用いることで吸着材作製過程においても環境負荷を低減できる合成法の条件探索も試みた。

ポリエチレン製の不織布(目付50g/m^2、繊維径13μm)の基材を窒素雰囲気下で電子線を20kGy照射したのち、グリシジルメタクリレート(GMA)およびTween20を純水と混合させて得られるエマルション溶液中で、40℃でグラフト重合を行った。次いで、GMAグラフト重合体にN-メチル-D(-)-グルカミン(NMDG)を転化させてホウ素除去用のグルカミン型吸着材を作製した。得られた吸着材(グルカミン官能基密度：1.5mmol/g, 20mg)を25℃から80℃に温調した0.1ppmのホウ素溶液30ml中で浸漬させて除去時の温度効果を検討した。

Fig.1にGMAのエマルショングラフト重合におけるグラフト率の反応時間依存性を示す。反応前後の重量増加により算出したグラフト率は時間とともに増加し、いずれの濃度においても、わずか1時間の反応で吸着材に必要な官能基量である150%に達した。モノマー濃度および反応時間をコントロールすることで、容易に目的のグラフト率が得られることがわかった。

得られたグルカミン型の吸着材の吸着温度依存性を検討するため、25℃から80℃に温調した0.1ppm、 pH6のホウ素溶液中に吸着材を浸漬撹拌させたところ、Fig.2に示すように、吸着温度の増加に伴い吸着効率が向上する傾向がみられた。これにより高温での吸着処理が除去効率を向上させる要因になりえることがわかった。

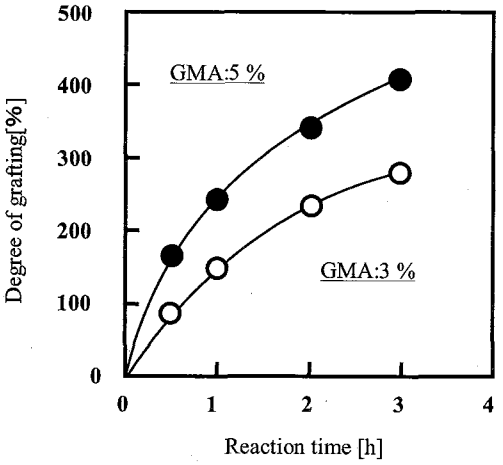


Fig.1 Effect of reaction time on degree of grafting in emulsion condition

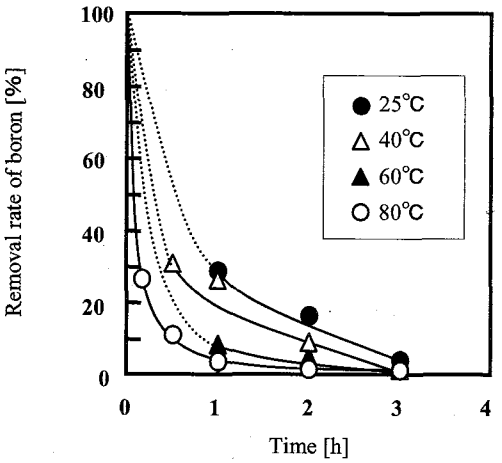


Fig.2 Effect of adsorption temperature on boron removal with 0.1ppm boron solution at pH6

References

1) M. Badruk, N. Kabay, and M. Demircioglu, Sep. Sci. Technol., 34, 2553 (1999).

2-04 Mercury Adsorbent Synthesized by Graft Polymerization onto Cellulose Nonwoven Materials

A. Sekine[a], Y. Suzuki[a], N. Seko[b] and M. Tamada[b]

[a]Oriental Engineering Co.Ltd.,[b]Environmental Industrial Materials Research Division,QuBS,JAEA

Abstract

Glycidyl methacrylate was grafted on cellulose nonwoven materials in its emulsion state. Amine-type adsorbents for mercury removal were synthesized by reacting the obtained GMA-grafted cellulose with ethylenediamine (EDA) and diethylenetriamine (DETA).The amounts of the amine contents were 2.9 mol/kg-adsorbent for EDA type and 2.8 mol/kg-adsorbent for DETA type. The adsorbents were put in the mercury solution of 100 ppb to evaluate the adsorption selectivity. The adsorption performance was the highest in an acidic region and the distribution coefficient in pH3 became 2.3×10^4 for EDA-type and 1.9×10^5 for DETA type, respectively.

近年、河川などの環境水中の重金属を除去可能な吸着材の開発が求められている。このような要望に応えるべく、これまでにポリエチレン(PE)製などの不織布を基材とする金属捕集材の研究開発に取り組み、環境排水中に含まれる重金属元素の除去を可能とする金属捕集材の作製に成功してきた。[1-3] しかし、石油製品であるPE製不織布は、石油資源への依存や廃プラスチックの処理などの問題があり、環境に対する負荷も大きい。一方、植物資源を原料とする生分解性高分子を基材として用いることができれば、上記の問題を克服でき、かつ環境負荷を低減することができると考えられる。そこで本研究では、バイオプラスチックであるセルロースを基材として、放射線グラフト重合法により吸着材の合成を試みるとともに、水銀に対する吸着性能を評価した。

セルロース不織布（目付: 30 g/m^2、繊維径: 20 μm）を基材に用い、グリシジルメタクリレート（GMA）を界面活性剤Tween20の存在下エマルション状態で放射線グラフト重合し、次いでエチレンジアミン（EDA）、ジエチレントリアミン（DETA）と反応させて水銀除去用吸着材を作製した。グラフト率（Dg）は反応前後の重量増加により算出した。得られた吸着材20 mgをpH調整した100 ppbの水銀溶液50 mlに入れ吸着試験を行い、分配係数を以下の式によって求めた。

分配係数= (吸着材中の金属濃度) / (溶液中の残存金属濃度)

本研究では100%から150%のグラフト重合体にアミン基を導入するために、線量10 kGy、反応温度40℃、1時間グラフト反応を行い、Tween20の濃度を0.05wt%に固定してグラフト率に対するモノマー濃度の依存性を検討した結果をFig. 1に示す。

その結果グラフト率にはGMA濃度依存性があり、各GMA濃度でのグラフト率を見ると、1%まではGMAがグラフトされにくいが、2%以後は急激にグラフト率が増加することが確認できた。本実験では、GMA濃度2%でグラフト反応させたものを用いた。次に、得られたグラフト率120%のGMAグラフト体をEDA及びDETAを用いて60℃で転化反応させたところ、1時間までは反応時間の増加に伴い官能基密度が増加するが、2時間以降はほとんど官能基量の増加は認められなかった。得られたアミン型の各吸着材（EDA: 2.9 mol/kg、DETA: 2.8 mol/kg）をpH3から12の範囲で、100 ppbに調製した水銀溶液中で所定時間浸漬撹拌させ、水銀に対する吸着性能評価を行った。pH5においては2時間で97%の水銀を吸着できた。浸漬2時間吸着材に吸着された水銀量を分配係数により評価した結果をFig. 2に示す。pH3付近の弱酸性領域において性能が最も高く、EDA型1.9×10^5、DETA型2.3×10^4になり、pH12の塩基性領域ではEDA型1.5×10^3、DETA型で2.6×10^2倍となった結果より、合成した水銀吸着材はpH2からpH9の領域での使用に適していることが分かった。

References

1) N. Seko et al., *Reactive & Functional Polymers*, 59 (2004) 235–2412.
2) M. Tamada et al., *Radiation Physics and Chemistry*, 71 (2004) 221–225.
3) N. Seko et al., *Nucl. Instr. and Meth. in Phys. Res. B*, 236 (2005) 21–29.

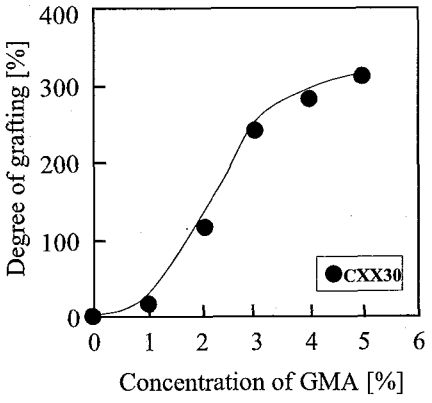


Fig.1 Effect of GMA concentration on degree of grafting by using cellulose nonwoven materials at 10 kGy, for 1h,at 40℃

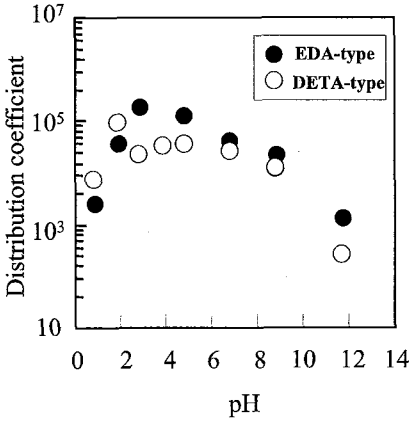


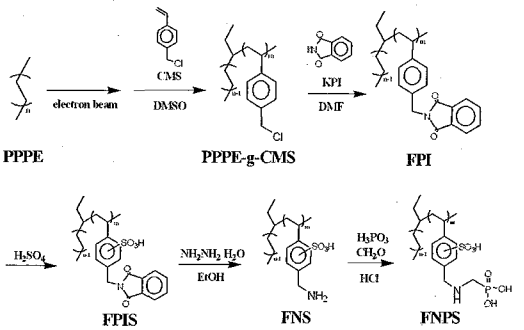
Fig.2 Distribution coefficient for amine-type adsorbents as a function of pH. Adsorption time of Hg was 2 h

2-05 Development of Bifunctional Chelating Fibers with High Performance in Metal Ion Adsorption Kinetics

A. Jyo[a], Y. Shibata [a], M. Tamada[b], N. Seko [b] and A. Katakai [b]

[a]Department of Applied Chemistry and Biochemistry, Kumamoto University,
[b]Environmental and Industrial Materials Research Division, QuBS, JAEA

Aminomethylphosphonate chelating resins, such as Duolite C467, Lewatit OC1060, and Purolite S940, have been used in the removal and recovery of various metal ions in wide fields of industries. However, the remaining drawback of these resins is slow kinetics in uptake of metal ions. In order to resolve the slow kinetic problem, we have developed an aminomethylphosphonate fiber of bifunctional type (named FNPS) according to the synthetic route shown in Scheme 1. FNPS has sulfonate groups in addition to aminomethylphosphonate groups.



Scheme 1 Synthetic route of the bifunctional fiber FNPS

The route in Scheme 1, which was established by trial and error changing the order of functionalization reactions, gave the satisfactory results for introduction of functional groups, compared with other tested routes. In the proposed route, chloromethylstyrene(CMS) was grafted onto trunk polyethylene coated polypropylene fiber(PPPE) by electron irradiation induced liquid phase graft-polymerization method as reported[1]. The grafted copolymer PPPE-g-CMS was reacted with potassium phthalimide, and the resulting FPI was treated with sulfuric acid for the introduction of sulfonate groups. The sulfonated intermediate FPIS was treated with hydrazine for hydrolysis of phthalimide moiety. The resulted FNS was converted into FNPS by Mannich condensation reaction.

Table 1 summarizes results of chemical analysis of FNPS. Relative standard deviations (RSD) of nitrogen, phosphorus contents are less than that of sulfur, indicating that control of the sulfonation is rather difficult compared with the introduction reactions of nitrogen and phosphorus.

Table 1 Summary of chemical analyses of FNPS

Contents of elements (mmol/g)			Acid capacity (meq/g)
Nitrogen	Phosphorus	Sulfur	
1.53(5.2)[a]	2.80(3.2)[a]	1.01(13)[a]	5.97(4.5)[a]

a) Values in parentheses are RSD in % (n=5). CMS content in PPPE-g-CMS was ca. 50 wt%.

Since phosphonic and sulfonic acids are diprotic and monoprotic acids, respectively, the acid capacity should be equal to $2m_p + m_s$; here, m_p and m_s are phosphorus and nitrogen contents, respectively. Calculated value of $2m_p+m_s$ is 6.61meq/g, which is higher than observed one 5.97 meq/g. by ca. 10%. However we do not have clear explanation on this discrepancy. The introduction of functional groups in each step was identified by FT-IR spectroscopy.

Column-mode uptake of Zn(II) was tested. Figure 1 shows the breakthrough profiles of Zn(II) at different flow rates of the feed. The feed was 0.01 M zinc sulfate of pH 2.0. Even at low pH of 2.0, FNPS was able to take up Zn(II) successfully. Although flow rates were changed from 50 to 1000 h^{-1} in space velocity, the shape of breakthrough curves was independent of the flow rates of the feed up to 1000 h^{-1}. Breakthrough capacities for Zn(II) up to C/C_o=0.05 were 0.72 - 0.85 mmol/g-fiber. Adsorbed Zn(II) on FNPS was quantitatively eluted with 1 M HCl and the repeated use of the column was possible.

References

1) A. Jyo, et al., Ind. Eng. Chem. Res., 43 (2004) 1599.

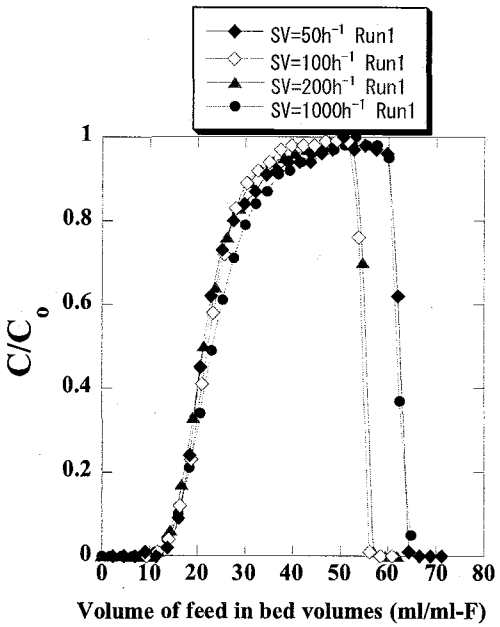


Fig. 1 Breakthrough profiles of Zn(II) in column-mode uptake of Zn(II) with FNPS at the different flow rates of the feed. Feed : 0.01 M $Zn(NO_3)_2$ pH 2. Column : FNPS (0.4 g in dry, 2.1ml in wet).

2-06 Development and Application of Fiberous Bifunctional Phosphonate-Sulfonate Cation Exchanger

K. Okada[a)], N. Seko [a)], M. Tamada [a)] and A. Jyo [b)]

[a)]Environment and Industrial Materials Research Division, QuBS, JAEA,

[b)]Department of Applied Chemistry and Biochemistry, Kumamoto University

Abstract

Bifunctional cation exchange fiber having both phosphonic and sulfonic groups was derived from the precursory fiber, which was prepared by co-graft polymerization of chloromethylstyrene and styrene onto polyethylene coated polypropylene fiber using the electron irradiation induced graft polymerization techniques. In column mode, up-take study of heavy metal ions such as Fe(III) and Pb(II) from strongly acidic feed, the bifunctional fiber exhibited excellent kinetic performances because of its high swelling ability in the wide pH range. In addition to strong adsorption ability, it demonstrated large capacity towards metal ions.

金属除去材料として、粒状の金属吸着樹脂が開発され、有害金属の除去、有用金属の回収プロセスに応用されている。粒子径0.5mm程度の金属捕集樹脂を用いるカラム分離プロセスでは、樹脂中への金属イオンの拡散が律速段階となるため、一時間あたりに充填樹脂の体積の10倍程度の体積の溶液から金属を吸着除去するのが限度となっている。これに対して放射線グラフト重合法によって合成した繊維状の金属捕集材では、繊維径が10-20μmであるため、従来の金属吸着樹脂に比較して、10～100倍ほどの処理速度が実現可能となった[1)]。しかし、弱酸性型吸着材であるホスホン酸型吸着材を例にとると、pH2以下の酸性領域ではホスホン酸基が弱酸であるため酸解離せず、吸着材の収縮が起こるため吸着容量・速度の双方が低下してしまうことが知られている。本研究では、ホスホン酸型吸着材に強酸性基であるスルホン酸基を導入し、二種の官能基の相乗作用により発現する金属吸着特性を評価した[2)]。

二官能性捕集材の合成は電子線前照射法によりポリエチレン被覆ポリプロピレン繊維にクロロメチルスチレンとスチレンを共グラフト重合した後、Arbusov反応を利用してホスホン酸基を導入し、クロロスルホン酸によりスルホン酸基を導入することにより合成した。また、比較の目的で、ホスホン酸基のみを有する一官能性ホスホン酸型捕集材も同様に合成した。得られた繊維状捕集材はカラム法とバッチ法により金属吸着特性の評価を行った。

本研究に用いた二官能性捕集材の化学構造をFig.1に示した。捕集材を用いたFe(Ⅲ)の吸着においては、Fe(Ⅲ)は配位子置換反応速度が遅いほか、複核水酸化物イオンを形成しやすいため、pH2程度の酸性領域からの吸着が必須であるため、膨潤性の低いイオン交換体では吸着の容量ならびに速度が低下することが知られている。二官能性、一官能性捕集材のそれぞれを充填したカラムを用いてFe(III)の吸着挙動を検討した結果をFig.2に示す。pH=1.8において、一官能性繊維では通液直後からFe(III) が漏出したが、二官能性捕集材では34ベッドボリュームまで漏出容量が増加した。これはスルホン酸基が全pH領域で解離するため、繊維がスルホン酸イオン間の反発により膨潤しFe(III)の繊維内拡散が容易になるとともにホスホン酸基との錯形成においても立体障害が減少するためと推察している。Pb(Ⅱ)などの金属吸着特性でも同様に、一官能性、二官能性捕集材では流速に依存せず良好な吸着挙動を示すが、二官能性繊維においてはホスホン酸基容量が小さいにもかかわらず大きな漏出容量を示した。また、選択性においては硫酸でpH=1に調製したNi(II)- Fe(III)溶液からの吸着挙動を評価したところ、Ni(II)の増加に伴いFe(III)の漏出容量は減少する傾向を示したが、Ni(II)の100倍モル共存下でもFe(III)を高速かつ選択的に吸着した。このことから、二官能性捕集材においては両官能基が金属イオン選択性に関与し酸性領域においても吸着が可能であることが明らかとなった。

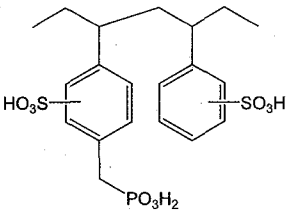


Fig.1 Structure of bifunctional fiberous adsorbent.

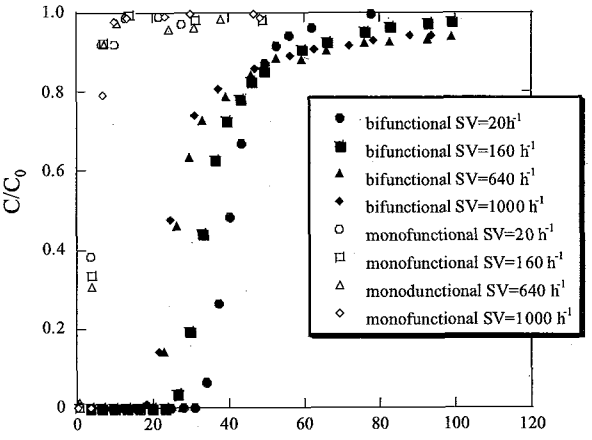


Fig.2 Effect of flow rate on breakthrough curves of Fe(Ⅲ)

Column; 1.5mL of fiber (0.4g),
Feeding solution:0.01M $Fe(NO_3)_3$ (pH=1.8)
SV means flow rate of solutions in space velocity(h^{-1})
C: Concentration of Fe(Ⅲ) in effluent
C_0: Concentration of Fe(Ⅲ) in feed

References

1) Shoji Aoki, Kenichi Saito, Akinori Jyo, Akio Katakai, and Takanobu Sugo, *analytical science,* **17** i205(2001).
2) Akinori Jyo, Kenji Okada,, 226th American Chemical Society National Meeting, Abstracts of Papers of CD rom version, Lecture No. I&EC62 (2003).

2-07 Cost Estimation of Uranium Collection from Seawater with Braid Type Adsorbent

M. Tamada[a], N. Seko [a], N. Kasai [a] and T. Shimizu [b]

[a] Environment and Industrial Materials Research Division, QuBS, JAEA,
[b]Environmental Science Research Laboratory, Central Research Institute of Electric Power Industry

Total amount of uranium in the seawater all over the world becomes 4.5 billion tons in spite of its extremely low concentration of 3.3 ppb. This amount covers 60,000 times of annual consumption of the uranium in the nuclear power plant in the world. To collect the uranium in the seawater, we synthesized a fibrous amidoxime adsorbent, which could adsorb uranium selectively in seawater, by radiation-induced graft polymerization. The stacks of 350 kg adsorbents were hang down from a floating frame moored at the offing of Aomori Prefecture in Japan. One kg of uranium was successfully recovered in 12 times immersion for three years[1]. It was found that the reduction of the uranium collection cost was necessary to realize the rational uranium cost. As a novel adsorbent, a braid type adsorbent was developed[2]. This adsorbent can be directly moored on the ocean floor and promising adsorbent for effective cost reduction. In the present report, the cost of the uranium collection from the seawater by this system was estimated.

The scale for the annual uranium collection was set to 1200 ton/year which corresponded to the fuel amount for six nuclear power plants of 1 million kW class. The performance of uranium adsorbent was 2 g-U/kg-adsorbent for 60 days soaking in the seawater. During the mooring, the adsorbent occupied the sea area of 1,031 km^2. The adsorbent was finally incinerated after six times' immersing. The soaking of 60 days was repeated six times. Totally, 360 days were spent for uranium collection in a year. After raising the adsorbent, the adsorbed uranium on the adsorbent was fractionally eluted by dilute acid. The cost of uranium collection was estimated by summation of those for the production process of the braid type adsorbents, the recovery process of the uranium in seawater, and the elution and the purification process of the uranium. Moreover, the effect of the adsorbent ability and the repetition usage on the cost reduction was investigated.

Figure 1 shows the effect of repetition usage on the uranium costs for adsorbent abilities of 2, 4, and 6 g-U/kg-adsorbent. The cost decreases proportionally by improving the adsorbent performance. However, the influence of the adsorbent durability becomes small as the increases of repletion number.

The uranium cost of 87,774 yen was reduced to 30,979 yen when the adsorbent ability of 2g-U/kg-adsorbent rose 6g-U/kg-adsorbent on the condition of six times' usage. This is because the cost of the adsorbent production and the recovery which occupy the uranium collection cost decreases similarly to the adsorbent performance.

The uranium cost became 57,633, 47,761, 40,093, and 34,073 yen for repetition usage of 12, 18, 30, and 60 times, respectively, at 2 g-U/kg-adsorbent. The cost for 18 repetition usage was reduced half of that for six times. In this case, the expenditure of the adsorbent production decreased remarkably although the costs for the recovery process and the elution and the purification were maintained.

In Okinawa sea area, 3g-U/kg-adsorbet was performed for 30 days' soaking. If this performance is converted to 60days, 4g-U/kg-adsorbent is expected. The cost for this adsorption ability becomes 25,000 yen in the 18 times' repetition usage.

References

1) N. Seko et al., Nuclear Technology 144 (2003) 274.
2) T. Shimizu et al., Journal of Civil Engineering in the Ocean 20 (2004) 617.

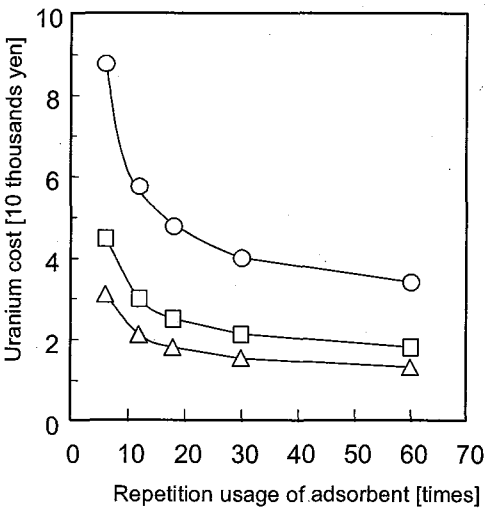


Fig.1 Effect of adsorbent durability on uranium cost; (○) 2 g-U/kg-adsorbent, (□) 4 g-U/kg-adsorbent, (△) 6 g-U/kg-adsorbent.

2-08 The Recovery Method of Scandium from Hot Spring Water

N. Kasai[a], N.Seko[a], M.Tamada[a] and E.Ichikawa[b]

[a] Environment and Industrial Materials Research Division, QuBS, JAEA
[b] Kusatsu-machi, Gunma-Prefecture

Abstract

Rare metals such as a scandium and vanadium are solved in the hot spring water. A fibrous phosphoric adsorbent was synthesized for recovery of scandium by using graft polymerization. The phosphoric adsorbent has high performance for scandium even in highly acidic condition. When the phosphoric adsorbent was dipped into the 100ppb scandium solution, 98% of scandium ions could be adsorbed within 2 hours. When the phosphoric adsorbent immersed in the 18ppb scandium of Yukawa-River and 40ppb of Yurikago-Bridge, the total amount of adsorbed scandium reached to 1.5g per 1kg-adsorbent.

1．はじめに

草津温泉は日本一の湧出量（約37,000リットル/分）を誇る酸性度の高い（pH2）温泉である。この温泉水中には稀少な金属が低濃度に溶存している。その中でもスカンジウムは，アルミニウム合金の耐熱性の向上や燃料電池の電解質に有用な元素として注目されている高価な金属である。現在スカンジウムは，100%海外に依存しており資源の確保が求められている。今回，低濃度で温泉中に溶存するスカンジウムの回収が可能な吸着材を用いた回収方法について発表する。

2．実験

スカンジウム回収用の吸着材は，放射線グラフト重合によりリン酸基を導入して作製した[1]。ポリエチレン製の不織布に電子線を照射したのち，グラフト率（Dg:反応前後の重量増加により算出）が60～70%，リン酸含有量4mol/kgの吸着材を作製した。

得られた吸着材20 mgを100ppbに調製した40 mlのスカンジウム溶液中でpHを変化させ酸性領域での吸着率と吸着時間依存性の予備試験を行った。

草津温泉での実験では温泉排水の集まる湯川（水温約30℃）とゆりかご橋付近（水温約95℃）の源泉に吸着材をプラスチックの網に入れて浸漬し，吸着試験を行った。

3．結果および考察

pH0.5から3の酸性域で100ppbに調製したスカンジウム溶液中で2時間浸漬撹拌した結果，pH1から3の範囲で高い吸着特性を示し，pH2では98％の回収率であった（Fig.1）。さらに，pH2に調製した40 ppbのスカンジウム溶液を36℃および92℃に保った恒温水槽中で2時間浸漬撹拌させた際の吸着時間依存性では，92℃において，わずか10分の接触で97％のスカンジウムを吸着した。このように，リン酸基を用いた吸着材が酸性領域で短時間にスカンジウムを吸着することが予備試験で明らかになった。

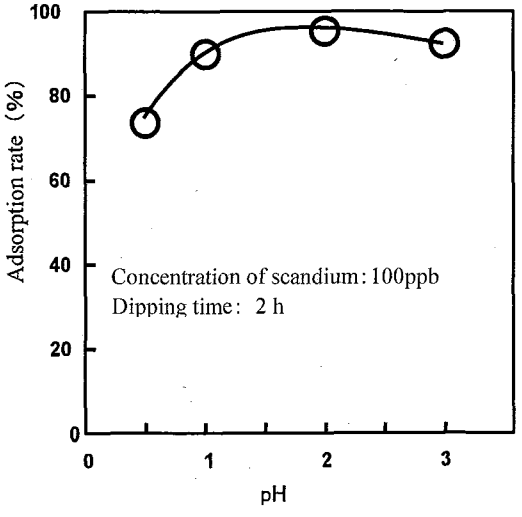


Fig.1 Relationship between pH and adsorption rate.

温泉水中に吸着材を浸漬し，浸漬時間と吸着材に吸着されたスカンジウムの量（吸着材1kgにスカンジウムが吸着された量に換算）を調べた結果をFig.2に示す。なお，温泉排水の湯川は18ppbのスカンジウム濃度でpH1.8，これに対して源泉のゆりかご橋は，40ppbのスカンジウム濃度でpH1.4である。湯川では吸着材1kgに対してスカンジウムの吸着量は0.2g（初期濃度の11,100倍）で飽和に達した。これに対し，ゆりかご橋は23時間で1.5ｇ（37,500倍）と高い吸着特性を示した。

高品位の鉱石中のスカンジウムの濃度は0.1g/kg程度であり，温泉水に浸漬することにより，湯川で２倍，ゆりかご橋で15倍の濃度のものが得られることが分かった。

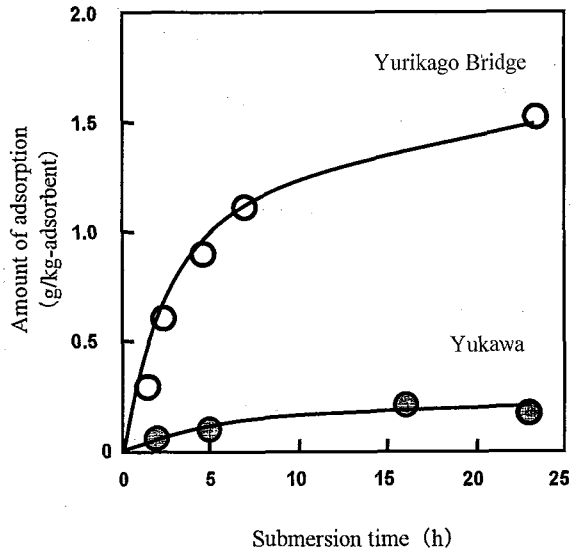


Fig.2 Relationship between submersion time and amount of adsorption.

References

1) Direct synthesis of Adsorbent having phosphoric acid with radiation induced graft polymerization, F. Basuki, N. Seko, M. Tamada, T. Sugo, T. Kume, J. Ion Exchange 14s (2003) 209-212.

2-09 Development of Equipment to Remove Cadmium from Waste of Scallop Processing by Graft Adsorbent

H. Nakai[a)], T. Temma[a)], M. Tamada[b)],
T. Sawamura[c)],T. Saito[c)], T. Honma[c)] and K. Sato[d)]

[a)]Hachinohe Technical Laboratory, Aomori Industrial Research Center,
[b)]Environment and Industrial Materials Research Division,QBS.JAEA,
[c)]Hachinohe National College of Technology, [d)]Kawasaki Plant Systems, Ltd.

Abstract

Removal technology for cadmium ion (Cd^{2+}) from the mid-gut gland in the scallop processing was developed by combining the Cd^{2+} leaching process with the malic acid solution and the Cd^{2+} adsorption with the iminodiacetic acid adsorbent synthesized with radiation-induced graft polymerization. Experimental equipment was assembled for removal of the Cd^{2+} from 20～40 kg of mid-gut gland. The Cd^{2+} in mid-gut gland was reduced from 25 mg/kg to 1.0 mg/kg after 24h treatment.

ホタテ貝の加工にともない廃棄される中腸腺はタンパク質や脂肪の他に，DHA や EPA などの有価物を含んでおり，その利用価値は非常に高い。しかし，中腸腺は有害金属であるカドミウムイオン（以下 Cd^{2+}と略記する。）を蓄積しているため，ほとんどが産業廃棄物として焼却処分されている。本研究では廃棄されている中腸腺をサプリメントや肥料・飼料等の資源として有効利用することを目的とし，Cd^{2+}を除去するための中腸腺処理装置を開発する [1)]。リンゴ酸による溶出処理と放射線グラフト重合法により作製した捕集材を応用して，中腸腺 30kg 程度の処理が可能な中腸腺処理装置を試作したので紹介する。

Fig.1 に試作した中腸腺処理装置の外観を示した。Cd^{2+}の除去効率を高めるため、リンゴ酸溶液により中腸腺からCd^{2+}を溶出させるとともに、溶出液を Cd^{2+}捕集カラムを通して循環させ、イミノ二酢酸型グラフト重合捕集材で Cd^{2+}を捕集するような循環除去法を採用した。主な基本仕様は次の通りである。処理量：20～40kg、溶出槽の容量：200L、カラム容積：5L（φ100mm×640mm）、温度制御範囲：室温～60℃、循環ポンプの最大流量：50L/min、最大許容圧力：0.5MPa

0.1M リンゴ酸溶液 150L が入った溶出槽の中に、粉砕していないボイル中腸腺 15kg（湿潤重量）を入れた網目状の籠を 2 段に重ねて投入した。溶液を撹拌するため、籠の下方からバブリングを行なった。カラムには直径 100mm，厚さ約 0.8mm のイミノ二酢酸型グラフト重合捕集材 800 枚を充填した。リンゴ酸溶液を 30℃に保ち、ポンプにより通液速度 3L/min（空間速度 SV＝36h^{-1}）でカラム（捕集材）に通液し循環させた。

中腸腺中の Cd^{2+}濃度を時間毎に測定した結果を Fig.2 に示した。中腸腺中の Cd^{2+}は最初 25mg/kg であるが，24 時間後には 1.0mg/kg 以下まで減少した。ビーカスケール実験と比べ、ほぼ同じ結果が得られた。試作した中腸腺処理装置において、スケールアップにより処理後の Cd^{2+}残濃度にバラツキが大きくなると懸念されたが、バラツキは 1.7mg/kg であり大きな問題ではなかった。バラツキを少なく出来たのはバブリングにより溶液が撹拌されたからと思われる。

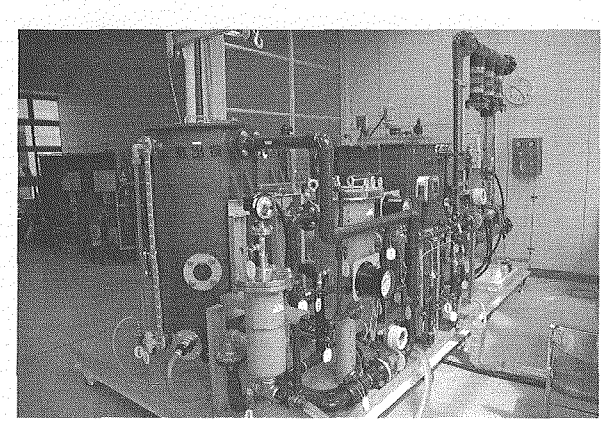


Fig.1 Appearance of equipment

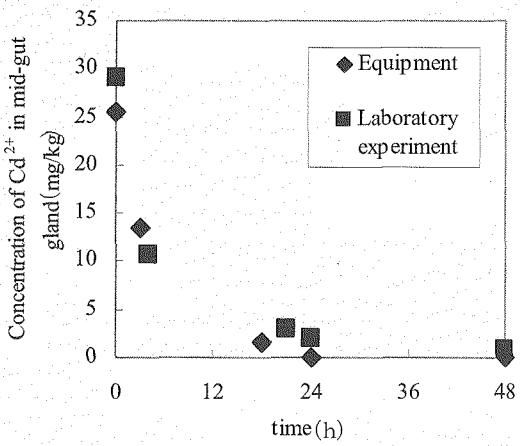


Fig.2 Concentration of Cd^{2+} in mid-gut gland

今後、Cd^{2+}除去のばらつき等のデータ収集や処理コストの試算を行う予定である。また、Cd^{2+}除去後のホタテ貝加工残渣を肥料や飼料、食品添加物、サプリメント等の資源への利用の検討を、青森県の農林系及び食品系の試験研究機関および民間企業との産学官連携により平成 18 年 4 月から 2 年間の予定で実施する。

【References】 1) H. Nakai, N. Seko, M. Tamada, T. Temma and M. Oguma, *J. Ion Exchange*,**15**,10-15 (2004).

【謝辞】本研究は独立行政法人新エネルギー・産業技術総合開発機構（NEDO）の平成 17 年度産業技術研究助成事業により実施したことを記し，感謝の意を表します。

2-10 Development of Grafting Adsorbent for Ultra Pure Water Production

T. Takeda[a] and M. Tamada[b]

[a]Kurashiki Textile Manufacturing Co., Ltd.
[b]Environment and Industrial Materials Research Division, QuBS, JAEA

Abstract

Fabric metal adsorbent synthesized by radiation-induced graft polymerization was investigated for ultra pure production. Effect of liner velocity on breakthrough capacities and effect of column length on breakthrough capacities were examined by column mode adsorption. In the metal concentration of 10ppb, the breakthrough capacities increased in proportion to linear velocity up to 400m/h .In addition breakthrough capacities increased in proportion to column length. The grafting adsorbent concentration was considered to be promising for ultra pure water production.

はじめに

放射線グラフト重合法によって得られる不織布状グラフト吸着材は、繊維径（１８μｍ）が小さいため繊維内への拡散が速く、高速で金属を吸着できる。ポリエチレン(PE)製の不織布を用いることにより、TOC（全炭素量）の溶出を低減化可能である。半導体や液晶の製造工程で使用される超純水は、ナトリウム、マグネシウム、ニッケル、亜鉛等の金属濃度を0.1ppt以下にすることが求められている。PE不織布から作製したスルホン酸型不織布状グラフト吸着材について、除去が難しいナトリウムを用いて、極低濃度における吸着除去特性を検討した。

実験方法

高密度ポリエチレン短繊維よりなる不織布（倉敷繊維加工㈱製）に、200kGｙの電子線を照射してグリシジルメタアクリレートをグラフトした後、スルホン酸基を導入しスルホン酸型グラフト不織布を得た。この吸着材の酸容量は3.12meq/ｇであった。合成した吸着材11.3mgを内径7ｍｍのカラムに高さが20ｍｍとなるように充填し、１N硝酸、純水、１N水酸化ナトリウムを用いてコンディショニングを行った後、10ppbのナトリウム溶液を調整し、線速度20、135、400、600、840m/ｈで通水し、破過点（カラムの出口濃度が入り口濃度の５％となった時点）及び線速度と破過点の関係をみた。また、吸着材を37枚（高さ75ｍｍ、424ｍｇ）と48枚（高さ95ｍｍ、542ｍｇ）をカラムに充填し、ナトリウム10ppb溶液を線速度400m/ｈで通水し、流路長の破過点への影響を調べ、不織布状グラフト吸着材の吸着特性を評価した。

結果及び考察

Fig.１に線速度と破過点の関係を示す。線速度の上昇につれて、400m/hまでは、破過容量が増加し、それ以降は減少した。これは、カラム内での乱流化の度合いが増すことにより接触確率が上がるために、破過容量が高くなると考えられる。最大の破過容量を与える400m/hの線速度は、現行の超純水処理材料の約３倍の処理速度である。

Fig.２に線速度が400m/ｈにおける流路長と破過点の関係を示す。流路長に比例して破過点が増加する現象が確認され、流路を長く設計することにより、金属吸着材料のライフが十分得られることが明らかとなった。

以上のことから、線速度を上げた乱流状態で、流路を長く設計した構造体に、処理水を通水することにより、極微量の金属を効率良く吸着除去することが明らかとなり、不織布状イオン交換体は超純水製造用の材料として適する見通しが得られた。

References

1) Y Koizumi, *et al.*,超超純水への挑戦：MEMBRANE、28、95 （2003）.

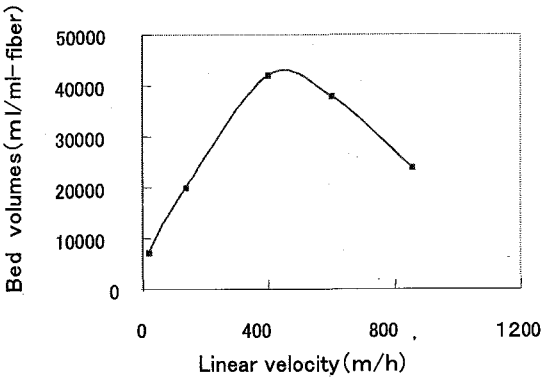


Fig.1 Effect of linear velocity on breakthrough point

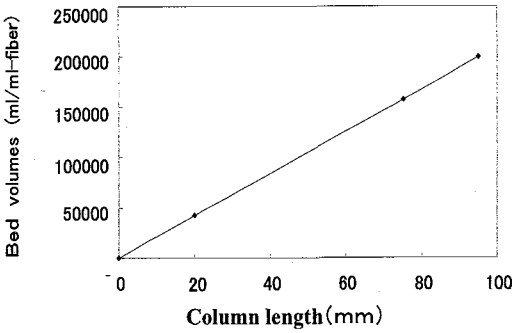


Fig.2 Effect of column length on breakthrough point

2-11 Preparation of Amidoxime-Type Chelating Fabric and Its Removal Performance of Toxic Heavy Metals

A.Katakai[a)], M.Tamada[a)], H.Nagamoto[b)], S.Ono[b)] and H.Miyagawa[b)]

[a)]Environment and Industrial Materials Research Division, QuBS, JAEA, [b)]Mitsui Mining & Smelting Co.LTD

Abstract

Heavy-metal-ion removal performance of the amidoxime-type fabric was evaluated by using a model polluted water containing zinc, cadmium, or lead ion. When acrylonitrile solution used as a monomer solution for radiation-induced graft polymerization was re-used five times, the degree of grafting was retained at 90% of an initial degree of grafting. The chelating fiber exhibited 3.6-fold adsorption capacity compared to a commercially available chelating resin. Removal of lead ion from the solution obtained by the washing of polluted soils in a batch mode demonstrated that lead concentration in the solution decreased below the environmental standard level for thirty minutes.

1. はじめに

工場排水や鉱山廃水などの重金属汚染水から有害重金属を除去する新しい浄化法として、放射線グラフト重合により合成したキレート繊維を用いた除去法が注目されている。この方法による重金属汚染水の処理は、従来の消石灰による中和凝集沈殿法[1)]で発生する有害重金属を含む水酸化物スラッジの処理を必要とせず、また、低濃度の重金属を処理するときに使用する市販のイオン交換樹脂やキレート樹脂が抱える処理速度の遅れの問題もなく、その上、取り扱いが簡便であるなどの優れた特徴を有している。本研究では、アミドキシム基を有するキレート繊維の放射線グラフト重合法による経済的な合成法と得られたキレート繊維の重金属汚染水からの亜鉛（Zn）、カドミウム（Cd）、鉛（Pb）などの除去性能について検討した。

2. 実験方法

既報にしたがって[2)]、電子線を200kGy照射したポリエチレン被覆ポリプロピレン製不織布にアクリロニトリル／メタクリル酸を共グラフトした。モノマー溶液の繰り返し使用を5回行い、キレート繊維の経済的な合成法を調べた。得られたグラフト繊維にヒドロキシルアミンを反応させてアミドキシム型キレート繊維（5.6mmol/g-ad）を作製し、重金属を含む模擬汚染水（Zn 100mg/L, Cd 20mg/L、pH 7）を用いて、バッチおよびカラム法により重金属除去性能を調べた。

3. 結果及び考察

モノマー溶液の繰り返し使用回数とグラフト率との関係について検討した。グラフト率は使用回数の増加に伴って低下する傾向を示すが、５回使用時で初回のグラフト率の90%を維持しており、このことからモノマー溶液の繰り返し使用によるキレート繊維の製造コスト低減化に見通しが得られた。

一方、キレート繊維を模擬汚染水50mlに入れ、12時間撹拌して重金属を吸着させた後、吸着前後の液中のZnおよびCd濃度を測定して平衡吸着量を求めた。キレート繊維の吸着量は80mg/g-adであり、比較として用いた市販キレート樹脂の吸着量22mg/g-adに対して3.6倍と優れた吸着性能を示した。次いで、キレート繊維を2mLのカラムに詰め、模擬汚染水を50h^{-1}の空間速度（SV）で通液して漏出曲線を得た。市販キレート樹脂についても、10h^{-1}のSVで通液して漏出曲線を得た。両漏出曲線をFig. 1, 2に示す。市販キレート樹脂はSVが10h^{-1}で漏出曲線が乱れるのに対してキレート繊維はその5倍の流速でも良好な漏出曲線を示し、イオン交換速度も吸着容量同様に優れていることが分かった。

さらに、汚染土壌の浄化処理液からのPbの除去試験を行った。Pbに汚染された土壌を洗浄処理した廃液（0.18mg/L）にキレート繊維を入れ、撹拌吸着による残存Pb量の時間変化を調べた。廃液中のPbの残存量は、撹拌開始30分で環境基準（>0.01mg/L）以下までに低下することが明らかになり、本キレート繊維が低濃度で高度な処理が必要な重金属汚染水の浄化材料として適していることが明らかになった。

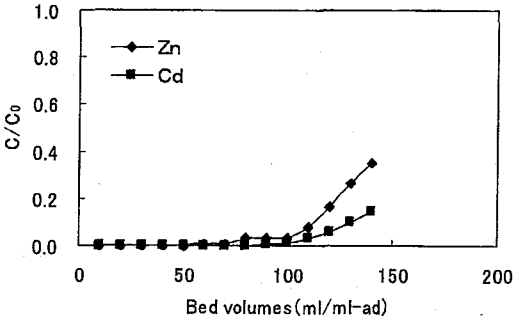


Fig. 1 Breakthrough curves of commercial chelate resin (SV 10h^{-1})
C/C$_0$:Effluent concentration/feed concentration

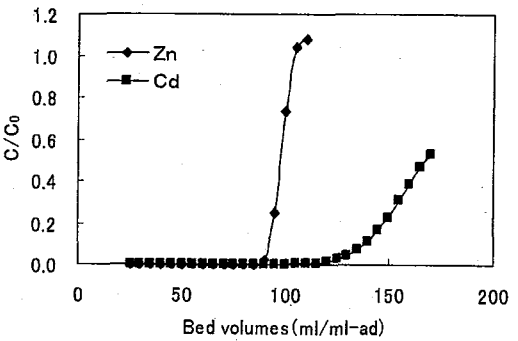


Fig. 2 Breakthrough curves of chelate fabric (SV 50h^{-1})
C/C$_0$:Effluent concentration/feed concentration

References

1) 吉野善彌監修：「水処理材と水処理技術」 シーエムシー出版 p. 2, p. 176 (2001)
2) 片貝秋雄, 玉田正男, 永本浩之, 宮川 博：日本イオン交換学会誌, 16, 122 (2005)

2-12 Removal of Ferric and Manganese Ions with Fibrous Iminodiacetic Acid Adsorbent synthesized by Graft Polymerization

Kazuya Tanaka[a)], Nobuhiro Anzai[a)], Noriaki Seko[b)], Masao Tamada[b)]
[a)] Anzai Co. Ltd., [b)] Environment and Industrial Materials Research Division, QuBS, JAEA

Abstract

Fibrous adsorbent having iminodiacetic acid was synthesized by radiation induced graft polymerization. The obtained adsorbent of 20 g was packed into column, 4cm in diameter and 50cm long and assembled in experimental equipment. The adsorption of Fe^{2+} and Mn^{2+} in the ground water was evaluated in the flow rate of 300, 1200 and 2500 h^{-1} space velocity. The adsorption capacities of Fe^{2+} and Mn^{2+} were independent of the flow rate. As a result, the removal rate of the graft fibrous adsorbent was 250 times faster than that of commercial ion exchange resin.

我が国の水道法による水質基準値は鉄0.3ppm、マンガン0.05ppmとなっている。特に、酒造用の割り水や仕込み用水は着色防止のために鉄を0.02ppm 以下にしなければならない。また、電子業界では、４メガビットのＬＳＩ製造用水では、鉄を含む総金属を0.002ppm以下まで除去することが不可欠である。

従来、鉄・マンガン除去法として、浄水場などの使用流量の大きい場合は空気または次亜塩素酸ナトリウム等による酸化と沈殿砂ろ過の組合せの気曝酸化法や接触酸化法がある。この方法では、第一鉄（Fe^{2+}）を溶解度の低い第二鉄（Fe^{3+}）に酸化し沈殿させて除去する方法であり、逆洗・沈殿と排泥の処理が必要であるため、立地面積は大きくなる。除去後の用水中の鉄・マンガン濃度は数10ppb が限界である。比較的小規模には、イオン交換樹脂法が用いられる。イオン交換樹脂法は、還元状態のFe^{2+}を直接捕集するため、ライン中に簡便に挿入できるなどの利点がある反面、除去処理速度が遅いという問題点がある。[1)]

本研究では、放射線グラフト重合法によりイミノ二酢酸型の繊維状捕集材を合成し、鉄・マンガンの模擬液および実地下水を用いてこれらの捕集除去性能を評価した。

摸擬液を用いたビーカースケールの試験では、従来のイオン交換樹脂の場合、空間速度10h^{-1}(空間速度=1時間あたりの通液量/樹脂及び捕集材体積)程度が処理速度の最大であるが、グラフト重合法により作製した繊維状捕集材は空間速度300h^{-1}においても、除去処理が可能であった。

4cmφ×50cmのカラムに捕集材を100cm^3（20g）充填し、このカラムを2本並列させるFig.1のような実験デモ機を作製し、実地下水を用いた除鉄、除マンガンの性能評価を行った。その結果、Fig.2 ,Fig.3（C_0:カラム入口の金属濃度、 C:カラム出口の金属濃度）に示すように空間速度(SV)によらず、捕集量に差異のないことがわかった。このことから、従来のイオン交換樹脂法と比較して、最大250倍の空間速度で通液処理できることを実証できた。したがって、装置の小型化、省スペース化を図ることが可能になる。

また、捕集材中に捕集させた鉄およびマンガンは、低濃度の酸（3.6%の塩酸）によって回収することが可能で、捕集材は繰り返し利用が可能になる.

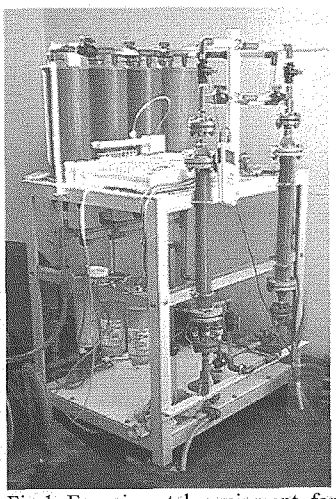


Fig.1 Experimental equipment for removal of Fe^{2+} and Mn^{2+}.

References

1) M. Takahashi *et al.*, "Development of removal method for ferric and manganese ions with fibrous graft-absorbent" Environmental Engineering Research 41 (2004) 229.

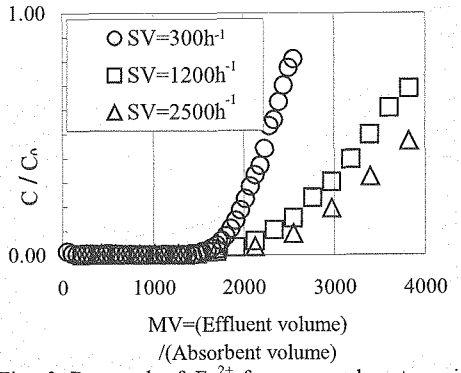


Fig. 2 Removal of Fe^{2+} from ground water with experimental equipment.

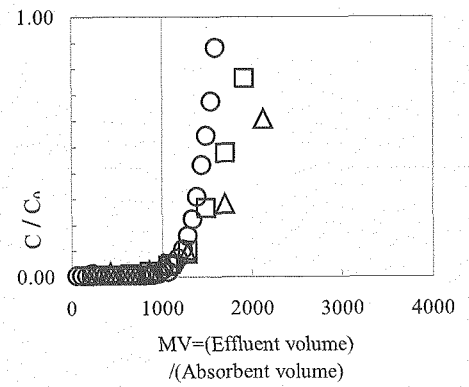


Fig. 3 Removal of Mn^{2+} from ground water with experimental equipment.

2-13 Off-On Biodegradability of Poly(3-hydroxybutyrate) Film Modified by Graft Polymerization

Y. Wada[a)], H. Mitomo[a)], N. Seko[b)] and M. Tamada[b)]

[a)] Graduate School of Engineering Gunma University
[b)] Environment and Industrial Materials Research Division, QuBS, JAEA

Abstract

Biodegradable polyester, poly(3-hydroxybutyrate) (PHB) is modified by grafting acrylic acid (AAc) and vinyl acetate (VAc) to control its biodegradability. Each PHB film grafted with AAc (PHB-g-AAc) and VAc (PHB-g-VAc) having a degree of grafting higher than 5% completely lost the enzymatic degradability. The enzymatic degradability of the PHB-g-AAc was recovered by thermal remolding. The highest enzymatic degradation rate was observed at degree of grafting of 12% after thermal remolding. The biodegradability of the PHB-g-VAc was also recovered after saponification. When the PHB-g-VAc film was saponified in the 0.05M NaOH solution at 8h, graft chains in PHB-g-VAc film became to biodegradable poly(vinyl alcohol). BOD-biodegradabilities of the saponified PHB-g-VAc increased rapidly with elapsed number of days. By saponification of the PHB-g-VAc, the resulting film can be degraded in the natural environment.

ポリ(3-ヒドロキシブチレート)(PHB)は生分解性を有する微生物産生脂肪族ポリエステルである。PHBの分解は、酵素PHBデポリメラーゼによって PHBの表面部分から優先的に分解されることが報告されている[1)]。本研究では、放射線グラフト重合技術を用いPHBフィルムにアクリル酸及び酢酸ビニルをグラフトし、得られたグラフトフィルムの酵素分解性について評価した。

PHBフィルムに電子線を10kGy照射後、所定の濃度のアクリル酸及び酢酸ビニル溶液と60℃で反応させることにより、グラフト試料を作製した[2)]。作製したアクリル酸グラフトPHBフィルム(PHB-g-AAc)はグラフト鎖をフィルム全体に混合することを目的とし、熱プレス機を用い190℃で再溶融熱処理を行った。また、酢酸ビニルグラフトPHB フィルム(PHB-g-VAc)は、グラフト鎖であるポリ酢酸ビニル(PVAc)を、生分解性を有するポリビニルアルコール(PVA)に転換することを目的とし、メタノール中にNaOH水溶液を0.05M加え25℃で8h鹸化処理を行った。PHB-g-AAcの再溶融熱処理前後及びPHB-g-VAcの鹸化前の酵素分解性について、*R. Pikettii*由来のPHBデポリメラーゼ(4μg)を含む0.1Mリン酸緩衝液(pH7.4)中、37℃で48時間酵素分解を行い評価した。鹸化前後のPHB-g-VAcについては、自然水(池の水)で分解実験を行い、BOD(Biochemical Oxygen Demand)生分解度を測定した。

PHB-g-AAc及びPHB-g-VAcの酵素分解性についてFig.1に示す。いずれの場合も、グラフト率の増加と共に生分解性は低下し、グラフト率が5%を超えると完全に酵素分解性が抑制された。これは、グラフト鎖がPHBフィルム表面を完全に覆ったことによる。また、PHB-g-AAcを再溶融熱処理することにより、PHBが表層に現れ、酵素分解性は向上することが確認された。

PHB-g-VAcの鹸化処理前後のBOD生分解度の測定結果をFig.2に示す。この結果、グラフト率5%及び15%の鹸化処理前フィルムは分解性を示さないのに対し、鹸化処理により分解性は再現することが確認された。これは、フィルム表面部分を覆っていた酢酸ビニルのグラフト鎖が鹸化されて、加水分解するPVAに変化したことにより分解可能になったと考えられる。

References

1) H. Abe, *et al.*, "Microscopic visualization on crystalline morphologies of thin films for poly(3-hydroxybutyric acid) and its copolymer", Polymer 41, 867 (2000).

2) Y. Wada, *et al.*, "Control of biodegradability of poly(3-hydroxybutyric acid) film with grafting acrylic acid and thermal remolding", J Appl. Polym. Sci. 101, 3856 (2006).

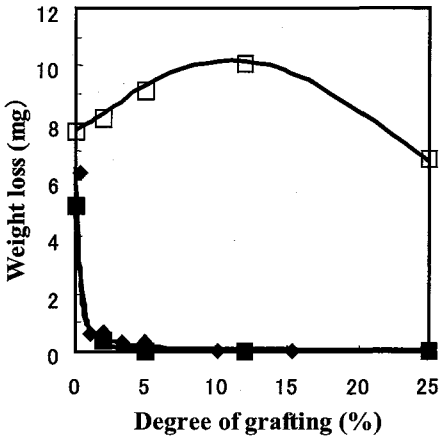


Fig.1 Enzymatic degradation of PHB-g-AAc and PHB-g-VAc. (■): PHB-g-AAc (□): PHB-g-AAc, after thermal remolding (◆): PHB-g-VAc

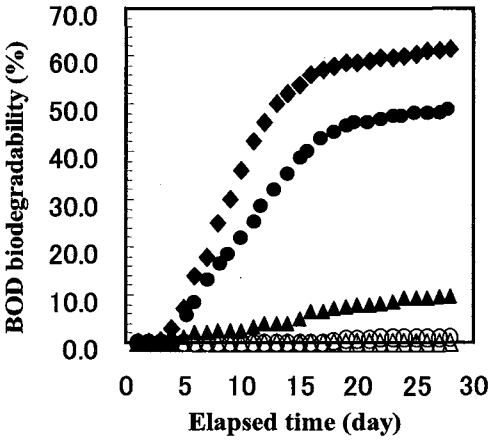


Fig.2 BOD biodegradability of PHB-g-VAc and saponified PHB-g-VAc. (◆): PHB, (○): Dg=3%, PHB-g-VAc (△): Dg=15%, PHB-g-VAc (●): Dg=3%, saponified PHB-g-VAc (▲): Dg=15%, saponified PHB-g-VAc

2-14 Metal Adsorption of Chitin / Chitosan Derivatives Hydrogels Crosslinked with Irradiation

N. Nagasawa[a)], Jarosław M. Wasikiewicz [b)], N. Seko[a)], T. Yagi[a)], L. Zhao[b)], H. Mitomo[b)], F. Yoshii[a,c)] and M. Tamada[a)]

[a)]Environment and Industrial Materials Research Division, QuBS, JAEA,
[b)]Faculty of Engineering, Gunma University, [c)]Industrial Collaboration Promotion Department, JAEA

Abstract

Radiation crosslinking of chitin / chitosan derivatives such as carboxymethylchitin (CMCt) and carboxymethylchitosan (CMCts) has been investigated. CMCt and CMCts of 40% concentration were irradiated by electron beams. The maximum gel fraction of those CMCht and CMChts reached 72%(75kGy) and 50%(100kGy) respectively. These gels absorpted water of 8.3g for CMCt and 21.2g for CMCts per 1 g of the dried gel. The absorption ability of various metal ions with these gels has been investigated. The highest adsorption of scandium and gold has been obtained for CMCt and CMCts gels, respectively.

1. はじめに

カニ・エビなどの甲殻類を原料とするキチン・キトサンは、特にアミノ基を有した天然資源で、水処理材、抗菌剤や人工皮膚材等の機能性材料として環境、農業や医療分野で応用されている。特に水処理材の金属吸着特性は、分子鎖中のアミノ基によるキレート作用に起因する。従来、キチン・キトサンのゲルは、主に化学薬剤よる橋かけ法で作製されている。最近、簡便で容易に橋かけできる手法として、水溶性のカルボキシメチル化キチン誘導体を高濃度ペーストで放射線照射してゲルを形成する放射線橋かけ法を見出し、抗菌活性を有することも明らかにしている[1,2)]。そこで、放射線で橋かけしたカルボキシメチル化キチン誘導体ゲルを作製し、金や白金等の有用金属イオン吸着特性を検討した。

2. 実験方法

試料は甲陽ケミカル(株)製のカルボキシメチルキチン（CMCt）［置換度0.83、脱アセチル化度24.6%］とカルボキシメチルキトサン（CMCts）［置換度0.91、脱アセチル化度84.0%］を使用した。試料を40%濃度の高濃度ペーストに調製後、フィルム状（1mm厚）に成形し、電子線を所定線量(10～200kGy)照射した。照射試料を蒸留水中に投入し、その不溶分からゲル分率を評価した。吸水率は48時間蒸留水中に浸漬させた重量変化より求めた。

ゲルの生分解性は、酵素や完全堆肥による分解試験や土壌埋設試験により評価した。作製ゲルの金属吸着特性は、100mLの金属イオン水溶液（100ppb, pH4.0）に乾燥ゲル50mgを2時間浸漬した後、その上澄み液の金属イオン濃度をICP-MSで測定後、初期水溶液と上澄み液との濃度差から評価した。

3. 結果及び考察

40%濃度のCMCht と CMChts の最大ゲル分率はそれぞれ72%(75kGy)と50%(100kGy)に達した。これらのゲルは、乾燥ゲル1g当たり8.3g（CMCt）、21.2g（CMCts）の吸水特性を有した。

酵素や完全堆肥による生分解試験や土壌埋設試験では、両キチン誘導体ゲルとも、ほぼ全部分解し、ゲル化しても生分解性を保持していた。

CMCt及びCMCts乾燥ゲルをpH4に調製した各種金属イオン水溶液について2時間浸漬後の最大金属吸着量をTable 1に示す。両ゲルは、金（Au）や銅（Cu）イオンを最も吸着する。また、CMCtゲルはスカンジウム（Sc）やカドミニウム（Cd）を、CMCtsゲルはバナジウム（V）を吸着することから、金属吸着選択性を有することがわかった。

Table 1 Metal adsorption of chitin and chitosan hydrogels

Kind of gel	CMCt		CMCts	
Kind of metal	Maximum amount of adsorption			
	%	μg/g	%	μg/g
Au	52.6	123.6	70.8	236.2
Cu	45.6	46.1	49.0	52.4
Cd	34.1	70.1	12.6	25.26
Pd	7.1	19.1	1.18	3.1
Pt	5.8	18.9	2.9	4.1
Sc	41.73	78.15	8.42	22.3
V	15.9	30.9	18.25	40.4

金属イオン水溶液のpHや他の金属イオン共存を変化して、CMCt とCMCts ゲルによる貴金属イオンについて吸着能力を検討した。CMCt とCMCtsゲルの金属吸着特性は、pHやイオン強度に依存する。金、パラジウム、白金の共存した金属溶液中では、両ゲルともpH2で金イオンを吸着し、pH4でパラジウムと白金を吸着することから、pHを低くすることにより、金イオンを効率よく分離できる。金属吸着部位は、金属イオン脱着挙動からイオン交換作用よりもむしろキレート作用が支配的であり、分子鎖中のアミノ基、アセチルアミド基、カルボキシル基と密接に関係していることがわかった。

カルボキシメチル化キチン誘導体の放射線橋かけゲルは、金、スカンジウム等の有用金属を吸着し、かつ生分解性を有した捕集材に応用可能である。

References

1) L. Zhao, H. Mitomo, N. Nagasawa, F. Yoshii, T. Kume. *Carbohydrate Polymers*, **51**, 169-175 (2003)
2) L. Zhao, H. Mitomo, M. Zhai, F. Yoshii, N. Nagasawa , T. Kume. *Carbohydrate Polymers*, **53**, 439-446 (2003)

2-15 Modification of Poly(lactic acid) by Radiation-induced Crosslinking

N. Nagasawa[a)], A. Kaneda[b)], T. Matsuzaki[b)], S. Kanazawa[c)], T. Yagi[a)], Tran Minh Quynh[b)], H. Mitomo[b)], F. Yoshii[a,d)] and M. Tamada[a)]

[a)]Environment and Industrial Materials Research Division, QuBS, JAEA, [b)]Faculty of Engineering, Gunma University, [c)]Sumitomo Electric Fine Polymer Inc. [d)]Industrial Collaboration Promotion Department, JAEA

Abstract

Poly(L-lactic acid), PLA was irradiated by electron beams (EB) in the presence of polyfunctional monomers (PFM) as crosslinking agent. After screening of the PFMs, triallyl isocyanurate (TAIC) at 3% concentration was found to be the most effective for crosslinking of PLA by irradiation technique. The crosslinked PLA obtained has heat resistance higher than 200 ºC. From this fact, the crosslinked PLA is applied on heat-shrinkable tube, cup and plate. The shrinkable tube has several advantages such as heat resistance and transparency. It is therefore proven that crosslinking technology is beneficial to expanding the application of PLA.

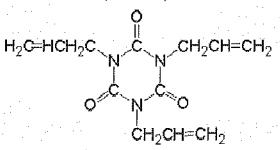
1. はじめに

太陽エネルギーを使って生物が合成し、大気中の炭酸ガスを増加させない資源循環型材料が注目されている。その中でもトウモロコシ等を原料とするポリ乳酸（以下PLAと略記）は、約170℃の高い融点を有し、透明性や機械的特性などが優れていることから、実用化に一番近い材料として有望視されている。しかし、PLAは約60℃を超えると熱変形し、強度が低下するという欠点があるため、耐熱性の向上が必要とされている。ここではPLAの耐熱性改善に対して、放射線照射による橋かけ構造を導入することを試みた。

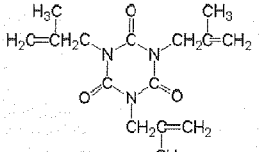
2. 実験方法

三井化学社製PLA（レイシアH-100J）に融点以上の温度（180℃）で様々な種類の橋かけ助剤（多官能性モノマー：PFM）を選択し、所定濃度を添加して混練した後、熱プレス機でフィルムを作製した。放射線処理は、γ線及び電子線を所定線量照射した。照射試料の橋かけ度合いは、クロロホルムに48時間浸漬し、溶解する成分を除去した後、不溶成分を乾燥して得られる重量変化であるゲル分率で評価した。また、橋かけPLAの熱的性質は伸び変形を測定する熱機械的分析で評価し、生分解性試験は37℃におけるプロテナーゼKによる酵素分解法によって評価した。

Triallyl isocyanurate **(TAIC)**



Trimethallyl isocyanurate **(TMAIC)**



Trimethylolpropane triacrylate (**TMPTA**)
$(H_2C=CHCO_2CH_2)_3CC_2H_5$

Trimethylolpropane trimethacrylate (**TMPTMA**)
$[H_2C=C(CH_3)CO_2CH_2]_3CC_2H_5$

1,6-hexanediol diacrylate (**HDDA**)
$[H_2C=CHCO_2(CH_2)_3-]_2$

Ethylene glycol bis [pentakis (glycidyl allyl ether)] ether, hydroxyl terminated (**EG**)
$[H_2C=C(CH_3)CO_2(C_2H_4O)-]_2$

Fig. 1 Strictures of polyfunctional monomers

3. 結果及び考察

ポリマー重量に対して3重量%濃度の各種PFM（Fig. 1）を添加してγ線照射したPLAのゲル分率を測定した結果をFig. 2に示す。PLA単独とTMAIC、TMPTMA、EGを添加した試料では、50kGy照射しても橋かけしないが、TAICとTMPTAでは、50kGy照射で80%のゲルが生成し、効果的に橋かけ反応が起きている。TAICはTMPTAよりも低い照射線量で効果的に橋かけ構造を導入できることがわかった。

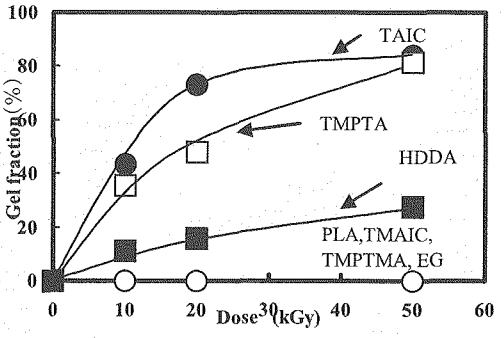


Fig. 2 Effect of PFMs on crosslinking of PLA by irradiation. Concentration of PFMs:3wt%

橋かけ前後の熱機械的分析の結果、未照射PLAでは、約60℃のガラス転移温度以上で急激に変形し、約100℃で測定不可能になる。3%TAIC濃度で50kGy 照射したPLAでは、約60℃で変形せず、200℃でも5%しか変形しないことから、橋かけ構造導入により耐熱性が極めて大きく向上することが分かった。橋かけ前後の生分解性を酵素分解測定により評価した結果、PLA単独と比較して約25%低下するが、生分解性は橋かけ構造を導入しても保持していることが分かった。放射線橋かけしたPLAを熱収縮チューブに応用した(Fig. 3）。橋かけPLAを200℃で2.5倍に膨張させ、室温で冷却固定すると熱収縮チューブができる。このチューブを160℃以上で再加熱すると、元の大きさに収縮して電線などの結束部分の保護材として利用できるため、生分解性熱収縮材への応用の見通しを得た。

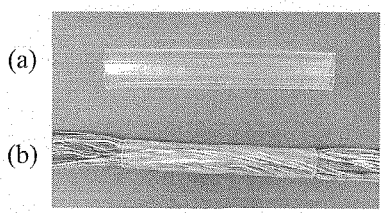


Fig. 3 Photographs of shrinkable tube of crosslinked PLA, (a) shrinkable tube and (b) example of using shrinkable tube.

2-16 Development of DNA-Derived Environmental Material by Gamma-Ray Irradiation

K. Furusawa[a)], E. Kita[a)], T. Dobashi[a)], N. Nagasawa[b)] and M. Tamada[b)]

[a)]Department of Biological and Chemical Engineering, Faculty of Engineering, Gunma University [b)]
Environment and Industrial Materials Research Division, QuBS, JAEA

Abstract

DNA-derived environmental cleanup material was prepared by gamma-ray irradiation on DNA and cross-linkable polymer mixtures. The gamma-ray cross-linkable biopolymers used for the study were carboxymethylcellulose (CMC), gelatin, bovine serum albumin (BSA), carboxymethylchitosan (CM-chitosan), and catinal. The DNA and biopolymer mixtures gelled homogenously after gamma-ray irradiation except for DNA + CM-chitosan mixture. Grams of acrydine orange adsorbed in dried gels decreased with increasing irradiation dose. The optimum irradiation dose for obtaining the maximum adsorption efficiency of the gel was determined as 10, 100, 10, and 30kGy, respectively, for DNA+gelatin, DNA+BSA, DNA+CMC, and DNA+Catinal.

1．はじめに

地球環境の化学物質による汚染は近年さらに深刻になっている。ダイオキシン類のような平面構造を有する化合物は、遺伝子の本体であるDNAにインターカレーション(選択的挿入)によって吸着するため、フレームシフト変異を引き起こす原因となっており、特に問題視されている。一方、DNAに対するダイオキシン類のインターカレーションを利用すれば、DNAを環境浄化材料として応用可能である。環境浄化材料としてのDNAの利活用のためには、DNAを水に対して不溶化することが必要である。本研究では、放射線架橋型の生体高分子とDNAの混合物にγ線を照射してDNAを不溶化することにより安定性の向上したDNA由来環境浄化材料を調製し、得られたゲルの発がん物質吸着性について調べた[1)]。

2．実験方法

実験に用いたDNAは、日本化学飼料より提供されたサケ白子由来高分子量DNA(平均塩基対数 10kbp)である。放射線架橋型の高分子として、カルボキシメチルセルロース(CMC)、ブタ表皮由来ゼラチン(gelatin)、牛血清アルブミン(BSA)、カルボキシメチルキトサン(CM-Chitosan)、塩化O-[2-ヒドロキシ-3-(トリメチルアンモニオ)プロピル]ヒドロキシエチルセルロース(Catinal HC-200)を用いた。DNAを0.25wt%、放射線架橋型高分子を10wt%含む混合水溶液を調製し、これらに対して10kGy/hの線量率のγ線を照射した。このようにして得られた各サンプルのゲル分率 G_f ($=w_n/w_i$、w_nは乾燥ゲルの重さ、w_iは未架橋分を含む乾燥ゲルの重さをそれぞれ表す。)と膨潤特性および発がん物質であるアクリジンオレンジ吸着特性について調べた。

3．結果及び考察

DNAと放射線架橋型の高分子の混合物に対してγ線を照射したところ、各サンプルとも常温において弾性を持つゲルが調製された。このゲルを50℃において2日間超純水に浸漬したところ、CM-ChitosanとDNAとの混合物のみが全て溶解し、他のサンプルでは弾性を持ったゲルのまま形状を保持していた。形状を保持した試料のゲル分率G_fの照射線量依存性をFig. 1に示す。各サンプルともにゲル化線量以上の照射を行うと、急激にゲル分率が上昇し、一定の値となる。タンパク質であるゼラチンおよびBSAとDNAとの混合物では、照射線量が高くなるにつれて、ゲル分率が1に近づき、ほぼ100%ゲル化する。一方、多糖類誘導体であるCMCおよびカチナールとDNAの混合物では、ゲル分率が最大でも0.6程度であった。以上の結果から、これらの混合物についてはγ線照射によって安定なゲルが調製されることがわかった。

乾燥試料1g当たりに吸着されたアクリジンオレンジのグラム数 C_{AO} の照射線量依存性をそれぞれの試料について Fig.2 に示す。どのサンプルについてもγ線照射線量が増加するほどアクリジンオレンジの吸着量が低下することがわかった。Fig.1 及び Fig. 2 の結果から最適照射線量は DNA+gelatin,DNA+BSA, DNA+CMC, DNA+Catinal についてそれぞれ 10, 100, 10, および30kGy であることが分かった。

References

1) K. Furusawa, E. Kita, T. Saheki, N. Nagasawa, N. Nishi, T. Dobashi, *to be submitted.*

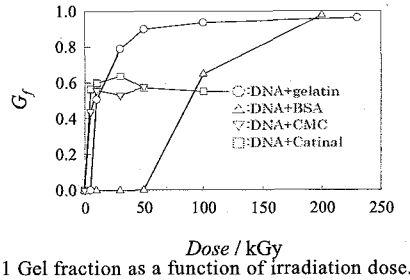


Fig. 1 Gel fraction as a function of irradiation dose.

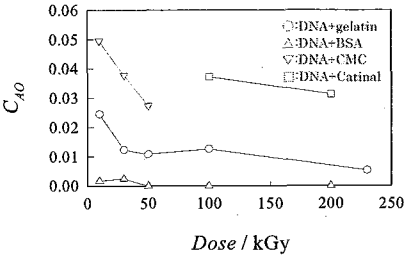


Fig. 2 Acridine orange absorbed in gel as a function of irradiation dose.

2-17 Enhancement of Plant Growth Activity of Irradiated Alginate

N. Nagasawa[a)], Le Q. Luan[b)], T. Yagi[a)], F. Yoshii[a,c)], T. Kume[d)], T. M. Nakanishi[b)] and M. Tamada[a)]

[a)]Environment and Industrial Materials Research Division, QuBS, JAEA, [b)]The Graduate School of Agricultural & Life Sciences, The University of Tokyo, [c)]Industrial Collaboration Promotion Department, JAEA, [d)]TARRI, JAEA

Abstract

The sodium alginate was irradiated by gamma-ray, and plant growth activity test and structural change of the product were studied. It was found that the concentration of 100mg/L of alginate irradiated at 75kGy in 4% aqueous solution was the highest for plant growth. Separation of the degraded product was performed using ultrafiltration membranes and found that fraction with molecular weight in the range of 1-3kDa (6-15 units) not only showed a remarkable effect on the plant growth, but also increased the activity of plant enzymes; *alcohol dehydrogenase, phenylalanine ammonia-lyase*. This fraction was stronger than one of the enzymatic degradation product. This differences proposed formation of carbonyl and carboxyl groups along with the main-chain scission.

1. はじめに

アルギン酸ナトリウム（Alg）は褐藻類から得られる多糖類で、化粧品や食品の乳化剤などに広く利用されている。これらAlgの分解によって得られるオリゴ糖は、植物生長促進、植物内の酵素活性増大などの新しい生物活性機能が注目されている。最近、放射線処理法は簡便で容易に分解できる手法としてオリゴ糖製造への利用が期待されており、照射Algの分子量変化や生成ラジカル挙動について報告してきた[1)]。本研究では、放射線分解によるAlgについて、高い植物生長活性を発現するための照射条件や放射線分解産物の構造について検討した。

2. 実験方法

試料はキミカ(株)製Alg(500cps)を使用し、所定濃度の水溶液に調製した。放射線処理は、粉末状態と水溶液状態でγ線を10kGy/hの線量率で所定線量(10～800kGy)照射した。照射したAlgの分子量変化をGPC測定で、構造変化をUV、FT-IR測定や還元糖及びカルボキシル基定量法により評価した。植物生長促進効果をキク、トルコギキョウ、宿根リモニウムの花やオオムギ、ダイズの穀物類を用いて、照射Alg添加による寒天培地での組織培養や0.1%Hyponex培養液での水耕栽培等で評価した。照射Algをメンブレンフィルターで5画分（F1:1000以下, F2:1000-3000, F3:3000-10000, F4:10000-30000, F5:30000以上）に分子量分画し、各分画による植物生長試験や生長促進に関連するアルコールデヒドロゲナーゼ（ADH）等の酵素活性試験を行った。

3. 結果及び考察

4%水溶液で照射したAlgを用いた植物生長促進効果試験を行い、線量は75kGy、添加濃度は100mg/Lが最適値であることを見出した。この条件を用いて、キク、トルコギキョウ、宿根リモニウムの寒天培地に照射Algを添加して25℃で25日間組織培養及び生育試験した結果、照射Algを添加することによって増殖率が、それぞれ18.8%（キク）、38.6%（トルコキキョウ）、39.3%（宿根リモニウム）と向上し、それぞれの草丈、根長、新鮮重も23.2%、39.4%、19.4%（キク）、14.4%、14.6%、8.1%（トルコキキョウ）、16.6%、9.7%、16.6%（宿根リモニウム）と増大した。穀類に対するAlg添加の水耕栽培では、オオムギで14.6%、ダイズで11.0%の新鮮重の増大が得られた。土に移植後、ハウス内栽培したダイズの生育は良好であり、7.4%のダイズ種子の増収が見られた。

また、オオムギに対する酵素分解物の最適濃度は300 mg/Lであり、照射分解物の100 mg/Lより高濃度が必要であり、照射分解物の比活性が高いことがわかった（Fig. 1）。

水溶液中で照射したAlgの分子量は、線量の増加と共に減少し、その分子量減少は照射試料の濃度に依存した。最も高い植物促進活性が得られる照射条件として、4%水溶液の75kGy照射が最適であり、得られた最適分子量は、約1.4万（未照射：60万）であり、その分解収率G値（100eV当たりの分解数）は、2.3であった。

照射Algを分子量分画した5画分の中で、F2画分（6-15量体）がオオムギの植物生長促進やADH酵素活性誘導の効果が最も高く、低濃度で効果が得られた。酵素分解の場合でも同様にF2画分が最も活性が高いが、このF2画分量は、酵素分解物では10%で、放射線分解では26%生成しており、4%水溶液75kGyの照射でF2の活性区分の生成量が多いことが、植物成長促進活性の高い要因であることを明らかにした。この相違は、照射Algでは本活性画分が特異的に蓄積することに加え、UV、FT-IRスペクトルや還元糖及びカルボキシル基定量法の結果で明らかにしたAlg分子鎖切断に伴うカルボニル基及びカルボキシル基が生じた新たな構造に起因しているものと考えられる。

Algの放射線分解生成物は、顕著な植物生長促進活性及び酵素誘導効果が発現することから、天然物由来の植物生長促進剤としての応用が期待できる。

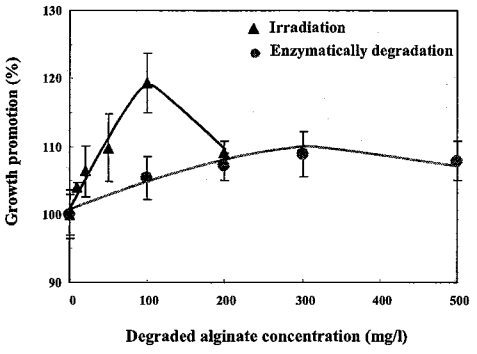


Fig.1 Concentration effect of irradiated sodium algnate on barley growth. Growth condition: water culture in 0.1% Hyponex® aqueous solution at 25 °C for 10 days. Growth promotion (%): Ratio of fresh weight of ten barley plants when unpromoted is assumed to be 100（g/g×100）

References

1) N. Nagasawa, H. Mitomo, F. Yoshii and T. Kume. *Polymer Degradation and Stability*, **69**, 279-285 (2000)

2-18 Cooperative Research on Radiation Processing of Natural Polysaccharides between VAEC and JAEA

A. Hiroki [a)], N. Nagasawa [a)], T. Yagi [a)], T. Kume [b)], F. Yoshii [a, c)] and M. Tamada [a)]

[a)] Environment and Industrial Materials Research Division, QuBS, JAEA, [b)] TARRI, JAEA,
[c)] Industrial Collaboration Promotion Department, JAEA

Abstract

Cooperative research between Vietnam Atomic Energy Commission (VAEC) and JAEA has been performed over a period of six years. In the cooperative research, natural polysaccharides such as alginate, chitin, and chitosan were irradiated by γ-ray to produce various functional materials. It was found that the alginate and the chitosan degraded with γ-irradiation were effective as a growth promoter for rice and carrot and an anti-bacterial agent, respectively. On the other hand, the hydrogels obtained by γ-irradiating carboxymethylchitosan aqueous solution in paste-like state showed a high adsorption capacity for Cu (II) ions as well as the anti-bacterial activity.

はじめに

海藻類や甲殻類を原料とするアルギン酸やキチン・キトサンなどの海洋性天然多糖類は、重要な天然資源として期待されている。海藻やカニ・エビなどが豊富にあるベトナムでは、これらの天然資源を利用した新しい生分解性材料の創製が切望されている。

原子力機構・量子ビーム応用研究部門ではこれまで高分子への放射線照射に伴う分解と高濃度溶液中での橋架け反応を制御して生分解性高分子材料を改質するなど、放射線照射技術に関する基礎的な研究を行ってきた[1, 2]。

ベトナムの豊富な海産天然資源と我々の持つ放射線照射技術を有効活用した新たな産業の創出を目的に、海産多糖類の放射線加工処理に関する研究協力が2000年9月より始まった。2003年9月より3年間の延長が行われ、現在第二期研究が行われている。ここでは、6年間の研究協力の中で見出されたいくつかの興味深い現象や、実用化に向けた研究成果を抜粋して報告する。

植物成長促進剤の開発

1.4 wt.%アルギン酸水溶液にγ線照射（最大 200 kGy）することにより、固体照射や従来の酵素分解法に比べ、簡便に低分子量化(分子量約220,000を2000にまで低下)できた。50, 100 kGy 照射したアルギン酸(分子量 8,000～10,000)を培養液に 20ppm 添加し、イネの生育を調べた結果を Fig. 1 に示す。100 kGy 照射した低分子量アルギン酸を添加すると、イネの成長が約 20%も促進されることが分かった。従って、低濃度でも高い成長促進作用を示す成分をγ線照射により作製することができた。

抗菌・抗カビ剤の開発

キトサンにγ線を照射し低分子量化させると、キトサンの持つ抗菌作用が増すことを見出した[3]。この知見を活用し、γ線照射（25 kGy）したキトサン（分子量約10,000）の1.5 wt.%水溶液をマンゴーやバナナの表面に塗布した結果、貯蔵期間を2～4倍も長くすることができた。

金属・有機物吸着材の開発

キトサン誘導体であるカルボキシメチルキトサン（CMCts）の30 wt.%水溶液（ペースト状）に50 kGy 以上γ線照射するとゲルが得られることを見出した。100 kGy 照射でゲル分率は50%、ゲルの膨潤度は20となった。乾燥したゲル(0.5 g)を0.1 M硫酸銅水溶液に入れたところ、Fig. 2に示すように溶液は薄青色から透明になった。2時間で完全に平衡に達し、銅イオン吸着能は約170 mg/g を示した。以上のことから、CMCts ゲルは抗菌活性のみならず高い金属吸着能を有することが分かった。

References

1) N. Nagasawa, et al., *Polym. Degrad. Stab.*, **69**, 279-285 (2000).
2) F. Yoshii, et al., *Nucl.Instr. and Meth. B*, **208**, 320-324 (2003).
3) S. Matsuhashi, et al., *J. Sci. Food Agric.*, **73**, 237-241 (1997).

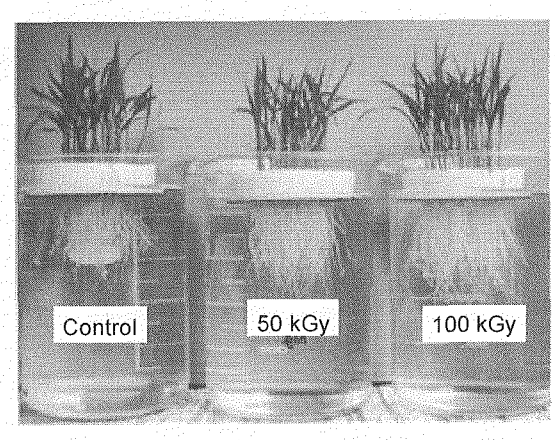


Fig. 1 Effect of irradiated alginate on rice growth. Rice was cultivated in hydroponic solution without alginate and with 20ppm of the irradiated alginate.

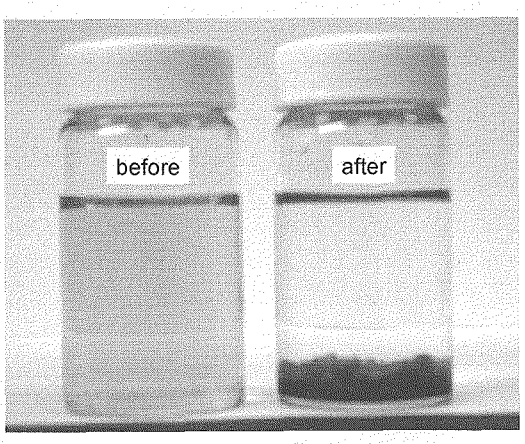


Fig. 2 Adsorption behavior of Cu (II) ions onto CMCts hydrogels. The dried gels were immersed into 0.1 M $CuSO_4$ aqueous solution (50 mL). Solution color: light blue (before) and clarity (after).

2-19 Radiation Effects on PTFE Moulding Powder

T. Yagi[a)], M. Tamada[a)], A. Udagawa[b)]

[a)] Environment and Industrial Materials Research Division, QuBS, JAEA ,[b)] PLACT Corporation

Abstract

Changes of mechanical properties of polytetrafluoroethylene (PTFE) were examined by means of γ-irradiation of the moulding powder prior to compression moulding. Shear strength and elongation at the break of PTFE increased 4 times with the increasing of radiation dose, whereas tensile strength maintained intrinsic value. Gas transmission rate of N_2 and O_2 were also considerably controlled to lower values. These results suggest that the radiation effects on PTFE moulding powder are useful for industrial applications.

1. はじめに

ポリテトラフルオロエチレン(PTFE)はテフロン(デュポン社の商品名)の名称でよく知られているフッ素樹脂である。PTFEは耐熱性、耐薬品性、電気絶縁特性および低摩擦抵抗などの優れた特性を持つため、チューブ、シート、ロッド、フィルムなどの工業製品に多数使用されている。

我々は成形用のPTFE原料粉末に室温で放射線照射を施し、成形後の材料特性に高機能・高靭性を付与する放射線改質技術の研究を進めている。成形用PTFE粉末(フィラー入りを含む)の照射効果について、圧縮成形法により得られた樹脂の引張り特性、引裂き強度、気体透過性などを報告する。

2. 実験方法

PTFEは旭硝子フロロポリマーズ(株)製モールディングパウダー(G350)およびガラス短繊維入り(15重量%)を用いた。照射はCo-60のγ線(1kGy/h)により所定線量(0.5～2kGy)行った。このときの照射は成形前の原料粉末と成形シートで行った。試料は保持圧30MPa、保持時間15分で50φmm x 70mmの円柱状に室温で圧縮成形し、これを温度360℃で2時間焼成を行い調製した。引張り試験は調製試料より厚さ0.5mmに切削したシート(ダンベル試験片)を用い、200mm/minの速度で行った。

3. 結果及び考察

一般に成形したPTFEは放射線照射(数kGy以上)により機械特性が急激に低下することが古くから知られている。しかし、放射線の照射量が1kGy以下の照射効果についてはあまり知られていないのが現状である。最近、PTFEの原料粉末に予め放射線を照射してから成形したシートと、常法により成形したシートに照射した場合で機械特性の線量依存性が大きく異なることが見出されている[1)]。すなわち、PTFEは成形後に照射した場合では線量の増大に伴って破断強度が急激に低下するが、原料粉末に照射してから成形したシートでは粉末の吸収線量が1kGy以下の場合、ほとんど低下がなく、1kGy以上の線量でも低下が抑制される。予め1kGy照射した原料粉末を用いて成形したシート試料の破断伸びおよび引裂き強度は照射により、それぞれ約1.6倍および約2倍に改質される。PTFE粉末にフィラーとしてガラス短繊維を複合したモールディングパウダーについて、機械特性と線量の関係をFig.1(成形シートに照射)およびFig.2(原料粉末に照射)にそれぞれ示す。成形したシートに照射した場合は破断強度の照射による低下が激しく、1kGy以下で半減する。破断伸びは0.5kGyまで僅かに増大するが、0.5kGyを超えると単純に低下する。一方、原料粉末に照射した場合、破断強度は0.5kGyまで変化がなく、2kGyでも半減値以上の値を示す。破断伸びは線量とともに増大し、2kGyで約2倍(未照射と比較)になる。引裂き強度は原料粉末に1kGyの照射で未照射に比べて約4倍の改質がみられる。気体透過性は0.5kGyの照射により、酸素および窒素とも減少するが、特に窒素に対しては1/4強まで減少する。原料粉末に照射するとPTFEの結晶融解熱量は20J/g(0kGy)から37J/g(2kGy)に大きくなる。このことから機械特性の改質には照射による結晶性の増加が寄与していると思われる。

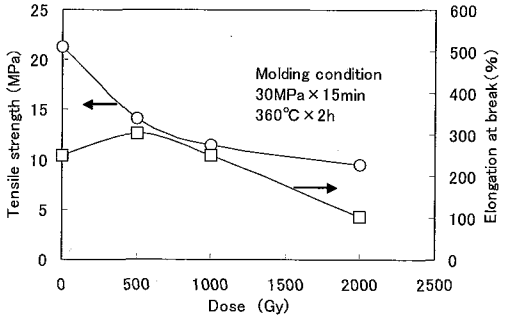


Fig.1 Elongation at break and tensile strength VS. γ-irradiation dose for PTFE sheet

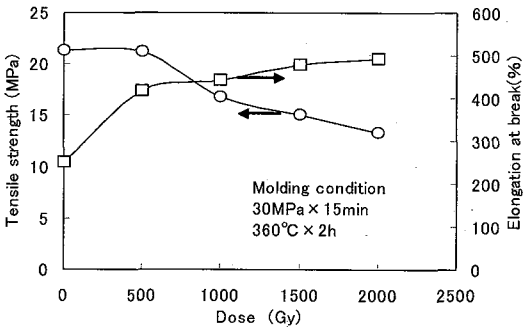


Fig.2 Elongation at break and tensile strength VS. γ-irradiation dose for PTFE moulding powder

References

1) 宇田川昂、池田重利、八木敏明
放射線と産業、No103、P.54-58(2004)

2-20 Hexyl Methacrylate-Based Monolithic Columns Prepared by Radiation-Induced Polymerization

Y. Ueki[a)], T. Umemura[b)], Y. Iwashita[c)], H. Hotta[c)], T. Odake[c)], K. Tsunoda[c)], A. Katakai[a)] and M. Tamada[a)]

[a)]Environment and Industrial Materials Research Division, QuBS, JAEA,
[b)]Department of Applied Chemistry, Graduate School of Engineering, Nagoya University,
[c)]Department of Chemistry, Faculty of Engineering, Gunma University

Abstract

Monolithic capillary columns for reversed-phase liquid chromatography were prepared by gamma ray-induced polymerization of hexyl methacrylate (HMA) and ethylene dimethacrylate in the fused silica capillaries, 0.25 mm in inner diameter. High separation efficiency of the monolithic columns were realized when the coulmns were prepared in the condition of 10 kGy irradaiation, total monomer concentration of 20% inclusive 25% crosslinker. The produced HMA-based monolithic columns were composed of adhered polymer particles, 1 μm and less than in diameter. The pressure drop of column, this 200 mm long, was below 2.0 MPa at linear velocity of 1 mm s^{-1}. The height equivalent to a theoretical plate was approximately 30 μm for the five kinds of alkylbenzenes.

簡便なマイクロカラム作製法としてゾルーゲル法やラジカル重合法により、全体にわたり数μm程度の貫通孔を持った連続多孔質分離媒体（モノリス）を細管内で直接合成し、利用するモノリスカラムの研究開発が注目を集めている[1-3]。我々の研究グループでは、これまでに有機ポリマー製のモノリス型キャピラリーカラムの作製とその高性能化に関する研究に取り組み、熱重合法により圧力損失が極めて低く、通常の100倍速での送液にも耐えうる高性能な有機ポリマー製モノリスカラムを開発してきた。[4-6] しかし、熱重合法では、重合時における温度分布の均一性や重合開始剤の分散性に問題があり、完全に均質なモノリスゲルの作製は困難であった。そこで本研究では、γ線を用いて細孔径が制御された均質なメタクリル酸ヘキシル製モノリスカラムを試みるとともに、作製したモノリスカラムの分離性能をアルキルベンゼン化合物の保持挙動を通して評価した。

モノリスゲルを構成する主鎖にはメタクリル酸ヘキシル（HMA）を用い、架橋剤にはジメタクリル酸エチレングリコールを使用した。これらを1-プロパノール、1,4-ブタンジオール、水の3成分からなる混合溶媒（細孔形成剤）に適宜混合し、モノマー反応溶液とした。窒素通気後、このモノマー溶液を溶融シリカキャピラリー管（内径: 0.25 mm, 長さ: 200 mm）に満たし、γ線照射（放射線源: ^{60}Co）により重合反応を行った。重合反応終了後、未反応のモノマーや細孔形成剤を取り除くため、エタノール、水の順で十分に洗浄し、目的とするメタクリル酸ヘキシル製逆相モノリスカラムを得た。試料には疎水性相互作用に基づき分離されるトルエン、エチルベンゼン、ブチルベンゼン、プロピルベンゼン、アミルベンゼンを使用した。

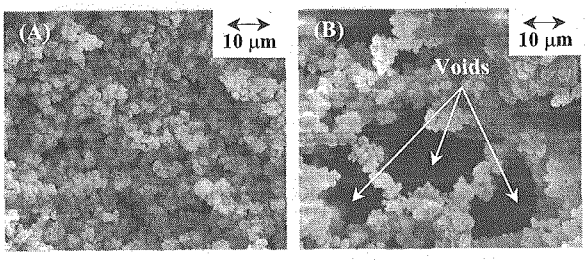


Fig. 1. SEM images of a cross section of HMA-based monolithic columns prepared by (A) radiation-induced polymerization and (B) thermal polymerization.

Fig. 1 に示すように、放射線重合法により作製したモノリスゲルは、粒径1 μm以下の微粒子ポリマー同士が結合したネットワーク構造を形成していた。また、本法により作製したモノリスゲルには、熱重合法において観察された直径20 μm程度の大きな空隙はなく、均質なモノリスゲルを形成していた。カラムの分離特性に及ぼす線量の影響について検討した結果、線量が5 kGyから200 kGyまで増加するにつれて、各種試料成分の保持時間ならびにカラム性能は減少した。そこで、本実験では最も良いカラム性能を示した線量10 kGyを最適線量とした。カラム性能に及ぼすモノリスゲル濃度の影響について検討した結果、モノマー濃度を20%、モノマー中の架橋剤割合を25%とした場合、低分子化合物に対して実用的に十分な分離能を有し、かつ圧力損失が低い（線流速が1 mm s^{-1}のとき、カラム背圧は1.7 MPa/200 mm）メタクリル酸ヘキシル製逆相モノリスカラムの作製に成功した（Fig. 2）。このときの理論段高は30 μm程度となった。

References
1) F. Svec, et al., *Anal. Chem.*, 64 (1992) 820–822.
2) H. Minakuchi, et al., *Anal. Chem.*, 68 (1996) 3498–3501.
3) F. Svec, et al., *Anal. Chem. A-Pages*, 78 (2006) 2100–2107.
4) Y. Ueki, et al., *Anal. Chem.*, 76 (2004) 7007–7012.
5) Y. Ueki, et al., *J. Chromatogr. A*, 1106 (2006) 106–111.
6) T. Umemura, et al., *Anal. Bioanal. Chem.*, *in press*.

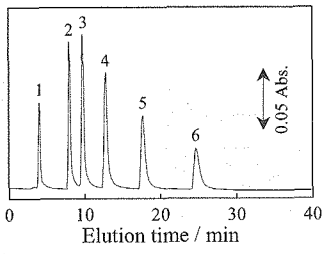


Fig. 2. Separation of a series of alkylbenzenes with HMA-based monolithic column. Mobile phase: acetonitrile–water (50:50, v/v), Linear velocity: 1 mm s^{-1}, Column temperature: 25°C, Detection: UV detection at 215 nm (on-column type UV detector), Sample: 1, uracil (unretained marker); 2, toluene; 3, ethylbenzene; 4, propylbenzene; 5, butylbenzene; 6, amylbenzene, Injection volume: 0.2 μL.

2-21 Development of Electron Beam Technology for the Treatment of PCDD/Fs in Municipal Waste Incinerator Gases

K. Hirota, M. Taguchi , T. Hakoda , and T. Kojima

Environmental and Industrial Materials Research Division, QuBS, JAEA

Introduction

The emission of polychlorinated dibenzo-*p*-dioxins (PCDD) and polychlorinated dibenzofurans (PCDF) has reduced after their new emission standards was promulgated. Typical way for reducing dioxin emission is to dismantle existing electric precipitators and install bag filters at municipal waste incinerators (MSWIs). However, a bag-filter system is required to control the temperature of incinerator gases. In addition, it is necessary to improve the incineration conditions, such as turbulence, temperature, and time to depress PCDD/F formation. The treatment of the filter trapping dioxins also has a risk of dioxin emission.

We have started experiments on electron-beam treatment of dioxins in MSWIs at a pilot scale. Electron-beam technology is based on the reactions with radicals, such as OH, e, N, and O, produced by the ionization and excitation of air components. The reactions can oxidize, namely decompose, pollutants. A second treatment is not necessary for an electron-beam system. Electron-beam technology is expected as a low cost and simple process method.

Experimental

The experiments were carried out at Takahama Clean Center treating 450t solid wastes in a day using 3 furnaces. The schematic flow of electron-beam facility is shown in Figure 1. An incinerator gas of 1,000 m^3_N/h was diverted from the downstream of a dry electric precipitator connected to one of the furnaces. Each furnace generates a 40,000 m^3_N/h flue gas when incinerating 150t/day. Electron beams were directly irradiated to the incinerator gases at a temperature of 200℃ through a 13 μm Ti foil attached to a reactor. The PCDD/F sampling was continued 4h during irradiation for their quantitative analyses.

Results and Discussion

The decomposition efficiencies of PCDD/Fs as a function of absorbed dose are shown in Figure 2. Our target of 90% decomposition efficiency was achieved at doses of 12 kGy for PCDD and 16 kGy for PCDF[1]. The discrepancy in the absorbed doses required for the 90% decomposition was solved when decomposition behavior for each PCDD/F homologue was analyzed. Initial decomposition G-values calculated from a plot of dose vs. the homologue concentration are available to compare their rate constants for reactions with OH radicals. The results showed the higher rate constants were obtained from lower chlorinated homologues, which is consistent with the results obtained theoretically. It was found that the PCDD homologues in the incinerator gases were decomposed through reactions with OH. The ring cleavage and the dissociation of ether bonds were probably the main pathway for the PCDD decomposition.

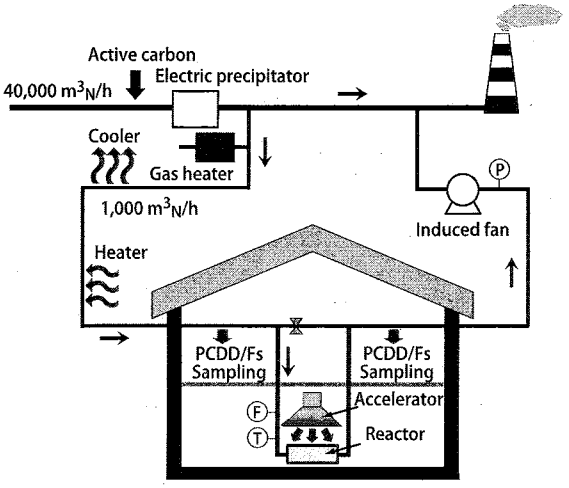


Fig.1 Schematic flow of electron-beam facility for PCDD/F treatment.

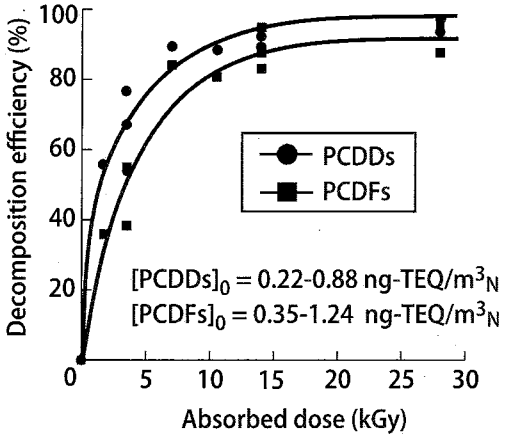


Fig.2 Decomposition of PCDD/FS in MSWI gases with electron beams.

In contrast, the decomposition behavior of PCDF homologues did not show any relations to their OH rate constants. *Tetra*-chlorodibenzofrun was produced after irradiation through the dechlorination of higher chlorinated homologues[2]. Dechlorination was likely to occur in the electron-beam treatment of PCDFs in the incinerator gases.

Based on the present studies, we estimated the annual cost for treating PCDD/Fs in MSWIs with electron beams. The cost for an electron-beam system is 7% lower than that for a bag filter system. Electron beam is a technologically and economically useful method to destroy PCDD/Fs in MSWIs.

References

1) K. Hirota, T. Hakoda, M. Taguchi, M. Takigami, H. Kim, and T. Kojima, *Environ. Sci. Technol.* 37 (2003) 3164.

2) K. Hirota and T. Kojima, *Bull. Chem. Soc. J.* 78 (2005) 1685.

2-22 Electron Beam Treatment of Formalin Sterilization Gas

A. Shimada[a)], T. Hakoda[a)], T. Kojima[a)], T. Takubo[b)], T. Iwasaki[b)] and S. Kinoshita[b)]

[a)] Environment and Industrial Materials Research Division, QuBS, JAEA, [b)]Iwasaki Electric Co., Ltd.

The sterilization of the clean room has been performed using an formalin/air mixture, which is prepared by vaporization of a commercially available formalin solution (water including about 37% of HCHO and about 5－10% methanol (CH_3OH)). The HCHO/air mixture in the clean room needs to be treated after its use for sterilization. In some food packaging factories, the formalin/air mixture at the HCHO concentration of 1200 ppmv in the clean room of 2000 m^3 is treated by circulating treated gas through the heat-catalyst reactor equipped in the room. The time to complete the treatment is, however, not short, for example, 2 or 3 d and it results in low operation efficiency. One of the reasons for such a long treatment time is that the heat-catalyst can work better at high HCHO concentrations and worse at low concentrations because HCHO may be oxidized only on the surface of the catalyst, not in the air containing gaseous HCHO. While, the method of making free radicals in the air such as electron beam (EB) is advantageous for such a low concentration gas treatment. In the present study, the EB processing for the formalin/air mixture treatment was studied to decrease the HCHO concentration from various initial values to 10 ppmv.

Air mixtures containing 90－1230 ppmv of HCHO with 30－340 ppmv of CH_3OH were irradiated by EB to the absorbed doses of 5－80 kGy. The concentrations of both HCHO and CH_3OH as a function of the dose are individually plotted as shown in Fig.1[1)]. The concentrations decreased with dose. The doses required to decrease HCHO concentrations to 10 ppmv were estimated to be 12, 32, 43, and 80 kGy for the initial HCHO concentration of 90, 300, 480, and 1230 ppmv, respectively, from the fitting curves in Fig.1.

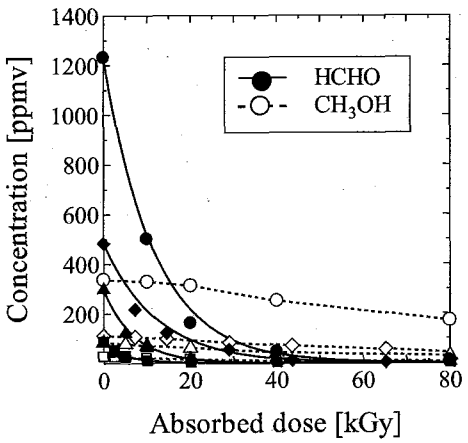


Fig.1 HCHO and CH_3OH concentrations in formalin/air mixtures as a function of dose

The relation between the initial HCHO concentration in air mixtures with CH_3OH and the dose for decreasing the HCHO concentrations to 10 ppmv, D [kGy], was derived from Fig.1, as shown in Fig.2[1)]. The relation for HCHO/air mixtures with CH_3OH can be well-represented by the following equation:

$$D = -4.2 \times 10^{-5}[HCHO]_0^2 + 1.2 \times 10^{-1}[HCHO]_0 - 1.2$$
$$[10\ \text{ppmv} \leqq [HCHO]_0 \leqq 1230\text{ppmv}] \quad (1)$$

Formic acid, CO, and CO_2 are produced by the irradiation of HCHO in air mixture, while CO and CO_2 are produced from CH_3OH in the air mixture. Formic acid can be collected with water scrubber and remaining CH_3OH can be removed with the scrubber. So, the scope of this study is limited to decrease the HCHO concentration to 10 ppmv.

The general equation was derived to estimate the time to complete the treatment in the clean room (t_{comp}), for any output of EB generator, the volume in the clean room, and the concentration of HCHO just after sterilization.

The t_{comp} is about 9 h when the output of EB is 12 kW (for example, accelerated voltage: 300kV, maximum current: 40mA), the volume of the clean room is 2000 m^3, and the concentration of HCHO just after sterilization is 1200ppmv. The t_{comp} by EB is about 25% of that by the heat-catalyst.

Such an EB processing can be applicable to improve the operation efficiency of the factories, for example food packaging factories.

Reference

1) Shimada, A.; Hakoda, T.; Kojima, T., *J. Chem. Eng. Jpn.*,Vol.39, No.9, (in press)

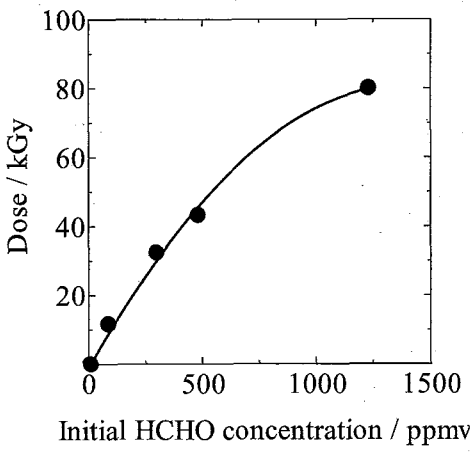


Fig.2 Absorbed dose required for decomposition of HCHO to 10 ppmv as a function of initial HCHO concentration before irradiation

2-23 Decomposition of Endocrine Disrupting Chemicals in Real Wastewater by ^{60}Co γ-Ray Irradiations

A. Kimura[a, b], M. Taguchi[a, b], Y. Ohtani[c], H. Hiratsuka[b] and T. Kojima[a, b]

[a]Environment and Industrial Materials Research Division, QuBS, JAEA, [b]Gunma University,
[c]Gunma Prefectual Institute of Public Health and Environmental Sciences

1.Introduction

Endocrine disrupting chemicals (EDCs) are widely spread into the water environment, and induce serious effects on living animals. We turns attention to 17 β-estradiol (E2) has the highest estrogen activity in water environment and *p*-nonylphenols (NPs) exhibits one of the highest estrogen activity among artificial chemicals. These EDCs were decomposed by ^{60}Co γ-ray irradiation[1), 2), 3)]. The treatment of real wastewater having the estrogen activity by use of γ-ray irradiation was investigated by the yeast two-hybrid assay (YTHA). Economic cost for the treatment of wastewater was evaluated.

2.Experimental

Three real wastewater samples were obtained from the different secondary effluents of water treatment plants with the activate sludge system. Model wastewater samples were prepared by adding E2 at 1.8 nmol dm^{-3} or NPs at 20 μmol dm^{-3} in wastewater having no estrogen activity collected at an effluent of a water treatment facility. The amounts of total organic carbon (TOC) in the model wastewaters were 1.02, 10.2 and 20.4 mg L^{-1}. The ^{60}Co γ-ray irradiations were carried out at 298 K using γ-ray sources at JAEA, Takasaki at the dose rates ranging from 133 to 1000 Gy h^{-1}. Analyses of real and model wastewater samples before and after irradiation were carried out with HPLC-MS and TOC analyzer. Human and medaka estrogen receptors were used for estimation of estrogen activities, hEA and mEA, respectively. Subtraction of hEA from mEA gives existence of the artificial EDCs in the real wastewaters.

3.Results and discussion

Little estrogenic compounds were included in the real wastewater sample (a) and (b) before irradiation, since hEA of these samples were lower than 1 ng dm^{-3} and mEA is high as shown in Fig. 1. Sample (c) include natural and artificial estrogenic compounds because of higher mEA and hEA. These samples were irradiated with γ-ray, and every mEA initially increased and then decreased, indicating that decomposition products also have the estrogen activity. Treatment of the real wastewater is required to decrease the estrogen activity to less than 1 ng dm^{-3}, which is a lower limit concentration of appearance of endocrine disrupting property. The doses for decrease in mEA of sample (a), (b) and (c) below 1 ng dm^{-3} were estimated at 100, 200 and 150 Gy, respectively.

E2 and NPs in the model wastewaters were decomposed by γ-ray irradiation. Although E2 at an initial concentration of 1.8 nmol dm^{-3} in pure water was decomposed at a dose of 10 Gy, decomposition of E2 in the model wastewaters required higher doses in the range of 50 to 200 Gy. The decomposition of NPs in the model wastewater was also gradual with the increase in the amount of TOC. Decomposition of EDCs in the model wastewater is assumed to be interfered by coexisting organic impurities.

Economical cost for decomposition of EDCs in secondary effluent at sewage treatment plants by use of electron beam is evaluated referring to the pilot plant experiments in previous work[4)]. Dose for the elimination of the estrogen activity of wastewater by electron beam is about 200 Gy as same as by ^{60}Co γ-rays. The treatment equipment for the recirculation of 10,000 m^3 day^{-1} is an electron beam accelerator at a total power of 280 kW (for example, 5 MeV, 56 mA). The total running cost for the initial investment and electric power for the equipment operation is estimated to be 17 yen m^{-3}. For example, the costs of the common treatment plants are in the range of 30 to 140 yen m^{-3}. The electron beam treatment equipment is considered to have the potentiality of the attachment to the other existing treatment plants.

References

1)A. Kimura et al., Radiat. Phys. Chem., 69, 295-301 (2004).
2)A. Kimura et al., Radiat. Phys. Chem., 75, 61-69 (2006).
3)A. Kimura et al., Radiat. Phys. Chem. in press
4)JAERI, JAERI-Research, 95-006 (1995).

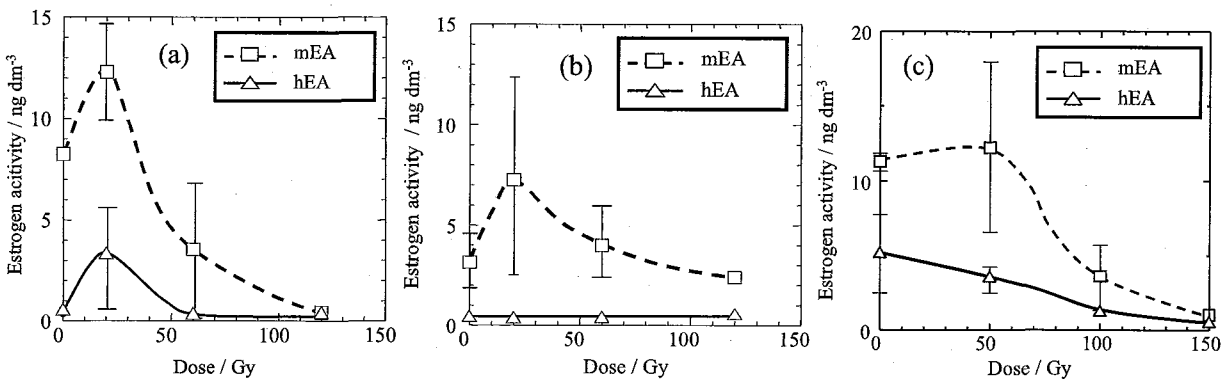


Fig.1 Estrogen activities of real wastewaters estimated using medaka estrogen receptor (Square) and human estrogen receptor (Triangle) after γ-ray irradiation.

2-24 Dependence of Differential Yields of Heavy Ion Induced OH Radicals in Water on Mass and Specific Energy of Heavy Ions, and Elapsed Time

M. Taguchi, and T. Kojima

Environment and Industrial Materials Research Division, QuBS, JAEA

1. Introduction

The oxidations of solutes in aqueous solutions are mainly induced by OH (hydroxyl) radicals formed from water molecules on heavy ion irradiation. Characteristics of the oxidations of solutes are strongly dependent on initial concentrations and spatial distributions of OH radicals. Clarification of reaction mechanisms of OH radicals is a critical point to interpretation of the radiation effects both in radiation chemistry and radiation biology. The heavy ion deposits its kinetic energy densely along and around its trajectory. The initial spatial distribution of OH radicals is the same as that of the energy deposition. OH radicals, however, disperse as time passed within their life, and this makes the interpretation of relevant chemical reactions very complicate. Investigations based on three influences, which are incident ion mass, specific energy in water, and elapse time after irradiation are indispensable to understand chemical reactions in the track.

2. Experimental

Phenol dissolved in water at 1-100 mM in concentration was used as sample solution after saturation with oxygen. The solution was put into an aluminum irradiation cell with an aluminum window.[1] Heavy ions used in this study were He, C and Ne ion provided from an AVF cyclotron in TIARA facility. Thin aluminum foils were used for reducing the incident energy of the ion. The sample solutions before and after irradiations were analyzed by high performance liquid chromatography with a reversed phase column.

3. Results and discussion

Three kinds of isomeric products (catechol, resorcinol, and hydroquinone) of phenol oxidized by OH radicals were commonly observed for the various energies of He, C, and Ne ions. Beside OH radicals, e^-_{aq} and H atoms react with oxygen to produce superoxide radicals, O_2^- and HO_2. The contribution of e^-_{aq} and H atoms can be ignored in this study, since these superoxide radicals react slightly with phenols to produce these oxidized products.

The number of oxidized products per a single ion, which is integration of differential G-value (G'-value) over entire trajectory, increased super-linearly with an incident energy of each ion. The G'-value of OH radicals is estimated by assuming that the mechanism of oxidations by ion irradiation is the same as that by γ-ray irradiation. The G'-values of OH radicals at the elapsed times of 1.5, 15 and 150 ns, which are time derived from scavenging capacity, k_{OH} [phenol], are shown in Fig. 1 for He ions. The G'-values are relatively large at the primary stage and decrease with time after the end of irradiation. The decreases of the G-values with time are generally observed for γ-ray and fast electron irradiations. OH radicals are consumed in consequence of reactions with e^-_{aq}, H atoms, and other transient species produced by irradiation. The G'-values of OH radicals decrease monotonously with decreasing specific energy, in other word LET, at the same elapsed time.

LET dependences of the G'-values of the OH radicals at 15 ns for each ion are shown in Fig. 2. The G'-values for He, C and Ne ions decrease with LET. However, their curves are not overlapped. LET gives the amount of deposited energy in a unit length along the trajectory but no information about energy distribution around trajectory. LET is not good parameter to comprehends reaction mechanism of OH radicals in track.

References

1) M. Taguchi, T.Kojima, Radiat. Res., 165, 455 (2005).

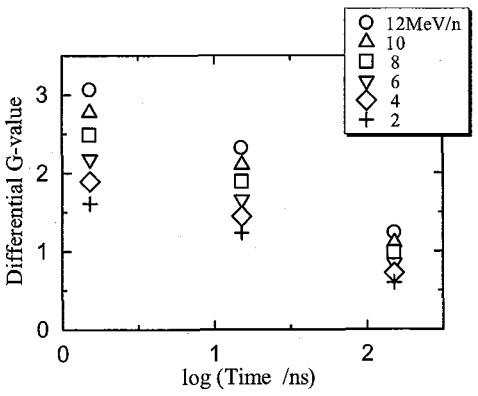


Fig.1 OH radical yield on specific energy as a function of elapsed time after He ion irradiation.

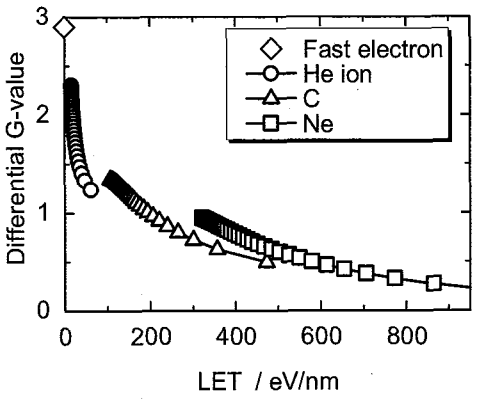


Fig.2 OH radical yield at 15ns after irradiation of fast electron, He, C, and Ne ion as a function of LET.

3 Biotechnology and Medical Application

3-01 *Deinococcus radiodurans* DNA Repair-Promoting Protein : Applications to Biotech Industry ····· 69
I. Narumi, H. Ohba, H. Sghaier, and K. Satoh
3-02 The Radiation Responsive Promoter of the *Deinococcus radiodurans pprA* Gene ····· 70
H. Ohba, K. Satoh, T. Yanagisawa and I. Narumi
3-03 Detection Method for Irradiated Foods Using ESR ····· 71
M. Ukai, M. Matsuura, T. Kume, Y. Kobayashi, M. Kikuchi and T. Sakashita
3-04 Detection of Oxidative DNA Damage Using Anti-8-OHdG Antibody
-A Useful Method to Distinguish Irradiated Foods- ····· 72
M. Kikuchi, A. Z. Mohd Dzomir, C. R. Gunawardane, M. K. Alam and Y. Kobayashi
3-05 Application of Hydrogel on Wound Dressing and Future View of Hydrogel ····· 73
F. Yoshii
3-06 Development of an Efficient Method for Mutation Induction in Plants ····· 74
Y. Hase, Y. Yokota, I. Narumi and A. Tanaka
3-07 DNA Damage Yields in Hydrated DNA after He Ion Irradiation ····· 75
A. Urushibara, N. Shikazono, K. Fujii and A. Yokoya
3-08 Study of Molecular Mechanism of Ion Beam Induced Mutations in the *Saccharomyces cerevisiae* ····· 76
Y. Matuo, S. Nishijima, Y. Hase, A. Sakamoto, A. Tanaka and K. Shimizu
3-09 Quantitative Analysis of DNA Double-Strand Breaks in Tobacco Protoplasts Irradiated with Helium, Carbon and Neon Ion Beam ····· 77
Y. Yokota, S. Yamada, Y. Hase, N. Shikazono, I. Narumi, A. Tanaka and M. Inoue
3-10 Comparison of the Mutation Inducing Effect between Ion Beams and Gamma Ray ····· 78
R. Morita, T. Morishita, H. Nakagawa, M. Nishimura, H. Yamaguchi, Y. Yokota, Y. Hase and A. Tanaka
3-11 Molecular Analysis of Ion Beam-Irradiated Orchids ····· 79
A. H. Affrida, A. Zaiton, A. Sakinah, B. Mohd Nazir, A. Tanaka, N. Shikazono, Y. Oono and Y. Hase
3-12 Selection of Rootstock Eggplant Resistant to Bacterial Wilt from Regenerants Derived from Ion Beam-Irradiated Microspores ····· 80
Y. Uchimura, K. Takata, Y. Saiki, K. Hirashima, T. Nakahara, Y. Hase, Y. Yokota and A. Tanaka
3-13 Mutation Induction from Osteospermum Leaf Cultures with Ion Beam Irradiation ····· 81
M.Iizuka, Y.Kimura, Y.Hase and A.Tanaka
3-14 Breeding of Stress-Tolerant Variety Series in Ornamentals by Ion Beam Irradiation ····· 82
M. Okamura, M. Momose, S. Watanabe, A. Shimizu, Y. Hase, Y. Yokota and A. Tanaka
3-15 The Optimum Dose of Ion Beam Irradiation to Tissue Cultured of Leaf Explants for Breeding Sugarcane ····· 83
F. Tohjima, T. Shirao, K. Ueno, M. Ooe, M. Yasuniwa, Y. Hase, A. Tanaka
3-16 Mutation Induction in Sugi Cedar and Hinoki Cypress by Ion Beam Irradiation ····· 84
K. Ishii, Y. Hosoi, Y. Hase and A. Tanaka

3-17 Mutation Induction in Garlic with Ion Beam Irradiation ····· 85
T. Tashiro, Y. Yamamoto, A. Tanaka and Y. Hase
3-18 Mutagenesis in Gynomonoecious Spinach (*Spinacia oleracea* L.) Plants and Selection of Low Oxalate Variants ····· 86
K. Murakami, N. Hata, Y. Yoshida, M. Masuda, A. Tanaka, N. Shikazono and Y. Hase
3-19 Effect of Ion Beam Irradiation on Coloration of Fruit Skin of Eggplant (Solanum melongena L.) ····· 87
N. Matsuzoe, T. Umeda, Y. Hase and A. Tanaka
3-20 Studies on Flower Color and Morphological Mutations from Chrysanthemum In Vitro Explants Irradiated with Ion Beams ····· 88
T.sato, H.Kagaya, Y.Hase and A.Tanaka
3-21 Induction of Mutation by the Ion Beam Irradiation to the Calluses of *Lilium* × *formolongi* Hort (*cv. White Aga*.) ····· 89
M. Kondo, K. Ogata, Y. Hase, Y. Yokota, I. Narumi and H. Kobayashi
3-22 Mutation Induction on Hybrid Limonium 'Moon Light' Using Ion Beams ····· 90
S. Chinone, Y. Hanaoka, K. Tokuhiro, K. Nakatsubo, M. Amano,Y.Hase, A. Tanaka and I. Narumi
3-23 Effects of Ion Beam Irradiation on Spore Germination, Mycelial Growth and Fruit Body Formation of *Pleurotus ostreatus* ····· 91
Y. Kawashima, T. Matsumoto, Y. Hase and Y. Yokota
3-24 Mutation Induction of Asiatic Hybrid Lily Using Ion Beam Irradiation ····· 92
N. Chiba, K. Arakawa, S. Nakamura, S. Suzuki, Y. Adachi, Y. Yokota and Y. Hase
3-25 Screening of Cadmium Resistant Rice Mutants Induced by Carbon Ion Irradiation ····· 93
T. Tsukamoto, H. Nakanishi, H. Hase, A. Tanaka, N. K. Nishizawa and S. Mori
3-26 Ion Beam Breeding of Rice Variety Suitable for Low Nitrogen Input ····· 94
H. Katayama, H. Kitamura, M. Mori, J. Nakagawa, T. Yoshida, T. Kawai, Y. Hase and A. Tanaka
3-27 Flower Color and Cluster Modification by Ion Beams in Chrysanthemum ····· 95
T. Nomizu, N. Furutani, Y. Hase, Y. Yokota and A. Tanaka
3-28 Mutation Induction in Azalea Using Ion Beam Irradiation and Its Gene Analysis ····· 96
N. Kobayashi, S. Sakamoto, A. Nakatsuka,Y. Hase and Y. Yokota.
3-29 Deletion of Minor Enzyme Activities of *Rhizomucor miehei* by Irradiation of Heavy-Ion Beam ····· 97
K. Sakai, H. Kobayashi, A. Oshima, S. Kato, K. Sato, Y.Hase, I. Narumi, T. Sakashita and Y. Kobayashi
3-30 Mutation Breeding of Koji Mold Induced by Ion Beams ····· 98
K. Ito, J. Takeichi, Y. Hanya, K. Satoh, Y. Hase T. Sakashita, Y. Kobayashi and I. Narumi
3-31 Analysis of Cellular Effects and Local Damage Induced by High LET Heavy Ions ····· 99
S. Wada, N. Hamada, T. Funayama, T. Sakashita, T. Kakizaki, Y. Yokota, Y. Hase and Y. Kobayashi
3-32 Recent Improvements of Heavy-Ion Microbeam System for Bystander Study ····· 100
T. Funayama, T. Kakizaki, S. Wada, Y. Yokota, T. Sakashita, N. Hamada and Y. Kobayashi

3-33 Late-Arising Loss of Clonogenicity in the Progeny of Cells Surviving High- and Low-LET Ionizing Radiations ····· 101
N. Hamada, S. Wada, T. Funayama, T. Sakashita , T. Kakizaki, M. Ni and Y. Kobayashi
3-34 Bystander Killing of Human Lung Cancer Cells by Heavy Charged Particle Irradiation ····· 102
K. Harada, T. Nonaka, N. Hamada, T. Funayama, H. Sakurai, T. Sakashita, S. Wada, H. Kawamura, M. Hasegawa, Y. Kobayashi and T. Nakano
3-35 Analysis of Radiation-Induced Apoptosis in Early *Drosophila* Embryos ····· 103
K. Tatei, T. Tamaki, H. Kawamura, N. Hamada, T. Sakashita, T. Funayama, S. Wada, T. Kakizaki, T. Nonaka, H. Obinata, T. Hattori, A. Ogawa, H. Kazama, T. Nakano, Y. Kobayashi and T. Izumi
3-36 Bystander Effect of High Linear Energy Transfer Charged Particle Radiation on Human Glioblastoma Cells ····· 104
S. Ishiuchi, M. Hasegawa, Y. Yoshida, N. Hamada, T. Funayama, S. Wada, T. Sakashita, Y. Kobayashi and T. Nakano
3-37 Effects of Heavy-Ion, UV-C, and X-Ray Irradiation on the Susceptibilities of Human Cells to HIV-1 Infection ····· 105
N. Shimizu, A. Oue, T. Ohtsuki, T. Mori, K. Yamaguchia, T. Nakamura, S. Wada, Y. Kobayashi and H. Hoshino
3-38 Effects of Heavy Ion Microbeam Irradiation on Isolated Single Fibers of Skeletal Muscle ····· 106
H. Yorifuji, M. Hino, S. Wada, Y. Tajika, Y. Morimura, N. Hamada, T. Funayama, T. Sakashita, T. Kakizaki and Y. Kobayashi
3-39 Research into the Radiosensitivity of Normal Brain Tissue ····· 107
Y. Suzuki, Y. Yoshida, K. Shirai, N. Hamada, T. Mizui, S. Noda, T. Funayama, T. Sakashita, Y. Kobayashi, T. Shirao, S. Ozawa and T. Nakano
3-40 Response of Associative Learning and Nervous System of *Caenorhabditis elegans* to Heavy Ion Beam Irradiation ····· 108
T. Sakashita, N. Hamada, M. Suzuki, T. Kakizaki, S. Wada, T. Funayama and Y. Kobayashi
3-41 Heavy Ion Microbeam Irradiation to the Central Nervous System of *Caenorhabditis elegans* and Development of Effect Prediction Simulator. Why is Associative Learning of *Caenorhabditis elegans* Promoted by Ionizing Irradiation? ····· 109
T. Sakashita, N. Hamada, M. Suzuki, T. Tsuji, T. Kakizaki, S. Wada, T. Funayama and Y. Kobayashi
3-42 Particle Number- and LET- Dependency of Bystander Effect through the Gap Junction Signalling in Human Normal Fibroblast Cells Exposed to Heavy-Ion Beams ····· 110
Y. Matsumoto, N. Hamada, M. Aoki, S. Wada, T. Funayama, T. Sakashita, T. Kakizaki, Y. Kobayashi and Y. Furusawa
3-43 Analysis of Molecular Mechanisms for Radiation-Induced Bystander Effects Using Heavy Ion Microbeams ····· 111
H. Matsumoto, M. Hatashita, A. Takahashi, N. Hamada, S. Wada, T. Funayama, T. Sakashita, T. Kakizaki and Y. Kobayashi

3-44 Chromosomal Aberrations by Medium-Mediated Bystander Effects Induced by High-LET Radiations ····· 112
K. Takakura, Y. Kanasugi, N. Hamada, S. Wada, T. Funayama, T. Sakashita, T. Kakizaki and Y. Kobayashi

3-45 Construction of Monitoring System for Biological Effects of Local Ionizing Radiation Using the Nematode *C. elegans* ····· 113
A. Higashitani, T. Sugimoto, C. Mori, Y. Suzuki, R. Saito, E. Ichiishi, T. Sakashita, N. Hamada, S. Wada, T. Kakizaki, T. Funayama and Y.Kobayashi

3-46 Ion Beam Irradiation has Different Influences on Glutathione Peroxidase of Cultured Human Retinal Vascular Endothelial Cells among ^{20}Ne, ^{12}C, and ^{4}He ····· 114
K. Akeo, N. Hamada, Y. Kobayashi, T. Funayama, T. Sakashita, Y. Akeo, K. Kawada and K. Tsubota

3-47 The Characteristics of Radiation-Induced Cell Responses in the Canine Spontaneous Tumor Cells ····· 115
T. Sano, S. Wada, K. Suzuki, M. Natsuhori, T. Kakizaki, T. Itoh, K. Nakazawa, Y. Kobayashi and N. Itoh

3-48 Effects of Heavy Ions and Gamma-Ray on the Tardigrade *Milnesium tardigradum* ····· 116
D. D. Horikawa, T. Sakashita, C. Katagiri, M. Watanabe, T. Kikawada,Y. Nakahara, N. Hamada, S. Wada, T. Funayama, S. Higashi, Y. Kobayashi,T. Okuda and M. Kuwabara

3-49 Regeneration Mechanism of Hemopoietic Organs in the Silkworm, *Bombyx mori*, after Heavy-Ion Irradiation : Analysis by Transplantation of the Irradiated Organs Using a Transgenic Silkworm Strain ····· 117
K. Kiguchi, K. Shirai, T. Sakata, K. Fukamoto, T. Kakizaki, S. Wada, T. Sakashita,T. Funayama, N. Hamada and Y. Kobayashi

3-50 Analysis of Local Irradiation of Heavy-Ion Microbeam Influence on Embryo or Yolk in the Silkworm, *Bombyx mori*, Egg by the Incidence of Somatic Mutation Appearing in the Larvae ····· 118
T. Furusawa, E. Suzuki, S. Nagaoka, H. Suzuki, N. Ishioka, N. Hamada, S. Wada, Y. Kobayashi, T. Sakashita, T. Kakizaki and K. Funayama

3-51 Identification of the Functional Tissues for Hydrotropism in Comparison with Those for Gravitropism ····· 119
Y. Miyazawa, H. Negishi, T. Sakashita, A. Kobayashi, T. Kaneyasu, A. Ooba, T. Funayama, S. Wada, N. Hamada, T. Kakizaki, Y. Kobayashi, N. Fujii and H. Takahashi

3-52 Circadian Rhythms in Resistance to γ Irradiation and Heavy Ion Beam in *Euglena* ····· 120
A. Bolige, T. Sakashita, T. Kakizaki, T. Funayama, N. Hamada, S.Wada, Y. Kobayashi and K. Goto

3-53 Analysis of the Maturation Process of Photosynthetic Activities in a Leaf Using Positron Emitting Tracer Imaging System (PETIS) ····· 121
S. Ishii, N. Kawachi, S. Fujimaki, N. Suzui and S. Matsuhashi

3-54 Interaction between Nitrogen Nutrients Acquisition Function and Distribution of Photosynthetic Products ····· 122
T. Ohyama, K. Sueyoshi, N. Ohtake, S. Ito, H. Ishibashi, T. Hara, T. Kimura, S. Matsuhashi, S. Fujimaki, N. Suzui, S. Ishii, N. Ishioka, S. watanabe, Y. Kawachi and T. Tsukamoto

3-55 Determination of Photosynthesis and Partitioning Rate Using by PETIS ····· 123
R. Suwa, S. Ishii, N. Kawachi, S. Fujimaki, N. Suzui, H. Sutou, S. Mathuhashi and K. Fujita

3-56 ^{52}Fe Tranlocation from the Roots to the Ear of Rice Using a Positron Emitting Tracer Imaging System (PETIS). ····· 124
T. Tsukamoto, H. Nakanishi, S. Watanabe, S. Matsuhashi, N. K. Nishizawa and S. Mori

3-57 Evaluation of Effect of Root Parasite on Nitrogen Translocation and Distribution in the Host Plant by Positron Emitting Tracer Imaging System (PETIS) ····· 125
H. Sekimoto, S. Honda, S. Katou, Y. Ochiai, K. Yoneyama, K. Yoneyama, Y. Takeuchi, N. Kawachi, S. Fujimaki, N. Suzui, S. Ishii, N. Ishioka and S. Matsuhashi

3-58 Imaging of Parallel Routes of Photoassimilate Transport in an Intact Plant Body ····· 126
S. Fujimaki, K. Sakamoto, N. Kawachi, S. Ishii, N. Suzui, N. S. Ishioka, S. Watanabe and S. Matsuhashi

3-59 Non-Invasive Imaging of Cadmium Transport in Crop Plants ····· 127
S. Fujimaki, S. Nakamura, N. Suzui, N. S. Ishioka, M. Chino and S. Matsuhashi

3-60 Positron Related Analysis of ^{13}N-Nitrate in Transgenic Rice Plant Over-Expressing Nitrate Transporter ····· 128
D. Sato, M. Mori, H. Katayama, H. Kitamura, T. Kawai, S. Fujimaki, N. Suzui,N. Kawachi, S. Ishii, S. Matsuhashi, T. Tanaka, T. Tsukamoto, N. K. Nishizawa and M. Mori

3-61 Effect of Cadmium on Translocation of Photoassimilates in Rice (*Oryza sativa* L.) ····· 129
N. Suzui, S. Fujimaki, N. Kawachi, S. Ishii and S. Matsuhashi

3-62 Impacts of Aluminum Ion for the Translocation of Signaling Molecule in Higher Plants ····· 130
T. Furuichi, S. Fujimaki, Y. Kawachi, N. Suzui, S. Ishii, N. Ishioka, S. Matsuhashi, Y. Yamamoto and M. Sokabe

3-63 Kinetic Analysis for Studying Photosynthesis in a Leaf Using $^{11}CO_2$ and Positron Emitting Tracer Imaging System ····· 131
N. Kawachi, K. Sakamoto, S. Ishii, S. Fujimaki, N. Suzui, N. S. Ishioka and S. Matsuhashi

3-64 Production of Radioisotopes for Nuclear Medical Application ····· 132
T. Katabuchi, S. Watanabe, N. S. Ishioka, S. Matsuhashi, Y. Iida, H. Hanaoka and K. Endo

3-65 The Sensitivity Evaluation of Anticancer Drug Using In-Air Micro PIXE, The 21st Century COE Program 'Biomedical Research Using Accelerator Technology' ····· 133
H. Kuwano, H. Kimura, K. Okada, S. Ma, A. Faried, M. Sohda, M. Nakajima T. Sakai, M. Oikawa, T. Satoh and T. Kamiya

3-66 The Targeting of the Chemotherapeutic Agents or Radiosensitizer by Radiation, Using the Liquid Core Microcapsules ····· 134
S. Harada, S. Ehara, K. Ishii, H. Yamazaki, S.Matsuyama, T. Kamiya, T. Satoh and M. Oikawa

3-67 Fluorine Uptake into the Human Tooth from the Thin Layer of F-Releasing Material ····· 135
H.Yamamoto, M.Nomachi, K.Yasuda, Y. Iwami, S. Ebisu, H. Komatsu, Y.Sugaya, T. Sakai, M. Oikawa, T. Satoh and T. Kamiya

This is a blank page.

3-01 *Deinococcus radiodurans* DNA Repair-Promoting Protein: Applications to Biotech Industry

I. Narumi [a)], H. Ohba [a)], H. Sghaier [a,b)] and K. Satoh [a)]

[a)] Radiation-Applied Biology Division, QuBS, JAEA, [b)]Faculty of Engineering, Gunma University

Deinococcus radiodurans is a non-pathogenic eubacterium that habits various environments on Earth. The most striking feature of *D. radiodurans* is its extreme radiation resistance. It shows the highest resistance to ionizing radiation among all living organisms: 100-fold and more than 1000-fold resistance compared to *Escherichia coli* and human cell, respectively. Previous studies revealed that *D. radiodurans* possesses high capacity for repairing ionizing radiation-induced DNA damage[1)]. However, the mechanisms underlying its radioresistance had yet to be determined. In 1999, The Institute for Genomic Research, USA, determined the genome sequence of *D. radiodurans*. The genome analysis, however, did not clarify the radioresistance mechanisms of this bacterium[1)].

We investigated *D. radiodurans* in order to clarify what gene is important for radioresistance. By analyzing the DNA damage repair-deficient mutant, KH311 (Fig. 1), a unique radiation-inducible gene (designated *pprA* for pleiotropic protein promoting DNA repair) responsible for loss of radiation resistance was identified. PprA protein, product of the *pprA* gene, had no similarity to any other known proteins hitherto. Subsequent biochemical studies revealed that PprA protein preferentially bound to ionizing radiation-induced DNA strand breaks, inhibited *E. coli* exonuclease III activity, and stimulated the DNA end-joining reaction catalyzed by ATP-dependent and NAD-dependent DNA ligases, thereby promoted DNA repair process at high efficiency. These results suggest that *D. radiodurans* has a radiation-induced non-homologous end-joining repair mechanism in which PprA plays a critical role[2)].

DNA cloning is one of the most frequently used methods in genetic engineering. DNA ligase is required to clone nucleic fragments into a DNA vector. Many biotech reagent manufacturers industrialize DNA ligase as a fundamental reagent. Therefore, we considered that a new biotech reagent would be developed by a combination of DNA ligase and PprA proteins. As a result of the transfer of technology, Nippon Gene Co., Ltd., Toyama, Japan, who licensed from our institute, released in November 2005 a new product "TA-Blunt Ligation Kit" which uses the PprA technology (Fig. 2). The newly released kit including the PprA technology is specialized in the ligation of PCR products and blunt-ended DNA fragments with which ligation was generally difficult. The inclusion of the PprA technology provides 10-fold increase in ligation efficiency compared to conventional products. Hereafter, a broad-ranging utilization of the PprA technology is expected in genetic engineering fields including genetic diagnosis and medication development.

References

1) I. Narumi, Trends. Microbiol. 11 (2003) 422.
2) I. Narumi et al., Mol. Microbiol. 54 (2004) 278.

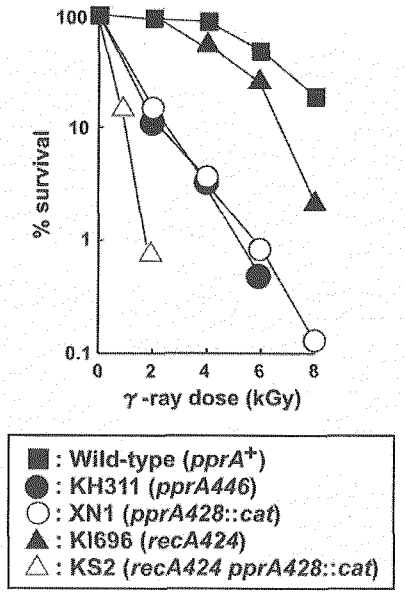


Fig.1 Sensitivity of *D. radiodurans* strain KD8301 (wild type), KH311 (*pprA* mutant), XN1 (*pprA* disruptant), KI696 (*recA* mutant) and KS2 (*recA* mutant plus *pprA* disruptant) to γ-rays. The percentage survival for each strain over the indicated range of doses was determined, and the mean from three independent experiments was plotted.



Fig.2 A highly-efficient DNA ligation kit "TA Blunt Ligation Kit" using the PprA technology which was released from Nippon Gene Co., Ltd., Toyama, Japan.

3-02 The Radiation Responsive Promoter of the *Deinococcus radiodurans pprA* Gene

H. Ohba [a], K. Satoh [a], T. Yanagisawa [b] and I. Narumi [a]

[a]Radiation-Applied Biology Division, QuBS, JAEA, [b]Faculty of Agriculture, Utsunomiya University

Abstract

In a previous study, we identified a novel radiation-inducible protein PprA that plays a critical role in the radiation resistance of *Deinococcus radiodurans*[1]. Despite the interest in mechanisms underlying radiation responses in *D. radiodurans*, little is known about the radiation responsive promoter for radiation-inducible proteins. In the present study, we constructed luciferase transcriptional fusions in an effort to delineate the upstream region of the *pprA* gene and to define the promoter region required for the induction of *pprA* expression following irradiation. This work provides useful insights into the radiation response mechanisms of *D. radiodurans*.

Introduction

放射線抵抗性細菌デイノコッカス・ラジオデュランスの優れたDNA二本鎖切断修復には、DNA損傷が生じた後に合成されるタンパク質が必要である。これまでに、デイノコッカス・ラジオデュランスの放射線抵抗性に中心的役割を担う新規放射線誘導タンパク質 PprA を同定した [1]。しかし、放射線応答の分子機構を明らかにすることが重要であるにもかかわらず、放射線誘導性タンパク質の放射線応答プロモーターについてはほとんど明らかにされていない。そこで本研究では、*pprA* 遺伝子プロモーターの放射線応答機構について解析を行った。

Methods

まず、*pprA* 遺伝子の転写開始点をプライマーエクステンション法により解析を行った。次に、放射線応答に関与するプロモーター領域の解析を行うために、大腸菌・ラジオデュランス間シャトルベクターにレポーターとしてルシフェラーゼ遺伝子を導入し、プロモーター活性測定用のレポーターベクターpRADN2 及び pRADN4 を構築した (Fig. 1.)。このベクターに *pprA* 遺伝子プロモーターフラグメントを挿入し、放射線照射後の *pprA* 遺伝子プロモーター活性の変動を解析した。さらに放射線応答機構の上位制御遺伝子と考えられている *pprI* 遺伝子 [2), 3)] を破壊し、*pprA* 遺伝子プロモーター活性に与える影響を解析した。

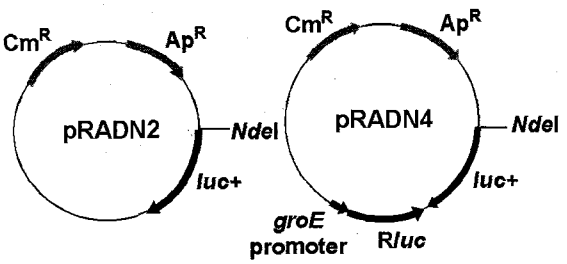


Fig. 1. Luciferase reporter vectors.

Results

プライマーエクステンション法により *pprA* 遺伝子の異なる3カ所の転写開始点 (-156、-154 及び-22) を同定した。さらに、これら 3 つの転写産物は放射線照射後の培養により転写産物量の増加がみられた。次に、放射線応答に関与するプロモーター領域を同定するため、ルシフェラーゼ遺伝子を用いたレポーターアッセイにより、放射線照射による *pprA* 遺伝子プロモーター活性の変動を解析したところ、遠位のプロモーターは-208 から-156 領域に、近位のプロモーターは-57 から-22 領域に存在すること、そして、-57 から-38 領域が最小必要プロモーター領域であることを明らかにした。さらに、部位特異的変異導入法による解析から、-33 位のチミンが放射線応答プロモーターの主要な塩基であることを明らかにした。さらに、*pprI* 遺伝子破壊株おいて *pprA* 遺伝子プロモーター活性がみられなかったことから、*pprA* 遺伝子の発現は *pprI* 遺伝子産物によりプロモーターレベルで制御されていることを明らかにした [4)]。

Discussion

今回構築したルシフェラーゼレポーターベクターは、プロモーター活性の解析において非常に有用であった。今回発見した *pprA* 遺伝子の二つの放射線応答プロモーターは、大腸菌のシグマ 70 配列とは全く異なることがわかり、さらに、デイノコッカス・ラジオデュランスにおいても、相同配列は確認できず、*pprA* 遺伝子特有の配列であることが明らかになった。

これまでの解析により PprI タンパク質は放射線応答機構の上位制御因子であると考えられているが、その詳細な機能は未だ解明されていない。本研究では PprI タンパク質が転写レベルで *pprA* 遺伝子プロモーターを制御していることが明らかになった。しかし、我々が行った精製 PprI タンパク質を用いた予備的実験により、PprI タンパク質と *pprA* 遺伝子の放射線応答プロモーター領域との結合は確認できなかった。本研究で同定した *pprA* 遺伝子の放射線応答プロモーターは、今後デイノコッカス・ラジオデュランスの放射線応答機構を全容解明していく上で非常に役立つであろう。

Reference

1) I. Narumi, et al., "PprA: a novel protein from *Deinococcus radiodurans* that stimulates DNA ligation", Mol. Microbiol., 54, 278 (2004).

2) A. M. Earl, et al., "The IrrE protein of *Deinococcus radiodurans* R1 is a novel rebulator of recA expression", J. Bacteriol., 184, 6216 (2002).

3) Y. Hua, et al., "PrI: a general switch responsible for extreme radioresistance of *Deinococcus radiodurans*", Biochem. Biophys. Res. Commun., 306, 355 (2003).

4) H. Ohba, et al., "The radiation responsive promoter of the *Deinococcus radiodurans pprA* gene", Gene, 363, 133 (2005).

3-03 Detection Method for Irradiated Foods Using ESR

M. Ukai[a, b], M. Matsuura[a], T. Kume[c], Y. Kobayashi[d], M. Kikuchi[d] and T. Sakashita[d]

[a] Hokkaido University of Education, [b] CREST-JST, [c] TARRI, JAEA
[d] Radiation-Applied Biology Division, QuBS, JAEA

Abstract

By electron spin resonance (ESR) spectroscopy, we revealed free radicals in irradiated foods. The representative ESR spectrum of irradiated food is composed of a sextet centered at g = 2.0, singlet at the same g-value and a singlet at g = 4.0. The first signal is attributable to a signal with hyperfine interactions of the Mn^{2+}. The second signal is due to an organic free radicals. The third signal may be originated from the Fe^{3+}. Upon γ-irradiation, new signals appeared. For the measure of irradiation effects, we proposed an advanced protocol for ESR detection of irradiated foods.

食品は保存時に微生物汚染されやすいため殺菌方法について多くの検討がなされてきた。放射線照射は効果的な殺菌法として国際的に認められている[1]。殺菌に必要な照射量は食品中の温度をほとんど上げない。そこで低温殺菌と称される。食品照射は食品の色や香りの劣化を最小限に留めることができる効果的な殺菌方法である。電子スピン共鳴（ESR）法は、放射線照射食品に関する品質表示の正しさを担保する検知技術に応用されており、EU では公定法として導入し照射の有無の判別を行っている。本研究では、照射誘導ラジカルの飽和挙動[2-4]を ESR により詳細に検討し、新規の照射食品検知法を確立した。

試料は胡椒、緑茶、紅茶、小麦粉、朝鮮人参、ネギ、パセリを用いた。照射はγ線を用い原研高崎研（現・日本原子力研究開発機構高崎量子応用研究所）において、5, 10, 30, 50kGy の各照射量で実施した。試料は 300mg を秤取、ESR 試料管（99.9%石英ガラス）に封入した。ESR 測定は ESR 分光器（JES-FE1XG, 日本電子 KK）を用い、マイクロ波の周波数は X バンド（9.3GHz）、共鳴磁場は 250 と 320 mT、掃引磁場は 500 と 100 mT とした。マイクロ波磁場を変化させ遂次飽和曲線を求める PSB 法[2]により電子スピン飽和挙動を検討した。

Fig. 1 に典型的な照射黒胡椒粉末試料の ESR 信号を示す。ESR 信号は胡椒の種類や形状に関わらず本質的に同一であった。本スペクトルは全長 500 mT の外部磁場掃引によって測定された。胡椒の ESR 信号は 3 成分であった。第一に、P_1で示した g = 2.0 における鋭く強い信号であり、これは有機フリーラジカルによる。第二に g = 2.0 を中心とする六本線（P_2）であり、これは Mn^{2+}イオンによる超微細構造線と同定できる。P_3で示した g = 4.0 の信号は Fe^{3+}による遷移金属イオンによるものである。P_2、P_3 の信号は観測されない試料もあったが、P_1 信号はすべての試料で観測された。照射量が増加するに従い P_1 の信号強度は強くなり、さらに P_1 に対称な位置に新規の信号（S_1、S_2）が得られた。試料によっては P_1 の高磁場側に S_1S_2 を観測した。これは triplet と推測される。S_1S_2信号は照射の判別に有用である。遂次飽和曲線から最大の ESR 信号強度（閾値）を与えるマイクロ波磁場を見出すことができた。この閾値を用い外挿法[2]により食品照射履歴を推定できた。本法は新規の厳密なる検知法として評価できた。

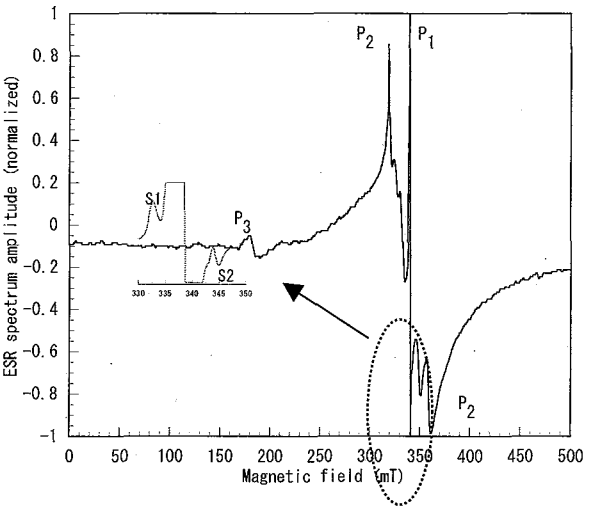


Fig.1 ESR spectra of the irradiated black pepper. The main signal was recorded by the magnetic field swept from 0 to 500 mT. The insert is an enlarged display to demonstrate the satellite peaks.

References

1) R. A. Molirs, Food Irradiations, John Wiley, p. 1 (2001).
2) M. Ukai, et al., "An ESR protocol based on relaxation phenomena in irradiated foods", Spectrochemica Acta, 63, 879 (2006).
3) M. Ukai, et al., "Free radicals in irradiated pepper: an electron spin resonance study", Appl. Magn. Reson., 24, 1 (2003).
4) M. Ukai, et al., "An electron spin resonance study of radical decay in γ-ray irradiated pepper by thermal treatments", Appl. Magn. Reson., 25, 95 (2003).

3-04 Detection of Oxidative DNA Damage Using Anti-8-OHdG Antibody -A Useful Method to Distinguish Irradiated Foods-

M. Kikuchi, A. Z. Mohd Dzomir[#], C. R. Gunawardane[$], M. K. Alam[*] and Y. Kobayashi

Radiation-Applied Biology Division, QuBS, JAEA

Abstract

Ionizing radiation has been used for reducing food losses and securing food safety. The development of versatile detection methods of irradiated foods is needed for appropriate management. In an effort to distinguish between irradiated and non-irradiated meats, a detection method of oxidative DNA base damages using chemiluminescence enzyme-linked immunosorbent assay with anti-8-hydroxy-2'-deoxyguanosine antibody was developed. The procedure of this method is not so complicated, and relatively short time is needed to obtain results without special techniques. For most of all foods containing DNA, this novel method should be applicable to detect the damaged DNA of irradiated foods. Application to beef meat irradiated with 3 kGy or higher was suggested to be detectable successfully.

食品照射は、食品や農産物に放射線を照射して殺菌、害虫駆除、芽止めなどを行うものである[1)]。我が国では世界に先駆けて照射によるジャガイモの芽止めが実用化されたが、これ以外には許可されていない[2)]。しかし諸外国で食品照射は食糧・農産物の保存と損耗防止及び食品の衛生化や食中毒防止に役立つ技術として、一般的に利用されるようになっている[3)]。今後予想される照射品目拡大に対応して、消費者の選択の自由の保障と適切な流通管理のために照射食品の検知法(照射履歴線量推定法)が必要である。すでにESR法[4)]やTL法[5)]などいくつかの検知法が開発され、EUの標準分析法等に採択されているが、高価な装置や熟練した技術が必要とされるなど、どれも一長一短がある。我々は、食品素材が共通に持つ成分の放射線による変化を照射食品識別の指標とすることを考え、DNA塩基損傷の主要な生成物のひとつである8-hydroxy-2'-deoxyguanosine (8-OHdG) を指標にした簡便な新規検知法の開発を行なった。

試料中の8-OHdG検出には酵素免疫測定法 (ELISA) を用いた。1次抗体として抗8-OHdG抗体を、2次抗体としてHorseradish peroxidase標識の抗マウス抗体を用い、検出は化学発光基質を用いて、Lumi-Imager F1で測定・定量を行なった。最初に、修飾塩基として8-OHdGを含むオリゴDNA、それを含まないオリゴDNAとその相補鎖DNAを合成し、反応の条件検討を行った。次に、市販の挽肉を購入し、高崎量子応用研究所のコバルト線源を用いて氷中で0～12 kGyの照射を行った。照射後の肉類は零下20℃の冷凍庫で保管し、DNA調製時に液体窒素下で磨砕後、DNeasy Tissue Kitを用いてゲノムDNAを分離し、ELISAに供した。

市販の抗8-OHdG抗体は、DNAを加水分解したヌクレオシドの8-OHdGと特異的に反応するとされている[6)]。この抗体を用いて高分子DNA中の8-OHdGの検出が可能かを検討するため、合成オリゴDNAをELISAで検出した結果、この抗体は合成オリゴDNA中の8-OHdGにも結合する事が確認された (Fig.1)。そこで、8-OHdGに対するELISAの実用性を検討するため、ガンマ線照射した食肉からDNAを分離して8-OHdG検出を行なった。その結果、吸収線量の増加とともにELISAによる化学発光が増加している事が確認され (Fig.2)、非照射肉から分離したDNAのシグナルと比較する事により3 kGy以上照射した食肉類の識別が可能であると考えられた。

今回開発したELISAによる8-OHdG検出法は、DNAを加水分解しないで検出できる方法であり、生物に普遍的に存在するDNAに生じた損傷を指標とするので汎用性があり、実験操作は簡便で多サンプルを同時に検出できる事から、照射食品のスクリーニング法として利用可能と考えられる。

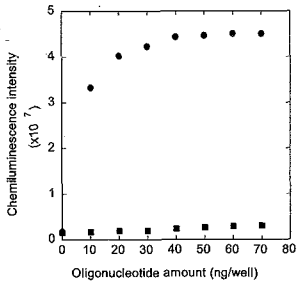


Fig.1 Chemiluminescence intensities between oligonucleotides corresponding to presence (●) and absence (■) of 8-OHdG.

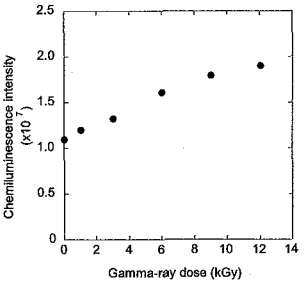


Fig.2 Detection of 8-OHdG in DNA isolated from irradiated beef using ELISA. Chemiluminescence intensity was increased with increasing doses.

References

1) International Consultative Group on Food Irradiation, "Facts about food irradiation" (1999).
2) 内海和久, "馬鈴薯芽止め事業30年目の現状紹介"食品照射 38, 73 (2003).
3) International Atomic Energy Agency, "Acceptance, control of and trade in irradiated food" (1989).
4) European Committee for Standardization, EN1786 (1996).
5) European Committee for Standardization, EN1788 (2001).
6) S. Toyokuni, et al. "Quantitaitve immunohistochemical detection of 8-hydroxy-2'-deoxyguanosine by a monoclonal antibody N45.1: its application to ferric nitriloacetate-induced renal carcinogenesis model", Lab. Invest. 76, 365 (1997).

MEXT研究員所属先
[#] MINTec-Sinagama, MINT, Malaysia.
[$] Institute of Post Harvest Technology, Sri Lanka.
[*] Institute of Food and Radiation Biology, BAEC, Bangladesh.

3-05 Application of Hydrogel on Wound Dressing and Future View of Hydrogel

F. Yoshii
Industrial Collaboration Promotion Department, JAEA

Abstract

Radiation crosslinked poly (vinyl alcohol) (PVA) hydrogel sheet was applied as a wound dressing to accelerate healing. The dressing was commercialized in July 2004. Furthermore, PVA gel protector to prevent shoe sore was commercialized. It was found that polysaccharide derivatives such as carboxymethylcellulose (CMC) undergo crosslinking under ionizing irradiation at high concentration, so called paste-like conditions. High degree of substitution (maximum 2.2) and high polymer concentration promote crosslinking.

1．ハイドロゲル創傷被覆材

創傷被覆材は、傷をシート状の材料で覆い外からの雑菌の混入を防止し、新生皮膚の生長を促進する製剤である。従来の傷の治療法は乾燥させ「かさぶた」を作るため、浸出液中の治癒因子が水分の蒸発により固まり失活し、新生皮膚は「かさぶた」の下から成長する。これに対し、ハイドロゲルで覆った湿潤環境では、治癒因子を含む滲出液を創面に保持できるため、治癒が円滑に進み、乾燥環境よりも治りが早くなる。最近このような湿潤環境の治療法が、有効とされてきている。

電子線橋かけ技術により開発した水分を多量に含む高強度で耐熱性のあるポリビニルアルコール（PVA）ハイドロゲルシートをモルモットの背部につくった2cm四方の傷に貼り、乾燥環境で治療するガーゼの場合と治癒の挙動を比較すると、傷はハイドロゲルの方が、ガーゼよりも治りが早く、傷に固着しないなどの特長があることを見出した。

これを医療用具として、事業化に発展させるため平成8年に科学技術振興事業団（現在の（独）科学技術振興機構、JST）の委託開発事業によりニチバン株式会社とハイドロゲルの連続生産システムの構築を目指し共同開発を行なった。ハイドロゲル素材のゲル強度、膨潤性及び安全性の確認、製造プロセスの確立、実製造機から得たハイドロゲルシートを用いた病院での臨床試験を行い良好な結果が得られた。これを基に厚生労働省から医療用具製造の承認を平成16年2月に受け商品名「ビューゲル」を製品化した[1]。同じゲルシートを用い靴擦れ（マメ）を防止するジェルプロテクターを同じ年に製品化した。

2．多糖類誘導体ハイドロゲルの合成とその特質

デンプンやセルロースのような多糖類及びその誘導体は放射線照射では分解のみが起き、放射線加工による有用な改質法はなかった。しかし、エーテル型誘導体の材料を「うどんや蕎麦」を作るときのように水と良く練り流動性のないペースト状で照射を行なうと橋かけ反応が起こることを見出した。CMCの置換度が1.3の橋かけ挙動をFig. 2 に示す[2]。ポリマー濃度が5%程度の水飴状の高粘度液体では分解が起き、濃度を上げ半固体状（10%以上）の照射で橋かけ反応が起こる。これを水に漬けると、吸水し高分子吸収体になる。CMCは、カルボキシメチル基の置換度が最も高い2.2であると60%という高い濃度でペース状試料を調整することができ橋かけ反応を行なうことができる。照射後乾燥したゲルは、水を400倍、生理食塩水を100倍吸水でき生分解性でもあることから、この特長を生かした販路の拡大を目指している。



Fig.1 Hydrogel wound dressing.

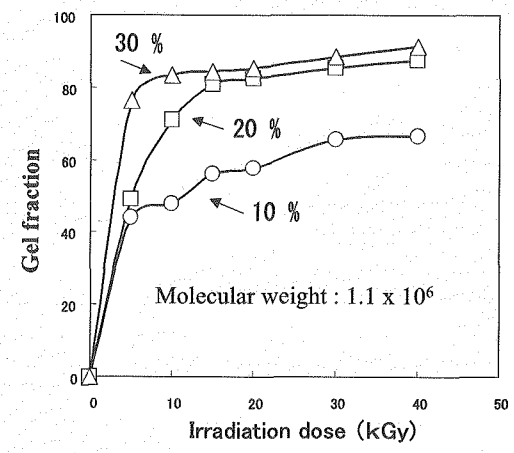


Fig.2 Radiation crosslinking of CMC at high concentration.

References

1) 磯部一樹、EBを利用したハイドロゲル創傷被覆材「ビューゲル」、コンバーテック、No.12, 58 – 61 (2004)

2) B.Fei, R.A.Wach, H.Mitomo, F.Yoshii, T.Kume, Hydrogel of biodegradable cellulose derivatives. I. Radiation-induced Crosslinking of CMC, J. Appl. Polym., Sci., **78**, 278 – 283 (2000).

3-06 Development of an Efficient Method for Mutation Induction in Plants

Y. Hase, Y. Yokota, I. Narumi and A. Tanaka

Radiation-Applied Biology Division, QuBS, JAEA

1. Introduction

The extensive analyses using model plant Arabidopsis showed that the ion beams have higher mutation frequency compared to low-LET radiations[1]. It was also shown that the ion beams frequently induce deletion-type mutations[2]. Furthermore, application of the ion beams for mutation breeding of new carnation and chrysanthemum varieties demonstrated that the ion beams have wide mutation spectrum and the ion beams can induce mutants without undesirable defects[3]. However, there are still unclear points in mutagenic effects of ion beams, that is, (1) Relationship between the property of ion beams and the mutation frequency or spectrum, e.g., which is better between carbon ion and helium ion for mutagenesis?, (2) Difference of the mutagenic effect when different tissue was used, e.g., which is better between leaves and petals as a material?, and (3) Mechanism for why the recessive homo mutants, such as chlorophyll deficient mutants, were obtained in the irradiated generation. In order to investigate these subjects, the experimental system that can detect a large number of mutations in vivo is needed. We have reported that the deletion-type mutation can be directly detected using long PCR technique[4]. Here, we tried to identify mutations in vivo using a marker gene.

2. Experimental procedure

The pPZP121 plasmid that harbors 35S::GFP (green fluorescence protein) construct was transformed into the wild-type Arabidopsis. Based on the segregation ratio and the southern blotting analysis, the transgenic plant homozygous for single insertion of T-DNA was obtained. The seeds of this line were sown on MS medium. At 3 days after sowing, they were exposed to the 320 MeV carbon ions with the dose of 0 ~ 100 Gy. Then, they were transplanted on rockwool. The GFP fluorescence was observed 1 month after irradiation.

3. Results and Discussion

The transgenic plants that continuously express GFP were exposed to the carbon ions at three days after seed sowing. It is expected that the GFP fluorescence disappear in part of these plants if the GFP gene was mutated. Actually, the GFP fluorescence disappeared in one plant derived from 15 Gy-irradiated 69 seedlings and in one of 43 control plants. In these plants, the expression of GFP gene was repressed only in the aboveground tissues, and the GFP fluorescence was retained in the roots of these plants. The 577 plants derived from dry seeds irradiated with 150 Gy of carbon ions were also observed but we could not identify the GFP fluorescence-disappeared plants. We concluded it is difficult to investigate large number of mutations by this method. The other marker genes in that the mutations can be positively selected will be used in the future experiment.

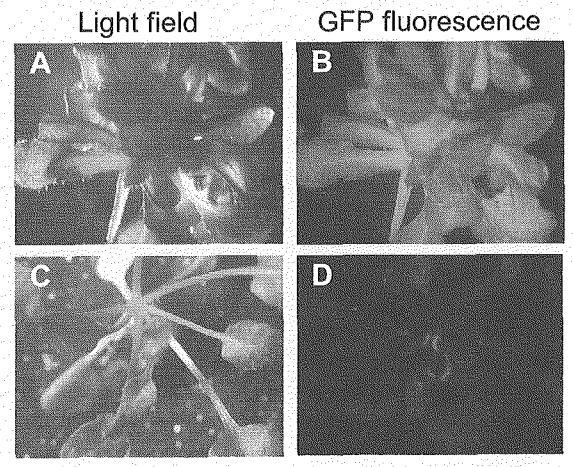


Fig.1 A, B; Control plants that continuously express green fluorescence protein (GFP). C, D; Transgenic plants in that the GFP fluorescence disappeared.

References

1) N. Shikazono et al., Genetics 163 (2003) 1449.
2) N. Shikazono et al., Genetics 157 (2001) 379.
3) M. Okamura et al., Nuc. Instr.Meth. B 206 (2003) 574.
4) Y. Hase et al., TIARA annual report 2004 (2005) 94.

3-07 DNA Damage Yields in Hydrated DNA after He Ion-Irradiation

A. Urushibara, N. Shikazono, K. Fujii and A. Yokoya

Advanced Science Research Center, JAEA

Ionizing radiation causes various types of DNA lesions, such as strand breaks, base lesions and, in particular, biologically relevant complex damage known as cluster damage sites, which consist of two or more elemental lesions within one or two helical turns of DNA [1]. Clustered DNA damage sites are considered to be less readily repaired than isolated lesions and therefore may induce serious genetic changes in living cells. The complexity of clustered damage is proposed to increase on increasing the ionizing density of the radiation (LET). The direct effect of low LET radiation is considered to produce 30-40% of the lesions in cells[2]. This value is known to reach 70% when cells are irradiated with α-particles[2]. Few investigations have been systematically undertaken to elucidate the nature of lesions produced by the direct effects of radiation with varying ionizing density.

To gain insights on the nature of lesions induced by the direct effect of the radiation, yields of single- and double-strand breaks (ssb's and dsb's), and base lesions for hydrated plasmid DNA were measured after exposure to He ion particles with varying LETs. The use of hydrated DNA eliminates the indirect effect of radiation arising from irradiation of bulk water. Base lesions were detected as the additional strand breaks after treatment of irradiated DNA with two glycosylases, Nth and Fpg proteins, which convert the oxidative base lesions into an ssb.

The yield of prompt ssb after exposing hydrated plasmid DNA to He ion particles with a LET of 19 keV/μm is 6.85 X 10^{-11} ssb/Gy/Da (Fig. 1). The yield is found to be similar for He ion particles with LETs of 63 and 95 keV/μm. This value of around 7 X 10^{-11} ssb/Gy/Da is comparable to that obtained after γ- irradiation [3]. While the yield of prompt ssb does not alter with varying LET values from 19-95 keV/μm, the yield of prompt dsb increases as the LET increases (Fig. 2). Consequently, the ratio of prompt ssb to dsb decreases as the LET increases, indicating that strand breaks in close proximity, which would produce dsb's, are more readily induced at higher LET.

Results of enzymatically induced ssb/dsb reveal that the amount of base lesions susceptible to cleavage by Nth and/or Fpg becomes less as the LET gets higher (Fig. 1 and Fig. 2). Although we cannot fully disregard the possibility that the number of damaged bases is actually reduced at higher LET, we favor the interpretation of base lesions being clustered and thus becoming less readily cleaved by the glycosylases. Inhibition of excision of damaged bases within a cluster has been indeed demonstrated using purified enzymes[4]. When samples are irradiated with the same dose, an increasing fraction of plasmids are unirradiated, and therefore undamaged, with increasing LET since fewer particles are needed to deposit the same amount of energy. This fact may also make the detection of enzymatically induced ssb's difficult in the current assay.

In summary, we propose that DNA lesions in hydrated plasmids become more readily clustered with increasing LET of the radiation.

References

1) Goodhead, D. T. Int. J. Radiat. Biol. 65 (1994) 7.
2) de Lara, C. M., et.al, P. Radiat. Res. 144 (1995) 43.
3) Yokoya, A., et.al. Am. Chem. Soc. 31 (2002) 8859.
4) Weinfeld, M.,et.al. Radiat. Res. 156 (2001) 584.

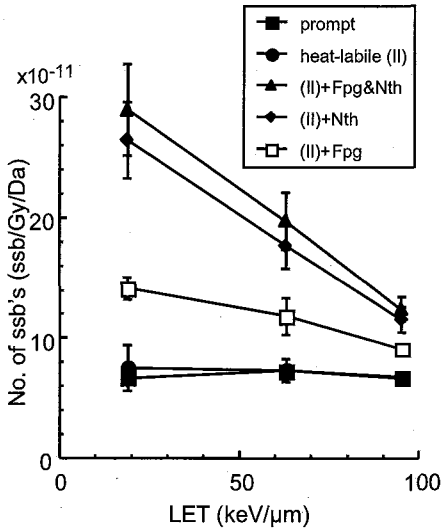


Fig.1 LET dependence of the yields of prompt and enzymatically induced single strand breaks.

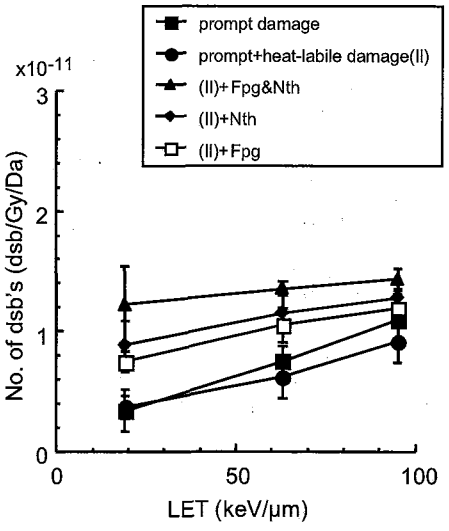


Fig.2 LET dependence of the yields of prompt and enzymatically induced double strand breaks.

3-08 Study of Molecular Mechanism of Ion Beam Induced Mutations in the *Saccharomyces cerevisiae*

Y. Matuo[a)], S. Nishijima[a)], Y. Hase[b)], A. Sakamoto[b)], A. Tanaka[b)] and K. Shimizu[c)]

[a)] Graduate School of Engineering, Osaka University, [b)]Radiation-Applied Biology Division, QuBS, JAEA, [c)]Radioisotope Research Center, Osaka University

Breeding technology using mutations induced by ion beam irradiation has undergone major developments, and has been applied in various fields. In this study, the budding yeast *Saccharomyces cerevisiae* was used as a model eukaryotic organism to elucidate the molecular mechanism of the mutagenesis caused by ion beams. The resultant mutation sites were identified and their mutation spectrums were compared with those of mutation sites induced by gamma-rays.

S. cerevisiae strains used in this study were S288C(*RAD*$^{+}$), G160/2b(*rad52*). The yeast strains were irradiated with carbon ions ($^{12}C^{5+}$; 220 MeV) with the dose 10 to 300 Gy, and LET is 107 keV/μm. Carbon ion beam was generated from AVF cyclotron in JAEA. Selection of *ura3* cells was accomplished by plating the cells on the media containing 5-fluoroorotic acid [1)]. The mutation sites of *ura3* mutants were determined by DNA sequencing.

The results show that the optimum dose for mutagenesis by carbon ion beams is 100 Gy. The ion beams at 100 Gy generate mutations 168.5 fold more than spontaneous mutation. The *URA3* regions (804bp) of mutants were sequenced. Mutations generated by ion beams were dominantly transversion, whereas mutations of spontaneous generation were mainly transition. The transversion / transition ratio in the *WILD* type was 5.0 and the ratio in the *rad52* type was 4.0 (Table 1).

Moreover, the fact that GC to TA transversions largely observed suggests that the mutations by ion beams resulted from oxidative damage such as formation of 8-oxodGTP mainly[2)].

The remarkable feature of yeast mutations induced by carbon ions was that the mutation sites were localized near the linker regions of nucleosomes, whereas mutations induced by gamma-ray irradiation were located uniformly throughout the gene. The mutation sites are localized on several regions with 170bp to 186bp interval. Yeast nucleosomes are very closely spaced, with a repeat length of 162±6bp, resulting in a linker length of only 15-20 pb, and their precise chromatin structure has been characterized. This interval may correspond to nucleosome structure[3)].

An important advantage of a forward mutation system such as the one used here is its ability to identify the mutational sequence context. While there were no specific sequence contexts in the carbon-ion induced mutations, C residues in the 5'-AC(A/T)-3' sequence had a tendency to change (Table 1, 21 of 51 mutations).

Additionally, we obtained no large deletions and duplications, whereas ion-induced mutations in *Arabidopsis thaliana* were mainly short deletions and rearrangements[4)].

References

1) D. Burke, et al., in 'Methods in Yeast Genetics' Cold Spring Harbor Laboratory Press (2000) pp7-15
2) H. Kasai et al., Analysis of a form of oxidative DNA damage, 8-hydroxy-2'-deoxyguanosine, as a marker of cellular oxidative stress during carcinogenesis, Mutat. Res. 387 (1997) 147-163.
3) C.L. White et al., Structure of the yeast nucleosome core particle reveals fundamental changes in internucleosome interactions, EMBO. J. 20 (2001) 5207-5218.
4) N. Shikazono et al., Analysis of mutations induced by carbon ions in *Arabidopsis thaliana*, J. Exp. Bot. 56 (2005) 587-596.

Table 1 Type of mutation induced by carbon-ion and gamma-ray irradiations.

Mutations class	Ion Beam *Wild* type		Ion Beam *rad52* type		Gamma ray *Wild* type		Gamma ray *rad52* type	
	Number	Percentage	Number	Percentage	Number	Percentage	Number	Percentage
Total	**51**	**100.0%**	**32**	**100.0%**	**31**	**100.0%**	**24**	**100.0%**
Base substitution								
Transitions	**7**	**13.7%**	**6**	**18.8%**	**6**	**19.3%**	**6**	**25.0%**
GC : AT	**7**	**[100%]**	**6**	**[100%]**	**6**	**[100%]**	**4**	**[67%]**
AT : GC	0	[0%]	0	[0%]	0	[0%]	2	[33%]
Transversions	**35**	**68.6%**	**24**	**75.0%**	**21**	**67.8%**	**13**	**54.1%**
GC : TA	**21**	**[63%]**	**19**	**[79%]**	**13**	**[62%]**	**6**	**[47%]**
GC : CG	**12**	**[31%]**	**3**	**[13%]**	**3**	**[14%]**	**2**	**[15%]**
AT : CG	1	[3%]	1	[4%]	5	[24%]	3	[23%]
AT : TA	1	[3%]	1	[4%]	0	[0%]	2	[15%]
Del. And Insertion	**9**	**17.6%**	**2**	**6.2%**	**4**	**12.9%**	**5**	**20.9%**

3-09 Quantitative Analysis of DNA Double-Strand Breaks in Tobacco Protoplasts Irradiated with Helium, Carbon and Neon Ion Beam

Y. Yokota[a)], S. Yamada[b)], Y. Hase[a)], N. Shikazono[a, c)], I. Narumi[a)], A. Tanaka[a)] and M. Inoue[b)]

[a)] Radiation-Applied Biology Division, QuBS, JAEA, [b)] Graduate School of Agriculture, Kyoto Prefectural University, [c)] Advanced Science Research Center, JAEA

Ion beam has large biological effects such as mortality, chromosome aberration and mutation in plants compared with low-LET radiation. However, the mechanism of DNA damages is unclear until now. In this study, initial induction of DNA double-strand breaks (DSBs), the most lethal DNA damages induced by radiation, was quantitatively analyzed in tobacco protoplasts irradiated by ion beams with different linear energy transfers (LETs).

Protoplasts were prepared from tobacco BY-2 cells according to the previous report[1)] and irradiated by gamma rays, helium, carbon and neon ions. Physical properties of radiation are shown in Table 1. After lysis of irradiated protoplasts in a proteinase buffer, DNA fragments that were generated by radiation-induced DSBs were separated between 1.6 Mbp and 6.6 kbp by a pulsed-field gel electrophoresis. The electrophoresis pattern of the DNA fragments was visualized by staining with SYBR Green I, and the image was recorded using a CCD video camera. From the image, the number (=DSB yield) and size (=interval between neighboring DSBs) of DNA fragments were obtained according to the report[2)].

The number of DSBs (Gbp^{-1}) linearly increased in the dose-range between 0 and 2000 Gy. DSB yields Gbp^{-1} Gy^{-1} depended on LET and the relative biological effectiveness reached maximum at 124 and 241 keV/μm carbon ions (Fig. 1). In normal human fibroblasts irradiated with nitrogen ions, the RBEs based on initial DSB yields reached maxima at LETs of 80 and 125 keV/μm and gradually decreased at 175 and 225 keV/μm[2)]. These results suggest that LETs required for maximal RBEs are higher in tobacco cells than in human cells, although it must be considered that the ion species are different between these studies. This suggestion may be explained by the following idea: DSBs are difficult to induce through radicals in tobacco protoplasts and the LETs needed to induce DSBs efficiently are higher in tobacco protoplasts than in human cells. The DNA fragmentation patterns of gamma rays and helium ions were almost the same as the random fragmentation pattern (Fig. 2, panel A). This means that low-LET radiation randomly induces DSBs on tobacco chromosomes. On the contrary, the DNA fragmentation patterns of carbon and neon ions were different from that of gamma rays, and they yielded short DNA fragments more frequently than gamma rays (panels B and C). This suggests that high-LET carbon and neon ions induce more closely spaced DSBs on tobacco chromosomes than do gamma rays by interactions between an ion track structure and higher-order chromatin structure. From these results, it is considered that the difference in initial induction of DSBs is one of the causes giving the large biological effects to high-LET ion beams.

References

1) Y. Yokota et al., Radiat. Res. 163 (2005) 520-525.
2) E. H glund et al., Int. J. Radiat. Biol. 76 (2000) 539-547.

Table 1. Physical properties of radiation.

Radiation	Sample type	Incident energy [a] (MeV/amu)	LET (keV/um) [a] Mean	Range
Gamma rays	Plug	-	0.2	0.2 - 0.2
Helium ions	Plug	24.7	9.4	8.9 - 10.1
	Suspension	11	17.7	17.5 - 17.9
Carbon ions	Plug	25.9	94.8	76 - 126
	Suspension	15	124	121 - 127
	Suspension	7.2 [b]	241	217 - 269
	Suspension	4.4 [b]	431	315 - 657
Neon ions	Suspension	11.4	440	411 - 473

[a] In the cell position.
[b] Modulated using nickel plates as an absorber.

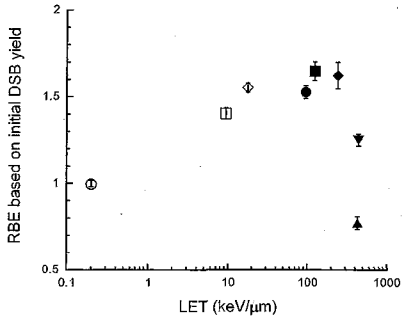


Fig. 1 LET-RBE relationship for initial DSB yields (Gbp^{-1} Gy^{-1}). Each symbol means 0.2 keV/μm gamma rays (○), 9.4 (□) and 17.7 (◊) keV/μm helium ions, 94.8 (●), 124 (■), 241 (♦) and 431 (▲) keV/μm carbon ions, and 440 keV/μm neon ions (▼).

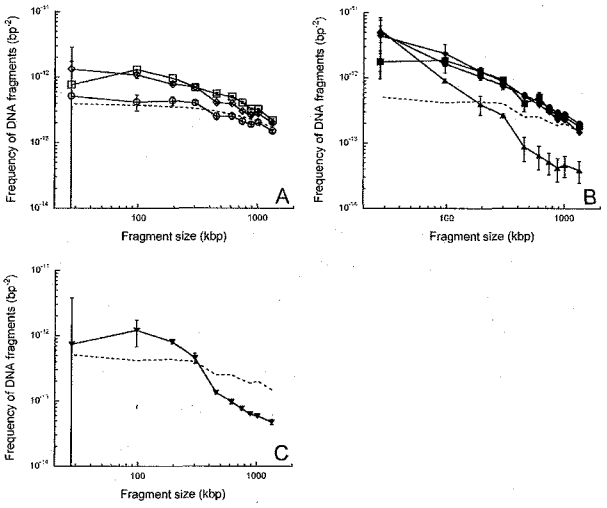


Fig. 2 Relationship between the frequency of DNA fragments at 200 Gy and fragment size for gamma rays and helium ions (panel A), carbon ions (panel B) and neon ions (panel C). Symbols are same as Fig. 1. In panel A, the random fragmentation pattern is depicted as the dotted line. In panels B and C, the fragmentation pattern of gamma rays is shown as the dotted line.

3-10 Comparison of the Mutation Inducing Effect between Ion Beams and Gamma Ray

R. Morita[a)], T. Morishita[a)], H. Nakagawa[a)], M. Nishimura[a)], H. Yamaguchi[b)], Y. Yokota[c)], Y. Hase[c)], and A. Tanaka[c)]

[a)]National Institute of Agrobiological Sciences, [b)]National Institute of Floricultural Science,
[c)] Radiation-Applied Biology Division, QuBS, JAEA

Recently, accelerated ions has been used as a novel mutagen for various plant species. However, few studies of ion-induced mutation have been carried out in plants[1)2)]. In the present investigation, carbon ion and gamma ray induced wx mutants in rice were examined to reveal the mutation at the DNA levels.

Dry seeds of rice (cv. Nipponbare and Hitomebore) were irradiated with doses of 40 Gy (carbon ions) and 200-250 Gy (gamma rays). Six wx mutants were obtained from rice M2 and M3 seeds by screening with KI_2 staining (Table 1). Genomic DNA was extracted from dry seeds. Wx genes were amplified by using five pair of primers, because of the difficulties involved with PCR amplification of the whole gene using a single pair of primers. Mutants that generated 5 PCR fragments similar in size to those of wild type were classified as having point-like mutations, and mutants that generated no fragments were classified as having rearrangements (inversions, translocations, and large deletions).

A total of 3 independent carbon ion induced and 3 independent gamma ray induced mutants were analyzed. Of the 3 carbon ion induced mutants, 1 had point-like mutations and 2 had rearrangements. Of the 3 gamma ray induced mutants, 2 had point-like mutations and 1 had rearrangements.

Sequencing analysis revealed that all point-like mutants had deletion. G040-10H had a 6 bp deletion in the 5th exon. G041-11H had a 2 bp deletion in the 2nd exon, and C092-1E had a 4 bp deletion in the 12th exon, respectively (Fig 1). Because of all deletions were found in exon, we concluded that these deletions have induced wx mutation,

Rearrangements were examined by PCR analysis. In 03C32040Gy, bands were not generated when using primers F1 and R1, indicating that the rearrangement should be between primer F1 and primer R1. In 02C22040Gy, the rearrangement should be between primers F1 and R3. In 02 γ 200Gy, the rearrangement should be between F1 and R1.

It has been reported that carbon ions induced both point-like mutation and rearrangement in Arabidopsis[2)]. In this report, we have shown that same mutation can also be induced in rice.

References

1) K. Naito et al. Genetics 169 (2005) 881
2) N. Shikazono et al. J. Exp. Bot. 56 (2005) 587

Table 1 wx mutants used in this study

wx mutant lines	mutagen	original cultivar
G040-10H	gamma-ray	Nipponbare
G041-11H	gamma-ray	Nipponbare
02 γ 200Gy	gamma-ray	Nipponbare
C092-1E	Carbon ion	Hitomebore
03C32040Gy	Carbon ion	Hitomebore
02C22040Gy	Carbon ion	Hitomebore

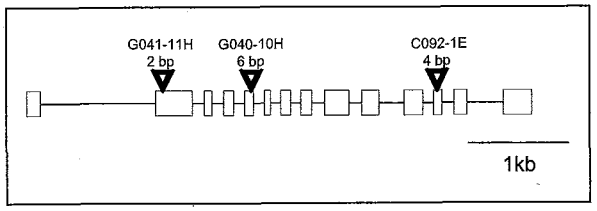


Fig. 1 Deletion in Wx gene. Boxes and horizontal lines indicate exons and introns of the Wx gene. Triangles indicate the positions of deleted nucleotides.

3-11 Molecular Analysis of Ion Beam-Irradiated Orchids

A. H. Affrida [a], A. Zaiton [a], A. Sakinah [a], B. Mohd Nazir [a], A. Tanaka [b], N. Shikazono[b], Y. Oono [b] and Y. Hase [b]

[a]Agrotechnology and Biosciences Division, Malaysian Institute for Nuclear Technology Research (MINT), [b] Radiation-Applied Biology Division, QuBS, JAEA

Mutation induction by ion beam provides an alternative for improvement of orchids. The protocorm-like bodies (PLBs) of two orchid species; *Dendrobium mirbellianum* and *Dendrobium crumenatum* were irradiated with 320 MeV $^{12}C^{5+}$ ions, accelerated by AVF Cyclotron at Japanese Atomic Energy Agency (JAEA), Japan, at various doses ranging from 0 to 12.0 Gray (Gy)[1]. Since no morphological change was detected, Amplified Fragment Length Polymorphism (AFLP) technique[2] was used to analyse the irradiated orchids. This PCR-based DNA fingerprinting technique involves digestion of DNA with restriction enzymes, ligation of adapter and selective amplification using primer with one (pre-amplification) and three (selective amplification) arbitrary nucleotides. The fingerprinting of the control and mutant lines were compared in order to detect their genetic difference.

AFLP assays were performed using AFLP Analysis System I (Invitrogen, USA) according to the manufacturer's instructions. Genomic DNA extracted from fresh leaf was digested with *Eco*RI and *Mse*I and ligated with *Eco*RI and *Mse*I adapter provided in the kit. DNA was amplified with *Eco*RI and *Mse*I primers followed by analysis with a denaturing 6% polyacrylamide gel electrophoresis and silver staining.

The three combinations of *Eco*RI and *Mse*I primers each with three arbitrary nucleotides used in this analysis were E-AGC & M-CTG, E-ACC & M-CTT and E-ACG & M-CAT. Primer sets E-AGC & M-CTG and E-ACG & M-CAT successfully produced fingerprinting in both species. No amplification was obtained with primer set E-ACC & M-CTT. (Table 1 and Fig. 1).

In *D. crumenatum,* polymorphisms were detected in all doses. The highest number of polymorphic bands was observed in DNA of seedlings irradiated at dose 4.0 Gy. However, DNA polymorphisms were also observed among the different unirradiated controls (data not shown). These unirradiated controls originated from seeds collected from different plants. It was reported that there are slight morphological differences in the flowers of these plants. The polymorphisms detected in the DNA profile suggest that the plants might have different genotypes. Polymorphism due to somaclonal variations induced during tissue culturing process is also a possibility.

In conclusion, AFLP analysis has successfully detected polymorphisms in irradiated seedlings of *D. mirbellianum* and *D. crumenatum*. More primer sets need to be tested to confirm genetic variations among the irradiated seedlings. Seedlings that showed polymorphisms during the AFLP analysis will be carefully monitored for morphological changes.

Table 1 Size of polymorphic bands generated by primer combinations E-AGC/M-CTG and E-ACG/M-CAT in *D. mirbelliannum* and *D. crumenatum* irradiated at different doses. N.D,: not detected.

Irradiation dose (Gy)	Size of Amplified DNA (bp)			
	D. mirbelliannum		*D. crumenatum*	
	E-AGC/ M-CTG	E-ACG/ M-CAT	E-AGC/ M-CTG	E-ACG/ M-CAT
2.0	1200	480 500	520	350 620
4.0	650	N.D.	350 530 650	320 350
6.0			350 650	320 500
8.0	N.D.	N.D.	350	320 500
10.0	N.D.	N.D.	650	320 500
12.0	320 580	400		

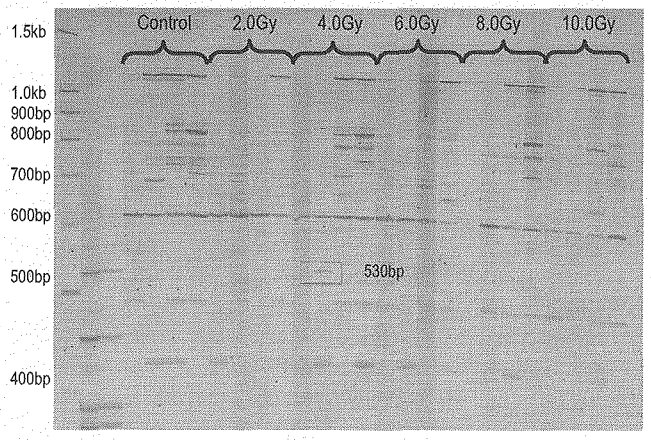


Fig. 1 AFLP analysis of control and irradiated *D. crumenatum*. A polymorphic band of 530 bp (red box) was clearly seen in 4.0 Gy plant.

References

1) Mohd Nazir, B et al., TIARA annual report 2004 (2005) 45.
2) Vos, P. et al., Nucleic Acids Res. 23 (1995). 4407.

3-12 Selection of Rootstock Eggplant Resistant to Bacterial Wilt from Regenerants Derived from Ion Beam-Irradiated Microspores

Y. Uchimura[a)], K. Takata[a)], Y. Saiki[a)], K. Hirashima[a)], T. Nakahara[a)], Y. Hase[b)], Y. Yokota[b)] and A. Tanaka[b)]

[a)]Department of Agricultural Biotechnology, Fukuoka Agricultural Research Center, [b)]Radiation-Applied Biology Division, QuBS, JAEA

1. Introduction

Bacterial wilt caused by *Ralstonia solanacearum* is the adverse soilborne disease for eggplants to die. To prevent eggplants from this disease, grafting onto rootstock varieties of *Solanum integrifolium* is the common practice. But bacterial wilt is differentiated into five bacterial groups in respect of pathogenicity to *S. integrifolium*[2)]. No rootstock variety had highly resistance to all bacterial groups, especially bacterial group IV as well as superior cultivation characteristic in Fukuoka prefecture. The purpose of this study was to breed rootstock eggplant resistant to bacterial wilt. In our previous work, we developed the method of mutation breeding that obtained regenerants from ion beam-irradiated microspores of *S. integrifolium*[1)]. This paper evaluated the regenerants which developed no symptoms against bacterial wilt of group IV.

2. Materials and Methods

A total of 261 regenerants were derived from ion beam-irradiated microspores of *S. integrifolium*[1)]. Bacterial wilt development was caused by inoculating 50 ml of group IV of *R. solanacearum* (10^8 cfu/ml in distilled water) into soil having the plants. As a susceptible control, non-irradiated seedling of *S. integrifolium* was used. We selected the plants which developed no symptoms against bacterial wilt following first evaluation on pots, and secondary evaluation by transplanting the resultant regenerants in field, because degree of resistant to the disease was variable by temperature, moisture and other factors.

3. Results and Discussion

All susceptible control developed symptoms of bacterial wilt as withering with rapid wilting in both evaluations (Fig.1). Most of the regenerants also developed the symptoms. Degree of resistant to the disease didn't significantly differ in radiation and dose. But some regenerants showed improvement in resistant to bacterial wilt over *S. integrifolium*. As a result, three regenerants that did not show any symptoms in both evaluations were selected. Secondary evaluation with other 18 regenerants are still being conducted presently (Table 1). Further, we continue to evaluate the progeny of the resulted regenerations for resistant to other bacterial groups and their agronomical characteristics.

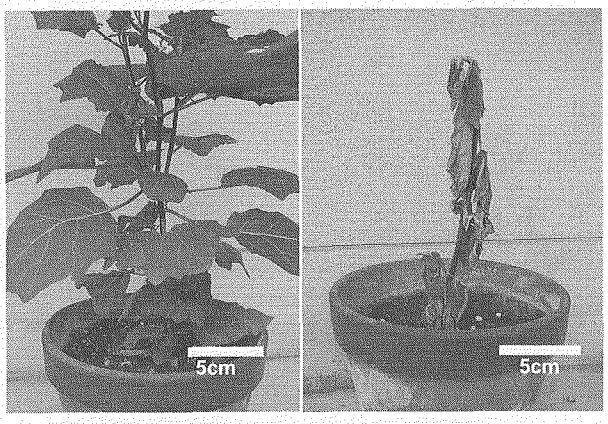
4. References

1) K. Takata et. al., TIARA annual report 2004(2005) 48.
2) K.Ozaki et. al., Bull, Chugoku Natl. Agric. Exp. Stn. 10(1992)49.

Table 1 Selection of resistant *S. integrifolium* regenerants to bacterial wilt.

Radiation	Dose (Gy)	First evaluation on pot		Secondary evaluation in field	
		Number of regenerants		Number of regenerants	
		evaluated	selected	evaluated	selected
Control[1)]		18	0	6	0
$^{12}C^{5+}$	1	51	11	2	0
	2	30	5	2	1
$^{12}C^{6+}$	1	104	10	7	1
	2	76	7	4	1
Total		261	33	15[2)]	3

1) Control ; seedling of *S. integrifolium* (susceptible variety).
2) Fifteen from 33 regenerants of first evaluation were used for secondary evaluation.



A B

Fig. 1 Regenerants from ion beam-irradiated microspores shows enhanced resistance to bacterial wilt. A; Resistant, B; Susceptible

3-13 Mutation Induction from Osteospermum Leaf Cultures with Ion Beam Irradiation

M.Iizuka [a], Y.Kimura [a], Y.Hase [b] and A.Tanaka [b]

[a]Gunma Agricultural Technology Center, [b]Radiation-Applied Biology Division, QuBS, JAEA

Introduction

Ion beams, which have a higher linear energy transfer (LET) than X and gamma rays, are one of efficient mutagenic agents, and applicable to mutation breeding of many horticultural crops. However, there have been few studies on the effects of ion beam irradiation on induction of mutation in vegetables and ornamental crops. The lethal dose of the $^{4}He^{2+}$ and $^{12}C^{5+}$ ion beam irradiation to strawberry, hydrangea and spiraea seed became clear [1),2)].
In Gunma Prefecture, Osteospermum cultivation is prosperous and its quality has obtained high evaluation. We think that the mutation breeding of Osteospermum is effective. Ion beams were irradiated to Osteospermum for the purpose of getting variation of the flower color and character. Here we examined the effects of ion beam irradiation on germination of Osteospermum.

Materials and Methods

Osteospermum in greenhouse were used as plant materials. Young leaves were excised, and the surface was sterilized by immersing in 70% ethyl alcohol for 1 min, followed by 1%(W/V) sodium hypochlolite solution for 15 min and then rinsed three times in distilled water. The leaf segments were cultured on modified Murashige and Skoog's (MS) medium supplemented with 0.1 mg/l NAA and 1 mg/l BA. The samples covered with Kapton film were irradiated with carbon ion beam (220 MeV $^{12}C^{5+}$ and 320 MeV $^{12}C^{6+}$) at various doses (2 to 150 Gy). After irradiation the leaf segments were transferred to the fresh medium and cultured at 25 °C and 16 hr-photoperiod. Regeneration rate was investigated after 40-50 days of culture.

Results and Discussion

Osteospelmum leaf segments was not able to regenerate following irradiation with 20 Gy or more[3),4)]. Therefore, it was thought that the irradiation of 1～5Gy was effective.

Hundreds of individuals grew, and three of them having a mutation in color of the flower on the other side of the petal have been selected so far[5)].

Thousands individuals were raised until now this year, and 21 individuals which have variation in a form and color were selected (Table1,fig.1). The color which applies the color of a flower to white, cream, deep yellow, and an orange appeared. And there was also a mutant containing a stripe. Dwarf and variegated leaf were seen with the form.

In this study, many Osteospelmum mutants were acquired by the ion beam. The ion beam is very effective in the breeding of Osteospelmum.

References

1) M. Iizuka et al. TIARA Annual Report 1998 (1999)30-31
2) M. Iizuka et al. TIARA Annual Report 2000 (2001)45-46
3) M. Iizuka et al. TIARA Annual Report 2001 (2002)42-43
4) M. Iizuka et al. TIARA Annual Report 2002 (2003)40-41
5) M. Iizuka et al. TIARA Annual Report 2003 (2004)50-51

Table 1. Mutants in Osteospelmum by the irradiation of $^{12}C^{5}$+ and $^{12}C^{6}$+ ion beams

Radiation	No. of hardening	No. of mutants	
$^{12}C^{5}$	865	color	13(1.5)[z]
		plant type	4(0.5)
$^{12}C^{6}$	758	color	2(0.3)
		plant type	2(0.3)

[z]The percent is shown in the parenthesis.
Color variation is dark yellow 6, light yellow 3, orange 3, light brown 2, and white 1.
Plant type variation is dwarf 5 and variegated leaf 1.

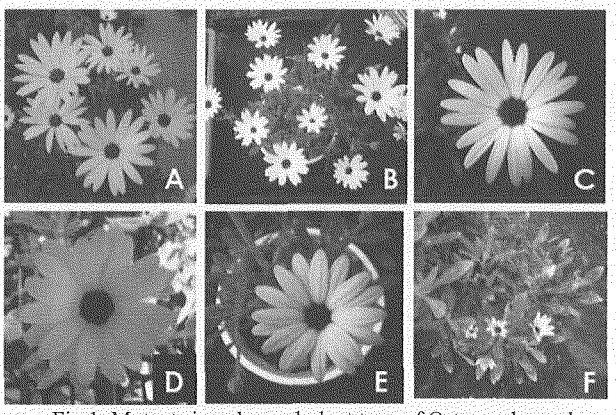


Fig.1. Mutants in color and plant type of Osteospelmum by the irradiation of ion beams.
A : Normal B : White C : Light yellow
D : Orange E : Light brown F : Dwarf

3-14 Breeding of Stress-Tolerant Variety Series in Ornamentals by Ion Beam Irradiation

M. Okamura[a)], M. Momose[a)], S. Watanabe[a)], A. Shimizu[a)], Y. Hase [b)], Y. Yokota [b)] and A. Tanaka [b)]

[a)]Plant Laboratory, Kirin Agribio Co., LTD., [b)]Radiation-Applied Biology Division, QuBS, JAEA

Ion beam breeding can induce a wide variety of flower-color and -shape mutants, and the combined method of ion beam irradiation with tissue culture is useful to obtain commercial varieties in a short time[1]. The potential of ion beam breeding and its application to produce stress tolerant variety series in ornamentals is discussed.

1. Production of color mutants in disease resistant carnation and their DNA analysis.

Superior varieties of spray carnation, "Vital series" and "Beam cherry", have been developed by the irradiation of 220 MeV carbon ion beams from TIARA cyclotron at JAEA-Takasaki. "Vital series" are the color family of the parent variety "Vital", consisting of red, pink, light pink, dark pink, salmon, bi-colored and yellow (Fig. 1). Most of the "Vital series", red, pink, light pink, dark pink, salmon and bi-colored retained good characteristics of parent "Vital" such as resistance to disease and insects, high productivity and long vase life. "Beam cherry" is the mutant of "Vital" with round petals and strong stem (Table 1). It also retained desirable characteristics of "Vital"[2].

The DNA contents of these mutant series have been analyzed by flow cytometer. Color mutants of "Vital"; red, pink, light pink, dark pink, salmon and bi-colored, have almost the same DNA contents; from –0.5% to +0.2% difference as compared with the parent. However, DNA contents of "Beam Cherry" and "Barbara" are +1% and –4% different from "Vital", respectively. It is interesting that only "Beam Cherry", that has stronger stem and higher volume than the parent, showed higher DNA content.

Transposable elements are considerably related to mutations because of their potential ability to transpose. Increasing knowledge on the relationship between mutated genes and transposable elements would improve mutation breeding. Transposable elements dTdic1 was found in carnation[3], so the behavior of dTdic1 was examined by PCR using DNA extracted from both leaves and petals of the mutants.

Only yellow mutant showed considerable difference from parent "Vital" in the behavior pattern of dTdic1. It possibly shows that large change occurred in DNA or chromosomes of the yellow mutant. The other mutants had almost the same pattern as the parent. In this study, relation between dTdic1 and mutation generation was not clear.

2. Mutation generation in stress tolerant petunia "Wave".

Spreading type petunia 'Purple Wave' is very popular in America, Europe and Japan. It has resistance to rain and heat tolerance. Seeds were irradiated with 320 MeV carbon ion beams. Growth rate of the shoot was examined after 1 month. The median growth dose of plants from ion beam-irradiated seeds was around 22 Gy. Plants derived from irradiation were cultivated in the greenhouse and their flower color and shape were examined. Flower color mutants such as pure white, rose vein, blue, light red and striped were obtained at 30 Gy to 40 Gy

After vegetative propagation, characteristics of the color mutants have been examined in the field. All mutants showed good resistance to rain and heat tolerance.

A wide spectrum in flower color and shape was observed in mutants derived from ion-beam irradiation, while the mutants retained the desirable characteristics of the parent such as disease resistance, stress tolerance etc. In preliminary test of standard carnation "Komachi" which is a superior variety with long vase life, mutants with little fading of the flower color have been obtained by 320 MeV carbon ion beam irradiation. These results show that ion beams have advantage to breed stress-tolerant variety series in ornamentals in a short time.

Since carnation is one of the big 3 flowers and petunia has become biggest gardening crop, these results show that ion beams have a great impact on the plant seed and seedling business.

References

1) M. Okamura et al., Nucl. Instr. Meth. B 206 (2003) 574.
2) M. Okamura et al., In J. Teixeira da Silva (ed.) Floriculture, Ornamental and Plant Biotechnology Vol. I, Global Science Books (2006) 619
3) Y. Ito et al., Plant Cell Physiology 43 (2002) 578.

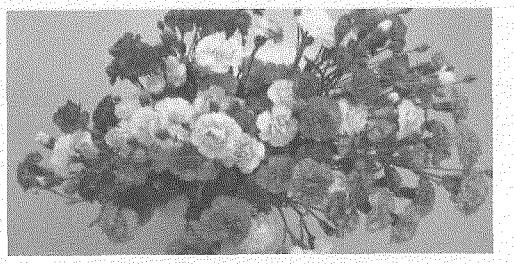


Fig.1 "Vital series" bred by ion beam breeding.

Table 1 Characteristics of the new varieties by ion beam breeding.

Varieties	Petal type	Productivity	Stem strength	Fusarium resistance
Beam Cherry	round	high	hard	resistant
Vital	serrated	high	middle	resistant
Barbara	serrated	middle	hard	middle

3-15 The Optimum Dose of Ion Beam Irradiation to Tissue Cultured of Leaf Explants for Breeding Sugarcane

F. Tohjima [a], T. Shirao [a], K. Ueno [a], M. Ooe [a], M. Yasuniwa [b], Y. Hase [c] and A. Tanaka [c]

[a] Kagoshima Biotechnology Institute, [b]Kagoshima Prefectural College of Agriculture,
[c]Radiation-Applied Biology Division, QuBS, JAEA

Abstract

Sugarcane cultivar "Ni17" has hard and harmful hair on its leaf sheath. We have intended to induce hairless or few hair mutants using ion beam irradiation to tissue cultured of leaf explants. In this study, we studied optimum doses of three ion beams for the effective mutation induction using JAEA AVF cyclotron. The efficiency of regeneration from callus, the mutation ratio of nursery plants and the selection ratio in field were observed. The optimum doses for each ion beam were 1 Gy of $^{12}C^{5+}$ at 220 MeV, 2 Gy of $^{12}C^{6+}$ at 320 MeV and 6 Gy of $^{4}He^{2+}$ at 100 MeV, respectively. We have selected 37 few hair mutants among the 6,575 regenerated plants in 2005. Furthermore, we have continued characteristic investigation and field test of the selected mutants.

サトウキビ品種“Ni17”は株出し適性が高く，耐風性も強い[1]。しかし，葉鞘部に着生する毛群（第57毛群）が粗剛であるため，収穫や採苗時の作業に障害をきたしている。そこで，イオンビーム照射による変異誘発により毛群の少ない優良系統の育成を図った。

“Ni17”の幼葉組織の切片を2,4-D 濃度 0.5～1 mg/l のカルス誘導培地に置床し，約一週間後にイオンビーム 320MeV・$^{12}C^{6+}$，220MeV・$^{12}C^{5+}$，100Mev・$^{4}He^{2+}$（以下C320，C220，He100）を照射した。照射回数（反復数）はC320が4回，C220及びHe100は1回であった。照射後，カルス，不定胚を経由し再生させた植物体を発根処理し，順化を行った。

各線種及び線量ごとに（順化個体数/置床葉片数）の値を算出し，無照射時の値を100%とする相対値を個体再生率と定め，各線種における線量と植物体再生への影響を検討した。その結果，反復間で差はあったがC320照射時の個体再生率は，2Gy照射で約75%，3～4Gy照射で50%以下となった。C220照射時の個体再生率は，2Gy照射で50%となり4Gy照射では25%以下となった。また，He100照射時の個体再生率は，7～8Gyの間の照射線量で約50%であり，炭素イオン（C320・C220）よりも個体再生率への影響は小さかった。今回用いた各線種はLETの大きい順にC220＞C320＞He100となるが，照射線量に対する個体再生率の低下はLET値に依存する傾向が認められた（Fig. 1）。

2004年9月～2005年4月に順化後，鉢上げした炭素イオンビーム照射個体（6,575個体，無照射を含む）から，主として毛群の有無を基準とするガラス室内での幼苗検定により355個体を初期選抜した。これらをほ場に定植した後，8月に生育調査，11月に毛群及び生育調査を行い，毛群が少なく生育の良好な有望個体37個体を選抜した。これらは現在もさらに生育特性に関して選抜中である。選抜された有望個体の照射条件はC320では0.5～2Gyが多く，2Gyが最も多かった。また，C220では1Gyが多かった（Table 1）。

品種“Ni11”の多芽体にヘリウムイオンを照射して変異誘発を行った出花らの報告[2]と比べ，品種“Ni17”の幼葉に炭素イオンを照射して変異を誘発した今回の結果は，より低線量で変異の出現が認められた。イオンビームを利用した単一形質改良の場合はできるだけ低線量の照射が望ましい。従って培養葉片への照射に炭素イオンビームを利用する場合は個体再生率の低下や生育に影響が少なく，変異出現率の高い線量としてC220は1Gy，C320は2Gy程度が適当であると考えられた。また，ヘリウムイオンビームを利用する場合は生育への影響は調査中であるが，He100では6Gy程度が適当であると考えられた。

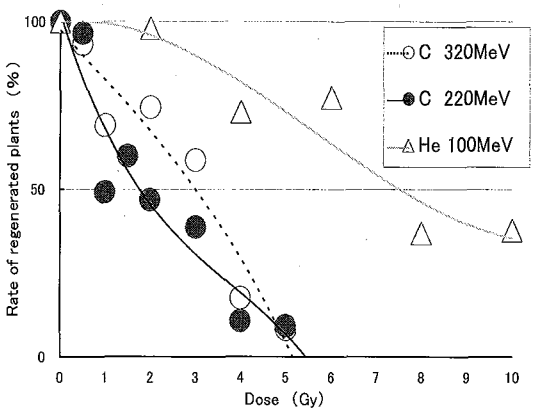


Fig.1 Effect of carbon and helium ion beams on rate of regenerated plants

References

1) M.Takemure et al., 鹿児島県農業試験場研究報告 32 (2004) :81.
2) K.Degi, et al., TIARA annual report 2003 (2004):48.

Table 1 The number of tested and selected plants in 2004~2005

Radiation	Energy	Dose	No. of regenerated plants	No. of hairless or few hair mutant	Mutation rate	No. of selected plants at open field	Selection rate
	(MeV)	(Gy)			(%)		(%)
		0	1,585	32	2.0	2	0.1
		0.5	493	40	8.1	7	1.4
		1	1,335	125	9.4	8	0.6
		1.5	390	23	5.9	2	0.5
$^{12}C^{6+}$	320	2	900	82	9.1	11	1.2
		3	72	2	2.8	0	0.0
		4	180	18	10.0	3	1.7
		5	4	0	0.0	0	0.0
		8	11	0	0.0	0	0.0
		10	14	0	0.0	0	0.0
		sub-total	4,984	322	6.5	33	0.7
		0	333	1	0.3	0	0.0
		1	516	17	3.3	3	0.6
		2	607	8	1.3	0	0.0
$^{12}C^{5+}$	220	3	33	0	0.0	0	0.0
		4	53	6	11.3	1	1.9
		5	29	1	3.4	0	0.0
		10	20	0	0.0	0	0.0
		sub-total	1,591	33	2.1	4	0.3
		Total	6,575	355	5.4	37	0.9

3-16 Mutation Induction in Sugi Cedar and Hinoki Cypress by Ion Beam Irradiation

K. Ishii [a], Y. Hosoi [a], Y. Hase [b] and A. Tanaka [b]

[a]Department of Molecular and Cell Biology, Forestry and Forest Products Research Institute, [b]Radiation-Applied Biology Division, QuBS, JAEA

Sugi cedar (*Cryptomeria japonica* D. Don) and Hinoki cypress (*Chamaecyparis obtusa* Sieb. et Zucc.) are the most important plantation forest trees in Japan. In these tree species with long life cycle, mutation is supposed to be promising in shortening the breeding time. Mutants such as male-sterile to solve the problem of pollinosis are promising.

Ion beam is expected to increase the mutation frequency and wide spectrum, since it has a high LET (linear energy transfer). The combination of ion beam irradiation and tissue culture was beneficial for high frequent mutation induction[1]. In the previous report, we have obtained the xantha (yellowish color) and wax rich mutants in Hinoki cypress by ion beam irradiation[2].

In this study, we tried to induce the mutants by irradiation of the in vitro cultured buds of Sugi cedar and shoot primordia of Hinoki cypress with $^{4}He^{2+}$ and $^{12}C^{6+}$ heavy ion beams.

In vitro cultured buds on half-strength LP medium of Sugi cedar originally collected from arboretum in Forestry and Forest Products Research Institute, Tsukuba, Ibaraki, were used. Shoot primordia of Hinoki cypress were also used for the experiments. They are cultured on CD medium supplemented with 10 μ M 6-benzylaminopurine and 0.03 μ M naphthalene acetic acid (NAA). Fresh buds or shoot primordia were subcultured on the medium in petri dish (35 x 10 mm) which was covered with Kapton film. They were irradiated with 50 MeV $^{4}He^{2+}$ or 320 MeV $^{12}C^{6+}$ ion beams delivered from the AVF cyclotron at TIARA in JAERI-Takasaki. After irradiation the shoot primordia were subcultured to the new media for assessing the surviving rate and detecting mutation.

Regenerated Sugi cedar trees were grown in the greenhouse and treated with gibberellic acid (GA) at 100 ppm in July to induce the formation of male flowers. After 3 months, male flower induction was checked with each tree. Surviving trees were checked again for male flower formation by GA treatment in the next year.

Shoot primordia irradiated with He ion beam were further irradiated with 0.6 mW/cm^2 of UVB in the Raytron (Nippon Ikakikai, RTP-220-NC). Surviving shoot primordia were subcultured to check the morphological characters.

Surviving rate of in vitro cultured buds of Sugi cedar and shoot primordia of Hinoki cypress irradiated with 5 to 20 Gy $^{4}He^{2+}$ and 0.5 to 5 Gy $^{12}C^{6+}$ ion beams decreased as the amounts of irradiation increased. Five Gy $^{12}C^{6+}$ ion beams caused more damage to Hinoki shoot primordia than $^{4}He^{2+}$ in the same dose. There was plastid mutation like albino and partial light-green leaves in Sugi cedar (Fig. 1). Wax rich shoots appeared in Hinoki cypress culture. Shoot elongation from surviving buds was suppressed with irradiation of 2 and 5 Gy $^{12}C^{6+}$ ion beams. Among the regenerated plantlets which have been habituated and grown in a greenhouse for further assessing experiments to detect mutants, there were many plantlets which did not survive in the next year. Assessing the sterile mutants by spraying gibberellic acid for inducing flowers indicated that male flowers were induced normally in Sugi cedar with 5 Gy but sometimes very few with 10 Gy $^{4}He^{2+}$ ion treatment. There were few male flower mutants among them (Fig. 2).

Among the regenerated plantlets of Hinoki cypress after UVB treatment, wax rich mutants were observed. We described also the albino, xantha and wax rich mutants from irradiated shoot primordium of Hinoki cypress[2].

So far, we observed putative UVB resistant wax rich mutants of Hinoki cypress, few male flower mutants of Sugi cedar, and plastid mutants for both conifers by ion beam irradiation. Further confirmation experiments of mutation of forest trees are necessary.

References

1) S. Nagatomi et al., TIARA annual report 5(1996)50.
2) K. Ishii et al., TIARA annual report 2003(2004)56.

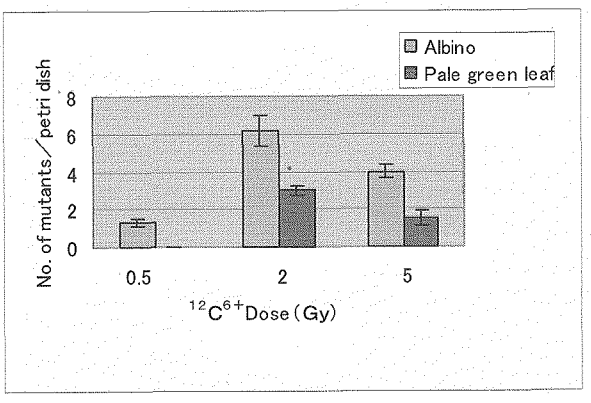


Fig.1 Plastid mutation of Sugi cedar .

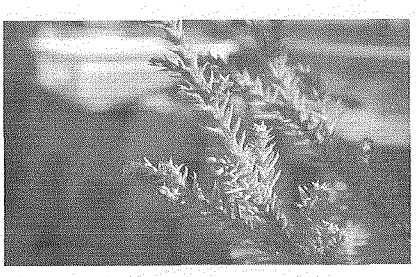


Fig.2 Few male flower mutants of Sugi cedar.

3-17 Mutation Induction in Garlic with Ion Beam Irradiation

T. Tashiro[a], Y. Yamamoto[b], A. Tanaka[c] and Y. Hase[c]

[a]Faculty of Horticulture, Chiba University, [b]Yokkaichi Agriculture Center, Yokkaichi City,
[c]Radiation-Applied Biology Division, QuBS, JAEA

Introduction

Garlic belongs to the Alliums family. Since it is sexually sterile and propagated vegetatively, the positive breeding is difficult. We have established a practical novel micro propagation system that enhances the propagation of viable bulblets *in vitro*. This micro propagation system is an effective method to proliferate, select and plant in the field[1]. The Ion beam irradiation is expected to be increase the mutation frequency and widen the spectrum, since ion beam is a high linear energy transfer (LET) radiation and can deposit a high energy on a target as compared to a low LET radiation such as gamma rays[2]. The purpose of this study is to develop an effective method for ion beam breeding in garlic and to obtain desirable mutants, especially that of volatile sulfur compounds. In this paper, we report the effects of ion beam on plantlet regeneration from the irradiated callus induced from basal plates of garlic bulbs and characterization of regenerated plantlets.

Materials and Methods

The compact and granular callus-like embryogenic callus was used for experiments. These calluses were induced from basal plates of garlic bulbs (*Allium sativum* L. cv Fukuchi-howaito), which were placed in a 20mm-diameter, 15cm-length tubes containing MS medium supplemented with 2,4-D 0.5 mg/l, sucrose 30 g/l and gelrite 2 g/l in November 2003. The calluses were placed in plastic Petri dish, 1~2 mm thickness in 60 mm diameter containing MS medium supplemented with a plant growth regulator. The Petri dishes were covered with Kapton film, and then irradiated with 50 MeV $^{4}He^{2+}$ and 320 MeV $^{12}C^{6+}$ ion beams at dosages of 0.1, 0.2 and 0.5 Gy at the TIARA AVF cyclotron in JAERI. The calluses, after the irradiation, were transferred to the medium for shoot differentiation. The experiments were performed under 3000 lux (day/night of 16/8 hrs.) at 25℃. The plantlets obtained after 5 months, were cleared of roots and leaves. The bulblets were dried and kept at room temperature until seeding. The round and good bulblets were selected and sown on the seed beds in the closed breeding system and cultured. The plantlets were then transferred to 11 cm diameter breeding pots on Nov. 9th 2005 and acclimated in the green house. The acclimated plants were transferred to the experimental field of Chiba University on Feb. 22nd 2006. In 2006 May 1st, we observed the appearance of growing plants. Ploidy levels of the regenerated plantlets were determined by Flow cytometry analysis using a Partec PAS flow cytometer equipped with a mercury lamp.

Results and Discussion

1) Effects of callus irradiation on regenerated plantlets

The number of regenerated plantlets was depended on the dosages of the carbon and helium ion beams. In the carbon ion beam, the numbers of regenerated plantlets per gram callus decreased with increasing dosage (218 at 0.1 Gy, 154 at 0.2 Gy, and 30 at 0.5 Gy). In the helium ion beam, the numbers of regenerated plantlets at 0.1Gy was lower (191 per gram callus) than the control, but regenerated plantlets in the other two dosages were higher (446 at 0.2 Gy and 330 at 0.5 Gy). The number of regenerated plantlets was 274 in non-irradiated treatment.

2) The characterization of regenerated plants from the irradiated callus

Generally, a normal acclimated plant was over 25 cm plant in height and with 6 leaves which had normal color and shape, and the bulb was more than 2 cm diameter. The variants produced by ion beam irradiation had different morphological characters such as dwarf, multiple shoot, variegated leaves, shrink leaf and thickening-less bulb. There were no differences in the tendency of variant type rate between carbon and helium ion beams at different dosages. Change of in ploidy level was found in acclimated plants by FCM analysis. Almost all of the nuclei were at the 2C level in the normal type leaves, whereas 4C and 2C level were observed in the variant leaves in both shoot type and bulb type.

References

1)Y.Yamamoto et al., Inte. Plant Propagators Soc. 7 (2000)17.

2) A.Tanaka et al., Int. J. Radiat. Biol. 72(1997) 121.

3-18 Mutagenesis in Gynomonoecious Spinach (*Spinacia oleracea* L.) Plants and Selection of Low Oxalate Variants

K. Murakami[a)], N. Hata [a)], Y. Yoshida [a)], M. Masuda [a)], A. Tanaka [b)], N. Shikazono [b)]
And Y. Hase [b)]

[a)]Department of Applied Plant Science, Faculty of Agriculture, Okayama University,
[b)] Radiation-Applied Biology Division, QuBS, JAEA

Spinach (*Spinacia oleracea* L.) is one of the indispensable leaf vegetable in Japan for its good cooking adaptability and high nutritious value. However, it accumulates large amounts of oxalate, which is detrimental to human health. Although several attempts have been conducted, there has been little success in its reduction by cultivation techniques, while a variety with significantly low oxalate content has not been found. Mutation breeding could be a potential strategy for producing a new variant with low oxalate content.

Spinach is a typical dioecious species, but there are spontaneously a few gynomonoecious plants with the capacity for self-fertilization, which can be applicable to mutation breeding programs. A stable occurrence of hermaphroditic flowers in gynomonoecious plants is economically important for their practical application in spinach mutation breeding programs; the expression of gynomonoecy was reported to be affected by genetic and/or environmental factor. For an efficient harvest of self-fertilized seeds in spinach, the effect of temperature on the expression of gynomonoecy was studied by employing selfed-seed populations from three plants in which the degree of gynomonoecy were different. It was concluded that an efficient harvest of self-fertilized seeds in mutation breeding programs may be achieved by applying selected lines with strong expressions of gynomonoecy, and by their cultivation at 25℃ after induction of bolting at 20℃ under 16-h photoperiod[1), 2)].

This study was conducted to evaluate mutagenesis in gynomonoecious spinach (*Spinacia oleracea* L.) plants for inducing low oxalate variants. Gamma-ray and ion beams of 220 MeV $^{12}C^{5+}$ and 50 MeV $^{4}He^{2+}$ were used as mutagen in seed irradiation. Optimum dosages for irradiation were determined to be about 100 Gy, 15-20 Gy and 150-200 Gy in gamma-ray, $^{12}C^{5+}$ and $^{4}He^{2+}$, respectively. In M_2 generation, there was one line segregating albino seedlings, one line segregating xantha seedlings and two lines segregating viridis seedlings, which indicates that recessive mutation could be expressed in M_2 generation due to the capacity for self-fertilization of gynomonoecious plants in an otherwise dioecious spinach. To save on labor and time for analysis, selection of low oxalate variants in M_2 generation was conducted by a two-step selection which consisted of the first analysis of bulked leaves from 2 plants as one specimen followed by the second analysis of selected individual plants. In the first analysis of 813 specimens, we selected 13 specimens as low and 9 specimens as high in oxalate content. In the second analysis, there was consistency in the distribution of low and high oxalate content corresponding to the first screening, indicating that selection of low oxalate variants could be achieved by this two-step selection with half the labor and time for analysis as compared to non-bulked method. However, there were no clear differences in distribution of oxalate content between M_3 progenies of plants selected as low or high oxalate content (Fig. 1), suggesting that the low oxalate content in plants isolated in M_2 generation was not of a genetic origin.

In the present study, 1) self-fertilized seed production system for mutagenesis and/or shortening breeding cycle, 2) mutagenesis in gynomonoecious plants with gamma-ray or ion beams, 3) two-step selection for effective screening of low oxalate variants were established. In order to increase the frequency of selection of the mutants, it is of great effectiveness to employ the line with approximately 100% gynomonoecious trait and irradiate their seeds at optimum dosage. To explore a variant with obvious deviation from the successive variation of oxalate content in the M_2 generation, as well as to pursuit a progenies of low oxalate content with accompanying recurrent mutagenic treatment, even if it has no obvious deviation from the successive variation, will lead to the final goal of this study, that is to obtain a novel variant with low oxalate content by mutagenesis in spinach.

References

1) N. Hata et al , J. Japan. Soc. Hort. Sci. 74 (2005) 228.
2) N. Hata et al , J. Japan. Soc. Hort. Sci. 75 (2006) 141.

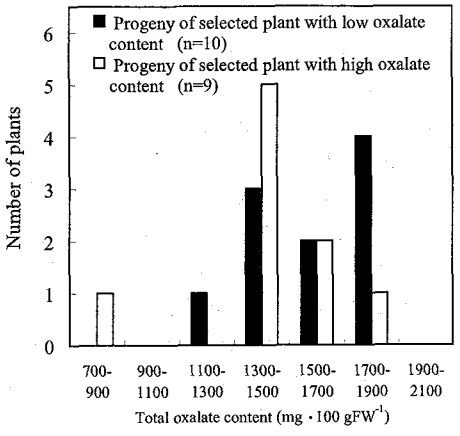


Fig.1 Distribution of oxalate content in M_3 progenies of the plants selected as low and high oxalate content in M2 generation. Black and white bars show progeny of the plant selected as low oxalate plants (658 mg/100 gFW) and high oxalate plants (1966 mg/100 gFW) in M_2 generation, respectively.

3-19 Effect of Ion Beam Irradiation on Coloration of Fruit Skin of Eggplant (*Solanum melongena* L.)

N. Matsuzoe[a)], T. Umeda[a)], Y. Hase[b)] and A. Tanaka[b)]

[a)]Faculty of Environmental and Symbiotic Sciences, Prefectural University of Kumamoto
[b)]Radiation-Applied Biology Division, QuBS, JAEA

Abstract

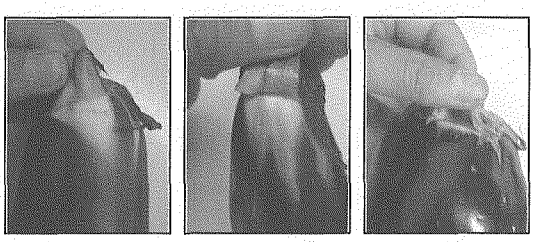
Fruit color is one of the important qualities in eggplant (*Solanum melongena* L.). Then, Anthocyanin of fruit in eggplant is also an important antioxidant for human health. Quality and quantity of light effects on the coloration of fruit skin of eggplants. We have reported the cultivars/lines of eggplant in the dark treatment were grouped into three pigmentation types (photoreceptive, non-photoreceptive and middle type) for photosensitivity to fruit coloration. *Solanum* melongena cvs. 'Kitta' (middle type) and 'Kumamoto-naga' (photoreceptive) were used for the experiments. Dry seeds of the cultivars were irradiated with ion beam (220 MeV $^{12}C^{5+}$) with the doses of 25 and 50 Gy at TIARA. M2 seeds derived from self-pollination of the M1 plants were germinated in the greenhouse and the seedlings were transplanted in the field. The photosensitivity to fruit coloration was assessed by color of the skin under the calyx, where is the absence of light. We found that 33 mutant plants changed their photosensitivity to fruit coloration in M2 generation. Two mutant plants were in cv. Kumamotonaga and 31mutant plants were in cv. Kitta.

ナス（*Solanum melongena* L.）は1200年前に我が国に渡来し、昔から日本人に食されてきた野菜の一つで、現在でも利用度が高い食材である。ナスの果実品質を評価する場合、果色は重要な要素の一つである。また、果色の黒紫色の原因物質であるアントシアニン色素は機能性成分として注目されている。一方、紫外線カットオフフィルムはアザミウマ等の害虫の発生防止を目的に、ハウス栽培の被覆資材に利用されている。しかし、ナスの果実の着色（アントシアニン色素の生成）は光環境と深い関係がある。即ち、ナスの果色発現は光環境の影響を受け、浴光時間が少ないと果色が悪くなる[1)]。また、ナスの果皮のアントシアニン色素の生成には光質として370nm前後の紫外線が必要である[2)]。さらに、290nm以下の紫外線を除去するビニルを被覆したハウスでは露地栽培と同様に着色するが、380nm以下の紫外線を除去するガラス温室では着色が悪くなることが報告されている[3)]。このように、ナスの品種の多くは果実の着色に紫外線を必要とするため、紫外線カットオフフィルムはナス栽培に利用されていないのが現状である。

筆者らは、ナス果実の着色は光環境の影響を受けるが、その程度は品種・系統で大きく異なることを報告した[4)]。即ち、果実への暗黒により果色が白色化するタイプⅠ（‘熊本長’）、影響が少ないタイプⅡ（米ナス系品種やバングラデシュから導入した‘Singhnath’）、並びに着色は低下するもののある程度の着色が見られるタイプⅢ（‘橘田’や‘筑陽’）があることを明らかにした。なお、タイプ判別は果実のヘタ下の紫の着色の有無によりできる（第１図）。本研究では、ナス果実の着色（アントシアニン色素の生成）と光環境との関係に与えるイオン照射の影響を明らかにすることを目的とした。

ナス品種‘熊本長’と‘橘田’を供試した．TIARA において乾燥種子にイオン照射(220 MeV $^{12}C^{5+}$, 25 and 50 Gy)した。照射した種子（Ｍ１個体）の自家受粉から得られた種子（Ｍ２）を発芽・育苗後，露地栽培した。果実の着色と光環境との関係（着色に光が必要又は不要）は第１図に示すようにへた下の着色で評価した。

‘橘田’では対照区（非照射区）には紫の着色が認められるが、イオン照射 25Gy では 22 個体、50Gy では９個体に紫の着色が認められなかった。‘熊本長では’ 対照区（非照射区）には紫の着色は認められないが、イオン照射 25Gy では２個体で着色が認められた。このことから、イオン照射は、ナス果実のアントシアニン生成に関する光感受性に影響を与えることが示唆された。



‘Kumamoto-naga’ ‘Kitta’ ‘Black Beauty’

Fig. 1 Color of fruit skin under calyx

Table 1 Effect of ion beam irradiation on coloration on fruit skin under calyx

		Coloring of purple on the skin under the calyx		
Cultivar	Dose(Gy)	−	+	++
Kitta	0(Plant)	0	0	2
	25	22	16	2
	50	9	1	0
Kumamoto-naga	0	2	0	0
	25	73	1	1
	50	26	0	0

Coloring of purple on the skin under the calyx: − :absence (white), ＋:slight presence, ++:presence (See Fig 1 ‘Kitta’)

References

1)T. Hagiwara, “ナスの果色に就いて”, 農業之研究, 36, 94(1942)

2)Y. Matsumaru et al., “ ナス果皮のアントシアニン含量に及ぼす光透過性を異にした種々の被覆資材の影響”, Environ. Cntrol in Biol, 9, 91(1971)

3)T. Toki, “温度及び紫外線管理による果菜類栽培の革新的技術開発”,農業技術, 46, 66(1991)

4)N. Matsuzoe et al., “果実への暗黒処理がナスの果色と果皮のアントシアニン組成に及ぼす影響”, J. Japan Soc. Hort. Sci., 68, 138(1999)

3-20 Studies on Flower Color and Morphological Mutations from Chrysanthemum In Vitro Explants Irradiated with Ion Beams

T.Sato[a)], H.Kagaya[a)], Y.Hase[b)] and A.Tanaka[b)]

[a)]Akita Prefecture Agricultural Experiment Station
[b)]Radiation-Applied Biology Division, QuBS, JAEA

Abstract

To get a yellow or white color mutant from chrysanthemum cultivar "Natsuyasumi" (purpulish red flower), we previously irradiated the petal and got a pinkishness mutant. In this study, we irradiated the pinkishness mutant with ion beam again. As a result, we got new white and yellow mutants.

輪ギク品種'夏休み'は、秋田県の気象条件に適し、開花調整をおこなわなくとも、需要が多い８月に開花がそろう特性がある。しかしながら、花色が赤紫であるため、８月出荷に要求される白色および黄色品種への改良が望まれている。一方、イオンビームの照射により、これまでにキク、カーネーション、バラなどで変異体が獲得されている[1)]。我々は、'夏休み'培養物にイオンビームを照射し、薄桃色の花色変異体を得ている[2)]。

本試験では、得られた薄桃色突然変異系統に再度イオンビームを照射して、白色または黄色の花色変異体の作出を試みた。

供試材料として放射線を照射した'夏休み'花弁由来再分化植物体から選抜した薄桃色系統(NNX-50-W-1およびNPI220-20-W-2)の花弁ならびに節培養物を用いた。外植片を培養し、2-3日後にイオンビームを照射した。照射は、日本原子力開発機構高崎量子応用研究所のAVFサイクロトロンを用い、$^{12}C^{5+}$ 220MeVおよび$^{12}C^{6+}$ 320MeVのビーム条件でおこなった。照射後、再分化植物体を発根・馴化し、圃場に展開して、花色変異体の生育特性調査、ならびに選抜をおこなった。

その結果、$^{12}C^{5+}$ 220MeV 10Gyのイオンビーム照射花弁(NPI220-20-W-2)からの再分化植物体において、黄色変異系統 NPIW2-NPI320-10-Y-2 と白色変異系統 NPIW2-NPI320-10-W-1 および W-2 を選抜した(Fig. 1)。

白色変異系統 NPIW2-NPI320-10-W-1 の花色は、供試材料 NPI220-20-W-2 の花弁に見られた赤みが消え、白であった。また、開花時期も'夏休み'と同程度であった。しかしながら、草丈が低くなる傾向が見られた。また、NPIW2-NPI320-10-W-2 は、花色が白であったが、草丈が低く、開花日も'夏休み'より１ヶ月ほど遅かった(Table 1)。

黄色の花色変異体 NPIW2-NPI320-10-Y-2 ならびに、昨年度選抜した NPIW2-NPI320-10-Y-1 は、花色が鮮橙黄で、開花も'夏休み'と同程度であるが、草丈が低かった。さらに NPIW2-NPI320-10-Y-1 は花径の減少や花形の乱れが観察されたため、選抜を中止した。

以上の結果から、白色変異体への線量を減じた放射線の再照射は、草丈低下などの不必要な変異が現れてしまったが、昨年まで得られなかった黄色の花色変異体が得られたことから、目的形質の獲得に有効であると考えられた。

選抜した、白色変異系統 NPIW2-NPI320-10-W-1 および W-2、ならびに黄色変異系統 NPIW2-NPI320-10-Y-1 および Y-2 は、それら単独での使用が困難なため、交雑のための育種素材として供することとした。

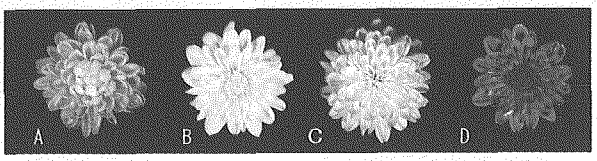


Fig. 1 Selected flower color mutant.
A : NPIW2-NPI320-10-Y-2 B : NPIW2-NPI320-10-W-1
C : NPI220-20-W-2 D : "Natsuyasumi"

Table 1 Character of flower color mutants.

mutant	flowering time	high (cm)
NNX-50-W-1	Aug. 6	127.5
NPI220-20-W-2	Aug. 6	126.3
NPIW2-NPI320-10-W-1	Aug. 4	84.5
NPIW2-NPI320-10-W-2	Sep. 7	62.5
NPIW2-NPI320-10-Y-1	Aug. 6	81.5
NPIW2-NPI320-10-Y-2	Aug. 6	85.2
"Natsuyasumi"	Aug. 4	128.3

Refrences

1) S.Nagatomi, et al., TIARA annual report (1995) 50.

2) T.Sato, et al., JAERI-Review (2003) 81.

3-21 Induction of Mutation by the Ion Beam Irradiation to the Calluses of *Lilium* × *formolongi* Hort (*cv. White Aga.*)

M. Kondo [a], K. Ogata [a], Y. Hase [b], Y. Yokota [b], I. Narumi [b] and H. Kobayashi [a]

[a] Niigata Agricultural Resarch Institute Biotechnology Division
[b] Radiation-Applied Biology Division, QuBS, JAEA

We have been working on producing marketable blue lilies. It has been impossible to produce blue lilies by crossbreeding or mutation, because they lack flavonoid 3',5'-hydroxylase (F3'5'H), which is necessary for synthesis of the blue pigment, delphinidin. Therefore, we developed an *Agrobacterium*-mediated transformation system for lilies[1]. For the marketing of the blue lilies, we have to regulate the spreading of the pollen to prevent them from crossing with other lilies, because they are genetically modified plants. The aim of this study is to producce male-sterile lilies. In the present study, we exposed calluses of a lily to $^{4}He^{2+}$ beams from the AVF cyclotron and investigated the effects on the calluses.

Filaments of lilies were cultured on a callus proliferation medium. The cultures were maintained at 25°C in the dark. The calluses induced from the filaments were maintained by subculturing monthly onto the same fresh medium under the same conditions. The penetration range of 50 MeV $^{4}He^{2+}$ from an AVF cyclotron (JAEA) was 1.45 mm. The diameter of the induced calluses was about 10.0 mm or more. Therefore, we crushed the calluses to about 1.0 mm diameter by squashing on stainless steel sieves of 1.29 mm mesh (the mesh size of 16) and filtration through them. The crushed calluses were placed on a modified callus proliferation medium and covered with sterilized Kapton film (7.5 μ m in thickness, 45 mm square in size, Toray-Dupon, Japan), and exposed at total doses of 0-10 Gy of 50 MeV $^{4}He^{2+}$ or 100 MeV $^{4}He^{2+}$ beams from the AVF cyclotron. The exposed calluses were transferred to a liquid culture medium and cultivated. The Cultures were placed on a rotary shaker (90 rpm) and maintained at 25°C in the dark. The Calluses were maintained by subculturing weekly in the same fresh medium under the same condition. The volume of the calluses was measured 28 days after the ion beam exposure.

It has been suggested that the irradiation doses that suppressed the proliferation rate to 50-90% were effective in induction of mutations in cultured plant tissues [2,3]. In the irradiation of 50 and 100 MeV $^{4}He^{2+}$, the doses of 0.2-0.6 and 0.25-0.5 Gy suppressed the proliferation rate of the calluses to 50-90% of the non-irradiated control, respectively (Fig. 1 and 2). We assumed from these results that the doses of 0.2–0.6 Gy of 50 MeV $^{4}He^{2+}$ and 0.25–0.5 Gy of 100 MeV $^{4}He^{2+}$ were appropriate for obtaining mutants. At present, the ion beam irradiation, regeneration, acclimatization and planting to a field are in progress to select male-sterile mutants of lily (Fig. 3).

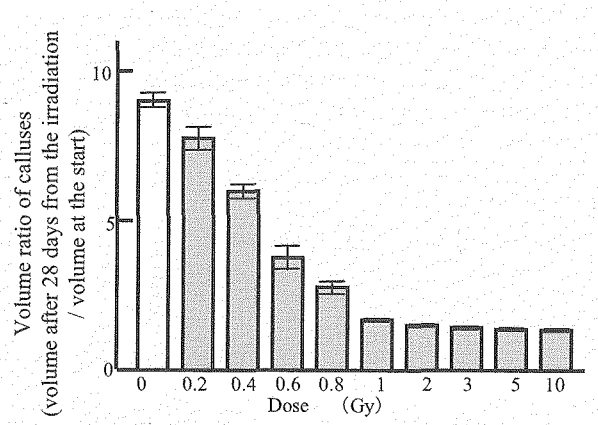


Fig.1 Effects of 50MeV $^{4}He^{2+}$ exposure on the growth of calluses. Values represent the means of 3 experiments. (Bar = standard deviation)

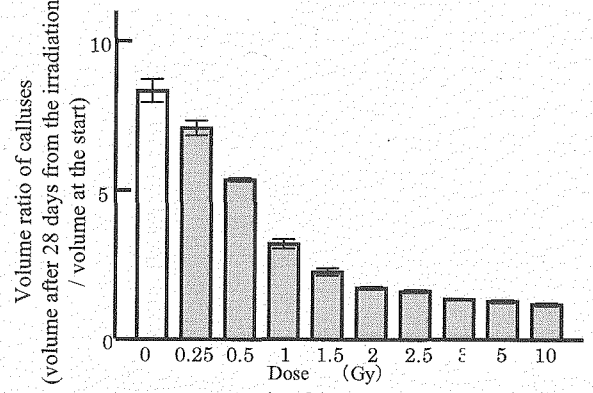


Fig.2 Effects of 100MeV $^{4}He^{2+}$ exposure on the growth of calluses. Values represent the means of 3 experiments. (Bar = standard deviation)



Fig.3 Ion beam-irradiated plants of "White Aga" were planted and grown in a field in order to investigate the pollen fertility.

References

1) Y. Hoshi et al. Plant Cell Rep. 22 (2004) 359.
2) M. Okamura et al. Nuclear Instr. Meth. B 206 (2003) 579.
3) S. Nagatomi et al. TIARA annual Report 1995 (1996) 50.

3-22 Mutation Induction on Hybrid Limonium 'Moon Light' Using Ion Beams

S. Chinone[a)], Y. Hanaoka[a)], K. Tokuhiro[a)], K. Nakatsubo[a)], M. Amano[a)],Y.Hase[b)], A. Tanaka[b)] and I. Narumi[b)]

[a)]Kaneko Seeds LTD., [b)]Radiation-Applied Biology Division, QuBS, JAEA

Abstract

The influences of ion beams irradiation to in vitro shoots on mutation induction in hybrid Limonium 'Moon Light' were investigated. In vitro shoots were irradiated with 320 MeV carbon and 50 MeV helium ion. Carbon ion beam had a high effect on the frequency of rooting and the growth of shoots, and the suitable dose was estimated to be around 4 Gy. Mutation on flower colour and growth characteristic weren't obtained by both ion beams irradiation. We estimated that this result were caused by that the number of materials irradiated with ion beams was insufficient and/or methods for ion beams irradiation to materials was inappropriate.

1. はじめに

*Limonium latifolium*や*L.bellidifolium*などとの種間交雑によって育成されたハイブリッド・スターチスは，主に添え花として利用されている．本研究では花が紫色の'ムーンライト'の花色の幅を広げることを目的にイオンビームを照射した．

2. 材料および方法

無菌的に培養を行っている'ムーンライト'の多芽体を1本のシュートに分割し，発根培地を分注した60mmシャーレに置床した．

イオンビーム照射は日本原子力研究開発機構イオンビーム照射研究施設（TIARA）のAVFサイクロトロンを用いて，炭素（$^{12}C^{6+}$,320 MeV）およびヘリウム（$^{4}He^{2+}$,50 MeV）を照射した．照射線量は$^{12}C^{6+}$で2，4，8，16および32Gy，$^{4}He^{2+}$で10，20，40，80および160Gyとした．照射後は新しい発根培地に移植し，移植1ヵ月後に調査を行った．調査後，発根している培養体の順化を行い，順化2ヵ月後にパイプハウスに定植し，開花検定を行った．

3. 結果および考察

1）培養体への影響：シュートや根の生育などへの影響は$^{12}C^{6+}$照射の方が$^{4}He^{2+}$照射より大きかった．

$^{12}C^{6+}$照射による発根率は0，2および4Gyの線量で100%であったが，8Gy以上の線量では低下した．シュートの生育は，4Gyで対照区と比べてわずかに抑制された．8Gy以上の線量になると生育は著しく抑制され，発根せずに枯死する個体が認められるようになった（Fig.1, Fig.2）．

$^{4}He^{2+}$照射による発根率は，対照区と10Gyで95～100%であったが，20Gy以上になると60～80%と低下した（データ略）．シュートの生育は，10Gyで生育抑制はわずかであったが，20Gy以上では枯死する個体が多くなった．

このことから，$^{12}C^{6+}$での適正線量は4Gy付近，$^{4}He^{2+}$での適正線量は10Gy付近であると推察された．

2）開花特性への影響：$^{12}C^{6+}$を照射し，正常に生育した136個体および$^{4}He^{2+}$を照射した228個体の開花検定を行った（Tab.1）．花色や生育特性に関する変異個体は認められなかった．イオンビーム照射による変異率は，カーネーションの花色や花弁の変異で3%程度[1)]であることが報告されているが，本実験では，供試個体数が少なかった，もしくは供試材料の大きさや照射の方法が適切でなかったため，変異個体が作出されなかったのではないかと推察された．

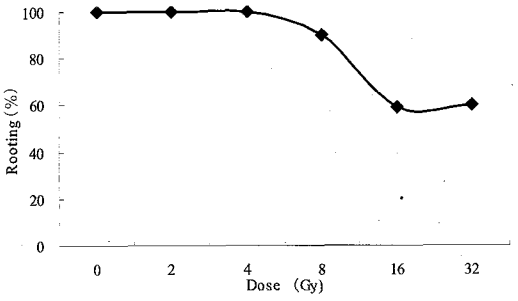


Fig.1. Influence of 320 MeV carbon ion beam irradiation to in vitro shoots on rooting in hybrid Limonium 'Moon Light'.

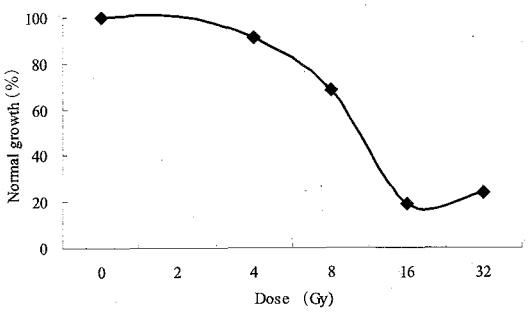


Fig.2. Influence of 320 MeV carbon ion beam irradiation to in vitro shoots on growth in hybrid Limonium 'Moon Light'.

Tab.1. The number of plants planted in the Greenhouse.

Dose (Gy)		No. of plants	Dose (Gy)		No. of plants
Control		10	Control		10
$^{12}C^{6+}$	2	41	$^{4}He^{2+}$	10	53
	4	38		20	42
	8	29		40	45
	16	8		80	36
	32	10		160	42
Total		136	Total		228

Reference

1) M. Okamura, et al., Wide variety of flower-color and shape mutants regenerated from leaf cultures irradiated with ion beam, Nuclear Instruments and Methods in Physics Research B, 206, 574-578 (2003).

3-23 Effects of Ion Beam Irradiation on Spore Germination, Mycelial Growth and Fruit Body Formation of *Pleurotus ostreatus*

Y. Kawashima[a)], T. Matsumoto [a)], Y. Hase [b)]and Y. Yokota [b)]

[a)]Gunma Prefectural Forestry Experiment Station, [b)]Radiation-Applied Biology Division, QuBS, JAEA

The mushroom varieties have been improved through clonal selection from wild species and crossing between strains. Since these methods require long terms, it is essential to establish more effective methods for breeding of mushrooms.

The ion beams, which have a higher linear energy transfer (LET) than X-rays and gamma rays[1)], are one of the efficient mutagen, and have been applied for mutation breeding of many horticultural and ornamental crops[2)]. However, there are few studies of ion beam irradiation in mushrooms[3)].

We previously reported the effect of ion beams on the growth of basidiomycete *Lyophyllum decastes* (Fr.:Fr) Sing[4)]. The germination rate of the irradiated spore slightly decreased at 350 Gy of $^{12}C^{6+}$ ion beams, and few spore germinated at the dose of 600 Gy. The mycelial growth and the regeneration rate of fruit bodies also decreased as the irradiation dose increased. Here, we report the mutagenic effect of ion beams in *P.ostreatus*.

Basidiomycete *Pleurotus ostreatus* (Jacq.:Fr.) Kummer grow in hardwood. The habitat is, often in large clusters, usually on stumps and fallen or standing trunks of broad-leaved trees, especially beech. Common, edible and tastes good. Distribution is over the whole world. *P.ostreatus* is characterized by the fruit bodies with unique stalk attached to the pilei which opens up like an oyster shell during the morphogenesis. Hence these fungi are also popularly called "oyster mushrooms" .

The segments of fresh fruit body and spore were taken from GPO-76, the wild species of *P.ostreatus* that was collected in the central part of Gunma Prefecture. They were cultured on modified Potato Dextrose Agar (PDA) medium in 5 cm φ petri dishes. The samples were irradiated with carbon-ion beam (320 MeV $^{12}C^{6+}$) with the doses of 100 to 1000 Gy. After irradiation, mycelial growth and germination rate of spore were investigated for 2 weeks. Then, the fruit body segments were transferred to the culture medium and were allowed to form fruit bodies. The culture medium for fruit body formation were made of saw - dust from hard wood and rice bran, mixed in the ratio of 10:2 (g/g) and watered to raise the final moisture content to 65%. The mixtures were packed 550 g each into 850 ml Polypropylene bottles (62 mm diameter × 16 cm hight). A hole about 2 cm in diameter that reached to the bottom of the bottle was made in the medium. The bottles were sterilized at 121C° for 45 min before inoculation. The cultivation room was kept at 22C° dark. When the vegetative mycelia extended throughout the bottle, usually 30 days after inoculation, the surface of the mediums were scratched and removed (kinkaki treatment). The bottles were filled with water for 2 hours, and then the extra water was drained off. Then, the atmosphere was changed to 15C°, 90% relative humidity and 350 lux illumination. The fruit bodies were formed around 50 days after kinkaki treatment. The yields were measured as fresh weight grams, and each average value was calculated.

As the irradiation dose increased, the germination rates and the mycelial growth decreased. At the dose of 400 to 500 Gy in $^{12}C^{6+}$ ion beams, the regeneration rate started to decrease and at the dose of 600 Gy and over, few spore germinated. At the dose of 700 Gy and over, no mycelial growth was observed. There was no significant difference between the yields of the irradiated and the control fruit bodies. Some morphological changes were observed in the fruit bodies. For example, the fruit bodies shown in Fig.1 extended unintentional direction, and the fruit bodies shown in Fig.2 are larger and longer compared to the control fruit bodies.

We are performing cytological studies to investigate horticultural values of the regenerated fruit bodies.

References

1) A. Tanaka et. al., Int. J. Radiat. Biol 72 (1997) 121-127.
2) N. Kudo et. al. TIARA Ann. Rep. 16(1998) 62-64.
3) H.Akaishi et. al. TIARA Ann. Rep. 18(2000) 56-57.
4) Y.Kawashima et.al. TIARA Ann. Rep. 18(2004) 96-97.

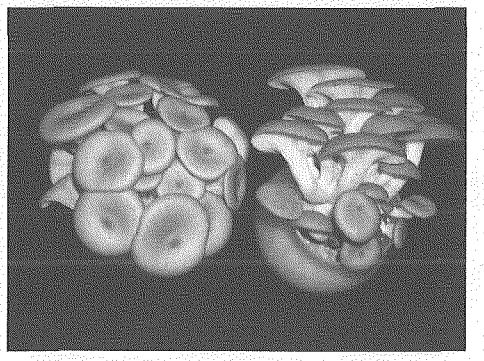


Fig.1 Fruit body of *P.ostreatus*, regenerated from 100 Gy-irradiated mycelia (left) and control (right).

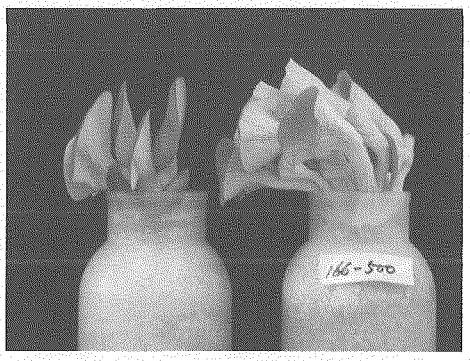


Fig.2 Fruit body of *P.ostreatus*, regenerated from 500 Gy-irradiated mycelia (right) and control (left).

3-24 Mutation Induction of Asiatic Hybrid Lily Using Ion Beam Irradiation

N. Chiba [a)], K. Arakawa [a)], S. Nakamura [a)], S. Suzuki [a)], Y. Adachi [b)], Y. Yokota [c)] and Y. Hase [c)]

[a)]Miyagi Prefectural Agriculture and Horticulture Research Center
[b)] Miyagi Prefectural Ogawara Region Agricultural Improvement and Development Center
[c)]Radiation-Applied Biology Division, QuBS, JAEA

Abstract

We examined two hundreds fifty-two M_1 plants that were derived from carbon ion irradiated ramentam of Asiatic hybrid lily. Mutation was observed at flower shape, flower color, spots on tepals and leaf shape. Estimated mutation induction rate was 4.5% and 4.1% at 0.5Gy and 1.0Gy respectively. These results suggest that mutation induction using carbon ion beam is an effective method for development of novel cultivars in Asiatic hybrid lily.

スカシユリ（Asiatic hybrid lily）は，エゾスカシユリ（*Lilium dauricum*），イワトユリ（*L. maculatum*），ヒメユリ（*L. concolor*）など，東アジア一帯に自生する原種に由来する交配群である[1)]。これまでに花の色素の組み合わせや，花弁の斑点の数を少なくすることを主要な育種目標とし，品種が開発されてきた[2)]。しかし，既にほとんどの交配可能な組み合わせで育種が行われているため，近年では新規性の高い品種が作出困難な状況にある。そこで，イオンビームを利用した突然変異育種により，新たなスカシユリの育種母本の作出を試みた。

直径６cmのシャーレに無菌培養で育成した黄色系スカシユリ品種のりん片80枚を置床したものを２枚用意した。これらをAVFサイクロトロンにより，炭素イオン$^{12}C^{6+}$（320MeV）線量0.5Gyと１.0Gyの条件で１枚ずつ照射した。その後にりん片から形成した球根をＭＳ培地で培養して，突然変異系統M_1世代を育成した後，これらをほ場で栽培，開花時に形質の変化を調査した。

炭素イオンを照射した80枚のりん片から，0.5Gyで178系統，1.0Gyで74系統，合計252系統のM_1世代を得た（Table 1）。無照射のりん片に比べ，照射したりん片から形成した球根の数は少なく，照射の影響が見られた。照射後の球根の生育は，培養中の２～３葉期までは，無照射のものより劣ったが，以後は回復した。

確認できた変異をTable１とFig.1，2に示した。スカシユリの花皮片は，大きく開いているのが特徴であるが，同属別種のテッポウユリ（*L. longiflorum*）のように，開花後も花皮片が筒状の突然変異が見られた。花色の突然変異については，黄色が濃くなったＭ１系統が出現した。花皮片の斑点の数は，一般に，多すぎると好まれない傾向にある。本調査では斑点が変化した８系統のM_1を得た。これらの花皮片には全く斑点が無いか，その数が減少していた。葉形については，葉の幅が狭いM_1系統が見られた。これらの結果から，諸形質における突然変異の出現率は，0.5Gyで4.5%，1.0Gyで4.1%と推定された。

スカシユリの交配群の中には，花皮片が筒状の品種が無いため，本試験で得られた花皮片が筒状の突然変異体は，育種母本として利用できる可能性がある。花皮片の斑点にイオンビームが影響することを利用して，斑点の数を少なくする改良技術も可能と考えられる。

References
1) A.C. Leslie, “The international lily register, 3rd edition” ,The Royal Horticultural Society, London, (1982).
2) M. Yamagishi, “スカシユリ花色の遺伝様式” ,農業および園芸 80: 1267-1271 (2005).

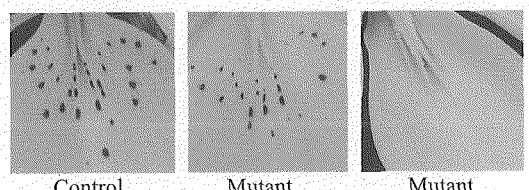
Table 1 Number of observed mutation induced by carbon ion beam.

		Dose(Gy)	
		0.5	1.0
No. of investigated M_1		178	74
Observed mutation	Flower shape	1	0
	Flower color	0	1
	Spots on tepals	6	2
	Leaf shape	1	0



Control Mutant

Fig. 1 Flower shape mutant induced by carbon ion beam (right) and control (left).



Control Mutant Mutant

Fig.2 Changes in spots on tepals between mutants (right and center) and control (left).

3-25 Screening of Cadmium Resistant Rice Mutants Induced by Carbon Ion Irradiation

T. Tsukamoto[a, c], H. Nakanishi[b], H. Hase[c], A. Tanaka[c], N. K. Nishizawa[a, d] and S. Mori[b]

[a]Department of Global Agricultural Sciences, The University of Tokyo, [b]Department of Applied Biological Chemistry, The University of Tokyo, [c] Radiation-Applied Biology Division, QuBS, JAEA, [d]Core Research for Evolutional Science and Technology (CREST), JST

1. Introduction

Cadmium (Cd), being a highly toxic metal pollutant of soils, inhibits root and shoot growth and yield production, affects nutrient uptake and homeostasis, and is frequently accumulated by agriculturally important crops including rice with a significant potential to impair animal and human health.

The aim of this work is to isolate rice mutants that lack translocation of Cd to the grain. In order to make it, we selected Cd resistant rice mutants that lack absorption of Cd from roots or translocation of Cd to shoots.

2. Experimental procedure

Dry rice seeds of rice (*Oriza sativa* L. cv. Nipponbare) were used. The irradiation apparatus for seeds, connected to a vertical beam line of the TIARA AVF cyclotron, was used for the 320 MeV carbon ion irradiation. The carbon ion irradiation with the doses of 50 Gy was performed under atmospheric pressure within 3 min. M_1 seeds were grown to maturity and harvested. About 2500 M_2 seeds were used for the first screening of Cd resistant assay.

For a pilot study, about 2500 seeds of non-irradiated rice "Nipponbare" were cultured in the fertilized soil containing 0, 100, 250 and 500ppm Cd in a growth chamber under a mixture of incandescent and fluorescent lamps with a 14 h light (30 °C)/10 h dark (25 °C) regime and a photon flux density of 320 μmol m^{-2} s^{-1}, respectively. After 3 weeks, the growth was observed.

For first screening, about 2500 M_2 seeds were cultured in the fertilized soil containing 250 and 500ppm Cd in a growth chamber. After 3 weeks, the survival plants were isolated.

3. Results and discussion

In order to investigate optimum concentration of Cd for rice "Nipponbare", about 2500 seeds of wild type "Nipponbare" were cultured in the fertilized soil containing 0, 100, 250 and 500ppm Cd, respectively. In all treatments of Cd, the growth of plants was suppressed (Fig. 1). A remarkable suppression of growth at 500ppm was observed. Therefore, we adopted 500ppm as the optimum concentration for Cd resistant assay to obtain mutants efficiently.

In order to obtain Cd resistant rice mutants, about 2500 M_2 seeds were cultured in the fertilized soil containing 250 and 500ppm Cd. After 3 weeks, 51 rice plants survived. These plants were transferred to the fertilized soil without Cd for harvesting M_3 seeds.

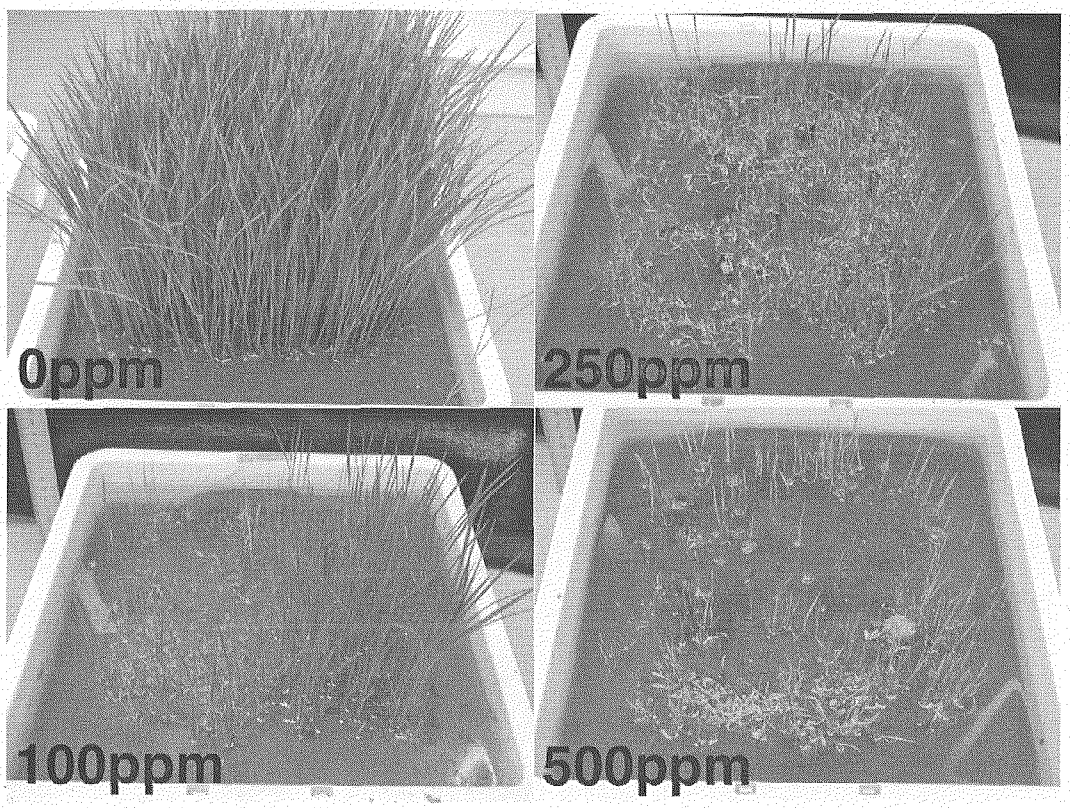


Fig. 1
The effect of Cd concentration on the growth of wild type "Nipponbare". "0ppm, 100ppm, 250ppm and 500ppm" indicate each concentration of Cd, respectively,

3-26 Ion Beam Breeding of Rice Variety Suitable for Low Nitrogen Input

H. Katayama [a)], H. Kitamura [a)], M. Mori [a)], J. Nakagawa [a)], T. Yoshida [a)], T. Kawai [a)], Y. Hase [b)], and A. Tanaka [b)]

[a)]Shiga Prefecture Agricultural Technology Promotion Center,
[b)]Radiation-Applied Biology Division, QuBS, JAEA

1. Introduction

In Shiga Prefecture, eutrophication of Lake Biwa caused by nitrogen is a serious problem. The data estimated by Shiga Prefectural Government at 2000 was reported that 16 % of nitrogen flowing into Lake Biwa is caused by agricultural drainage.[1)] Therefore, Shiga prefecture enacted "the ordinance for promotion of harmony between agriculture and natural environment" that could decrease the fertilizers and pesticides.

We aimed the breeding of the rice plants that maintain stable yield under low input of nitrogen fertilizer.

It has been reported that the ion beam can induce novel mutations for crop breeding.

Therefore, we have started to breed the rice cultivar suitable for growing in low nitrogen condition. Here, we investigated the effects of carbon-ion irradiation on the growth in rice.

2. Experimental procedure

2-1.

The hulled rice seeds (*Oryza sativa* L. cv. Akinouta) were placed on plastic dishes with embryo upward and they were exposed to the 320 MeV carbon ions with the doses of 20, 40, 60, 80, and 100 Gy. The irradiated seeds were cultured and the progeny seeds (M2) were obtained. The seeds were cultured in conventional fertilizer condition (basal fertilizer N=2.0 kg/10a and ear fertilizer N=2.0 kg/10a) or no fertilization condition. The growth was examined in heading stage and maturing stage.

Table 1. Growth examination in progeny line (M2) of rice seeds irradiated by 320 MeV carbon ions with different doses

Dose (Gy)	fertilizer condition	Numbers	culm length (cm)	contrast *	panicle length (cm)	contrast *	panicle number (number/stub)	contrast *
0	conventional	10	96.7 a		19.5 ab		19.3 a	
20		15	95.0 a		19.8 b		19.2 a	
40		8	93.7 a		19.5 ab		20.1 ab	
60		16	95.3 a		19.6 ab		21.4 b	
80		8	93.1 a		19.0 a		20.9 ab	
100		3	92.9 a		19.7 ab		21.7 ab	
0	no	10	84.6 ab	0.87	19.3 a	0.99	15.1 a	0.78
20		15	85.9 b	0.90	19.2 a	0.97	16.0 a	0.83
40		8	82.3 ab	0.88	18.8 a	0.97	15.6 a	0.78
60		16	82.1 a	0.86	19.1 a	0.97	16.8 a	0.79
80		8	83.8 ab	0.90	18.5 a	0.98	16.2 a	0.77
100		3	81.6 ab	0.88	19.5 a	0.99	16.7 a	0.77

* Numbers are the ratio to the results in the conventional condition.

** English small letter represents the significance of the difference at 5% level by the method of tukey.

2-2.

We reported that the suitable dose to obtain mutants in our rice cultivars is 40 Gy[2)]. Therefore the hulled rice seeds (*Oryza sativa* L. cv. Akinouta and Daiiku-1743) were exposed to the 320 MeV carbon ions with the dose of 40 Gy. The progeny seeds (M2) were cultured in low fertilizer condition (basal fertilizer N=0kg/10a and ear fertilizer N=2.0 kg/10a). The mutants were selected in maturing stage.

3. Results and discussion

3-1.

Compared to the conventional fertilizer condition, the culm length was shortened by 10% and panicle number was reduced by about 20%, in the no fertilization condition. However, the panicle length was similar in both fertilizer conditions (Table.1).

It is thought that the culm length was shortened and the panicle number was increased as the dose increased, although the difference is not significant.

3-2.

The difference of four weeks in heading stage and blooming stage was found in M2 population by outside. However, since there is no difference in morphology in most M2 plants, we could not distinguish the environmental factor and genetic factor. Therefore, we first selected the mutants on the basis of the panicle length that is not influenced by environmental factor (Table.2). And then, they were selected again by the ear weight.

The mutants that show high nitrogen absorption ability will be selected.

4. References

1) Biwako Environment Division; Shiga Prefecture, Environment of Shiga.,21 (2002)

2) H. Kitamura et al.,IARA annual report 2004 (2005) 2.23

Table 2. Selection by panicle length of progeny line (M2) of rice seeds irradiated by 320 MeV carbon ions with 40 Gy

Cultivar	Numbers	Selection numbers	Selection rate(%)
"Akinouta"	13358	2794 a	20.9
'Daiiku 1743'	7904	1746 b	22.1

a: No. of plants that have panicle length with more than 20 cm.
b: No. of plants that have panicle length with more than 19cm

3-27 Flower Color and Cluster Modification by Ion Beams in Chrysanthemum

T. Nomizu[a)], N. Furutani[a)], Y. Hase[b)], Y. Yokota[b)] and A. Tanaka[b)]

[a)]Kyoto Prefectural Institute of Agricultural Biotechnology,
[b)]Radiation-Applied Biology Division, QuBS, JAEA

Abstract

The purpose of our study is to determine the optimum ion beam irradiation dose for the formation of shoot primordium or somatic embryo which were taken from petal segments of three chrysanthemum cultivars (H13, H42 and 'Shiroyamate'). Petal segments were cultured on MS medium and then irradiated with 220 MeV carbon ions, accelerated by AVF cyclotron at JAEA at doses of 1-32 Gy. The suitable dose for shoot primordium formation of H13, H42 and 'Shiroyamate' were 2, 2 and 4 Gy, respectively. The suitable dose for embryogenesis of H42 was 2 Gy. The plants are regenerated and will be evaluated their horticultural values in the future study.

盆コギクは、仏花として出荷期幅が決まっており、赤・白・黄の3色セットが求められている。しかし天候による開花変動が大きく、産地では危険分散のために多くの品種が作付けされている。

こうした中で、イオンビームを用いた突然変異育種法はガンマ線やX線などの放射線を用いた育種と比較して幅広い変異を示すことが知られており[1)]、キクでは既にいくつかの品種が育成されている。

本研究では、開花変動の少ない赤色の盆コギクを用いて、イオンビーム照射と培養により草姿や開花特性を同じくする白・黄の盆コギクを育成するために、花弁に照射するイオンビームの照射条件を検討した。

京都府農業総合研究所で育成された赤色の盆コギクH13及びH42と白色の在来品種'白山手'の花弁を3～5 mmに調整し、H13はNAA 10 mg/lとBA 10 mg/l、H42はNAA 1 mg/lとBA 1 mg/l及び白山手はNAA 10 mg/lとBA 3 mg/lを添加したMS培地を10ml含む60 mmシャーレに置床し、日本原子力研究開発機構（高崎市）の照射施設AVFサイクロトロンにおいて、加速粒子は12C5+、エネルギー220 MeVで0～32 Gyの範囲で照射した。照射後に同組成の培地を含む90 mmシャーレに置床し、25℃、連続照明下で8週間培養し、苗条原基の形成率を調査した。また、H42についてはNAA 10 mg/lとBA 20 mg/lを含むMS培地を用いて上記の方法でイオンビームを照射し、5週間後に不定胚の形成率及び形成数を調査した。

イオンビームの線量がH13、H42及び'白山手'の花弁切片からの苗条原基形成に及ぼす影響を調査した(Table 1)。苗条原基は全ての線量区で形成されたが、形成率は線量が増加するにつれて減少し、H13では4 Gy、H42では16 Gy、'白山手'では8 Gyで急激に低下した。

次に、イオンビームがH42の花弁からの不定胚形成に及ぼす影響を調査した（Table 2)。H42の花弁はイオンビームの線量が8 Gyまでは不定胚形成が見られたが、16 Gy以上では不定胚形成は見られなかった。不定胚の形成率は2 Gy、形成数は1 Gyのイオンビーム照射で急激に減少した。

この結果、苗状原基形成及び不定胚形成の効率などを考慮すると、H13及びH42は2 Gyまで、'白山手'は4 Gyまでが適当であると考えられる。今後、再生植物体について花色等の特性を調査する予定である。

Table 1. Effect of carbon ion beam ($^{12}C^{5+}$) irradiation on shoot primordium formation from petal segment

Cultivars	Doses (Gy)	Percentage of petal forming shoot primordium
H13	0	32.1
	1	44.8
	2	20.4
	4	14.8
	8	12.0
	16	16.8
	32	8.0
H42	0	66.8
	1	66.1
	2	66.0
	4	38.7
	8	54.5
	16	38.6
	32	17.1
'Shiroyamate'	0	100
	1	100
	2	100
	4	92.0
	8	32.6
	16	47.4
	32	54.3

Petal segments (3-5 mm) were irradiated carbon ion beam, and then they were cultured in shoot primordium formation medium at 25℃ for 8 weeks under continuous light.

Table 2. Effect of carbon ion beam ($^{12}C^{5+}$) irradiation on somatic embryogenesis from petal segment in H42

Doses (Gy)	Percentage of petal forming embryo	No. of embryos per petal
0	93.5	13.7
1	93.8	6.0
2	73.8	3.7
4	33.3	2.8
8	4.5	1.5
16	0	0
32	0	0

Petal segments (3-5 mm) were irradiated carbon ion beam, and then they were cultured in embryogenesis Medium at 25℃ for 5 weeks under continuous light.

Reference

1) S. Nagatomi, et. Al., TIARA Annual Report 6:41-43 (1998)

3-28 Mutation Induction in Azalea Using Ion Beam Irradiation and Its Gene Analysis

N. Kobayashi[a], S. Sakamoto[a], A. Nakatsuka[a], Y. Hase[b] and Y. Yokota[b].

[a] Faculty of Life and Environmental Science, Shimane University
[b] Radiation-Applied Biology Division, QuBS, JAEA

1. Introduction

Ion beams are powerful and efficient mutagenic tools with high linear energy transfer (LET) and have been applied to mutation breeding of many horticultural crops. Some kinds of mutations of flower color, flower shape, leaf shape and other traits were reported by ion beam irradiation[1, 2].

In this study, ion beams were irradiated to azalea seeds and cultured leaf segments to induce flower color and shape mutation. Additionally, we try to research the key genes of ion beam induced mutations as a final purpose; homeotic genes related to flower shape and organ mutation and anthocyanin biosynthesis genes related to flower color mutation that we already isolated [3,4].

2. Materials and Methods

About one hundred of seeds of *Rhododendron kaempferi* were irradiated with carbon ion beam (220 MeV $^{12}C^{5+}$) at various doses (0 to 200 Gy, Fig. 1). After the irradiation, seeds were sowed on wet filter paper in tissue culture dishes. The germination rate was evaluated after 21 days.

R. pulchrum 'Sen-e-oomurasaki' in pot was used as explants materials. Fungicide treated young leaves were excised and the surface was sterilized by immersing in 70% ethylalcohol for 30 seconds, followed by 10% (w/v) sodium hypochlorite solution for 10 minutes (including 3 minutes treatment of Ultra sonic automatic washer) and then rinsed four times in distilled water. The leaf segments were cultured on modified 1/2 Murashige and Skoog's medium supplemented with 2 μM NAA and 9 μM TDZ in the test tube[5]. After a few days, the explants were transplanted on the high concentration agar medium for the transportation and covered the tissue culture dishes with Kapton film. The transported samples were irradiated with carbon ion beam (220 MeV $^{12}C^{5+}$) at various doses (0 to 128 Gy, Table). After the irradiation the leaf segments were transplanted the initial medium and cultured at 22±1°C and 16 hours-photoperiod. The regeneration rates of shoots and callus were investigated after three months.

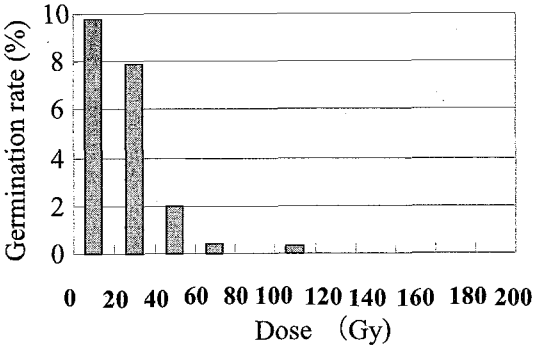


Fig. 1. Dose response of germination rate in *R. kaempferi* at 21days after sowing.

3. Results and Discussion

As a preliminary experiment, we confirmed effective does of carbon ion beam irradiation for *R. kaempferi* seeds. The seeds germinated at ranges from 0 to 100 Gy and they were not able to germinate with more than 120 Gy irradiation. Therefore, the second irradiation was applied narrow doses (0 to 90 Gy) in the same condition. The germination rates were strongly downed from the range of 20 Gy and the optimal irradiation condition may be around these doses for *R. kaempferi* seeds. Further studies using another species are needed to compare these results.

Except 16 Gy irradiated leaves, the regeneration rate of *R. pulchrum* 'Sen-e-oomurasaki' decreased according to the ion beam strength. The explants of 128 Gy irradiation were not able to regenerate shoot and callus (Table 1). For the further detail experiment, it is necessary to resolve some problems of cultured materials during transportation; high temperature damages and culture media dissolution.

4. References

1) M. Iizuka et al. JAEA-Review 2005-001, 50-51.
2) M. Kato et al. JAEA-Review 2005-001, 81-83.
3) Y. Kii et al. 2005. J. Japan. Soc. Hort. Sci. 74 (Suppl.2): 289 (In Japanese).
4) F. Shiba et al. 2005. J. Japan. Soc. Hort. Sci. 74 (Suppl.2): 291 (In Japanese).
5) S. Sakamoto et al. 2005. J. Japan. Soc. Hort. Sci. 74 (Suppl.2): 310 (In Japanese).

Table 1. Regeneration rates of shoot and/or callus from *R. pulchrum* 'Sen-e-oomurasaki' leaf segments at three months after irradiation.

Dose	shoot	shoot primodia and callus	callus	leaf damage index
0Gy	0/19 (0%)	3/19 (15.7%)	18/19 (89.4%)	3.1
4Gy	1/23 (4.3%)	4/23 (17.3%)	21/23 (91.3%)	2.8
8Gy	0/22 (0%)	3/22 (13.6%)	14/22 (63.6%)	3.0
16Gy	0/18 (0%)	0/18 (0%)	5/18 (27.7%)	3.0
32Gy	0/21 (0%)	3/21 (14.2%)	11/21 (52.3%)	2.5
64Gy	0/21 (0%)	1/21 (4.7%)	11/21 (52.3%)	2.4
128Gy	0/11 (0%)	0/11 (0%)	0/11 (0%)	2.6

Leaf damage index was visually evaluated.
0; no damage (all green) to 5; completely browning

3-29 Deletion of Minor Enzyme Activities of *Rhizomucor miehei* by Irradiation of Heavy-Ion Beam

K. Sakai[a)], H. Kobayashi [a)], A. Oshima [a)], S. Kato[a)], K. Sato[b)], Y.Hase[b)], I. Narumi[b)], T. Sakashita [b)] and Y. Kobayashi [b)],

[a)]Tokyo Research Laboratory, Meito Sangyo Co.,Ltd. [b)] Radiation-Applied Biology Division, QuBS, JAEA

Cheese is one of the most important dairy food produced from milk and various kind of cheese are produced worldwide(16.5 million ton, FAO report)[1)]. Rennet, a kind of enzyme, can hydrolyse the amide bond of *k*-casein (Phe105-Met106) very specifically and causes milk coagulation. Rennet is traditionally extracted from the fourth stomak of young ruminants. As increasing cheese production, microbial proteases originated from *Rhizomucor pusillus(Rh. pusillus)* and *Rh. miehei* have been developed. Also fermentation produced chymosin (FPC or clone chymosin) has already developed[1)]. Because FPC produced cheese gains only limited public acceptance yet and BSE issue of animal rennet, demands for microbial non-genetically modified organism coagulant is increasing again.

Microbial coagulant contains many kind of enzymes as contaminants, amongst of them lipase affects severely cheese flavor and amylase limits utilizing whey, a chemical inactivation process should be necessary[2)]. Breeding a mutant with low side-activities or without them is very important from economical standpoint because such mutant strain enables abbreviation of activity losing process. Heavy-ion irradiation is expected to induce a different mutagenesis by its high linear energy transfer (LET) comparing to UV and gamma-ray irradiation and chemical mutagene.

Sporangiospore of the coagulation enzyme producing strains of *Rh. miehei* was harvested from an agar plate culture and was spread on petri dish with an aid of diluted Triton X100. Spores(10^7 per dish) were dried over Silica gel and then their water activity was adjusted over saturated NaCl solution at 6℃. Dried spores were covered with Kapton film and stored until irradiation of heavy-ion beam at TIARA HY-1 port. Every heavy-ion beam of $^{4}He^{2+}$ (50MeV), $^{12}C^{5+}$(220MeV), $^{20}Ne^{7+}$(350MeV) and $^{40}Ar^{13+}$ (460MeV) was irradiated at dose range from 20 to 1000Gy. The spores were suspended again in sterile water and were cultivated on yeast extract-glucose agar plate (YG plate) to determine a survival rate. Colony of mutant strains grown on YG plate were transferred to YG slant medium and cultivated for 7days. A small portion of felt-like mycelium was scraped off and inoculated to soya flower-starch producing medium. Milk coagulating activity was assayed with 10%(w/v) skim milk containing 10mM $CaCl_2$ at 35℃. Lipase and amylase activities of fermented broth were detected respectively by spotting the broth on emulsified olive oil-agar plate or potato starch-agar plate.

The sporangiospore suspension was spread on petri dish with a diluted Triton X-100 so that the sporangiospore tends to aggregate because its surface hydorophobicity. Although spores would be overlapped each other in the sample preparation, it is considered that the depth of stacked spores might within the range of each ion because the survival rates after irradiations was reproduced. Irradiation to spread spore on a petri dish was more effective to process much samples than that fixed on membrane[3)].

The result obtained was shown in Fig.1.The dose response of C and Ne ion was about ten times sensitive than that of He and Ar ion. At the same dose of 200Gy, both C and Ne ion irradiation gave a survival fraction of about 1%, whereas both He and Ar ion did a rate of about 10%. This result is good agreement with the reports that C or Ne ion have larger relative biological effectiveness than He or Ar.

Lipase activity and amylase activity production of survived spores have checked by plate assay method. Hallow was formed on each plate by spotting fermented broth of the spores. Although no mutant lacking neither lipase nor amylase was isolated among the preliminary several hundreds strains, a few light-red colored colonies were found. It was reported that this color was caused by a auxotrophic mutation in adenine synthesis of *Aspergillus oryzae*[4)]. The same mutation should be occurred in *Rh. miehei* by heavy-ion irradiation and there is a possibility isolating mutant strains that lacks lipase or amylase activity.

We intend isolation of lipase-less mutant by irradiation of C or Ne ion beam at a dose from 100 to 200Gy in 2006.

References

1) Fox, P.(2004) Cheese Chemistry, Physics and Microbiology
2) Garg, S. (1994) Food reviews International,10,313-355
3) Amsal, A. (1999) Food Sci. Technol., 5(2), 153-155
4) Feng, J. (2004) Biosci.Biotechnol.Biochem., 68(3), 656-662

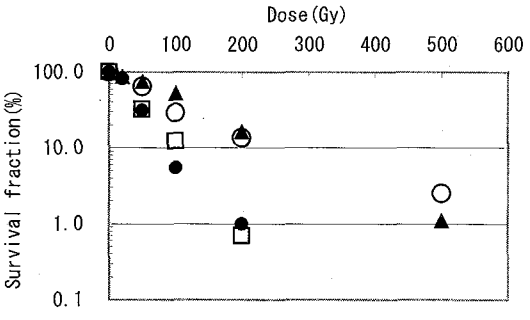


Fig. 1. Dependence of Survival Fraction on Dose and Species of Ion.

Dried spore were irradiated by He (○), C (□), Ne (●) and Ar (▲). After treatment, every spore was suspended again in sterile water to give appropriate number of vital spore a Y-G plate.

3-30 Mutation Breeding of Koji Mold Induced by Ion Beams

K. Ito[a)], J. Takeichi[a)], Y. Hanya[a)], K. Satoh[b)], Y. Hase[b)] T. Sakashita[b)], Y. Kobayashi[b)] and I. Narumi[b)]

[a)]R&D Division, Kikkoman Corporation. [b)]Radiation-Applied Biology Division, QuBS, JAEA

Introduction

Koji molds, *Aspergillus sojae and Aspergillus oryzae*, are a very important microorganism in the industry used for brewing of soy sauce. In soy sauce production, proteases and peptidases are key enzymes. These enzymes hydrolyze proteins of soybean and wheat to peptides and amino acids, which form the basis for the taste of soy sauce. Therefore, many soy sauce researchers have tried improvement related to the enzyme production of koji molds. Recently, recombinant DNA techniques have been developed to improve koji molds. However, the utilization to foods of these techniques is difficult in Japan from the viewpoint of the public acceptance. For this reason, it is still important to improve koji molds by traditional mutation. There are problems that traditional mutation due to the usual mutagens, UV, NTG and X-rays, leads to much inconvenient mutation. Consequently, almost mutants simultaneously have inconvenient characters, slow growth rate, low activity of other enzymes etc, even if high protease activity was acquired. Then, we focused on mutation by ion beam. It is known that this method induce targeted mutations with a very small number of inconvenient mutation, in spite of high mutation frequency because of its high linear energy transfer (LET). For the purpose of obtaining protease overproducing mutant without inconvenient characters, we employed ion beam method for mutational breeding of koji molds. In this report, we investigated survival rate and mutation frequency of *A. sojae* IFO4241 to determine optimal irradiation condition of ion beam mutations.

Materials and Methods

(1)Survival rate

Survival rate was calculated by comparing the number of colonies with or without irradiation. The suspensioncontaining of 10^2-10^6 conidia were spread on Malts agar medium (Kyokuto Seiyaku) and incubated at 30°C for 6 hours for germination. Germinated conidia were irradiated with 50MeV ^{4}He (LET was 17.5 keV/μm), 220MeV ^{12}C(121.8keV/μm),350MeV ^{20}Ne (440.8 keV/μm) ion beams accelerated by AVF cyclotron at JAEA, in a dose range of 10-500 Gy. Irradiated conidia were cultured at 30°C for 3 days. The number of colonies was counted.

(2)Mutation frequency

Mutation frequency was measured by counting the number of Pyrithiamine (PT) resistant colonies[1)]. PT resistant mutants were selected on Czapex-Dox medium (BD Falcon) containing 0.2 μg/ml pyrithiamine.

(3)Sequence analysis of *thiA* gene of PT-resistant mutants

The *thiA* gene that is involved in PT-resistance of *A. sojae* from mutants was amplified by PCR using primers (5′-GGGGTGACGATGAGCCGCTCTT-3′and 5′-GGGCAATTGATTACGGGATCCCAT-3′) and the genomic DNA as a template. The amplified fragments were sequenced by BECKMAN COULTER CEQ2000 and mutation sites were decided.

Results and Discussion

(1)Survival rate and mutation frequency

Figure 1 shows the survival rate of *A. sojae* IFO4241 irradiated with each ion beam. The survival rate to ^{4}He ion beam was similar to that of ^{20}Ne ion beam, whereas that of ^{12}C ion beam was remarkably low. The comparison of the maximum mutation frequency after irradiation is shown in Table1. The maximum mutation frequency with ^{12}C ion beam irradiation tended to be higher than that of other ions and was ten times higher than that with UV irradiation. Unlike in the case of plants, the maximum mutation frequency irradiated with each ion beam, except for ^{20}Ne ion beam, was observed on the irradiation condition that the survival rate was below 10^{-2}.

(2) Sequence analysis of *thiA* gene of PT-resistant mutants

It has been reported that the deletion mutation frequently occurs due to ion beam irradiations. To investigate the type of mutations caused by ion beam in koji molds, the *thiA* gene of PT-resistant mutants were sequenced. In 33 PT-resistant mutants, 4 resistant mutants depended on *thiA* gene mutation, and all mutations were base substitutions. All sites of base substitution were different. The number of base substitutions in *thiA* gene, which were obtained by ion beam irradiation, was smaller than that of UV irradiation.

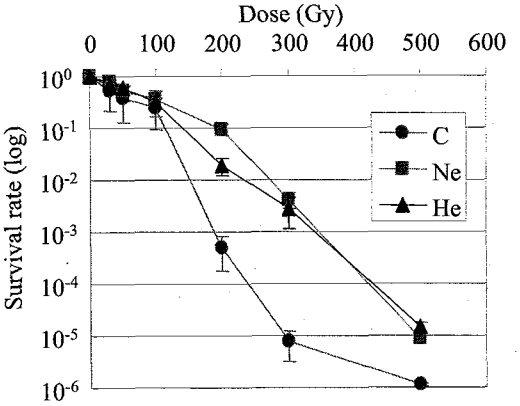


Fig.1 Survival rate of germinated conidia after irradiation with ion beams in *A. sojae* IFO4241.

Table.1 Comparison of the maximum mutation frequency.

	He (300Gy)	Ne (200Gy)	C (200Gy)	UV
Mutation Frequency ($\times 10^{-5}$)	3.56	1.88	5.60	0.26

The dose which detected the maximum mutation frequency of each ion is shown in parentheses. The germinated conidia were exposed to UV with a germicidal lamp. The survival rate of UV irradiation condition which detected the maximum mutation frequency was 0.12.

Reference

1) T. Kubodera et al. FEBS Lett., 555(3), 516-20 (2003).

3-31 Analysis of Cellular Effects and Local Damage Induced by High LET Heavy Ions

S. Wada [a, b], N. Hamada [a, b], T. Funayama [b], T. Sakashita [b], T. Kakizaki [c], Y. Yokota [b], Y. Hase [b], and Y. Kobayashi [a, b]

[a] Department of Quantum Biology, Division of Bioregulatory Medicine, Gunma University Graduate School of Medicine, [b] Radiation-Applied Biology Division, QuBS, JAEA, [c] Department of Veterinary Medicine, Kitasato University

Radiation-induced cell death is thought to result from DNA damage. Radiation-induced residual unrepaired and misrepaired DNA damage lead to genetic instability and cell death. Especially apoptosis, that is programmed cell death, is induced through activation of DNA damage signals. Now many research of this pathway is proceeding. Recently several studies have suggested that one of signal transduction of radiation-induced apoptosis could also mediate cell membrane damage and this pathway is the sphingomyelin–ceramide signal transduction. The pathway is considered that radiation-induced membrane damage activates sphingomyelinases that convert sphingomyeline of cell membrane into ceramide without DNA damage signals and ceramide generated from cell membrane serves as a second messenger in inducing apoptosis. It was suggested, however, radiation also induces other pathway for apoptosis by ceramide. The mechanism is ceramide synthase pathway by mediation of DNA damage signals, radition-induced DNA damage increase ceramide level by the synthesis of ceramide through the activation of the ceramede synthase. For this reason, Sphingomyelin–ceramide signal transduction pathway of radiation-induced apoptosis from cell membrane is not known in detail. So, because microbeam apparatus can irradiate a specific area of target cells, it is considered to be effective means for elucidation of the pathway by membrane/cytoplasm damage. In this study we investigated apoptosis induced by selective membrane/cytoplasm irradiation using the microbeam irradiation apparatus.

Chinese hamster ovary (CHO-K1) cells were grown in Ham's F12 medium supplemented with 10% serum on the CR-39 plate that is ion-track detector. For selective cytoplasm/membrane irradiation, these cells were exposed to 11.2 MeV/u ^{40}Ar ions provided by the AVF cyclotron using heavy ion microbeam irradiation apparatus at TIARA, JAEA-Takasaki. After irradiation, CR-39 plates were etched form the opposite side of the cells with KOH-ethanol solution at 37°C to visualize ion tracks. Then, we observed each irradiated cells and induction of apoptotic cells was detected by the TUNEL assay after 72 hrs. To observe the localization of ceramide in the cells, ceramide was detected by immunohistochemical method.

To confirm cytoplasm irradiation, the phase-contrast microscope image of irradiated cell was overlaid with etched ion pits image (Fig.1). ^{40}Ar ions traversed cytoplasm only. We could deposit radiation damage on membrane/cytoplasm only using microbeam apparatus. Fig. 2 shows the change of apoptotic fraction induced by cytoplasm irradiation after 72hrs. Apoptotic fraction induced by cytoplasm irradiation was about 1.4% and higher than that of control. This result indicates that apoptosis was induced by even cytoplasm irradiation. When the localization of ceramide in the cells by cytoplasm irradiation was observed, ceramide and etched ion pits were observed at nearly same position. It was considered that ceramide was generated at damage site of cytoplasm.

These results indicate that radiation induces apoptosis and production of ceramide without mediation of DNA damage signals.

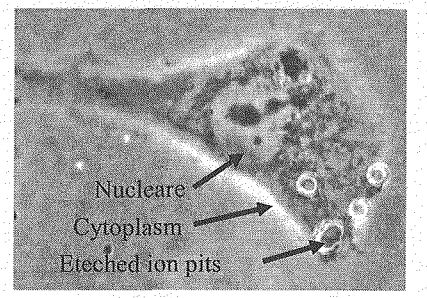


Fig. 1. Picture of an irradiated cell overlaid with an etched ion pits image. The microscope image of irradiated cells was overlaid with the image the etched ion pits obtained at the same field. ^{40}Ar ions traversed cytoplasm only.

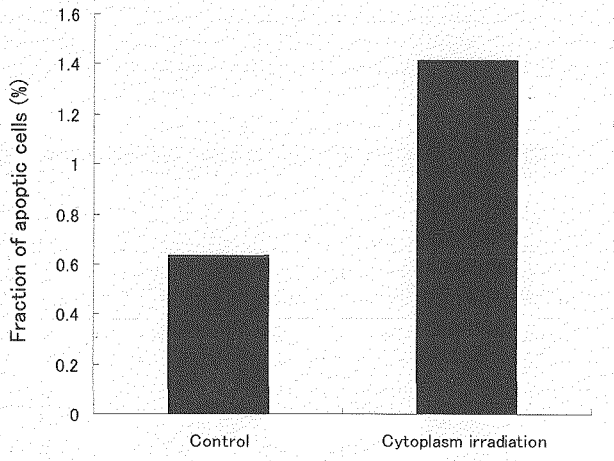


Fig. 2. Apoptotic fraction induced by cytoplasm irradiation after 72hr. Apoptotic fraction induced by cytoplasm irradiation is higher than that of control.

3-32 Recent Improvements of Heavy-Ion Microbeam System for Bystander Study

T. Funayama [a)], T. Kakizaki [a)], S. Wada [a, b)], Y. Yokota [a)], T. Sakashita [a)], N. Hamada [a, b)] and Y. Kobayashi [a, b)]

[a)] Radiation-Applied Biology Division, QuBS, JAEA, [b)] Department of Quantum Biology, Division of Bioregulatory Medicine, Gunma University Graduate School of Medicine

Introduction

Heavy-ion microbeam system enables target irradiation of various biological samples from cell to individual with a microbeam of minimum 5 μm in diameter. Using this system we had been carried out many kind of biological applications.

Analysis of molecular mechanisms of bystander effect is one of the most important subjects in recent radiobiological field, and target irradiation of cells with microbeam is considered as a most effective means to solve this issue. However, our system had had a limitation in targeting accuracy and irradiation speed. In addition, the limitation of beam time interfere the rapid progress of the study.

Therefore, we had improved our system to adopt the effective analysis of bystander mechanisms. Here, we report our improvements in three major points.

Upgrading performance of cell targeting system

Automatic sample stage and focus control unit of cell targeting system are very important parts for assuring targeting accuracy of the system. However, we had not been able to maximize its performance because of the miss-action of focus control unit caused by aged deterioration. Therefore, we renewed focus control unit of cell targeting system with newly designed one. According to this replacement, we developed new stage driver software, and optimized the performance of stage movement by tuning software code. With this optimization, amount of time required for each single stage action were shortened, and total throughput of cell irradiation was significantly increased. We consider that this improvement of stage system will bring us more numbers of cells irradiated within beam time, and help us to promote analysis of molecular mechanisms of bystander effect.

Micro-laser interface for off-beam irradiation

Our heavy-ion microbeam system had contributed to the analysis of radiation-induced bystander effect, and it will also be anticipated to contribute in future. However, the analysis of bystander effect will become more complicated, and will be consider to require more beam time for analysis. Nevertheless, it is apparently difficult to increase beam time sufficient enough for carrying out complete analysis, so that we will not be able to run molecular analysis satisfactorily by limited beam time of the AVF cyclotron. Therefore, to overcome this difficult situation, we introduced a UV micro-laser interface on our cell targeting system to use as *off-beam* irradiation source.

Our UV laser interface was incorporated into the *offline2* microscope system, which is a part of cell targeting system of heavy-ion microbeam. This laser interface can irradiate cells with laser light of 365 nm wavelength using optics of microscope, and its spot size is minimum 1 μm in diameter. It is known that irradiation of UV laser of 356 nm wavelength induces DNA double strand break in targeted region of cell nucleus, and its efficiency can be enhanced by DNA labeling by bromo-deoxy-uridine (BrdU).

To confirm that UV laser irradiation induces DNA double strand break on irradiated nucleus region, we irradiated CHO-K1 cells that were treated with the media containing thymidine analogue BrdU (50 μM) for 6 hours to label its DNA. Prior to irradiation, we registered the coordinates of target cells to irradiation software, thereafter the center of cell nucleus were irradiated by UV laser of 1 μm in diameter. After irradiation, the cells were incubated for 15 min at 37°C, fixed, and then immunostained by antibody specific to phosphorylated histone H2AX (γH2AX). Thereafter, the stained cells were revisited according to registered coordinate, and fluorescent images were obtained by cooled CCD camera.

In the stained irradiated cells, we detected clear γH2AX foci in the center of the cell nucleus. The result suggested that we become able to induce DNA double strand break not only by heavy ion irradiation, but also by UV-laser, which do not restricted by beam time. DNA double strand break is now considered as a key trigger of induction of bystander effect, so that our *off-beam* irradiation method will be a useful means to accelerate molecular analysis of the bystander effect.

Improvement of post-irradiation analysis software

We had developed and utilized software for post-irradiation analysis that automatically obtains images of irradiated cells continuously after irradiation. However, this software had adopted only to obtain phase-contrast images of cell, so that it was difficult to utilize it to immunostaining analysis of irradiated cell that requires fluorescent imaging. Therefore, we incorporated software codes of controlling cool CCD still camera that is attached on *offline2* microscope. This incorporation of fluorescent image acquisition made efficient the analysis of immunostained cell image, so that it will become a great help for molecular analysis of bystander effect.

Additionally, we also incorporated the function of controlling target irradiation of UV micro-laser that was mentioned above, thus now the software become not only for post-irradiation analysis, but also for whole process of bystander analysis, which included from induction of DNA double strand break to biological response of bystander irradiation.

This improvement of software not only contribute to take a lot of advantages on analysis of bystander mechanisms, but also expected a technical feed back to develop our new cell targeting system of heavy-ion focused microbeam.

3-33 Late-Arising Loss of Clonogenicity in the Progeny of Cells Surviving High- and Low-LET Ionizing Radiations

N. Hamada[a, b, c], S. Wada [a, b, c], T. Funayama [c], T. Sakashita [c], T. Kakizaki [c], M. Ni [c] and Y. Kobayashi [a, b, c]

[a]Department of Quantum Biology, Gunma University Graduate School of Medicine, [b]The 21st Century Center of Excellence Program for Biomedical Research Using Accelerator Technology, [c]Radiation-Applied Biology Division, QuBS, JAEA

Abstract

There is increasing evidence that ionizing radiation persistently perturbs genomic stability and induce delayed reproductive death in the descendents of survivors, however, dependence of these inductions upon linear energy transfer (LET) is still largely unknown. We have examined the cell killing effectiveness of gamma-rays (0.2 keV/μm) and six different beams of heavy ion particles with LET values wide-ranging from 16.2 to 1610 keV/μm in primary normal human diploid foreskin fibroblasts. First, irradiated confluent density-inhibited cultures were subjected to primary colony formation, revealing that relative biological effectiveness (RBE) based on the primary 10% survival dose peaked at 108 keV/μm, and that inactivation cross section increased proportionally up to 437 keV/μm. Secondly, cells harvested from primary colonies further underwent secondary colony formation, showing that delayed reproductive death occurred in a dose-dependent fashion. While the RBE based on the secondary 80% survival dose peaked at 108 keV/μm, very little difference between LET was observed in the RBE based on the secondary survival at primary 10% survival dose. Our present results indicate that delayed reproductive death arising only during secondary colony formation is independent of LET and is more likely to be dependent upon initial damages having being fixed during primary colony formation.

重イオン粒子は、線エネルギー付与（LET）の低い光子に比べ、生物学的効果比（RBE）が高く、さらに、物理学的な線量分布の集中性に優れていることから、がんの放射線治療に臨床応用されている。しかしながら、がん病巣の内部および周囲には正常細胞が混在しているため、放射線治療を実施する際に正常細胞への照射は避けられない。このことから、重イオン粒子がヒト正常細胞に及ぼす生物効果を詳細に解析する必要がある。長い間、放射線の生物効果は、核に照射された細胞においてのみ認められると考えられてきたが、近年では、細胞質に照射された細胞、さらには、照射生存子孫細胞（遺伝的不安定性）や照射周囲の細胞（バイスタンダー効果）にまで及ぶことが明らかになってきた。放射線照射生存子孫細胞には、照射後の分裂を経た後に遅延的に、増殖死、遺伝子突然変異、染色体異常などが引き起こされることが知られている。コロニー形成能の喪失を指標としたRBEは100-200 keV/μmのLETで最大に達することが広く知られている一方で、遅延的増殖死のLET依存性はこれまで全く明らかにされていない。そこで、本研究では、ヒト正常二倍体線維芽細胞における放射線誘発遅延的増殖死のLET依存性を2次コロニー形成能の喪失を指標として解析することを目的とした。

細胞周期による感受性のばらつきを軽減させるため、そして、細胞間相互作用はストレス応答に重要な役割を果たしている[1]ことから、ヒト正常二倍体線維芽細胞であるAG01522細胞を1x10^4 cells/cm^{2}の密度で播種後、4・7・9日目に培地交換し、11日目に放射線照射実験に使用した。^{60}Coγ線を基準放射線として、また、LETが異なる6種の重イオン粒子をTIARAにて、照射した。放射線照射後1時間以内に再播種し、1次コロニーを8ディッシュずつ形成させた。1次コロニーの内、4ディッシュは染色後に計数し、残りの4ディッシュからはコロニーを回収・再播種し、さらに2次コロニーを形成させた。

1次コロニーにおいて生存率は線量依存的に低下した。また、γ線（0.2 keV/μm）の10%生存線量（D_{10}）に対する6種の重イオン粒子（16.2-1610 keV/μm）のRBEは、100 keV/μm近傍で最大となった[2]。このことから、線量あたりの細胞殺傷効果にLET依存性があることが確認された。一方、光子または粒子あたりの生物効果を示す指標である不活化断面積が、0.2-437 keV/μmの範囲では、両対数上で直線的に増加した[2]。

2次コロニーにおいても線量依存的な生存率の低下が認められ、γ線の80%生存線量に対する重イオン粒子のRBEも100 keV/μm近傍で最大となった[2]。このことから、線量あたりの遅延的増殖死の誘発にもLET依存性があることが示された。一方、1次コロニーにおいて同一の生存率を与えたD_{10}における2次コロニーの生存率は、LETによらず同一であることがわかった[2]。

1次コロニー、2次コロニーともにRBEは100 keV/μm近傍で最大に達したことから、遅延的増殖死にもLET依存性があることが初めて解明された。一方、1次コロニーのD_{10}における2次コロニーの生存率がLETに非依存性であったことは、遅延的増殖死の起因となる損傷が1次コロニー形成期間に固定されることを示唆している。遅延的に死に到る細胞は照射後に繰返し分裂できることから、その起因は、チェックポイントがかかるような重篤なDNA損傷ではなく、放射線照射後に観察されるクロマチンの構造変化[3]などを由来として形成されるゲノム上の潜在的不安定領域であると考えられる。また、本研究で指標としたコロニー形成能の喪失は、長期の増殖停止あるいはアポトーシスや壊死の程度を反映していることから、今後はコロニー形成能を喪失する機序とそのLET依存性をより詳細に解明していく必要がある。

References

1) N. Hamada, et al., "Gap junctional intercellular communication and cellular response to heat stress", Carcinogenesis 24, 1723 (2003)
2) N. Hamada, et al., "LET-dependent survival of irradiated normal human fibroblasts and their descendents", Radiat. Res. 166, 24 (2006)
3) N. Hamada, et al., "Histone H2AX phosphorylation in normal human cells irradiated with focused ultrasoft X rays: Evidence for chromatin movement during repair", Radiat. Res. 166, 31 (2006)

3-34 Bystander Killing of Human Lung Cancer Cells by Heavy Charged Particle Irradiation

K. Harada[a)], T. Nonaka[a)], N. Hamada[b,c)], T. Funayama[c)], H. Sakurai[a)], T. Sakashita[c)], S. Wada[b,c)], H. Kawamura[a)], M. Hasegawa[a,d)], Y. Kobayashi[b,c)] and T. Nakano[a)]

[a)]Department of Radiation Oncology, [b)]Department of Quantum Biology, Gunma University Graduate School of Medicine, [c)]Radiation-Applied Biology Division, QuBS, JAEA, [d)]Department of Radiation Oncology, Nara Medical University School of Medicine

Abstract

We have here examined clonogenic survival of confluent human lung cancer A549 cells exposed to X-rays or 220 MeV $^{12}C^{5+}$ charged particles. Targeted exposure of 0.001-0.005% of cells within the confluent population were resulted in 8-15% reduction of surviving fraction, suggesting that the induced bystander responses are involved in mechanism of cell death by heavy particles.

重イオンビーム照射は線量分布の集中性が良好で従来のX線やγ線よりも高い細胞致死効果が得られることから、放射線治療において病巣の制御のみならず正常機能の保持も可能となりうる治療手段として期待されている[1)]。しかし、重イオン照射による高い殺細胞効果の詳細なメカニズムや照射された細胞から非照射細胞へのシグナル伝達によって引き起こされるバイスタンダー効果については十分に解明されていない。本研究ではヒト肺癌由来の細胞株を用いて重イオンビーム照射後のバイスタンダー効果の誘導について検討し、重イオンビーム照射による細胞死の機序の一端を解明する。

細胞はヒト肺癌由来の細胞株であるA549を用いた（p53 statusは野生型）。X線照射は群馬大学大学院のMBR-1505（140 kVp、92.89 cGy/分、日立社製）、重イオン照射は原子力機構TIARAの細胞局部照射装置および深度制御種子照射装置にて行った（220 MeV $^{12}C^{5+}$、108 keV/μm）。照射後の細胞生存率はコロニー形成法で検討した。X線および深度制御種子照射装置（ブロードビーム）によるコロニー形成法では35mmのディッシュに照射2日前に$5x10^5$個の細胞をまき、照射当日にコンフルエントの状態であることを確認し照射した。細胞局部照射装置（マイクロビーム）を用いた照射では照射2日前に$5x10^5$個の細胞を35 mmディッシュの底面に固体飛跡検出材（CR-39）をワセリンにて貼付したグラスベースディッシュ上に準備し、照射前にコンフルエントであることを確認し実験を行った。標的細胞はディッシュ中の1個、5個、25個の細胞をランダムに選択し、照射するイオンの数はひとつの細胞あたり1個、5個、10個とした。X線、ブロードビーム、マイクロビームいずれにおいても照射後は60 mmのディッシュに至適個数の細胞をtriplicateでまきなおし、14日後に細胞を固定・染色した後、コロニー数をカウントし、非照射細胞の生存率を対照とし細胞生存率を検討した。

ブロードビームを用いた実験で220 MeV $^{12}C^{5+}$の細胞生存曲線は直線的であったが、X線および220MeV $^{12}C^{5+}$のD_0（37%生存線量）／D_{10}（10%生存線量）はそれぞれ1.59 Gy／4.00 Gy、1.23 Gy／2.39 Gyであった（Fig. 1）。

マイクロビームを用いた実験では、選択的に1つの細胞にのみイオンを照射した際の細胞生存率は非照射細胞とほぼ同様であった。照射細胞数をディッシュ内の5-25個、また各細胞への照射イオン数を5-10個とすると照射していない細胞の生存率に比較し統計学的に有意に低下した（Fig. 2、9-15%の低下）。

本実験ではディッシュ全体の細胞のうち0.001-0.005%という極少数の細胞を重イオンビームで照射した時、ディッシュ全体の細胞生存率が有意に低下する結果がえられた。このことは重イオン照射による細胞死のメカニズムに照射細胞から非照射細胞へのバイスタンダー効果が深く関与していることを示唆していると思われた。

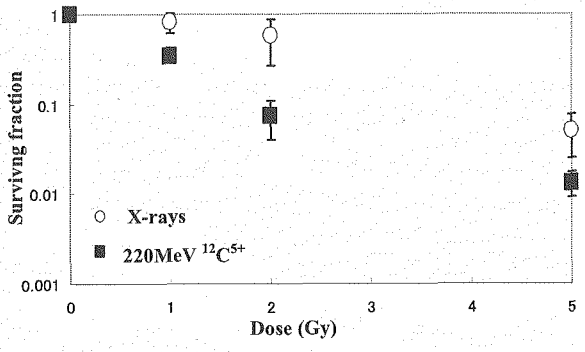


Fig. 1. Survival curves for p53 wild-type human lung cancer cells (A549) exposed to 150-kVp X-rays, 220-MeV $^{12}C^{5+}$ions, tested by a clonogenic assay. The data are presented as the means and standard errors of more than three independent experiments.

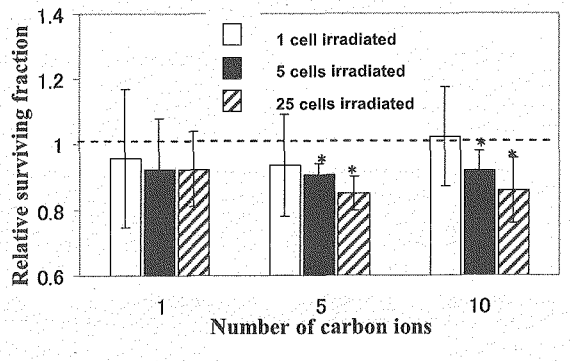


Fig. 2. Relative surviving fraction of confluent density-inhibited culture of A549 cells where 1-25cells were irradiated with 1-10 carbon ions. The surviving fraction of the nonirradiated A549 control was normalized as 1 (*, P<0.05 compared with nonirradiated A549 control).

References

1) D. Schulz-Ertner, A. Nikoghosyan, C. Thilmann, T. Haberer, O. Jakel, C. Karger, G. Kraft, M. Wannenmacher, J. Debus. Results of carbon ion radiotherapy in 152 patients. Int J Radiat Oncol Biol Phys. 58 (2004) 631-640.

3-35 Analysis of Radiation-Induced Apoptosis in Early *Drosophila* Embryos

K. Tatei[a)], T. Tamaki[b)], H. Kawamura[b)], N. Hamada[c,d)], T. Sakashita[d)], T. Funayama[d)], S. Wada[d)], T. Kakizaki[d)], T. Nonaka[b)], H. Obinata[a)], T. Hattori[a)], A. Ogawa[a)], H. Kazama[b)], T. Nakano[b)], Y. Kobayashi[c,d)] and T. Izumi[a)]

[a)]Department of Molecular Biochemistry, [b)] Department of Radiation Oncology, [c)] Department of Quantum Biology, Gunma University Graduate School of Medicine, [d)] Radiation-Applied Biology Division, QuBS, JAEA

Apoptosis is the evolutionary conserved process required for normal development and adaptive response to cellular injury. It has been established that p53 functions as the principal transcription factor that is activated in response to DNA-damaging stress. However, recent studies have shown that certain cell types lacking *p53* can also undergo apoptosis when treated with ionizing radiation or UV. Mechanisms for *p53*-independent apoptosis are poorly understood, although much studies suggested that ionizing radiation including heavy-ion particle causes DNA double-strand breaks and also membrane and/or cytoplasmic damage. In mammalian cells, three genes, *p53*, *p63* and *p73*, form the family and have partially overlapping functions. *Drosophila* might be suitable for studying *p53*-independent process because of the lack of other family members within the fly genome.

In *Drosophila*, there is no detectable developmental cell death during the first 7 hours after the egg laying corresponding to the mid-gastrula stage. Therefore, it is advantageous if we could observe radiation-induced apoptosis in the early embryo because of no developmental apoptosis. We irradiated 0-3 hours embryos after egg laying with ion, X-rays and UV followed by 5 hour incubation at 25°C. TUNEL assay was employed for detecting apoptosis. TUNEL positive cells were detected in blastula (Fig. 1) and gastrula stage of embryos. This result indicates that apoptotic machineries also exist in the early stages of embryo although there was no developmental programmed cell death.

Next, we investigated the *p53* dependency of the irradiation-induced apoptosis in the early embryo. It has been reported that irradiation-induced apoptosis in the imaginal discs is severely diminished in *p53* mutant flies. The existence of the *p53*-independent apoptosis has not been clearly shown in *Drosophila*. Embryos from *p53* mutant, $p53^{5A\text{-}1\text{-}4}$ that lacks transcriptional activity, were irradiated with 100 mJ/cm^2 of UV-B followed by 5 hour incubation at 25°C in the dark. Numerous TUNEL positive cells were observed in the embryo (Fig. 2). We also observed that UV and X-ray irradiations induce *Ark* (*Apaf-1 related killer*, *Drosophila Apaf-1* ortholog) expression in the *p53* mutant embryos (data not shown).

Our results showed that heavy ion, X-rays and UV could induce apoptosis in the early *Drosophila* embryo. We also showed that irradiation induced apoptosis still occurs in the embryo lacking *p53* activity. These data indicate that molecular pathway for *p53*-independent apoptosis exists in the early *Drosophila* embryo. The high frequency of apoptotic cells in *p53* mutant embryos suggests that the *p53*-independent pathway plays a pivotal role in the early embryo. Further studies are required for characterizing the molecular mechanism of the *p53*-independent apoptosis.

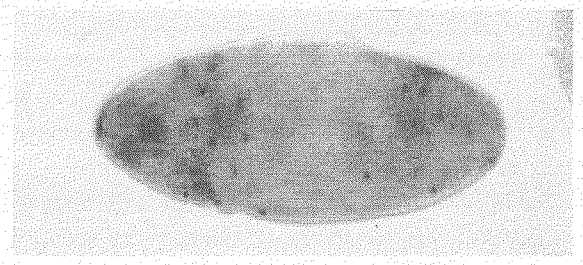


Fig.1 Heavy ion irradiation induced apoptosis in the early *Drosophila* embryo.
Embryos collected for three hours were exposed to heavy ion beam, and then staged for 5 hours. Apoptosis was detected by TUNEL assay.

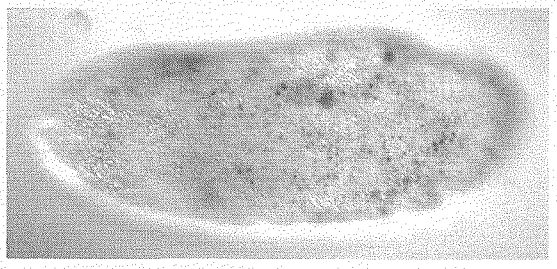


Fig.2 UV-B irradiation induced apoptosis in the early *Drosophila* embryo lacking *p53* gene.
Embryos from $p53^{5A\text{-}1\text{-}4}$ were irradiated with 100 mJ/cm^2 of UV-B. Embryos were fixed and subjected to TUNEL assay 5 hours after irradiation.

3-36 Bystander Effect of High Linear Energy Transfer Charged Particle Radiation on Human Glioblastoma Cells

S. Ishiuchi[a,c], M. Hasegawa[b,c], Y. Yoshida [b,c], N. Hamada[b,c,d], T. Funayama[d], S. Wada[d], T. Sakashita[d], Y. Kobayashi[b,c,d] and T. Nakano[b,c]

Departments of [a]Neurosurgery and [b]Radiation Oncology, Gunma University Graduate School of Medicine, [c]The 21st Century Center of Excellence Program for Biomedical Research Using Accelertor Technology, [d]Radiation-Applied Biology Division, QuBS, JAEA

Abstract

High linear energy transfer (LET) charged particle radiation such as ^{12}C-ion beams, ^{20}Ne- ion beams and ^{40}Ar-ion beams is a new modality for the treatment of X-ray resistant cancers. Here we investigated the radiation-induced bystander effect on human glioblastoma cells using a CGNH-89 cell line. We irradiated individual charged-particles to target cells by a microbeam from cyclotron at JAEA Takasaki, and monitored DNA double strand breaks by γH2AX as a marker. We found bystander responses were induced in the neighboring non-irradiated cells. These results explained marked cytotoxity of heavy ions on human glioma cells.

Glioblastoma(GBM)は低 LET(linear energy transfer)放射線であるγ線や X 線に対して、通常外照射、ライナック定位放射線照射、ガンマナイフ照射あるいはサイバーナイフ照射いずれの形式を問わず治療抵抗性である。一方、一部臨床応用がすでに開始されている炭素線を用いた重粒子線に代表される高 LET 放射線に対する GBM の生物学的効果については十分に解析されていない。我々が物理線量 1 Gy (ブロード照射) に対するコロニー形成能試験の生存曲線より算定した生物学的効果比は、X 線：炭素線：アルゴン線＝1：4.4：7.5 と重粒子線は X 線と比較して高い殺細胞効果を示した[1]。本研究では、同じ物理線量を照射した場合に質量の大きい重イオンがより細胞障害性が高い理由を見出すために、ヒト神経膠芽腫細胞株(CGNH-89)[2]を材料とし、マイクロビーム照射装置を用いて、非照射細胞と照射細胞を厳密に分け照射し、各種重イオンの腫瘍に対する放射線効果を検討した。評価は、ヒストン H2AX の serine139 のリン酸化を認識する抗γH2AX 抗体により、腫瘍細胞の DNA 損傷形式を解析した。

照射線源は、日本原子力研究開発機構・高崎量子応用研究所イオン照射研究施設 TIARA の AVF サイクロトロンで加速された重イオンのうち 220 MeV ^{12}C、260 MeV ^{20}Ne、及び 460 MeV ^{40}Ar を用いた。CR-39 試料を準備しマイクロビーム照射を行い、照射1, 2, 6, 12, 18, 24 時間後に 4%パラフォルムアルデヒド固定しγH2AX 染色を施行した。各種、重イオンは細胞核周囲の細胞質に 1, 5, 10 個照射した。

コントロールの非照射細胞群ではγH2AX の染色はび慢性で あった。被照射細胞は照射直後より徐々にγH2AX の foci を認め 16 時間後までに foci は拡大明瞭化し、照射イオン数に関わらず、周囲の細胞にも被照射細胞同様なγH2AX の foci が検出された(Figure)。同じ物理線量を照射した場合に質量の大きい重イオンがより細胞障害性が高い理由の背景に、被照射細胞周囲の腫瘍細胞に引き起こされ、抗γH2AX 抗体にて認識される double strand breaks の bystander 効果の可能性が示唆された。

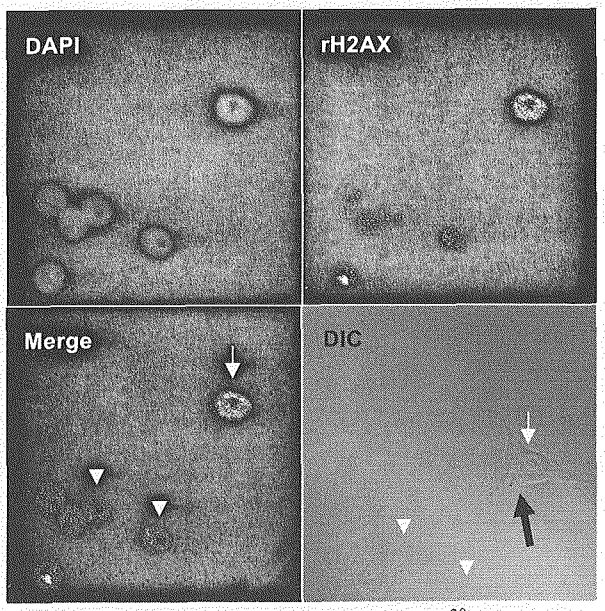


Fig.1 Images of cell at 12 hr after five ^{20}Ne-particles irradiation. Arrows and arrow heads (white) in Marge image and differential interference (DIC) image indicate same cell. Arrow (black) in DIC indicates irradiated-site of 260 MeV ^{20}Ne. Irradiated cells and non-irradiated cells indicated clear fluorescence foci by γH2X staining.

References

1) S. Ishiuchi, M. Hasegawa, N. Hamada, T. Funayama, S.Wada, T. Sakashita, Y. Kobayashi and T. Nakano. "Cytotoxic effect of high linear energy transfer charged particle radiation on human glioblastoma cells", TIARA Annual Report 2004 JAEA-review 2005-001, 169-170

2) S. Ishiuchi, et al. Nat. Med. 8, 971-978 (2002).

3-37 Effects of Heavy-Ion, UV-C, and X-Ray Irradiation on the Susceptibilities of Human Cells to HIV-1 Infection

N. Shimizu[a)], A. Oue[a)], T. Ohtsuki[a, b)], T. Mori[a, b)], K. Yamaguchi[a, b)], T. Nakamura[a, b)], S. Wada[b, c)], Y. Kobayashi[b, c)] and H. Hoshino[a, b)]

[a)]Department of Virology and Preventive Medicine and [b)]21st Century COE Program, "Biomedical Research using Accelerator Technology", Gunma University Graduate School of Medicine and [c)] Radiation-Applied Biology Division, QuBS, JAEA

Irradiation with heavy-ion has been shown to have different effects on human cells from those with X-ray and UV-C. Effectiveness of heavy-ion irradiation in cancer therapy has been documented well. However, only little knowledge has been compiled about cellular responses such as changes of signal transduction and gene expression when human cells were irradiated with heavy ions. We have examined the usefulness of heavy ion irradiation as a research tool in virology. The entry mechanism of human immunodeficiency virus type-1 (HIV-1) into target cells mediated by the main receptor CD4 and the coreceptor CCR5 has not been sufficiently elucidated yet. Some reports showed that infection of human cells with HIV-1 is mediated by the process of double strand break/repair, which may be specifically induced by heavy ion irradiation. The aim of this study is to find out new factors involved in HIV-1 infection by using heavy-ion irradiation.

NP-2/CD4/CCR5 cells, which are human glioma cells transduced with CD4 and CCR5, were used in this study[1)]. NP-2/CD4/CCR5 cells were irradiated with carbon (C) ion, UV-C or X-ray at different doses. Expression of CCR5 and CD4 on the cell surface was detected by flow cytometry using anti-CCR5 or anti-CD4 monoclonal antibody. Irradiated NP-2/CD4/CCR5 cells were exposed to a CCR5-using (i.e. R5-tropic) HIV-1 strain, Ba-L, 48 hour after irradiation. The susceptibilities of NP-2/CD4/CCR5 cells to HIV-1 were determined by indirect immunofluorescence assay (IFA) or Western blot analyses both of which detect HIV-1-related antigens expressed in the infected cells. Reverse-transcribed genomic DNA of HIV-1 in the infected cells was also detected by PCR using oligonucleotide primers having sequences of the *env* gene. Proliferation and conditions of the cells irradiated and/or exposed to HIV-1 were microscopically observed.

Results obtained by flow cytometric analyses showed that expression levels of CCR5 and CD4 on NP-2/CD4/CCR5 cells were hardly affected by irradiation not only with C-ion but also with UV-C or X-ray. C-ion irradiation induced giant cell formation of NP-2/CD4/CCR5 cells, although their proliferation was remarkably inhibited. Results obtained by IFA and Western blot analyses showed that the susceptibility of NP-2/CD4/CCR5 cells to HIV-1 Ba-L strain was enhanced several-fold as compared with those of non-irradiated cells when the cells were irradiated with C ion at 0.5 and 1.0 Gy (Fig. 1A). The susceptibility to HIV-1 was, however, reduced when the cells were irradiated with C ion at 2.0 and 4.0 Gy. When NP-2/CD4/CCR5 cells were irradiated with UV-C or X-ray, the susceptibilities to HIV-1 were enhanced. Results obtained by PCR showed that amounts of the reverse-transcribed DNA of HIV-1 in NP-2/CD4/CCR5 cells were increased when the cells were irradiated with heavy ion at 0.5 and 1.0 Gy, but decreased at 2.0 and 4.0 Gy (Fig. 1B). Amounts of the reverse-transcribed DNA of HIV-1 in NP-2/CD4/CCR5 cells were decreased by irradiation with UV-C and X-ray.

In this study, we show that heavy ion irradiation at low doses has enhancing effects on the susceptibility of NP-2/CD4/CCR5 cells to HIV-1. This enhancing effect was specifically detected when the cells were irradiated with heavy ion but not with UV-C and X-ray. Enhancement of HIV-1 infection may be accomplished by up-regulation of viral incorporation into the cells or reverse-transcription of the viral genomic RNA. Thus, heavy-ion irradiation will be a useful tool to analyze the mechanism of HIV-1 infection in human cells.

Reference

1) Soda, Y., et al., Biochem. Biophys. Res. Comm. 258: 313, 1999

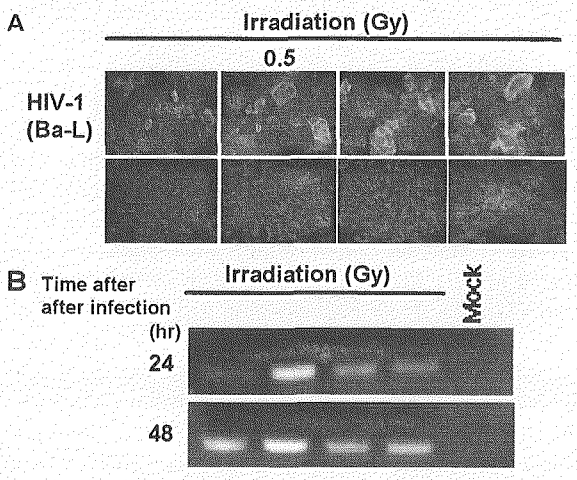


Fig. 1. The susceptibilities of NP-2/CD4/CCR5 cells to HIV-1. (A) NP-2/CD4/CCR5 cells were irradiated with C ion at different doses and exposed to HIV-1 Ba-L strain 48 hour after irradiation. The cells infected with HIV-1 were detected by IFA after 48 hour after viral exposure. (B) The susceptibilities of NP-2/CD4/CCR5 cells to HIV-1 were examined by PCR detecting reverse-transcribed genomic DNA of HIV-1. Total DNA of NP-2/CD4/CCR5 cells were extracted at 24 and 48 hour after viral exposure and HIV-1 DNA was detected by PCR.

3-38 Effects of Heavy Ion Microbeam Irradiation on Isolated Single Fibers of Skeletal Muscle

H. Yorifuji[a)], M. Hino[a,b)], S. Wada[c)], Y. Tajika[a)], Y. Morimura[a)], N. Hamada[b,c,d)], T. Funayama[c)], T. Sakashita[c)], T. Kakizaki[c)] and Y. Kobayashi[c,d)]

[a)]Department of Neuromuscular and Developmental Anatomy, Division of Bioregulatory Medicine, Gunma University Graduate School of Medicine, [b)]The 21st Century Center of Excellence Program for Biomedical Research Using Accelerator Technology, [c)] Radiation-Applied Biology Division, QuBS, JAEA, [d)] Department of Quantum Biology, Division of Bioregulatory Medicine, Gunma University Graduate School of Medicine

The muscular dystrophy is a heterogeneous group of hereditary disease characterized by progressive muscle weakness and wasting. Main lesions of the muscular dystrophy are degeneration and necrosis of the skeletal muscle. Recently, the progress of the molecular genetics has elucidated a variety of affected genes and their products of muscular dystrophy. Many of these proteins are localized to the basal lamina, plasma membrane and its undercoat and may contribute to plasma membrane integrity. During the cycle of contraction-relaxation, plasma membrane is injured and then the injury is rapidly repaired even in the normal muscle. In the muscle of many types of muscular dystrophy, the injury is thought to be more severe and cause Ca^{2+} influx into muscle cells, which finally results in muscle degeneration. However, the detailed molecular mechanism of the injury-repair process remains to be elucidated. In this study, to clarify the injury-repair process, we used heavy ion microbeam to damage the isolated skeletal muscle fibers and observed the lesions by electron microscopy.

Single muscle fibers were isolated from mouse extensor digitorum longus (EDL) and flexor digitorum brevis (FDB), and were plated on CR-39 plastic cover slips. Irradiated heavy ions were ^{40}Ar (11.2 MeV/amu), ^{20}Ne (12.8 MeV/amu) and ^{12}C (18.3 MeV/amu) which were provided by AVF-cyclotron at TIARA (Takasaki Ion Accelerator for Advanced Radiation Application) in JAEA. The irradiated muscle fibers were fixed at various time points after irradiation. After embedding in Epon 812, ultra thin sections were cut, stained by uranyl acetate and lead citrate, and examined by a transmission electron microscope.

Muscle fibers fixed at the shortest time point (2 minutes after the end of irradiation) showed the irregular protrusions and invaginations of the plasma membrane and fragmented basal lamina at the heavy ion-microbeam irradiated region (Fig.1). In the cytoplasm, irregular distribution of thin filaments was found near the plasma membrane. Thick filaments irregularly scattered around the periphery of the groups of thin filaments (Fig.1). Sarcoplasmic reticula near the irradiated regions showed distended appearance with flocculent material within the lumen. Disarrangement of thick and thin filaments and distended sarcoplasmic reticula may result from local leakage of Ca^{2+} into cytosol. Many autophagic vacuoles can be seen at 7 minutes after the irradiation. These vacuoles become more prominent and showed more variety at 22 minutes. We also examined the permeability of the plasma membrane, however, it is not increased by heavy ion irradiation as judged by the invasion of the fluorescent-dextran (MW 10,000) and Evans blue (MW 961). The difference between ion species (^{40}Ar, ^{20}Ne and ^{12}C) in the influence on muscle fiber is not qualitative but rather quantitative.

In conclusion, the main influences of irradiation of heavy ion beam on skeletal muscle fibers are the change of the fluidity of the plasma membrane and local leakage of Ca^{2+} into cytosol.

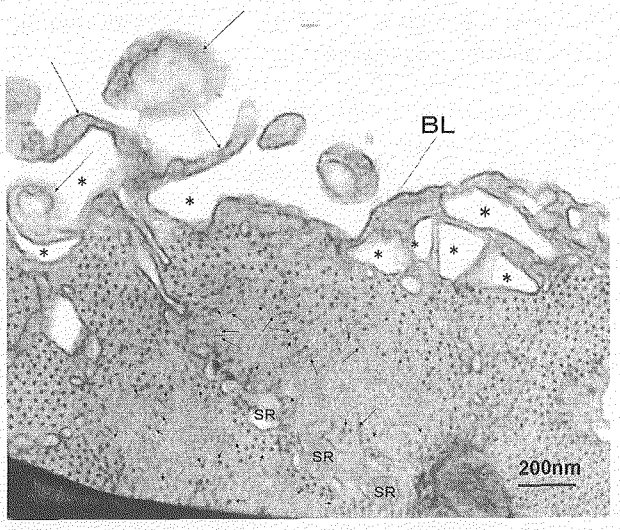


Fig.1 Electron microscopy of the ^{40}Ar irradiated region of muscle fiber fixed at 2 minutes after the end of irradiation. Irregular protrusions (long arrows) and invaginations (*) of the plasma membrane and fragmented basal lamina (BL) are seen. Thick filaments irregularly scatter around the periphery of the groups of thin filaments (short arrows) or lie oblique (arrowheads). Distended sarcoplasmic reticula (SR) are also seen.

3-39 Research into the Radiosensitivity of Normal Brain Tissue

Y. Suzuki[a)], Y. Yoshida[a,d)], K. Shirai[a)], N. Hamada[b,d,e)], T. Mizui[c)], S. Noda[a)], T. Funayama[e)], T. Sakashita[e)], Y. Kobayashi[b,d,e)], T. Shirao[c)], S. Ozawa[d)] and T. Nakano[a,d)]

Depertments of [a)]Radiation Oncology, [b)]Quantum Biology and [c)]Neurobiology and Behavior, Gunma University Graduate School of Mediceine, [d)]The 21st Century Center of Excellence Program for Biomedical Research Using Accelertor Technology, [e)]Radiation-Applied Biology Division, QuBS, JAEA

Abstract

Damage to normal brain tissue caused by irradiation has not been studied in detail. In this study, we investigated the effect of X- and ^{12}C-irradiation on cultured normal neurons (immature and mature) and cultured organotypic brain slice tissues. The radiosensitivity of immature neurons was significantly higher than that of mature neurons. The effect of ^{12}C-irradiation on immature neurons was about 6 times higher than that of X-irradiation. In organotypic slice culture, X- and ^{12}C-irradiation induced the remarkable morphological change, especially, in the external granule cell layer. The effect of ^{12}C-irradiation was about 2 times higher than that of X-irradiation.

悪性度の高い脳腫瘍では、腫瘍を制御するのに十分な放射線量が正常脳組織の耐用線量をはるかに上回っている。そのため、脳腫瘍の放射線感受性について検討するのみでなく、正常組織の耐用線量を上げる（放射線感受性を下げる）研究が不可欠と考えられる。しかしながら、現在までに、血流や各種生体内物質の影響を受けないような状態での脳正常組織の放射線感受性については、ほとんど分析されていない。今回、脳正常組織の放射線に対する反応を胎児ラットから摘出した培養正常脳神経細胞（実験①）および小脳培養切片（実験②）の放射線に対する反応について検討した。

＜実験①＞

胎生 18 日目のラット海馬より神経細胞を採取し、Banker 法にて培養した。未熟神経細胞(培養 7 日目)は X 線 0～30 Gy、220 MeV 炭素線 0～10 Gy の照射を行い、成熟神経細胞(培養 21 日目)は X 線 0～30 Gy を照射した。照射後 12 時間の各細胞を 4%パラフォルムアルデヒドで固定し、DAPI および TUNEL 蛍光染色法を用いて、放射線により誘発される核濃縮およびアポトーシスの頻度を計測した。

30 Gy の X 線を照射した結果、未熟神経細胞の核濃縮像は非照射時の 15.4%から 46%と有意に増加した（$p < 0.001$）。一方、成熟神経細胞について同様に実験した結果、核濃縮像は非照射時（29.6%）と照射時(31.5%)では有意な違いは認められなかった。未熟神経細胞は成熟神経細胞より放射線感受性が高く、神経細胞の成熟度により放射線感受性に違いがあることが確認された[1)]。

未熟神経細胞は、X 線及び炭素線照射によりアポトーシスが誘発され、それは線量依存的であった。また、炭素線の効果は X 線に比し約 6 倍強く、神経細胞の放射線誘発アポトーシスにおける X 線照射に対する炭素線照射の生物学的効率比（RBE）は約 6.0 と推定された(Fig. 1)。

＜実験②＞

生後 10 日目の未熟なラットから小脳を取り出し、～600 μm に薄切し、特殊な培養皿上で培養した。培養後 1 日目の切片に X 線 0～20 Gy、炭素線 0～20 Gy の範囲で照射を行い、照射後 1～24 時間で経時的に固定した。その後、パラフィン包埋切片を作成し、ヘマトキシリン・エオジン(HE)染色を行うことで形態学的変化について検討した。

X 線および炭素線照射により、小脳皮質の一部に形態異常が引き起こされた。特に、発達中の小脳皮質に存在する外顆粒細胞層が照射による影響をもっとも受けやすく、層の異常拡大が認められた(Fig. 2)。この層拡大について測定したところ、炭素線の効果は X 線に比し約 2.0 倍強く、小脳皮質外顆粒細胞層の異常拡大を指標とした場合の X 線照射に対する炭素線照射の RBE は約 2.0 と推定された。

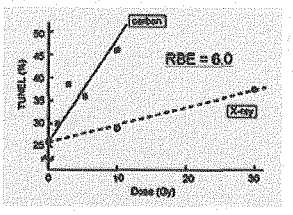


Fig.1 Relationship between dose and apoptosis by X- and ^{12}C-irradiation in immature neurons.

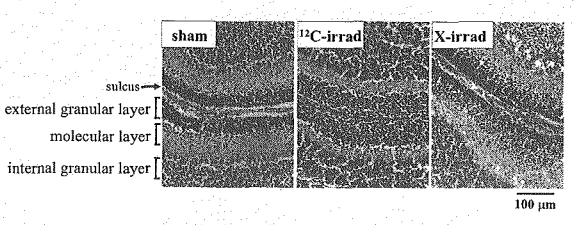


Fig.2 Images of organotypic slices at 12 h after X- and ^{12}C-irradiation of 10 Gy (HE stain).

この研究は、群馬大学 21 世紀 COE プログラム「加速器テクノロジーによる医学・生物学研究」より援助を受けている。

References

1) Shirai K, et al. "Differential effects of x-irradiation on immature and mature hippocampal neurons in vitro", Neurosci Lett. 399, 57-60 (2006)

3-40 Response of Associative Learning and Nervous System of *Caenorhabditis elegans* to Heavy Ion Beam Irradiation

T. Sakashita [a)], N. Hamada [a, b, c)], M. Suzuki [d)], T. Kakizaki [a)], S. Wada [a, b, c)], T. Funayama [a)] and Y. Kobayashi [a, b, c)]

[a)]Radiation-Applied Biology Division, QuBS, JAEA, [b)]Department of Quantum Biology, Gunma University Graduate School of Medicine, [c)]The 21st Century Center of Excellence Program for Biomedical Research Using Accelerator Technology, [d)] Japan Society for the Promotion of Science

Abstract

It has been reported that the radiation-induced impairments of learning and memory in mammals are mainly caused by suppression of hippocampal neurogenesis. On the other hand, alterations of neurotransmitter activity in rat brain after ionizing irradiation suggest impairments of function in the central nervous system (CNS) except for hippocampus. However, direct measurement of the impairments is difficult in mammals. Thus, our goal of the present study is to understand at the functional level when and how ionizing radiation affects CNS, using the adult stage of *Caenorhabditis elegans* with no newborn neuron and a simple learning behavior, i.e. food-NaCl associative learning. The animals were irradiated with broad beams of C ions (0 - 500 Gy), which were included in cosmic rays. We observed a remarkable decrease of chemotaxis index just after irradiation in the food-NaCl associative learning conditioned animals. The result suggests that plastic parts of the nervous system related food-NaCl associative learning are sensitive to C ions. Microbeam irradiation experiments are in progress.

現在、放射線による学習と記憶の障害は主に海馬における新生ニューロンの生成抑制に起因すると報告されている[1)]。また、電離放射線照射によるシナプスのナトリウムチャネル特性の変化[2)]やドーパミンの伝達異常[3)]は、海馬以外（新生ニューロンを含まない）の神経系中枢域における学習に関わる障害を示唆する。しかし、哺乳動物を用いて海馬以外の神経系中枢域での放射線照射効果を直接調べることは難しい。そこで、本研究では神経系のモデル生物として知られる線虫を用いて、新生ニューロンの影響を考慮しなくてもよい成虫段階での放射線照射の影響を、神経系中枢機能のひとつである連合学習[4)]に着目して調べることを目的とした。本研究では、線虫のFood-NaCl連合学習*を対象とし、宇宙環境で重要な重イオン線に対する影響を調べた。

NGM寒天培地にて20 ℃で孵化後約3日間飼育した成虫段階の線虫を、すべての実験に用いた。線虫のNaClに対する化学走性を集団試験により評価した。指標には、化学走性指標（C.I.）**を用い、あらかじめNaClの濃度勾配を与えた寒天培地プレート上に15分間置いた後の集団について、NaClに対する化学走性を評価した。220 MeV Cイオンブロードビームを Food-NaCl連合学習の条件付けを開始後30 - 60分経過した線虫に照射した。連合学習への経時的な影響を調べるために、照射直後、1時間後、3時間後、5時間後に集団化学走性試験を実施した。また、20μmφのコリメーターにて形成した220 MeV Cイオンマイクロビームをアジ化ナトリウムで麻酔をかけ固定した線虫の咽頭部分（神経系中枢域）に照射した。照射後速やかに緩衝液にて洗浄し麻酔から回復させるとともに、FoodなしNaClあり寒天培地にてFood-NaCl連合学習のための条件付けを行った。照射による一過性の影響を評価するために、2時間の条件付け後に、集団化学走性試験を実施した。

Cイオンブロードビーム照射直後において、線虫の化学走性は線量の増加に伴って低下した。照射後1時間から3時間にかけては、100 Gyを照射した線虫では、非照射線虫の化学走性の変化に徐々に近づく経時的な変化を示した。一方、300、500 Gyを照射した線虫では、化学走性が低下したまま維持される結果となった。照射から5時間経過後には、線量に関わりなく同程度の化学走性を示した。これらの結果は、新生ニューロンを持たない線虫において、Cイオン照射により神経系中枢機能に異常が発生することを示唆している。また、^{60}Co γ線照射実験の結果と比較すると、照射直後の化学走性の低下に関してCイオン照射実験でも同様の傾向が観察されたが、γ線照射実験で観られた（1）300 Gyを照射した線虫の連合学習の再開、（2）500 Gyにおける顕著な化学走性の回復と停止といった経時的な変化が、Cイオンブロードビーム照射実験では観察されなかった。γ線とCイオン照射の結果の違いについての原因は分からないけれども、ラットの味覚嫌悪学習に関してもγ線と重イオンとの照射効果の間に同様の傾向が報告されている[3)]。今後の検討が必要である。Cイオンマイクロビームの神経系中枢域（咽頭近傍）への照射によるFood-NaCl連合学習の影響に関しては、現在までに、神経系中枢域へのCイオンビーム照射によりNaClに対する化学走性に異常が起こらないことを確認した。現在、連合学習に関するデータを蓄積中である。

* 線虫には0.1 - 100 mMのNaClに誘引される化学走性があるが、Food（大腸菌）とNaClの4つの組み合わせで条件付けを行うと、Foodがなく NaClがある寒天培地上に数時間置いた場合においてのみ、NaClに対する化学走性が低下するように変化する。

** C.I. =｛（高濃度のNaClスポットに移動した個体数）－（対照の位置を中心としたスポットに移動した個体数）｝÷（プレート全体の個体数）

References

1) J. Raber, et al., "Radiation-induced cognitive impairments are associated with changes in indicators of hippocampal neurogenesis", Radiat Res. 162, 39 (2004).
2) M. J. Mullin, et al., "Ionizing radiation alters the properties of sodium channels in rat brain synaptosomes", J Neurochem. 47, 489 (1986).
3) B. M. Rabin, et al., "Heavy particle irradiation, neurochemistry and behavior: thresholds, dose–response curves and recovery of function", Adv. Space Res. 33, 1330 (2004).
4) S. Saeki, et al., "Plasticity of chemotaxis revealed by paired presentation of a chemoattractant and starvation in the nematode *Caenorahabditis elegans*", J. Exp. Biol. 204, 1757 (2001)

3-41 Heavy Ion Microbeam Irradiation to the Central Nervous System of *Caenorhabditis elegans* and Development of Effect Prediction Simulator. Why is Associative Learning of *Caenorhabditis elegans* Promoted by Ionizing Irradiation?

T. Sakashita [a)], N. Hamada[a, b, c)], M. Suzuki[d)], T. Tsuji[e)], T. Kakizaki [a)], S. Wada [a, b, c)], T. Funayama [a)] and Y. Kobayashi [a, b, c)]

[a)]Radiation-Applied Biology Division, QuBS, JAEA, [b)]Department of Quantum Biology, Gunma University Graduate School of Medicine, [c)]The 21st Century Center of Excellence Program for Biomedical Research Using Accelerator Technology, [d)] Japan Society for the Promotion of Science, [e)] Biological Systems Engineering Laboratory, Hiroshima University

Abstract

We investigated the effects of ionizing radiation on the food-NaCl associative learning using *Caenorhabditis elegans*, well known as a model organism for a nervous system. Normally, *C. elegans* moves towards NaCl, but animals show behavior to avoid NaCl when they have experienced starvation and NaCl simultaneously. This behavior has been termed "associative learning". The results of γ-ray irradiation experiments revealed the followings: (1) Radiation responses occurred only in the animals conditioned with starvation and NaCl, (2) The changes consisted of early- and late-phase components. In addition, the preparation of animals for heavy ion microbeam irradiation has been developed for the food-NaCl associative learning of *C. elegans*. Using the preparation, we found that chemotaxis towards NaCl was not affected by the targeted irradiation to the nervous ring of *C. elegans*. Furthermore, the simulation model that reflected a neuron network of food-NaCl associative learning has been developed.

はじめに

神経系のモデル生物として知られる線虫(*Caenorhabditis elegans*)を用いて、food-NaCl連合学習[1)]に対する放射線照射の影響を調べた。前世紀半ばには、すでに神経系中枢域への放射線照射が、学習などの神経系中枢機能の抑制をもたらすことが知られていた。しかし、その原因については、未だ十分な理解に至っていない。現在、放射線照射による神経系中枢機能の抑制の要因として、放射線照射に伴う海馬における新生ニューロンの生成低下[2)]が考えられている。しかし、海馬以外の神経系中枢における影響についてはまったくわかっていない。

そこで、我々は、新生ニューロンの影響を考慮しなくてもよい成虫段階の線虫を用いて、神経ネットワーク自身への放射線照射の影響を明らかにすることを目的として、特に神経系中枢機能である連合学習に着目し研究を開始した。当初、^{60}Coγ線照射により連合学習が促進する結果が得られた(連合学習の定義に沿った解釈)。しかし、その後の詳細な実験と解析により、線虫のfood-NaCl連合学習のγ線照射に伴う促進は、一過性であることが明らかになった。そのため、当初予定した計画を変更し、"γ線照射に対する線虫のfood-NaCl連合学習の応答解析"をまず実行し、放射線応答現象の再検討を行った。

結果及び考察

1) γ線照射に対する線虫のfood-NaCl連合学習の応答

はじめに、^{60}Coγ線を用いて、線虫のfood-NaCl連合学習の放射線応答を調べた。その結果、連合学習に伴うNaClへの化学走性の変化が、学習時の放射線照射においてのみ大きく変動する傾向が観察された(但し、NaClへの化学走性に影響がでない線量域。非学習時には放射線の影響はなし)。また、照射直後に化学走性が低下(連合学習の進行、又は、化学走性の攪乱を意味する)し、その後、学習が停止するなどの応答が観られた。以上の結果から、我々は、線虫のfood-NaCl連合学習の放射線応答が、(1)学習時の照射により特異的に観察されるものであること、(2)照射後の応答には2つの時間的なフェーズが存在することを初めて明らかにした。

2) 重イオンマイクロビームを線虫の神経系中枢の特定領域に照射する実験系の構築と応答解析

次に、γ線の照射実験により明らかとなった線虫の連合学習の放射線応答が、神経系中枢域への重イオン照射によって生じるものかどうかを確かめるために、放射線を微小領域に照射することが可能な重イオンマイクロビームによる照射実験を進めている。現在までに、神経系中枢域への重イオンビーム照射によりNaClに対する化学走性に異常が起こらないことを確認した。

3) 線虫神経系中枢ネットワークのシミュレータ開発

最後に、神経系中枢機能への放射線照射効果を神経ネットワークの応答として理解するために、線虫のfood-NaCl連合学習に関与するであろう神経細胞間の結合をコンピュータ上に再現した。そして、この神経ネットワークの結合を、Suzukiらの方法[3)]に基づき、遺伝的アルゴリズムによって調整することで、線虫の化学走性をシミュレート可能な初期モデルを構築した。

まとめ

本研究により、線虫の連合学習の放射線応答が、連合学習の条件付けの際にだけ生じる特異的なものであること、その応答には、初期と後期の2つのフェーズが存在することを明らかにすることができた。また、重イオンマイクロビームを線虫の神経系中枢域に照射する実験系の構築、シミュレータの初期モデルの開発を達成した。

References

1) S. Saeki, et al., "Plasticity of chemotaxis revealed by paired presentation of a chemoattractant and starvation in the nematode *Caenorahabditis elegans*", J. Exp. Biol. 204, 1757 (2001)

2) J. Raber, et al., "Radiation-induced cognitive impairments are associated with changes in indicators of hippocampal neurogenesis", Radiat Res. 162, 39 (2004).

3) M. Suzuki, et al., "A model of motor control of the nematode *C. elegans* with neuronal circuits", Arti. Int. in Med. 35, 75 (2005).

3-42 Particle Number- and LET- Dependency of Bystander Effect Through the Gap Junction Signalling in Human Normal Fibroblast Cells Exposed to Heavy-Ion Beams

Y. Matsumoto[a, b], N. Hamada[c, d, e], M. Aoki[a], S. Wada[e], T. Funayama[e], T. Sakashita[e], T. Kakizaki[e], Y. Kobayashi[c, d, e] and Y. Furusawa[a]

[a]Heavy-ion Radiobiological Research Group, National Institute of Radiological Sciences, [b]Graduate School of Medicine, Chiba University, [c]Department of Quantum Biology, Division of Bioregulatory Medicine, Gunma University Graduate School of Medicine, [d]The 21st Century Center of Excellence (COE) Program on Biomedical Research using accelerator technology, [e]Radiation-Applied Biology Division, QuBS, JAEA

Abstract

When cells were irradiated with ionizing radiation, non-irradiated cells around irradiated cells showed same biological effect, for example apoptosis, DNA damage, chromosomal aberration, and these phenomena are called bystander effect. Bystander effect is caused by two major pathway, gap junction signalling or medium-mediated signalling. The correlation of these pathways with bystander effect, and some transmission agents of the effect were reported in many papers. But the existence of the particle number- or LET-dependency of the effect is still a matter of debate. In this experiment, we demonstrated that the particle number-dependency of bystander effect was observed in AG01522 cells exposed to carbon ion beams with LET of about 100keV/μm, and suggested that existence of the LET-dependency of this effect.

放射線を細胞に照射した場合，周囲の非照射細胞にもバイスタンダー効果として被曝した細胞からの影響が現れることが判っている[1)]。バイスタンダー効果は活性分子種や特殊な信号伝達物質によって被曝細胞から周囲の細胞に影響が及んでいるものと考えられる。この伝達経路としては培地を介した液性伝達経路と細胞間チャンネル信号伝達経路を介した信号伝達が考えられており，その詳細については不明な点が多かったが，一連の研究により，バイスタンダー効果へのこれらの経路の関与及びその伝達に関わる物質の存在が明らかとなってきた[2-8)]。

世界の多くの施設の装置はｐ、α粒子を用いておりLETを広い範囲で変えることは出来ないが，国内ではPF-SPICE- TIARA等多施設を利用することで，LETを数keV/umから数千keV/umまで変えることができ，LET依存性の研究が可能である[9)]。

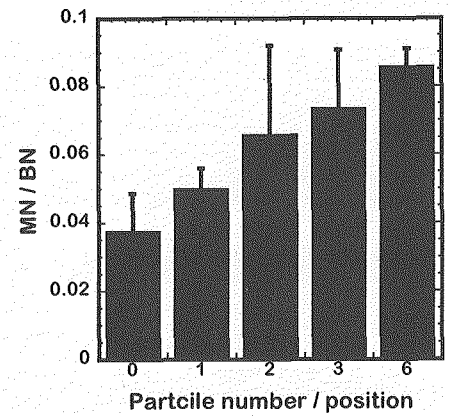


Fig. 1 particle number-dependency of bystander effect in AG01522 cells exposed to C-ion irradiations

ヒト正常繊維芽細胞AG01522を用い，照射時にサンプルディッシュ1枚あたり約70万個の細胞が存在する条件で、このうち7 x 7の合計49点（照射面中心を原点として，2.5mm間隔）にマイクロビームを照射した。バイスタンダー効果の有無については，染色体異常を指標とし，微小核形成を計数した。先にLETが400keV/μm以上のネオンイオン及びアルゴンイオンを用いて行った実験では，各点1粒子ずつの照射で飽和レベルの微小核が誘発され，各点2-4粒子の照射でも誘発頻度は変わらなかった。一方，LETが約150keV/μmのカーボンイオンを用いた場合、照射粒子数の増加と微小核誘発頻度との間に相関が見られた（Fig.1）。先に報告したネオンおよびアルゴンビーム照射による結果と合わせて，高LET領域（400keV/μm以上）で見られなかったバイスタンダー効果の粒子数依存性が，中程度のLET（約150keV/μm）では見られることが示唆された。しかし，現在バイスタンダー効果の粒子数依存性の有無については意見が分かれている。本実験データは2粒子照射時のエラーバーが大きいため，取得した他のサンプルの早急な解析が必要であり，またその他の粒子数（3粒子，8粒子，12粒子）についても解析を行い，実験データの検証を行う必要がある。

Reference

1) Targeted cytoplasmic irradiation induces bystander response. PNAS 101: 13495-13500 (2004).
2) Bystander effect in lymphoma cells vicinal to irradiated neoplastic epithelial cells: Nitric oxide is involved. J. Radiat. Res. 45: 1-7 (2004).
3) Bystander effect on cell growth stimulation in neoplastic HSGc cells induced by heavy-ion irradiation. Radiat. Envirnm. Biophys. 42: 183-187 (2003).
4) Role of gap junctional intercellular communication in radiation-induced bystander effect on human fibroblast cell. Radiat Res 160: 64-69 (2003).
5) Bystander effect induced by counted high-LET particles in confluent human fibroblasts: a mechanistic study. FASEB J 17: 1422-1427 (2003).
6) Sper/NO-induced reversible proliferation inhibition and cycle arrests associated with a micronucleus induction in HSG cells. Nitric Oxide: Biol. Chem. 8: 83-88 (2003).
7) Nitric oxide-mediated bystander effect induced by heavy-ion in human salivary grand tumor cells. Int J Radiat Biol 78: 837-844 (2002).
8) Medium-mediated bystander effects on HSG cells co-cultivated with cells irradiated by X-rays or a 290 MeV/u carbon beam. J Radiat Res 42: 305-316 (2001).
9) Single particle irradiation system to cell (SPICE) at NIRS. Nucl. Instr. Meth. B 210: 292-295 (2003).

3-43 Analysis of Molecular Mechanisms for Radiation-Induced Bystander Effects Using Heavy Ion Microbeams

H. Matsumoto[a)], M. Hatashita[a)], A. Takahashi[b)], N. Hamada[c,d,e)], S. Wada[c,d,e)], T. Funayama[e)], T. Sakashita[e)], T. Kakizaki[e)] and Y. Kobayashi[c,d,e)]

[a)]Faculty of Medical Science, University of Fukui, [b)]Nara Medical University School of Medicine, [c)]Gunma University Graduate School of Medicine, [d)]The 21st Century Center of Excellence Program for Biomedical Research Using Accelerator Technology, [e)]Radiation-Applied Biology Division, QuBS, JAEA

Abstract

A classical paradigm of radiation biology asserts that all radiation effects on cells, tissues and organisms are due to the direct action of radiation. However, there has been a recent growth of interest in the indirect actions of radiation including the radiation-induced adaptive response, the bystander effect, low-dose hypersensitivity, and genomic instability, which are specific modes of stress exhibited in response to low-dose/low-dose rate radiation. However, mechanisms of these phenomena are not fully known. The objective of this project is to elucidate molecular mechanisms of the bystander effect using heavy ion microbeams in JAEA. We found that the foci of γH2A.X were formed in the unirradiated cells in the target colony including the irradiated cell 30 min after irradiation with 260 MeV ^{20}Ne beams and that this formation of the foci was almost completely suppressed by the addition of NO specific scavenger, c-PTIO. Also we found that the foci of γH2A.X were formed in the unirradiated cells in the untargeted colonies 6 h after irradiation with 260 MeV ^{20}Ne beams and that this formation of the foci was almost completely suppressed by the addition of c-PTIO. Our findings demonstrate that NO is an initiator/mediator for evoking heavy ion microbeam-induced bystander effects.

低線量／低線量率放射線に対して生物が示す特異的な応答様式の一つに放射線誘発バイスタンダー効果がある。放射線誘発バイスタンダー効果とは、放射線が通過した細胞の近傍に存在する全く放射線が通過していない細胞において観察される放射線による生物効果であるが、この分子メカニズムは十分に明らかにされていない。我々は、日本原子力研究開発機構において開発された重イオンマイクロビーム細胞照射システム（細胞局部照射装置）を用いて放射線誘発バイスタンダー効果の分子メカニズムを明らかにすることを計画した。

１．実験方法

1. 細胞：ヒトがん細胞(H1299 細胞[1)]、A-172 細胞)およびヒト正常線維芽細胞(AG1522 細胞)を用いた。
2. 培養：中央に 12 mm 径の孔の開いた 35 mm ディッシュの内面中央に 20 mm 四方の CR-39 樹脂をワセリンで固定したものを使用した。また CR-39 樹脂の表面を collagen コートして細胞を培養した。2 x 10^5 cells/ml の細胞懸濁液 5 μl を CR-39 樹脂上に 5 箇所スポットし(1000 cells/colony)、3 時間後に培地を 3 ml 添加し、15~20 時間培養したものを照射実験に供した。
3. 照射：Funayama ら[2)]が確立した方法に従って、中央にスポットしたコロニーの細胞 1 個に 5~10 粒子の 260 MeV ^{20}Ne を照射した。また対照実験として 260 MeV ^{20}Ne のブロードビームにおいても照射した。
4. 細胞の固定および染色：照射後、細胞を 37°C で培養し、0.5、3、6 および 12 時間後にメタノール／アセトン混液(1:1)で固定し、リン酸化型 H2A.X (γH2A.X)抗体およびリン酸化型 NBS1 抗体を用いた蛍光抗体染色法により染色し、蛍光顕微鏡下で観察した[3)]。

２．結果及び考察

1. 標的コロニーにおける H2A.X のリン酸化：ヒトがん細胞において、照射 30 分後、非照射細胞において細胞当たり数個の γH2A.X フォーカスが認められた。このフォーカス形成は一酸化窒素(NO)ラジカル消去剤である c-PTIO の添加により消失した。
2. 非標的コロニーにおける H2A.X のリン酸化：ヒトがん細胞において、照射 6 時間後、非標的コロニー内の細胞において細胞当たり 1ー2 個の γH2A.X のフォーカスが認められた。このフォーカス形成は c-PTIO の添加により消失した。
3. 非照射細胞における γH2A.X フォーカス形成のメカニズム：ヒト正常線維芽細胞(AG1522 細胞)を中央および周辺 4 箇所、計 5 箇所に播種し、中央の標的コロニー内の 1 細胞に照射した場合の標的コロニー内および周辺の非標的コロニー内の非照射細胞における γH2A.X のフォーカス形成を c-PTIO、誘導型 NO 合成酵素阻害剤 aminoguanidine およびギャップ結合阻害剤 lindane 存在下で現在検討している。
4. ブロードビーム照射による γH2A.X および NBS1 フォーカスの形成：ヒト正常線維芽細胞(AG1522 細胞)を CR-39 樹脂全体に播種し、3 Gy 相当の 260 MeV ^{20}Ne ブロードビームを照射し、γH2A.X およびリン酸化型 NBS1 のフォーカス形成を二重蛍光抗体染色法により観察した。その結果、照射 6 時間後において γH2A.X およびリン酸化型 NBS1 のフォーカス形成部位が一致して認められた。この手法を用いてマイクロビームで観察された非照射細胞での γH2A.X フォーカスの場所に NBS1 がリクルートされているのか否かを現在検討している。

References

1) Z. H. Jin, et al., Int. J. Radiat. Oncol. Biol. Phys. **59**, 852 (2004).
2) T. Funayama, et al., Radiat. Res. **163**, 241 (2005).
3) A. Takahashi, et al., Cancer Res. **64**, 8839 (2004).

3-44 Chromosomal Aberrations by Medium-Mediated Bystander Effects Induced by High-LET Radiations

K. Takakura[a)], Y. Kanasugi[a)], N. Hamada[b,c)], S. Wada[b,c)], T. Funayama[b)], T. Sakashita[b)], T. Kakizaki[b)] and Y. Kobayashi[b,c)]

[a)]Physics Department, International Christian University, [b)]Radiation-Applied Biology Division, QuBS, JAEA, and [c)]Department of Quantum Biology, Division of Bioregulatory Medicine, Gunma University Graduate School of Medicine

Our study aims to investigate the chromosomal aberrations induced by medium-mediated bystander effects and the role of the catalytic subunit of DNA-dependent protein kinase (DNA-PKcs) in the bystander effects[1)]. The recipient normal human fibroblast cells were treated with conditioned medium that was harvested from donor fibroblasts exposed to low-linear energy transfer (LET) X-rays and high-LET heavy ions.

The recipient cells were treated for 12 h with conditioned medium, which were harvested from donor cells at 24 h after exposure to 10 Gy of soft X-rays (5 keV/μm) and ^{20}Ne ions (437 keV/μm), followed by analyses of chromosome aberrations in recipient cells with premature chromosome condensation methods. To examine the role of DNA-PKcs, cells were treated with its inhibitor LY294002 (LY)[2)]. As shown in Fig. 1, increased frequency of chromosome aberrations in recipient cells treated with conditioned medium from irradiated but not un-irradiated donor cells were observed irrespective of radiation types. Bystander induction of chromosome aberrations in recipient cells was mitigated when donor cells were treated with LY before irradiation, and was exacerbated to the contrary when recipient cells were treated with LY before treatment of recipient cells with conditioned medium from irradiated donor cells.

From these results, it is suggested that the induction of bystander chromosome aberrations are partially reparable by DNA-PKcs-mediated DNA damage repair machinery, such as non-homologous end-joining repair pathways and that the bystander signals from donor cells are regulated by through the DNA-PKcs. The strong participation of nitric oxide (NO) in the bystander effects were also examined using scavenger 2-(4-carboxyphenyl)-4,4,5,5-tetramethyl-imidazoline-1-oxyl-3-oxide (c-PTIO), though the results are not shown in detail in this report.

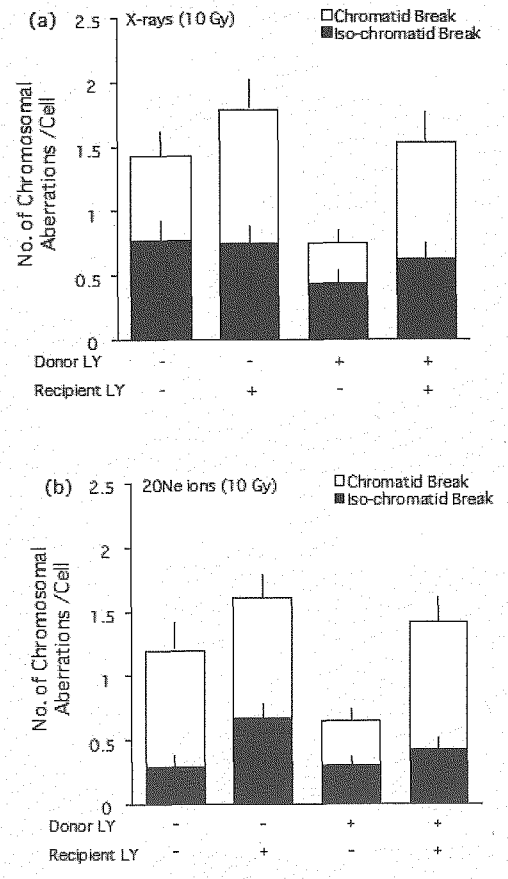


Figure 1. Effect of LY294002 (LY) on induction of chromosome aberrations in recipient cells when donor cells were irradiated a) with soft-X rays and b) with high LET Ne ion beams. Open and closed columns represent iso-chromatid breaks and chromatid breaks, respectively. LY+ and LY– indicate the treatment with and without LY, respectively. These data are presented as means and standard errors of three independent experiments where >40 cells were analyze.

References

1) Nagasawa H, Huo L, Little JB. Int J Radiat Biol. 79 (2003) 35.

2) Okayasu R, Takakura K, Poole S, Bedford JS. Journal of Radiation Research. 44 (2003) 329.

3-45 Construction of Monitoring System for Biological Effects of Local Ionizing Radiation Using the Nematode *C. elegans*

A. Higashitani [a)], T. Sugimoto [a)], C. Mori [a)], Y. Suzuki [a)], R. Saito [b)], E. Ichiishi [b)], T. Sakashita [c)], N. Hamada [c)], S. Wada [c)], T. Kakizaki [c, d)], T. Funayama [c)] and Y. Kobayashi [c, d)]

[a)]Graduate School of Life Sciences, Tohoku University, [b)]New Industry Creation Hatchery Center, Tohoku University, [c)]Radiation-Applied Biology Division, QuBS, JAEA, [d)]Graduate School of Medicine, Gunma University

Our previous study shows that the microbeam irradiation of 220 MeV 12C particles delivered from the azimuthally varying field (AVF) cyclotron at the Takasaki Ion accelerators for Advanced Radiation Application (TIARA) of the Japan Atomic Energy Agency (JAEA) is useful in characterizing tissue-specific, local biological response to radiation in the nematode *Caenorhabditis elegans* as an experimental model. DNA damage induced cell cycle arrest and apoptosis were observed in the locally irradiated region of the germline cells. However, we could not observe bystander effect in the germline cells for induction of the arrest and apoptosis in the non-irradiated neighboring region by the microbeam irradiation[1,2]. In contrast, in mammalian systems, many bystander effects have been observed[3-8]. In particular, the recent report indicates that unirradiated cells up to 1 mm distant from irradiated cells showed a significant bystander effect for induction of micronucleated and apoptotic cells in reconstituted human skin tissue[8]. The 1 mm distance is just identical to the body size of *C. elegans* adult hermaphrodite. A possible reason for the absence or recuction of bystander effect in *C. elegans* may be due to lack of communication between completely different organs and / or the defined part in the same organ. The germline cells may be isolated and protected from radiation-induced bystander responses. Therefore, we focus to further study bystander effect in other somatic tissues such as gut and muscle in *C. elegans*.

To construct the monitoring system for biological effects of local ionizing radiation, at first, DNA microarray analysis for transcriptional alterations after irradiation of ionizing radiation with the nematode 22K genechip. About 50 genes were up-regulated by the irradiation (Fig. 1). One of the up-regulated genes was a member of small heat shock gene *hsp-16*. The *hsp-16* promoter *lacZ* (β-galactosidase) fusion has been constructed for monitoring several environmental stresses including heat shock[9]. To specify differences between high-temperature stress and radiation effect, at first, we monitored the *lacZ* expression at different temperatures. The results indicated that the *lacZ* positive cells could appear at more than 28℃, suggesting the radiation experiments must carry out at less than 27℃ (Fig. 2). In addition, apoptosis related genes *ced-13* and *egl-1* were specifically up-regulated by the irradiation.

We are now constructing and applying each gene fusion system to study the biological effects of local ionizing radiation including bystander effect in somatic tissues.

References

1) S. Sugimoto et al., Int. J. Radiat. Biol. 82 (2006) 31.
2) A. Higashitani et al., TIARA annual report 2004 (2006) 136.
3) H. Zhou et al., Proc. Natl. Acad. Sci. USA. 97 (2000) 2099.
4) H. Matsumoto et al., Radiat. Res. 155 (2001) 387.
5) C. Shao et al., FASEB J. 17 (2003) 1422.
6) A.I. Kassis, Hum. Exp. Toxicol. 23 (2004) 71.
7) H. Matsumoto et al., Biol. Sci. Space 18 (2004) 247.
8) O.V. Belyakov et al., Proc. Natl. Acad. Sci. USA. 102 (2005) 14203.
9) E.G. Stringham and E.P. Candido, J. Exp. Zoology 266 (1993) 227.

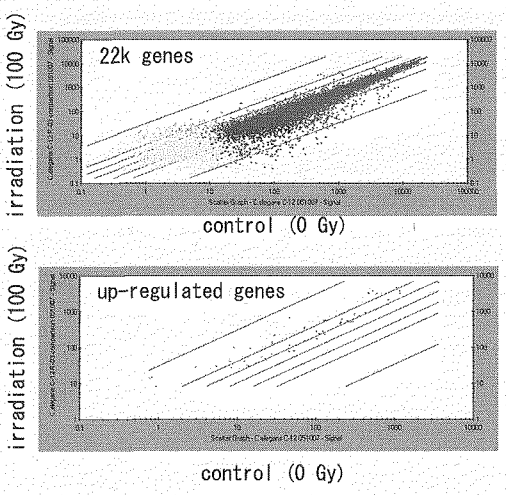


Fig.1 DNA microarray analysis for transcriptional alterations after ioninzing radiation in the nematode *C. elegans*. x, y axes indicate the signal strength of each microarray probe after hybridization.

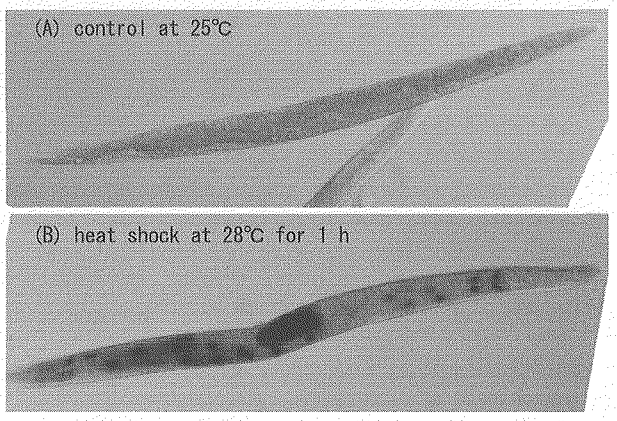


Fig.2 A small heat shock protein gene *hsp-16-lacZ* fusion is useful for stress responses.

3-46 Ion Beam Irradiation has Different Influences on Glutathione Peroxidase of Cultured Human Retinal Vascular Endothelial Cells among ^{20}Ne, ^{12}C, and ^{4}He

K. Akeo [a, b], N. Hamada [c, d], Y. Kobayashi [c, d], T. Funayama [c], T. Sakashita [c], Y. Akeo [a], K. Kawada [a] and K. Tsubota [b]

[a]Akeo Eye Clinic, [b]Department of Ophthalmology, Keio University School of Medicine, [c] Radiation-Applied Biology Division, QuBS, JAEA, [d]Department of Quantum Biology, Division of Bioregulatory Medicine, Gunma University Graduate School of Medicine

We previously reported that irradiation of visible light and hyperoxia had more influence on growth of cultured aortic endothelial cells than that of cultured retinal pigment epithelial cells because of oxidative stress[1-3]. Since then, we have studied the effects on retinal endothelial (RE) cells instead of aortic endothelial cells.

Glutathione peroxidase (GPX), a selenium-dependent and lipid peroxide-scavenging enzyme that effectively reduces lipid peroxides with the concomitant oxidation of glutathione is distributed in mitochondria[4]. Faucher et al. measured the expression of two Bcl-2 family members, Bax and Bcl-2, in a human endothelial like cell-line overexpressing the organic hydroperoxide-scavenging enzyme GPX, in the absence of any apoptotic/oxidant stimulus, and showed that overexpressing an antioxidant gene such as GPX in endothelial cells is able to change the basal mRNA and protein Bax levels without affecting those of p53 and Bcl-2. This phenomenon could be useful to antiatherogenic therapies that use antioxidants with the aim of protecting the vascular wall against oxidative stress injury[5]. The gamma ray (^{60}Co) causes ionization uniformly in the whole irradiated tissue. We found out that high dose of gamma irradiation prevented programmed cell death regulated by p53 and Bcl-2 genes in the ciliary body dissected from living body, and was useful for preservation of organ after culture by the protective influence of inflammatory reaction[6].

The irradiation is known to result in a dose-dependent decline in the activities of GPX in the skin of mice[7]. We reported at the annual meeting of Japanese Ophthalmological Society and TIARA last year that gamma ray irradiation decreased the expression of GPX in the RPE cells but it might be possible for the ion beams to induce the expression in order to protect from the damage of cell membrane due to the accumulation of energy at narrow areas.

The damage of RE cells is one of the pathological findings in senile macular degeneration and diabetic retinopathy. Oxidative stress such as light damage or ischemia could be the triggers of these diseases. We investigate how the ion beams with the different reaching depth in tissue influence GPX against the oxidative stress in the RE cells using LightCycler system as a real time-reverse-transcriptase polymerase chain reaction (RT-PCR).

Established human RE cells in vitro were exposed to an ionization radiation that is induced by acceleration of the ionizing atom of ^{20}Ne, ^{12}C, and ^{4}He. We obtained the RE cells after 0, 4, 8, 24 hr of the irradiation and extracted total cellular RNA and cDNA was synthesized. We used the Primer3 website to design the primers for RT-PCR amplification of the cDNA of GPX and 18S RNA. The reactions were carried out at the following temperature: 95°C, for denaturation; 60°C, for annealing; and 72°C, for extension for 17–27 cycles. After mixing the cDNA, primer, and SYBR green, the expression of 18S RNA and GPX was measured using the LightCycler system.

The technology of this system is extremely innovative and enables rapid and simultaneous evaluation PCR experiments. Fluorometric analysis of the formed PCR products was performed as a real-time measurement either continuously or at specifically defined time points during each PCR cycle. The experimental protocol contained five cycle programs: program 1, reverse transcription of the template RNA; program 2, denaturation of the cDNA/RNA hybrid; program 3, cDNA amplification; program 4, melting curve analysis (for product identification); program 5, cooling of the rotor and thermal chamber. The analyses could be monitored online, i.e., directly during the reaction, with the user-friendly LightCycler software.

The expression of GPX in RE cells was increased by the exposure to ion beam irradiation (50 MeV ^{4}He and 220 MeV ^{12}C) after 0, 4, and 24 hr of the irradiation. The ion beam by 350MeV ^{20}Ne might induce the expression of GPX each time after 0, 4, 8, and 24 hr of the irradiation because of the damage of cell membrane according to the high LET. It is possible for ion beam irradiation to induce the defense mechanism against lipid peroxidation in RE cells by the expression of GPX.

REFERENCES

1) K. Akeo et al., Exp. Eye Res. 49 (1989) 335
2) C. K. Dorey et al., Curr. Eye Res. 9 (1990) 549
3) K.Akeo et al., Ophthalmic Res. 24 (1992) 357
4) K. Watanabe, Tran.Soc Pathology Jpn 76 (1986) 39.
5) K. Faucher et al., Mol Cell Biochem. 277 (2005) 81
6) K. Akeo et al., Exp. Animals. 55 (2006) 375.
7) J.G. Chandra et al., Clin Chim Acta 332 (2003) 111

3-47 The Characteristics of Radiation-Induced Cell Responses in the Canine Spontaneous Tumor Cells

T. Sano[a)], S. Wada[b)], K. Suzuki[a)], M. Natsuhori[a)], T. Kakizaki[a,b)], T. Itoh[a)], K. Nakazawa[a)], Y. Kobayashi[b)] and N. Itoh[a)]

[a)]Department of Veterinary Radiology and Radiation Biology, Kitasato University, [b)] Radiation-Applied Biology Division, QuBS, JAEA

Abstract

Even in the veterinary medicine, animal's survival time extends, and cancer becomes a main reason of the death. There are several therapeutic procedures for the cancer patients, it is expected the chance of the application of the radiation therapy will increase in the future. The purpose of this study is to evaluate about the radiation sensitivity of the canine spontaneous tumor cell lines as a basic research for the advanced radiation therapy in the veterinary medicine. Each cells were irradiated by X ray (250kVp, 0.8Gy/min, LET 1.0keV/μm) and carbon beam (220MeV, 6.0Gy/min, LET 108keV/μm). After each given dose (range between 1～8Gy), cells were harvested and survival fractions were evaluated by the Clonogenic assay. The relative biological effectiveness (RBE) of carbon beams compared with X-rays was investigated by the each surviving fraction. The radiation sensitivity was H, F, and S in the high order. The differentiation of the sensitivity order was not observed, but a cell resisted to X-rays irradiation tended to show more sensitivity to carbon beam irradiation. All RBE were converged at 4, and there are several degree of relationship between the beam character, radiation sensitivity, and RBE.

現在獣医学領域においても動物の寿命の延長・高齢化が進み人と同様、癌による死亡が大部分を占めるようになった[1)]。飼い主の意識の変化などにより、愛犬もしくは愛猫が癌になった場合、様々な治療法の中から生体への侵襲が少なく患者の高い生活の質（QOL；Quality of Life)の維持が可能な放射線治療が選択される機会は今後さらに増加すると考えられ、さらには陽子線や炭素線を用いた高度放射線治療を望む声も多くなると予想される。放射線治療を行うにあたり個々の腫瘍あるいは個体の放射線感受性をあらかじめ予測し評価することができれば、個々の患者に対し適切な線量や照射間隔を考慮した放射線治療プロトコールを作成することが可能となり、個々の患者へのオーダーメイド放射線療法の実施が可能となる[2, 3)]。そこで本研究では、獣医学領域における高度放射線治療実現のための基礎的研究として、イヌ株化腫瘍細胞に対する放射線照射の影響の詳細な評価のために、Clonogenic assayを用いたX線および炭素線照射に対する細胞反応および生物学的効果の比較を行った。実験にはイヌの自然発生腫瘍由来の株化腫瘍細胞３種(S;扁平上皮癌由来、F;線維肉腫由来、H;血管周皮腫由来）を用い、これにX線（250kVp, 0.8Gy/min, LET 1.0keV/μm）を2,4,6,8Gyおよび炭素線（220MeV, 6.0Gy/min, LET 108keV/μm）を1,2,4,6Gy照射し、Clonogenic assayを用いて生存率の算出を行った。またClonogenic assayにより得られた生存曲線をLQモデル（Liner Quadraticモデル）にあてはめ、シミュレーション解析を行った。基準放射線としてX線を、対象とする放射線に炭素線を設定しD10における生物学的効果比（RBE；Relative Biological Effectiveness）の違いと生存率の変化に対するRBEの変動について調べた。生存曲線の分布より放射線感受性は高い順にH>F>Sとなり、感受性の順に線質による違いは認められなかった（Fig.1）。炭素線の照射により生存曲線の形状はより直線に近づき、全ての細胞に対する生物学的効果の増大が示された。中でも最も放射線抵抗性であったSにおける変動が大きく、より抵抗性を示す細胞において炭素線照射の影響は増大するものと考えられた。RBEは全ての細胞で約4となり、生存率の変化に対するRBEの変動は生存率の減少に伴い一定の値に収束していく傾向が確認された（Fig.2）。放射線により誘導される細胞死すなわち放射線感受性との間には明らかではないものの、ある程度の関連性を有する可能性が確認された。しかしより詳細な評価のためには、今後より多くの細胞・組織を用い、実際の腫瘍症例に対するデータとして還元するための更なる基礎研究が必要であると思われた。

Fig. 1.

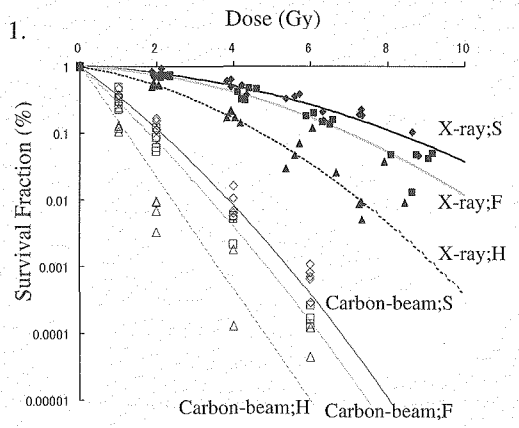
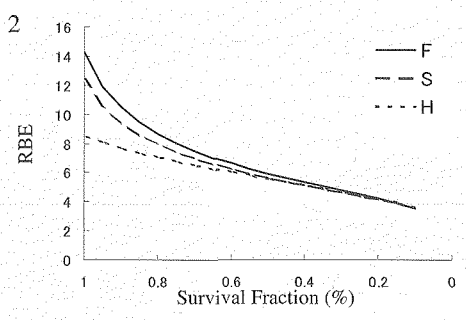


Fig. 2



References

1) Englewood, C.O., Animal health survey. pp.12(1986).
2) Bock C, Dube A, Greulich KO, Gupta PK.Mutat Res., 439(2), 171 (1999).
3) 原田良信. Isotope News. 585 (2003).

3-48 Effects of Heavy Ions and Gamma-Ray on the Tardigrade *Milnesium tardigradum*

D. D. Horikawa [a, b, c], T. Sakashita [c], C. Katagiri [d], M. Watanabe [b], T. Kikawada [b], Y. Nakahara [b], N. Hamada [c, e], S. Wada [c, e], T. Funayama [c], S. Higashi [a], Y. Kobayashi [c, e], T. Okuda [b] and M. Kuwabara [f]

[a]Graduate School of Environmental Earth Science, Hokkaido University, [b]Anhydrobiosis Research Unit, National Institute of Agrobiological Sciences (NIAS), [c]Radiation-Applied Biology Division, QuBS, JAEA [d]Institute of Low Temperature Science, Hokkaido University, [e]Department of Quantum Biology, Graduate School of Medicine, Gunma University, [f]Graduate School of Veterinary Medicine, Hokkaido University

Tardigrades (Fig. 1 A) are tiny animals whose body length ranges from 0.1 to 1.0 mm and inhabit various kinds of environments. Almost all terrestrial tardigrade species can enter "anhydrobiosis", an ametabolic state induced by dehydration. Anhydrobiotic tardigrades (Fig. 1 B) show considerable tolerance to a variety of extreme environmental conditions, such as low and high temperatures (-273°C to +151°C), vacuum, high pressure (< 600 MPa) and organic solvents[1]. They also have been known to tolerate exposure of high doses of X-rays and gamma-rays[2),3)]. However, there are no reports concerning effects of heavy ions on tardigrades. In the present study, in order to gain additional knowledge about radio-tolerance of hydrated and anhydrobiotic tardigrades, we examined survival ability after irradiation with heavy ions as well as gamma-rays using a tardigrade species *Milnesium tardigradum*.

M. tardigradum was gained from mosses on asphalt pavements in Ibaraki, Japan. Hydrated or anhydrobiotic animals were irradiated with gamma-rays (0.2 keV) from ^{60}Co sources at the doses of 500 Gy to 7000 Gy or irradiated with ^{4}He (50 MeV, 16.3 keV/m) at the doses of 500 to 8000 Gy at Japan Atomic Energy Agency (JAEA), Takasaki. Survival was checked at 2, 24 and 48 h after irradiation (hydrated animals) or after rehydration (anhydrobiotic ones). LD_{50} at 2, 24 and 48 h was estimated by means of linear regression analysis between the survival rate and radiation dose.

LD_{50} values after irradiation with gamma-rays at 48 h and with heavy ions at 24 and 48 h were somewhat higher in hydrated *M. tardigradum* compared to anhydrobiotic one (Table 1). This survival pattern in *M. tardigradum* was opposite to those in other anhydrobiotic animals[4,5]. It is difficult to explain the survival pattern in the case of *M. tardigradum*, since anhydrobiotic animals having little water contents (1.1% wt./wt.) are expected to be damaged less by the indirect action of radiation compared to hydrated animals (water content: 80.7% wt./wt.). In contrast to other anhydrobiotic animals, *M. tardigradum* contains low concentration of trehalose (< 0.2% wt./dry wt.) in the anhydrobiotic state. The presence of different amounts of a disaccharide sugar "trehalose" may responsible for the different degree of radiation tolerance between tardigrades and other anhydrobiotic animals, because trehalose has protective effects against radiation[6].

Furthermore, there was an overall tendency of LD_{50} values in both hydrated and anhydrobiotic animals for heavy ions to be higher than those for gamma-rays (Table 1). This result indicates that *M. tardigradum* is more tolerant to heavy ions than that to gamma-rays. This characteristic may be unique in tardigrades, because high-linear energy transfer (LET) heavy ions is thought to be more detrimental than low-LET gamma-rays[7].

To understand the mechanisms of radiation tolerance, further studies to estimate reproductive ability or DNA damages after irradiation in hydrated and anhydrobiotic tardigrades are needed.

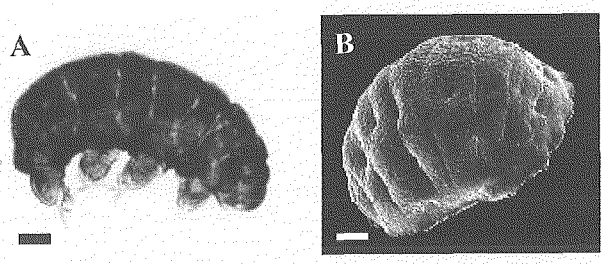


Fig. 1 A tardigrade species *Ramazzottius* cf. *varieornatus* in hydrated (A) and anhydrobiotic (B) states.
Scale bar = (A) 50 μm (B) 20 μm

References

1) JC. Wright, Zool. Anz. 240 (2001) 563-582.
2) R. May et al., Bull. Biol. de la Fran. et de la Belg. 98 (1964) 349-367.
3) KI. Jonsson et al., Int. J. Radiat. Biol. 81 (2006) 649-656.
4) T. Iwasaki, J. Radiat. Res. 5 (1964) 91-96.
5) M. Watanabe et al., Int. J. Radiat. Biol. (2006) *in press*.
6) K. Yoshinaga et al., Biosci. Biotech. Biochem. 61 (1997) 160-161.
7) EJ. Hall, Radiobiology for the radiologist, Ed. 4 (1994)

Table 1 LD_{50} at 2, 24 and 48 h after irradiation of gamma-rays or ^{4}He in *M. tardigradum*.

		LD_{50} (Gy)		
Radiation	State	2 h	24 h	48 h
Gamma	Hydrated	5500	5200	5000
	Anhydrobiotic	5500	5400	4400
$^{4}He^{2+}$	Hydrated	7800	6300	6200
	Anhydrobiotic	7900	5400	5200

3-49 Regeneration Mechanism of Hemopoietic Organs in the Silkworm, *Bombyx mori*, after Heavy-Ion Irradiation: Analysis by Transplantation of the Irradiated Organs Using a Transgenic Silkworm Strain

K. Kiguchi[a], K. Shirai[a], T. Sakata[a], K. Fukamoto[b], T. Kakizaki[b], S. Wada[b], T. Sakashita[b], T. Funayama[b], N. Hamada[b] and Y. Kobayashi[b]

[a]Department of Applied Biology, Faculty of Textile Science and Technology, Shinshu University,
[b]Radiation-Applied Biology Division, QuBS,JAEA

We previously demonstrated that locally-targeted irradiation of the silkworm, *Bombyx mori*, with heavy-ions resulted in marked damage of the larval hemopoietic organs (HPOs), but that these were subsequently regenerated with high frequency[1]. Regeneration is thought to occur by one of two different processes. The first process involves the phagocytosis of damaged cells from the irradiated HPOs by hemocytes in circulation[2], while the second arises from the cellular proliferation and differentiation of the hemopoietic stem cells, although the mechanism by which this occurs is not yet well understood. In order to clarify the origin of the stem cells responsible for the regeneration of heavy-ion-irradiated HPOs, we conducted transplantation experiments of the organs using transgenic silkworm larvae, which were characterized by GFP(green fluorescence protein) expression in most tissues and cells including hemocytes. Here we suggest that the stem cells responsible for regeneration may also originate from the hemocytes in circulation.

A laboratory colony of the *pnd pS* silkworm strain was used for experiments. A transgenic silkworm strain expressing the GFP gene, a gift from Dr. T. Tamura, which was transformed using the GAL4/UAS system[3] was also used. The HPOs on the left side of the *pnd pS* larvae (4th instar, day 2) were selectively exposed to ion beams (^{12}C, 18.3 MeV/u, LET=116.4, 100 Gy) as described previously[1,2]. Twelve hours after irradiation, the imaginal wing discs and attached HPOs were quickly excised from the irradiated left thoracic region and implanted into transgenic silkworm larvae (4th instar, day 2) to allow regeneration. The implanted organs were recovered from the host larvae six days later (5th instar, day 4), fixed in Carnoy's solution, embedded in paraffin and sectioned following routine methods. Anti-GFP antibody (MBL) was used to assess GFP localization in the regenerated organs immunohistochemically.

As shown in Fig. 1, GFP-signals were clearly detected in those HPOs that regenerated after heavy-ion irradiation. This finding suggests that the hemocytes expressing GFP in circulation, invade the implanted HPOs where they are involved in regeneration. As mentioned previously, two processes may be responsible for regeneration. First, the injured cells must be removed from the irradiated HPOs to eliminate any damaged tissue and the hemopoietic stem cells must then proliferate and differentiate. However, the question then is what are the hemopoietic stem cells derived from? The results obtained in this experiment suggest that stem cells may originate from one of the hemocytes in circulation, possibly prohemocytes. However, the possibility exists that they are derived from healthy cells within the HPOs that might have escaped damage by irradiation.



Fig. 1. Immunohistochemical detection of GFP-signals in the regenerated HPOs.
Arrow indicates the regenerated HPOs that expressed GFP. Bar indicates 100 μ m. WD: wing disc.

References

1) Ling, E. *et al.*, I. Insect Biotechnol. Sericol. 72, 95-100 (2003)
2) Ling, E. *et al.*, Devlop. Comp. Immunol. 30, 531-543 (2006)
3) Imamura, M. *et al.*, Genetics 165, 1329-1340 (2003)

3-50 Analysis of Local Irradiation of Heavy-ion Microbeam Influence on Embryo or Yolk in the Silkworm, *Bombyx mori*, Egg by the Incidence of Somatic Mutation Appearing in the Larvae

T. Furusawa[a)], E. Suzuki[a)], S. Nagaoka[b)], H. Suzuki[c,d)], N. Ishioka[d,e)], N. Hamada[f)], S. Wada[f)], Y. Kobayashi[f)], T. Sakashita[f)], T. Kakizaki[f)] and K. Funayama[f)]

[a)]Center for Bioresource Field Science, Kyoto Institute of Technology, [b)]Fujita Health University, [c)]Japan Space Forum, [d)]Graduate School of Med. And Dental Sci, Kagoshima University, [e)]Japan Aerospace Exploration Agency, [f)] Radiation-Applied Biology Division, QuBS, Japan Atomic Energy Agency,

The exposure of diapause eggs to X-rays or heavy ion particles resulted in somatic mutations appearing as white spot(s) on the black integument during larval stage[1)]. In this system utilizing the P^S gene as an index of radiation exposure, incidence of somatic mutation was clearly estimated as individual level dependently on both dose and LET. It has not been cleared whether the somatic mutation will be induced by direct hit of the heavy particles to embryo or indirect of these to yolk by bystander effect. This leads us to examine the incidence of the somatic mutation by local hit of heavy ion particles to embryo or yolk in *Bombyx* eggs.

The eggs (P^S/p) were kept at 25℃ for first 10 days after oviposition, and then at 5℃ for 70 days to terminate diapause. These diapause-terminated eggs were transferred again to 25 ℃ for resumption of embryogenesis. Carbon ion beam (0.5 Gy and 3.0 Gy) was irradiated to the day 2 after the resumption of embryogenesis, and locally to 20 μm^2 of the center (yolk) of the egg at 112 keV/μm and of embryo at 119 keV/μm. After the irradiation, the newly hatched larvae were reared on an artificial diet throughout all stages, and we counted the number of larvae with white spot(s) on the black integument to examine the incidence of somatic mutation. The incidence of somatic mutation was higher in embryo irradiated to the beam than in the center of yolk to the beam.

Furthermore, we examined the incidence of the somatic mutation in detail when the ion beam was irradiated to head-thorax and caudal portion of embryo, and the yolk region at the center of the eggs. In this experiment, the eggs were kept at 25℃ for the first 18 days after oviposition to enter diapause status, and then at 5 ℃ for 97 days to terminate diapause. For the resumption of embryogenesis, these eggs were transferred to 25℃, and 2 days later carbon beam was irradiated to each portion.

The incidence of the somatic mutation was 5~7% in the non-irradiated eggs. In contrast, the higher incidence was observed in the head-thorax and caudal portion of embryo, and the yolk region at the center of the eggs (Fig. 1). Especially, the irradiation of carbon beam (3 Gy) to the caudal portion of embryo resulted in about 30% incidence. It was interest that the incidence elevated

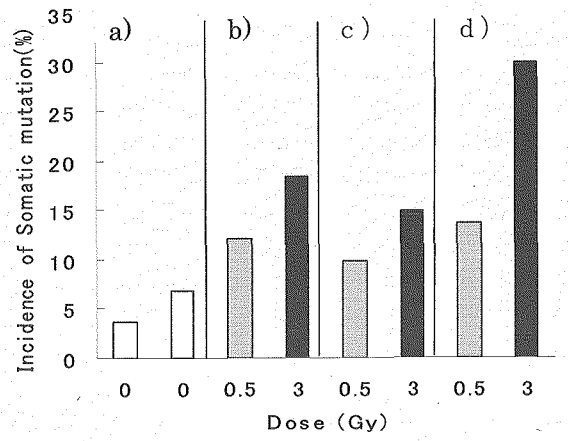


Fig. 1. Local irradiation of carbon beam to the silkworm egg and the incidence of somatic mutation. a) Non-irradiation (control), b) Center of egg , c) Head-thorax portion and d) Caudal portion of embryo.

with the increase of irradiation dose when carbon beam hits at almost center of the egg which contains only yolk granules. Since the results suggested the bystandar effect, now we are investigating the interaction between the frequency of somatic mutation and irradiation of a heavy ion particle to the center of egg.

References

1) E.Kotani, T.Furusawa, S.Nagaoka, K.Nojima, H.Fujii, Y.Sugimura, M.Ichida, E.Suzuki, A.Nagamatsu, T.Todo and M. Ikenaga. J. RDIAT.RES., **43**, SUPPL., S193-S198 (2002)

3-51 Identification of the Functional Tissues for Hydrotropism in Comparison with Those for Gravitropism

Y. Miyazawa[a)], H. Negishi[a)], T. Sakashita[b)], A. Kobayashi[a)], T. Kaneyasu[a)], A. Ooba[a)], T. Funayama[b)], S. Wada[b)], N. Hamada[b,c)], T. Kakizaki[b,d)], Y. Kobayashi[b,c)], N. Fujii[a)] and H. Takahashi[a)]

[a)]Graduate School of Life Sciences, Tohoku University, [b)] Radiation-Applied Biology Division, QuBS, JAEA,
[c)]Graduate School of Medicine, Gunma University, [d)]Department of Veterinary Medicine, Kitasato University School of Veterinary Medicine and Animal Sciences

Abstract

Hydrotropism is a response of roots to a moisture gradient. Despite its importance on acquirement of water and nutrients, functional tissue for hydrotropism is hardly uncovered. To approach this problem, we intended to identify the functional tissues responsible for hydrotropism, in comparison with gravitropism. We irradiated either laser beam or heavy-ion beam to root tissues and monitored the changes in tropic responses. Laser beam irradiation to either elongation zone or columella cells resulted in marked decrease in both tropic curvatures. Similar effect was observed when heavy-ion beam was irradiated to elongation zones. Irradiation of either beam to elongation zone resulted in a decrease in root growth. However, the heavy-ion beam irradiation to columella cells affected neither root tropism nor growth. Considering the non-destructive cell inactivation effect of heavy-ion beam, our results suggest that cells in both columella and elongation zone are necessary for expression of both tropisms, but the biological processes that occur inside the respective cells are different.

植物が固着性生物であるにも関わらず現在まで地上で繁栄してきた背景には，植物が周囲の環境を感受・応答する形態形成能力を進化の過程で獲得してきたことが挙げられる．こうした形態形成能力の一つである重力屈性は，植物が恒常的に存在する重力を利用することで，地上部を負の重力方向に伸ばすことで光を，地下部を正の重力方向に伸ばすことで養水分を効率よく獲得する生長制御法である．また，植物の根は重力屈性能に加え，水分勾配に対して水分屈性能を発現し，自身を高水分側へと屈曲・伸長させる．重力屈性は古くから研究されており，根に関しては根冠（コルメラ細胞）のアミロプラストが重力方向に沈降することで感受が起こり，その後伸長領域でオーキシンが偏差分布することにより，屈曲が生じることが明らかとなっている．その一方で水分屈性に関しては，古くからその存在は示唆されていたものの，地上において重力方向と水分が分布する方向が同一であるため解析が困難であった．

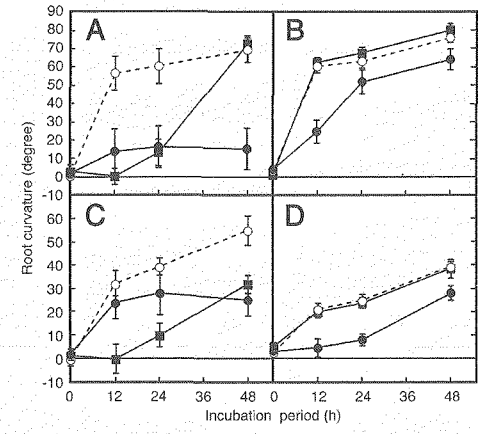


Fig.1 Effects of either heavy-ion micro beam or laser irradiation on root tropic responses. A, B: Effect of either laser (A) or heavy-ion beam (B) irradiation on gravitropism. C, D: Effect of either laser (C) or heavy-ion beam (D) irradiation on hydrotropism. Tropic responses of roots with their elongation zones irradiated (●), and with their columella cells irradiated (■), as well as no irradiation roots(○), are shown. Data are means ± SE.

しかし近年，エンドウの重力屈性欠損突然変異体を用いた解析により水分屈性の存在が実験的に証明されるとともに，エンドウ，キュウリなどを用いて，重力屈性が水分屈性に干渉すること，水分勾配の感受が根端で起こること，屈曲時に伸長領域においてオーキシン誘導性遺伝子の偏差的発現が起こることが明らかにされてきた．また最近になり，シロイヌナズナを用いた水分屈性実験系も確立され，シロイヌナズナは地上重力下でも水分屈性が重力屈性の干渉を逃れて発現することが明らかにされ，この際に，シロイヌナズナにおいては，コルメラ細胞内のアミロプラストの消失による重力感受能力の低下が起こることが明らかとなっている．しかしながら，水分屈性において根端のどの部位がどのような形で水分屈性に機能するかは，その重要性にも関わらず分かっていないのが現状である．

そこで本研究では，水分屈性において機能する細胞群とそこでの生体反応を同定することを目的として実験を行った．方法としては，シロイヌナズナ根端に対しレーザー照射及び重イオンビーム照射を行い，特定の数細胞を破壊し，それらの個体について重力屈性および水分屈性を確認することにより行った．Fig.1に示すように，細胞そのものを破壊するレーザー照射をコルメラ細胞および，伸長領域に対して行った結果，重力屈性，水分屈性ともに顕著な屈曲角度の低下が確認された．また，伸長領域に照射したサンプルに関しては顕著な伸長量の低下も観察された．このことは，両細胞群の存在が刺激の感受，シグナル伝達と偏差的な伸長による屈曲に必須であることを示している．また，細胞を非破壊的に不活化する重イオン（$^{12}C^{5+}$:220 MeV）マイクロビーム（直径 180 μm, 500 Gy相当量）を伸長領域に照射したところ，レーザー照射と同様に伸長量および屈性能の低下が認められ，屈性発現における伸長領域での偏差的な遺伝子発現の必要性を支持する結果が得られた．一方で，重イオンマイクロビームをコルメラ細胞に照射したところ，両屈性において有意な伸長量，屈性能の低下は認められなかった．これらの結果は，水分屈性，重力屈性ともに，それらの発現過程でコルメラ細胞，伸長領域の細胞群が機能することを明確に示すとともに，両細胞群における屈性発現に伴う生体反応には大きな差異があると考えられた．

3-52 Circadian Rhythms in Resistance to γ Irradiation and Heavy-Ion Beam in *Euglena*

A. Bolige [a], T. Sakashita [b], T. Kakizaki [b], T. Funayama [b], N. Hamada [b,c,d], S.Wada [b,c,d], Y. Kobayashi [b,c,d] and K. Goto [e]

[a] United Graduate School of Agricultural Science, Iwate University, [b] Radiation-Applied Biology Division, QuBS, JAEA, [c] Department of Quantum Biology, Gunma University Graduate School of Medicine, [d] The 21st Century Center of Excellence Program for Biomedical Research Using, [e] Laboratory of Biological Rhythms, Obihiro University of Agriculture and Veterinary Medicine

Abstract

We report a novel finding of circadian rhythms in resistance to γ irradiation and heavy-ion (C-ion) beam in *Euglena gracilis* (Klebs Z). They persisted for several days under continuous darkness at a constant temperature, and the most resistant phases occurred 2-4 h before subjective midddays, at which circadian rhythms in UV resistance and anti-oxidative capacities become maximal. Whereas the rhythms were apparent at all the fluences we examined, amplitudes were maximal, 45% (γ) and 20% (C ion), when the rhythms were studied using LD50. Suvival after irradiation did not depend on temperatures of *Euglena* at the time of irradiation, indicating that it did not involve enzymatic protection; the same also holds for circadian UV resistance. On the other hand, higher temperatures of *Euglena* after irradiation, particularly γ irradiation, enhanced cell death, suggesting an involvement of temperature-dependent process. The resistance to γ and C ion were enhanced by a slightly different set of non-enzymic antioxidants, but they resembled each other in that a combination of glutathione, L-cysteine and β-carotene was most effective, suggesting non-enzymic anti-oxidative mechanisms different from either UV-C or UV-B resistance. We moreover found that the resitance to higher fluences involved ass-yet-unidentified mechanisms as well as non-enzymic anti-oxidation. Particularly, the non-enzymic antioxidants succeeded in persistently enhancing survival after lower fluences of γ radiation, whereas they failed to do so after higher fluences; they just delayed death, as lower temperature after irradiation do so.

概日リズムはシアノバクテリアからヒトまで普遍的に存在する生物の重要な特性であり、予知的な環境適応として機能している。ユーグレナ（*Euglena gracilis* Z）では、UVC 耐性や UVB 耐性、及び抗酸化能の全般（脂溶性 and/or 水溶性の一重項酸素消去能・ヒドロキシルラジカル消去能が主観的真昼に最大となるよう概日リズムによって制御されている。ただし、主観的真昼より 2～4 時間前に最大抗酸化能を示す弱い成分も認められる。ストレス因子や時間因子の全くない恒常環境で、生物の放射線耐性や重イオン耐性がどのような経時変化を示すのか、全く未知である。本研究では、ユーグレナを用いてこの問題に取り組む。

本研究では、ユーグレナを6～8万細胞/mL になるまで25 °C 、6 Klx 恒明（白色蛍光灯）で培養し、恒暗に移した。恒暗中の様々な時点でγ線や220 MeV ^{12}Cイオンを照射し、中性赤を用いて生死判別を行った。その生存率をもって耐性の基準とした（C イオン は照射直後、γ線は一日後）。

γ線とCイオンのLD_{50}は最強耐性の位相で各々2200、1200 Gy、最弱耐性の位相で各々1500, 1000 Gy であった。

恒暗下に、γ線耐性と C イオン耐性は同一位相の概日リズムを示した。その位相は、抗酸化能や UV 耐性のリズムに比べ 2～4 時間ほど先行したものとなっている。C イオン耐性リズムの振幅はγ線耐性リズムに比べると格段に低い。

γ線とCイオン照射を行う温度（0、25 °C）が生存率に影響しないとの結果から、この耐性には酵素的な防御反応が殆ど関与していないと考えられる。これに対し、照射後に低温（4 °C）放置した場合には、25 °C で保存した場合より 10～60 %ほど高い生存率を示し、温度依存的な生命活動が死を促進する可能性が示された。このことは、γ線照射の場合により顕著に認められる。

γ線耐性と C イオン耐性に関わる抗酸化機作を明らかにするため、各種抗酸化剤の耐性増強効果を調べた。γ線耐性増強には還元型グルタチオン、GSH－エチルエステル、システイン、ヒスチジンなどが有効であった。また、β－カロテンやリコピンも少なからず有効であった。

C イオン耐性増強に有効であったのはシステイン、N－アセチルシステイン、ルチン、アスコルビン酸、還元型グルタチオン、GSH－エチルエステル、トロロックス、β－カロテンやリコピンなどの抗酸化剤である。

したがって、γ線耐性や C イオン耐性には水溶性や脂溶性のラジカル消去能と一重項酸素消去能が総合的に関与しているものと考えられる。

ただし、両耐性は互いに異なる抗酸化機作も関係している。例えば、γ線耐性増強に有効な抗酸化剤は C イオン耐性増強にも有効であったが、逆に C イオン耐性増強に有効なアスコルビン酸、N－アセチルシステイン、ルチン、トロロックスなどはγ線耐性増強には殆ど無効だからである。

600 Gy のγ線照射の場合、還元型グルタチオン、システイン、β－カロテンとヒスチジンを組み合わせて投与することによって、概日位相に関わらず生存率は約 95 %まで増加した。しかし、1000 Gy のγ線照射の場合、最弱位相の生存率は 91 %まで増加するにとどまった。

一方、300 ～600 Gy の C イオン照射の場合、還元型グルタチオン、システインやβ－カロテンを同時投与することによって、概日位相に関わらず生存率は約 92 %以上まで増加した。しかし、800 Gy のγ線照射の場合、最弱位相の生存率は 75 %まで増加するにとどまった。

低線量で照射の場合、γ線耐性も C イオン耐性も非酵素的な抗酸化能だけで説明できるが、高線量照射の場合には、抗酸化能以外の要因も関係している可能性が示されたことになる。

3-53 Analysis of the Maturation Process of Photosynthetic Activities in a Leaf Using Positron Emitting Tracer Imaging System (PETIS)

S. Ishii, N. Kawachi, S. Fujimaki, N. Suzui and S. Matsuhashi

Radiation-Applied Biology Division, QuBS, JAEA

1. Introduction

In general, the activities of CO_2 fixation and photosynthate export in a leaf increase along with the development of the leaf. However, the development does not progress uniformly in the whole leaf. There are an immature region and a mature one at the same time in the leaf during the developing process. Therefore, spatial and temporal analysis is needed for understanding the relationship between the activities and the development.

The Positron Emitting Tracer Imaging System (PETIS) is a tool that can visualize sequentially the movement of radioactive tracer in a living plant. Translocation of the photosynthate in higher plants has been studied previously with PETIS [1].

In this study, as a temporal and spatial analysis, we attempted not only to visualize the movement of photosynthate in a leaf but to estimate a map of the activities of CO_2 fixation and photosynthate export in the whole leaf based on PETIS data.

2. Materials and Methods

Hemp plants (*C. sativa* L. var. sativa) were grown for 30 days at 25 °C with a daily light-dark cycle of 16-8 hr.

In this study, we selected two leaves from each test plant. One was "expanded leaf", the largest expanded leaf, which should have completely developed. The other was "young leaf", the adjacent upper leaf, which should still have an immature region. Approximately 80 MBq of $^{11}CO_2$ gas was fed separately to the young leaf and to the expanded leaf of each test plant and the images of ^{11}C movement were respectively obtained by PETIS for 2hr (Fig. 1). The interval between the feedings was 3 hr sufficient for the decay of ^{11}C (half-life: 20.4 min) to the background levels.

3. Results and Discussion

We regions of interest (ROIs) with a size of 5 mm square over the leaf area on the PETIS data as shown in (Fig. 2 (left)). The time-activity curves (TACs), the time courses of radioactivity within the respective ROIs, were generated (Fig. 2 (right)).

Based on the TACs, the activity of CO_2 fixation and that of the photosynthate export were separately estimated for each ROI. As shown in Fig. 3, the distributions of the estimated activities were mapped (Only the case with the fixation activity in the young leaf is shown).

As a result, it was revealed that the distribution pattern of the export activity was quite different between the young leaf and expanded leaf although that of the fixation activity was similar. Based on this fact, we concluded the activity of CO_2 fixation and that of photosynthate export do not complete their maturation concurrently.

Reference

1) S. Matsuhashi, S. Fujimaki, N. Kawachi, K. Sakamoto, N.S. Ishioka and T. Kume, *Soil Science and Plant Nutrition* **51**, 417-423, 2005

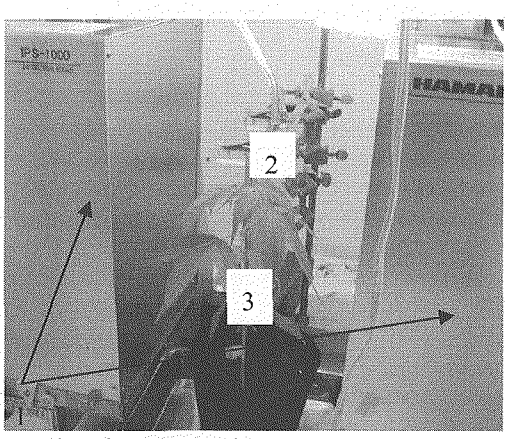


Fig. 1: Setting of PETIS experiment
1: Pair of γ-ray detectors, 2: $^{11}CO_2$ feeding gas-cell, 3: Test plant

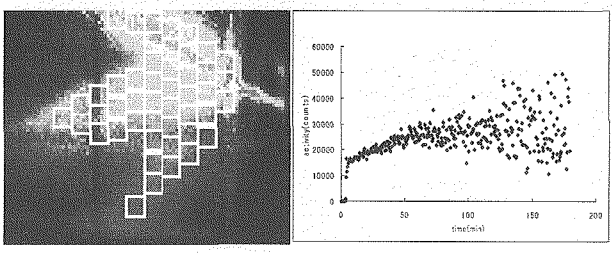


Fig. 2: The example of ROIs and TAC
5 mm square ROI were drawn on leaf image (left panel) and the example of regional time activity curve generated from each ROI (right panel)

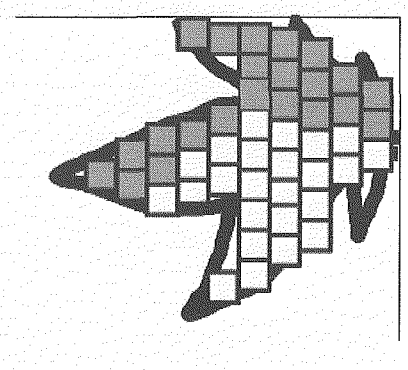


Fig. 3: Distribution map of the activity of CO_2 fixation at the each ROI on young leaf

3-54 Interaction between Nitrogen Nutrients Acquisition Function and Distribution of Photosynthetic Products

T. Ohyama[a)], K. Sueyoshi[a)], N. Ohtake[a)], S. Ito[a)], H. Ishibashi[a)], T. Hara[a)], T. Kimura[a)], S. Matsuhashi[b)], S. Fujimaki[b)], N. Suzui[b)], S. Ishii[b)], N. Ishioka[b)], S. watanabe[b)], Y. Kawachi[b)] and T. Tsukamoto[b)]

[a)] Faculty of agriculture Niigata university,
[b)]Radiation-Applied Biology Division, QuBS, JAEA

As nodulated leguminous crops grow, they assimilate both gaseous nitrogen and combined nitrogen. Combined N especially the NO_3^- form inhibits all phases of nodulation and the N_2 fixation process, although the mechanisms have not been fully elucidated. Tungstate is a non-essential element for plant growth, which exerts harmful effects on plants. When tungstate is applied to the plant medium, it competes with molybdate and inhibits some enzymes, which have a Mo cofactor in the active site such as nitrate reductase and nitrogenase. Application WO_4^{2-} to the culture medium disturbed nitrate transport to the shoot[1)]. In this report WO_4^{2-} was introduced into cut end of petiole of primary leaf and investigated that $^{13}NO_3^-$ transport from root to shoot was inhibited or not.

Soybean (cv. Williams) seeds were inoculated with *Bradyrizobium japonicum* strain USDA110 and cultivated hydroponically with N free medium. 13 days after sowing (DAS), introducing treatment was performed as follows; Water contained 1mM sodium tungstate was fed to a cut end of petiole of primary leaf. Control was fed distilled water. From 14 DAS plants were fed 1 mM nitrate in the culture medium. After 18 DAS $^{13}NO_3^-$ was supplied to the root and radioactivity was monitored at shoot for 40 min using PETIS. After Analysis by PETIS, the radioactivity of a whole plant was observed with a BAS.

Figure 1A shows the ^{13}N distribution of whole plants 40min after application of ^{13}N labeled nitrate. Introduced WO_4^{2-} to the primary detected ^{13}N signals same as control plants. Transport of ^{13}N from root to shoot detected by PETIS was also same level between control and WO_4^{2-} treatment (Fig.1 B). Those results indicated that introduced tangstate to the primary leaf petiole was not disturbed nitrate transport from root to shoot.

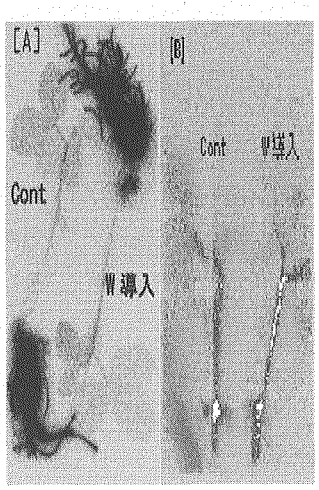


Fig. 1 [A] Distribution of ^{13}N in whole plant 40 min after applied ^{13}N labeled nitrate to the culture medium. Radioactivity was detected by BAS. [B] Average PETIS image during ^{13}N experiment period.

Cont means introduce distilled water from cut end of primary leaf petiole and W means introduce 1mM sodium tungstate. Introduce treatments applied 6 days before ^{13}N experiment.

Reference

1) Yamazaki et al. TIARA annual report (2003) 112-114

3-55 Determination of Photosynthesis and Partitioning Rate Using by PETIS

R. Suwa[a)], S. Ishii[b)], N. Kawachi[b)], S. Fujimaki[b)], N. Suzui[b)], H. Sutou[b)], S. Matsuhashi[b)]
And K. Fujita[a)]

[a)]Graduate school of Biosphere Sciences Hiroshima University
[b)]Radiation-Applied Biology Division, QuBS, JAEA

Abstract

Carbon is an indispensable nutrition source for crop. Until now, it has been impossible to measure carbon fixation and translocation simultaneously in real time repeatedly in intact plant. Using the technologies of PETIS, We are able to visualize the real time fixation and translocation of carbon in tomato plant. We used $^{11}CO_2$ to monitor localization of fixed ^{11}C in leaf.

光合成による葉の CO_2 固定能力については、ガス交換法が一般的に用いられ、同化炭素の葉から外部への以降は、^{13}C や ^{14}C などの同位体元素の存在割合から定量されることが一般的である。光合成による炭素の固定は、その後の移動のための力となるため、両者は密接に関連している。本実験では、^{11}C を用いた、各種環境条件の変化に対する葉の応答を調査するにあたり、その比較方法の是非について検討した。

葉が検出器の視野に入るようにトマトを設置し、20MBq の $^{11}CO_2$ を葉を囲むアクリル箱内に供給すると共に PETIS による測定を、150 μ mol/sec/m^2 の照明条件下で開始した。その 5 分後に照明を切った。Fig. 1 に、測定期間中のγ線積算画像を示した。図 1 から、植物を囲う箱全体、箱内の植物の存在していない空気流入出口側の 2 点に ROI とり、タイムアクティビティーカーブを Fig. 2 に示した。ROI1 で、$^{11}CO_2$ 供給により高濃度の ^{11}C を含む空気が流入したため急激な上昇を示した。ROI2、および 3 から、$^{11}CO_2$ がアクリル箱内から全て流出する時間は 15 分以降であった。植物の固定炭素が葉から外部へ移行する割合は、指数関数的であるため、測定開始後 15 分から 120 分までの値を Y=a+e(-b×t)に示した。Y はその時間における植物葉 ^{11}C 保持量、a は定数、b は 1 分あたりの減少割合、t は測定開始後の時間（分）として示した。その結果を以下に示した。

$Y = e^{(-0.0053 \times t)}$　　$R > 0.99$

植物体に対する葉への光照射は測定開始後 5 分で消灯したので、消灯時のγ線強度の値が葉での光合成による ^{11}C 固定量であるとした。また、同様の実験を同一植物体を用いて同一条件で後に 2 回行った。

1 回目、2 回目、3 回目のそれぞれの光合成による炭素固定量は相対γ線量として、145826、153082、164043 であった。また、作成されたそれぞれの式から求めた 1 時間当たりの葉からの転流率は、1 回目、2 回目、3 回目の $^{11}CO_2$ 供給実験で 27.7%、28.2%、28.2%であった。一連の実験を同一条件下で繰り返し行った結果、光合成速度、転流速度ともに、同様の結果を示した。この方法を用いて、以後、各種環境条件での葉の生理機能の応答について、解析を行うこととした。

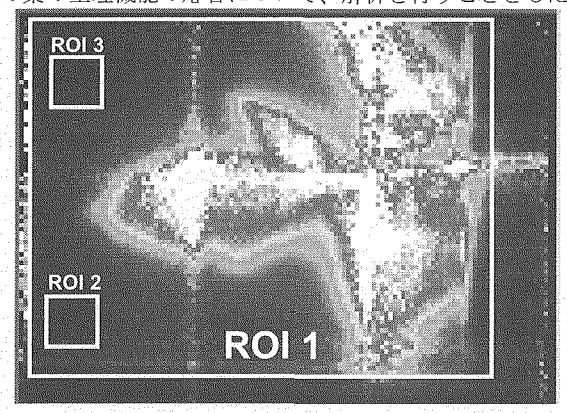


Fig.1 Integrated γ-ray activity during monitoring
ROI 1: Assimilated ^{11}C in the leaf
ROI 2: Relative $^{11}CO_2$ imput
ROI 3: Relative $^{11}CO_2$ output

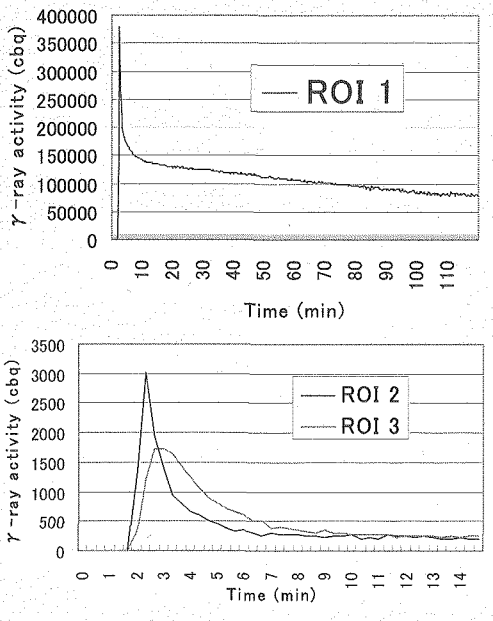


Fig.2 γ-ray activity at ROI 1,2 and 3

3-56 ^{52}Fe Tranlocation from the Roots to the Ear of Rice Using a Positron Emitting Tracer Imaging System (PETIS).

T. Tsukamoto[a), c)], H. Nakanishi[b)], S. Watanabe[c)], S. Matsuhashi[c)], N. K. Nishizawa[a, d)] and S. Mori[b)]

[a)]Department of Global Agricultural Sciences, The University of Tokyo, [b)]Department of Applied Biological Chemistry, The University of Tokyo, [c)]Radiation-Applied Biology Division, JAEA, [d)]Core Research for Evolutional Science and Technology (CREST), JST

1. Introduction

Iron (Fe) is an essential nutrient for plants. However, little is known how Fe is translocated in rice plants especially to the ear after absorption from roots. In addition, the real-time measurement of translocation of Fe to the ear has not been documented in plants. To study the pathway of Fe to the ear, we traced ^{52}Fe in rice plants (*Oryza sativa* L. cv. Nipponbare) of 3 weeks after flowering by positron emitting tracer imaging system (PETIS).

2. Experimental procedure

Rice (*Oriza sativa* L. cv. Nipponbare) were hydroponically cultured in a growth chamber under a mixture of incandescent and fluorescent lamps with a 14 h light (30 °C)/10 h dark (25 °C) regime and a photon flux density of 320 μmol m^{-2} s^{-1}. The nutrient solution was renewed once a week. The absorption experiments were performed about 3 months after germination and 3 weeks after flowering.

A rice plant was supplied with 20 mL of culture solution in polyethylene bags. The plants and the bags were fixed an acrylic board and placed between a pair of PETIS detectors in a chamber at 30°C under 65% humidity and a light density of 320 μmol m^{-2} s^{-1}. $^{52}Fe^{3+}$-deoxymugineic acid (DMA) (about 2 MBq) was added to culture solution. The ear and the flag leaf were monitored by PETIS for 14 h.

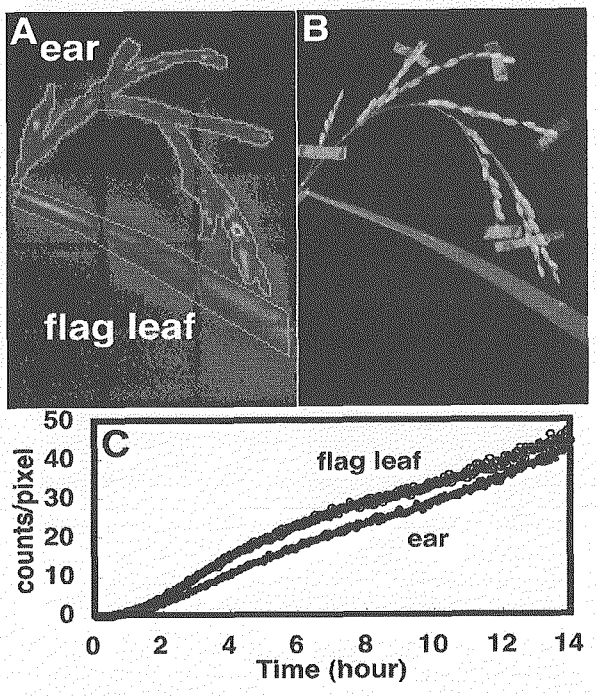


Fig. 1 ^{52}Fe translocation to the ear of rice. (A) Accumulative PETIS image. (B) Gross image of rice plant. (C) Time course of radioactivity of ^{52}Fe in the ear and flag leaf.

3. Results and discussion

In order to clarify the pathway of Fe from the roots to the ear of rice, $^{52}Fe^{3+}$-DMA was fed to roots of a rice plant, and translocation of ^{52}Fe was monitored using PETIS method. ^{52}Fe was translocated to both the ear and the flag leaf within 14 h (Fig. 1A). The time course of radioactivity in the ear and the flag leaf (indicated in Fig. 1A) was extracted from the PETIS data (Fig. 1C). ^{52}Fe radioactivity arrived simultaneously at both the ear and the flag leaf. This result suggests that ^{52}Fe was not translocated from the roots to the ear *via* the flag leaf within 14 h. The autoradiography image showed the shoots that were not visualized by PETIS (Fig. 2). In shoots, the nodes were strongly labeled. It was reported that the nodes contained the elliptical, diffuse and anastomosing vascular bundles, and the xylem transfer cells were found in the elliptical bundles[1)]. Therefore, ^{52}Fe might be transferred from xylem to phloem in the nodes. It was reported that *OsYSL2*, which is an Fe^{2+}-nicotianamine complex transporter gene in rice, is expressed in ear[2)]. It is assumed that *OsYSL2* plays an important role in Fe accumulation in ear.

References

1) S. Y. Zee et al., Aust. J. Bot. 20 (1972) 41.
2) S. Koike et al., Plant J. 39 (2004) 415.

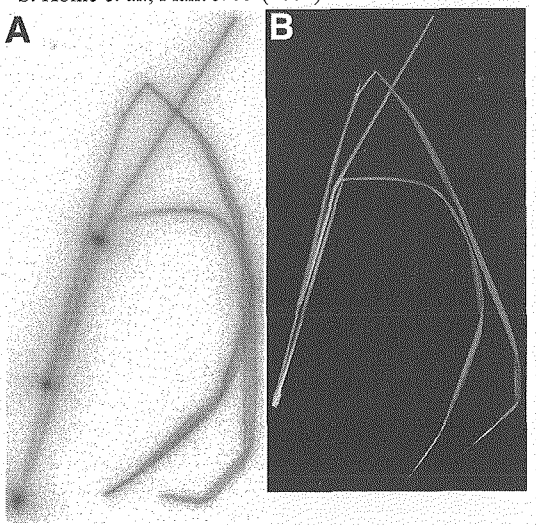


Fig. 2 ^{52}Fe translocation from the roots of rice plants. (A) Image of autoradiography. (B) Gross image of rice plant.

3-57 Evaluation of Effect of Root Parasite on Nitrogen Translocation and Distribution in the Host Plant by Positron Emitting Tracer Imaging System (PETIS)

H. Sekimoto[a], S. Honda, S. Katou[a], Y. Ochiai[a], K. Yoneyama[a], K. Yoneyama[b], Y. Takeuchi[b], N. Kawachi[c], S. Fujimaki[c], N. Suzui[c], S. Ishii[c], N. Ishioka[c] and S. Matsuhashi[c]

[a]Faculty of Agriculture, Utsunomiya University, [b]Weed Science Center, Utsunomiya University, [c]Radiation-Applied Biology Division, QuBS, JAEA

1. Introduction

Broomrapes (*Orobanche* spp), root holoparasites, can cause enormous damage before their scapes appear above ground, because their infestation occurs underground. As a consequence, efficient control is extremely difficult and infestation frequently results in a severe reduction of crop yields.

It was known that nitrogen fertilizer application reduced the crop damage caused by these root parasites[1,2]. Ammonium has the toxicity or inhibitory effect. On the contrary, it is known that nitrate markedly promoted production and excretion of germination stimulants for root parasitic plants in the host roots[3].

To share the absorbed nitrogen with host plant would be one of strategy for survival of root parasites. Then, translocation of ^{13}N-nitrate or ^{13}N-ammonium in the root systems of red clover (*Trifolium pratense* L.) infected by broomrapes (*Orobanche minor* Sm.) was examined by a positron emitting tracer imaging system (PETIS).

2. Materials and methods

To make root systems of red clover infected by broomrapes, broomrape seeds were sown on the root system of red clover in the rock-wool with NH_4NO_3 media. Also they are grown for 90 days, when broomrapes have infected enough and formed tubers, red clover plants with broomrapes were transplanted to the culture solution[4]. They were grown in a growth chamber (continuous light 350 μmol $m^{-2}s^{-1}$ at 25C) for 3 days.

Red clover roots were used with or without a tuber of broomrape, and fixed between two acrylic boards and placed midway between a pair of PETIS detectors. The end of the roots which hanged out of the boards was soaked with 10 mL of the culture solution. About 150 MBq of ^{13}N-nitrate or ^{13}N-ammonium were added to the culture solution to feed them, and ^{13}N translocation in root and shoot of host plant (red clover) and a broomrape tuber was monitored using PETIS for 90 min.

3. Results and discussions

It was observed that distribution ratio of ^{13}N originated from $^{13}NH_4^+$ in *Orobanche* was higher than that from $^{13}NO_3^-$, implying that $^{13}NH_4^+$ would stagnate more than $^{13}NO_3^-$ in *Orobanche* (Fig. 1). However, the distribution ratio of activity in *Orobanche* to all activity in the root system was almost same in both $^{13}NO_3^-$ and $^{13}NH_4^+$, suggested that $^{13}NH_4^+$ would not be attracted by *Orobanche* necessarily superior to $^{13}NO_3^-$. It would be caused by the trait of slow translocation of NH_4^+, because NH_4^+ is transformed to amino acid in the root.

On the other hand, the distribution ratio of $^{13}NH_4^+$ in the shoot to in the whole *Orobanche*- infected plant was lower than in the no-infected plant, indicating that *Orobanche* would take $^{13}NH_4^+$ that moved from root to shoot away easily compared with $^{13}NO_3^-$.

References

1) B.E. Abu-Irmaileh, Weed Sci. 42 (1994) 57-60
2) G.N. Dhanapal, P.C. Struik, M. Udayakumar and P.C.J.M. Timmermans, Agron. Crop. Sci. 176 (1996) 335-359.
3) K. Yoneyama, Y. Takeuchi amd T. Yokota, Physiol.Plant.112 (2001) 25-30.
4) T. Tadano and A. Tanaka, Jpn. J. Soil Sci. Plant Nutr. 51 (1980) 399-404

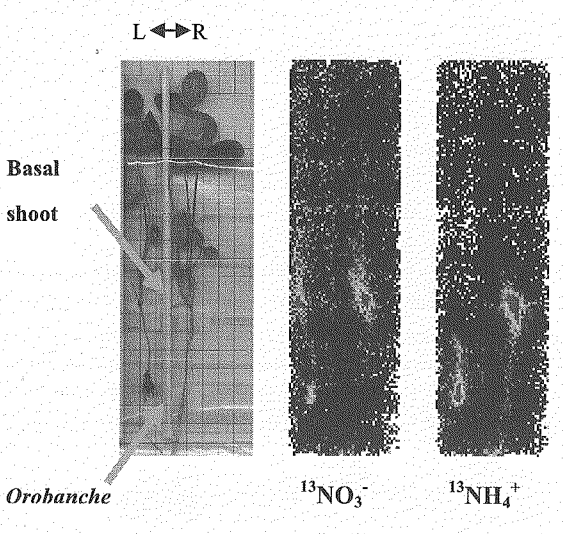


Fig.1 Distribution of $^{13}NO_3^-$ and $^{13}NH_4^+$
Orobanche-infected (Left), no-infected plants (Right)

3-58 Imaging of Parallel Routes of Photoassimilate Transport in an Intact Plant Body

S. Fujimaki, K. Sakamoto, N. Kawachi, S. Ishii, N. Suzui, N. S. Ishioka, S. Watanabe and S. Matsuhashi

Radiation-Applied Biology Division, QuBS, JAEA

Introduction

Two corresponding concepts, "source" and "sink", have been used to explain the balance of allocation of photoassimilates in plant physiology. The source indicates organs which supply carbohydrates to other parts of the body. In contrast, the sink indicates those which demand the carbohydrates. In agricultural fields, it is commonly performed to remove a part of fruits in order to enlarge the rest of them. This is a typical example of artificial modification of the source-sink balance, and demonstrates that the relationship between source and sink is one of the most important themes in the agricultural and biological studies. However, it is difficult to identify practically which leave, root, or fruit acts as a source or a sink, or how each source or sink organ is connected to other ones for transportation of nutrients in an intact plant body. It is partly because these situations vary, depending on the spatial relationships and the growth of the respective organs and of the routes between them.

Positron Emitting Tracer Imaging System (PETIS) is one of a few non-invasive methods which enable to monitor the transportation of substances in a plant body. In the present study, we focused on the source-sink connections in an intact plant body and visualized them using PETIS.

Materials and Methods

Three-week-old hemp plants (*Cannabis sativa* L.) were used in this experiment. $^{11}CO_2$ mixed with ambient air was fed to the largest expanded leaf of the test plant and the distribution of ^{11}C-photoassimilates was serially monitored by every 20 seconds as one frame for 360 frames (2 hours in total) using PETIS. The light and temperature conditions were kept during the experiment. After several hours, ^{11}C (the half-life is 20.4 min) activity had decayed to background levels, then the same experiment was performed except that the $^{11}CO_2$ gas was fed to the lower adjacent leaf of the same plant.

Results and Discussion

It was demonstrated that ^{11}C-photoassimilates were transported upward to the apical bud and downward to the roots in both cases when the $^{11}CO_2$ gas was fed to the largest expanded leaf (Fig. 1) and to the lower adjacent leaf (Fig. 2). The same results were obtained from more than three individuals. It should be noted that the two streams of photoassimilates shown here should be exist in parallel in the actual plant body, although these images are separately displayed. Observed in detail, the results indicated that there were streams with opposite directions in the region between the nodes to which the fed leaves were attached. In general, it is known that there can be such streams with opposite directions even in the same vascular bundle. It seems reasonable to consider our results representing streams within parallel routes, *i.e.* sieve tubes.

Time-activity curves, temporal changes of the tracer amount in specific regions of interest, at the nodes were generated from the PETIS data and analyzed. As a result, the flow speeds of both streams at this internode region were estimated as approximately 1 cm min^{-1}. Assumed that the resistance in the sieve tubes was the same in both cases, the result would indicate that pressure slopes with opposite directions and similar steepness existed within parallel sieve tubes in this internode region. This implies the degree of independence between the two streams was sufficiently high to maintain the respective pressure slopes, in other words, the connection of the two routes was sufficiently low. We have previously reported that the source-sink balance affects the flow speeds of photoassimilates within sieve tubes [1], and we consider that the present study should mark the beginning of quantitative studies of the source-sink connections.

Reference

1) S. Matsuhashi, S. Fujimaki, N. Kawachi, K. Sakamoto, N.S. Ishioka and T. Kume, *Soil Science and Plant Nutrition* **51**, 417-423, 2005

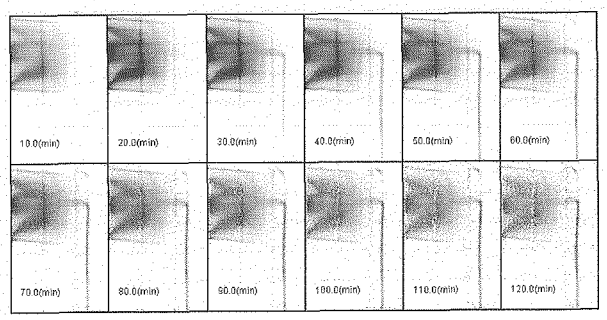


Fig. 1 Stream of ^{11}C-photoassimilates from the largest expanded leaf.

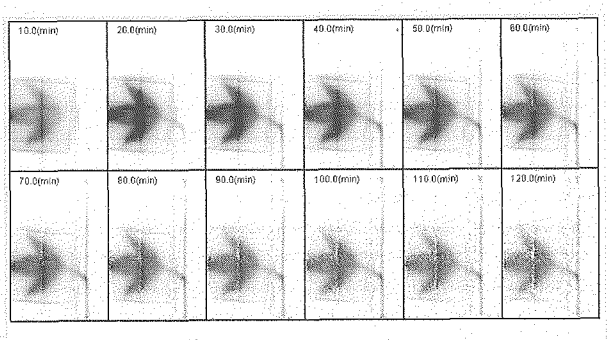


Fig. 2 Stream of ^{11}C-photoassimilates from the lower adjacent leaf of the largest expanded leaf.

3-59 Non-Invasive Imaging of Cadmium Transport in Crop Plants

S. Fujimaki [a)], S. Nakamura [b)], N. Suzui [a)], N. S. Ishioka [a)], M. Chino [b)] and S. Matsuhashi [a)]

[a)] Radiation-Applied Biology Division, QuBS, JAEA
[b)] Faculty of Bioresource Sciences, Akita Prefectural University

Introduction

Presently, cadmium (Cd) pollution of soil and foods is serious problem in the world. In particular, it is an urgent need to reduce the pollution of rice in Japan. Repression of Cd transport in rice plants and decontamination of soil can be major measures against the problem. Recently, phytoremediation is drawing attention as a method for decontamination of soil. This method is to make plants to uptake Cd from the contaminated soil and to accumulate it in their aerial portion, and harvest the plants. Therefore, comprehension of dynamics of Cd transport in plant bodies will be a pivotal step to realize the two measures above described, *i.e.* the repression of Cd transport in rice plants and the phytoremediation. However, the dynamics, including absorption at roots, transportation via vascular system and accumulation in various organs, remain unclear.

Positron Emitting Tracer Imaging System (PETIS) is one of a few non-invasive methods which enable to monitor the movements of substances in a plant body. In this study, we employed PETIS to visualize Cd transport in intact crop plants and analyzed the dynamics with the obtained image data.

Materials and Methods

We selected ^{107}Cd as the radionuclide for the tracer experiment, and developed the method of production, including bombardment with an ion-beam and chemical purification (described in detail by Ishioka et al. in this issue[1)]). Rice (*Oryza sativa* L. cv. Nipponbare) and sorghum (*Sorghum vulgare* L.) plants were grown hydroponically for four weeks and two weeks after sowing, respectively. We selected sorghum as a model plant for phytoremediation. The test plants were fed hydroponic cultures containing ^{107}Cd (and certain levels of non-radioactive Cd in some cases), and the serial images of ^{107}Cd distribution in the aerial portion were obtained with the PETIS apparatus by every 4 minutes for over 24 hours. Time courses of the absorption of water and the tracer by the plants were also monitored serially. All the settings were placed in growth chambers to maintain the appropriate temperature, light and humidity during the PETIS experiment. Time-activity curves, temporal changes of the tracer amount in specific regions of interest, were generated from the PETIS data. These data were combined with the time courses of water and tracer absorption, and analyzed.

Results and Discussion

We successfully obtained fine serial images of Cd transport in the test plants (Fig. 1, only the data with rice is shown). It was demonstrated that Cd arrived to the shoot of the rice plants within approximately 1 hour, then it was accumulated strongly in the basal region of the shoot, which consists of a short stem and meristems, and little was transported toward the upper leaves. The analysis of the time-activity curves revealed the linear correlation between the Cd concentrations in the culture and the rates of Cd uptake, and provided quantitative estimation of the proportion of the Cd amount accumulated in the basal region to those absorbed from the culture.

Reference

1) N.S. Ishioka et al., TIARA annual report 2005 (2006, this issue).

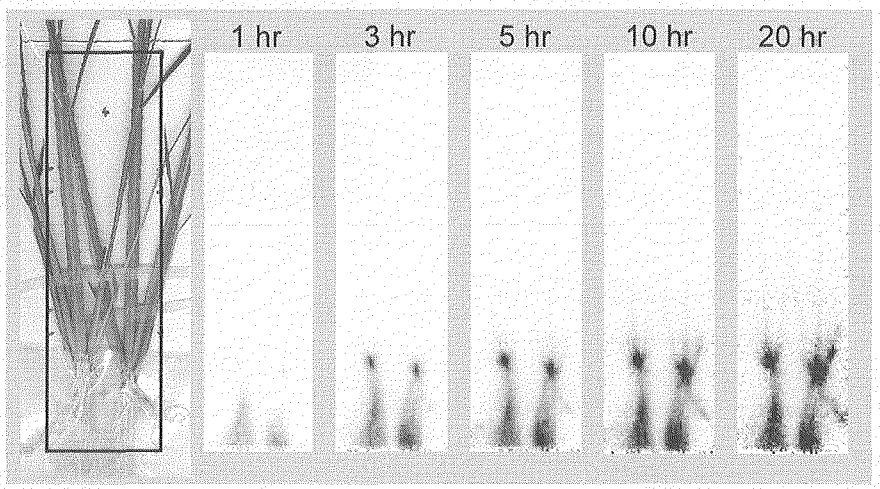


Fig. 1 Serial images of Cd transport in rice plants. Each image is integration of 15 original frames, corresponding to 1 hour.

3-60 Positron Related Analysis of ^{13}N-Nitrate in Transgenic Rice Plant Over-Expressing Nitrate Transporter

D. Sato[a)], M. Mori[a)], H. Katayama[a)], H. Kitamura[a)], T. Kawai[a)], S. Fujimaki[b)], N. Suzui[b)], N. Kawachi[b)], S. Ishii[b)], S. Matsuhashi[b)], T. Tanaka[c)], T. Tsukamoto[d)], N. K. Nishizawa[d)] and M. Mori[e)]

[a)]Shiga Prefecture Agricultural Technology Promotion Center, [b)]Radiation-Applied Biology Division, QuBS, JAEA, [c)]Nagasaki Agricultural and Forest Experiment Station, [d)]Faculty of Agricultural and Life Sciences, The University of Tokyo [e)]Research Institute for Bioresources and Biotechnology, Ishikawa Prefectural University

1. Introduction

Nitrogen is the most important element for growth in higher plants. However, the excessive fertilizers applied to the farming fields cause the water pollution. Therefore, we aimed the breeding of the rice plant suitable for low input of nitrogen fertilizer. To examine the physiological importance of a putative rice high-affinity nitrate ion transporter (*OsNRT2*) which involves nitrate uptake at external low nitrate concentrations, we constructed transgenic plant (NRT2 plant) that OsNRT2 mRNA over-expressing.

Our previous study with PETIS (Positron Emitting Tracer Imaging System) using $^{13}NO_3^-$ as a tracer was suggested that the NRT2 plants have improved the ability to absorb nitrate[1)].

In this study, germanium semiconductor detector that is suitable for multiple samples for statistical analysis was used for evaluation of the ability of NRT2 plant nitrate uptake.

2. Materials and Methods

The *OsNRT2* in binary vector, pMLH7133-RNRT2, was transformed into rice (*Oryza sativa* L. cv. Yumeoumi). Seeds of wild-type rice (WT plant) and NRT2 plant were germinated on a paper towel. The seedlings of rice were grown hydroponically (1/2 Kimura B medium) in an incubator (light/dark, 16 h/8 h, 30°C/25°C, 250 μmol photon m^{-2} s^{-1}) for 3 weeks. The third aged seedlings of rice were nitrogen-starved for 24 hours, and then the culture medium was replaced by the tracer media containing $^{13}NO_3^-$ (1.5–3.0 MBq mL^{-1}), which is produced by using the TIARA AVF cyclotron. After $^{13}NO_3^-$ absorption for 10 min, the only aerial part was put into a polyethylene bag, and the radioactivity of the sample was measured with the germanium semiconductor detector.

Before the nitrogen uptake experiment, it was confirmed that there was no significant difference of the dry weight of the root between NRT2 plants and WT plants.

3. Results and Discussion

The radioactivity of $^{13}NO_3^-$ accumulated in the aerial part of the plants for 10 min were NRT2 = 13355 ± 1668 and WT = 8145 ± 867 (Count/DW of root/10 min, mean ± SE, n=8), respectively.

The results indicate that NRT2 plants absorbed 1.6 times as much ^{13}N-NO_3 per time and per dry weight of root as WT plants. Our previous results with PETIS showed that NRT2 plants absorbed larger volume of ^{13}N-NO_3 than WT plants but the distribution pattern in the aerial parts was similar. Considering both the results together, it is concluded that the *OsNRT2* gene product acts as a nitrate ion transporter in rice plants for nitrate uptake from the soil, but not for nitrate distribution within the aerial part.

References

1) D. Sato et al., TIARA annual report 2004 (2005) 159

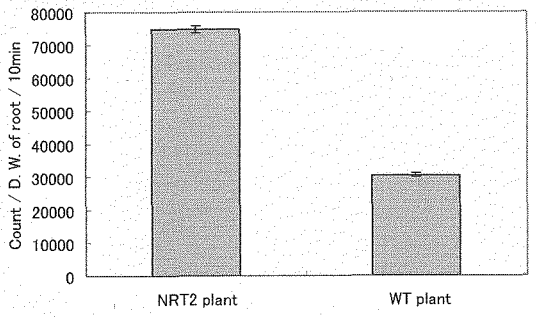


Fig. 1 $^{13}NO_3^-$ uptake into NRT2 and WT rice plants determined by germanium semiconductor detector.

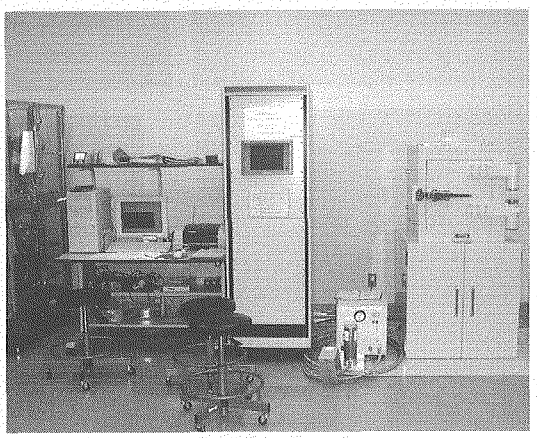


Fig. 2 Germanium semiconductor detector analysis

3-61 Effect of Cadmium on Translocation of Photoassimilates in Rice (*Oryza sativa* L.)

N. Suzui, S. Fujimaki, N. Kawachi, S. Ishii and S. Matsuhashi

Radiation-Applied Biology Division, QuBS, JAEA

Introduction

Cadmium (Cd) is a major environmental pollutant, which accumulates in agricultural soils, and is a toxic element to all organisms. In plants, the most sensitive symptom of Cd toxicity is stomata closure, followed by the inhibition of photosynthesis. On the other hand, it has been reported that Cd treatment increases carbohydrate content of source organ[1]. This contradictory result could be due to the inhibition of translocation of photoassimilates by Cd. However, direct evidence has not been reported.

Thus, in this study, we have attempted to evaluate the effect of Cd on translocation of photoassimilates by using $^{11}CO_2$ and noninvasive measurement device, the Positron Emitting Tracer Imaging System (PETIS).

Materials and Method

Rice plants (*Oryza sativa* L. cv Nipponbare) were germinated and grown hydroponically in nutrient solution without Cd for 4 weeks. Plants were transferred to the nutrient solution containing 0 (control), 10 and 100 μM of Cd, and cultured for 1 day before PETIS experiment.

In a set of PETIS experiments, five to six of Cd-treated plants were placed between a set of PETIS detectors in a growth chamber. The upper half of the largest expanded leaf of each plants was inserted into a "gas-cell", a clear acrylic box for feeding $^{11}CO_2$ gas. 100 MBq of $^{11}CO_2$ was supplied to the gas-cell and the translocation of ^{11}C-photoassimilates was monitored using PETIS for 1 hour (Fig. 1).

For the evaluation of flow rate of photoassimilates in each plant, an "arrival time" of ^{11}C-photoassimilates to the basal part of shoot (basal region) was defined as the following procedures: (1) Time-activity curve, i.e. time course of ^{11}C-radioactivity in the basal region was generated from the serial images of each plant (Fig. 2a). (2) Initial slope of the rising ^{11}C-photoassimilates concentration was estimated by a linear least-square method using the time-activity curve (Fig. 2; dotted line). (3) The value of the x-axis intercept of approximated line was defined as ^{11}C-arrival time (Fig. 2b; arrow).

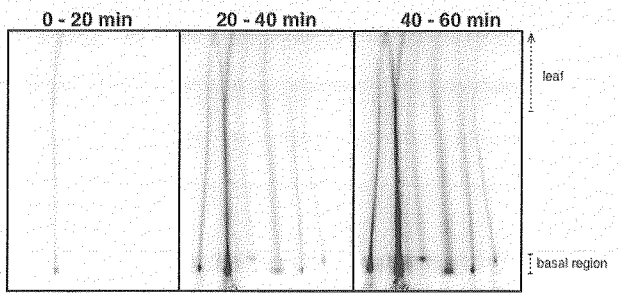


Fig. 1. Serial images of translocation of ^{11}C-photoassimilatess. Each image was integration of 120 serial images obtained every 10 seconds by PETIS. In this example, Cd concentrations in the nutrient solutions were: 10, 0, 100, 10, 100, 0 μM (from left to right).

Results and Discussion

The serial images of translocation of ^{11}C-photoassimilates from leaf to shoot were obtained (Fig. 1). We conducted four sets of PETIS experiment using 24 different plants treated with 0, 10, 100 μM of Cd, and evaluated the flow rate of ^{11}C-photoassimilates of each plant with the value of ^{11}C-arrival time.

The correlation between the Cd concentration in nutrient solution and the ^{11}C-arrival time was summarized in Table 1. As shown in this table, the arrival times of ^{11}C-photoassimilates from leaf to basal region in the Cd-treated plants were longer than those of control plants. This result indicates that Cd exposure for 1 day causes the inhibition of translocation of photoassimilates in rice plant.

References

1) JL. Moya et al. Photosyn. Res. 36 (1993) 75-80

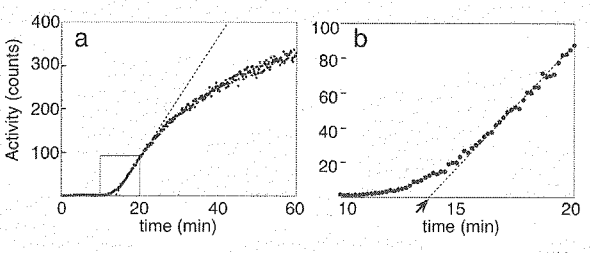


Fig. 2. Typical time-activity curve for accumulation of ^{11}C-photoassimilates in the basal region. (a) is shown at high magnification in (b). Dotted line is the approximated line of the initial slope. Arrow shows the defined "^{11}C-arrival time".

Table 1. ^{11}C-arrival times to the basal region of rice plants treated with 0 (control), 10, 100 μM Cd.

Cd concentration in nutrient solution (μM)	0	10	100
^{11}C-arrival times (min)	15.4 ± 1.0	20.3 ± 1.5[a]	24.8 ± 1.6[b]

Mean ± standard error of six (0 μM) or eight (10, 100 μM) replicates. Arrival times significantly different from control were indicated by a ($p < 0.05$) and b ($p < 0.01$).

3-62 Impacts of Aluminum Ion for the Translocation of Signaling Molecule in Higher Plants

T. Furuichi [a], S. Fujimaki [b], Y. Kawachi [b], N. Suzui [b], S. Ishii [b], N. Ishioka [b], S. Matsuhashi [b], Y. Yamamoto [c] and M. Sokabe [a]

[a] Graduate School of Medicine, Nagoya University, [b] Radiation-Applied Biology Division,, QuBS, JAEA, [c] Research Institute for Bioresources, Okayama University

In plants, photosynthesized sugars are utilized not only as carbon sources but also as signal molecules for growth and development. In addition to the widely studied functions in metabolic processes, the signaling function of sugars has recently been focused on. In leaves of *A. thaliana* expressing aequorin, the level of cytosolic calcium ion (Ca^{2+}) concentration ($[Ca^{2+}]_{cyt}$) was raised in response to sugar but not unmetabolizable analogues of it [1]. This response is observed in autotrophically grown plants, but not in heterotrophically grown plants, and the mRNA level of sucrose-H^+ symporters in the former is clearly higher than that in the latter. Using a simultaneous real time imaging system for movements of sugar molecules and aequorin luminescence in *A. thaliana* mature plants, which consists of a PETIS (positron emitting tracer imaging system) for measuring radioactivity of ^{18}F-deoxyglucose (^{18}FDG) and a VIM-camera system (a CCD camera equipped with an intensifier) for detecting aequorin luminescence, the movement of sugar molecules and the aequorin luminescence in leaves were simultaneously analyzed [2]. The time course of ^{18}FDG translocation into the leaf was roughly comparable to aequorin luminescence reflecting an increase in $[Ca^{2+}]_{cyt}$, indicate that sugar molecule may directly play as a sort of signaling molecule.

Aluminum (Al) is the most abundant metal element in the crust of earth, and free Al ions (Al^{3+}) are the main factor in the inhibition of root elongation in acidic soils. In the Al^{3+}-induced inhibition of root elongation, Al^{3+} primary accumulates in root meristem and causes the inhibition of cell elongation. Although, the molecular mechanisms for these symptoms have not been fully elucidated. As a nature of trivalent cations, Al^{3+} reversibly block the voltage-gated and mechanosensitive Ca^{2+}-permeable channels.In the long distance, sugar-mediated signal transduction in plants, the TPC1 Ca^{2+}-permeable channels participate in the sugar-induced $[Ca^{2+}]_{cyt}$ increase [3], implying that plant TPC1 channels plays important role(s) in sugar-mediated signal transduction. Moreover, interestingly, Al^{3+} specifically or more effectively inhibits the plant TPC1 channels [4]. According to those evidences, Al^{3+} may inhibit sugar-mediated signal transduction for the sink-source transition and growth regulation. To obscure the impacts of Al^{3+} for the sugar-signaling in roots, translocation of sugars from leaves to roots were investigated. To monitor this, ^{11}C-labeled CO_2 ($^{11}CO_2$) was synthesized at TIARA. To start the positron imaging using PETIS detectors, 100 MBq of $^{11}CO_2$ were applied to the airtight acryl chamber which including whole seedlings. To mimic the impact of Al^{3+} in acidic soils, tobacco seedlings grown by hydroponics with an acidic mineral solution (Ruakura medium without sucrose, pH 4.3) were pretreated with or without Al^{3+} for 21 Hrs. As an impact of Al^{3+}, translocation of ^{11}C (immobilized by photosynthesis and mainly converted to sucrose) was inhibited in Al^{3+}-treated plant, hence it was clearly translocated in untreated plant (Fig. 1). These results may indicate that Al^{3+}-dependent inhibition of sucrose transition into the root promote the inhibition of root elongation. Further analysis for the molecular mechanism of Al^{3+}-impact for sugar translocation and the relationship with the other nutritional and mineral uptake (such as nitrate, potassium and sodium), photosynthetic activity may necessary to elucidate the molecular mechanism of Al^{3+}-toxicity.

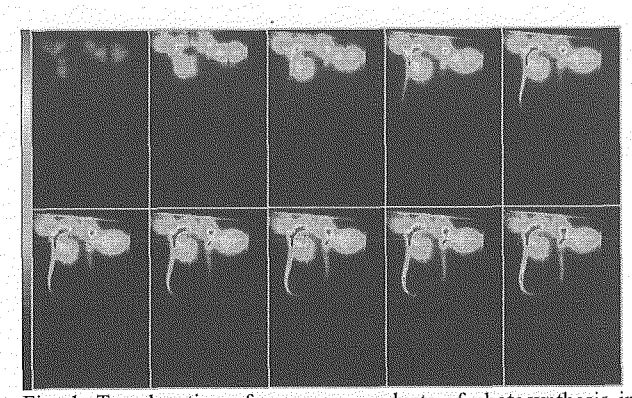


Fig. 1. Translocation of sugars as products of photosynthesis in tobacco seedlings. Seedlings were incubated with (right in each frame) or without (left in each frame) 200 μM $AlCl_3$ for 21 Hrs. The γ-rays emitted from decaying positrons from ^{11}C were counted over time using the coincident method with the paired detectors for 120 min. Counts are luminescence was integrated for every 12 min (left to right and up to down panels).

References

1) T. Furuichi et al., Plant Cell Phyisiol.,42 (2001) 1149.
2) T. Furuichi., TIARA annual report 2003 (2004) 128.
3) T. Furuichi et al., Plant Cell Phyisiol.,42 (2001) 900.
4) T. Kawano et al., Biochem Biophys Res Commun. 324 (2004) 40.

3-63 Kinetic Analysis for Studying Photosynthesis in a Leaf Using $^{11}CO_2$ and Positron Emitting Tracer Imaging System

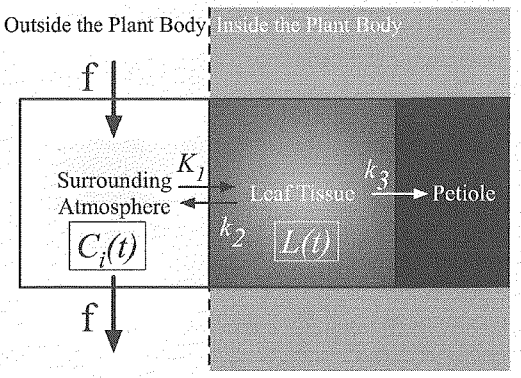
N. Kawachi, K. Sakamoto, S. Ishii, S. Fujimaki, N. Suzui, N. S. Ishioka and S. Matsuhashi

Radiation-Applied Biology Division, QuBS, JAEA

In vivo imaging technologies with appropriate mathematical model analysis allow the quantitative measurement of the physiological functions. However, in the field of plant physiology, few methods for model analysis using positron imaging have been established, and a majority of the experimental methods are used for qualitative analysis omparison between control and test plants.

The positron emitting tracer imaging system (PETIS) and $^{11}CO_2$ have been used for imaging the photosynthesis process in plant leaves. Further, ^{11}C kinetics facilitate the estimation of the physiological function parameters of photosynthesis. In order to analyze the photosynthetic performance with regard to the carbon photoassimilation rate, K_1 (/min), and sucrose export rate, k_3 (/min), we analyze photosynthesis by the compartmental model[1], which has been one of the most successful analysis methods for tracer kinetic modeling in the field of nuclear medicine. A schematic compartmental model for the proposed method is shown in Fig. 1. Based on the use of synthesized $^{11}CO_2$ in TIARA and the PETIS, we investigate a new analysis method for quantifying the rate constants of photoassimilation and sucrose export of a test leaf.

Noninvasive PETIS measurements were performed using a hemp leaf under dark (as $^{11}CO_2$ gas input) and two light (as leaf response) conditions sequentially. In data analysis, a region of interest (ROI) for the leaf was drawn around the leaf on the integrated $^{11}CO_2$ image (Fig. 2 (a)). The ROI was superimposed on the dynamic images acquired as input images to generate the input time-activity curve $C_i(t)$. The ROI was also superimposed on the other dynamic images of the leaf scan, and the time-activity curves of the leaf



$$\frac{dL(t)}{dt} = (K_1 - k_2) \cdot C_i - (k_2 + k_3 + \lambda) \cdot L(t) \quad \text{, (Eq. 1)}$$

Fig.1 A schematic illustration of the compartment model for the analysis of photosynthesis and a differential equation of instantaneous equilibrium of carbon dynamics. The photosynthetic system is simplified into three compartments, and the arrows indicate the carbon compound flows.

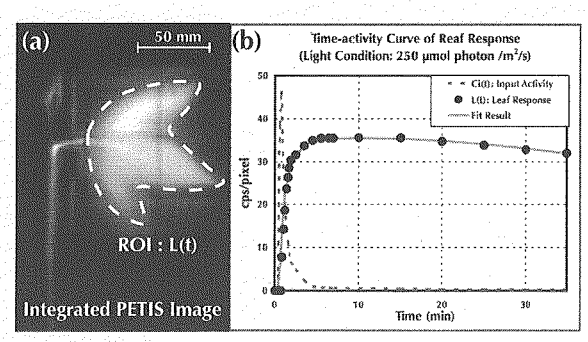


Fig.2 (a) ROI selection on the test leaf. The leaf ROI was placed on the integrated PETIS image to generate the time-activity curves. (b) Measured and predicted time-activity curves. The time-activity curve of the input (dashed line) and leaf response (black dot) were measured by the PETIS. The solid line indicates the theoretical prediction obtained by the present kinetic analysis.

response were generated for $L(t)$. K_1 and k_3 for the leaf were estimated by using the two time-activity curves and fitting to the eq. 1 by the nonlinear least-squares method (Fig. 2 (b)).

As shown in this figure, the data and estimated curves for the leaf response are in good agreement; in other words, there are almost no errors between the time-activity curves of the PETIS dynamic data and the estimated ones. This indicates that the present kinetic model appropriately expresses the carbon kinetics during photosynthesis with parameters K_1 and k_3, despite the use of a simplified model.

The results obtained from the sequential PETIS measurements are summarized in Table 1. In general, there is a tendency for CO_2 assimilation to increase for light conditions; our results for the parameter K_1 indicate a similar tendency of the photoassimilation. Parameter k_3 is a factor that contributes toward decreasing the ^{11}C in the ROI, that is, the transfer of sucrose. The *source ability*, which is one of the most important parameters in physiological and agricultural researches, is expressed by the factor $K_1 \times k_3$. This data also increase with the photon irradiance.

Table 1

Condition (μmol photon /m²/s)	70	250
K_1 Photoassimilation Rate	0.306	0.829
k_3 Sucrose Export Rate	0.00983	0.0132
$K_1 \times k_3$ *"Source Ability"*	3.0×10^{-3}	1.1×10^{-2}

References

1) N. Kawachi et al., IEEE NSS/MIC CR 2005(2006) 2908.

3-64 Production of Radioisotopes for Nuclear Medical Application

T. Katabuchi[a)], S. Watanabe [b)], N. S. Ishioka [b)], S. Matsuhashi [b)], Y. Iida [c)], H. Hanaoka [c)] and K. Endo [d)]

[a)]21st Century COE Program and Subdivision of Quantum Biology, Gunma University Graduate School of Medicine, [b)] Radiation-Applied Biology Division, QuBS, JAEA, [c)]Department of Bioimaging Information Analysis, Gunma University Graduate School of Medicine, [d)]Department of Diagnostic Radiology and Nuclear Medicine, Gunma University Graduate School of Medicine

We have been trying to produce the radionuclides, ^{64}Cu and ^{67}Cu, at the JAEA-Takasaki. ^{64}Cu is an positron emitter having a half life of 12.7 h. Research has demonstrated that ^{64}Cu is a suitable nuclide for the positron emission tomography[1)]. On the other hand, ^{67}Cu is a β^--decay nuclide which has a suitable β-particle energy to treat small tumors[2)]. The physical half-life is 2.58 days long enough for ^{67}Cu-labeled agents to accumulate at tumor sites. Those copper nuclides can be delivered to tumors by two types of agents. A first group of agents is monoclonal antibodies targeting tumor-related antigens. A second group is diacetyl-bis(N4-methylthiosemicarbazone) (ATSM), which delivers copper to tumors based on different mechanism from Cu-labeled antibodies[1)]. The final goal of this project is to assess the effectiveness of imaging and therapy using ^{64}Cu- and ^{67}Cu-labeled agents. We started production and separation of those target in 2005 at JAEA-Takasaki.

We produced those copper nuclides using an AVF cyclotron at JAEA-Takasaki. ^{64}Cu was created through the nuclear reaction ^{64}Ni(p,n)^{64}Cu using 20 MeV proton beam[3)]. Enriched ^{64}Ni (enrichment: 99.6%) in the chemical form of ^{64}NiO was used as a target. The target was typically irradiated at a beam intensity of 5 μA for 2 hours. The produced ^{64}Cu was chemically separated from the target material by ion-exchange chromatography method. An anion exchange column filled with AG1-X8 (0.6 cm ID, 20 cm long) was conditioned with 6M HCl. After application of 6M HCl solution of irradiated nickel target into the column, washing was performed with 35mL 6M HCl. Then ^{64}Cu was eluted with 8mL 2M HCl. The yield of ^{64}Cu was approximately 900 MBq at the end of bombardment (EOB). 450 MBq of ^{64}Cu was obtained after chemical separation. The production yield was enough for preclinical studies using mice.

^{67}Cu was created through the nuclear reaction ^{68}Zn(p,2p)^{67}Cu using 70 MeV proton beam[4)]. The target is enriched ^{68}ZnO powder (enrichment: 98.7%). The ^{68}Zn target encapsulated in the quartz tube was mounted in an aluminum target holder which cooled the target front and back with circulating helium gas and water, respectively. The target was typically irradiated at a beam intensity of 3μA for 4 hours. Chemical separation of ^{67}Cu was done by ion-exchange chromatography. Three columns of AG50W-X8, Chelex 100 and AG1-X8 were prepared. A column (1.2 cm ϕ × 14 cm long) of the cation exchange resin AG50W-X8 was conditioned with 36 mL of 8M HCl. A column (1.2 cm ϕ × 8 cm) of Chelex-100 was prewashed with 40mL 6M HCl and then conditioned with 50mL 0.001M HCl. A column (0.6 cm ϕ × 20cm long) of the anion exchange resin AG1-X8 was prewashed with 15mL 2M HCl and conditioned with 15mL 6M HCl. After irradiation, the quartz tube containing ^{68}ZnO powder was opened and then the ^{68}ZnO inside the tube was dissolved in 25 mL concentrated HCl. The solution was applied to the AG50W-X8 column to remove ^{66}Ga and ^{67}Ga and washing was performed with 2mL 6M HCl. The eluate was evaporated to complete dryness, transformed into the solid form of $ZnCl_2$. Then 3mL water was added to dissolve the $ZnCl_2$. A solution of $ZnCl_2$ is weak acid (pH ~ 4) because of hydrolysis reaction forming the $[Zn(OH)Cl_2]^{2-}$ ion. This pH allows us to apply the solution to the Chelex-100 column. After applying the solution, 50 mL 0.001M HCl was run over the Chelex-100 column and the first 35 mL eluate was collected for recycling the ^{68}Zn. The bulk of Zn flows through the column whereas Cu stays in the column. ^{67}Cu was eluted with 16 mL 6M HCl. The first 4mL of the eluate was discarded and the rest was collected as a Cu fraction. The Cu fraction was evaporated to dryness and the residue was dissolved with 0.5 mL 6M HCl. The solution was loaded onto the AG1-X8 column and washing was performed with 19mL 6M HCl. Then elution of ^{67}Cu was carried out with 4mL 2M HCl. The yield of ^{67}Cu was 97 MBq at EOB and 33MBq of ^{67}Cu was obtained after chemical separation. Further improvement of ^{67}Cu production yield is required for preclinical studies. At the present, we need to cool down the irradiated target to reduce the radioactivity from mainly gallium isotopes for two days. We are developing a remote system to perform the first ion-exchange removing gallium remotely, allowing experimenters to start chemical separation right after irradiation.

References

1) A. Obata et al., Nucl. Med. Biol. 32 (2005) 21.
2) Ilse Novak-Hofer and P. A. Schubiger, Eur. J. Nucl. Med. 29 (2002) 821.
3) F. Szelecsenyi et al., Appl. Radiat. Isot. 44 (1993) 575.
4) T. Stoll et al., Radiochim. Acta 90 (2002) 309.

3-65 The Sensitivity Evaluation of Anticancer Drug Using In-Air Micro PIXE, The 21st Century COE Program 'Biomedical Research using Accelerator Technology'

H. Kuwano[a)], H. Kimura[a)], K. Okada[a)], S. Ma[a)], A. Faried[a)], M. Sohda[a)], M. Nakajima[a)]
T. Sakai[b)], M. Oikawa[b)], T. Satoh[b)] and T. Kamiya[b)]

[a)]Department of General Surgical Science, Gunma University, Graduate School of Medicine,
[b)]Department of Advanced Radiation Technology, TARRI, JAEA

Abstract

Esophageal squamous cell carcinoma (ESCC) has high sensitivity for chemoradiotherapy compared with other cancer of the digestive system, and it is important to separate responder from non-responder for chemoradiotherapy. We tried applying in-air micro-PIXE (PIXE) as one of methods to evaluate the sensitivity of anticancer drug. We found the intracellular platinum element (Pt) could be detected in ESCC cell lines treated by Cisplatin (CDDP) with PIXE. Detection of Pt using PIXE required about 1.0×10^3 times higher dose of CDDP than IC50 in the treatment. We had to incubate cancer cells in the medium including CDDP for a short period, 60 min, for examples, because the viability of cancer cells was lost for high cytotoxicity. Although there were some problems in the research up to date, we hope that the sensitivity assay of anticancer drug using PIXE will be established and our study will develop as translational research.

近年、様々な癌において分子生物学的なアプローチにより数多くの研究が行われているが未だに不明な点が多い。特に癌における元素動態やその分布においては殆ど知られていない。そこで我々は大気マイクロPIXE(以下PIXE)を用いて、癌悪性度の評価や抗癌剤に対する感受性の評価を試みることとした。

食道癌は独特な生物学的特徴を有する癌である[1)]。化学放射線療法が効果的な癌の一つであり、そのresponderとnon-responderを選別することは、個別化治療において重要な課題になっている。我々は分子生物学的アプローチによる食道癌患者における化学放射線療法の感受性評価法を検討し報告している[2)]。我々は既存の感受性評価法にPIXEの技術を融合させることにより、さらに精度の高い感受性評価法を開発できないかと考えた。

我々はこれまでの検討で、シスプラチン処理した食道癌細胞株を試料として、PIXEを用いた測定により、細胞内プラチナ元素(以下Pt)の検出が可能であることを見出した。

続いて、感受性の相違によるシスプラチン投与後の細胞内元素動態を比較するため、基礎実験としてシスプラチン感受性試験食道癌細胞株を用いてシスプラチン感受性試験(MTT assay)を行い、高感受性株(TE-2)と低感受性株(TE-13)を見出した。この差異につき細胞周期およびアポトーシスの面からも、FACSやDNA fragmentation assayを行い確認している。また、抗癌剤耐性に関わるとされる遺伝子(MDR1、MRP1、MRP2)について、RT-PCRを行い両細胞株におけるmRNAの発現を検討した結果、3遺伝子ともTE-2に比しTE-13における発現が有意に増加していた。

様々なシスプラチン投与濃度と時間を組み合わせ、試料作成を行い、PIXEを用いたシスプラチン感受性評価における試料の最適化を目指した。シスプラチンを細胞内のPt分布として評価するには、感受性評価に用いられるIC50より、かなり高濃度での投与が必要であった。ただし、この濃度での長時間投与ではほとんど全ての細胞がviabilityを失うため、高濃度短時間投与、具体的には、マイラー膜上に細胞を生着させ、2.0mMのシスプラチン含有メディウムで1時間incubationし、洗浄後凍結乾燥したサンプルにて、比較的短時間の照射でPt分布の安定したdetectが可能であった。

高濃度シスプラチンの短時間投与が最適であることを見出したが、問題はこの高濃度シスプラチン投与がどの程度の生物学的な意義を有するかであり、今後の更なる検証が必要となる。続いての問題はPIXEで核の局在を把握できるかである。シスプラチンは核内に取り込まれ、DNAに結合し架橋を作ることにより、その合成を阻害し細胞分裂を抑制する。つまり、感受性に直接関与するのは核内のPt分布であると考えられる。したがって、PIXEを用いてプラチナ分布を解析する際、同時に核の局在を把握して、より高精度の感受性評価につなげるため、BrdUを用いた核標識の応用を検討していく予定である。イオン分布の客観的評価法としての定量化が必要不可欠であるが、標準試料の適用等で解決を試みたい。最終目標はPIXEを用いた抗癌剤感受性評価法を確立し臨床に還元することである。

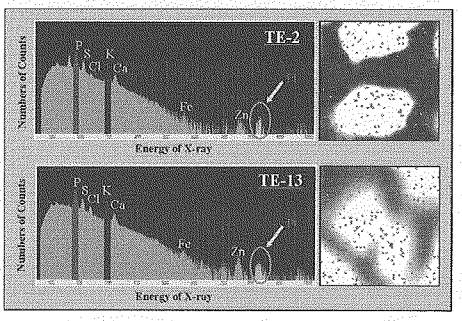


Fig.1 X-ray spectrum of each ion and distribution of intraceller platinum ion in ESCC cell lines. In left side, the accumulation is identified in the energy area of platinum ion in both cell lines. In right side, platinum dot is overlaid to smoothed phosphate area.

References

1) Distinctive clinicopathological characteristics in esophageal squamous cell carcinoma. Kuwano H., et al., Ann Thorac Cardiovasc Surg. 2003 Feb;9(1):6-13.
2) Pretreatment evaluation of combined HIF-1alpha, p53 and p21 expression is a useful and sensitive indicator of response to radiation and chemotherapy in esophageal cancer. Sohda M., et al., Int J Cancer, 2004. 110(6):838-44.

3-66 The Targeting of the Chemotherapeutic Agents or Radiosensitizer by Radiation, Using the Liquid Core Microcapsules

S. Harada [a], S. Ehara [a], K. Ishii [b], H. Yamazaki [b], S.Matsuyama [b], T. Kamiya [c], T. Satoh[c] and M. Oikawa [c]

[a]Department of Radiology, School of Medicine, Iwate Medical University, [b]Department of Quantum Science and Energy Engineering Tohoku University, [c] Department of Advanced Radiation Technology, TARRI, JAEA

Our previous study reports that liquid core microcapsules made from alginate[1] and hyaluronic acid[2] is capable of emitting its core by radiation, which lead to localize the drugs containted in its core by radiation. However, the composition between alginate[1] and hyaluronic acid[2] that bring about the maximum emission rate, remains unclear. In this study, the composition of liquid core microcapsule between alginate and hyaluronic acid for the maximum emission of its core was researched using micro PIXE camera.

The 0.2% solution of alginate was mixed into the 0.002, 0.02, 0.1, or 0.2 % solution of hyaluronic acid supplemented with 0.05 mg of carboplatin (Pt containing anticancer drug). Those materials were well kneaded in the agar pestle. The mixture was atomized into 0.34mMOL of calcium chloride solution, and then polymerized for 5 min. The number of microcapsules was counted, using the hemocytometer. Finally, the number of microcapsules was adjusted to $1.0X10^7$/0.1ml. The 3ml of microcapsule's suspension were poured into the dish (3cm in diameter) equipped with mylar film (0.1μm in thickness). The dish was irradiated using ^{60}Co γ ray at single dose of 2 Gy. Immediately after irradiation, the suspension of microcapsules was frozen by liquid nitrogen through isopentane, and dried in vacuum at $1.0X10^{-3}$ Torr. The mylar film containing microcapsules was used for the target of micro PIXE camera.

The morphology the microcapsules were imaged by micro PIXE camera, and shown in the Fig. 1. The shape of microcapsule was imaged basing on the Ca distribution and the liquid core was done on that of Platinum. The emission of liquid core was determined basing on the two criteria: 1) jet like eruption of carboplatin; and 2) scattered distribution of carboplatin. There were only emission of liquid core of microcapsule when the 0.2% solution of alginate was mixed into the 0.1% solution of hyaluronic acid. In the other composition of alginate and hyaluronic acid, no remarkable emission of liquid core of microcapsules was observed.

It is considered that there is a suitable composition of alginate and hyaluronic acid, whose rate was 2 alginate to 1 hyaluronic acid in weight. As the considerable reason for this phenomena, there might be a balance between the pore formation by decomposition of hyaluronic acid[2] and the pushing power by shrinkage of alginate[1], brought by irradiation.

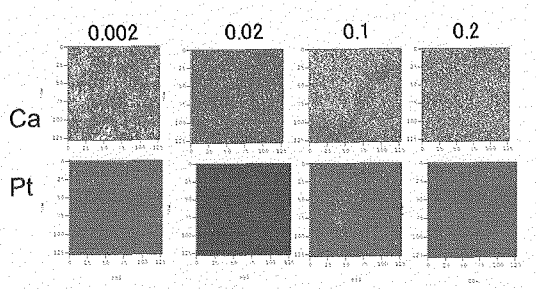


Fig.1 The distribution of Ca and Pt. The shape of microcapsules were imaged by Ca, and its liquid core was done by Pt. The row represents the kind of trace elements and the lengthwise represents the contamination of hyaluronic acid.

References

1) Thu, B. Gaserod, O. Paus, D. Mikkelsen, A. Skjak-Braek, G. Toffanin, R. Vittur, F. Rizzo, R., Biopolymers. 53(1) (2000) :60

2) Go Matsumura, Anthony Herp, and ward Pigman, Radiato.Res. 26 (1966) 735.

3-67 Fluorine Uptake into the Human Tooth from the Thin Layer of F-Releasing Material

H.Yamamoto [a)], M.Nomachi [b)], K.Yasuda [c)], Y. Iwami [a)], S. Ebisu [a)], H. Komatsu [d)], Y.Sugaya [b)], T. Sakai [e)] M. Oikawa [e)] T. Satoh [e)]and T. Kamiya [e)]

[a)] Graduate School of Dentistry, Osaka University, [b)] Graduate School of Science, Osaka University, [c)] The Wakasa Wan Energy Research Center, [d)] Graduate school of Dental Medicine, Hokkaido University, [e)] Department of Advanced Radiation Technology, TARRI, JAEA

Using PIGE (TIARA, JAPAN) technique, we have studied the fluorine (hereinafter F) distribution in human tooth to clear the quantitative correlation between F concentration in the tooth and the prevention effect on the progress of dental caries [1~3]. We report here F uptake into the human tooth from the thin layer of F-releasing low viscous resin (FLVR). The thin layer coating technique is often used at the dental clinical application to acquire the rigid adhesion between the filling material and tooth[4].

The crown of human tooth was horizontally cut. The dentin of cut surface was firstly applied with four kinds of FLVR about 50~150μm in thickness following the instruction of manufactures. The non-F-releasing and F-releasing filling resins were also hardened respectively on the cut surface applied with four kinds of FLVR thin layer. The Groups of non-F-releasing filling material (LITE FIL IIP) are G1 (A) (FL-Bond and LITE FIL IIP), G2 (A) (REACTMER BOND and LITE FIL IIP), G3 (A) (XENO Bond and LITE FIL IIP) and G4 (A) (PROTECT LINER F and LITE FIL IIP). The Groups of F-releasing filling material are G1 (B) (FL-Bond and BEAUTIFIL), G2 (B) (REACTMER BOND and REACTMER PASTE), G3 (B) (XENO Bond and XENO CF PASTE), and G4 (B) (PROTECT LINER F and TEETHMATE F-1). The treatment and the measurement of specimens are as same as previously reported[1]. The F uptake from the specimens after one month was estimated in the form of 2D map. The max F concentration and F penetration depth in the tooth were analyzed. The penetration depth means the distance where showed until about 500 ppm F.

The X-ray image and 2D mapping, and concentration of F and Ca of G4 (A) and G4 (B) were shown in Fig.1. F penetration was observed in all of teeth of G1 (A) ~ G4 (A) groups, where F were released and supplied to tooth only from FLVR thin layer. The values of max F concentration in the tooth and F penetration depth were in order of F concentration contained in FLVR. Between the groups of applied material, G1 (A) and G1 (B) or G4 (A) and G4 (B), F uptake showed the significant difference (Fig.2, Fig.3).

The penetration of F was observed in the whole tooth specimen. The FLVR was useful for F uptake into the tooth, and F distribution depended on the kinds of thin layer of FLVR and filling resin. Therefore, the selection of the low viscous F-releasing and filling resin combination in the clinical application should be determined depending on their characteristic properties. One of the fundamental data, which is useful for the analysis of F transportation relating to the prevention of caries, was obtained.

References

1) T. Sakai, et al., Biol. Trace Element Res. 77 (1999) 71.
2) M. Nomachi et al., TIARA Annual report 1998 (1999) 226.
3) H. Yamamoto et al., Nucl. Instr.and Meth. B 231 (2005) 300.
4) B. Van Meerbeek et al., Oper Dent. 28 (2003) 647.

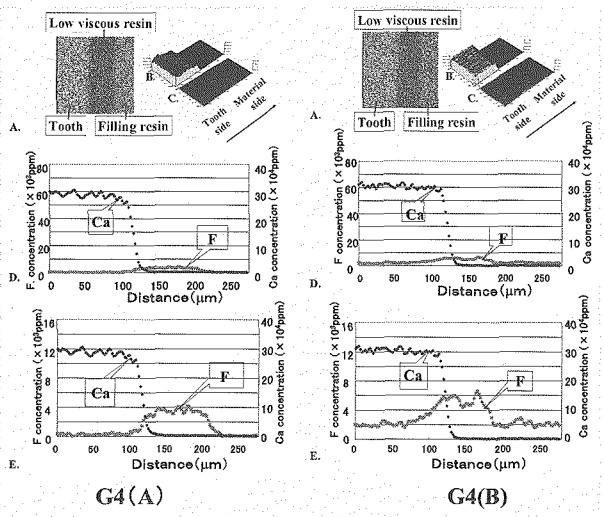


Fig.1 F penetration from 'PROTECT LINER F' to the tooth
A: X-ray image. B: 2D mapping of Ca. C: 2D mapping of F.
D: Concentration of average values of F and Ca in the measurement area. The direction is shown by an arrow in 'C'.
E: Enlarged fluoride concentration in 'D'.

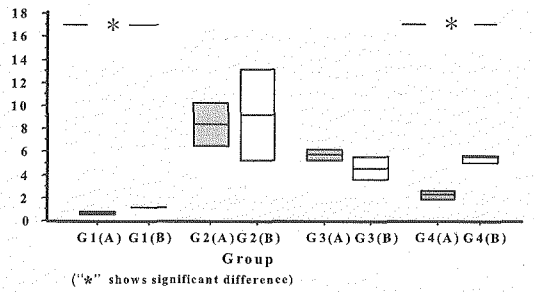


Fig.2. Maximum concentration of F penetrated into the tooth

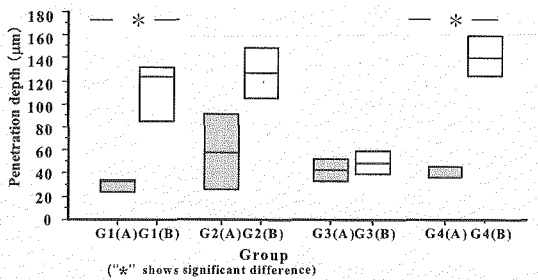


Fig.3. Penetration depth of F into the tooth

This is a blank page.

4 Advanced Materials, Analysis and Novel Technology

4-01 Development of the Heavy Ion Beam Pulse Radiolysis ····· 141
T. Kondoh, J. Yang, K. Kan, Y. Yoshida, H. Shibata, M. Taguchi and T. Kojima
4-02 LET Effect on Irradiation of Hydroxy Imide Compounds in Alcohol Solution ····· 142
S. Nakagawa, N. Ohta, M. Taguchi and T. Kojima
4-03 Preparation of Submicron Copper Wires in Ion Track-Etched Membranes of Thermally Stable Polyimide: Effect of Electrodeposition Temperature on Their Morphology ····· 143
H. Koshikawa, M. Asano, T. Yamaki, M. Yoshida and Y. Maekawa
4-04 Gas Separation SiC Membrane Developed from Precursor Polymers by Radiation Curing ····· 144
R.A. Wach, M. Sugimoto and M. Yoshikawa
4-05 1-D Crosslinked Polymer Nanowires Prepared by Single Particle Nanofabrication Techniques ····· 145
S. Seki, S. Tsukuda, S. Tagawa, M. Sugimoto, T. Sato, M. Oikawa and T. Sakai
4-06 Characterization of Carbonizing Processes of Titanium Thin Films by Carbon-Implantation ····· 146
Y. Kasukabe, T. Yamamura, J. J. Wang, N. S. Nishida, S. Yamamoto and M. Yoshikawa
4-07 Ion-Induced Luminescence of Cr-Doped Alumina ····· 147
A. Inouye, S. Nagata, T. Shikama, S. Yamamoto and K. Takano
4-08 Effects of Hydrogen and Hydroxyl on Ion Beam Induced Luminescence of Ceramics ····· 148
S. Nagata, S. Yamamoto, A.Inouye, B. Tsuchiya, K. Toh, K.Takano, M. Yoshikawa and T. Shikama
4-09 Spectroscopic Analysis of Si Bombarded with C_{60} Ions ····· 149
H. Naramoto, S. Sakai, K. Narumi, V. Lavrentiev, Y. Maeda, K. Takahiro, K. Kawatsura, S. Nishibe, N. Hasuike, H. Harima, Y. Baba, S. Yamamoto, N. Hirao and H. Kudo
4-10 Raman Analysis of Damage of C_{60} Thin Films by Fast Ion Bombardment ····· 150
K. Narumi, S. Sakai, H. Naramoto and Y. Maeda
4-11 Chemical State Analysis of Vacancy-Impurity Complexes by Positron Annihilation Spectroscopy ··· 151
M. Fujinami, K. Oguma, T. Akahane, A. Kawasuso and M. Maekawa
4-12 Characterization of Ion Beam-Induced Quantum Structures Using a Slow Positron Beam ····· 152
M. Maekawa, R. S. Yu and A. Kawasuso
4-13 Analysis of Light Elements in Carbon Materials ····· 153
Y. Horino, Y. Mokuno, A. Chayahara, H. Yasui, K. Awazu, S. Yamamoto, K. Narumi and H. Naramoto
4-14 Radiation-Induced Luminescence from TiO_2 by Ion Irradiations ····· 154
S. Kitazawa, S. Yamamoto, M. Asano, Y. Saitoh and S. Ishiyama
4-15 Disorder Analysis of Laser Crystal Surfaces Irradiated by a Neutral Argon Beam ····· 155
A. Sugiyama, S. Yamamoto and K. Takano
4-16 Application of X-Ray Photoelectron Spectroscopy to Characterization of Metallic Nanoclusters Formed by Ion Implantation-III ····· 156
K. Takahiro, S. Oizumi, K. Kawatsura, T. Isshiki, K. Nishio, S. Nagata, S. Yamamoto, K. Narumi and H. Naramoto
4-17 Cr Ion Irradiation Effects on Hydrogen Storage Characteristics of Pd ····· 157
H. Abe, R. Morimoto, H. Uchida and H. Itoh

4-18 Visible Photoluminescence of ZnO Rods Grown on Cu Implanted Substrate ····· 158
A. Takeyama, S. Yamamoto, M. Yoshikawa and H. Ito
4-19 Blister Formation in Rutile TiO_2 (100) Films by Helium Irradiation ····· 159
S. Yamamoto, K. Takano, A. Inouye and M. Yoshikawa
4-20 Improvement of Gasochromic Properties in Tungsten Oxide by Ion Irradiation ····· 160
K. Takano, A. Inouye, S. Yamamoto and M. Yoshikawa
4-21 Hydrogen Sensing Characteristics of Ag Implanted WO_3 ····· 161
A. Takeyama, S. Yamamoto, M. Yoshikawa and H. Ito
4-22 Improved Separation of Cadmium-107 from Silver Cyclotron Targets by Precipitaion Method ····· 162
N. S. Ishioka, S. Fujimaki, N. Suzui, S. Nakamura and S. Matsuhashi
4-23 Synthesis of Hydrophilic Endohedral ^{133}Xe-Fullerenol by Using Higher Fullerene ····· 163
S. Watanabe, T. Katabuchi, N. S. Ishioka and S. Matsuhashi
4-24 Deuteron-Induced Activation Cross Section Measurement of Fe, Cr, Mn, Ni and Au for IFMIF Accelerator ····· 164
M. Nakao, N. Kubota, K. Ochiai, H. Sudo, N.S. Ishioka and T. Nishitani
4-25 Production of Radioisotopes for Nuclear Medicine Using Ion Beam Technology and Its Utilization for Both Therapeutic and Diagnostic Application in Cancer ····· 165
Y. Iida, H. Hanaoka, T. Katabuchi, S. Watanabe, N. S. Ishioka, S. Matsuhashi, N. Oriuchi, T. Higuchi, M. Miyakubo and K. Endo
4-26 Nuclear Reaction Micro-Analysis of Boron Doped Steel ····· 166
H. Shibata, Y.Kohno, T.Satoh, M.Oikawa, J.Haga and T.Sakai
4-27 Measurement of Three-Dimensional Structure of Biological Samples by STIM for PIXE Analysis ··· 167
T. Satoh, T. Sakai and M. Oikawa
4-28 Analysis of Radiation-Induced Cell Death In Vivo by Micro Particle-Induced X-Ray Emission (Micro PIXE) ····· 168
M. Hasegawa, H. Sakurai, S. Ishiuchi, T. Tamamoto, I. Asakawa, M. Shin, M. Oikawa, T. Satoh, T. Kamiya, K. Arakawa and T. Nakano
4-29 Studies on the Cadmium Distribution of Acute Cd Toxicity in Testis Using In-Air Micro Particle Induced X-Ray Emission (PIXE) ····· 169
T.Kusakabe, T.Nagamine, H.Takada, K.Nakazato, K.Suzuki, K.Nakajima, T.satoh, M.Oikawa and K.Arakawa
4-30 Analysis of Boron Distribution in 9L Gliosarcoma Cells Using Particle Induced γ-Ray Emission (PIGE) ····· 170
K. Endo, T. Yamamoto, Y. Shibata, K. Tsuboi, A. Matsumura, H. Kumada, K. Yamamoto, T. Sakai, T. Satoh, M. Oikawa, Y. Ohara and K. Ishii
4-31 Standard Reference Material for Determination of Platinum in Biological Materials by Micro Beam PIXE ····· 171
Y. Iwata, K. Ishii, M. Fukuda, T. Kamiya, T, Satoh, M. Oikawa and T. Sakai
4-32 Development of In-Air On/Off -Axis STIM ····· 172
K. Inomata, K. Ishii, R. Oyama, H. Yamazaki, S. Matsuyama, K. Yanai, E. Sakurai, T. Kamiya, T. Sakai, T. Satoh, M. Oikawa and K. Arakawa

4-33 Fundamental Research of Highly Sensitive PIXE by Grazing Exit X-Ray Measurement ····· 173
K. Tsuji, S. Yamamoto, T. Sakai, M. Oikawa, T. Sato and K, Arakawa
4-34 Micro-Machining of Resists on Silicon by Proton Beam Writing ····· 174
N. Uchiya, T. Harada, M. Murai, H. Nishikawa, J. Haga, T. Sato, M. Oikawa,T. Sakai, Y. Ishii ,
M. Fukuda, T. Kamiya and S. Yamamoto
4-35 Thermal Stability of Deformation and Refractive Index Change in Silica Glass Induced by
Ion Microbeam ····· 175
H. Aiba, T. Nakamura, Y. Ohki, M. Murai, H. Nishikawa, M. Oikawa, T. Satoh and
K. Arakawa
4-36 Measurement of Structure and Charge States of Swift Carbon Cluster Passing Through
a Thin Foil ····· 176
A. Chiba, Y. Saitoh, K. Narumi, M. Adachi and T. Kaneko
4-37 TOF Mass Spectrometry of Secondary Ions from HOPG Target Bombarded by Fast C and
Au Cluster Ion Beams ····· 177
H. Shibata, H. Tsuchida, A. Itoh, Y. Saitoh, A. Chiba, M.Adachi, T. Kamiya and K. Narumi
4-38 Effect of 1.66 MeV/atom Au Cluster Ion Irradiation in Si Single Crystals ····· 178
A. Iwase, T. Nakatani, F. Hori, Y. Saitoh, A. Chiba, K. Narumi and R. Oshima
4-39 Highly Sensitive Surface Contaminant Analysis Using Pulsed Cluster Ion Beams ····· 179
K. Hirata, Y. Saitoh, A. Chiba, K. Narumi, Y. Kobayashi and T. Kamiya
4-40 Aerosol Formation Induced by Proton Irradiation to Air ····· 180
Y. Oki, N. Osada, Y. Kanda, S. Yokoyama, K. Sato, K. Manabe, A. Endo, H. Noguchi,
H. Kaneko, Su. Tanaka and T. Iida
4-41 Measurement of Double Differential Fragment Production Cross-Section Induced
by Ten's MeV Nucleons ····· 181
T. Oishi, T. Sanami, M. Hagiwara, M. Baba, S. Kamada, T. Okuji, Y. Iwamoto, S. Tanaka and
H. Nakashima
4-42 Development of Monitor and Dosimeter Applicable to High-Energy Neutrons ····· 182
A. Endo, T. Sato, D. Satoh, Y. Shikaze, Y. Tanimura, J. Saegusa, M. Tsutsumi,
Y. Yamaguchi, H. Kaneko, K. Oda, Y. Imasaka, M. Notsu, H. Tada, H. Tawara, K. Eda,
K. Takahashi and M. Baba
4-43 Easy Measurement Technique for 2D Distribution of Fluence Using GAF-Film and PC-Scanner ···· 183
T. Agematsu and H. Hanaya
4-44 Preliminary Study on Applicability of B3 Film Dosimeter for Two Dimensional Dose Distribution
Using a PC-Scanner ····· 184
H.Hanaya and T.Agematsu
4-45 Focused Microbeam Formation for Heavy Ion Beam from AVF Cyclotron (II) ····· 185
W. Yokota, T. Satoh, M. Oikawa, T. Sakai, S. Okumura, S. Kurashima, N. Miyawaki,
H. Kashiwagi, T. Kamiya and M. Fukuda
4-46 Design of Age-related Macular Degeneration (AMD) Treatment System Using
a Carbon Ion Beam ····· 186
H. Shimada, M. Oikawa, T. Satoh, T. Sakai, T. Agematsu, S. Okumura, M. Taguchi, T. Sato,
Y. Horiuchi, H. Katoh, K. Yusa, M. Fukuda, T. Kamaiya, S. Kishi, T. Nakano and K. Arakawa

4-47 Development of Ion-Induced Fluorescence Measurement Technology at the External Light Ion Microbeam System ····· 187
M. Oikawa, T. Satoh, J. Haga and T. Sakai
4-48 Formation of a Large-Area Uniform Ion Beam Using Multipole Magnets ····· 188
Y. Yuri, N. Miyawaki, T. Kamiya, W. Yokota, K. Arakawa and M. Fukuda
4-49 The Effect of Support Gas in Fullerene (C_{60}) Ion Production ····· 189
K. Yamada, K. Ohkoshi, Y. Saitoh, K. Mizuhashi and W. Yokota
4-50 Development of All-Permanent-Magnet ECR Ion Source for the JAEA Cyclotron ····· 190
K. Yoshida , T. Nara , Y. Saitoh and W. Yokota
4-51 Improvement of the Cyclotron System for Microbeam Formation ····· 191
N. Miyawaki, S. Okumura, S. Kurashima, H. Kashiwagi, K. Yoshida, I. Ishibori, Y. Yuri, T. Nara, T. Agematsu, W. Yokota and M. Fukuda
4-52 Development of Beam Generation and Irradiation Technology for Electrostatic Accelerator ····· 192
K.Ohkoshi, S.Uno, A.Chiba, K.Yamada,Y.Saitoh, Y.Ishii, T.Sakai, T.Satoh and K.Mizuhashi

4-01 Development of the Heavy Ion Beam Pulse Radiolysis

T. Kondoh[a)], J. Yang[a)], K. Kan[a)], Y. Yoshida[a)], H. Shibata[b)], M. Taguchi[c)] and T. Kojima[c)]

[a)]ISIR, Osaka University, [b)] Faculty of Engineering, Kyoto University,
[c)] Eenvironment and Industrial Materials Research Division, QuBS, JAEA

Abstract

The heavy ion beam is a high LET radiation. Ion beam gives large energy into the materials at some constant depth. As a result of above thing, ion beam can excite materials high densely (High density excitation effect). The characteristic of this ion beam was used to develop the new technology such as the material and the medical application. Ion beam pulse radiolysis is developing for elucidation of the initial process of ion beam induced chemical reaction. Our unique measurement method is developing using a scintillator and the photon counting method. Transient optical absorption of the pyrene's cation radical which was induced by irradiation of 220MeV C^{5+} ion was measured.

イオンビームは高 LET 放射線であり、電子線など低 LET 放射線と大きく異なり、物質中を直進し一定の深さで大きなエネルギーを与える。その結果、物質を高密度に励起できる（高密度励起効果)。このイオンビームの特性を利用して新規イオンビームプロセスを開発し、材料、医学等の領域に応用することは、非常に重要視されている。しかし、これらの応用技術を発展させるには、イオンビームによって生成されるカチオンラジカル、電子、励起分子など初期の短寿命活性種の挙動を明らかにし、イオンビーム初期過程を解明することが必要である。イオンビームの特徴である高密度励起効果は、照射直後の活性種の分布や自己減衰過程に反映される。低 LET 放射線に比べて活性種がはるかに高密度であるため、再結合や化学反応が、非常に短い時間領域で起こることが予測される。本研究では、高感度測定可能なフォトンカウンティング法による過渡吸収実験を考案した。TIARA のパルス性能を活用した世界でも数少ない時間分解分光法を開発し、ナノ・ピコ秒時間領域の反応初期過程の解明を行っている。

Fig. 1 に、HX ポートに設置された試料セルとフォトンカウンティング法による吸収分光測定システムを示す。本実験では、AVF サイクロトロンからの 220MeV C^{5+}イオンを用いた。イオンビームは、チョッパーにより 1/6 に間引いた。イオンビームは、金属箔窓と試料液面に設置されたシンチレーターを通過し試料に入射した。イオンビームがシンチレーターを通過する際の発光を分析光とし、光ファイバーを通して光測定系に導いた。シンチレーターには CaF_2 (940ns, 435nm)を用いた。これまでの研究では、分析光強度（I_0）を正確に測定する事が困難だった。これはイオンビームが光源であると同時に励起源であることが原因であった。この問題を解決するために、測定する波長領域で、吸収も発光もほとんどない塩化メチレンをサンプルの溶媒として用いた。これにピレンなどの溶質を溶解し、更にイオンビームが誘起した溶質の活性種だけの時間挙動を調べた。

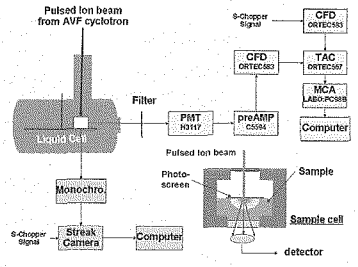
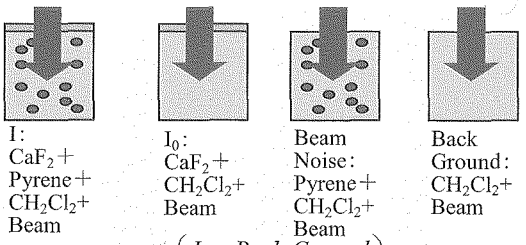


Fig. 1 Measurement system of ion beam induced optical absorption



$$O.D. = \log\left(\frac{I_0 - Back\ Ground}{I - Beam\ Noise}\right) \quad .....(1)$$

Fig.2 Procedure of optical absorption measurement

Fig. 2 に光吸収測定のプロセスを示した。この場合の、ピレン由来のイオンビーム誘起活性種の過渡光吸収強度は（1）式で計算される。

Fig. 3 に 220MeV C^{5+}イオン照射により生成した、塩化メチレン中のピレンカチオンラジカルの過渡光吸収挙動を示した。青線は 1mM ピレン－塩化メチレン溶液で、赤線が 10mM、黒線が 100mM のピレン濃度の場合である。測定波長は 440nm であり、ビームカレントは 0.07nA とした。ビームカレントが多いと光シグナルが予想外に速い減衰挙動だった。これは、シンチレーターの発光寿命のメーカー値が、X 線などの低 LET 放射線で測定されたものであり、高カレントイオンビームでは高密度励起になるためと考えている。また、各測定の積算時間を同一にすると、1mM ではピレンカチオンラジカルはノイズレベルだが、ピレン濃度 10mM では、有意に光吸収が立ち上がった。ピレン濃度 100mM の場合も同様であった。しかし、吸光度はピレン濃度に比例はしなかった。イオンビームが生成するピレンカチオンラジカル濃度の飽和が起こっていると考えている。測定点が少ないので今後詳細に測定し検討する。

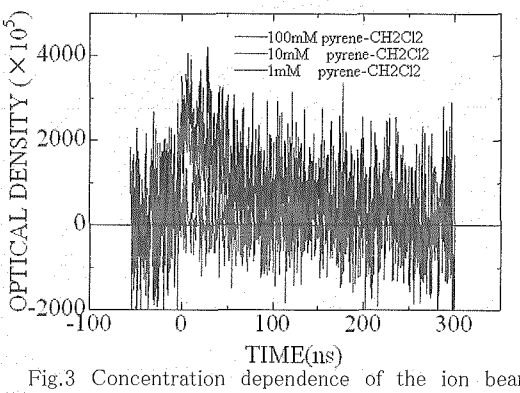


Fig.3 Concentration dependence of the ion beam induced optical absorption of cation radical of Pyrene

4-02 LET Effect on Irradiation of Hydroxy Imide Compounds in Alcohol Solution

S. Nakagawa[a], N. Ohta[b], M. Taguchi[c] and T. Kojima[c]

[a]Tokyo Metropolitan Industrial Technology Research Institute, [b]Hiroshima Univ.,
[c] Environment and Industrial Materials Research Division, QuBS, JAEA

Abstract

Hydroxymaleimide was irradiated in 2-propanol with 200 MeV C-ion beam from the AVF cyclotron in the TIARA Facility. Degradation efficiency of hydroxymaleimide irradiated by C-ion decreased rather than γ-irradiation. Appearant G-value of degradation of hydroxymaleimide decreased with decreasing incident energy of C-ion. These results suggest that the degradation efficiency of hydroxymaleimide decreased with increasing LET. Hydroxysuccinimide, the main product by γ-irradiation, was produced little and unknown product newly appeared by C-ion irradiation. The lower concentration of cations diffusing out of the spur will control the reaction mechanism under C-ion irradiation.

1. はじめに

マレイミド($C_2H_2(CO)_2NH$)は、光化学重合反応の開始剤として利用されてきたが、放射線化学的な反応に関する研究例はほとんどない。一方、ヒドロキシマレイミド($C_2H_2(CO)_2NOH$)を2-プロパノール中でγ線照射したところ、ヒドロキシスクシンイミド($C_2H_4(CO)_2NOH$)が効率よく生成し、その生成機構はヒドロキシマレイミドの励起三重項状態を経由することが示唆された[1]。そこで、2-プロパノール中でのヒドロキシマレイミドの放射線照射による反応機構をさらに調べるため、イオン照射を行った。

2. 実験方法

ヒドロキシマレイミドを2-プロパノールに溶かし（0.1モル%）、窒素置換した試料に原子力開発機構TIARA施設内AVFサイクロトンのCイオン(220MeV)およびＨｅイオン(100MeV)を照射した。また、試料の上にアルミ箔を置き、入射イオンのエネルギーを変えて、照射エネルギー依存性を調べた。照射試料は、真空乾燥した残留物をアセトニトリルで溶解したのち、高速液体クロマトグラフ（カラムCDS、移動相アセトニトリル:水＝60：40）で分析した。

3. 結果及び考察

γ線およびCイオン照射でのヒドロキシマレイミド及び生成物の濃度変化をFig.1およびFig.2に示す。ヒドロキシスクシンイミド以外の生成物として、液体クロマトグラフの保持時間で示した化合物が確認された。γ線照射での分解のＧ値は0.5であり、Cイオン照射では1/10以下であった。また、γ線照射では、６割のヒドロキシマレイミドがヒドロキシスクシンイミドに変化したが、イオン照射では、ヒドロキシスクシンイミドの生成は激減し、保持時間4.7分の生成物が確認された。ヒドロキシマレイミドの三重項状態はヒドロキシマレイミドのカチオンと電子の再結合反応により生成しており、LETの大きいイオン照射では、スパー外に拡散できるカチオン種の濃度が減少するため、ヒドロキシスクシンイミドの生成量が減少したと考えられる。

Ｃイオンの初期エネルギーに対する見かけのＧ値をFig.3に示す。初期エネルギーの増加に伴い、Ｇ値はわずかに増加することがわかった。これは、ＬＥＴの増加で微分Ｇ値が減少することを意味する。

今後、Ｈｅイオン(50MeV)照射など、異なるLETにおける照射効果のを調べる予定である。

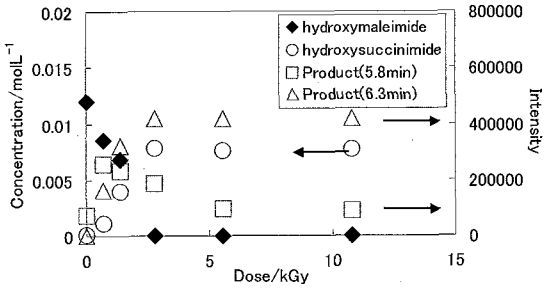


Fig.1 Dose dependence of concentrations of hydroxymaleimide γ-irradiated in 2-propanol.

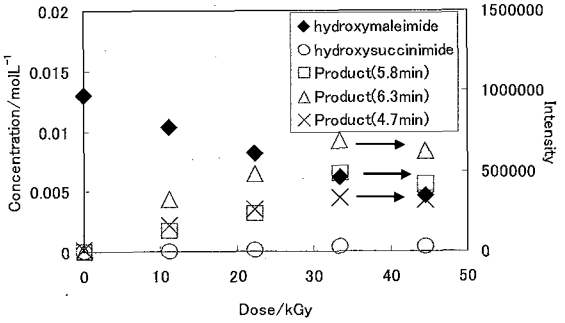


Fig.2 Dose dependence of concentrations of hydroxymaleimide irradiated by C-ion in 2-propanol.

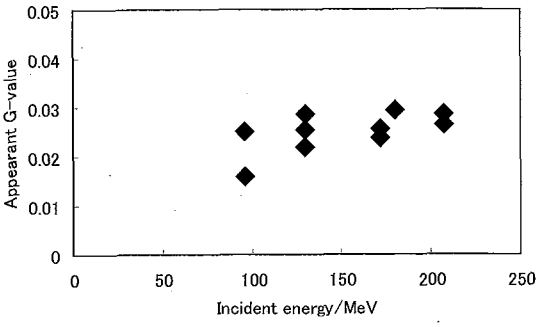


Fig.3 Dependences of appearant G-value on incident energy of C-ion.

Reference

1) S. Nakagawa, “Solvent effect on irradiation of hydroxymaleimide”, 日本化学会第８５春季年会予稿集

4-03 Preparation of Submicron Copper Wires in Ion Track-Etched Membranes of Thermally Stable Polyimide: Effect of Electrodeposition Temperature on Their Morphology

H. Koshikawa, M. Asano, T. Yamaki, M. Yoshida and Y. Maekawa

Environment and Industrial Materials Research Division, QuBS, JAEA

The damaged region created along the path of swift heavy ions in polymers is susceptible to a proper etchant, resulting in the formation of through-holes with nanometer-to-micrometer diameters. This so-called ion track membranes of thermally and mechanically stable polymers have been developed for applications to electronic devices through hybridization with metals and semiconductor alloys by electroplating[1,2]. In this study, anisotropically conducting membranes were prepared by electrochemical deposition of copper (Cu) wires into the cylindrical pores with diameters of 0.5-2 μm in the polyimide (PI)-based ion track membrane. We report here the effect of deposition temperature on the morphology of the resulting submicron Cu wires.

Commercially-available PI films (Kapton, thickness: 12 μm) were irradiated by 450 MeV $^{129}Xe^{23+}$ with fluences of 3×10^5 and 3×10^7 ions/cm^2 from the AVF cyclotron at the TIARA facility. According to the established procedure[3], the PI ion track membranes with 0.5-μm diameter cylindrical pores were then prepared by the 1.5 hour etching in a pH12 aqueous sodium hypochlorite (NaClO) solution at 60°C. Successive layers of gold (25 nm) and Cu (20 μm) were coated on one side of the ion track membranes as a cathode[4]. The Cu wires were deposited within the pores of the ion track membranes onto the Cu cathode by electrochemical plating in a pH1 aqueous solution of 1.3 M copper sulfate ($CuSO_4$) with periodic potential modulation (–0.2 V; 6 sec, 0.2 V; 1 sec). The deposition temperature was controlled at room temperature, 50 and 80°C by a thermostat water bath. The PI film was removed from the Cu electrode using a NaClO solution at 60°C for 30 min. The geometry of the wires was estimated by scanning electron microscopy (SEM) observation.

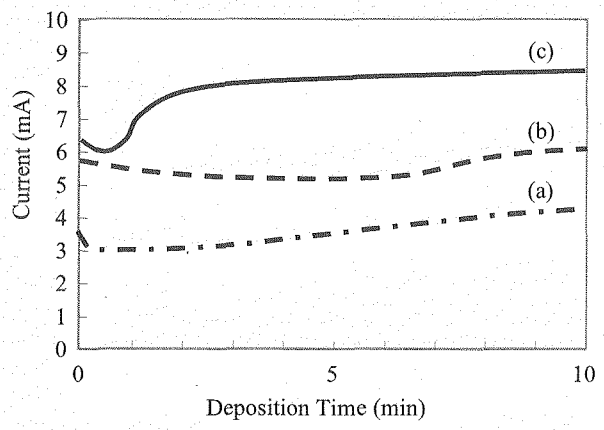


Fig. 1 Current vs. time curve during the electrodeposition of the Cu wires at room temperature (a), 50 (b) and 80 °C (c).

Figure 1 shows deposition current vs. time curve obtained when the Cu wires were prepared at different temperatures. As the temperature rose, the higher current was obtained over the deposition time. The current usually corresponds to the rate of the electroplating because it originates from the reduction of Cu^{2+} in the $CuSO_4$ solution. Thus, it is assumed that the supply of Cu^{2+} to the growing wire surface is a rate-determining step for the deposition process. In theory[5], the mean velocity of particles in a continuous medium, v, is proportional to the square root of the absolute temperature, T, as expressed by the following equation: $v = (3RT/M)^{1/2}$, where R and M denote the gas constant and the mass of an ion, respectively.

Figure 2 compares the SEM images of the Cu wires prepared at room temperature, 50 and 80°C. The wire surface appeared to be smoother at the higher deposition temperature. In line with the above discussion, the amount of Cu^{2+} at the surface should be large enough to be compactly deposited in the case of high-temperature electroplating. On the other hand, the Cu^{2+} mobility at low temperatures is probably too low to keep up with the wire growth occurring within the pores. As shown in fig.2a, this leads to the formation of the Cu wires consisting of loosely assembled with small grains.

References

1) Y. Suzuki et al., Chem. Mater., 14 (2002) 4186.
2) Y. Maekawa et al., Polymer, 45 (2004) 2291.
3) C. Trautmann et al., Nucl. Instr. and Meth. in Phys. Res. B 111 (1996) 70.
4) D. Dobrev et al., Nucl. Instr. and Meth. in Phys. Res. B 149 (1999) 207.
5) W. J. Moore, "Physical Chemistry", Prentice-Hall, Tokyo, (1962) 216.

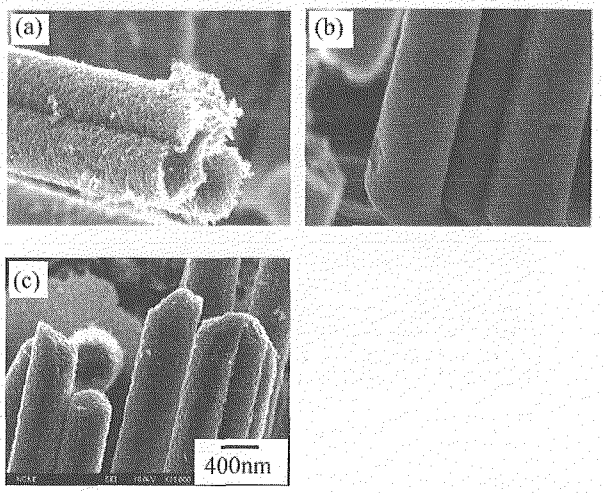


Fig. 2 SEM images of the copper wires deposited at room temperature (a), 50 (b) and 80 °C (c).

4-04 Gas Separation SiC Membrane Developed from Precursor Polymers by Radiation Curing

R.A. Wach, M. Sugimoto and M. Yoshikawa

Environment and Industrial Materials Research Division, QuBS, JAEA

Our previous research work on radiation curing of preceramic polymer coatings revealed that the admixture of 5-20 wt% of PVS into PCS improves the quality of the final SiC surface after pyrolysis[1]. Plasticization of the film by PVS allows for the development of smoother coating on the substrate during solvent evaporation, and reducing formation of cracks and pinholes during pyrolysis. This has a significant practical relevance since the void-free membrane structure is expected to increase gas separation factor. Therefore, a blend of PCS containing 20% of PVS was utilized to form coatings on porous Al_2O_3 substrate.

SiC produced from preceramic polymer by EB oxidation (1.8 MGy in air atmosphere) and following pyrolysis at 1123 K in Ar atmosphere displays fully amorphous structure. The cross-section of a coated plate is presented in Fig. 1. A flawless interface between SiC and γ-alumina shows good adhesion of SiC film to the substrate. Table 1 presents the distribution of Al and Si atoms evaluated from 1-4 areas indicated in the cross-section image. The significant decreasing of Si atom content occurs at the surface of γ-alumina support but some Si atoms are deposited in the porous support.

Nitrogen, hydrogen and helium gases permeation tests were conducted by a vacuum method. Permeance of two types of samples is presented in Fig. 2. The membrane was formed by two- (sample 1) or four-times (sample 2) spin coating (900 rpm) of 2.5% cyclohexane solution of PCS80/20PVS, irradiation and firing. In the case of sample 1, the developed film was of insufficient quality with several pinholes observed by SEM at high magnification. As a result of defective surface a high gas flux was accomplished and low separation ratio, close to that characteristic for Knudsen diffusion mechanism, which is about 3.7 for H_2/N_2. The permeation took place essentially through the defects of the coating layer instead of desired permeation through thickness of the SiC membrane itself.

For the membranes formed by four times coating He and H_2 permeance at room temperature is less than 1×10^{-9} $mol\cdot sec^{-1}\cdot m^{-2}\cdot Pa^{-1}$. Nevertheless, the apparent dependence of the permeability on the temperature is observed. Samples demonstrate temperature activated permeation behavior. Determined values of activation energy for sample 2 (PCS80/20PVS) are 5.2, 5.7, 1.2 for He, H_2 and N_2, respectively. They are characteristic for molecular sieving mechanism, which indicates that the permeation takes place throughout pore-like structure. Presently obtained data confirms activated permeation mechanism, and supports the presumption that amorphous SiC film functioning as a porous structure was fabricated. Accordingly, perm-selectivity at 298-523 K was in the range of 41-249 and 35-206 for He/N_2 and H_2/N_2, respectively. Produced SiC coating film still contains a few percent of oxygen but its performance is superior to other known SiC membranes.

Table 1. Relative Al and Si atomic content measurd by EDS in the areas specified in Fig. 1

Element / area No.	1	2	3	4
Al	0.04	0.06	0.86	0.97
Si	0.96	0.94	0.14	0.03

References

1) R.A. Wach et al., *Key Eng. Mater.*, 317 (2006) 573.

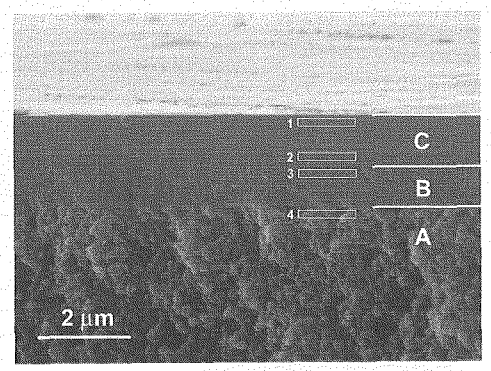


Fig.1 SEM picture of a cross-section of the coated plate. PCS 80/20 PVS blend in 5% cyclohexane solution spin-coated at 1000 rpm. The cross-section components are denoted as: A – α-alumina, 100 nm grade; B – γ-alumina, 10 nm grade; C – SiC coating. Areas 1-4 were evaluated by EDS.

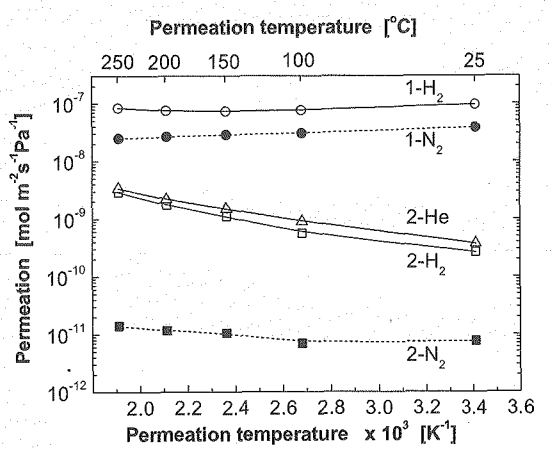


Fig.2. Permeance through membranes coated two (1) and four-times (2)

4-05 1-D Crosslinked Polymer Nanowires Prepared by Single Particle Nanofabrication Techniques

S. Seki[a)], S. Tsukuda [a)], S. Tagawa [a)], M. Sugimoto [b)], T. Sato [c)], M. Oikawa [c)] and T. Sakai [c)],

[a)]The Institute of Scientific and Industrial Research, Osaka University, [b)]Environment and Industrial Materials Research Division, QuBS, JAEA, [c)]Department of Advanced Radiation Technology, TARRI, JAEA

High energy charged particle irradiation of polystyrene and polysilane derivatives is shown to cause crosslinking reactions leading to the formation of a polymer gel containing cylindrical nanostructures of regular length and thickness. The deposited energy density in a charged particle track controlled the spatial distribution of crosslinks of polymer molecules. The radial variation in dose along each ion track results in the formation of cylindrical structures with nm-sized radius of the cross-section.[1-3] These cylindrical structures are well visualized as worm-like structures (nanowires). The similar schema for the formation of the nanowires have been demonstrated for the charged particle irradiation of a variety of polymeric materials including π-conjugated polymers, polymers for hydrogels, and proteins. The present results represent the potential utility of this technique for single-particle fabrication of nano-structures with sub-nanometer spatial resolution.

The nanowires based on polystyrene (PS) can be visualized by atomic force microscopy (AFM), as shown in Fig. 1. After the development procedure, the nanowires lie prostrate on the substrate surface, and are overlapped giving the entangled structures in some cases as shown in Fig. 1(c). It should be noted that the range of incident particle in the polymer media were set far longer than the thickness of the polymer films in all cases, thus all incident particles were passing through the polymer films and stopped in the substrates. The length of the nanowires reflects the thickness of the original polystyrene film, whereas the thickness (cross-section) of the nanowires increases with the molecular weight of the polystyrene. The average molecular size of the polymer is therefore a primary factor determining the thickness of the nanowires. However, the nanowire thickness also increased with LET of the ion beam, as the high-LET 500 MeV $^{197}Au^{31+}$ beam produced thicker wires than those prepared using the low-LET 400 MeV $^{84}Kr^{18+}$ beam.

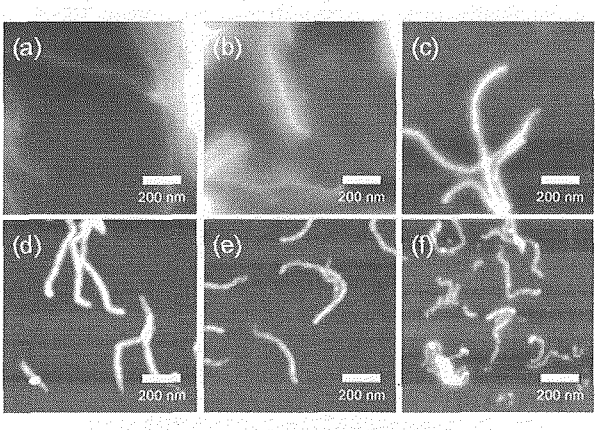


Fig.1 AFM micrographs of nanowires based on polystyrene (PS) showing the variation in size with molecular weight and the type of ion beam. The nano-wires were formed by 450 MeV $^{129}Xe^{23+}$ beam irradiation to (a) a PS8 (Mn = 1.1 × 10^6) (b) a PS7 (Mn = 6.8 × 10^5) and (c) a PS4 (Mn = 1.2 × 10^5) thin films at 1.0 × 10^9 ions/cm^2. The nanowires were also formed by (a) 500 MeV $^{197}Au^{31+}$, (b) 450 MeV $^{129}Xe^{23+}$ and (c) 400 MeV $^{84}Kr^{18+}$ beams irradiation to PS3 (Mn = 5.15 × 10^4) thin films at (d) 5.1 × 10^8, (e) 6.9 × 10^8, and (f) 1.1 × 10^9 ions/cm^2.

The radii of the nanowires were determined by AFM as r_1 and r_2 which were defined as the half-width at half-maximum and the half height of the AFM traces of the nanowire cross-section, respectively. The values of r_1 and r_2 are typically observed as 11.3 and 3.4 nm for the nanowires based on PS1(Mn = 2.1 × 10^3). The ration of r_1/r_2 showed considerable increase with the molecular weight of the polymers. The values of r_2 were much lower than r_1, showing that the nanowires formed an elliptical cross-section due to sagging onto the substrate surface after development. Assuming that the nanowire cross-section is a simple ellipse, the nominal radius r is defined as follows to facilitate discussion of the distribution of deposited energy and crosslinking reactions on an ion track[4].

$$r = \sqrt{r_1 \times r_2} \qquad (1)$$

The experimental nominal r and theoretical chemical core radius (r') are in good agreement for thicker nanowires, but the experimental values are much larger for thinner nanowires. This can be attributed to variations in the efficiency of energy leakage from the core to the penumbra area, and the size of molecules with respect to the wire diameter. The ion track model employed in the present paper is highly simplified, treating the deposited energy density in the core region as constant values. In reality, however, the energy density in the penumbra increases close to the boundary with the core, which will affect the efficiency of energy leakage from the core in a radius-dependent manner. The effect of relative molecular size can be seen in the shapes of the nanowires, where wires formed in low molecular weight polymer are worm-like, whereas those in high molecular weight films are rod-like[5]. These effects of energy leakage and the shape and size of polymer chains must be considered in discussion of the deposited energy density. The present results also demonstrate the possibility of single-particle fabrication of nano-structures with sub-nanometer spatial resolution.

References

1) S. Seki, et al., *Adv. Mater.* 2001, **13**, 1663.
2) S. Tsukuda, et al., *J. Phys. Chem.B* 2004, **108**, 3407.
3) S. Seki, et al., *Macromolecules*, 2005, **38**, 10164.
4) S. Tsukuda, et al., *Appl. Phys. Lett.* 2005, **87**, 233119.
5) S. Seki, et al., *J. Am. Chem. Soc.* 2004, **126**, 3521.

4-06 Characterization of Carbonizing Processes of Titanium Thin Films by Carbon-Implantation

Y. Kasukabe [a, b], T. Yamamura [b], J. J. Wang [b], N. S. Nishida [b], S. Yamamoto [c] and M. Yoshikawa [c]

[a]Center for International Exchange, Tohoku University, [b]Department of Metallurgy, Tohoku University, [c]Environment and Industrial Materials Research Division, QuBS, JAEA

Titanium carbide (TiC) films are a class of materials with many desirable physical properties, including extreme hardness, high melting point, excellent electrical conductivity, magnetic susceptibility and so on, making them outstanding candidates for many applications in various environments. Recently, it was reported that these properties were related to crystallographic textures and/or orientations of TiC films[1]. Therefore, much interest has been focused on crystallographic orientation and epitaxial growth of TiC. As for epitaxial growth mechanism of TiC, especially the atomistic mechanism of carbonizing processes by C-implantation is not understood clearly. Observation of the crystallographic structural change of deposited Ti films (~100 nm thick) during C-implantation was made by using transmission electron microscope (TEM) for the purpose to elucidate the carbonizing processes of Ti films. The Ti films were deposited by an electron beam heating method onto NaCl (001) surfaces held at room temperature (RT).

The deposited Ti films consisted of (03・5)-oriented hcp-Ti (lattice constants: a=0.296 nm, c=0.471 nm) and (110)-oriented CaF_2 type TiH_x ($x \approx 1.5$; lattice constant: a=0.441 nm). Carbon ions (C^+) with 26keV were implanted into the deposited Ti films in a 400kV analytical and high resolution TEM combined with ion accelerators at JAEA-Takasaki[2]. The H atoms which constituted TiH_x were released from the as-deposited Ti films during the early stage of C-implantation. Figures 1(a) and 1(b) show, respectively, a typical electron diffraction pattern (ED) and a bright field (BF) image taken from the C-implanted Ti film with C/Ti=0.54. Figures 1(c) and 1(d) are dark field (DF) images taken from the 002 and 020 reflections of (110)- and (001)-oriented TiC_y, respectively. It can be seen from Fig. 1(a) that hcp-Ti (lattice constants: a=0.299 nm, c=0.479 nm) and NaCl-type TiC_y (lattice constant: a=0.432 nm) coexist in this film. Furthermore, the band-like contrast region elongated in the <110> direction of the NaCl substrate indicated by white arrows is composed of (110)-oriented TiC_y crystallites. On the other hand, (001)-oriented TiC_y crystallites grow preferentially outside the band-like contrast region. Therefore, it can be considered that (110)-oriented TiC_y grown in the band-like contrast region is formed by carbonizing (110)-oriented TiH_x in the unimplanted Ti film, accompanied by the release of H atoms. On the other hand, (001)-oriented TiC_y grown outside the band-like contrast region would be transformed from (03・5)-oriented hcp-Ti in Ti films by C-implantation. Orientation relationship between (03・5)-oriented hcp-Ti sublattice and (001)-oriented fcc-Ti sublattice is shown in Fig. 2. In order to form the fcc sublattice by the hcp-fcc transformation, the atoms on the (00・1)-plane including B, A and Q atoms in Fig. 2 have to be shifted from position B to position B*, the center of gravity of triangle BAQ. The hcp sublattice is transformed into fcc-Ti sublattice with inheritance of square atomic arrangement that corresponds to EFJK atoms shown in Fig. 2. The results of TEM observation indicated that (001)- and (110)-oriented TiC_y are epitaxially formed by the transformation of (03・5)-oriented hcp-Ti and (110)-oriented TiH_x, respectively.

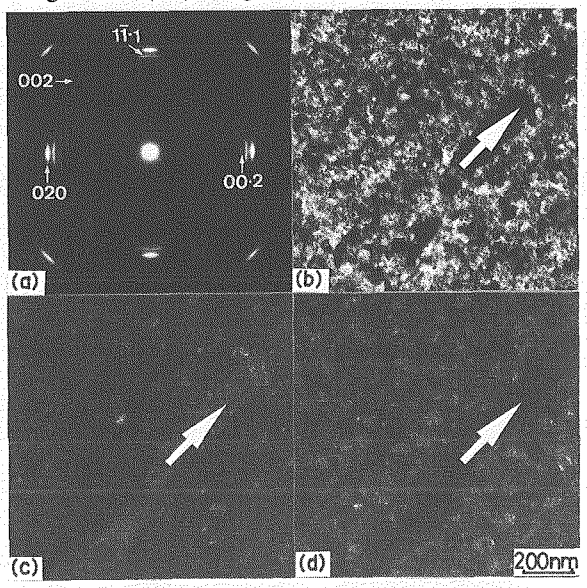


Fig.1 ED pattern (a) and BF image (b) and DF images (c) and (d) taken from a C-implanted Ti film with C/Ti = 0.54.

References

1) Z. Chen, S. S. Perry, A. Savan, P. M. Adams and S. V. Didziulis, J.Vac. Sci. Technol. A 23 (2005) 234.
2) H. Abe et al., JAERI-Research 96-047 (1996) 1.

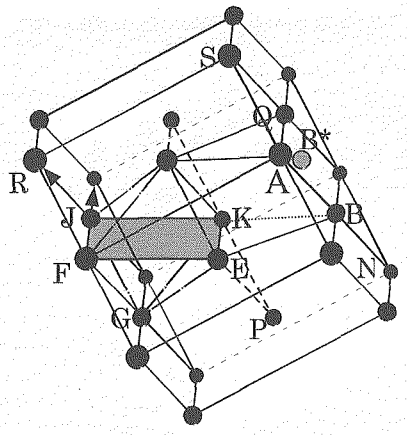


Fig.2 Schematic representation of orientation relationship between hcp-Ti and fcc-Ti.

4-07 Ion-Induced Luminescence of Cr-Doped Alumina

A. Inouye[a], S. Nagata[b], T. Shikama[b], S. Yamamoto[c] and K. Takano[c]

[a]School of Engineering, Tohoku University
[b]Institute for Materials Research, Tohoku University
[c]Environment and Industrial Materials Research Division, QuBS, JAEA

Abstract

Luminescence from oxides, such as Cr doped alumina (ruby), induced by energetic particles can be used for detecting flux, fluence and energy distribution of α particles (3.5 MeV) generated by D-T reaction in a fusion reactor. Previously, we found that the ion-induced luminescence of ruby (R-line) decreased by nuclear collisions. In the present study, we examined thermal recovery of the R-line luminescence intensity in ruby and of the defects in α-Al_2O_3 single crystal during heat treatment. It was found that the damaged luminescence centers did not recover up to the temperature of 900 K, when the displacements per unit volume in the sample was accumulated up to about 20 vacancies/nm^3 by H^+ or He^+ ion irradiation. Ion channeling measurements suggested that the displaced O atoms mainly caused dechanneling in the α-Al_2O_3 single crystal.

放射線照射によって発光する酸化物のなかで、クロム添加アルミナ（ルビー）は Cr^{3+}に由来する強い可視赤色発光（R-line）を示すことから、核融合炉内の DT 反応によって生成される 3.5 MeV のα粒子に対する光学式荷電粒子モニターの検出材料として利用することが考えられている。このため、keV～MeV 領域の軽イオン照射に対するルビーの発光特性を調べることは極めて重要である。これまでに、クロム添加アルミナの R-line 発光中心は入射イオンの核衝突によって消滅することを明らかにしてきた。今回は、焼鈍による発光強度および結晶の回復傾向を調べ、発光中心の消滅に起因する欠陥の種類について検討を行った。

本実験では、0.5 wt% : Cr が添加されたアルミナ焼結体（AF995R、Desmarquest、仏国）を試料として用いた。入射エネルギーを 3 keV～3 MeV の範囲でH^+またはHe^+イオンを、最大照射量 1x10^{22} ions/m^2 まで照射し R-line 発光を測定した。さらに照射後、10 分の等時焼鈍を大気中、1300 K まで行い、照射前と焼鈍後の発光強度の比較も行った。一方で、同様な条件で照射および焼鈍を行った単結晶α-Al_2O_3（0001）に対して、1 MeV の He^+イオンを用いた RBS / チャネリング法によって結晶性を評価し、照射による損傷や焼鈍による回復挙動について検討を行った。

3 keV～3 MeV まで変化させた H^+または He^+イオンを照射した試料に対して、焼鈍によるイオンビーム誘起発光強度の回復挙動と照射量との関係を Fig.1 に示す。縦軸には照射前における R-line 発光強度の 10%回復した焼鈍温度、横軸には照射によって累積されるはじき出し密度の計算値（TRIM98）をそれぞれ示している。入射イオン種および入射エネルギーに関わらず、R-line 発光強度の回復挙動とはじき出し密度の関係は一貫した傾向が見られた。低照射量領域では 700 K 以下の比較的低温で発光強度が回復するが、はじき出し密度が約 20 個/nm^3 以上になると急激に回復しにくくなる傾向が明らかとなった。

一方で、10 keV の He^+イオンを 1x10^{20} ions/m^2 まで照射および照射後の焼鈍を行った単結晶α-Al_2O_3 に対して結晶性評価を行った結果を Fig.2 に示す。照射を行うとアルミ原子に比べ酸素原子に由来する後方散乱収量が増加しやすい傾向にあった。また、照射試料を 500 K で焼鈍を行うと若干ながら酸素原子の回復が観測でき、900 K で焼鈍を行うとアルミ原子を含んだ結晶全体が回復することが確認できた。

以上の結果から、低照射領域では主に酸素原子のはじき出しによって R-line 発光中心が消滅するが、照射量が増加するとともにアルミ原子を含んだ欠陥集合体が形成されることで R-line 発光中心は 900 K 以下の温度では回復しないと考えられる。

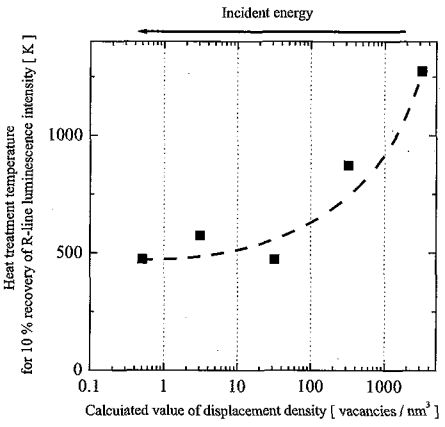


Fig.1. The Heat treatment temperature for 10 % recovery of R-line luminescence intensity was plotted against the displacement density accumulated by 3 keV ~ 3 MeV H^+ or He^+ ion irradiation.

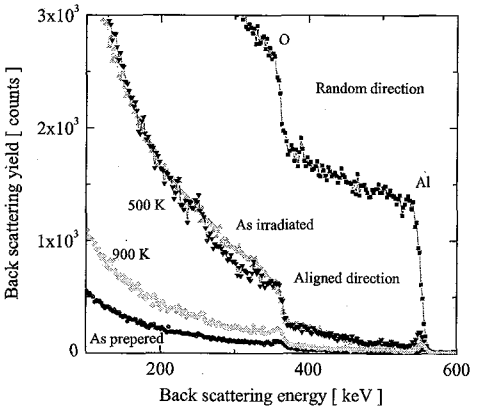


Fig.2. The crystal structures of the α-Al_2O_3 single crystal before and after 10 keV He^+ ion irradiation up to 1 x 10^{20} ions/m^2 were observed by ion channeling method.

4-08 Effects of Hydrogen and Hydroxyl on Ion Beam Induced Luminescence of Ceramics

S. Nagata[a)], S. Yamamoto[b)], A.Inouye[a)], B. Tsuchiya[a)], K. Toh[a)], K.Takano[b)], M. Yoshikawa[b)] and T. Shikama[a)]

[a)]Institute for Materials Research, Tohoku University,
[b)]Environment and Industrial Materials Research Division, QuBS, JAEA

The in-situ luminescence measurements during ion bombardment are powerful methods to measure dynamic process involved damage creation and relaxation in ceramics. Previously we reported that the 2.7 eV luminescence corresponding to the $B_{2\alpha}$ oxygen deficiency centers was more intense in silica glasses containing less OH under H and He ion irradiation[1)]. In the present experiment, we examined relation between $B_{2\alpha}$ centers and non-bridging oxygen hole center (NBOHC) in connection with the formation of E′ centers.

Samples of SiO_2 glasses studied were commercially available fused and synthesized silica glasses having different OH concentration, produced by Toshiba Ceramics, Co. Ltd., with a size of 10 mm x 10 mm and a thickness of 0.5 mm. A beam of 1MeV H ions was incident on the sample to a fluence of about 1 x 10^{17} H/cm^2, with a flux density of about 10^{13} ions/cm^2. The ion induced luminescence was transmitted by optical fibers inserted in the vacuum chamber or by an optical window, and was detected using a monochrometer equipped with a CCD camera. Absorption spectra were measured after the ion irradiation, with a spectral range of 200-800 nm.

Normalized intensities of 2.7 and 1.9 eV luminescence form low-OH (1 ppm) and high-OH (800 ppm) silica glasses are shown in Fig. 1, plotted against the incident 1 MeV H ion fluence. The intensity of 2.7 eV luminescence increased with increasing the H ion dose to 10^{17} H ions/cm^2. Dose dependence behavior of the 2.7 eV luminescence was similar for both silica glasses, while the higher intensity was observed for the low-OH silica.

In contrast to the fluence dependence of the 2.7 eV luminescence, the 1.9 eV luminescence corresponding to NBOHCs in high-OH silica saturated at a dose about 1x10^{15} H ions/cm^2.

The 5.1 eV absorption corresponding to the $B_{2\alpha}$ band, was very weak for low-OH silica and almost absence for high-OH silica, while the intense 2.7 eV luminescence was observed by excitation of the ion beam and 5 eV photon. This suggests that the 2.7 eV luminescence is a quite sensitive probe to detect a $B_{2\alpha}$ center. The absorption intensity of E′ centers (5.4 and 5.8 eV absorption corresponding to E'_{β}, and E'_{γ} centers, respectively) was higher for high-OH silica, below 1x10^{16} H/cm^2. Also, the intensity of the 4.8 eV absorption was higher for high-OH silica, as well as 1.9 eV luminescence. The 4.8 eV absoption is known to be assigned to a NBOHC or a Peroxy radical (POR). Thus the paramagnetic oxygen deficient or excess defects were more effectively created in high-OH silica, while non-magnetic $B_{2\alpha}$ centers were created in low-OH silica glasses. In contrast to the ion irradiation, absorption intensity due to E′ centers and NBOHCs became much smaller in silica glasses containing more OH, in case of Gamma-ray irradiation[2)]. The larger optical absorption in high-OH silica in the present results can be attributed to the effective ion-induced dissociation of OH and transformation of $B_{2\alpha}$ centers to paramagnetic E′ centers.

References
1) S. Nagata, S. Yamamoto, K. Toh, B. Tsuchiya, T. Shikama, J. Nucl. Mater. 329-333 (2004)1507-1510.
2) Y. Kawaguchi, N. Kuzuu, J. Appl. Phys. 80 (1996)5633-5638

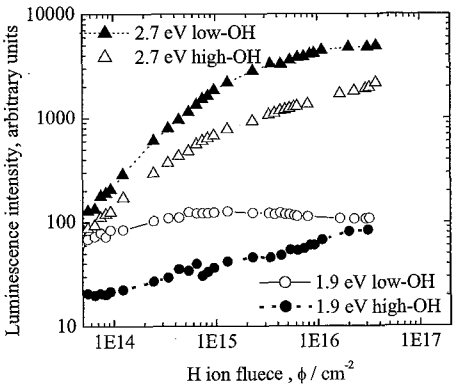


Fig.1. Fluence dependence of the intensity of 2.7 and 1.9 eV luminescence from low-OH (1 ppm) and high-OH (800 ppm) silica glasses under 1 MeV H ion irradiation.

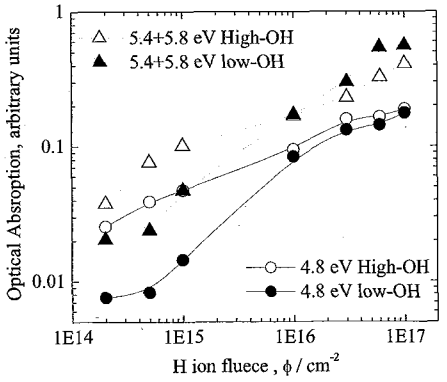


Fig.2. Fluence dependence of peak absorption intensity for low-OH (1 ppm) and high-OH (800 ppm) silica glasses by 1 MeV H ion irradiation.

4-09 Spectroscopic Analysis of Si Bombarded with C_{60} Ions

H. Naramoto[a)], S. Sakai[a)], K. Narumi[a)], V. Lavrentiev[a)], Y. Maeda[a,b)], K. Takahiro[c)], K. Kawatsura[c)], S. Nishibe[c)], N. Hasuike[c)], H. Harima[c)], Y. Baba[d)], S. Yamamoto[d)], N. Hirao[e)] and H. Kudo[f)]

[a)]Advanced Science Research Center, JAEA, [b)]Graduate School of Energy Science, Kyoto University, [c)]Graduate School of Science & Technology, Kyoto Institute of Technology; [d)]Quantum Beam Science Directorate, JAEA, [e)]Nuclear Engineering, Ltd.; [f)]Graduate School of Pure & Applied Sciences, University of Tsukuba

Abstract

Surface-sensitive analysis was performed on Si(100) bombarded with 10-100keV C_{60} ions by employing Resonant Raman spectroscopy(RSS), Rutherford backscattering spectrometry(RBS) and X-ray Photo electron Spectroscopy(XPS). RSS with 266nm laser reveals the evidence of dynamic competition between amorphization and recrystallization during C_{60} ion bombardments, and the size of recrystallized nano-crystallites can be controlled by changing the C_{60} ion dose. XPS analysis suggests the possible formation of some Si carbide at deeper region. Co atoms implanted into C_{60} film were pushed into rather deeper region by annealing (300-570K), and the activation energy for Co diffusion was estimated to be 0.74eV with RBS analysis.

C_{60}と遷移金属元素の混合物では、電子の授受による結合形成と歪誘起による結合解除の相反する過程が競合して、様々な新しいナノ構造物質が形成される [1, 2]。この場合、C_{60}の同素体変換 [3]や分子鋳型の素材の C_{60} の選択的除去など、エネルギービームを利用した物質処理 [4]が重要な役割を果たす。我々は、混合物構成要素の C_{60} を入射イオンにして、分子構造が崩壊する近傍のエネルギー領域での衝撃効果を、結晶性の Si 及び C_{60} を標的にして調べてきた。

本報告では、10-100keV の C_{60}^+を Si 結晶に照射した場合の表面構造・状態の変化を、共鳴ラマン分光法、イオンチャネリング法及光電子分光法により調べた結果を記す。また、イオン注入法を利用した C_{60} 薄膜中の Co の拡散の活性化エネルギーの評価法についても言及する。

数 10keV の C_{60}^+等を Si(100)標的に RT 近傍で照射した。Si 表面近傍の結晶性評価には、2MeVHe$^+$イオンの<100>軸チャネリング効果を用い、結合状態の解析のために共鳴ラマン分光装置（京都工芸繊維大）及び放射光利用光電子分光装置（KEK/PF/BL27A）を利用した。Co を注入した C_{60} 薄膜の拡散挙動の解析には、2MeVHe$^+$イオンに RBS 法を用いた。

C_{60}^+イオンをSi(100)に照射した場合：数10keVC_{60}^+を照射した試料に対して、散乱角を105度に設定してチャネリング実験を行い、20keVC_{60}^+イオン照射により誘起される結晶格子の乱れは$5\times10^{13}C_{60}/cm^2$程度の照射量で飽和する事を確認した。更に波長の異なる紫外光領域のレーザー（266、364nm）を入射して、共鳴ラマン測定を行った。その結果、Fig. 1 に示す様に、表面数nm近傍の変化に敏感な266nm光を用いることにより、照射量により敏感に変化する照射効果を検出できた。Fig. 2は、ラマンピーク位置のシフトと幅の拡がりから、残存するSiナノ結晶のサイズと照射量との関係を評価したものである。照射により残存する結晶領域は急激に減少して8nm程度のサイズまで減少するが、それ以降はほぼ照射量に比例して、徐々にで平衡に達することが理解される。つまり、単一イオン照射の場合と異なり、C_{60}^+イオン照射では、高温照射の場合に似て、結晶化も起こる事を示している。一方PF27Aでの光電子分光実験からは、Si-Cの結合状態を示唆する結果が得られた。

Co$^+$イオンをC_{60}薄膜結晶に照射した場合：注入したCoをマーカーにしてRBS法でCoの拡散挙動を調べた。その結果、活性化エネルギーとして0.74eVを持ち、300-570Kの温度領域で、Co原子はより深部へと移動することを見出した。

References

1) S. Sakai et al., Mater. Trans. 46 (2005)765.
2) V. I. Lavrentiev et al., Chem. Phys. Lett. 424 (2006) 101.
3) K. Narumi et al., Fullerenes, Nanotubes and Carbon Nanostructures 14 (2006) 429.
4)H. Naramoto et al., Phys. Sol. St. 44 (2002) 668.

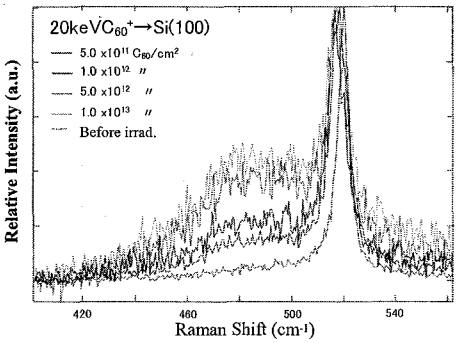


Fig. 1: UV resonant Raman spectra for Si irradiated with 20keV C_{60} at the different doses. The 266nm light was employed.

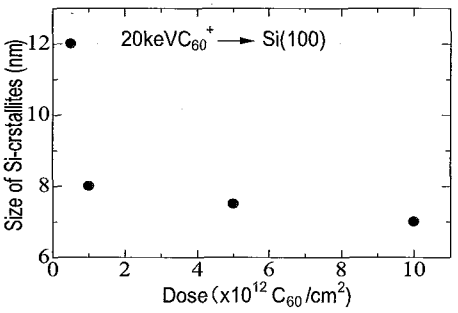


Fig. 2: Size change of Si-crystallites in amorphized layer as a function of 20keV C_{60}^+ fluence.

4-10 Raman Analysis of Damage of C_{60} Thin Films by Fast Ion Bombardment

K. Narumi [a], S. Sakai [a], H. Naramoto [a] and Y. Maeda [a, b]
[a]Advanced Science Research Center, JAEA, [b]Graduate School of Energy Science, Kyoto University

Abstract

Damage of C_{60} thin films irradiated with 380-keV H^+, 7-MeV C^{2+}, 360-keV Ar^+, and 2.1-MeV Ar^{6+} has been analyzed with Raman spectroscopy. Damage cross sections have been estimated by analysis of fluence dependence of the peak-intensity ratio of the $A_g(2)$ mode. The dependence of the cross section on the stopping power of C_{60} indicates that the damage of the molecule is dominated by nuclear collisions. Temperature dependence of the $A_g(2)$ mode of irradiated films shows that the broadening of the $A_g(2)$ mode with increasing fluence is not due to the polymerization of the C_{60} molecules.

C_{60}固体に対するイオン照射効果は、高速のイオンを照射した時に、個々のC_{60}分子がどうなるのか、さらに、その分子の配置はどうなるのか、といった興味の下、研究が行われ、これまでの報告では、イオン照射によってC_{60}分子が壊れ、最終的にはC_{60}固体が非晶質炭素になることがわかっている。[1,2] また、C_{60}分子の破壊と並行してC_{60}ポリマーが生成すると考えられてきた。[3] 本研究では、ラマン分光法による解析結果に基づいて、依然議論の余地が残っていると考えられるC_{60}分子の損傷機構（原子核との衝突、電子励起のどちらが主な過程か）について議論するとともに、イオン照射によるポリマー化について検証した。

Si(100)、(111)基板上に真空蒸着法によって作製したC_{60}薄膜に対して、室温で380 keV H^+、7 MeV C^{2+}、360 keV Ar^+、2.1 MeV Ar^{6+}イオンを照射した。照射量は、イオン種・エネルギーに応じて1×10^{12} /cm^{2}から7×10^{16} /cm^{2}の範囲で選択した。また、それぞれの場合において、入射イオンの飛程に比べてC_{60}薄膜の厚さを十分薄くしたので、ほとんどの入射イオンが薄膜を透過でき、薄膜中にとどまる入射イオンの効果は無視できる。イオン照射後、薄膜をラマン分光法で評価した。ラマン分光測定は、Ar^+レーザーからの波長488 nmの光を励起光として用いた。

C_{60}薄膜のラマンスペクトルの照射量依存について、照射量に対する$A_g(2)$モードのピーク収量の変化より、C_{60}分子の損傷断面積を求めた。この損傷断面積と核的阻止能S_n、電子的阻止能S_eとの関係をプロットした結果をFig. 1に示す。図中実線は、損傷断面積とS_nの関係を最小自乗法でフィットした結果を表し、$S_n^{1.1}$に比例する直線である。一方、S_eについてはS_nほど明確な依存性が認められず、特に380 keV H^+の場合を除くと、S_eが断面積にほぼ依存しないという結果が得られた。これらの結果より、本研究で照射したイオン種・エネルギーの場合、C_{60}分子の損傷断面積は核的阻止能と強い相関を持ち、このことはC_{60}分子の損傷が主に原子核との衝突によることを示唆するものと考えられる。

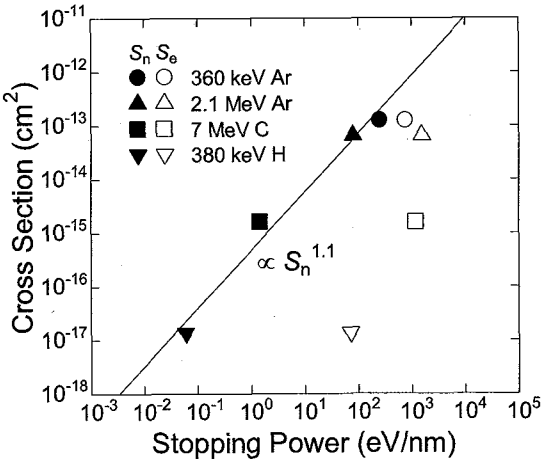


Fig. 1 Dependence of the damage cross section on both the nuclear stopping power S_n and the electronic stopping power S_e. The solid line was obtained with the least-squares method.

Fig. 2に7 MeV C^{2+}を5×10^{14} /cm^{2}照射した試料のラマンスペクトルの温度依存を示す。測定は真空中で行った。この照射量の領域では、照射量の増大に伴って$A_g(2)$モードの低波数成分の増大が観測され、イオン照射によるポリマー化に由来するものと考えられてきた。[3] C_{60}ポリマーは~180°Cで分解し、$A_g(2)$モードの低波数成分が消失するが、Fig. 2の結果は、この温度を越えても、$A_g(2)$モードの低波数成分が消失しないことを示している。従って、従来ポリマー化によると考えられていたイオン照射による$A_g(2)$モードの形の変化は、ポリマー化によるものではなく、損傷を受けたC_{60}のラマンスペクトルを反映しているものだと考えられる。

References

1) R.G. Musket, R.A. Hawley-Fedder, W.L. Bell, Radiat. Eff. Defects **118** (1991) 225.
2) S. Prawer, K.W. Nugent, S. Biggs, D.G. McCulloch, W.H. Leong, A. Hoffman, R. Kalish, Phys. Rev. B **52** (1995) 841.
3) J. Kastner, H. Kuzmany and L. Palmetshofer, Appl. Phys. Lett. **65**, 543 (1994).

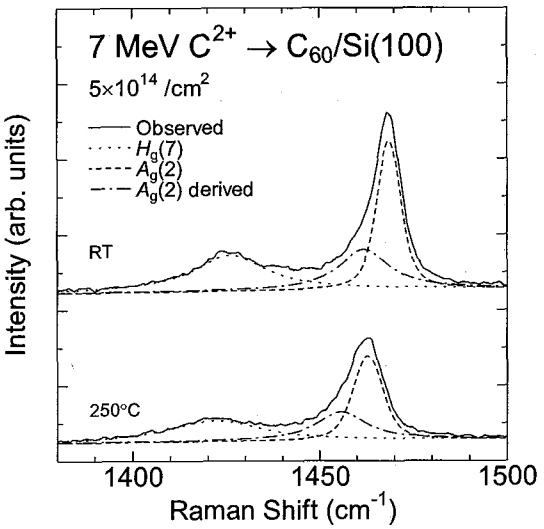


Fig. 2 Raman spectra measured at room temperature (RT) and 250°C for C_{60} films irradiated with 7-MeV C^{2+}, 5.0×10^{14} /cm^2. The broken lines correspond to Voigt-line-fit analyses assuming three components, $Hg(7)$, $Ag(2)$ and a $Ag(2)$-derived lower-frequency component.

4-11 Chemical State Analysis of Vacancy-Impurity Complexes by Positron Annihilation Spectroscopy

M. Fujinami[a)], K. Oguma[a)], T. Akahane[b)], A. Kawasuso[c)] and M. Maekawa[c)]

[a)]Chiba University, Dept. of Applied Chemistry, [b)]NIMS, [c)]Advanced Science Research Center, JAEA

Abstract

Positron annihilation spectroscopy (PAS) is a sensitive probe for studying the electronic structure of defects in solids. Transition-metal contaminants are ubiquitous in Si devices and gettering has proved very effective to trap the contaminants. PAS is applied to analyze the defects and their coupled elements simultaneously. A Cz-Si wafer was implanted 3 MeV Si ions (dose: 1E14 /cm^2) and the Cu ion implantation was done into the back side (200 keV, 1E14 /cm^2). Subsequently the samples were annealed under nitrogen atmosphere at various temperatures for 1 hour to realize the Cu diffusion. A high intensity at the high-momentum part in annihilated γ-rays is recognized in the sample annealed at 600°C and the profile is very similar to that for the bulk Cu. According to SIMS, 85% of the implanted Cu atoms are accumulated in the Si^+ implanted region. It is directly proved that the vacancy clusters trap Cu atoms. An annealing at 700°C, the trapped Cu are released and oxygen atoms are coupled with vacancy clusters.

半導体デバイスが緻密化するにつれ工程で混入する遷移金属汚染の除去が問題になる。そこでデバイス領域外に不純物金属を効果的にゲッタリングする最適な欠陥の探求が盛んである。従来の測定法では欠陥と不純物金属との相互作用の直接的な証拠は得られず，ましてやTEMで観察できない微小空孔（数個以下）との相互作用も不明のままであった。陽電子消滅法は空孔を検出しその化学状態の情報を与え，局所分析も可能である。そこで，本研究では陽電子消滅法によりSi中の銅と空孔の相互作用を調べることを目的とした。

CZ-Si(100)ウエハのミラー面に自己Si^+イオンを3 MeV，1×10^{14} /cm^2，室温にて注入した。Si^+の平均注入深さは2.4 μmであり，注入層は非晶質化してはいない。次に裏面にCu^+イオンを200 keV，1×10^{14} /cm^2，室温にて注入した。その後，窒素中でから800℃の範囲で1時間アニールした。

Cu^+イオンを注入した試料裏面の$S-E$カーブおよびCoincidence Doppler broadening(CDB)測定から，400℃程度から空孔とCuの複合体が形成し，500℃でその強度が増加することがわかった。またSも高い値を示し，空孔を含んでいる。600℃のアニールにより，CDBの比率曲線は無処理のSiとほぼ同一となり，空孔－Cu複合体は解離して空孔も消滅した。自己イオンを注入したSiミラー面において，裏面にCuを注入した試料としていない試料とを比較した。500℃までは両者に変化はなく，S値が単調に増大しており空孔のクラスター化が起こっていた。600℃で両者に大きな差が観測された。Fig. 1にCDB比率曲線を示す。Cu未注入ではCDB比率曲線の高運動量成分には何ら変化がみられないが，Cu注入試料では高運動量成分にCu特有の構造が確認された。SIMSの結果(Fig.2)は注入したCuの85%が自己イオン注入領域に濃縮されることを示した。CDBの結果は，裏面で解離したCuが解離・拡散しミラー面近傍の空孔クラスターに捕獲されている様子を陽電子により初めて直接観察することができたと言える。一方で700℃ではSIMSではCuは測定されず，CDB比率曲線もCu未注入試料と同じく空孔－O複合体の生成が帰属された。600℃では空孔はCuと結合したが，700℃ではOと結合し安定化すると考えられる。他の報告[1,2]では700℃で10個程度の空孔クラスターとCu複合体の形成が報告されている。この不一致は，ゲッタ能が空孔サイズに依存していることを示唆していると考えている。

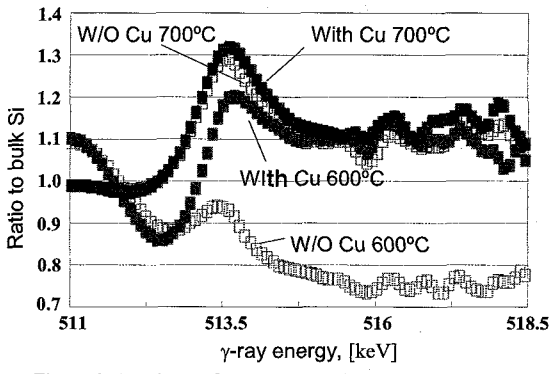


Fig. 1 Coincidence Doppler broadening ratio curves for the annealed samples

一方で同様の実験をNiについても実施した。Niの注入面でのCDB測定においても，ミラー面においても空孔－Ni複合体の形成は認められなかった。SIMS測定によれば注入したNiの20%程度はミラー面の注入領域に捕獲されていることが示されたが，必ずしも空孔に捕獲されているわけでない。これらのCuとNiの違いが何に起因しているのかは未解明である。

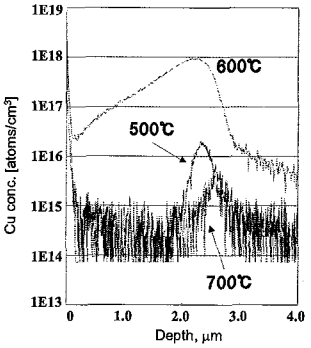


Fig. 2 Cu profiles for the sample annealed by SIMS measurement.

以上，本法によりゲッタリングにおける空孔－不純物複合体の直接検出に成功し，CuとNiの違いについても明確に示すことができた。

References

1) R. Krause-Rehberg *et al.*, "Impurity gettering by vacancy-type defects in high-energy ion-implanted silicon at R_p/2", Appl. Phys. Lett. 77, 3932 (2000)

2) R. Krause-Rehberg *et al.*, "Improved defect profiling with slow positrons", Appl. Surf. Sci., 194, 210 (2002).

4-12 Characterization of Ion Beam-Induced Quantum Structures Using a Slow Positron Beam

M. Maekawa, R. S. Yu and A. Kawasuso

Advanced Science Research Center, JAEA

Abstract

Effects of oxygen ion implantation into silicon carbide (SiC) have been examined using slow positron beam to investigate the formation mechanics of a two-dimensional quantum structure. The Doppler broadening of annihilation radiation and positron lifetime measurements showed that radiation defects were removed and a SiO_2 layer was formed by post-implantation annealing at 1400°C. An interface layer, which resembles that of the SiO_2/SiC produced by conventional thermal oxidation, was also found.

一定領域への高濃度イオン注入により照射イオンの析出や空孔クラスタリングが起った場合、量子井戸、量子ドット、ナノキャビティなどの量子構造が形成される。我々はこのような材料に対し、空孔型欠陥や異種原子クラスターの存在に敏感な陽電子消滅法を適用し、イオンビーム誘起量子構造の形成消滅メカニズムの解明を目指している。

今年度は、まず2次元量子井戸構造として、炭化ケイ素(SiC)への酸素イオン打ち込みによる埋め込み酸化膜に着目した。このようなSiCウエハは実用応用面でも高性能デバイス用ウエハとして研究が進められている。酸素イオン打ち込み法はSiプロセスで実績のある手法であり、SiCへも適用可能なことが報告されているが[1]、形成された埋め込みSiO_2膜や表層SiC層の照射損傷についてまだ十分に調べられているとはいえない。そこで陽電子消滅法を適用し、埋め込み酸化層や界面近傍の欠陥評価を試みた。

試料は、n型4H-SiC(0001)基板に200 keVの酸素イオンを打ち込んで作製した。期待される埋め込みSiO_2膜の形成領域は表面から200～400 nmの領域であり、対応する陽電子の打ち込みエネルギーは4～7 keVであった。照射量は1×10^{18}cm^{-2}とし、照射損傷の残留を避けるため600℃の高温注入とした。照射後、アルゴン雰囲気中で1400℃の熱アニールを施した。この試料に対し、エネルギー可変低速陽電子ビームによる運動量分布測定（Sパラメータ、Wパラメータ測定）及び陽電子消滅寿命測定を行った。

照射直後においては、酸素注入領域においてSパラメータが上昇し、多数の空孔型欠陥が存在することが明らかとなった。特に3keV付近の表面近傍領域でのSパラメータの上昇が著しく、イオン照射により大きな欠陥が生成していると思われる。酸素イオン打ち込み領域(7keV付近)のS、Wパラメータは、バルクSiO_2の値(S:1.13、W:0.95)[2]とは異なっており、酸化膜の形成は不十分であると思われる。しかし照射後の熱アニールによって3～6 keVでのS及びWパラメータはバルクSiO_2の値とほぼ同じ値にまで変化した。これは埋め込み酸化膜層の形成を示している。陽電子消滅寿命測定からは、およそ1.4nsという特徴的に長い寿命成分が測定された。これは、バルクSiO_2のポーラス構造でのオルソポジトロニウム消滅由来の成分(1.6ns)に相当すると考えられる。これらより、形成した埋め込み酸化膜はバルクSiO_2同様のアモルファス構造を持っていることが推測される。しかし、バルクSiO_2と比較すると寿命がやや短いことから、依然欠陥を含んでいるものと推測される。

陽電子打ち込みエネルギーが7keVより深い領域ではWパラメータは上昇する。これは熱アニールにより、陽電子が酸素の価電子と消滅する確率が増加したことを示している[2]。これより、埋め込み酸化膜層とSiC基板の間には、熱酸化SiO_2/SiC界面同様の酸素ダングリングボンドを伴ったSiO_2/SiC界面中間層が形成されていると思われる[2]。この

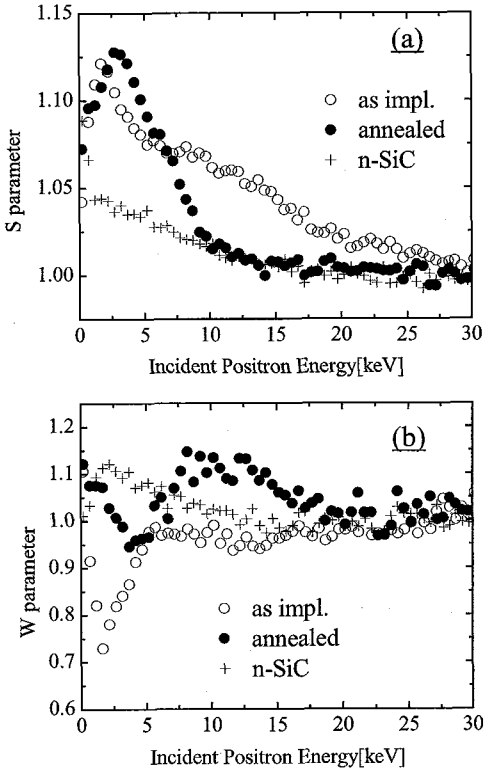


Fig. 1 (a) S parameter and (b) W parameter for the virgin SiC, as-implanted SiC and implanted SiC after annealing at 1400 °C. The implantation dose is 1.0×10^{18} cm^{-2}. Both S and W parameters are normalized to the average values of bulk SiC at high energy regions (E>20 keV).

SiO_2/SiC界面領域での寿命は391psとなり、熱酸化SiO_2/SiC界面の値(451ps)に相当するものとなった。

以上より、酸素イオン打ち込み法によりSiC中に埋め込み酸化膜が形成されることがわかった。また、酸化膜と基板SiCの間には欠陥を伴った界面中間層が発生することが明らかとなった。陽電子消滅法は材料中に形成される酸化膜や界面などの薄膜2次元構造の検出と特性評価に有効であることが確認された。

References

1) N. P. Barradas, C. Jeynes and S. M. Jackson, Nucl. Inst. Methods **B136-138**, 1168 (1998).

2) M. Maekawa, A. Kawasuso, M. Yoshikawa, A. Miyashita, R. Suzuki and T. Ohdaira, Phys. Rev. **B73**, 014111 (2006).

4-13 Analysis of Light Elements in Carbon Materials

Y. Horino[a)], Y. Mokuno[a)], A. Chayahara[a)], H. Yasui[b)], K. Awazu[b)],
S. Yamamoto[c)], K. Narumi[d)] and H. Naramoto[d)]

[a)] National Institute of Advanced Industrial Science and Technology, [b)] Industrial Research Institute of Ishikawa, [c)] Environment and Industrial Materials Research Division, QuBS, JAEA,
[d)] Advanced Science Research Center, JAEA

Abstract

Carbon materials are well known for their excellent properties and many applications are being under intense study. The plasma enhanced chemical vapor deposition (PECVD) using hydrocarbon gas is the most used method to synthesize carbon materials. So hydrogen will be involved during processing and they will influence properties of carbon materials. In order to investigate the influences, we examine the distribution of hydrogen at near surface region in some carbon materials by a nuclear reaction analysis (NRA). The preliminary study indicates that the contamination from residual gases in the vacuum system prevented us from obtaining right information. So we have reformed the vacuum system to avoid surface contamination. We have checked the system by using hydrogen implanted silicon wafer. We could obtain a profile of the implanted hydrogen which was consistent in calculated one by the TRIM code.

DLC(diamond like carbon)やダイヤモンドなどの炭素系薄膜材料は、通常炭化水素系のガスを用いた気相合成で作製されるため[1)]、水素が含有され、材料特性に関係があることが分かってきた。そのため、水素の量・分布を評価することは炭素系新奇材料の創製に不可欠なものと考えられる。しかし、水素の分析は、特に数十 ppm オーダーの微量の定量分析は非常に困難で、水素の材料特性に対する影響の詳細な研究は行われていないのが現状である。

本研究では、炭素系材料に対する水素の影響を検証するために、炭素系薄膜材料中の水素分布を定量的に測定し、材料特性との関連を調べることを目的とする。そのため、エネルギー6～8MeV の ^{15}N（窒素同位体）と水素との共鳴核反応法（NRA）を利用した。水素分布を定量的に測定し、本方法の定量下限や深さ分解能を評価する。また、水素の吸着量や深さ分布と材料特性との関連を明らかにする。

測定に用いた共鳴核反応は、$^{1}H(^{15}N, \alpha\gamma)^{12}C$ で、共鳴エネルギー（E_R）=6.385MeV、共鳴幅＝1.8keV である。Fig.1 に示すように、エネルギーE_0で入射したプローブイオン（^{15}N）が試料中でエネルギーを失いながら進行し、エネルギーがE_Rになると水素との核反応が起こり、約 4.4MeV のガンマ線が放出される。エネルギー損失量が水素の存在する深さ、検出されるガンマ線が水素量の情報を有し、プローブイオンのエネルギーをスキャンすることで深さ方向の水素分布を得ることができる。共鳴幅が非常に狭いため、深さの分解能は主に ^{15}N イオンのエネルギー拡がりで決まり、今回は約 5nm であった。この方法により各種炭素材料の水素分布測定を行った。これまでの分析の結果、分析チャンバーの真空度が良くないと、残留ガスからの表面吸着などにより測定結果に影響があることが分かった。そのため、チャンバーの改良による超高真空環境を実現し、その後分析を進めた。

Fig.2 に、Si ウェハに 2keV H イオンを 5×10^{15}ions/cm^2 注入したもの（■）、多結晶ダイヤモンド（▲）、およびダイヤモンド単結晶（○）を分析した結果を示す。いずれの場合も約 6.49MeV 近傍にピークが観察された。これらは材料表面に吸着している水素に相当する。このピーク幅は、真空度が悪かった場合と比較して、約 1/2 になった。図中のエネルギーは使用した加速器の表示をそのまま用いている。そのため実際のエネルギーより数 10keV 程度のずれがある。この場合、6.49MeV 付近が試料表層、約 6.52MeV 以上が試料内部に相当する。

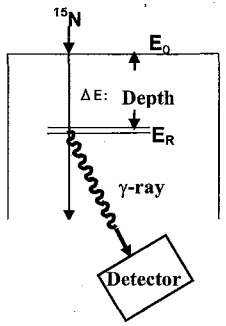


Fig.1 Illustration of the measurement

Si の場合、表面と注入の分布が明瞭に分かり、TRIM で計算した飛程 44nm とほぼ一致した。多結晶ダイヤモンドの場合、内部の水素量は約 0.2at%であるが、ダイヤモンド単結晶の場合、表面のピーク以外は、S/N 比による測定限界以下であるため、正しい量は不明である。今後、定量限界等を明らかにする。

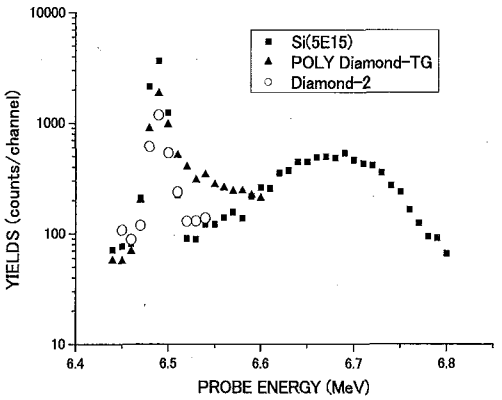


Fig.2 Hydrogen profiles measured by the NRA. The samples were silicon wafer implanted by 2keV H with a dose of 5×10^{15}ions/cm^2 (■), polycrystalline diamond (▲) and single-crystalline diamond (○).

References

1) Y. Mokuno, A. Chayahara, Y. Soda, Y. Horino and N. Fujimori, Diamond and Related Materials **14**, 1743 (2005).

4-14 Radiation-Induced Luminescence from TiO_2 by Ion Irradiations

S. Kitazawa[a], S. Yamamoto[b], M. Asano[b], Y. Saitoh[c] and S. Ishiyama[d]
[a]Division of Fuels and Materials Engineering, NSED, JAEA, [b] Environment and Industrial Materials Research Division, QuBS, JAEA, [c] Department of Advanced Radiation Technology, TARRI, JAEA, [d] JST

Abstract

Radiation-induced luminescence (RIL) produced by ion irradiations at room temperature has been used to study photon emission from titanium dioxide (TiO_2) targets. The kinetic energies of ions were from 10 to 30 keV. The targets were produced by the methods; sol-gel, direct oxidation, anodic oxidation and pulsed laser deposition. The atomic lines from titanium and oxygen, visible bands at 2.0 and 2.6 eV due crystalline defects, and a UV band at 3.9 eV from transitions in crystal were observed in the UV-visible spectra. The bands which were fitted by three Lorentz curves were analysed to investigate the excitation mechanism of RIL. The dependences of the irradiation ion species and projectile energies, and the target conditions were investigated. This study indicates the potential of titanium dioxide as a radiocatalyst.

酸化チタン(IV) (TiO_2) は、光機能物質として、広く研究・開発され、多くの分野で実用化されている。特に、光触媒としては、太陽光で作用するために、非常に大きな実用性の可能性がある。また、高速のイオンが衝突したときに蛍光すれば、その蛍光により光触媒性が発現する可能性がある。これは、月面に多く存在するチタンを用いた湿式太陽電池や放射性廃棄物の再利用化などの放射線触媒研究への糸口にもなる。

イオン照射励起ルミネッセンス(RIL)測定は、原研高崎TIARA内のECRイオン源を用いて行った。実験装置の概略図をFig. 1に示す。イオン源から、イオンが引き出され、90度磁石で電荷・質量分析され、トランスポート系を通り衝突真空槽に導かれる。ビームラインのベース圧力は、10^{-5} Paであった。イオン源からターゲットの距離は約3mであった。これは、10keVで酸素イオンを引き出したときには、およそ10^{-5}秒で通過する距離である。これ以上短い寿命のイオン源内で生成した準安定状態のイオンは、ターゲット上には飛んでこないことになる。イオン種は、酸素、窒素とアルゴンを用いた。イオン電流強度は、基板上で10～20マイクロアンペア程度であった。ビームの形状は、ターゲット上で、5x10mm程度の楕円形だが、それ以上に広がる成分もあった。ターゲットは、１辺が２cmの８角形のアルミニウム製リボルバー型のホルダーに取り付けた。RILは、標的から４５度、約３０cm離れたところに、レンズを用いてファイバー入力に集光した。真空槽と大気の間には、溶融石英のビューポートが有り２５０nm以下の波長では、透過がほとんどない。分光システムは、Czerny-Turner型の分光器に、光ファイバーを用いたもので、分解能は、2nm以下である。試料の酸化チタンTiO_2は、ルチル単結晶の他に、ゾル・ゲル法、直接酸化法、陽極酸化法、パルスレーザー蒸着法などの方法で作製した試料を用いた。

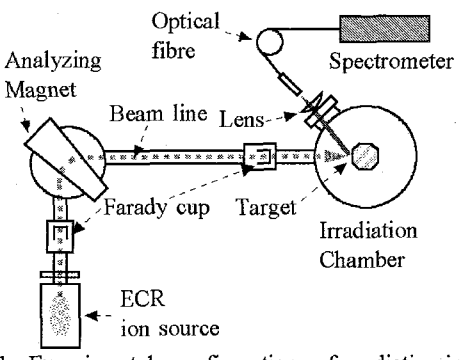


Fig. 1 Experimental configuration of radiation-induced luminescence (RIL) system of optical emission spectroscopy by highly charged ion irradiations.

N^+を10keVで加速し、ゾル・ゲル法と直接酸化法で作製した標的試料に照射したときのスペクトルは、Fig. 2のようになった。それぞれの強度は、スペクトル全体の積分した値で規格化している。スペクトル中には、数多くの鋭いピークを持つラインと、広いバンドの２種類が現れた。ラインは、Tiおよび0原子からの蛍光で、良く知られている値によりアサインすることが出来、図中の分光記号で記してある[1]。バンドは、３つ観測され、3.8eV付近のものはTiO_2結晶の格子間遷移で、2.0と2.6eV付近のものはともに格子欠陥によると考えられる。ラインは、固体内またはスパッタされた原子からの蛍光であり、標的試料の状態にはほとんど依存性がない。これに対して、バンドは二酸化チタン結晶内の発光機構を反映している。すなわち、バンドを分解して、その幅や高さなどを比較することにより、蛍光のメカニズムを知ることができる。ここで、入射粒子のエネルギー（10～30keV）や様々なイオン種（O, N, Ar）、また標的試料を作製方法の違いにより様々な状態で実験を行った[2]。

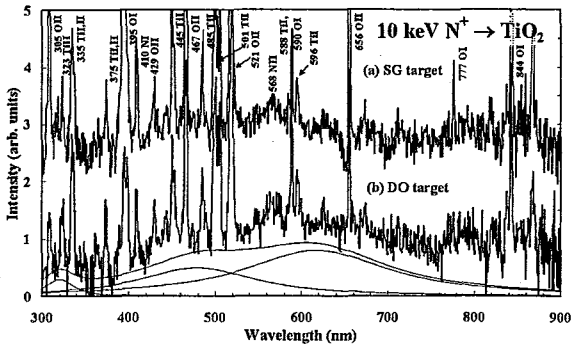


Fig.2 RIL spectra from TiO_2 targets by 10 keV N^+. The targets were produced by sol-gel (SG) derived method (a) and direct oxidation (DO) method (b). The dotted lines are four fitted Lorentz curves, and the solid line is their sum

References

1) Sin-iti. Kitazawa, Shunya Yamamoto, Masaharu Asano, Yuichi Saitoh, Shintaro Ishiyama, "Radiation-induced luminescence from sol-gel anatase TiO_2 by 10 keV O^+ irradiation", Nucl. Instrum. Methods Phys. Res. B, 232, 94-97 (2005).

2) Sin-iti. Kitazawa, Shunya Yamamoto, Masaharu Asano, Yuichi Saitoh, Shintaro Ishiyama, "Radiation-induced luminescence from TiO_2 by 10, 20 and 30 keV oxygen ion irradiations", Nucl. Instrum. Methods Phys. Res. B. *accepted*.

4-15 Disorder Analysis of Laser Crystal Surfaces Irradiated by a Neutral Argon Beam

A. Sugiyama[a)], S. Yamamoto[b)] and K. Takano[b)]

[a)] Advanced Photon Research Center, QuBS, JAEA,
[b)] Environment and Industrial Materials Research Division, QuBS, JAEA

Heat resistive and multifunctional optical elements have been expected to improve the laser performance of solid-state lasers. To create those kinds of element, we have been studied the bonding method of laser crystals[1-3]. In the series of bonding developments, we recently started to use new method called SAB[4] (Surface Activation Bonding). In this method, a neutral argon beam is used for the cleaning and creating dangling bonds on the surfaces in the initial step. After contacting the surfaces, a heat treatment is applied to enforce the bonding strength. To study morphological surface change caused in these processes, disorder and heat-recovery analyses of the surface were carried out by means of XPS (X-ray Photo Spectroscopy) and RBS (Rutherford Backscattering Spectrometry) methods in TIARA.

Thin α-sapphire substrates of 300 μ m in thickness were irradiated by the neutral argon beam. The process has four different parameters of a discharge voltage, a discharge current, an irradiated time, and an irradiated angle to the specimen. To clear the influence by these parameters, first, the discharge voltage was changed in a range of 0.6 to 2 keV under the condition that holds the same etching amount of 30 nm. In the second, the irradiated angle was varied from 9 to 37 degree with the fixed parameters of 2 keV, 200 mA, and 10 min. In addition, we made heat treatment for the samples at different temperature from 723 to 1723 K.

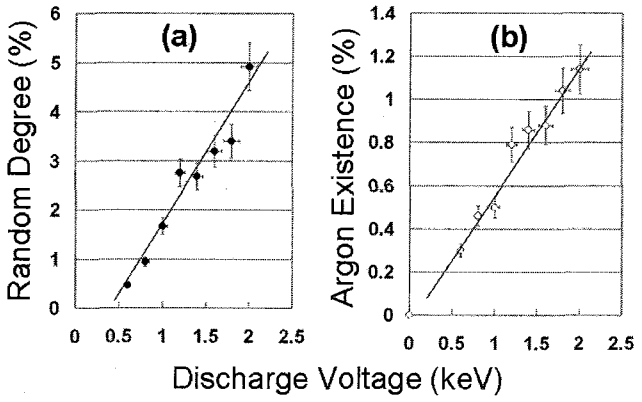


Fig. 1 Random degree of crystal and argon existence in the irradiated surfaces as a function of discharge voltage: (a) by RBS measurements; (b) by XPS measurements.

Random degree of the crystal surface was calculated from the measured values of Al (1.10MeV) spectra in two different alignment configurations of the probe $^4He^+$ beam generated from a single-ended accelerator. Argon existence also shown in Fig. 1 was estimated from the spectra of Al(2p), O(1s), Ar(2p). In this XPS method, the probe depth is assumed to around 2.5 nm. The same upward tendency shown in Fig. 1 appeared in another measurement for incident angle variation of the argon beam. This measurement indicates that around 10 degree incident beam may be adequate for the reduction of surface damage. On the other hand, RBS measurements of heat-treated samples showed that disordered crystal lattice starts recovering with an increase of heat treatment temperature. Argon existence was also reduced to the marginal detection when the sample was heated at 1537 K. Fig. 2 shows the morphological surface changes observed by AFM (Atomic Force Microscope). With these basic results, we will optimize the argon beam parameters required for minimum surface damage which brings about the good laser crystal bonding.

References

1) A. Sugiyama et al., Jpn. Weld. Soc. 75 (2006) 9.
2) A. Sugiyama et al., Appl. Opt. 37 (1998) 2407.
3) A. Sugiyama et al., Ceramics Int. 31 (2005) 1085.
4) T. Suga, Mater. Jpn. 35 (1996) 496.

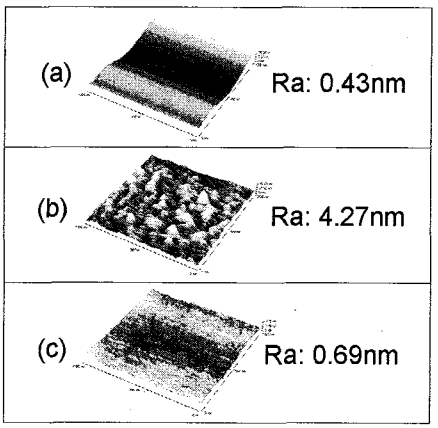


Fig. 2 Morphological change observed by AFM: (a) before irradiation; (b) after irradiation; (c) after heat treatment at 1573 K for 10 hr. Each viewing area was 1x 1 μ m. Ra indicates the roughness of the surfaces.

4-16 Application of X-Ray Photoelectron Spectroscopy to Characterization of Metallic Nanoclusters Formed by Ion Implantation-III

K. Takahiro[a)], S. Oizumi[a)], K. Kawatsura[a)], T. Isshiki[a)], K. Nishio[a)], S. Nagata[b)], S. Yamamoto[c)], K. Narumi[d)] and H. Naramoto[d)]

[a)]Kyoto Institute of Technology, [b)]Institute for Materials Research, Tohoku University, [c)]Environment and Industrial Materials Research Division, QuBS,JAEA [d)]Advanced Science Research Center, JAEA

Ion implantation is very promising for the formation of nanoclusters because of its ability to control the type and concentration of the implanted atoms. Usually implanted atoms as well as defects distribute non-uniformly along depth, resulting in the depth-dependent nucleation and growth of nanoclusters. It is, therefore, necessary to examine the depth-dependent size distribution of nanoclusters. Cross sectional transmission electron microscopy (XTEM) is often used to directly investigate their size. However, much effort and time have to be paid to prepare specimens for XTEM observation. Alternatively, X-ray photoelectron spectroscopy (XPS) can be used to estimate the size of nanoclusters. In XPS of Au nanoclusters, for example, the spin-orbit splitting between $5d_{5/2}$ and $5d_{3/2}$ increases with increasing their average size. In this work, the $5d$ splitting was measured on Au nanoclusters embedded in Al_2O_3 and SiO_2 to estimate the cluster size.

A single crystalline sapphire (α-Al_2O_3) and fused silica (SiO_2) were commercially available from Shinkosha and Sendai-Sekiei, respectively. Au^+ ions with an energy of 500 keV were implanted into these matrices to a fluence of 4×10^{16} cm^{-2}. Au implantation was performed using a tandem accelerator at Tohoku University. The depth distributions of implanted atoms were analyzed by using Rutherford backscattering spectrometry (RBS) with 2-MeV He ions from a single-end accelerator at TIARA. The etching rate by Ar ions in XPS analysis was determined by the Au depth profile obtained from RBS measurements. XPS analysis using non-monochromatized Mg Kα radiation was performed with JEOL 9010. To obtain depth profile of XPS binding energies for the implanted Au, the surface of implanted samples was etched with 0.8-keV Ar ions from a sputter-etching gun equipped with JEOL 9010. XTEM was conducted with JEM-2000EX operating at 200 kV to directly observe Au nanoclusters.

Figure 1 shows Au $5d$ spin-orbit splitting measured on Au implanted in Al_2O_3, together with Au concentration, as a function of sputtering time or depth in Al_2O_3. The $5d$ splitting is found to be correlated strongly with the Au concentration. As the Au concentration increases, the $5d$ splitting becomes larger, indicating that the Au nanoclusters with the larger size tend to be formed in the vicinity of the projected range of Au ions. The Au cluster size can be estimated by the $5d$ splitting-size relationship which is derived from literatures[1,2].

In Fig. 2, the Au cluster sizes estimated with XPS and TEM are plotted as a function of depth in Al_2O_3. The cluster sizes are estimated with XPS to be 1—2 nm, good agreement with results obtained from TEM. Furthermore, the XPS reveals the presence of Au clusters 0.8 ± 0.1 nm in diameter at depths 60—70 nm and 130—150 nm, while no cluster is visible for TEM observation. In Au-implanted SiO_2, the cluster sizes are estimated with XPS to be 1.5—5 nm, somewhat larger than those observed with TEM. This discrepancy may be arisen from size modification due to coalescence and/or disintegration of Au nanoclusters during Ar sputter etching.

References

1) S. B. DiCenzo et al., Phys. Rev. B 38 (1988) 8465.
2) H.-G. Boyen et al., Phys. Rev. Lett. 94 (2005) 016804

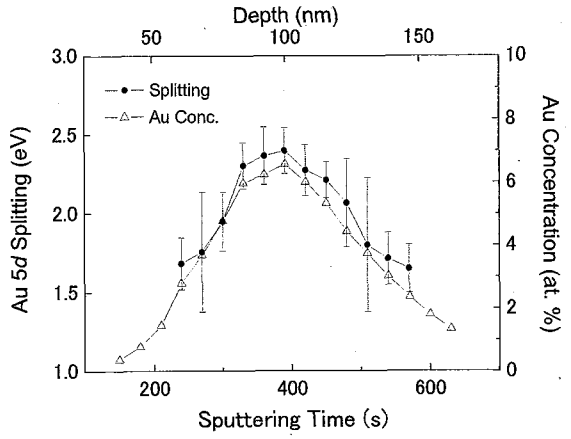


Fig.1. Au $5d$ spin-orbit splitting and Au concentration as a function of sputtering time (or depth in Al_2O_3).

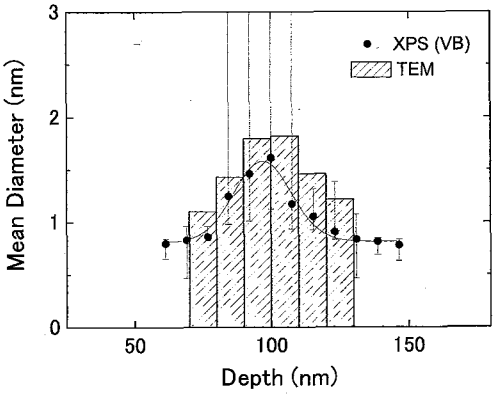


Fig. 2. Mean diameters of Au nanoparticles obtained by XPS and TEM as a function of depth in Al_2O_3.

4-17 Cr Ion Irradiation Effects on Hydrogen Storage Characteristics of Pd

H. Abe[a)], R. Morimoto[b)], H. Uchida[b)] and H. Itoh[a)]

[a)] Environment and Industrial Materials Research Division, QuBS, JAEA
[b)] Department of Applied Science, Graduate School of Engineering, Tokai University

Regarding the hydrogen storage in Pd, it was reported that the hydrogen absorption rate was improved by surface modification due to ion irradiation[1, 2]. It was also reported that Cr atoms contribute to the surface activation of hydrogen storage materials[3]. Thus, hydrogen storage characteristics of Pd are expected to be significantly improved by irradiation of Cr ions. In this study, we have examined the Cr ion irradiation effects on the hydrogen absorption rate of Pd.

Pd sheets with the purity of 99.99 %, and the size of 7.5 x 7.5 x 0.1 mm^3 were used in our experiments. Prior to ion irradiation, all samples were annealed for an hour at 1173 K in a flowing pure N_2 gas (99.9998 % purity). Cr ion (Cr^+) irradiation into Pd samples was made at an acceleration energy of 350 keV in a dose range up to 1 x 10^{17} cm^{-2} at room temperature in TIARA, JAEA. N and Ar ions were also irradiated at 350 keV for comparison with Cr^+ irradiation. For the electrochemical measurements of Pd samples, an Hg/HgO was used as the reference electrode in an open cell. Details of the electrochemical measurements have been reported elsewhere[4].

Figure 1 shows hydrogen absorption curves of Pd samples before and after Cr^+ irradiation. As the Cr^+ dose increased from 1 x 10^{14} cm^{-2} to 1 x 10^{17} cm^{-2}, the hydrogen absorption rate increased. Figure 2 shows the comparison among hydrogen absorption curves of Pd irradiated with 350 keV N^+, Ar^+ and Cr^+ at 1 x 10^{17} cm^{-2}. The sample irradiated with Cr^+ exhibited a much higher rate than the N^+ and Ar^+ irradiated samples. Regarding the N^+ and Ar^+ irradiation effects, the increases of the hydrogen absorption rate were reported to be ascribed to an increase in hydrogen trapping sites, which accelerate hydride nucleation and growth in the surface region. However, a quite high hydrogen absorption rate observed in the Cr^+ irradiated sample is hardly explained only by an increase in the hydrogen trapping sites, because the concentration of such trapping sites generated by the Cr^+ irradiation is though to be comparable to those by N^+ and Ar^+ irradiation. It is most likely that the enhancement in the hydrogen absorption due to Cr^+ irradiation is caused by surface activation due to high concentration doping of Cr into Pd as well as introduction of hydrogen trapping sites. Further investigations are necessary to clarify the mechanisms of the Cr^+ irradiation effects.

References

1) H. Abe, A. Uedono, H. Uchida, A. Komatsu, S. Okada and H. Itoh, Mat. Sci. Forum, 363-365 (2001) pp.156-158.
2) H. Abe, R. Morimoto, F. Satoh, Y. Azuma and H. Uchida, J. Alloys Comp., 404-406 (2005) pp. 288-292.
3) F. Suzuki, S. Takahashi, A. Yamagiwa and H. Uchida, J. Alloys Comp., 356-357 (2003) pp. 336-339.
4) H.H. Uchida, Y. Watanabe, Y. Matsumura and H. Uchida, J. Alloys Comp., 231 (1995) pp. 679-683.

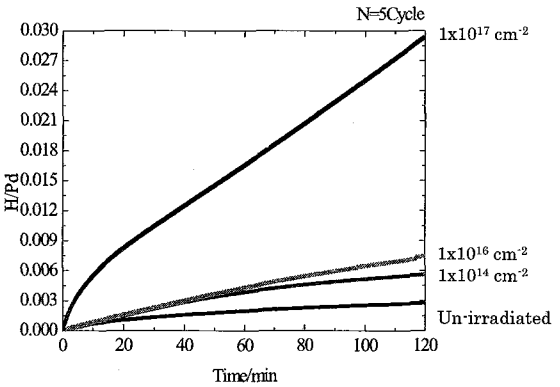


Fig.1. Hydrogen absorption curves of Pd irradiated with 350 keV Cr^+ at doses of 1x10^{14} cm^{-2} to 1x10^{17} cm^{-2}. The curve of the unirradiated Pd is also shown for comparison.

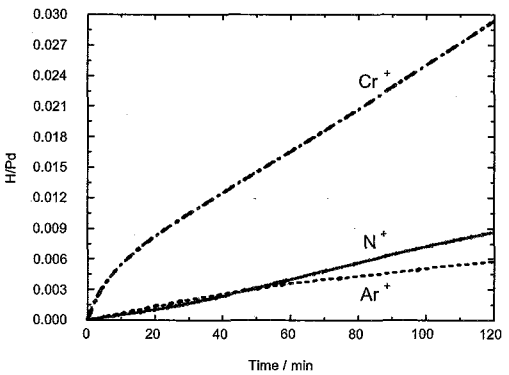


Fig.2. Comparison of hydrogen absorption curves of Pd samples irradiated with 350keV N^+, Ar^+ and Cr^+ at 1 x 10^{17} cm^{-2}.

4-18 Visible Photoluminescence of ZnO Rods Grown on Cu Implanted Substrate

A. Takeyama, S. Yamamoto, M. Yoshikawa and H. Ito

Environment and Industrial Materials Research Division, QuBS, JAEA

ZnO thin film shows a green broad luminescence and it has been expected as a phosphor material for Field Emision Display (FED)[1]. The luminescence has been thought to be originated from lattice defects of ZnO, such as oxygen vacancy or Zn interstitials, which strongly affected by the grain size and morphology of the film[2]. Therefore, the luminescence is very sensitive to fablication roots and this make difficult to control the luminescence peak wavelength. In addition to this inherent problem in ZnO, thin film phosphor could not offer high luminescence efficiency as required for the phosphor material, because the surface area derived from its flatness is small. On the other hand, rod like ZnO (ZnO rod) phosphor could offer high luminescence efficiency by its large surface area. In this report, we show a novel technique to fablicate ZnO rods with controlling its luminescence peak wavelength.

ZnO rods were grown on Si substrate and annealed Cu ion implanted Si substrate. The Cu fluence of 2.2 x10^{16} atoms/cm^2. Cu-implanted substrate was annealed at 500℃ for 20 minutes. The XRD pattern obtained for both substrates after the growth showed ZnO rods were grown perpendicular to the substrate along the c-axis.

Figure 1 is a photo luminescence (PL) spectra of ZnO rods. In fig. 1, the peak wavelength for the rods grown on the Cu-implanted substrate annealed for 20 minutes was approximately 20 nm shorter than that of the un-implanted substrate. On the other hand, UV luminescence peak, which is related to the transition of an electron from conduction band to valence band, is nearly the same for the rods grown on both substrates, and this means they have almost the same band gap energy. As is well known, the visible luminescence of ZnO rods was influenced by the distribution of lattice defects. Therefore, the blue shift of the peak wavelength indicates that a distribution of lattice defects of ZnO rods grown on Cu-implanted substrate was different from that of un-implanted substrate.

Figure 2 was Raman spectra of the ZnO rods. The peak at 437 cm^{-1} is the high-frequency E2 phonon mode, which represents the wurtzite structure of ZnO[3]. The Raman peak shift for un-implanted substrate was nearly consistent with this wavenumber. Although the lattice parameter and crystal strucutre of ZnO are much different from those of Si, the Raman spectrum indicates ZnO rods grown on un-implanted substrate were not strained. This seems the strain derived from lattice mismatch between the substrate and ZnO rods was relaxed as the rods were grown. On the other hand, for 20 minutes annealed Cu-implanted substrate, the peak shifted longer than 437 cm^{-1}. This indicates ZnO rods grown on the Cu-implanted substrate were strained compressively along a-axis, the orthogonal direction to c-axis. In contrast to the un-implanted substrate, Cu-implanted substrate was recrystallized while it was annealed at 500℃ followed by the growth of ZnO rods at 930℃. The crystal structure and lattice parameter of the substrate dynamically changed during the recrystallization, and this introduced continuously the strain into ZnO rods. It also prevented relaxing of ZnO rods, and allowed continuous redistribution of lattice defects.

References

1) Y. Nakanishi et al., App. Surf. Sci. 142 (1999) 233.
2) J.D. Ye et al., Appl. Phys. A 81 (2005) 759.
3) S.J. Chen et al., J. Cryst. Growth 247 (2003) 357.

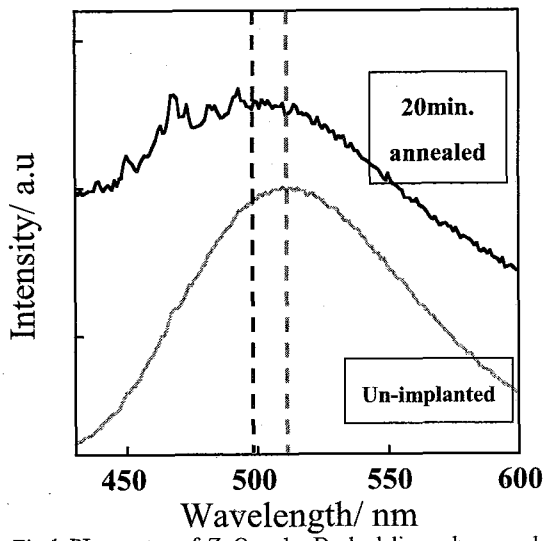


Fig.1 PL spectra of ZnO rods. Dashed lines show peak wave lengths for each spectrum.

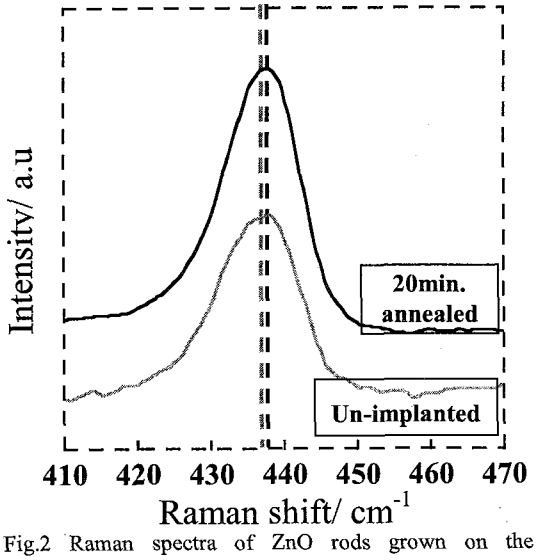


Fig.2 Raman spectra of ZnO rods grown on the un-implanted and annealed Cu-implanted substrates.

4-19 Blister Formation in Rutile TiO_2 (100) Films by Helium Irradiation

S. Yamamoto [a)], K. Takano [a)], A. Inouye [a, b)] and M. Yoshikawa [a)]

[a)]Environment and Industrial Materials Research Division, QuBS, JAEA,

[b)] School of Engineering, Tohoku University

The photocatalytic properties of titanium dioxide (TiO_2) have attracted much interest from the viewpoints of basic science and applications. For the improving photocatalytic activity of TiO_2 films, modification of surface features and fabrication of effective large surface area are required. The implantation of helium into materials can be used to produce specific microstructures on surface region, such as bubbles, blisters and craters, with unique properties for application such as catalysis. In this study, irradiation energy and fluences of helium ion for blister formation in rutile TiO_2 (100) films were investigated.

TiO_2 films were deposited on α-Al_2O_3 (0001) substrates by pulsed laser deposition (PLD) using a KrF excimer laser in an O_2 atmosphere. In this study, ~300 nm thick TiO_2 films were deposited at 500°C under oxygen pressure of 2 Pa. The preparation of TiO_2 films was described previous reports in detail [1, 2)]. The deposited TiO_2 films were irradiated at room temperature with 1~4 keV helium ions up to fluence range from 1×10^{16} to 2.3×10^{17} ions/cm^2. The surface morphology of the deposited films was observed using an AFM (SPA400, SII). The film thickness and composition were determined by RBS analysis using a 3 MV single-stage-accelerator at JAEA/Takasaki. The photo-induced superhydrophilicity of blister formed TiO_2 films were examined by measurements of contact angle against water as a function of He fluence.

Figure 1 shows AFM images (2 μm × 2 μm) of the rutile TiO_2 (100) films (a) unirradiated, (b) irradiated at room temperature, respectively. The films were irradiated with 4 keV helium ions to a fluence of 1.0×10^{17} ions/cm^2. From Fig. 1 (a), smooth surface was observed in unirradiated TiO_2 (100) film. In the case of irradiated at room temperature, many blisters were recognized on the TiO_2 (100) film surface. Mean diameter of these blisters was 123 nm, mean height was 20 nm, and areal density was about 2.2×10^9/cm^2. The mean diameter of helium blisters was almost the same when the helium ion fluence was changed from 2.0×10^{16} to 2.0×10^{17} ions/cm^2 in present experiment. But the mean height of blisters slightly increased with increasing the fluence of helium ions[3, 4)]. Also helium blisters were observed at higher than 2 keV irradiation energy.

In general, TiO_2 films lose photocatalytic properties by ion irradiation. Thus, heat treatment is essential for recovery of photocatalytic properties. The AFM observations confirm that the helium irradiated TiO_2 films with heat treatment at 673 K for 6 h maintain the blister formation. Figure 2 shows the change in contact angle against water as a function of He fluence. One can recognize that contact angle against water of the film degreases with the He fluence. On increasing the fluence of helium, the photo-induced superhydrophilicity of TiO_2 films was improved. The result suggests that the blister formation in rutile TiO_2 films by helium irradiation is useful for improving photocatalytic properties.

References

1) S. Yamamoto, et al., Thin Solid Films 401 (2001) 88.
2) S. Yamamoto, et al., J. Crystal Growth 237-239 (2002) 569.
3) S. Yamamoto, et al., Transaction of the Materials Research Society of Japan 30 (2005) 789.
4) S. Yamamoto et al., TIARA annual report 2004 (2005) 220.

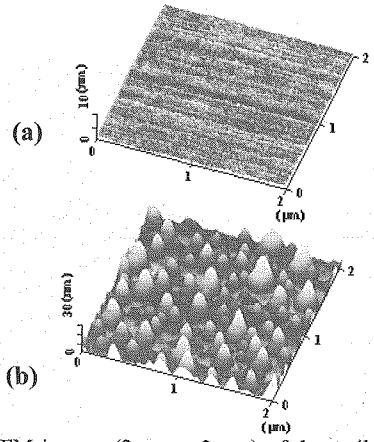


Fig.1 AFM images (2 μm × 2 μm) of the rutile TiO_2 (100) films (a) unrradiated, (b) irradiated at room temperature. The film samples were irradiated with 4 keV helium ions to a fluence of 1.0×10^{17} ions/cm^2.n air.

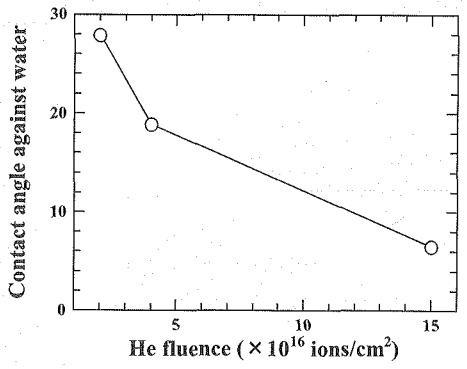


Fig.2 The change in contact angle against water was measured as a function of He fluence. The film samples were irradiated with 4 keV helium ions at room temperature and then heat treated at 673 K for 6 h in air.

4-20 Improvement of Gasochromic Properties in Tungsten Oxide by Ion Irradiation

K. Takano[a)], A. Inouye[a, b)], S. Yamamoto[a)] and M. Yoshikawa[a)]

[a)]Environment and Industrial Materials Research Division, QuBS, JAEA
[b)]School of Engineering Tohoku University

Abstract

Gasochromic properties for hydrogen gas on tungsten oxide thin films have been investigated for optical hydrogen gas sensors. The gasochromic properties are considered to relate to oxygen vacancies or defects in the tungsten oxide. In this study, it is tried to make oxygen vacancies or defects in the tungsten oxide thin films by H^+ and He^+ beam irradiation, to investigate the relation between the amount of fluency and the gasochromic properties. The coloration for 1 % hydrogen in 99 % argon gas was measured by time resolved optical spectroscopy with 630 nm light. The coloration is enhanced with the increasing fluence, over $1x10^{14}$ ions/cm^2.

本研究グループでは、酸化タングステン（WO_3）薄膜の水素吸着により透過率が変化する特性（ガスクロミック特性）を利用した、光学式水素センサー[1)]の研究開発を行っている[2)]。酸化タングステンのガスクロミック特性は、結晶内の酸素原子の欠陥によって発現すると考えられている[3)]。そこで、本研究では新しい試みとして、作製したWO_3薄膜に対して、高エネルギーのイオンを照射することにより、酸化タングステンの結晶内に酸素原子の欠損を意図的に作り、水素による着色率の照射量依存性を調べ、ガスクロミック特性との関係を検討した。酸化タングステン薄膜は、高周波マグネトロンスパッタ法を使用して石英基板上に、0.5μmの厚さに堆積した。同一ロットのWO_3薄膜に対し、入射エネルギー40 keVと200 keVのH^+イオン、および入射エネルギー40 keVのHe^+イオンを、それぞれ $1x10^{15}$ 個/cm^{2}から$1x10^{17}$ 個/cm^{2}まで照射した。$1x10^{16}$個/cm^{2}以上イオンを照射すると、薄膜は薄緑色から青色へ変色した。これは、酸化タングステン中の酸素原子が欠損した為であると考えられる[4)]。次に、照射量とガスクロミック特性との関係を調べるために、水素に対する触媒金属であるパラジウムを薄膜の表面上に30 nm積層し、アルゴンガスで希釈した濃度 1 % の水素を暴露した時の、630 nmの可視光の透過光強度 $I(t)$ を測定した。Fig. 1は、入射エネルギー40 keVのH^+イオンを照射した膜の、透過光強度比 $I(t)/I(0)$ の時間変化を示す。透過光強度比は、未照射（成膜直後）の薄膜では水素を暴露してもほとんど変化しないが、照射を行うと80 %以下に減少（着色）し、ガスクロミック特性が向上していることが分かる。Fig. 2は、入射エネルギー40 keVと200 keVのH^+イオン、および入射エネルギー40 keVのHe^+イオンを、３つのロットの薄膜に対してそれぞれ照射した場合の、水素暴露から30分後の透過光強度比 $I(30)/I(0)$ を示す。入射エネルギー、照射イオン種、に関わらず、照射により透過光強度比は未照射膜に比べて減少する傾向にあり、ある照射量で極小値を取ることが予想される。この結果から、入射エネルギー、照射イオン種、イオン照射量の制御により、薄膜のガスクロミック特性を2倍以上改善できる事が分かった。酸化タングステンのガスクロミック特性は、原子組成比（W/O）と関連性があることが報告されている[5)]。今後は、イオン照射による酸素原子に関連した欠陥生成のメカニズムを明らかにすると共に、透過光強度比が極小となる原子組成比（W/O）が得られるような、欠陥量が導入できるイオン照射技術の研究開発を行う。

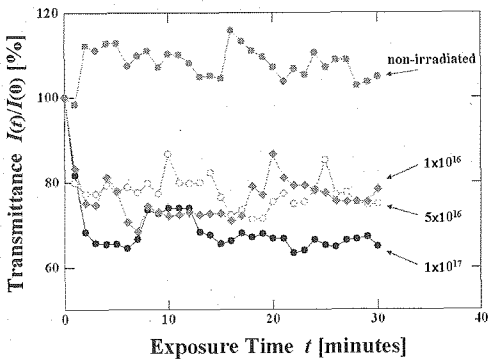


Fig. 1 Transmittance for 1 % hydrogen of the tungsten oxide thin films irradiated by 40 keV H^+. Coloration of irradiated films increase than that of non-irradiated film.

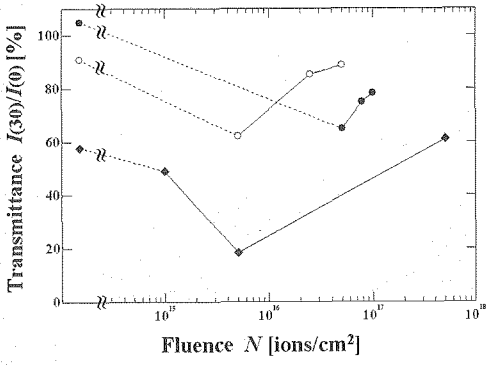


Fig. 2 Fluence dependence of the Transmittance for 1% hydrogen on the tungsten oxide thin films irradiated by 40 keV H^+, 40 keV He^+ and 200 keV He^+ irradiation.

References

1) K. Ito and T. Ohgami, Appl. Phys. Lett. 60 (1992) 938.
2) K. Takano, A. Inouye, S. Yamamoto, M. Yoshikawa, A. Sugiyama, Trans. Mater. Res. Soc. Jpn. 31 (2006) 223.
3) A. Georg, W. Graf, R. Neumann, V. Witter, Thin Solid Films 384 (2001) 269.
4) L. Berggren and Gunnar A. Niklasson, Solid State Ionics 165(2003) 51.
5) M. Stolze, B. Camin, F. Galbert, U. Reinholz, L. K. Thomas, Thin Solid Films 409 (2002) 254.

4-21 Hydrogen Sensing Characteristics of Ag Implanted WO_3

A. Takeyama, S. Yamamoto, M. Yoshikawa and H. Ito

Environment and Industrial Materials Research Division, QuBS, JAEA

Abstract

Hydrogen sensitivity of the sensor, which consisted of tungsten oxide (WO_3) and catalysts layer (gold (Au) and platinum), was slightly improved by a silver (Ag) ion implantation into WO_3. This improvement of the hydrogen sensitivity indicates the catalytic activity of Au dispersed on an ion-implanted WO_3 was improved. However, its hydrogen sensing velocity was smaller than the hydrogen sensor, which consisted of un-implanted WO_3 and catalysts layer. This seems the lattice transformation of the ion-implanted WO_3 which occurred when it faced to hydrogen, was disturbed by implanted Ag atoms inside WO_3.

酸化タングステン(WO_3)を用いた光学式水素センサは、水素との接触による着色によって水素を検知可能であり、火災・爆発の恐れのない安全な水素センサとして注目されている[1]。センサ表面には水素分子を原子状にしてWO_3と反応させるための金属触媒（白金やパラジウム）が蒸着されているが、これに加え金を蒸着するとセンサの応答特性が向上するとの報告がある[2),3)]。一方、酸化物上の金属触媒の効果は、酸化物と金属触媒との相互作用に大きく影響され、制御された雰囲気下で熱処理を行なうことにより大幅に向上する可能性がある[4)]。本研究では、水素導入時にWO_3の抵抗変化を測定し、銀(Ag)イオン注入がWO_3上の金の触媒効果を向上させ水素センサの応答特性を改善する可能性について探った。WO_3の抵抗は水素との接触による着色により低下するため、これを測定することにより水素への応答特性の評価が可能である。

φ20mm x 2mmの大きさのWO_3ペレットに対し、室温で銀イオンを注入した。注入エネルギーは350keV、注入量は5×10^{15}atoms/cm^{2}である。イオン注入したペレットをセンサ作製に適した大きさに分割した後、イオン注入による損傷を回復しWO_3の結晶化を促すため、これをアルゴン雰囲気中600℃ 1 時間熱処理した。熱処理後、ペレット表面に金薄膜5nmを蒸着しアルゴン雰囲気中で600℃、10分間熱処理した。さらに熱処理後のペレット表面に白金薄膜を10nm蒸着し水素センサを作製した。熱処理後のペレットのX線回折(XRD)パターンにはWO_3のピークが確認され、WO_3の損傷が回復していることが確認された。センサの応答特性の比較のため、未熱処理のAgイオン注入ペレットおおび未注入のWO_3ペレットを用いて同様に水素センサを作製した。こうして作製したセンサを測定チャンバ内に設置し、2%水素導入時のセンサの表面抵抗の変化を測定してセンサの応答特性を評価した。

Fig. 1に水素センサの応答特性の変化を示す。水素導入前後のセンサの抵抗をR_0、Rとすると水素に対する応答特性はR/R_0で定義される。イオン注入ペレットに蒸着する金の膜厚を5nm (曲線2)から10nm (曲線3)に厚くすると、応答特性が改善されることがわかる。これは、金が応答特性を改善することを示唆している。

一方、未熱処理のAgイオン注入ペレット（Ag^+ un implanted）は応答特性が悪く応答速度も低いが、金蒸着後熱処理すると応答特性は向上し（曲線2）、金蒸着後熱処理した未注入ペレット(曲線1)と同程度の特性を示すことがわかる。しかし未熱処理の未注入ペレット（WO_3 un-annealed）と比べると、応答速度はかなり低い。水素検知時のセンサにおいては、①触媒上で水素分子が水素原子に解離し、②水素原子がWO_3中に拡散してWO_3の結晶構造が変化し抵抗が下がる（R/R_0が小さくなる）、という二つの反応が起こると考えられている[1)]。イオン注入ペレット上の金および白金の触媒効果が劣化して①の反応速度が低下したと仮定すると、イオン注入ペレットの応答特性（曲線２）は未注入ペレットのそれ（曲線１）に比べ悪化することが予想されるが、実際には逆にやや向上している。このことは、イオン注入ペレット上の金の触媒効果が、未注入ペレットのそれに比べてわずかに向上したことを示している。従ってイオン注入ペレットの応答速度の低下は触媒上での水素の解離に起因するものではなく、WO_3の構造変化が妨げられることによると考えられる。この原因としては、注入したAgイオンがWO_3と固溶体を形成し、水素がWO_3の結晶格子内へ侵入するのを妨害していることが考えられる。より注入量の大きいペレットを用いて作製したセンサの応答速度が低いことも、この原因によると思われる。

以上の結果から、Agイオン注入はWO_3上の金の触媒効果を向上させるが、逆に水素センサの応答速度を低下させることがわかった。今後、応答速度を向上させるためには、さらに熱処理条件を探る必要がある。

References

1) H. Nakagawa, et al., "A room-temperature operated hydrogen leak sensor", Sens. Actuators B 93, 468 (2003).
2) M. Ando, et al., "Optical hydrogen sensitivity of noble metal–tungsten oxide composite films prepared by sputtering deposition", Sens. Actuators B 76, 13 (2001).
3) S.J. Ippolito, et al., "Hydrogen sensing characteristics of WO_3 thin film conductometric sensors activated by Pt and Au catalysts", Sens. Actuators B 108, 154 (2005).
4) J. Fan, et al., "Influence of the oxidative/reductive treatments on the activity of $Pt/Ce_{0.67}Zr_{0.33}O2$ catalyst", Appl. Surf. Sci. 245, 162 (2005).

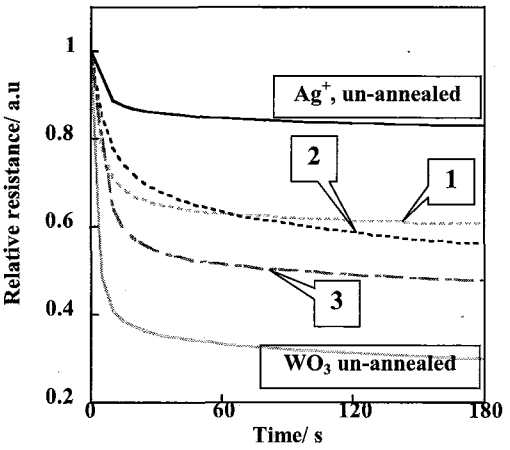


Fig.1 Plot of a relative resistance vs. time.
Pellets were annealed after Au deposition.
1. WO_3 deposited with 5nm Au.
2. Ag-implanted WO_3 deposited with 5nm Au.
3. WO_3 deposited with 10nm Au.

4-22 Improved Separation of Cadmium-107 from Silver Cyclotron Targets by Precipitaion Method

N. S. Ishioka [a], S. Fujimaki [a], N. Suzui [a], S. Nakamura [b] and S. Matsuhashi [a]

[a] Radiation-Applied Biology Division, QuBS, JAEA,
[b] Faculty of Bioresource Sciences, Akita Prefectural University

INTRODUCTION

Cadmium (Cd) is a toxic heavy metal found in a variety of industrial and environmental settings. It is well known that the Cd which was accumulated in the liver and kidneys causes diseases such as kidney dysfunction, emphysema, osteomalacia and osteoporosis due to chronic exposures.

Recently, a problem of cadmium pollution in food has attracted considerable attention as public concern related to the human health in the world. In order to avoid Cd absorption via food, it is important that we understand the mechanisms of absorption and translocation of Cd in agricultural products. The increasing interest in the element Cd in rice, particularly in Japan, stimulates a need to develop convenient and reproducible methods to trace this element.

^{107}Cd is regarded as one of the best radionuclides used for the direct determination of the dynamic statistics of the Cd in plants by means of the Positron Emitting Tracer Imaging System. Our earlier work illustrated that no-carrier-added ^{107}Cd can be produced using the ^{107}Ag(p,n)^{107}Cd nuclear reaction.[1] In the present work, we have improved the radiochemical separation method which is suitable for routine production.

EXPERIMENT

Using radioactive tracers of ^{109}Cd ($T_{1/2}$: 453 d) and ^{106m}Ag ($T_{1/2}$: 8.3 d), the separation of Cd from silver (Ag) was accomplished by a precipitation method with hydrochloric acid (HCl).[1] ^{109}Cd and ^{106m}Ag can be produced by proton bombarding a natural silver (Ag) sheet; the Ag target was irradiated for 30 min at a beam current of 2 μ A.After the irradiation, the Ag target was dissolved in 4 ml of 14 M HNO_3. The mother solutions which contained several kBq of the radioactive tracers and 0.8 g of Ag were prepared. The radiochemical separation yields were determined from various conditions: HCl concentrations, addition time and presence of light. Figure 1 shows the gradient method which adds HCl having concentration gradient. Activity of each sample was determined by gamma-ray spectrometry using a HPGe detector coupled to SEIKO 7600 MCA.

RESULTS AND DISCUSSION

Table 1 shows the recovery yields of ^{109}Cd at precipitation conditions. No ^{106m}Ag impurities were detected all the separation methods. The results show that the proposed method completely separates nanogram-amounts of Cd from gram-amounts of Ag. Using the gradient-method, the radiochemical recovery of ^{109}Cd was 92%. On the other hand, the recovery yields of ^{109}Cd were about 89% and 75% by constant-method which was used precipitator of 0.2M HCl and 2M HCl, respectively. From the results of condition a. and b., it can be found that the high recovery yields were provided with low concentration of hydrochloric acid by short time. In addition, it was seen that the yields was degreased by shading in the condition a. and c.. From the above mentioned, we concluded that the gradient method in a condition with light is suitable for routine production of ^{107}Cd. The method requires only a filtration and evaporation to dryness of relatively convenient volumes. It is much quicker and more efficient than the formerly used method to spend HCl by the constant concentration.

References

1) N. S. Ishioka, S. Fujimaki, N. Suzui, S. Matsuhashi, The abstract of the 40th Annual Meeting on Radioisotope and Radiation Research (2005), p. 20.

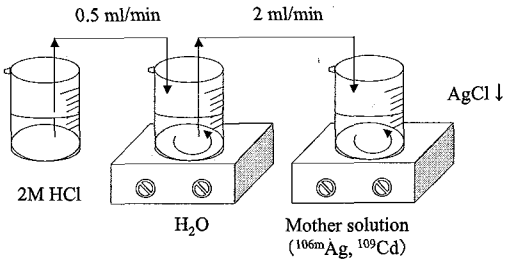


Fig. 1. Gradient method: injection of HCl with concentration gradient

Table 1. Radiochemical recovery yields of ^{109}Cd after precipitation separation; a comparison of light and shade conditions

	concentration and flow rate (HCl)	^{109}Cd recovery yields		^{106m}Ag	time	total volume
a.	0.2M HCl, 5 ml/min	89% (light)	78% (shade)	No detected	10 min.	76 ml
b.	2M HCl, 0.1 ml/min	75% (light)	78% (shade)	No detected	50 min.	31 ml
c.	Gradient method	92% (light)	77% (shade)	No detected	10 min.	28 ml

4-23 Synthesis of Hydrophilic Endohedral ^{133}Xe-Fullerenol by Using Higher Fullerene

S. Watanabe, T. Katabuchi, N. S. Ishioka and S. Matsuhashi

Radiation-Applied Biology Division, QuBS, JAEA

1. Introduction

Endohedral fullerenes encapsulating a radioisotope within a fullerene cage have a possibility of being new radiopharmaceuticals. In order to realize this, hydrophilic fullerene derivatives, which allow *in vivo* investigations, have to be synthesized from hydrophobic fullerenes, in addition to the encapsulation of radioisotopes emitting β- or γ-rays available for therapy or diagnosis. We have reported a method of synthesizing hydrophilic endohedral ^{133}Xe-fullerenols (^{133}Xe@C_{60}(OH)$_x$ and ^{133}Xe@C_{70}(OH)$_x$),[1] which would be applied to the therapy of bone cancer, because ^{133}Xe emits a β-ray with the maximum energy of 0.346 MeV and fullerenol is concentrated in bone tissues.

For the therapeutic purpose, the separation of endohedral ^{133}Xe-fullerenes from empty fullerenes is necessary, because endohedral ^{133}Xe-fullerene derivatives without empty fullerene derivatives can be effectively concentrated in target tissues. However we had not succeeded in the separation on ^{133}Xe@C_{60} and ^{133}Xe@C_{70}. Recently, we described the production of endohedral ^{133}Xe-higher fullerenes (^{133}Xe@C_{76} and ^{133}Xe@C_{84}) by implantation of ^{133}Xe ions into C_{76} and C_{84} fullerene targets, and a possibility of the separation of endohedral ^{133}Xe-higher fullerenes from empty fullerenes by high performance liquid chromatography.[2] Therefore, this paper aims at the synthesis of hydrophilic endohedral ^{133}Xe-fullerenols (^{133}Xe@C_{76}(OH)$_x$ and ^{133}Xe@C_{84}(OH)$_x$) from the endohedral ^{133}Xe-higher fullerenes (^{133}Xe@C_{76} and ^{133}Xe@C_{84}).

2. Experimental

Fullerene targets for ion implantation were made by vacuum evaporation of fullerene (C_{76} or C_{84}) on Ni foils. Implantation of ^{133}Xe ions into the targets was carried out with an isotope separator at an acceleration energy of 30 keV. After ion implantation, the fullerene on the target was dissolved in *o*-dichlorobenzene. The solution was filtered through a membrane filter with 0.2 μm pore size (Millipore, JGWP) to remove insoluble materials. The filtrate was used to synthesize endohedral ^{133}Xe-fullerenol.

The synthesis of endohedral ^{133}Xe-fullerenol (^{133}Xe@C_{76}(OH)$_x$ and ^{133}Xe@C_{84}(OH)$_x$) was carried out by the method described in the literature.[3] Four milliliters of the *o*-dichlorobenzene solution containing ^{133}Xe@C_{76} or ^{133}Xe@C_{84} was stirred for 12 h with 50 μL of tetrabutylammonium hydroxide (TBAH, 40% in water) and 0.5 mL of 14 M KOH solution by a rotary evaporator. After the stirring, the *o*-dichlorobenzene solution was removed *in vacuo* at 80°C. In this operation, the KOH phase was also evaporated. One milliliter of pure water was added to the evaporated residue and stirred to dissolve the evaporated residue. Some parts of the evaporated residue were not dissolved. To remove the TBAH and KOH, the supernatant of the solution was passed down a size-exclusion gel chromatography column with Sephadex G25 Fine using water as an eluent. The effluent from the column contains ^{133}Xe@C_{76}(OH)$_x$ or ^{133}Xe@C_{84}(OH)$_x$.

The ^{133}Xe radioactivity of ^{133}Xe@C_{76}(OH)$_x$ or ^{133}Xe@C_{84}(OH)$_x$ was measured by γ-ray spectrometry to determine the recovery defined as a percentage of the amount of ^{133}Xe@C_{76}(OH)$_x$ or ^{133}Xe@C_{84}(OH)$_x$ to that of original ^{133}Xe@C_{76} or ^{133}Xe@C_{84}.

3. Results and Discussion

The recovery of the ^{133}Xe@C_{60}(OH)$_x$, ^{133}Xe@C_{70}(OH)$_x$, ^{133}Xe@C_{76}(OH)$_x$ and ^{133}Xe@C_{84}(OH)$_x$ was 1.6%, 2.1%, 12% and 17%, respectively, together with our previous data of ^{133}Xe@C_{60}(OH)$_x$ and ^{133}Xe@C_{70}(OH)$_x$. In the previous experiment, we have confirmed that most of the encapsulated ^{133}Xe atoms release from the fullerene cage during the reaction time of 12h.

In this study, the recovery was found to increase with the number of carbon atoms in fullerene. We assumed that the order of the recovery related to the amount of releasing ^{133}Xe atoms from the fullerene cage. Therefore, we determined the amount of releasing ^{133}Xe atoms from fullerene cage during the reaction time of 12h.

The release of ^{133}Xe atoms on ^{133}Xe@C_{60}(OH)$_x$, ^{133}Xe@C_{70}(OH)$_x$, ^{133}Xe@C_{76}(OH)$_x$ and ^{133}Xe@C_{84}(OH)$_x$ was 77%, 64%, 43% and 34%, respectively. From this result, it was confirmed that the order of the recovery related to the amount of releasing ^{133}Xe atoms from the fullerene cage.

The recovery of 17% for ^{133}Xe@C_{84}(OH)$_x$ is still low. In order to increase the recovery, we will examine the optimum conditions in the synthesis of ^{133}Xe@C_{76}(OH)$_x$ and ^{133}Xe@C_{84}(OH)$_x$.

References

1) S. Watanabe, N. S. Ishioka, T. Sekine, H. Kudo, H. Shimomura, H. Muramatsu, T. Kume, *J. Radioanal. Nucl. Chem.*, **266** (2005) 499.
2) S. Watanabe, T. Katabuchi, N. S. Ishioka, S. Matsuhashi, H. Muramatsu, , *J. Radioanal. Nucl. Chem.*, in press.
3) D. W. Cagle, S. J. Kennel, S. Mirzadeh, J. M. Alford, L. J. Wilson, *Proc. Natl. Acad. Sci.*, **96** (1999) 5182.

4-24 Deuteron-Induced Activation Cross Section Measurement of Fe, Cr, Mn, Ni and Au for IFMIF Accelerator

M. Nakao[a)], N. Kubota[a)], K. Ochiai[a)], H. Sudo[b)], N.S. Ishioka[c)] and T. Nishitani[a)]
[a)]Division of Fusion Energy Technology, FRDD, JAEA, [b)]Tokyo Nuclear Services Co. Ltd.,
[c)]Radiation-Applied Biology Division, QuBS, JAEA

1. Introduction

In the design of the International Fusion Materials Irradiation Facility (IFMIF), long-term operation with total facility availability of at least 70 % is required[1]. However, activation of structural materials by deuteron beam limits maintenance, which causes lower facility availability. Thus it is essential to prepare deuteron-induced activation cross section database and to select low activation materials based on it. So far, we have measured excitation functions of 22 kinds of reactions for Al, V, Fe, Ni, Cu, Ta, and W targets.[2), 3)] In this work, we measured those of 8 reactions for Fe, Ni, Cr, Mn and Au targets. Deuteron-induced activities of nuclides produced in SS316 and F82H were also measured to validate the measured cross sections totally.

2. Experimental procedure

Deuteron irradiation experiment was performed at the LA1 station of an AVF cyclotron in the TIARA facility. In the experiment, we adopted a stacked-foil activation technique to measure cross sections at different energy points simultaneously. Each energy point was the averaged value derived from the energy loss in the sample, which was calculated by the IRACM code system[4]. The deuteron fluence was estimated from the measured ^{65}Zn activity and the ^{nat}Cu(d,x)^{65}Zn reaction cross section data reported by Takacs et al.[5] After irradiation and suitable cooling time, gamma-rays emitted from the irradiated samples were measured with a High-Purity Ge detector. Activation cross sections were derived from these photo-peak yields of gamma-rays. In the same way, activities of each nuclide produced in the alloy foils by 39.5 MeV deuterons were measured.

3. Activation cross sections

Measured excitation function of the ^{nat}Fe(d,x)^{54}Mn reaction is shown in Fig. 1. The results were compared with other experimental values and two types of calculation ones which were the data library computed by the ALICE-F code[6] (ACSELAM) and were computed by the TALYS code[7] (TALYS). The present data agreed with the previous data and TALYS within a factor of 1.5 although ACSELAM is 5 times as small as the present data. We have also obtained the activation cross sections; ^{48}V and ^{52}Mn from d+^{nat}Cr; ^{54}Mn from d+^{55}Mn; ^{52}Mn and $^{55, 56, 57}$Co from d+^{nat}Fe; $^{55, 56, 57}$Co and $^{60, 61}$Cu from d+ ^{nat}Ni; ^{194}Au from d+^{197}Au in 26-47 MeV range.

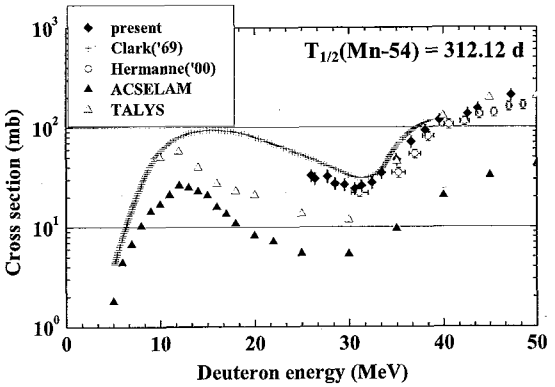


Fig. 1 Excitation function of the ^{nat}Fe(d,x)^{54}Mn reaction.

4. Induced activity of SS316 and F82H

The activities for SS316 and F82H in each nuclide were compared with the calculated values derived from the measured cross sections in our work. For ^{54}Mn and ^{181}Re, the calculated values were 50% larger than the measured ones. For ^{48}V, ^{52}Mn, ^{56}Co and ^{57}Co, the calculated values were in agreement with the measured ones within 14%.

5. Summary

We have completed the projected cross section measurement of 30 kinds of reactions for Al, V, Cr, Mn, Fe, Ni, Cu, Ta, W and Au targets in 2005. It is confirmed that the induced activity in SS316 and F82H could be evaluated with 14 % accuracy although further considerations are needed for the activities of ^{54}Mn and ^{181}Re in F82H.

References

1) IFMIF International Team, JAERI-Tech 2003-005 (2003).
2) M. Nakao, et al., AIP Conf. Proc. 769 (2005) 1489.
3) M. Nakao, et al., JAEA-Review 05-001 (2005) 283.
4) S. Tanaka, et al., JAERI-Data/Code 97-019 (1997).
5) S. Takacs, et al., Nucl. Inst. Meth., B 174 (2001) 235.
6) T. Fukahori, JAERI-M 92-039 (1992) 114.
7) A. J. Koning, et al., NRG Report 21297/04.62741/P (2004).

4-25 Production of Radioisotopes for Nuclear Medicine using Ion Beam Technology and Its Utilization for Both Therapeutic and Diagnostic Application in Cancer

Y. Iida [a)], H. Hanaoka [a)], T. Katabuchi [b, d)], S. Watanabe [d)], N. S. Ishioka [d)], S. Matsuhashi [d)], N. Oriuchi [c)], T. Higuchi [c)], M. Miyakubo [c)] and K. Endo [c)]

[a)]Department of Bioimaging Information Analysis, [b)]21st Century COE Program and [c)]Department of Diagnostic Radiology and Nuclear Medicine, Gunma University Graduate School of Medicine
[d)]Radiation-Applied Biology Division, QuBS, JAEA

Abstract

Radioimmunotherapy (RIT) becomes one of the most promising treatments for cancer therapy. Recently, because various radioisotopes are being used for RIT, the efficient tailor-made therapy is thought to be possible. The high energy ß-particle-emitter, such as ^{90}Y (2.28MeV), seems particularly well suited for the treatment of relatively large tumor masses, but the middle energy ß-particles, such as ^{67}Cu (0.18 – 0.58MeV), may have an advantage in treating small lesions. In this study, we prepared ^{67}Cu and evaluated its potential of application for RIT in tumor bearing mice. Our results of tumor localization studies show that ^{67}Cu was expected to be suitable for RIT.

現在、放射性薬剤を体内に投与して治療を行う内用放射線療法に用いられる放射性核種（RI）は^{131}Iのみであるが（^{90}Y、^{89}Sr、^{186}Reなどが臨床使用への検討段階にある）、治療での有効性が期待されるRIは他にも多数存在する[1)]。一方で、内用放射線療法の治療効果は標的となるがん組織の大きさ、状態と放射線のエネルギーとのバランスに左右され、個々の標的に対して最も効率的なエネルギーが存在する可能性が示唆されている[2)]。すなわち、性質の異なる種々のRIを利用することで、個々の病態に適した個別化医療を実現できる可能性がある。そこで原子力機構AVFサイクロトロンを用いて新規治療用RIを製造し、がん治療における有効性を調べるとともに、個々のがん組織に対して最も高い治療効果を示すRIを探索し、最適な治療を実現するための個別化医療の可能性を基礎的に検討する。

新しい治療用RIとしてまず^{67}Cuの製造を試みた。^{67}Cuは半減期61.9時間、主なβ線のエネルギーが0.391、0.483、0.576 MeVのRIで、高い治療効果が期待できる。また、臨床で利用されつつある^{90}Yとほぼ同等の半減期（^{90}Yの半減期は64.1時間）を有する一方、放射線のエネルギーは大きく異なるため（^{90}Yのβ線のエネルギーは2.28 MeV）、治療効果を比較するのに適している。さらに、低酸素腫瘍に集積する化合物としてCu-ATSMが報告されており[3)]、^{67}Cu-ATSMを用いたがん治療に適用できる。最初、^{64}Ni(α, *p*)^{67}Cu反応により^{67}Cuの製造を試みたが、収量が低いことから（1.5時間で約3.4 MBq）、^{68}Zn(*p*, *2p*)^{67}Cuにより製造することとした。その結果、^{67}Cuは5時間で48 MBqが得られ、化学分離による不純物除去の検討を行った[4)]後、以降の実験に使用した。

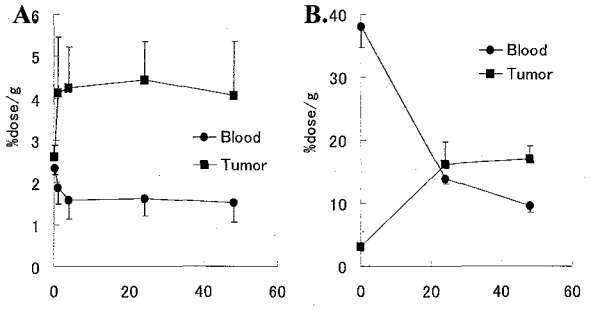


Fig.1 Biodistribution of (A) ^{67}Cu-ATSM in nude mice bearing HT-29 tumor xenografts and (B) ^{67}Cu-TETA-NuB2 in SCID mice bearing B-cell lymphoma RPMI1788. For each time point, data were acquired from five animals.

まず、^{67}CuをATSMと混和することにより^{67}Cu-ATSMを合成した。標識はHPLCおよびTLCで確認し、標識率、放射化学的純度は95%以上であった。HT-29腫瘍細胞をヌードマウスに移植後、^{67}Cu-ATSM 7.4～11.1 kBqを尾静脈から投与し、経時的に放射能の分布を調べた（Fig. 1A）。^{67}Cu-ATSMは投与直後から高く腫瘍組織に移行し（投与1時間で4.2 %dose/g）、この集積は投与48時間後も維持された。

次に、悪性リンパ腫の標的となるCD20を抗原とする抗体：NuB2に^{67}Cuを結合させ、その体内動態を、CD20陽性細胞を移植したSCID マウスを用いて検討した。抗体とRIの結合には1,4,8,11-tetraazacyclotetradecan- N,N',N'',N'''-tetraacetic acid (TETA)を用いた。検討の結果、^{67}Cu-TETA-NuB2は投与24時間で16.3 %dose/g、48時間で17.0 %dose/gと高い腫瘍集積性を示した（Fig. 1B）[5)]。

^{67}Cu標識薬剤の体内動態の検討結果から、これらの放射性薬剤の投与により高い腫瘍抑制効果が得られることが予測された。

References

1) Barbet J, et al., "Which radionuclides will nuclear oncology need tomorrow?", Eur. J. Nucl. Med. Mol. Imaging 33:627-30 (2006).
2) van Dieren EB, et al., "Absorbed dose distribution of the auger emitters ^{67}GA and ^{125}I and the beta-emitters ^{67}CU, ^{90}Y, ^{131}I, and ^{186}RE as a function of tumor size, uptake, and intracellular distribution.", Int. J. Radiat. Oncol. Biol. Phys. 36:197-204 (1996).
3) Fujibayashi Y, et al., "Copper-62-ATSM: a new hypoxia imaging agent with high membrane permeability and low redox potential.", J. Nucl. Med. 38:1155-60 (1997).
4) Katabuchi T., et al., "Production of 67Cu at JAEA-Takasaki for Nuclear Medical Application.", Proc. The Second International Symposium on Biomedical Research Using Accelerator Technology, Maebashi, Japan, p. 80 (2005).
5) Iida Y., et al., "Preclinical Evaluation of Radiolabeled Anti-CD20 Monoclonal Antibody, NuB2, for Cancer Therapy.", Proc. Eur. J. Nucl. Med. Mol. Imaging 32:suppl1 S206 (2005).

4-26 Nuclear Reaction Micro-Analysis of Boron Doped Steel

H.Shibata[a], Y.Kohno[b], T.Satoh[c], M.Oikawa[c], J.Haga[c] and T.Sakai[c]

[a] Graduate School of Engineering, Kyoto University, [b] Department of Materials Science and Engineering, Muroran Institute of Technology, [c] Department of Advanced Radiation Technology, TARRI, JAEA

An addition of trace amount of boron to steel materials improves mechanical properties. Behavior of boron additive, however, is not sufficiently understood because of the difficulty of microscopic analysis, although boron treatment may substantially prevent hydrogen from segregating at grain boundaries.

A proton microbeam from 3MV single ended electrostatic accelerator of TIARA facility was used for microanalysis of trace amount of boron. The mapping techniques of a trace amount of boron (several tens ppm) distribution by detecting γ-ray emitted from ^{10}B (p, α'γ) ^{7}Be and α-particle from ^{11}B (p, α) ^{8}Be nuclear reaction have been developed [1,2].

In this study in-air microanalysis system has been used for simultaneous γ-ray and X-ray measurements. The measurement system is described elsewhere[3]. For α-particle measurements, an annular type SSD detector (Canberra ANFD 300-20-300RM) has been installed in just front of sample inside the chamber as shown in Figure 1. As this setting disturbs X-ray measurement, simultaneous measurements of α-particle and X-ray become impossible. A typical current of several pA at the beam diameter of about 1μm was used for mapping area of 50 μm x 50 μm. The overall resolution of the proton beam can be kept nearly 1μm.

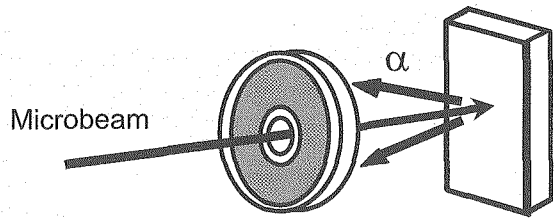


Fig.1. Schematic view of experimental setup for α-particle measurements.

Several types of steel specimens containing trace amount of boron were prepared for microanalysis. These steel samples divided in three categories. The first (category A) contained trace amounts of C, Si, Mn, P, S N and B. The second (Category B) contained these trace elements and rather rich amounts of Cr, W, Co, V. The third (category C) contained trace amounts of C, Si, Mn, P, S, Cr and V. The samples containing the same boron concentration in these categories could not be prepared this time. So, steel specimens containing 100 ppm (A1), 50 ppm (A2), 40 ppm (B1), 20 ppm (B2) boron bombarded by 1.7 MeV proton microbeam for γ-ray detection and sample containing 34 ppm boron (C1) bombarded by 1.32 MeV H_2^+ microbeam for α-particle detection, and these compared the appearance of boron distribution. In case of γ-ray measurements, X-rays from the same samples were also measured simultaneously for heavier elemental analysis.

An image of boron was obtained by gating to 428 keV γ-ray signals and a typical image of boron was shown in previous report [4]. This steel sample contained 50 ppm boron and heavier metal elements. Figure 2 shows boron distribution in iron containing 34 ppm boron which was obtained by detecting α-particle signals peaked at ~3.7MeV. The image was taken for 200 μm x 200 μm area scanned by ~ 2 μm$^{\phi}$ H_2^+ beam (middle) and 50 μm x 50 μm area scanned by about 1μm$^{\phi}$ beam (right and left hand side).

In Fig.2, many blocks of boron are observed. This phenomenon is caused by segregation of boron atoms doped in steel materials. This segregation may be appeared along with iron grain boundaries. Sizes of these blocks are from several mm to ~10 μm in diameter. In this study, any grains cannot be imaged, therefore, these blocks cannot be determined their locations. As intensities of γ-ray and α-particle signals also does not calibrate to the absolute value of boron density, concentration of boron in a block cannot be estimated. Though three samples (A1, A2 and C1) show the segregation of boron, B1 and B2 show uniform distribution. A1, A2 and C1 samples contain heavy elements, Cr and V, however B1 and B2 samples does not contain any heavy elements. We can conclude that heavy elements such as Cr and V affect the segregation of boron.

X-rays from iron samples were also measured, and lines of ingredients, such as Cr, W, Co, V, etc. were observed. Images of these elements show uniform distributions.

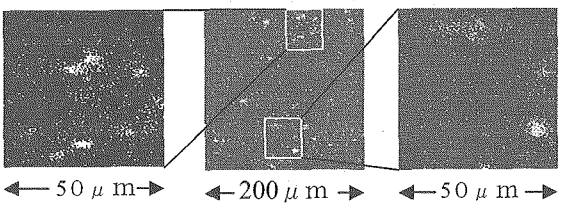


Fig.2. A typical α-particle image of 34 ppm boron contained in a steel specimen bombarded by 1.32 MeV molecular hydrogen microbeam

References

1) G.Demortier, Nucl. Instrum. Meth. Phys. Res. B 104 (1995) 244.
2) W.J.Trompetter,A.G.Reyes,I.C.Vickridge, A.Markwitz, Nucl. Instrum. Meth. Phys. Res. B 158 (1999) 568.
3) T.Sakai, T.Kamiya, M.Oikawa, T.Sato, A.Tanaka, K.Ishi, Nucl. Instrum. Meth. Phys. Res. B 190 (2002) 271.
4) H.Shibata, Y.Kohno, Y.Hosono, A.Amemiya, T.Satoh, M.Oikawa, and T.Sakai, JAEA-Review 2005-001, TIARA Annual Report 2004 (2005) 301-303.

4-27 Measurement of Three-Dimensional Structure of Biological Samples by STIM for PIXE Analysis

T. Satoh, T. Sakai and M. Oikawa

Department of Advanced Radiation Technology, TARRI, JAEA

Introductin

When biological samples which have thickness variation and internal constitution are analyzed with an in-air micro -PIXE system[1], X-ray yields have to be corrected using to X-ray production cross sections and linear attenuation coefficients. Because it is difficult to correct X-ray yields by micro-PIXE analysis by itself, three-dimensional distribution of an intracellular matrix must be accurately taken with spatial resolution of a few microns. Therefore, we used Scanning Transmission Ion Microscopy (STIM)[2], which can measure it easily using a particle detector located just behind the sample in the atmosphere. In our previous study[3], the elemental map by micro-PIXE for a spherical sample could be corrected by STIM under the assumption the ratio of major elements in the sample was constant. Though X-ray yields from symmetric and uniform samples can be fully corrected by STIM only, the rotation of a sample is required in the case of samples which have internal structure. If there are projection maps by STIM in all directions, the tomograms can be acquired in the same way as CT scan. This method is called STIM-CT[4]. To get three-dimensional distribution of intracellular matrix, we attempted STIM-CT of plant cells in this study.

Experiment

The schematic diagram of our experimental apparatus is shown in Fig. 1. The 3MV single-ended accelerator and the micro-PIXE system at the TIARA were used. The 3 MeV proton microbeams were scanned over a target. The diameter of the microbeam was 1 μm. Polycarbonate foil 5 μm thick was used as a beam extraction window. A target was glued on the needle which was rotated by 180° at intervals of 15°. A surface barrier detector was placed just behind the target. Every data set consisting of the particle energy measured by the detector and the bombardment position measured as the beam scanning voltages was recorded and digitalized by a PC. Cultured and dried cells of pennycress (*thlaspi caerulescens*) were used as targets. Figure 2 is a photograph of the test sample.

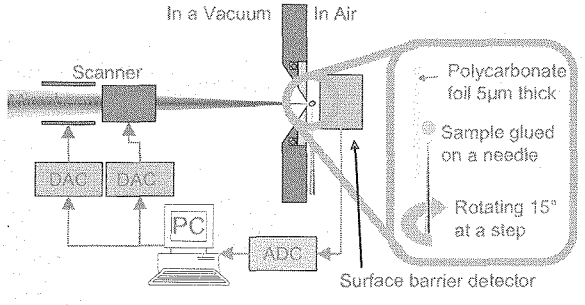


Fig. 1 Schematic diagram of our experimental apparatus. A sample was glued on a needle.

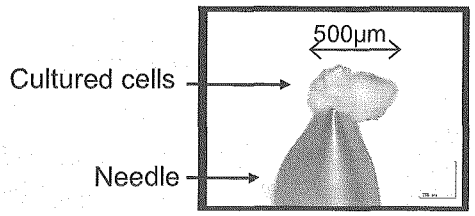


Fig. 2 Optical microscope image of the target. The upper part is a mass of cultured cells. The lower part is the tip of a needle.

Results

Figure 3 shows a projected image measured by STIM. The needle was turned by a step at 15° after this image was measured. This procedure was repeated eleven times, so that twelve projected images were obtained. The tomographic image at A line in Fig. 3 is shown in Fig. 4. It was successfully reconstructed by the back projection method with Shepp and Logan filter.

Acknowledgement

The authors wish to thank Professor Sekimoto (Utsunomiya University) for preparation of the samples.

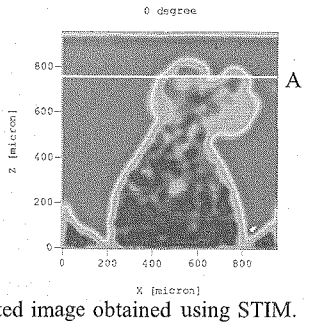


Fig. 3 Projected image obtained using STIM. There were 12 similar images (0°, 15°, 30°, 45°, 60°, 75°, 90°, 105°, 120°, 135°, 150°, 165°) per sample.

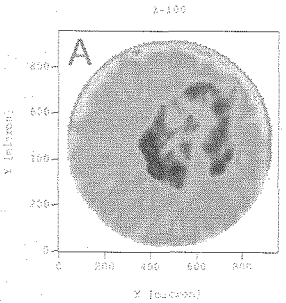


Fig. 4 Tomographic image at line A in Fig. 3. This was obtained by the back projection method.

References

1) T. Sakai, et al., Int. J. PIXE Vol. 10 Nos. 3 & 4 (2000) 91.
2) J.C. Overley, et al., Nucl. Instr. and Meth. B30 (1988) 337.
3) T. Satoh, et al., Nucl. Instr. and Meth. B249 (2006) 234.
4) C. Michelet, et al., Nucl. Instr. and Meth. B150 (1999) 173.

4-28 Analysis of Radiation-Induced Cell Death In Vivo by Micro Particle-Induced X-Ray Emission (Micro PIXE)

M. Hasegawa[a,c,d], H. Sakurai[a,c], S. Ishiuchi[b,c], T. Tamamoto[d], I. Asakawa[d], M. Shin[a,c], M. Oikawa[c,e], T. Satoh[e], T. Kamiya[c,e], K. Arakawa[c,e] and T. Nakano[a,c]

[a]Departments of Radiation Oncology and [b]Neurosurgery, and [c]21st Century COE Program, Gunma University Graduate School of Medicine, [d]Department of Radiation Oncology, Nara Medical University School of Medicine, and [e] Department of Advanced Radiation Technology, TARRI, JAEA

Abstract

A human ependymoblastoma, a human glioblastoma, and a human small cell lung cancer (SCLC) transplanted to nude mice were irradiated with 200 kV X-rays. Tumors were excised 3, 4.5, or 6 hours after 10Gy irradiation, and samples were prepared for evaluating the changes of elements associated with cell death, especially apoptosis and necrosis, by using a micro-particle-induced X-ray emission (micro-PIXE). Phosphorus (P), potassium (K), chlorine (Cl), and sulphur (S) were shown in the nuclei and the cytoplasm of tumor cells. Apoptosis was frequently induced 3-6 hours after irradiation in the ependymoblastoma, but no significant change of elements was demonstrated compared with the non-irradiated tumors. Necrosis was often found in the glioblastoma and the SCLC, and P, K, Cl, and S were decreased in those areas.

アポトーシスや壊死に代表される細胞死については、分子生物学レベルで解明が進んでいるが、放射線によって誘発される細胞死についても関与するシグナル伝達、遺伝子、蛋白のレベルの変化が明らかにされつつあり、さらに細胞内外の元素の分布、動態も重要と考えられている。大気マイクロPIXE(Particle Induced X-ray Emission)によって細胞内元素の分布の画像化が可能となったので、本研究ではまず組織標本での検索技術を確立することを目的として、凍結切片の急速乾燥標本を作製して検索した。次にその有用性を具体的に明らかにすることを目的として、放射線照射前後のin vivoの細胞死、特に壊死、アポトーシスにおける元素分布の変動を解析して検討した。

ヒト由来でヌードマウス可移植性の上衣芽腫(p53野生型)、ヒト膠芽腫、ヒト小細胞肺癌（p53変異型）を雄性ヌードマウス(BALB/cA-Jcl nu/nu)皮下に移植して、200 kV X線10 Gy (Stabilipan 2, Siemens)で10Gy 1回照射後、3時間、4.5時間、6時間に摘出して、5μ、10μの凍結切片を作成し、マイラー膜に貼付後、急速に乾燥固定した標本を作製して、大気PIXEで検索した。さらに観察後の標本をヘマトキシリンで染色して、光学顕微鏡で検索し、同一標本における元素分布と組織所見（特に壊死、アポトーシス）を対比した。

対照群腫瘍（非照射）では、3種類のいずれの腫瘍でも胞巣にほぼ一致してリンP、カリウムK、クロールCl、硫黄Sの分布を認め、細胞質、核のいずれにも分布していると思われたが、カルシウムCa、ケイ素Si、鉄Feの分布には細胞との有意な相関は認められなかった。一部の標本には粒状のCaが散見されたが、組織所見との有意な相関は認められなかった。膠芽腫および小細胞肺癌の非照射群では小壊死巣が散見され、これに一致してP、K、Cl、Sの有意な低下を認めた。

照射群腫瘍では、上衣芽腫、10Gy照射後3～6時間にアポトーシス誘発を光学顕微鏡で高率に認め、TUNEL陽性であったが、PIXEでは5μおよび10μ厚のいずれの標本でも、対照群と比較して有意な変化は指摘できず、基本的には対照群とほぼ同様な所見であった(Fig. 1)。膠芽腫および小細胞肺癌では、照射群でも小壊死巣が散見され、壊死や組織欠損部分に一致してP、K、Cl、Sの有意な低下を認めたが(Fig. 2)、Ca、Si、Feには有意な変化を認めなかった。

大気マイクロPIXEの腫瘍組織レベルの応用についての検討で、壊死巣の描出が可能であることを示し、放射線生物学分野における有用性を示唆できた[1]。ただし、組織(in vivo)に関しては、これまでの検索方法では光学顕微鏡に比較して分解能が劣るので、アポトーシスに伴う元素の変化を明らかにするためにはさらに検討が必要である。

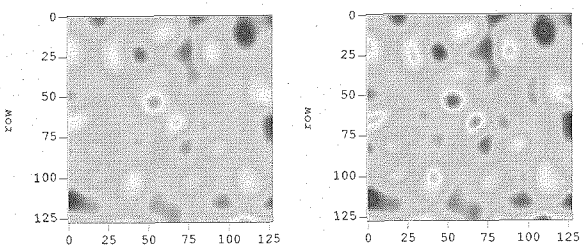


Fig. 1 Distribution of phosphorus (left) and potassium (right) in the ependymoblastoma 6 hours after 10Gy irradiation.

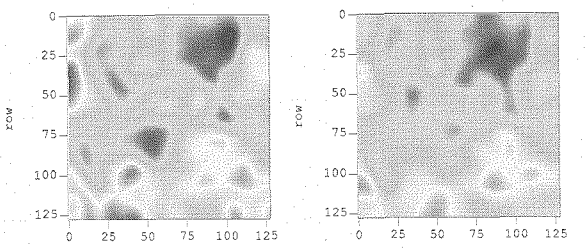


Fig. 2 Distribution of phosphorus (left) and potassium (right) in the gliobalstoma 6 hours after 10Gy irradiation.

References

1) T. Nakano、K. Arakawa、M. Hasegawa、T. Kamiya、et al. Research of disease onset mechanism by determining the distribution of intracellular trace elements using an in-air micro-PIXE analyzer system. Int J PIXE (submitted).

4-29 Studies on the Cadmium Distribution of Acute Cd Toxicity in Testis Using In-Air Micro Particle Induced X-Ray Emission (PIXE)

T.Kusakabe [a,b], T.Nagamine [a,b], H.Takada [a,b], K.Nakazato [a], K.Suzuki [a], K.Nakajima [a], T.satoh [c], M.Oikawa [b,c] and K.Arakawa [b,c],
[a] School of Health Sciences, Faculty of Medicine, Gunma University, [b]21st Century COE Program, Gunma University, [c]Department of Advanced Radiation Technology, TARRI, JAEA

Abstract

Cadmium (Cd) is an industrial and environmental pollutant that is toxic to cells and organs . Cd is also well known to induce apoptosis and necrosis in liver, edema in lungs, and hemorrhagic necrosis in testis .

To clarify the mechanism of acute Cd toxicity in testis, we have analyzed intracellular distribution of metal elements such as Cd, Fe, Cu, Zn using in-air micro PIXE.

The rats were injected a single intraperitoneal injection (i.p.) of $CdCl_2$(1mg/kg) and sacrificed at 6,12,24h .

The testis Cd concentration determined by ICP-MS was significantly increased after Cd injection in 6 h. In-air micro PIXE showed marked accumulation of Fe in interstitium and seminiferous tubules 6h after Cd injection.

At 12h after an injection of Cd , the blood testiculus barrier (BTB) was injured, and Cu and Fe were accumulated in the circumference of basement membrane of seminiferi tubuli. In addition, the increased TBARS concentration in testis was observed after Cd injection in 24h.

Summary: The findings suggest that Fe may participate in Cd-induced testis damage through production of reactive oxygen species.

1. はじめに

重金属の一種であるカドミウム（Cd）は世界各国で使用され環境中に多く排出されており、特に精巣に対して非常に高い感受性を示し、血管内皮の障害を生じさせ精巣の出血性壊死を引き起こすことが報告されている。

また、Cdによる直接のDNA障害ではなく金属の曝露により生成される活性酸素種が引き金となり精巣の障害が生じることも報告されている。また、Leydig細胞における脂質過酸化物と鉄の増加が生じることから組織障害への陽イオンの関与も示唆されている。本研究においてCdの急性暴露における精巣障害と精巣組織中の金属元素変動の解明を試みたので報告する。

2. 実験方法

Wistar ラット(350-400g)に体重1kgあたり1mgのCdを１回腹腔内投与し、コントロール群は生理食塩水の腹腔内投与を行った。

投与後6,12,24時間後にエーテル深麻酔下にて屠殺後、精巣を摘出し-80℃に保存した。その後クリオスタットにて15 μ mに薄切し、常温下でマイラーフィルム(10 μ m)上にて乾燥し大気マイクロPIXE分析を行った。

大気マイクロPIXE分析は日本原子力研究開発機構高崎量子応用研究所イオン照射研究施設（TIARA）の大気マイクロPIXE分析システムを用いて分析を行い、3MVシングルエンド加速器より発生させた加速電圧3.0MeVのプロトンマイクロビームを用い45分間照射を行った。

また、精巣組織中のCd濃度を精巣組織を湿式灰化後ICP-MSを用いて測定し、酸化ストレスの指標としてThiobarbituric Acid Reactive Substances(TBARS)濃度を測定した。

3. 結果及び考察

Cd投与後における精巣組織中のCd濃度は6時間後から有意な上昇を示し12時間後に最大値を示した。また、精巣組織中のTBARS濃度は組織中のCdの濃度増加とともに増加した。これらのことからCdによる精巣の組織障害に酸化ストレス(ROS)が関与することが示された。

また、大気マイクロPIXE法による分析結果からCdの組織中の濃度増加とともに精巣組織中の鉄の分布の増加が確認されCdによる組織障害への鉄の関与が示唆された。

また、投与12時間後において銅と鉄の精細管の上皮における集中が確認された(Fig1)。組織学的所見から精細管の障害が生じていることが確認されていることから、血液精巣関門（BTB）の崩壊により銅や鉄が精細管内に流入し精巣の組織障害を強めていることが示唆された。

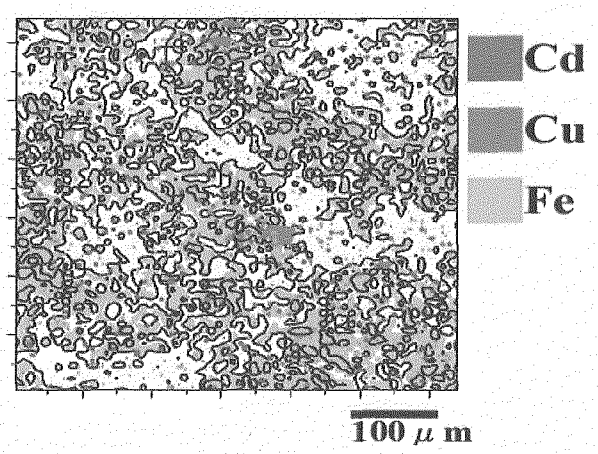


Fig1. Element maps of testis analyzed by in air Micro-PIXE . The rats were injected a single intraperitoneal injection (i.p.) of $CdCl_2$(1mg/kg) and sacrificed at 12h after an injection. . Marked accumulation of Cu and Fe was shown in the circumference of basement membrane of seminiferi tubuli.

4-30 Analysis of Boron Distribution in 9L Gliosarcoma Cells Using Particle Induced γ-ray Emission (PIGE)

K. Endo[a)], T. Yamamoto[a)], Y. Shibata[a)], K. Tsuboi[a)], A. Matsumura[a)], H. Kumada[b)], K. Yamamoto[b)], T. Sakai[c)], T. Satoh[c)], M. Oikawa[c)], Y. Ohara[c)] and K. Ishii[d)]

[a)]Department of Neurosurgery, Institute of Clinical Medicine, University of Tsukuba, [b)]Department of Research Reactor, NSRI, JAEA, [c)]Department of Advanced RadiationTechnology, TARRI, JAEA, [d)]School of Engineering, Tohoku University.

Abstract

We have applied micro particle induced X-ray emission (micro-PIXE) to determine inter- and intracellular distribution of boron (^{10}B) and Gadolinium (^{157}Gd). Because the energy of micro-PIXE from ^{10}B is too low, we employed a method to detect gamma-ray produced from the nuclear reaction of ^{10}B, namely particle induced gamma-ray emission (PIGE). We showed the results of inter and intracellular distribution of boron elements in tumor tissue using micro-PIGE. However, further investigation is necessary to obtain higher spatial resolution and the optimization of the measurement time or the improvement of the sampling methods should be investigated. In future, this method will be applied to analyze the intracellular micro-distribution of the capture element and development of new drugs for NCT.

悪性脳腫瘍に対する放射線治療法の一つとして硼素中性子捕捉療法（Boron Neutron Capture Therapy: BNCT）の臨床研究が進められている。そしてこの治療法の効果は腫瘍細胞内における硼素元素の分布状態に大きく影響を受けると考えられているため、これを解明することは効果的なBNCTのためには重要である。これまでにも硼素元素の腫瘍内での分布やその動態の研究が報告されてきたが、これを画像的に明らかにした報告はまだないのが現状である[1,2]。

そこで本研究ではTIARAのSingle-ended acceleratorを用い、特にγ線を測定するparticle induced γ-ray emission （PIGE法）を導入することで、9Lgliosarcoma腫瘍細胞における硼素元素（^{10}B）の分布状態を細胞レベルで測定することを目的とした。

実験方法は、まずラットの皮下に予め9Lgliosarcoma腫瘍細胞を移植し、２週間増殖させる。十分に増殖後硼素含有薬剤（BSH）を尾静脈内より投与する。硼素が腫瘍細胞に取り込まれた１２時間後に腫瘍細胞を摘出し、凍結後薄切標本を作製しマイラー膜上に固定、ここにマイクロビームを照射し測定した。通常のparticle induced X-ray emission（PIXE）法での硼素元素の特性X線エネルギーは小さく測定が困難なため、今回核反応により発生するγ線を測定するPIGE法を用いることで硼素元素（^{10}B）を直接測定することが可能となった。

測定結果はFig. 1に示す如く、黒いドットで示される硼素元素の分布は、腫瘍細胞（淡灰色で示される部分）分布に多く一致して観察された。これより硼素含有薬剤BSHは腫瘍細胞に取り込まれている可能性が示唆された。しかしまだ最終的な目的としている細胞内器官と硼素元素分布との相関関係の確定には至っていない。また腫瘍細胞の存在していない箇所からも硼素元素が測定されている。これらの測定結果から本当に腫瘍細胞内に取り込まれた結果なのか、あるいは固定時の手技上の問題などで周囲に湧出などしてしまった部分をも測定した結果なのかなどまだ明確ではない。これらを解明するために、今後は試料の急速凍結固定など固定方法の工夫、または正常組織・細胞における硼素元素分布の測定結果との比較など、今後も実験を予定している。

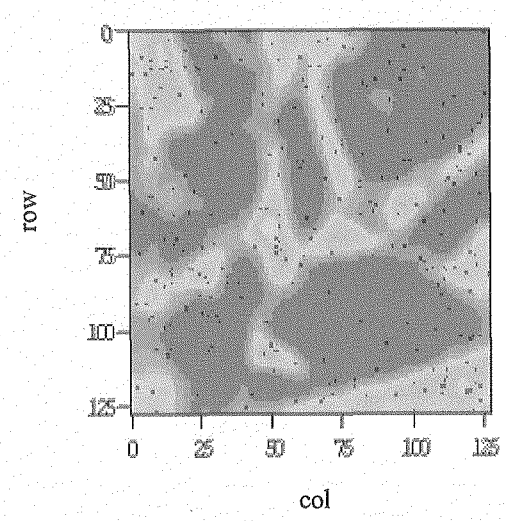


Fig.1. Superimposed image of 9L gliosarcoma cells and the distribution of boron elements.

References

1) Coderre JA, Chanana AD, Joel DD, Elowitz EH, Micca PL, Nawrocky MM, Chadha M, Gebbers J-O, Shady M, Peress NS, Slatkin DN: Biodistribution of boronophenylalanine in patients with glioblastoma multiforme: Boron concentration correlates with tumor cellularity. Radiat Res 149: 163-170 (1998).

2) Wegden M, Kristiansson P, Ceberg C, Munck af Rosenschoeld P, Auzelyte V, Elfman M, Malmqvist KG, Nilsson C, Pallon J, Shariff A: Nuclear microprobe analysis of the selective boron uptake obtained with BPA in brain tumour tissue. Nucl Instr and Meth in Phys Res B 219-220: 67-71 (2004).

4-31 Standard Reference Material for Determination of Platinum in Biological Materials by Micro Beam PIXE

Y. Iwata[a)], K. Ishii[b)], M. Fukuda[c)], T. Kamiya[c)], T, Satoh[c)], M. Oikawa[c)] and T. Sakai[c)]

[a)]Department of Chemistry, Faculty of Education and Human Studies, Akita University
[b)]Department of Quantum Science and Engineering, Graduate School of Engineering, Tohoku University
[c)] Department of Advanced Radiation Technology, TARRI, JAEA

Abstract

Standard Reference Material (SRM) is indispensable to the calibration of apparatus and the evaluation of the accuracy and precision of analytical technique. Previous work, we showed utilities of several macro porous cation-exchange resins for micro PIXE analysis. In this work, we made SRM containing the known amount of platinum in anion-exchange resin. Macro porous anion-exchange resin, Macro-Prep 25Q (BioRad) was suspended in 2 M HCl and added the known amount of $PtCl_6^{2-}$. The concentration of Pt in the resin was 20-200 ppmv. Individual particle of the resin was subjected to 3 MeV proton bombardments by micro beam system of TIARA. It was found the macro porous nature of the resin (pore size; 72.5nm) allows $PtCl_6^{2-}$ ion to access the exchange sites located throughout the matrix. This SRM is similar to biological cell because it is spherical in shape and its matrix elements are carbon, oxygen and hydrogen. This SRM made of macro porous resin has a possibility for use as pseudo-biological SRM for micro beam PIXE.

PIXE分析を含め、ほとんどの機器分析において、装置の校正や分析結果の相互比較のために標準物質(SRM)は、不可欠である。これまで、粒径が25から100μmで球状の陽イオン交換樹脂に、微量元素を付着させたSRMを作成し、TIARAマイクロPIXEシステムと日本アイソトープ協会仁科記念サイクロトロンセンター（NMCC）ノーマルPIXE分析システムを用い、生体試料分析に対する有効性を報告してきた。この検討では、TIARAにおける Cu、Zn等の生体必須元素の画像化の下限値（5ppm程度）を求めた[1)]。また粒径25ミクロンの多孔質の構造を持つマクロポーラス型陽イオン交換樹脂に、微量の金属陽イオンを球体全体に均一に付着させた粒子状試料の作成に成功し、分析感度、分解能、照射安定性において優れたSRMになりえることを示した。

一方白金は、装飾用、触媒として需要が高く、またその錯体は抗ガン剤として研究やその臨床利用が行われている。このため、本連携研究の群馬大医チームをはじめとして、白金の細胞内分布がマイクロPIXEシステムで研究されている[2)]。そこで本研究では白金化合物として安定な塩化白金酸(IV) ($PtCl_6^{2-}$) を選び、この陰イオンをマクロポーラス型陰イオン交換樹脂に吸着させることで白金分析用SRMの開発を検討したので報告する。

マクロポーラス型陰イオン交換樹脂（Macro Prep 25Q：四級アンモニウム型 粒径25 μm 、ポアサイズ725Å、BIORAD）の約10mlを50mlのガラス遠沈管にとり、純水を加えて懸濁させた。3000rpmで5分間遠心分離し、上澄みを除いた。この操作を3回繰り返した後、同様の操作を2M塩酸で3回繰り返した。2M 塩酸に懸濁した陰イオン交換樹脂を10mlメスピペットにとり一昼夜放置し樹脂を沈降させ、樹脂の体積を測定した。樹脂0.5 ml含む懸濁液1.0 mlをガラスバイアルにとり、$PtCl_6^{2-}$の標準溶液（２M 塩酸溶液）を加え、15時間以上穏やかに振とうした。樹脂体積あたりの白金含有量は、20－200 ppmvとした。樹脂は、懸濁液の状態で保存した。このように、一定体積の樹脂と目的元素の白金標準溶液を混合するだけで、簡便にSRMを調製することができた。今回は$PtCl_6^{2-}$の樹脂への吸着を促進するために2M硝酸酸性下で振とうしたが、他の陰イオンの陰イオン交換樹脂の吸着反応は、分配現象としてよく研究されている。本法は大部分の-2、-3価の陰イオンに適用できると期待される。この有用性をNMCCならびにTIARAで確認した。

NMCCにおけるノーマルPIXE分析用のため、この陰イオン交換樹脂の懸濁液を薄膜状に加工した。懸濁液0.2 μlを水約５ml で希釈し、すぐに孔径10 μm のニュークリポアポリカーボネートフィルター上に吸引濾過した。濾過の面積は２ cm^2であった。顕微鏡観察により、フィルター上に均一に樹脂が分布していることを確かめた。ビーム径2mmの3MeV プロトンビームを照射した。添加した白金量に対する、単位照射電荷量あたりのX線の強度を測定し白金添加量の定量性が優れていることが確かめられた。40μCの連続照射でも安定性に優れていた。

TIARAマイクロPIXEシステム分析用のため、マイラー膜を貼り付けたターゲットホルダー上に、樹脂の懸濁液を付着させた。キムワイプのこよりで水分を吸い取った。実体顕微鏡下顕微鏡下で、樹脂が重なり合わないように、口径1mmのターゲット上に楊子を使って樹脂をばらまいた。3MeV プロトンビームをサブミクロンに絞り、スキャンエリアを60 x 60あるいは30 x 30 μm とし大気中100-800 nCの照射を行った。

TIARAマイクロPIXEシステムによる、マクロポーラス型陰イオン交換樹脂中の白金の画像をFig. 1 に示す。白金添加量は200ppmv、スキャンエリアは29 x 29 μm、照射電荷量は400 nCである。白金の分布は、樹脂が球体とした場合とよく一致しており、樹脂内に白金が均一に分布していることが確かめられた。白金の添加量を20－200ppmvと変化させたが、樹脂内の白金の分布を画像化できた。このSRMは生体細胞に類似の大きさ、形状、元素組成を持つマトリックス中に、正確量の白金を含むため、抗がん剤の細胞内分布の定量化への応用が期待される。

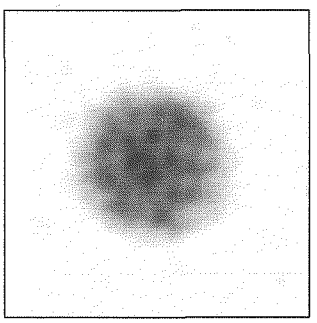


Fig. 1 PIXE image for Pt in Macro-Prep 25Q by Micro Beam System

References

1） Y. Iwata, K. Ishizawa, T. Sakai, T, Satoh, M. Oikawa, JAERI-Review, 2004-25, 278-279

2） 木村仁、桑野博行他、第1回高崎量子応用研究シンポジウム要旨集 p173

4-32 Development of In-Air On/Off -Axis STIM

K. Inomata [a], K. Ishii [a], R. Oyama [a], H. Yamazaki [a], S. Matsuyama [a], K. Yanai [b], E. Sakurai [b], T. Kamiya [c], T. Sakai [c], T. Satoh [c], M. Oikawa [c] and K. Arakawa [c]

Department of Quantum Science and Energy Engineering, Tohoku University [a]
Department of Pharmacology, Tohoku University School of Medicine [b]
Department of Advanced Radiation Technology, TARRI, JAEA [c]

PIXE (Particle Induced X-ray Emission) is a powerful method for the analysis of trace elements. Micro-PIXE is capable of providing spatial distributions of elements on the micron scale by focusing the beam spot to within 1 μ m. In-Air Micro-PIXE has been developed at the TIARA.

In order to carry out accurate quantitative analysis in In-Air Micro-PIXE, it is necessary to take account of the X-ray self absorption in the sample. STIM (Scanning Transmission Ion Microscopy) is helpful for the measurement of the thickness and density of the sample. In STIM, the energy of particle after passing through the sample is measured and the energy loss is estimated. In the case of thin target sample, the energy loss is proportional to $\Sigma N_i Z_i$ δx where Z_i and N_i are the atomic number of an element i and the number of the element i per unit volume, respectively and δx is the thickness of target sample, which can be approximated by $\delta x \Sigma N_i A_i$ /2 ($Z_i \sim A_i$ /2 where A_i is the atomic mass of the element i). Therefore, the energy loss is approximately proportional to the product of the thickness δx and the density ρ ($=\Sigma N_i A_i$) of the sample. Because the incident particles passing through the sample are directly detected, STIM cannot be carried out with high beam intensity due to the limit of counting rate of detector, whereas PIXE requires the high beam intensity to detect very trace elements. We developed a peculiar method of STIM which can be carried out with In-Air Micro PIXE simultaneously. This peculiar STIM is called In-air on/off-axis STIM, which is reported here.

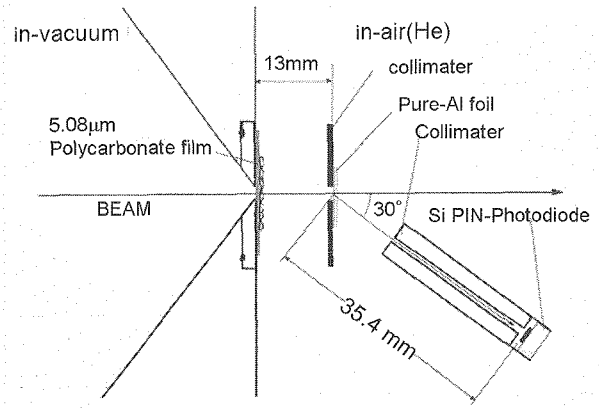


Fig.1. In-air on/off-axis STIM system

Figure 1 shows the experimental setup of the In-air on/off-axis STIM connected with the In-Air micro PIXE camera. Thin pure Al foil is placed at the position of 13 mm from the sample target foil of the In-Air micro PIXE camera and a Si PIN-photodiode detector of which the energy resolution is 14keV is set to look into this foil through a collimator of 1 mm in diameter at an angle of 30 degree with respect to the beam direction.

Since the counting rate can be reduced by measuring particles scattered with the Al foil instead of direct beams, In-air on/off-axis STIM can be carried out with high beam intensity. Moreover, In-air on/off-axis STIM does not interfere with In-air micro-PIXE analysis because an X-ray detector of the In-air micro-PIXE camera is placed to not look into the Al foil. The reason why Aluminum was selected as scattering element is that the natural abundance of Al^{27} is 100%. The STIM system is filled with He gas to decrease beam scattering and energy loss.

We demonstrated the performance of In-air on/off-axis STIM using RBL-2H3 cells. The distribution of density $\rho\delta x$[μg/cm^2] of RBL-2H3 cells derived from the energy spectra of In-air on/off-axis STIM is shown in Fig.2. Figure 3 shows the map of absorption correction factor calculated with the on/off-axis STIM data for Mg K-X-rays.

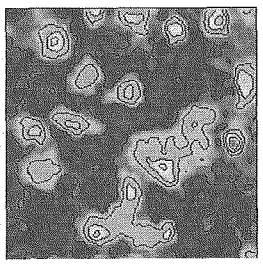


Fig.2. Map of $\rho\delta x$ [μg/cm^2].

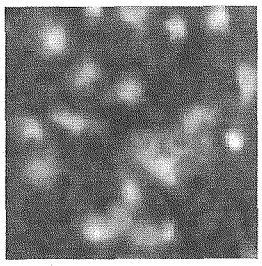
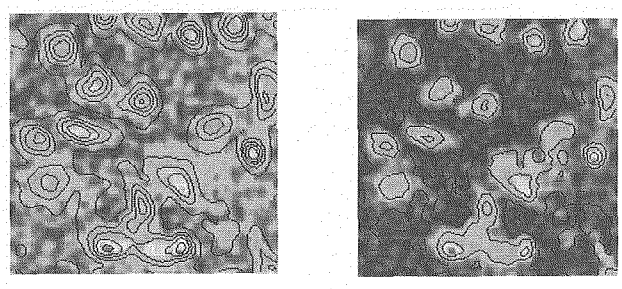


Fig.3. Map of absorption correction factor for Mg K-X-ray.



(a) (b)

Fig.4. Concentration image of Mg without absorption correction (a) and with correction (b)

Figure 4 (a) shows the concentration image of Mg element obtained by the In-air micro-PIXE camera without absorption correction. The corrected concentration image of Mg element is obtained by multiplying the image of Fig.4 (a) by the absorption correction factor of Fig.3 and is shown in Fig.4 (b). It was shown that the contrast of concentration of Mg is improved by absorption correction.

4-33 Fundamental Research of Highly Sensitive PIXE by Grazing Exit X-Ray Measurement

K. Tsuji[a)], S. Yamamoto[b)], T. Sakai[c)], M. Oikawa[c)], T. Sato[c)] and K, Arakawa[c)]

a) Osaka City University
b) Environment and Industrial Materials Research Division, Qu BS, JAEA
c)Department of Advanced Radiation Technology, TARRI, JAEA

Abstract

Grazing exit X-ray spectrometry is a surface sensitive method. Since X-rays emitted from inside sample are refracted at surface, such X-rays are stopped by a slit that was placed between the sample and the detector. Therefore, only the X-rays emitted from the sample surface are detected. This X-ray analytical technique was applied to PIXE. A precise rotating goniometor was installed to a sample vacuum chamber in order to control the exit angle. Thin Co films having different thicknesses were prepared and measured by grazing exit PIXE (GE-PIXE). A good linear relationship between Co film thickness and Co Ka intensity. This result indicates that GE-PIXE is a promising method for surface-sensitive quantitative method.

斜出射X線分析法は何らかの方法で励起された特性X線を固体表面からすれすれの角度で測定する方法である[1)]。試料中の深い場所で発生したX線は表面で屈折し、試料と検出器の間に設けたスリットにより遮断される。よって、検出器には届かない。結果として固体表面から発生したX線のみが観測されることになる。そこで、斜出射X線分析法は表面に敏感な方法として知られている。この方法の利点はマイクロビーム励起と組み合わせることができる点である。つまり、マイクロビームにより微小部分析を、斜出射法により表面分析を行えば、「微小部の表面分析」が可能となる。今回、この斜出射法をPIXEに応用した。

Fig. 1 には斜出射PIXE実験のために組み上げた装置図を示す。プロトンビームは試料に対して約45度に入射し、発生した特性X線はスリットを通してエネルギー分散型X線検出器で測定した。試料は高精度ゴニオメーターにより回転できる仕組みとなっている。なお、この角度制御は自動遠隔制御が可能となっている。

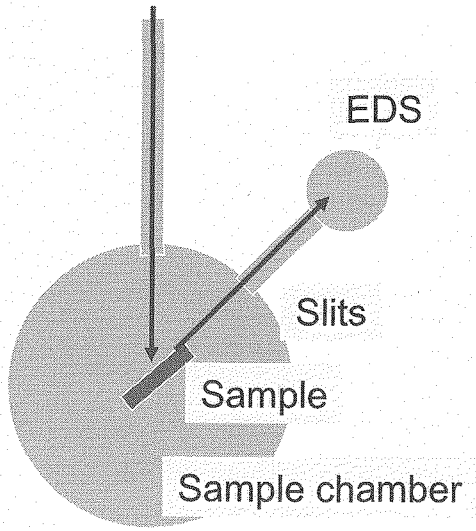


Fig.1 Experimental setup of grazing exit PIXE (GE-PIXE). The sample was attached to a precise rotating stage in a sample vacuum chamber to control exit angle. Characteristic X-rays were measured an energy dispersive X-ray detector through a slit.

試料としては膜厚の異なるCo薄膜をマグネトロンスパッタリング法にシリコン基板上に準備した。Fig. 2には斜出射PIXEにより発生したCo Kα線強度とCo薄膜の厚さとの関係を示す。この測定は取り出し角度を0.6度に固定して行った。両者には相関係数0.9988と良好な数値が得られた。このことは斜出射条件下において斜出射PIXE法は十分な定量性を有していることを示唆している[2)]。

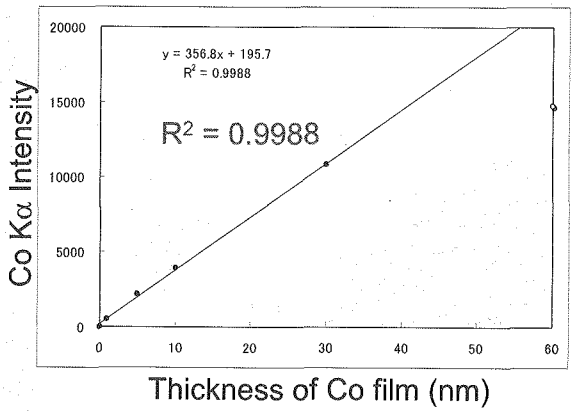


Fig.2 Relationship between thickness of Co thin films (X-axis). and Co Kα intensity (Y-Axis)

References

1) K. Tsuji, Grazing-Exit X-Ray Spectrometry, " XRay Spectrometry: Recent Technological Advances", edited by K. Tsuji, J. Injuk, R. E. Van Grieken, John Wiley & Sons, Ltd, p. 293-305, (2004).
2) K. TSUJI, "Grazing-Exit and Micro Wavelength-Dispersive X-Ray Spectrometry (GE-WDXRS and μ-WDXRS)", EXRS 2006, 19-23 June, 2006, Paris, France.

4-34 Micro-Machining of Resists on Silicon by Proton Beam Writing

N. Uchiya [a)], T. Harada [a)], M. Murai [a)], H. Nishikawa [a)], J. Haga [b)], T. Sato [b)], M. Oikawa [b)], T. Sakai [b)], Y. Ishii [b)], M. Fukuda [b)], T. Kamiya [b)] and S. Yamamoto [c)]

[a)]Department of Electrical Engineering, Shibaura Institute of Technology, [b)]Department of Advanced Radiation Technology, TARRI, JAEA, [c)]Environment and Industrial Materials Research Division, QuBS, JAEA

Proton beam writing (PBW) is a direct write technique for fabrication of micro- or nano-meter sized structures. Since the scattering of protons with energy of MeV order is suppressed compared with electrons, the PBW is a promising technique for the micro-machining of structures with a high aspect ratio[1)]. Compared with x-ray, extreme UV (EUV) light and electron beam, the proton beam has the following advantages. First, high-energy protons with energy of MeV order scatter less than low-energy electrons with energy of several tens of keV implanted into the same depth of materials. Second, the scanning of the proton beam enables a direct write process without expensive masks required for the exposure with the x-ray or the EUV light. Third, the depth of the proton penetrating into resist materials is controlled by the acceleration energy. Especially, based on the first advantage, the PBW is effective for micro-machining with a capability to produce structures on thick resist with a high aspect ratio[1, 2)].

We report the results of proton beam writing on positive and negative resists such as PMMA and SU-8 on silicon, respectively. After the developments, the micrometer-sized structures on silicon by the PBW were evaluated by scanning electron microscope (SEM).

We used a typical positive resist, PMMA and a negative resist, SU-8, both purchased from Micro Chem Corp. The PMMA was dropped and spin-coated at a speed of 1000 rpm on a silicon substrate. The spin-coated PMMA film was then baked at a temperature of 170 C for 30 min. The SU-8 was spin-coated at a speed of 2000 rpm on a silicon substrate and was prebaked at a temperature of 95 C for 3 min. Consequently, the PMMA film was 5 μm in thickness and the SU-8 film was 21 μm.

These resist films on silicon were subjected to the scanning of the 1.7 MeV focused proton beam with a 3-MV single-ended accelerator at the microbeam facility of TIARA, JAEA. The diameter of the proton beam was focused to about 1 μm, which is estimated on the basis of the secondary electron image from a nickel mesh. The fluence of the proton was counted as electrical charges per unit area (nC/mm^2) and controlled by exposure time, beam current and irradiation area in the ranges from 50 to 200 nC/mm^2. After the proton beam writing, the resists were developed and rinsed. In the case of the PMMA, the development with IPA-water (7: 3) was performed for 20 minutes and rinsed in demonized water[3)]. The SU-8 samples were developed for 3 minutes using an exclusive developer and rinsed in IPA. These samples were observed by the SEM and after Pt sputter coating to avoid charging of the samples.

Resists such as PMMA and SU-8 on silicon were scanned by PBW with various drawing patterns including a grid, circles, and dots. These patterns can be written over the area of 700 μm by 700 μm. Figure 1 shows an SEM image of the side wall of a grid patterned PMMA (fluence: 100 nC/mm^2). The irradiated area is removed in the case of the positive resist. A 1.1-μm-wide trench with a depth of 5 μm was observed. Formation of the vertical side walls can be ascribed to the small lateral scattering of protons and homogeneous distribution of the electronic stopping power at the relatively small depth of 5 μm. The smooth sidewall can be explained by the fact that the linewidth is insensitive to the current fluctuation around the fluence of 100 nC/mm^2.

Figure 2 is a SEM image of SU-8 developed after the irradiation at 1.7 MeV with a dot pattern (fluence: 100 nC/mm^2). Since the irradiated area remains for the negative resist after development, the structure of pillars was formed. The width of the pillar was 1.1 μm at the top and 2.2 μm at the bottom on the silicon substrate with a height of 21 μm. The increasing width of the pillars along the depth is ascribed to the lateral scattering and inhomogeneous depth distribution of the electronic stopping power. The angle of the sidewall against the surface of the substrate was 91.4 degrees that was close to 91.5 degrees estimated by SRIM simulation[4)]. This result shows that PBW is suitable for the micromachining of high aspect ratio structures.

The above mentioned feature such as vertical sidewall with smooth surface for the positive and negative resists confirmed that the PBW technique is useful for the micro-machining of thick resists with several tens of micrometers.

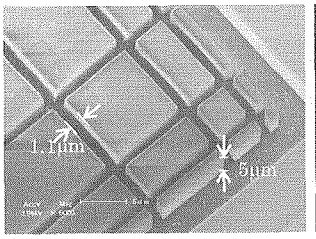


Fig.1 SEM image of 5-μm thick PMMA with grid pattern by PBW at 1.7 MeV (fluence: 100 nC/mm^2).

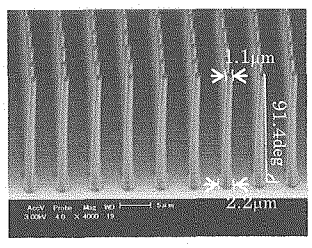


Fig.2 SEM image of 21-μm height SU-8 pillars by PBW at 1.7 MeV (fluence: 100 nC/mm^2).

References

1) S. V. Springham, T. Osipowicz, J. L. Sanchez, S. Lee, and F. Watt, Proc. SPIE Int. Soc. Opt. Eng. 3183 (1997) 128.
2) A. A. Bettiol, K. Ansari, T. C. Sum, J. A. van Kan, and F. Watt, Proc. SPIE Int. Soc. Opt. Eng. 5347 (2004) 255.
3) K. Ansari, J. A. van Kan, A. A. Bettiol, and F. Watt, Appl. Phys. Lett. 85 (3) (2004) 476
4) J. F. Ziegler, J. P. Biersack, and U. Littmark, The Stopping and Range of Ions in Solids, New York, 1985

4-35 Thermal Stability of Deformation and Refractive Index Change in Silica Glass Induced by Ion Microbeam

H. Aiba[a], T. Nakamura[a], Y. Ohki[a], M. Murai[b], H. Nishikawa[b], M. Oikawa[c], T. Satoh[c] and K. Arakawa[c]

[a] Department of Electrical Engineering and Bioscience, Waseda University, [b]Department of Electrical Engineering, Shibaura Institute of Technology, [c] Department of Advanced Radiation Technology, TARRI, JAEA

High-energy ion irradiation on silica glass can induce micro- or nano-scale structural and refractive-index change[1]. The latter can be used to fabricate fiber Bragg gratings and other devices. While UV light irradiation has been used to increase refractive index, the induced increment becomes smaller at temperatures above about 100 °C. In this paper, we show that the refractive index increment induced by ion microbeam irradiation has a superior thermal stability.

Ion microbeam irradiation was performed using a 3-MV single-ended accellerator in TIARA facility in TARRI, JAEA. Focused microbeam of H^+ ions (1.7 MeV) with a diameter of 1 μm was scanned over a surface of synthetic glass (Nippon Quartz, [OH]:1300 ppm) in dimensions of 3 x 3 x 10 mm^3 with mirror-polished front and side surfaces, up to a fluence of 5 x 10^{16} to 5 x 10^{17} ions/cm^2. The irradiated region is 30-50 μm in length included the sample edge and 10 μm in width. The ion-irradiated silica glass was sequentially annealed at temperatures from 500 °C to 1050 °C with intervals of 50 °C for 15 minutes at each temperature. After the thermal annealing, the depths of dents induced by irradiation on the irradiated surface and its side surface were examined by atomic force microscopy (AFM).

Figure 1 shows refractive index changes estimated from the depths of dents remaining after the thermal annealing done following the ion microbeam irradiation. The index shows a slight increase around 550 °C to 800 °C and then drops. About two thirds of the increment in refractive index induced by the ion irradiation remains after the annealing at 1000 °C and above.

The energy provided per unit volume by ion irradiation is expressed by the product of effective energy deposition and fluence[2]. Figure 2 shows the relation between this product and depth. All the data points before the thermal annealing (20 °C) are on a single straight line. Although not shown, the dents induced by He^+ ions are also on this straight line. Furthermore, the Raman scattering intensity corresponding to the emergence of Si-O three-membered rings in silica glass shows a similar dependence. From these facts, we conclude that the dents and refractive index increment are induced by the densification caused by the appearance of the three- or four-membered ring structure in silica glass that usually has five- or six membered rings[2].

In Fig. 1, the refractive index values are higher at about 550 °C to 800 °C than the original values. This indicates that Si-O bonds broken or deformed by the ion irradiation changed into high-density structure by the thermal effect, forming three- or four-membered rings.

It has been shown that the refractive index increment induced by the ion irradiation is controllable by the irradiation energy and thermal annealing, and that it is stable up to around 800 °C. This fact indicates that the ion-induced refractive index increment has a far higher thermal stability than that induced by UV light irradiation, which is mainly due to the Kramers-Kronig effect[3].

References

1) M. Hattori et al., Nucl. Instr. Meth. B210, 272-276 (2003)
2) T. Nakamura et al., Proceedings of the 2nd Space Environment Symposium, JAXA Special Publication, JAXA-SP-05-024, pp.115-119, December 2005
3) M. Douay et al., J. Lightwave Technology, Vol. 15, No. 8, 1329 (1997)

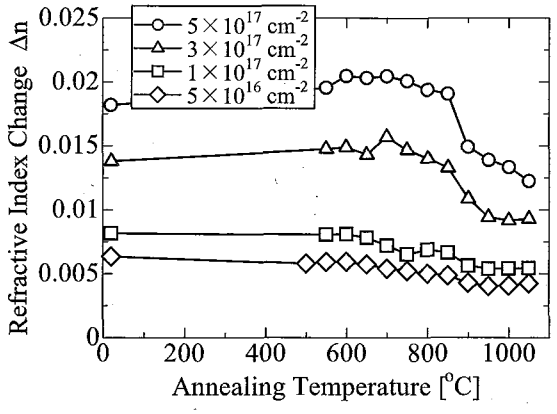


Fig.1 Refractive index changes estimated from depths of dents induced by ion microbeam irradiation as a function of annealing temperature.

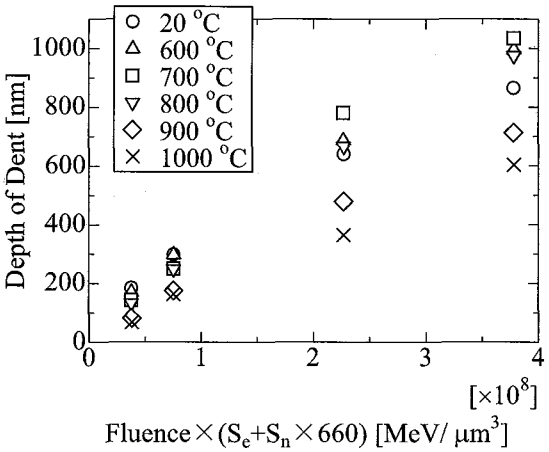


Fig.2 Depths of dents as a function of the product of effective energy deposition and fluence. S_e is the electronic stopping power and S_n is the nuclear stopping power.

4-36 Measurement of Structure and Charge States of Swift Carbon Cluster Passing Through a Thin Foil

A. Chiba [a)], Y. Saitoh [a)], K. Narumi [b)], M. Adachi [a)] and T. Kaneko [c)]

[a)] Department of Advanced Radiation Technology, TARRI, JAEA, [b)] Advanced Science Research Center, JAEA, [c)] Department of Applied Physics, Okayama University of Science

Abstract

The charge states were measured for the constituent ions of 1 MeV/atom C_3^+ passing through a carbon thin foil. The constituent ions of C_3^+ deflected by the electrostatic field were detected with a luminance plate position detector. Since the detected ion positions contain the information of charge states and the cluster structure, this measurement method enabled us to investigate the structure-dependence of the average charges in the cluster ions. The data clearly show that the measured average charge of C_3^+ ions in a linear-chain structure is larger than that in a triangle structure. Moreover we found that the average charge of the edge-position ions in a linear structure is larger than that in the middle-position ion. These experimental results are well supported by a recent theory on the cluster average charge.

MeV 領域のクラスターイオンが物質と衝突する際、複数の原子が極めて狭い領域に同時に衝突するため、単原子イオンとの衝突とは異なる特殊な相互作用をもたらす。その要因の一つは固体内の微少空間における隣接した原子／イオン間の干渉（近接効果）が考えられる。Brunelle らは薄膜透過後の解離した炭素クラスター構成イオンの平均電荷がクラスターサイズに依存することを初めて発見した [1]。この結果は、固体表面近傍における構成イオン間の近接効果の存在を示唆している。一方、炭素クラスターは、サイズが同じでも空間的構造が複数存在すると指摘されており、非常に興味深い。これまで、我々は薄膜を使ったクラスターの構造解析実験を通して、小規模なサイズの炭素クラスターに対し鎖状構造と環状構造が存在することを指摘している [2]。こうした構造の違いは、近接効果と空間的構造の相互関係における幅広い知識を与え、更にはクラスターイオンと物質との反応メカニズムの解明おいて重要な要素と考えられる。我々は C_3^+ に着目し、薄膜透過後のクラスター構成原子の荷電状態とその構造依存性について新たな知見を得た。

測定系の概念図を Fig.1 に示す。タンデム加速器で加速された高速クラスターイオン（1MeV/atom）は薄膜（1.1$\mu g/cm^2$～2.4$\mu g/cm^2$）を透過する過程で個々の単原子イオンに解離し、クーロン爆発によって核間距離が拡がっていく。膜中の構成イオンは一度荷電平衡に達し、エネルギーロスと共に平均電荷は減っていく。薄膜透過後の構成イオンは、平行平板電極（ΔV=30kV）で電荷に相応して偏向され、蛍光出力型の Multi-Channel Plate(MCP)で検出される。蛍光板上に発光点として表示されたイオンの検出位置から、各構成イオンの電荷を求めた。本測定系では、膜後の構成イオンが持つ電荷を測定すると同時に、平行平板電極と MCP 間の距離と電場強度及び構成イオンの電荷から、計算により偏向された軌道を修正し、偏向されない状態で MCP に入射すると予想される発光点の位置(Non-deflection points) を求めることができる。Non-deflection points の分布は解離前のクラスター構造に反映される。即ち、本測定系により解離前の構造と解離後の構成イオンの電荷を関連付けて議論することが可能となる。偏向された実際の検出点（Deflected points）と Non-deflection points の分布例を

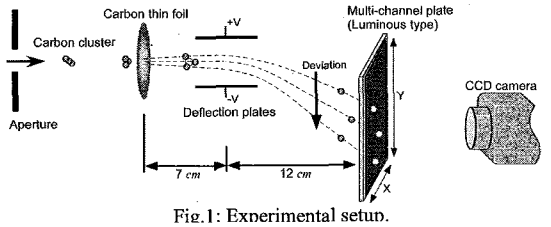


Fig.1: Experimental setup.

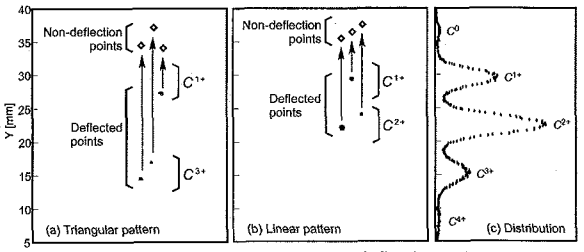


Fig. 2: Instances of calculated non-deflection points.

Fig.2 に示す。Fig.2(c)は解離した構成イオンが MCP に入射した位置の集積（約 10 万点）を X 方向に積分した電荷分布である。膜後の構成イオンの電荷は 0 から+4 まで確認できる。Fig.2(a)のような検出点の分布の場合、Fig.2(c)の電荷分布から各イオンの電荷は+1 と+3 であることが分かる。よって算出点は◇で示されるような正三角形の頂点にほぼ位置する。このような分布の場合、解離前のクラスター構造は環状構造であったと推定できる。また、Fig.2(b)のように算出点が直線上にほぼ等間隔に分布した場合、解離前の構造が鎖状構造であったと推定できる。構造毎に約 10,000 の検出点を解析した結果、Table 1 に示すように膜後のクラスター平均電荷は鎖状構造の方が環状構造よりも大きくなる。更に、鎖状構造において、両端に位置するイオンのほうが中心のイオンよりも平均電荷は大きくなることが分かった。実験結果は、膜中でのクーロン爆発と隣接するイオン場の影響を考慮したクラスター平均電荷の理論計算値と良い一致を見た。

薄膜中で解離した鎖状構造の中心イオンは両端のイオンによる近接効果により電離作用が著しく妨げられ、平均電荷がより小さくなったものと考えられる。言い換えると両端のイオンは中心イオンからのみ影響されるため平均電荷は環状構造のそれよりも更に大きくなり、結果として鎖状構造の平均電荷が環状構造よりも大きくなったと考えられる。以上のことから固体中でのクラスター構成原子の電離過程はクラスターの空間的相対性と強い相互関係にあることが分かった。

Table 1: Structure-dependence of cluster average-charge.

Foil $\mu g/cm^2$	Linear-chain	Ring	Center	Edge
1.1	1.86±0.02	1.80±0.02	1.78±0.03	1.90±0.03
2.0	1.90±0.01	1.85±0.01	1.81±0.02	1.94±0.02
2.4	1.96±0.03	1.89±0.02	1.86±0.04	2.01±0.03
2.4 (Cal.)	1.94	1.92	1.90	1.95

References

1) A. Brunelle, S. Della-Negra, J. Depauw, D. Jacquet, Y. Le Beyec, and M. Pautrat, Phys. Rev. A 59, 4456 (1999).
2) A. Chiba, Y. Saitoh, and S. Tajima, Nucl. Instrum. Method Phys. Res. B 232, 32 (2005).

4-37 TOF Mass Spectrometry of Secondary Ions from HOPG Target Bombarded by Fast C and Au Cluster Ion Beams

H. Shibata[a)], H. Tsuchida[a)], A. Itoh[a)], Y. Saitoh[b)], A. Chiba[b)], M.Adachi[b)], T. Kamiya[b)] and K. Narumi[c)]

[a)] Graduate School of Engineering, Kyoto University, [b)] Department of Advanced Radiation Technology, TARRI, JAEA, [c)] Advanced Science Research Center, JAEA

Recently the interaction of fast (high energy) cluster ions with solids has attracted attention in basic physics and application fields. As fast cluster ions can bombard a very small (atomic size) area of a solid surface by many atoms simultaneously and release large energy in a very short time (from femto- to pico-second region). This situation causes nonlinear effects or synergetic effects, which is unusual for single atom collision with solid targets.

Fast cluster ion beams used for the study of secondary ion emission processes were produced by the TIARA tandem accelerator. A time of flight (TOF) mass spectrometer combined with a pulsed cluster ion beam was used for a secondary ion measurement.

In this report we present some results of positive and negative secondary ion emission from a highly oriented pyrolytic graphite (HOPG) target bombarded by carbon and gold cluster ions.

The experimental system of TOF mass spectrometry was composed of a pulsed ion beam generating system and an ion flight time measuring system.

A chopper and two sets of slits installed in an injector beam line generated pulsed ion beams by chopping continuous cluster ion beams from an ion source. A square wave from a master pulse generator controlled a high voltage applied to parallel plate electrodes for chopping the beam. In this study pulsed cluster ion beams of 0.5 MeV/atom (~ 42 keV/amu) C_1^+ ~ C_8^+ ions and 1.67 MeV/atom (~ 8.5 keV/amu) Au^+ ~ Au_3^+ were used. The interval and width of the pulsed beam used in this experiment were 125 μs and ~100 ns, respectively. As averaged beam currents of pulsed beams could not be measured, continuous beam currents were measured before pulsing and were several 10 pA. The vacuum in a beam line and a chamber was kept at ~ 10^{-7} Pa to prevent cluster ions from breaking.

A linear type TOF mass spectrometer and a TAC (Time to Amplitude Converter) system for time measurement were adopted as a secondary ion mass spectrometric system. The TOF mass spectrometer composed of an extractor, a drift tube (~50cm long), an acceleration electrode and a multichannel plate (MCP) detector. A TTL output from the pulse generator was used as a start pulse and a secondary ion signal from the MCP was used as a stop pulse of the TAC measurement system. Typical mass spectrum was accumulated for 30 minutes. Sheet shaped targets were used and bombarded at an incident angle of 45 degrees. The secondary ions were extracted to the normal direction from the target. The target was bombarded by 5keV Ar ion beam from an ECR ion source for 10 ~ 20 minutes for cleaning of the HOPG surface.

Some results, mainly the total secondary ion yields except for yields of hydrogen ions from a HOPG target bombarded by carbon and gold cluster ions, will be discussed. Mass spectra of secondary ions emitted from a HOPG target bombarded by carbon cluster ions are described elsewhere [1)]. In case of Au^+, Au_2^+ and Au_3^+ ion bombardments the emitted positive and negative secondary ion mass spectra were not so different from each other, and secondary ions of large cluster sizes could not be seen.

Figure 1 shows the ratios of yields of positive and negative secondary ions except for hydrogen ions from the HOPG target bombarded by carbon (upside) and gold (downside) projectiles to the yield of positive ions for C_1^+ and Au_1^+ projectile. The yield of positive secondary ions for incident C_1^+ and Au_1^+ ion is unity. If the relation between the yield and cluster number n of incident C_n or Au_n is linear, the yield is n for C_n, or Au_n, as indicated by the "linear" curves in Fig.1. The values of yield ratio for each incident cluster ion are indicated by closed circles for positive secondary ions and triangles for negative ones in Fig.1. The yields of negative secondary ions for all incident cluster ions C_n^+ are about twice positive ion yields. The tendency is the same for gold projectiles as carbon case, but the yield ratio of negative ions to positive ions are about 20. The super-linear relation can be seen for carbon case, but the sub-linear relation can be seen clearly for gold case.

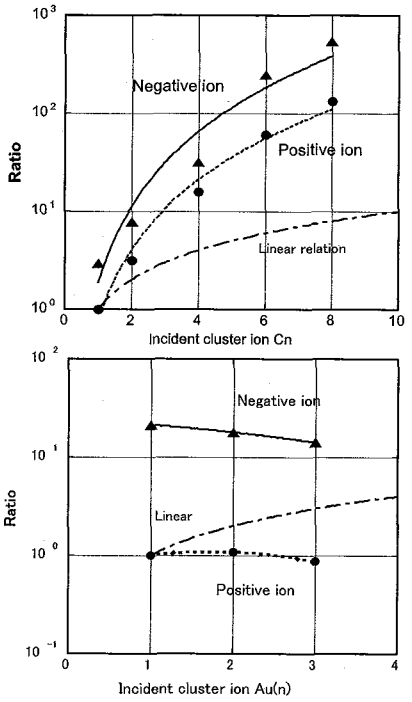


Fig.1. The ratio of yields of positive (▲) and negative secondary ions (●) emitted from HOPG target bombarded by carbon (upside) and gold (downside) incident ions. The yield of positive secondary ions bombarded by C_1^+ or Au_1^+ ion is unity.

References

1) TIARA Annual Report 2004 (2005) 346-347.

4-38 Effect of 1.66 MeV/atom Au Cluster Ion Irradiation in Si Single Crystals

A. Iwase[a)], T. Nakatani[a)], F. Hori[a)], Y. Saito[b)], A. Chiba[b)], K. Narumi[c)] and R. Oshima[d)]

[a)]Department of Materials Science, Osaka Prefecture University, [b)]Department of Advanced Radiation Technology, TARRI, JAEA, [c)]Advanced Science Research Center, JAEA, [d)] Osaka Nuclear Science Association

1. Introduction

Recently, irradiation effects of energetic cluster ions have been of great interest because of their exotic interactions with solids. In this paper, we report the defect production by Au cluster ions in silicon single crystals.

2. Experimental Procedure

Silicon single crystals were irradiated with Au+ monoatomic ions and with Au_n^+(n=2 and 3) cluster ions at room temperature. Incident energy of ions was 1.66 MeV/Au atom. Irradiation-induced defects were observed by using the dark field weal-beam method of transmission electron microscope (TEM). The fluence of ions was $1x10^{12}/cm^2$.

Results and Discussion

Figure 1 shows the dark field TEM image for unirradiated silicon. We do not find any defects in this specimen. Figure 2 shows the TEM images for Au^+ ion irradiation (a), Au_2^+ cluster ion irradiation(b) and Au_3^+ cluster ion irradiation. Although the number of irradiating Au atoms is the same, the irradiation effect is quite different. The density and the average size of defects, which can be observed as white spots in the TEM images, increase with increasing the cluster size. The experimental result implies that the cluster ion irradiation produces the larger number of defects than the monoatomic ion irradiation and/or that defects produced by the cluster ions are more thermally stable than those produced by monoatomic ions.

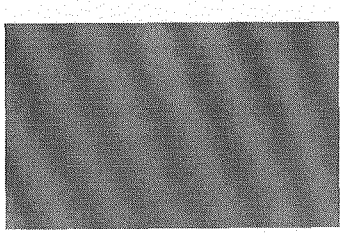


Fig. 1 TEM image for unirradiated silicon

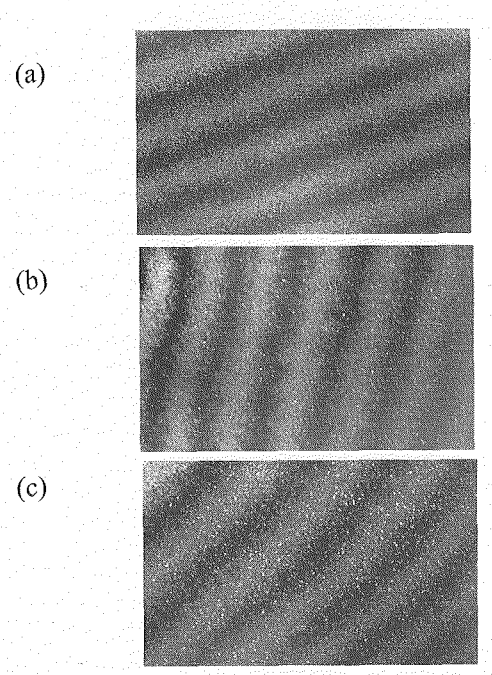


Fig. 2 TEM images of silicon for (a)Au^+ ion irradiation, (b) Au_2^+ ion irradiation and (c) Au_3^+ ion irradiation.

4-39 Highly Sensitive Surface Contaminant Analysis Using Pulsed Cluster Ion Beams

K. Hirata[a)], Y. Saitoh[b)], A. Chiba[b)], K. Narumi[c)], Y. Kobayashi[a)] and T. Kamiya[b)]

[a)]National Institute of Advanced Industrial Science and Technology (AIST), [b)]Department of Advanced Radiation Technology, TARRI, JAEA, [c)]Advanced Science Research Center, JAEA,

Time-of-flight (TOF) secondary ion mass spectrometry is one of the most powerful tools for surface analysis of materials. Mass analysis of secondary-ions is based on the phenomenon in which secondary ions are ejected from the surface when the primary ions bombard the target. We have applied pulsed cluster ion beams to TOF secondary ion mass spectroscopy. Cluster ion bombardments give different secondary ion emission yields from those for monoatomic ions because of their peculiar irradiation effect[1,2]. In this paper, we show that the emission yields of secondary ions originating from surface contaminants on metal are enhanced by cluster ion bombardments, which will be applicable to surface contaminant detection with high sensitivity.

Positive Secondary ion (P-SI) TOF measurements for a contaminated aluminum target were performed with a linear type TOF mass analyzer using pulsed monoatomic and cluster ion beams produced by a 3 MV tandem accelerator at the TIARA[2]. For quantitative comparison, TOF peak intensities should be scaled under the condition of the same number of incident primary atoms. For this purpose, the relative P-SI emission yield per incident atom was obtained by measuring incident beam current *Io* and P-SI current *Ip* under continuous direct current beam irradiation (Fig. 1). An electric potential lower than that at the sample (c) was applied to the metal plate (e) so that secondary electrons and negative-SIs emitted from the sample do not reach the metal plate. A grid (d) with lower electric potential than that at the plate (e) was placed between the sample and plate so as to eliminate the effect of those electrons on the *Ip* measurement that were emitted from the metal plate upon bombardment of the P-SI and neutral-particle. *Io* and *Ip* were measured, respectively, by a Faraday cup and the metal plate, which were connected to high-sensitivity electrometers. The number of detected P-SI per atom $Y_{d,P\text{-}SI}$ is given by $Y_{d,P\text{-}SI}=(\alpha\beta/e)(Ip/nIo)$, where α, β, n, and e are the absolute SI detection efficiency in the TOF measurement, the SI detection efficiency of the *Ip* measurement system, cluster number, and elemental charge, respectively. As α and β are invariant over the entire period of the measurements, we obtain $Y_{d,P\text{-}SI}=\gamma Ip/nIo$ (γ: constant). This indicates that the relative P-SI emission yield per incident atom Y_X for peak X can be compared between the spectra by scaling the total counts of each spectrum based on *Ip*/*nIo* of each bombardment condition.

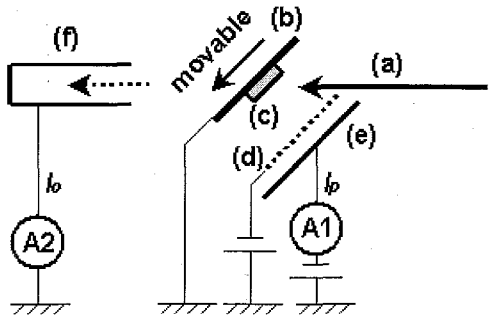


Fig. 1 Schematic diagram of the set-up for the *Io* and *Ip* measurements. (a) ion beam, (b) sample holder, (c) target, (d) grid, (e) metal plate, (f) Faraday cup, (A1) and (A2) electrometers.

Figure 2 shows the P-SI TOF spectra from *m*/*z* (mass to charge ratio)=20 to 30 of the aluminum target for (a) 0.5MeV-C_1^+ (0.5MeV/atom- C_1^+), and (b) 4.0MeV-C_8^+ (0.5MeV/atom-C_8^+), respectively. The relative intensity on the vertical axis is proportional to the SI emission yield per incident atom, as the total counts of the spectra are scaled based on *Ip*/*nIo* as described above. The peaks observed in Fig.3 can be attributed to ions of singly charged sodium ion (Na^+: *m*/*z*=23), and hydrocarbons ($C_2H_3^+$: *m*/*z*=27, and $C_2H_5^+$: *m*/*z*=29), originating from surface contaminants.

We see that the 0.5MeV/atom-C_8^+ impact provides a higher P-SI yield of Na^+ than the 0.5MeV/atom-C_1^+ impact although the primary ions of the same element bombard the same sample with the same velocity. The emission yield of Na^+ for the C_8^+ impact is ~15 times higher than that for the C_1^+ impact. Therefore, the yield is increased by a factor of ~15 in comparison with those expected under the assumption that each constituent atom of the cluster behaves as a monoatomic ion with the same velocity.

In conclusion, the use of a cluster ion instead of a monoatomic ion as a primary ion provides higher emission yields of secondary ions from surface contaminants in the secondary ion TOF measurements.

References

1) K. Hirata, Y. Saitoh, A. Chiba, K. Narumi, Y. Kobayashi, and K. Arakawa, Appl. Phys. Lett., **83**, (2003) 4872.
2) K. Hirata, Y. Saitoh, A. Chiba, K. Narumi, Y. Kobayashi, and Y. Ohara, Appl. Phys. Lett., **86**, (2005) 044105.

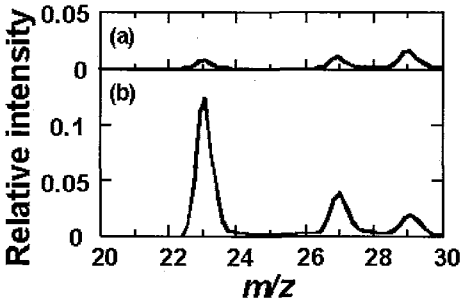


Fig. 2 Positive secondary ion TOF spectra of contaminated Al target for (a) 0.5MeV-C_1^+ (0.5MeV/atom-C_1^+), and (b) 4.0MeV -C_8^+ (0.5MeV/atom-C_8^+). The relative intensity on the vertical axis is proportional to the SI emission yield per incident atom.

4-40 Aerosol Formation Induced by Proton Irradiation to Air

Y. Oki[a], N. Osada[b], Y. Kanda[c], S. Yokoyama[d], K. Sato[d], K. Manabe[d], A. Endo[d], H. Noguchi[e], H. Kaneko[f], Su. Tanaka[g] and T. Iida[h]

[a]Research Reactor Institute, Kyoto University, [b]Graduate School of Engineering, Kyoto University, [c]High Energy Accelerator Research Organization (KEK), [d]Division of Environment and Radiation Sciences, NSED, JAEA, [e]Safety Administration Department, JAEA, [f]Department of Advanced Radiation Technology, TARRI, JAEA, [g]Nippon Advanced Technology Co., Ltd, [h]Graduate School of Engineering, Nagoya University

Abstract

Radioactive aerosols produced in air of accelerator rooms are one of sources of internal exposures in accelerator facilities. Their particle size is very important information for estimation of internal doses. The size is determined by that of non-radioactive aerosols produced through radiolytic processes of air because radioactive atoms formed in air are attached to the non-radioactive aerosols. In this work, to elucidate behavior of the radioactive aerosols in the accelerator rooms the particle size and number concentration of the non-radioactive aerosols were measured immediately after proton irradiation as a function of deposited energy to air by protons. The aerosol diameter was found to be 10-20 nm. Both the particle size and concentration increased with an increase in the deposited energy.

加速器室内では高濃度のエアロゾル生成がしばしば認められるが[1][2]、これは空気の放射線分解により誘起される現象と考えられている。一方、核反応により加速器室内空気中で生成する放射性原子の一部は、これらの(非放射性)エアロゾルに付着して放射性エアロゾルとなり空気中を輸送される。放射性エアロゾルの粒径などの情報は放射線防護に不可欠であるが、これらの理解のためには生成直後の非放射性エアロゾルの性状を解明することが有効である。

本研究では以上の観点から、実際に空気に陽子線を照射して非放射性エアロゾルを生成させ、生成直後のエアロゾル個数濃度や粒径分布を初めて測定した。さらに空気に付与されるエネルギーと生成濃度、粒径との関係を考察した。

照射は日本原子力研究開発機構高崎量子応用研究所イオン照射研究施設 (TIARA) で行った。AVF サイクロトロンから供給される 48 MeV の陽子線(1 nA～4 nA)を用いた。ビームと直交するようにガス導入管(ステンレス鋼薄肉管、内径 21 mm) を配置し、管内に高純度空気をマスフローコントローラーで制御して導入しながら、陽子線を照射した。陽子線は導入管を貫通し試料空気に照射される。生成されたエアロゾルは希釈されることなく層流のまま管内を移動し、測定器まで到達する。個数濃度と粒径分布の測定は、導入管の出口側に設置した SMPS (Scanning Mobility Particle Sizer、TSI 社 Model 3936) により、照射中連続して行った。なお照射位置での陽子数及びビーム形状は Al 板の放射化により測定した。

生成直後のエアロゾルの粒径は対数正規分布を示し、試料空気(流速:0.3 dm^3/min)に陽子線電流値 2nA で照射した場合、幾何中央径は約 15nm となった。照射中に繰り返しスキャンして得られた粒径分布を比較すると照射中はほとんど変化せず、エアロゾルが安定して生成することが確認された。

試料空気に付与されるエネルギーは、陽子線が貫通する照射管などの材質と試料空気の陽子線に対する阻止能より算出し、陽子線のビーム形状を考慮し補正した。

生成エアロゾルの個数濃度は、付与エネルギーが増加するに従い増加したが、その増加は次第に鈍化する傾向が見られた(Fig.1)。またエアロゾル生成には閾値があることが示唆された。試料空気流量一定時の陽子線電流値の増減と陽子線電流値一定時の試料空気の流量増減により付与エネルギーを変化させた。いずれの照射でも、単位体積あたりに同じエネルギーを付与するとほぼ同じ個数濃度が得られた。

個数濃度と粒径には正の相関が見られた(Fig.2)。Fig.2 で個数濃度が 0 である時の粒径を外挿すると 8 nm 程度となる。これはこの粒径以下の粒子は短時間で消滅することを示唆している。

なお、本研究は連携重点研究「陽子加速器施設における線量評価に関する研究」により行われた。

文献

1) K.Kondo, et al., Int.J.Appl.Radiat.Isot.,35 (1984) 939.
2) H.Muramatsu, et al., Int. J. Radiat. Appl. Instrum. Part A, 39 (1988) 413.

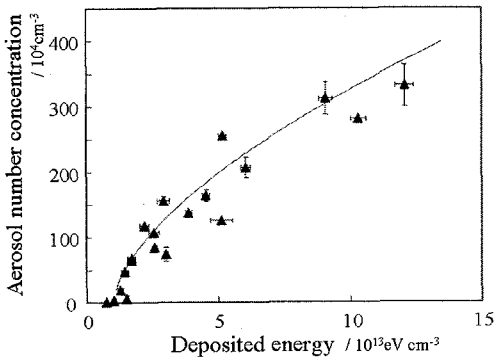


Fig.1 Relationship between deposited energy and aerosol concentration

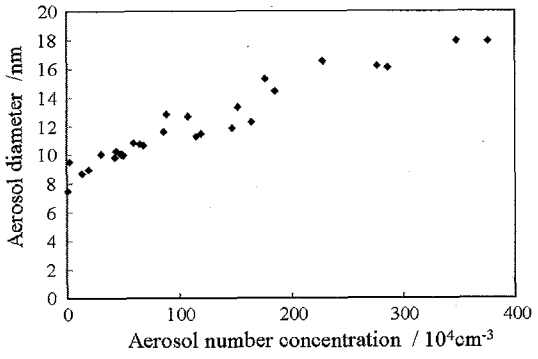


Fig.2 Relationship between aerosol concentration and diameter

4-41 Measurement of Double Differential Fragment Production Cross-Section Induced by Ten's MeV Nucleons

T. Oishi [a], T. Sanami [b], M. Hagiwara [a], M. Baba [a], S. Kamada [a], T. Okuji [a], Y. Iwamoto [c], S. Tanaka [d] and H. Nakashima [e]

[a]Cyclotron and Radioisotope center, Tohoku University, [b]Radiation Science center, High energy accelerator research organization, [c] Research Group for Applied Radiation Physics, JAEA, [d] Accelerator department, Nippon advanced technology., LTD, [e]J-PARK center, JAEA

In the evaluation of the single event effects which cause semiconductor memory errors, detailed knowledge of incident particles as charge, mass, angle, energy are necessary not only for primary particle but also secondary particle. Particularly fragments produced by middle-high energy nucleons are important due to the large liner energy transfer (LET). The reaction mechanisms for fragment productions are still uncertain for the reason attributed to the experimental difficulty as a small amount of produced fragments, large energy loss, short stopping range, high back ground of light particles and so on.

We have developed Bragg curve counter[1,2] (BCC) to obtain reliable experimental data of the fragment production. In this study, BCC have been improved to extend the dynamic range and applied to fragment production cross-sections measurements both in proton and the neutron induced reactions.

Figure 1 shows a schematic view of the BCC which is a cylindrical gridded ionization chamber. The fragments ionize the gas in the BCC and produce a number of free electrons in proportion to the energy deposit. The free electrons drift toward an anode electrode by the electric field in BCC keeping the shape of the ionization distribution (Bragg curve). Owing to the constant drift velocity of the free electrons, the time distribution of the anode signal corresponds to the reversed Bragg curve. Thus the fast part of anode signal is proportional to the Bragg peak that provides the information on the atomic number of the fragment. The integration of the whole anode signal represents the total charge that is proportional to the fragment energy. Besides, a time difference between cathode and anode correspond to the stopping range of fragments. In the measurements of protons induced reactions, samples were put on the sample changer outside of the BCC and the fragments enter the BCC along the axis through the entrance window (mylar 2.5 μm thick). On the other hand, in the neutrons induced reactions, the samples were installed inside to overcome lower neutron flux owing to the large solid angle[3,4].

In low energy region where the fragments cannot form Bragg peak, the particles identification using the stopping range was applied to extend the dynamic range. In high energy region where the fragments punch out the detector, the energy compensation method was developed to extend measurable energy by using the relationships of the incident energy and the deposited energy calculated by SRIM code for each particles. Using these methods, the dynamic range of the BCC was improved to become two times wider in maximum.

In the neutron experiment, a number of fragments emit to various directions because of putting samples into the detector. The signals from these fragments do not correspond to Bragg curve specific to a kind of particle. To solve this problem, segmented anode electrode which was divided the electrode into two parts of center and outer was developed. If the signal is obtained from the outer part, the fragments were omitted as oblique direction's events. As the results, the particle identification was improved and could obtain data in neutron induced reaction.

Figure 2 shows present results and calculations (PHITS) of double differential cross-sections of C(p, x) reactions. The calculations show underestimations in higher energy region. The result of C(n, x) reactions shows in Fig. 3. Similar results were obtained both in proton and the neutron induced reactions.

References

1) C.R.Gruhn, et al. Nucl. Instrum. Meth., 196 (1982) 33.
2) N.J.Shenhav and H.Stelzer, Nucl. Instrum. Meth., 228 (1985) 359
3) N.Ito, M.Baba, et al. Nucl. Instrum. Meth., A337 (1994) 474
4) T.Sanami, et al. Nucl. Instrum. Meth., A440 (2000) 403

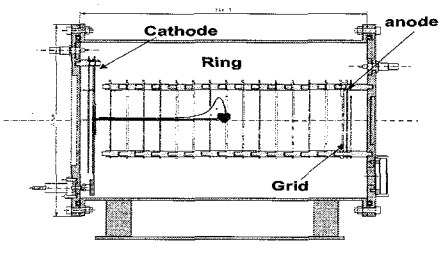


Fig.1 schematic view of the BCC.

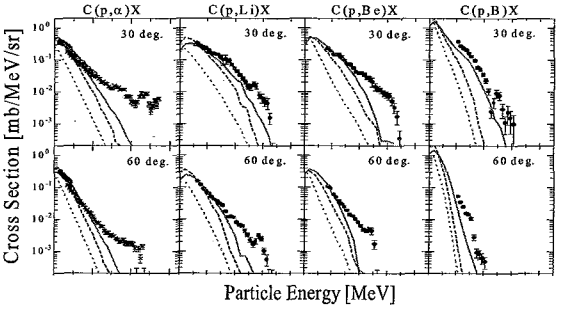


Fig. 2 Double differential cross-section of C(p, x) reaction.

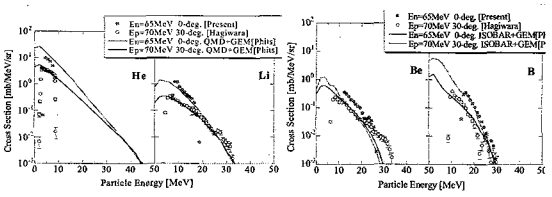


Fig. 3 Comparison of proton and neutron induced reactions.

4-42 Development of Monitor and Dosimeter Applicable to High-Energy Neutrons

A. Endo[a)], T. Sato[a)], D. Satoh[a)], Y. Shikaze[b)], Y. Tanimura[b)], J. Saegusa[b)], M. Tsutsumi[b)], Y. Yamaguchi[b)], H. Kaneko[c)], K. Oda[d)], Y. Imasaka[d)], M. Notsu[d)], H. Tada[d)], H. Tawara[e)], K. Eda[e)], K. Takahashi[e)] and M. Baba[f)]

[a)]Division of Environment and Radiation Sciences, NSED, JAEA, [b)]Department of Radiation Protection, NSRI, JAEA, [c)]Department of Advanced Radiation Technology, TARRI, JAEA, [d)]Faculty of Maritime Sciences, Kobe University, [e)]Radiation Science Center, KEK, [f)]Cyclotron and Radioisotope Center, Tohoku University

High intensity proton accelerator facilities have been developed in order to pursue frontier research in particle physics, life science, nuclear technology and so on. At these facilities, monitoring of high-energy neutrons produced through nuclear spallation is one of the key issues in radiation protection of workers and the public. We have developed a monitor and dosimeters applicable to high-energy neutrons, and have studied the calibration method of the instruments using the quasi mono-energetic neutrons in TIARA.

A new inventive radiation dose monitor, designated as DARWIN[1)] (Dose monitoring system Applicable to various Radiations with WIde energy raNges), has been developed for real-time monitoring of doses in workspaces and surrounding environments of high-energy accelerator facilities (Fig. 1). DARWIN is composed of a phoswitch-type scintillation detector, which consists of liquid organic scintillator BC501A coupled with ZnS(Ag) scintillation sheets doped with ^{6}Li, and a data acquisition system based on a Digital-Storage-Oscilloscope. DARWIN has the following features: (1) capable of monitoring doses from neutrons, photons and muons with energies from thermal energy to 1 GeV, 150 keV to 100 MeV, and 1 MeV to 100 GeV, respectively, (2) high sensitivity and prescision, and (3) ease of operation with a simple graphical user-interface. The performance of DARWIN was examined experimentally in TIARA, the Facility of Radiation Standard at JAEA and HIMAC at the National Institute of Radiological Sciences. The results of the experiments indicated the accuracy and high sensitivity of DARWIN for measuring dose rates from neutrons, photons and muons with wide energies.

In the development of personal dosimeters, a method has been established to design a radiator for more efficient detection of high-energy neutrons with a plastic nuclear track detector (PNTD).[2)] Subsequent to the proposal of a two-layer structured radiator to improve detection efficiency of high-energy neutrons, its availability has been investigated both experimentally and theoretically. An inner deuterized hydrocarbon (CD_2) layer adjacent to PNTD should play the role of both a radiator of deuterons recoiled there and a degrader for energetic protons recoiled in the outer layer of a CH_2 material. It was found that the energy dependence of the efficiency was changed sensitively by the thickness of the CD_2 layer. A best combination of CH_2 and CD_2 thickness was estimated under a condition of a constant total thickness. For example, the sensitivity could be flattened within 20% between about 5 and 70MeV by using 1 g/cm^2-CD_2 and 2 g/cm^2-CH_2. The developed radiator has successful improved detection efficiency and energy response of PNTD for measuring neutron dose.

In the study of calibration method of monitors and dosimeters for high-energy neutrons, the properties of neutron field were studied using the quasi-monoenergetic neutron irradiation field of 40-90 MeV in TIARA.[3)] The neutron beam profile at different distances from the target was investigated by using imaging plates with a polyethylene converter to measure the recoil protons produced in the converter. It was found from the results that the irradiation field area was fixed geometrically by the distance from the target and the diameter of the collimator exit and that the beam intensity within the irradiation field was in inverse proportion to the square of the distance from the target. The peak energy and energy spectrum of neutrons both inside and outside the irradiation field were measured by the time-of-flight method using a liquid organic scintillation detector. These results will be applied to develop a calibration filed which is traceable with the international standard for neutron energy more than 20 MeV.

References

1) T. Sato, et al., J. Nucl. Sci. Technol. 42 (2005) 768.
2) K. Oda, et al., Radiat. Meas. 40 (2005) 570.
3) Y. Shikaze, et al., Radiat. Prot. Dosim. submitted.

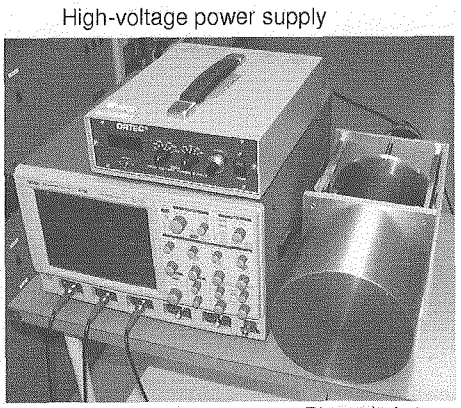


Fig.1 Overview of DARWIN. The phoswitch-type detector is composed of liquid organic scintillator coupled with ^{6}Li-ZnS(Ag) sheets. A LabVIEW based on-line analysis program with a simple graphical user-interface is installed in the data acquisition system.

4-43 Easy Measurement Technique for 2D Distribution of Fluence Using GAF-Film and PC-Scanner

T. Agematsu and H. Hanaya

Department of Advanced Radiation Technology, TARRI, JAEA

Abstract

We developed an easy measurement technique for 2D-distribution of relative ion beam fluence using GAF-chromic film and an image scanner for a personal computer. The thin active layer type GAF-film, HD-810, is usable for heavy ion beams with short range. We obtained dose response curves of the film irradiated by 2 MeV electron beam measuring with three color components of different model scanners. Each curve has a linear region from zero to some hundreds of Gy, depending on the model and the color, which is available to measurement of 2D fluence with high spatial resolution of the scanners.

材料科学やバイオ技術の研究開発でイオンビームを大面積均一照射する場合、２次元フルエンス分布を測定することは容易でない。比較的簡便なフィルム線量計による方法では、リアルタイム計測ができない欠点はあるものの、空間分解能において優れ、設置スペースが小さく、更に積分型であるという利点がある。しかし、２次元の吸光度分布測定が可能な分光光度計など(例:CS-9000クロマトスキャナ(島津製作所))が必要であり、線量測定を専門としないイオンビームユーザーは簡単に測定することができなかった。

我々は、医療分野で低線量γ線の線量測定などに応用されているGAFフィルム線量計(ISP社)と、吸光度測定器としてPCスキャナ(パソコン用画像スキャナ)を組合せた測定技術[1,2]に着目し、実用的で簡便かつ高空間分解能なイオンビームフルエンスの２次元相対分布測定技術を開発[3]した。GAFフィルム線量計は一般に流通しており入手が容易であるとともに、放射線による着色が可視であるため目視による確認とITVカメラによるリアルタイムな観察が可能である。今回用いたGAFフィルムHD-810は、サイクロトロンを用いたバイオ技術などの研究開発の照射実験で用いる線量に適合し、飛程の短い重イオンビームにも対応できる。

照射したGAFフィルムをPCスキャナで読み込んだ画像データはフリーソフト「BMP2CSV」を用いてRGB色成分ごとに8bit値・CSVファイルに変換し、「MS-Excel」を用いて吸光度(O.D.)換算した。いずれも簡単に入手できるソフトウェアであり、簡便にデータ処理が行える。

PCスキャナで測定した場合の線量応答のリニアリティーが良い範囲を調べるために、電子線(2MV)でGAFフィルムを照射し、PCスキャナで計測した色成分毎の結果をFig. 1に示す。PCスキャナがLiDE50 (Canon)の場合、R成分では200Gy程度まで、G成分では500Gy程度まで、B成分では1200Gy程度までの利用可能なリニアリティーがあることを確認した。

GAFフィルム自身の空間分解能は１μm以上であることが報告[4]されているが、従来の実用的な２次元分布測定可能な分光光度計CS-9000の測定空間分解能は0.4mmである。これに対してPCスキャナLiDE50の場合、光学解像度が1200dpi (0.021mm分解能)であり、高空間分解能な測定が可能である。同じ照射サンプルを分光光度計CS-9000とPCスキャナLiDE50で測定し比較した例をFig. 2に示す。両者の分布は一致しており、PCスキャナの高空間分解能が確認できる。

PCスキャナの機種による特性の違いについて調べた結果をFig. 1に示す。3LED方式(LiDE60)とCCD方式(GT9500 (EPSON))では読み取り方式が違うにも関わらず特性が似ている。一方で、LiDE50(3LED方式)ではこれらと大きく異なっている。従って、機種毎に校正用に照射したGAFフィルムを測定し、得られる線量応答カーブでリニアな範囲を使う必要がある。

本技術により、イオンビーム照射実験の基礎データとなる２次元フルエンス相対分布が、だれでも簡便かつ高空間分解能で測定できるようになった。

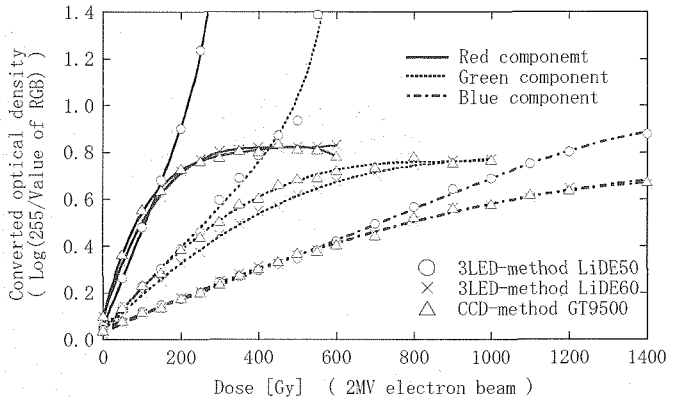


Fig. 1 Dose response for R, G and B components of different types of PC-scanners using GAF-film irradiated by 2-MeV electron beam.

References

1) Slobodan Devic, et al., Med. Phys. 31(9) (2004) 2392-2401.
2) M. A. Stevens, et al., Phys. Med. Biol. 41 (1996) 2357-2365.
3) T. Agematsu, et al., JAER-Review 2005-001 355-357.
4) T. Kojima, et al., Radiat. Phys. Chem., Vol.68 (2003) 975-980.

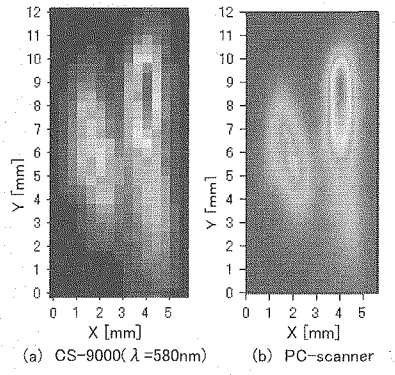


Fig. 2 Comparison of the spatial resolution of (a) 2D spectrophotometer and (b) PC-scanner. Fluence distribution maps of 320MeV-C ion beam spot on GAF-film were measured with these devices.

4-44 Preliminary Study on Applicability of B3 Film Dosimeter for Two Dimensional Dose Distribution Using a PC-Scanner

H.Hanaya and T.Agematsu

Department of Advanced Radiation Technology, TARRI, JAEA

Abstract

The 2D dose distribution measurement was tested by combining radiochromic film dosimeter and an image scanner for a personal computer. The combined system is cheap, easy to handle and allows speedy measurement with high spatial resolution. In the present preliminary study, dose response of B3 film for 2MeV electron beams was readout using the image scanner with RGB color components. The curve in the Green color component was linear up to 100kGy under the condition that B3 films are kept dry without heat treatment. This result meets the fundamental requirement for 2D dose distribution measurement system using B3 dosimeter with the image scanner.

材料科学やバイオ技術の研究開発でイオンビームを大面積均一照射する場合、２次元フルエンス分布を測定することは容易でない。そこで我々は簡便な測定方法としてGAFフィルム線量計(HD-810)とPCスキャナ(パソコン用画像スキャナ)を組合せた測定技術を開発[1]してきた。これにより線量測定を専門としないイオンビームユーザーでも簡便で高空間分解能な２次元フルエンス相対分布測定が可能となった。更に我々は、PCスキャナを組合せた測定方法でより広範囲なフルエンス(線量)に対応するため、各種フィルム線量計を用いる可能性を検討している。GAFフィルムではHD-810の線量範囲（カタログ:10Gy-400Gy）より低い線量にMD-55（2Gy-100Gy），HS（0.5Gy-40Gy），XR-T（0.1Gy-15Gy）などを用いる可能性があるが、今回は高い線量範囲の測定について、B3フィルム線量計[2,3](GEX社、2kGy-80kGy)を用いる可能性の検討を行った。

B3フィルムの線量応答特性を調べるために2MeVの電子線で照射を行った。Fig. 1にB3フィルムを分光光度計で測定した結果を示す。吸光度スペクトルは、GAFフィルムでは主に赤色(R)の吸収(青色の着色)が多くなるのに対して、B3フィルムでは主に緑色(G)の吸収(薄いピンク色の着色)が多くなる。Fig. 2にPCスキャナLiDE50(Canon)を測定器とした場合の線量応答特性を示す。ＲＧＢ色成分のうち、Gの信号強度が強く、青色（B）は弱く、Ｒでは適切な信号強度が得られないことがわかった。また、PCスキャナで測定した線量応答カーブは、照射時の湿度依存性を除くための包装状態(購入時のアルミフィルムによるパッケージ)で照射し、加熱処理(測定値の長期期間再現可とするためにメーカーが、提案するプロセス。;照射後60℃、15分)を行わない場合に、Gで比較的リニアで良い特性を示した。この傾向は、分光光度計（λ=554nm；B3フィルム専用測定器の測定波長）で測定しプロットした線量応答カーブでも同様の結果が得られており、B3フィルムの特性によることがわかる。

B3フィルムとPCスキャナ(LiDE50)の組合せた電子線の吸収線量の２次元相対分布測定は、照射時の湿度依存性を排除し、照射後の加熱処理を行わないことにより、線量応答カーブがリニアとなり、使用できる可能性があることがわかった。しかし、Ｂ３フィルムは、商品カタログでも電子線とγ線(35℃)で線量応答カーブの違いが示されており、線量率依存性などもある可能性がある。従って、B3フィルムは、各種条件：線質、線量率、照射湿度、温度などにより線量応答カーブが変化しているため、PCスキャナ測定法による線量応答のリニアな条件が限られていることがわかった。今後、B3フィルムとPCスキャナによるイオンビームの２次元フルエンス相対分布測定方法の実用性について、検討を進める予定である。

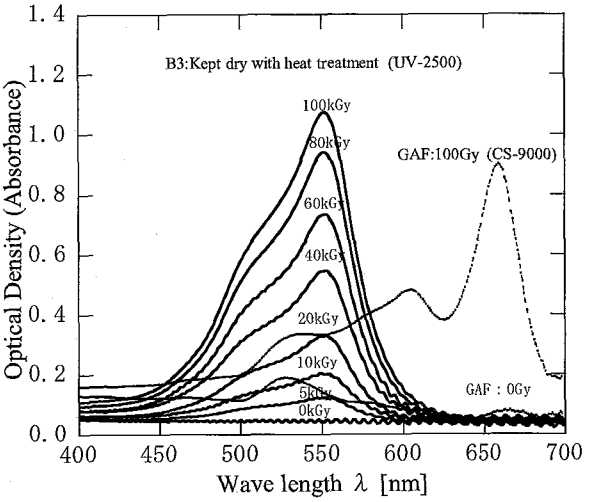


Fig.1 Optical density spectrum of B3 film and GAF film. Films are irradiated by 2MeV electron beam.

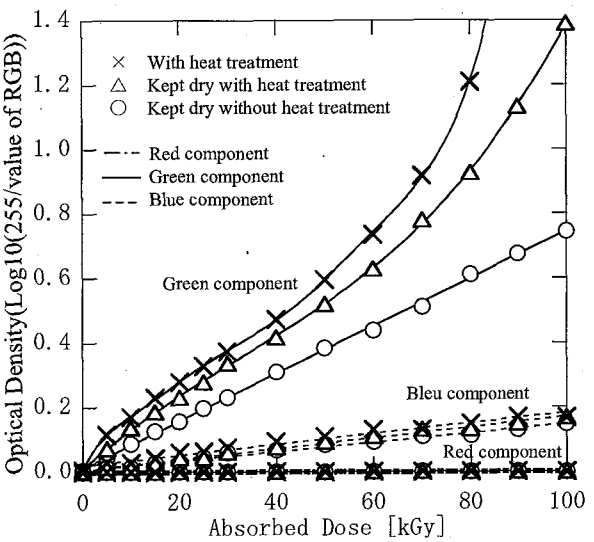


Fig.2 Dose response of B3 film with RGB component using PC-scanner (LiDE50). Films are irradiated by 2MeV electron beam.

References

1) T. Agematsu, et al., JAERI-Review 2005-001 355-357.
2) A.Miller, et al., Radiat.Phys.Chem.31(1988)491-496
3) ATEF A. ABDEL-FATTAH et al., Radiat.Phys.Chem.47 (1996)611-621

4-45 Focused Microbeam Formation for Heavy Ion Beam from AVF Cyclotron (II)

W. Yokota[a)], T. Satoh[a)], M. Oikawa[a,b)], T. Sakai[a)], S. Okumura[a)], S. Kurashima[a)], N. Miyawaki[a)], H. Kashiwagi[a)], T. Kamiya[a,b)] and M. Fukuda[c)]

[a)]Department of Advanced Radiation Technology, TARRI, JAEA,
[b)]Graduate School of Medicine, Gunma University, [c)]Research Center for Nuclear Physics, Osaka University

Overview

We are developing a focusing microbeam system[1)] at the HX course of the cyclotron at TIARA for application to biomedical research and study on single event phenomena of semiconductors for space application. A beam spot of less than 2 μm in diameter was successfully formed in fiscal 2004[2)] using 260-MeV $^{20}Ne^{7+}$ beam which was accelerated with a flat-top acceleration system. In fiscal 2005, nine experiments of microbeam formation were carried out, in seven of which the spots of 1.7 μm on average was obtained. It has further become possible to maintain this size of spot for some hours. Therefore we made test irradiation of bio-materials and semiconductor devices in the atmosphere for the first time.

We sometimes, especially in the coldest period of the year, had instability of the beam in intensity and position that caused difficulties in forming microbeam. It was found that the instability correlated to the change in temperature of cooling water for the ECR ion source, which might affect the plasma condition of the source.

The influence of vibration between the microbeam system and the irradiation device was considered on the basis of measurement.

Experiment and result

The energy spead $\Delta E/E$ of 260-MeV $^{20}Ne^{7+}$ beam was reduced to about 5×10^{-4}, a few tenth of the usual value[3)], using the flat-top acceleration system of the cyclotron[4,5)] in order to reduce chromatic aberration in the quadruplet quadrupole lens to focus the beam as small as 1 μm. The accelerated beam was transported to the microbeam formation system by tuning so that the beam was on the axis of the quadruple magnets of the transport system. And then it was, at first in the microbeam formation system, collimated with the micro slits to 5 μm. Its divergence was further limited by another slit system, and the beam was finally brought to the copper grid on the focal plane of the quadruplet quadrupole lens. The beam spot was scanned on the grid by the X-Y magnetic scanner. The secondary electrons emitted from the grid were detected by a plastic scintillator and the SEM image was taken. The lens currents were tuned while observing the SEM image to make it clearer for a smaller beam spot.

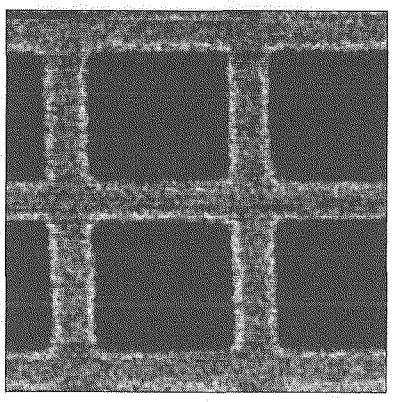


Fig.1 An example SEM image of a copper grid. The grid intervals are 25 μm and the black squares are empty.

An example of a clear SEM image is shown in Fig.1. Secondary electron emission is enhanced at a sharp edge and this brightened the grid edges. The beam spot diameter is determined as a FWHM of a peak in the secondary electron yield profile. The spot diameter was estimated at 1.2 μm in the case of the figure.

For irradiation in the atmosphere, a small chamber was used, on the bottom wall of which a copper grid, a window of a 7.5 μm thick Kapton for ions to get through into the air, were set. The chamber was connected to a flange of the microbeam line with the bellows and could be horizontally shifted. After microbeam was formed, the window was moved to the focal point and the microbeam was extracted into the air. The beam could not be focused for a long enough period in the test irradiation because of the instability arising from the ECR ion source. The test irradiation will be continued also in fiscal 2006.

Vibration and distortion of microbeam system parts

The vibration of the lens was measured with a laser displacement sensor. The amplitude of the vibration against the floor was from 0.2 to 0.6 μm when all the rotary pumps were switched off. The relative vibration amplitude of the irradiation apparatus to the lens will be larger if the apparatus is put on the floor because they vibrate independently. Therefore, the apparatus must be tightly fixed to the lens frame to reduce the relative vibration as less as possible.

The irradiation apparatus will contain a movable heavy part such as a motor-driven X-Y stage to move the target. The change of weight balance arising from the motion of the part may considerably shift the beam spot on the target. The shift of the beam spot against the copper grid was measured by putting a 10 kg weight on the lens frame and was roughly 5 μm/(kgf·m). A counter weight mechanism may be necessary to cancel the change of weight balance.

References

1) M. Oikawa, et al., Nucl. Instr. Meth. B210 (2003) 54
2) W. Yokota, et al., JAEA-Review 2005-001 (2004) 291
3) N. Miyawaki, et al., in this annual report
4) M. Fukuda, et al., Rev. Sci. Instrumn. 74 (2002) 2296
5) S. Kurashima, et al., JAERI-Review 2004-25 (2004) 313

4-46 Design of Age-Related Macular Degeneration (AMD) Treatment System Using a Carbon Ion Beam

H. Shimada [a,b], M. Oikawa [a,b], T. Satoh [b], T. Sakai [b], T. Agematsu [b], S. Okumura [b], M. Taguchi [c], T. Sato [d], Y. Horiuchi [d], H. Katoh [d], K. Yusa [e], M. Fukuda [f], T. Kamaiya [a,b], S. Kishi [d], T. Nakano [a,d] and K. Arakawa [a,b]

[a] 21st Century COE Program, Graduate School of Medicine, Gunma University, [b] Department of Advanced Radiation Technology, TARRI, JAEA, [c] Environment and Industrial Materials Research Division, QuBS, JAEA, [d] Department of Medicine, Graduate School of Medicine, Gunma University, [e] Research Center for Heavy Particle Medicine, Gunma University, [f] Research Center of Nuclear Physics, Osaka University.

1. Introduction

Age-related Macular Degeneration (AMD) with Choroidal Neovascularization (CNV) is a degenerative condition of the macula (the central retina). AMD is the leading cause of vision loss in fifty years of age and older. Manifestations of AMD include CNV, pigment epithelial detachment, subretinal hemorrhage and fibrovascular scar formation. As a result, the central vision deteriorates. In the worst cases, it causes a complete loss of central vision, making reading or driving impossible.

There is no established effective therapy for AMD at present. In selected cases with extramacular CNV, laser photocoagulation is effective for sealing leaking or bleeding vessels. Unfortunately, laser photocoagulation is not indicated for majority of cases with submacular CNV because it destroys the central retina as well, which results in severe visual loss. Recently, photodynamic therapy has proven to be effective in stopping abnormal blood vessel growth in some patients with AMD. This new type of laser treatment is far less damaging to the retina than laser photocoagulation and is the treatment of choice in many cases. However, it is perfect solution neither laser photocoagulation nor photodynamic therapy. The ideal treatment should be effective in sealing the CNV but should be non-invasive for the retina.

The aim of present research is development of a carbon ion microbeam therapy for AMD using a high precision carbon-ion microsurgery system. In this therapy, the diseased part (CNV) that exists very much in the local domain so as not to destroy the retina with which it covers on the diseased part is needed fir the technology that irradiates it in high accuracy.

2. Design of a Microbeam Irradiation Treatment System

In our research project, we have examined AMD treatment system, determination of an irradiation position, and have developed a detection device for an emission from eyeground, and so on. In the heavy-ion particle therapy of AMD, the affected part (CNV) of the eyeground is irradiated using a carbon ion microbeam after searching for an irradiation position. The CNV of AMD is cured by local irradiation using a sharp Bragg peak (~ 250 μm) of heavy-ion beam. An in-depth irradiation position is determined by the emission measurement from the ocular fundus using a microbeam. The range in-depth of ion beam is adjusted up to 2.0 mm every 50 μm in eyeground using several seats of thin PMMA (poly-methylmethacrylate) film as range shifters. The irradiation position is confirmed by a fundus camera having a long working distance and luminescent of contrast agent for fluorescent angiography (indocyanine green (ICG)). The fundus camera is in an early phase of development in this work.

3. Observation of Heavy ion induced emission of Indocyanine Green (ICG)

The measurement system that carbon ion beam (C^{5+}-220 MeV,C^{6+}-320MeV) irradiation experiment to ICG used for the irradiation positioning of this treatment system is set up in the HA port at the TIARA was used. The carbon ion beam irradiated the solution sample of ICG the luminescence of near infrared ray's area (~ 800 nm) from ICG was observed though it was very slight luminescence (see Fig.1). As a result, it has been clarified experimentally that ICG can be used for this irradiation positioning method.

The change in the emission intensity and spectrum of ICG into the ionic species, beam energy, and concentration of ICG is measured as a schedule for the future.

Table 1. Summary of irradiation system for AMD treatment.

Devices & Techniques	
Measurement of distance (from cornea to CNV)	Echo scan Optical coherence tomography
Confirmation of irradiation position	Fundus camera (long working distance)
Beam energy	Carbon, 96 MeV/u
Irradiation dose	Total: 20 GyE
Irradiation time	> 20 msec.
Beam diameter	Variable (> submillimeter)
Range control	Several seats of thin PMMA film
Adjustable beam range	2.0 mm
Interval of beam range	50 μm
Direction of beam adjustment	from choroids to retina

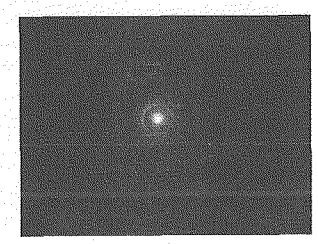


Fig. 1. This photograph is Luminescence of ICG in solution irradiated by ion beam. The concentration of ICG is 2 mg/mL in PBS almost equal to that of person's highest blood.

4-47 Development of Ion-Induced Fluorescence Measurement Technology at the External Light Ion Microbeam System

M. Oikawa, T. Satoh, J. Haga and T. Sakai

Department of Advanced Radiation Technology, TARRI, JAEA

Abstract

We are developing an ion-induced fluorescence measurement technology at the TIARA facility. Establishment of a new high-sensitivity beam diagnostics was required for progress of highly spatial resolution of microbeam. Therefore, we introduced a scanning transmission ion imaging (STI) as new beam diagnostics. Evaluation of STI method was performed by two kinds of experiments. In one experiment, sensitivity of STI was compared with conventional secondary electron imaging using SUS mesh (t=100 μm). In the other, estimation error for beam size was analyzed from one-dimensional profiles of luminous intensity. As a result, it has been confirmed that STI has higher sensitivity than secondary electron imaging. On the other hand, it was proved that the beam size was overestimated by the cause such as scattering from SUS mesh edge.

国内外の様々な加速器施設で磁気レンズ集束方式イオンマイクロビーム装置が整備され、その応用技術として、マイクロ PIXE、PIGE、RBS 等の分析実験や、イオン 1 個を任意の位置に照射するシングルイオンヒット実験など多種多様な用途・分野での利用が進められている。現在、TIARA の 3 MV シングルエンド加速器に接続されているサブミクロンマイクロビーム形成装置（SB ライン）では、従来の 2 次放射線を利用した分析手法に加えて、新たにイオンマイクロビームを励起源とした大気中蛍光分析技術の開発を進めている[1]。原理は生命科学分野で広く利用されている蛍光顕微鏡と同様であり、PIXE 法では測定できない分子等の電子状態の分布を観測することができる。そのため、PIXE 法と併用することができれば相補的に多くの情報を得ることが可能となる。さらに、蛍光顕微鏡の解像度は光の回折限界により制限され、200 nm 以下のものを観察できないが、励起源として 200 nm 以下に集束したイオンマイクロビームを用いれば、従来の解像度を超えた新しい蛍光観察技術を確立することが可能となる。本研究において、ビームの高空間分解能化（ナノビーム化）が必須であり、それに対応した高感度なビーム診断法の確立が求められている。従来用いている 2 次電子イメージング法は 2 次電子の発生量が多いため比較的高感度であり、1 画面の走査が数秒程度で済むため、リアルタイム計測が可能で集束パラメータの調整にも十分な追従性を有している。しかし、高空間分解能化した場合には、ターゲット上でのビーム電流が少なくなり、明瞭な 2 次電子イメージの取得が困難となる。そこで今回、高空間分解能化に対応できる高感度ビーム診断法の確立を目指し、現在開発中である大気蛍光分析技術を応用して、イオンの入射によりシンチレータが発する蛍光をビームの走査位置情報に基づき 2 次元マッピングする手法について検討を行った。実験は上述のサブミクロンマイクロビーム形成装置において、3 MeV の H^+を用いて行った。SUS メッシュ（0.1 mm 厚）の後方にシンチレータおよび光電子増倍管を設置し、ビームスキャナを用いてビームを 2 次元的に走査しながらシンチレータの発光強度の計測を行った。メッシュの孔の部分に照射された場合にはシンチレータが発光するが、他の部分にビームが照射された場合にはビームが透過しないためシンチレータは発光しない。そこで、発光強度分布をビームの位置制御情報と同時に測定することでメッシュの透過イオン像が得られ、ビームサイズの評価が可能となる。この透過イオンイメージングによるビームサイズ評価においては、従来法の電顕校正用 Cu グリッド（1000 lines/inch）の 2 次電子イメージングによりビームサイズが 0.8×0.6 μm^2 と見積もられたマイクロビームを使用した。ビームサイズ評価に先立ち、3 pA 以下の微少ビーム電流条件下における 2 次電子イメージングと透過イオンイメージングの検出感度比較を行ったところ、透過イオンイメージングの方が明瞭な像を取得することができた。この方法では、イオン 1 個ずつによる発光分布計測も原理的に可能であるため、極微弱電流時のナノビーム形成への適用に有利であることが確認された。次に透過イオンイメージングにより得られた SUS メッシュ像を解析し、ビームサイズの評価を行った。SUS メッシュ像において、孔部の発光強度の立ち上がりがビームサイズを反映していることから、X、Y 軸各々直線上の発光強度プロファイルを導き、それを 1 回微分してガウスフィッティングを行い、その半値幅を求めた。その結果 X=3.2 μm、Y=2.1 μm となり、2 次電子イメージングで見積もられたビームサイズよりも 1 μm 以上大きく評価された。この原因について調査するため、光電子増倍管をパルス出力に変更して透過イオンのエネルギー差を計測したところ、SUS メッシュの孔エッジ部での散乱成分に由来するエネルギーの低い（=発光強度の低い）領域が存在することが判明した (Fig. 1)。エッジによる散乱成分の空間的広がりを解析したところ、半値幅で 1.9 μm であり、透過イオンイメージングにおけるビームサイズの過大評価は散乱に起因すると結論付けられた。それは SUS メッシュの厚さや孔の工作精度に依存していると考えられる。

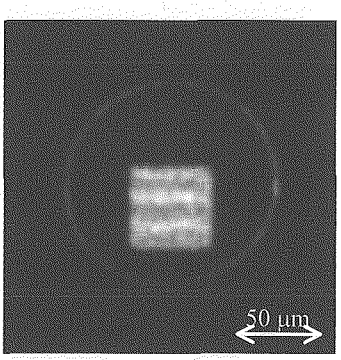


Fig. 1. Scanning Transmission Ion Microscopy (STIM) image of a low energy region in the SUS mesh. In this image, a white square shows an area of irradiation damage. It was introduced to the scintillator by scanning irradiation (scanning field of 50 μm × 50 μm) that made for a marker of the low energy region (= low luminous intensity area).

Reference

1) T. Sakai, et al., TIARA Ann. Rep. 2004, JAEA-Review 2005-01 (2006) p. 298.

4-48 Formation of a Large-Area Uniform Ion Beam Using Multipole Magnets

Y. Yuri [a], N. Miyawaki [a], T. Kamiya [a], W. Yokota [a], K. Arakawa [a] and M. Fukuda [b]

[a] Department of Advanced Radiation Technology, TARRI, JAEA,
[b] Research Center for Nuclear Physics, Osaka University

At the TIARA AVF cyclotron facility, various kinds of ion-beam irradiation techniques have been developed such as uniform beams and microbeams. As uniform irradiation, two types of systems are currently available: One is the raster scanning system using dipole magnets and the other the beam expansion system using thin foils. With the former, the local particle fluence rate is not continuous but depends on the scanning frequency. With the latter, it is difficult to achieve high uniformity for a large-area target. In order to compensate such drawbacks of existing irradiation systems, we are developing the *nonlinear focusing system* using multipole magnets. This system enables us to carry out high-accuracy uniform irradiation with a constant particle fluence rate over the whole of a large-area target.

Formation of the uniform beam can be achieved based on nonlinear focusing [1]. The transverse phase-space profile of the beam is bent into an "S-shape" by the odd-order nonlinear force produced by the magnet such as an octupole. Seen in the real space, the tail of the transverse distribution is folded into the inside and the profile then becomes uniform on a target. The nonlinear magnetic field actually couples ion motion in the two transverse directions. In order to make the coupling as weak as possible and to control in each direction independently, the cross-section of the beam has to be flat at the position where the multipole magnet is located. Two multipole magnets are, therefore, necessary to make the two-dimensional uniform distribution.

In order to confirm whether it is possible to realize beam uniformization at the TIARA AVF cyclotron beam line, we performed numerical simulations. Figure 1 shows the beta functions of the transport optimized for uniform beam formation using a couple of octupole magnets. A typical simulation result is depicted in Fig. 2. The figure clearly shows that the uniform area of 10cm×10cm is established and that the phase-space distribution is no longer elliptical but S-shaped. As shown in Fig. 3, the uniformity of less than several percent is attainable when the irradiation density is sufficiently high. We have also confirmed, through systematic simulations, that the dependence of the uniformity on the beam emittance and the energy spread below the order of 0.1% (typical value for beams extracted from an AVF cyclotron) is negligibly small.

This system will be utilized for ion-beam applications such as the evaluation of radiation resistance of electronic devices and the development of fuel cell membranes.

References

1) P. F. Meads, IEEE Trans. Nucl. Sci., NS-**30** (1983) 2838.

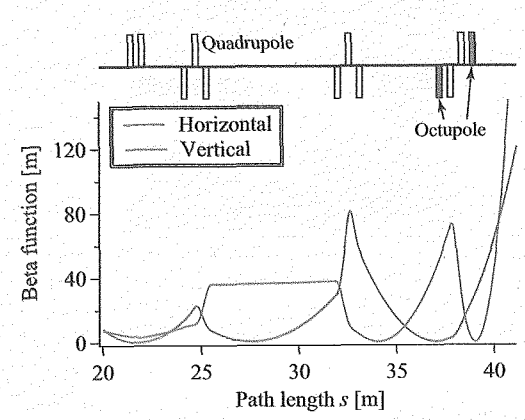


Fig. 1: Beta functions of the beam transport of the JAEA AVF cyclotron optimized for beam uniformization. Two octupole magnets are located at s=37m and s=39m. The exit of the cyclotron corresponds to *s*=0m.

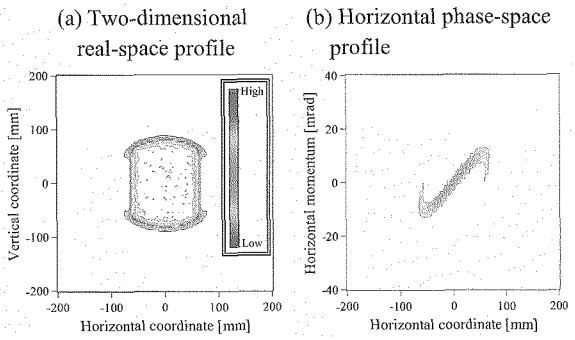


Fig. 2: Transverse beam profiles on the target when the two octupole magnets are turned on. H^+ beams with the kinetic energy of 100 MeV is assumed. The initial transverse distribution is Gaussian. The gradients of the two octupole magnets are -2.3×10^3 T/m^3 and 4.7×10^3 T/m^3.

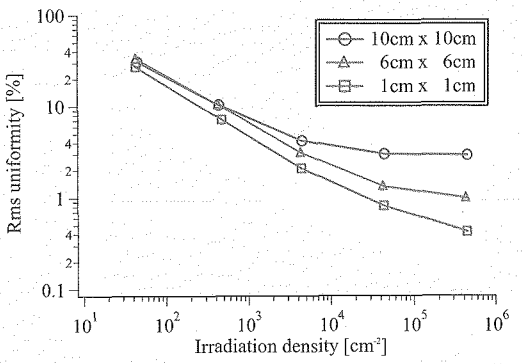


Fig. 3: Rms uniformity vs. the irradiation density. Simulation parameters are the same as in Fig. 2 except for the irradiation density. The uniformity is evaluated for three different areas around the beam axis at the target. It should be noted that the uniformity is better in the smaller area around the beam axis.

4-49 The Effect of Support Gas in Fullerene (C_{60}) Ion Production

K. Yamada, K. Ohkoshi, Y. Saitoh, K. Mizuhashi and W. Yokota

Department of Advanced Radiation Technology, TARRI, JAEA

The cluster ion irradiation provides various effects such as very low-energy implantation, extremely high yield sputtering, unique surface smoothing, low-damage surface cleaning and low temperature thin film formation, which do not easily take place in single-atom irradiation[1]. They are useful for surface fabrication and modification in the field of material development. The fullerene ion is a large cluster of carbon and is expected to emphasize these effects. A fullerene (C_{60}) ion beam of about 1 μA is accelerated with 400 kV ion implanter of TIARA, JAEA[2,3], and it is used to study analysis of the cluster ion irradiation effect[4] etc. However, the fullerene beam current should be much increased to permit application using the various effects mentioned above.

The fullerene ions are produced with a Freeman ion source[5] for the TIARA ion implanter. The dependence of beam intensity on the operation parameters is very different between fullerene ions and single-atom ions. For example, fullerene ion beam intensity decreases with increasing arc current, which is completely opposite of single-atom beam intensity. The beam current of C_{60}^+ is, therefore difficult to be maximized. Then, the correlation between support gas (Ne, Ar, and Xe) flow rate (measured as pressure in the evacuation chamber) and the beam current of C_{60}^+ was studied in order to make ion source parameter optimization for higher intensity of C_{60}^+.

An experimental setup is illustrated in Fig.1. Fullerene sample (Tokyo Chemical Industry Co., Ltd., C_{60}>99%) was vaporized in an oven at 410℃. A support gas was fed into a plasma chamber simultaneously with the fullerene vapor because fullerene vapor alone could not sustain stable arc discharge. The flow rate of support gas was controlled by a mass flow controller with the minimum rate of 0.2 cm^3/min. The fullerene ions were extracted at 4 kV, then C_{60}^+ was selected by a 90° analyzing magnet and accelerated to 200 keV.

A fullerene beam current with a conventional Faraday cup is measured at a smaller value than actual one because a large number of secondary positive ions produced by fullerene collision escape through the electron-suppression field. Therefore, we used a high-aspect ratio Faraday cup without an electron suppressor[3].

The result is shown in Fig. 2. The beam current of C_{60}^+ decrease with increasing support gas flow rate (decreasing pressure). In the case of Ne support gas, the beam current of C_{60}^+ was maximized in the vicinity of a pressure where arc discharge vanished. On the other hand, in the case of Ar and Xe support gas, arc discharge was sustained even at the minimum flow rate, where beam current was maximum. The ion beam current was higher in order of Xe, Ar, and Ne compared at the same pressure.

The result suggests that the heavier mass and the lower flow rate of the support gases bring higher C_{60}^+ current. The mass flow controller should be replaced by one with a smaller minimum rate for Ar and Xe, and other various gases should be examined to clarify the ionization mechanism in order to further increase fullerene ion beam current.

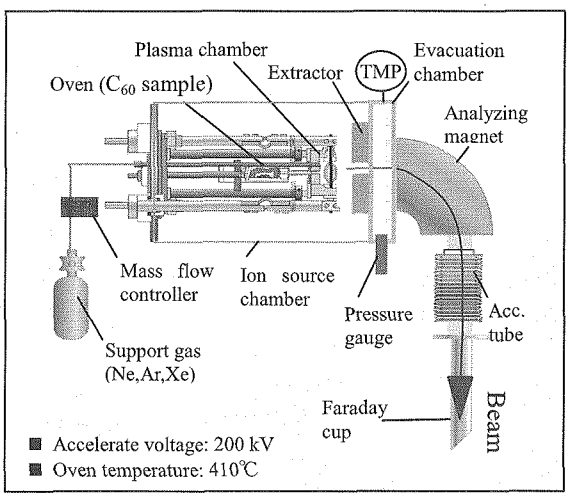


Fig.1 Experimental setup for fullerene ion production. Fullerene vapor and the support gas were fed into the plasma chamber. C_{60}^+ ion was selected by the analyzing magnet. The beam of C_{60}^+ was measured with the high-aspect ratio Faraday cup.

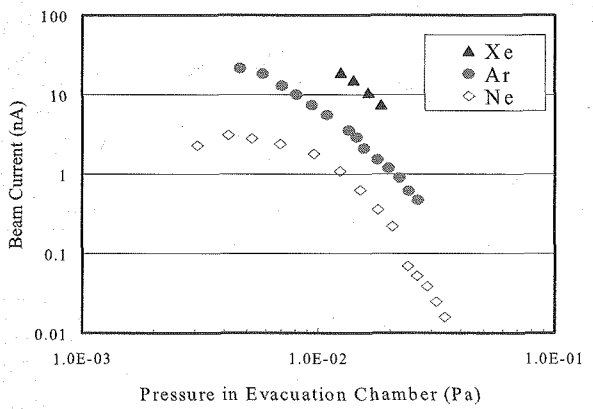


Fig.2 The beam current of C_{60}^+ as a function of pressure in the evacuation chamber.

References

1) I. Yamada, Nucl. Instr. Meth. B 148 (1999) 1
2) Y. Saitoh, S. Tajima, I. Takada, K. Mizuhashi, S. Uno, K. Ohkoshi, Y. Ishii, T. Kamiya, K. Yotumoto, R. Tanaka and E. Iwamoto, Nucl. Instr. Meth. B 89 (1994) 23
3) K. Ohkoshi, Y. Saitoh, T. Orimo, A. Ohmae, I. Takada and S. Tajima, JAERI-Review 2003-033 (2003) 323
4) H. Naramoto, V. Lavrentiev, K. Narumi and S. Sakai, JAERI-Review 2003-033 (2003) 225
5) J. H. Freeman and G. Sidenius, Nucl. Instr. Meth. 107 (1973) 477

4-50 Development of all-permanent-magnet ECR ion source for the JAEA cyclotron

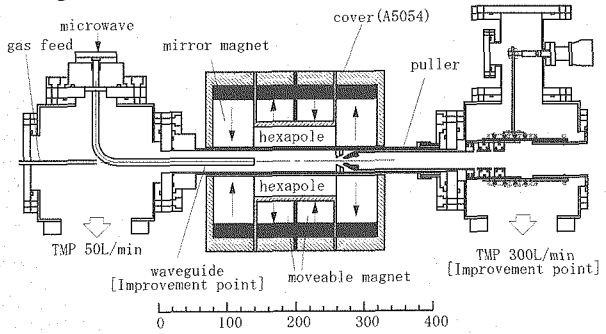
K. Yoshida, T. Nara, Y. Saitoh, W. Yokota

Department of Advanced Radiation Technology, TARRI, JAEA

A heavy-ion microbeam and a single-ion hit technique are being developed at the JAEA AVF cyclotron facility for elucidation of biofunctions and radiation response of semiconductor[1]. High stability of beam intensity is necessary for these techniques, both in a short time-range and in a long time range. However, the stability of the present ECR ion sources for the cyclotron, which are of an electromagnet type, is not satisfactory because the temperature of the coils rises with time and leads to change in the plasma condition. Therefore, we have started development of an all-permanent-magnet ECR ion source (LECR)[2].

The magnetic field distribution of a conventional permanent-magnet ECR ion source is fixed or difficult to change. That of LECR is easy to tune by moving the pieces of magnets, surrounding the hexapole magnet, in radial directions.

The schematic design of LECR is shown in Fig.1. The high voltage of extraction is generally applied to the whole of a permanent-magnet ECR ion source. The high voltage in the case of LECR is applied only to a plasma chamber for the reason that the position of the movable magnets is changed by hand. The bias voltage, which is effective to increase highly charged ions, can be applied to the waveguide insulated from the plasma chamber.



Microwave ---------- 14GHz (Max 125W)
Mirror (Max/Min) ---------- 8800G / 2200G
Hexapole (r=16mm) ---------- 8000G

Fig.1 Schematic view of the all-permanent-magnet ECR ion source (LECR) and the specification.

We did not obtain enough beam current for the original design of LECR. One reason is deterioration of vacuum in extraction chamber at the power of a microwave higher than 40W. Therefore a TMP (300ℓ/min) was installed in the extraction chamber. The vacuum of the extraction chamber improved from 8.0×10^{-5}Pa to 1.0×10^{-5}P. It might be another cause of low beam intensity that bias voltage did not effect enough because waveguide was far from plasma. Therefore the waveguide was lengthened by 60mm to set the leading edge close to the resonance zone.

The improvement of vacuum has enabled continuous running of the source at the maximum power (125W) of a microwave amplifier. The beam current of O^{5+} was increased from 1 to 15μ A and in addition, O^{7+} was observed for the first time. Table2 compares intensity of oxygen ion produced by the ECR ion sources[3] used at TIARA.

TABLE 1 Oxygen beam currents obtained by the ECR ion sources in TIARA (μA).

	O^{4+}	O^{5+}	O^{6+}	O^{7+}
HECR			200	70
OCTOPUS		116	120	10
MINI-13		11	1.9	0.023
LECR original design	2	1	0.6	<0.01
LECR modified	16	15	10	0.6

The charge distribution for LECR, which became similar to that of a large ECR ion source such as OCTOPUS, suggests appearance of the natural performance of LECR. Therefore we examined an effect of the movable magnets. Dependence of beam current of O^{6+} and H^+ on the movable magnet position is shown in Fig.2. The beam current of O^{6+} increased when the radial distance between the movable magnets and the hexapole was widened from 0mm to 50mm. On the other hand the beam current of H^+ is maximized at about 10mm.

This result suggests that the movable magnets may permit the optimum tune of the source parameter for each ion element and for each charge state as an electromagnet type ECR ion source dose.

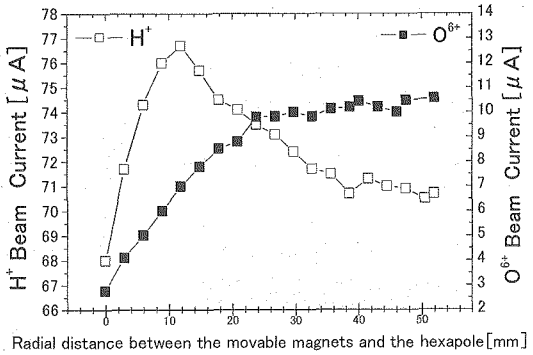


Fig.2 Dependence of the beam current on the radial distance of the movable magnets.

References

1) M.Fukuda et.al., Nucl. Instr & Meth. Phys. Res. B210, 33-36 (2003)
2) K.Yoshida et.al., JAERI Review,2004-025, 316 (2004).
3) W.Yokota et.al., JAERI Review,99-025, 259 (1999)

4-51 Improvement of the Cyclotron System for Microbeam Formation

N. Miyawaki[a)], S. Okumura [a)], S. Kurashima [a)], H. Kashiwagi [a)], K. Yoshida [a)], I. Ishibori [a)], Y. Yuri [a)], T. Nara [a)], T. Agematsu [a)], W. Yokota [a)] and M. Fukuda [b)]

[a)]Department of Advanced Radiation Technology, TARRI, JAEA,
[b)]Research Center for Nuclear Physics, Osaka University

Introduction

At the JAEA AVF cyclotron, a heavy ion microbeam about 10 μm in diameter formed by a beam collimator with an aperture is utilized for researches in biotechnology. For higher spatial resolution required with the progress of the researches, a focusing microbeam system with a quadruplet quadrupole lens is under developement[1]. The energy spread $\Delta E/E$ of the accelerated beam less than 0.02% in FWHM is necessary to reduce the chromatic aberration at the lens in order to achieve a goal beam size of 1 μm in diameter, while the typical energy spread of the cyclotron beam is around 0.1%. Therefore, the center region of the cyclotron was improved to control the beam phase and a flat-top (FT) acceleration system was developed to reduce the beam energy spread[2]. Since a highly stabilized beam is essential to decrease the fluctuation of the beam intensity, several improvements for the cyclotron, such as stabilization of the power supply, are in progress.

Beam stabilization

The power supply of the main magnet of the cyclotron was designed to have the stability of less than $\pm 1\times10^{-5}$, since the stability of the magnetic field is required to be $\pm 1\times10^{-5}$ for the normal operation. Furthermore beam intensity decreased with operating time due to the magnetic field changed by increasing magnet temperature. We, therefore, have stabilized the magnet temperature[3] and achieved the magnetic field stability of $\pm 5\times10^{-6}$. But we have experienced disappearance of the beam in the microbeam formation system, where the beam is controlled on strict conditions. We found two possible causes: the temperature fluctuation of the cooling water at the ion source and the change in the main magnetic field of the order of 10^{-6}. For the later, we applied a precise temperature control unit with a Peltier device to the feedback circuit of the power supply of the main magnet in order to reduce the change of the magnetic field. The current stability of the power supply has been improved from $\pm 1\times10^{-5}$ to $\pm 2\times10^{-6}$, as a result, as shown in Fig. 1.

Reduction of beam energy spread

A broader beam phase width gives a larger difference of energy gain to ions, because of the sinusoidal voltage waveform acceleration. A FT waveform, generated by superimposing a fifth-harmonic voltage waveform on the fundamental one, has been applied to reduce the difference of the energy gain. The FT voltage region within about 14 rf degrees was successfully observed in the test operation. An analyzing system[4], which consist of a deflecting magnet, three sets of slits and semiconductor detectors, was developed to measure the beam energy spread. With use of the improved center region, of the FT voltage wave and of the analyzing system, the beam energy spread was reduced to 0.05%, as shown in Fig.2, which is a half of the ordinary value.

References

1) M. Oikawa, et al., Nucl. Instr. and Meth. B210 (2003) 54.
2) M. Fukuda, et al., Rev. Sci. Instrum. 74 (4) (2003) 2293.
3) S. Okumura, et al., Rev. Sci. Instrum. 76 (2005) 033301.
4) S. Okumura, et al., Proc. 17th Int. Conf. on Cyclotrons and Their Applications, Tokyo, Japan 410 (2004).

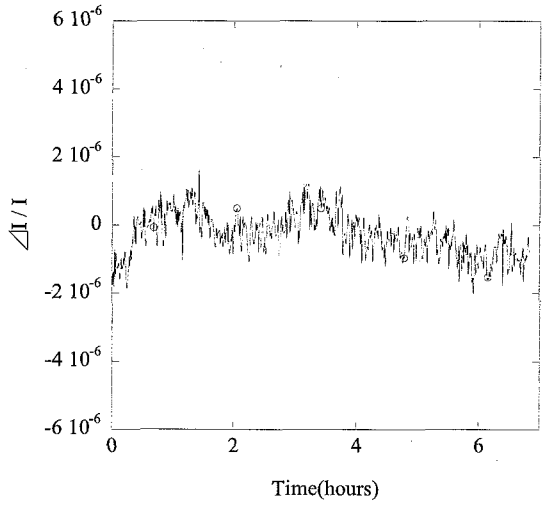


Fig.1 Current drift of the power supply for the main magnet. Applying a temperature control unit with a Peltier device to the feedback circuit, the stability of the output current is improved.

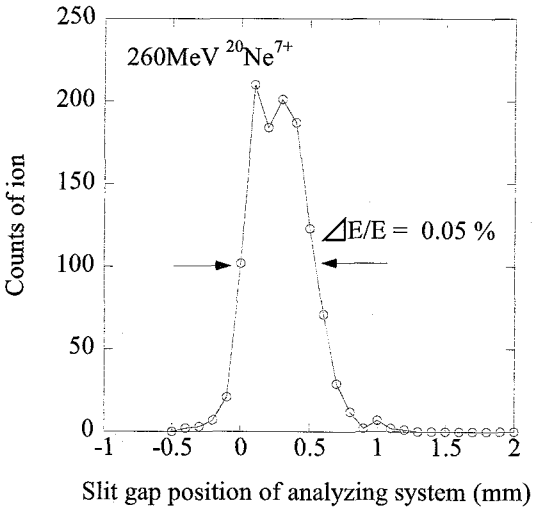


Fig.2 Beam intensity distribution measured with the beam energy analyzing system. The difference of 1 mm in the abscissa corresponds to ΔE/E of 0.1 %.

4-52 Development of Beam Generation and Irradiation Technology for Electrostatic Accelerator

K.Ohkoshi, S.Uno, A.Chiba, K.Yamada,Y.Saitoh, Y.Ishii, T.Sakai, T.Satoh and K.Mizuhashi

Department of Advanced Radiation Technology, TARRI, JAEA

Abstract

Three electrostatic accelerators (a tandem, a single-ended and an ion implanter) at a TIARA facility have developed about beam generation and irradiation technology as follows for the frontier irradiation experiments.
[1]To increase usable energy of cluster beam by the tandem accelerator, we have tried generation and acceleration of multiply charged gold(Au) cluster beam. As a result, we succeed in acceleration Au_3^{2+} ion of about 70pfA at the target.
[2]To improve cluster beam transmission to a charge exchange stripper of the tandem accelerator, we have studied an effect of cluster beam transmission by changing the stripper gaseous species. As a result of the comparative test on three kinds of gas(N_2, SF_6, CO_2), the better transmission date of the gas which the molecular weight is small was obtained.
[3]It was confirmed that the resolution of developed measurement system of beam energy spreads was about 5×10^{-5} using $dE/E=2\times10^{-4}$ beam from single-ended accelerator. In addition, we have installed a chamber for the beam energy measurement at the straight beam line of the tandem accelerator.

1．クラスターイオンの生成・加速技術の開発

TIARA[1]タンデム加速器におけるクラスターイオンのエネルギー領域の拡大が、多価のクラスターイオンを用いて可能であるかを利用頻度の高い金のクラスターについて調べた。負のクラスターイオンを正イオンへ荷電変換する際、そのほとんどは解離してしまう。解離せずに+1価のイオンに荷電変換される率は数%以下であるが、+2価になるのは非常に少なく、ビーム輸送が困難である。そこで、半導体検出器（SSD）を用いて、+2 価のクラスターイオンを検出し、輸送パラメータの調整を行った。その結果、ターゲット上で Au_3^{2+}を 70 pfA 程度検出することに成功し、利用可能な最大エネルギーを 6 MeV から 9 MeV に拡大することができた。

また、荷電変換時のクラスターイオンの解離率を改善する目的で、炭素クラスターイオンを用いて荷電変換ガス種と解離率の間に依存性があるかを N_2、CO_2、及び SF_6 について調べた。Fig. 1 に N_2 と SF_6 のガス圧に対する C_8 クラスターイオン透過率を示す。各ガス種での最適ガス圧（ピーク値比較）におけるクラスターイオンの解離の割合は、通常使用している N_2 に対して CO_2 が 1.2 倍、SF_6 が 1.4 倍と質量数が大きくなるほど高くなっており、クラスターイオンに対する荷電変換ガスとしては、質量数の小さなものが適すると示唆する結果を得た。

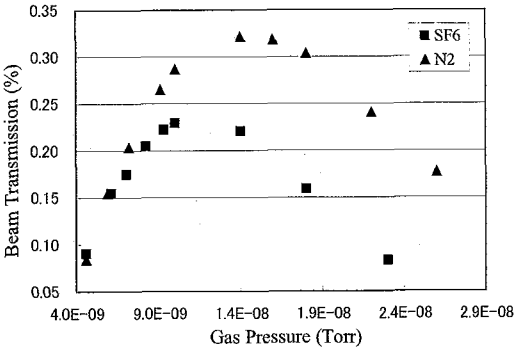


Fig.1 Relationship between gas(N_2,SF_6) pressure and C_8 beam transmission.

2．高精度ビームエネルギー計測技術の開発

共鳴核反応幅がそれぞれ 150eV, 300eV 以下と小さな核反応 $^{27}Al(p,\gamma)^{28}Si$、$^{24}Mg(p,\gamma)^{25}Al$を用いて静電加速器の電圧校正やエネルギー幅測定を目的とした計測技術の開発[2]によって、これまで 3MV シングルエンド加速器について評価を行ってきた。ビームエネルギーの安定化技術開発の結果のために、分析電磁石によりエネルギー幅を $dE/E=2\times10^{-4}$ に制限したビームを用いて測定系の分解能を評価した結果、5×10^{-5}程度であることを確認した。

今後、$dE/E=5\times10^{-5}$ 程度のビームにより測定系の分解能の再確認を行う等、計測技術の開発を進めるとともに、並行して加速器のエネルギー高安定化技術開発を進める。

3．タンデム加速器のビームエネルギー測定技術の開発

タンデム加速器では、ペレットチェーンのインバーター制御化など電圧安定度の向上に向けた技術開発[3]を進めている。エネルギー評価を頻繁に行う必要から、共鳴核反応法によるエネルギー測定専用チェンバーを分析電磁石の0°ラインに新設した。0°ラインでは各種のビームが混在するが、共鳴核反応 $^{1}H(^{15}N,\ \alpha\gamma)^{12}C$ 及び $^{27}Al(p,\gamma)^{28}Si$ を用いてエネルギーの校正を行うことができる。測定の結果、前者は電圧計(GVM)2.1MV に対し 0.88%、後者は 0.496MV に対し 2.82%と電圧表示に対し低目の値であった。今後、タンデム加速器特有の荷電変換に伴うエネルギーロスやスプレッド及びターゲット厚による影響評価を行う予定である。

4．ECR イオン源を用いた多価イオン加速

イオン注入装置では、材料へのイオン注入深さの制御範囲を拡大させるため、小型 ECR イオン源を搭載して多価イオン生成を行っている。今回は、MIVOC (Metal Ion from Volatile Compounds) 法[4]により、Tris(Methylsily) methane の試料を用いてシリコン(Si)の多価イオン発生を試みた。その結果、3 価が 3.6μA、5 価が 0.9μA 発生することに成功し、イオン注入装置で Si の MeV 領域の照射を可能とした。

Reference
1) Y.Saitoh, S.Tajima, et al., Nucl.Instum.Methods phys.Res. B89, 23(1994)
2)Y.Ishii, A.Chiba, et al., JAERI-Review 2004-025, P326 -327
3)K.Mizuhasi, et al., JAERI-Review 2004-025, P321-323
4)H.Koivisto, J. rje and M.Nurmia, Nucl.Instrum.Methods. B94 ,291(1994)

5 Status of Irradiation Facilities 2005

5-01 Safety Measures, Utilization Condition and Introduction of New Utilization System in TIARA Facility ····· 195
Y. Nakamura, K. Nishimura, H. Takizawa, M. Hosono, H. Kaneko, H. Watanabe, H. Tachibana, S. Kaneya, S, Mochizuki, M. Kawabata, M. Iijima and K. Daikubara

5-02 Operation of JAEA AVF Cyclotron System ····· 196
T. Nara, T. Agematsu, I. Ishibori, S. Kurashima, K. Yoshida, S. Okumura, N. Miyawaki, K. Kashiwagi, Y.Yuri, W. Yokota M. Fukuda, K. Akaiwa, To. Yoshida, S. Ishiro, Y. Arakawa, Tu. Yoshida, S. Kanou, A. Ihara and K. Takano

5-03 Operation of the Electrostatic Accelerators ····· 197
K.Mizuhashi, S.Uno, K.Ohkoshi, A.Chiba, K.Yamada, Y.Saitoh, Y.Ishii, T.Satoh, T.Sakai, W.Yokota, T.Kitano, T.Takayama, T.Orimo, S.Kanai, A.Ohmae, M.Kouka and M.Ishii

5-04 Radiation Control in TIARA ····· 198

5-05 Radioactive Waste Management in TIARA ····· 199
J.Yoshii, N.Higuchi

5-06 Utilization of the Electron Accelerator and Gamma-Ray Irradiation Facilities ····· 200
T. Kanazawa, H. Kaneko, N. Haneda, H. Hanaya, R. Yamagata, H. Seito, S. Koyama , T. Yamaguchi, I. Kawashima, N. Yagi and M. Takagi

5-07 Operation of the Electron Accelerators ····· 201
H. Kaneko, H. Hanaya, N. Haneda, R. Yamagata, H. Seito, T. Kanazawa, T. Yamaguchi, I. Kawashima and N. Yagi

5-08 Operation of the Co-60 Gamma-Ray Irradiation Facilities ····· 202
N. Haneda , R. Yamagata, H. Kaneko, H. Hanaya, H. Seito, T. Kanazawa, S.Koyama, I. Kawashima, N. Yagi, M. Takagi and T. Yamaguchi

This is a blank page.

5-01 Safety Measures, Utilization Condition and Introduction of New Utilization System in TIARA Facility

Y. Nakamura, K. Nishimura, H. Takizawa, M. Hosono, H. Kaneko, H. Watanabe, H. Tachibana, S. Kaneya, S, Mochizuki, M. Kawabata, M. Iijima and K. Daikubara

Department of Advanced Radiation Technology, TARRI, JAEA

Abstract

Several safety measures in the TIARA facility, were carried out such as the repair of surface deteriorated concrete layer on the roof of the research building, the installation of barrier-free slope and handrail at the front entrance, and so on. The number of experimental subjects increased rapidly for recent a few years, however in 2006, this value reduced contrarily. A new utilization system for radiation facilities in JAEA is scheduled to be introduced from fiscal year of 2006. Prior to the introduction, we investigated the framework of this system. The utilization part is divided into internal, external and flexible use. Then the experimental subjects are collected twice for a year according to new this system. A TIARA annual report 2004 consisted of 412 pages was issued and the last 14th TIARA research review meeting was held successfully at Takasaki city gallery.

TIARA施設の安全確保

定期1ヶ月及び3ヶ月巡視点検等を確実に実施し、放射線施設の安全確保を実現した。主要な施設関係整備内容としては、イオン照射研究棟屋上コンクリート表層剥離部分(約190m^2)の補修、作業エリア雨漏れの調査及び対象外壁亀裂部分の補修、大型機材庫床沈下間隙部分(5～6cm程度)のCaulking剤充填補修、省エネ及び暗所対応用人感センサー付き照明(13灯)の設置、玄関御影石部分の滑り止め(バーナー火炎熱射による目荒らし)加工、バリアフリー用スロープ・手摺りの設置(Photo.1参照)、外部利用者用ネットワークの構築(光ファイバーケーブルの敷設及びファイヤーウォールの設定)、等々を実施した。

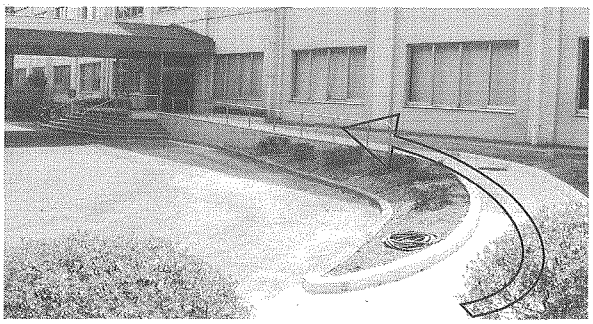


Photo. 1 Installation of barrier-free slope and handrail at front entrance of TIARA building

施設利用状況及び利用支援等

2006年度を含むTIARA施設全体の実験利用課題の件数推移をFig. 1に示す。課題総数は、2001年度まで100件前後で推移していたが、2002年度以降増加に転じ、2005年度では133件に急増していた。なお、2006年度上期分の総件数は、新制度移行に伴い103件まで減少した。2005年度の年間利用時間合計は、サイクロトロンで2486hであり、研究分野別内訳ではバイオ技術が1064h (42.8%)を占め、次に宇宙環境材料が378h、基盤技術及びマシンスタディーがいずれも312hであった。一方、静電加速器では458日が年間総利用日数であり、このうち無機機能材料が143日(31.2%)、次に基盤技術、宇宙環境材料及び原子力材料が、それぞれ86日、68日及び67日の順であった。

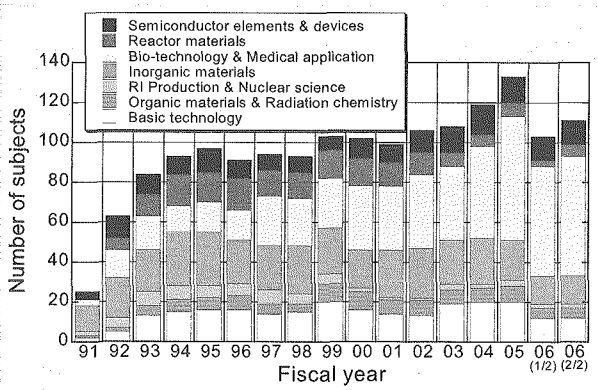


Fig. 1 Yearly shift of the number of experimental subjects occupied in individual research field.

2006年度から導入される新たな施設利用制度では、利用種別は自己使用枠(機構内利用)と施設共用枠(外部利用)とに大別されるが、TIARA施設では利用運営の柔軟・利便性を向上させるため、独自に第3の有効利用枠を導入した。この新利用制度の主要内容は、1)各枠の利用比率は加速器毎に事前に目標設定、2)課題募集は2回/年(上期及び下期)、3)有効利用枠は各期に2回程度設定、等々である。また、新利用制度における施設利用や課題募集方法等を具体的に検討するとともに、「高崎研施設利用委員会」(略称)及び「TIARA等専門部会」を組織し、それらの結果について審議依頼した。

2006年度上期の利用割当/申込時間(配分比率)は、サイクロトロンの自己使用枠部分が1013.5h/1890.5h(0.536)、施設共用枠部分が60h/60h(1.0)、また静電加速器では同様にそれぞれ194日/319日(0.608)及び14日/14日(1.0)であった。

さらに、利用窓口業務等の平成15～17年の最近3年間における月平均値は、宿泊申込者が約50人、指定登録・解除者は30～40人、見学者は100～130人でほぼ定常値を示している。一方、ガラスバッジ及びIDカードの発給・返却数は、15～60件と大幅に増加している。

成果普及活動

2005年度TIARA施設利用の研究成果概要を総括したTIARA Annual Report 2004(JAEA-Review 2005-001)を編集・発行した。この報告書は、全412ページ(カラー含む)であり、約450部を関係箇所に配布した。また、第14回TIARA研究発表会が、6月23日と24日の両日高崎シティギャラリーで開催され、口頭発表10件、ポスター発表108件、参加者327名であった。

その他

TIARA施設の省エネ対策[1]の一環として、5月連休時における装置立ち上げ時期の延伸を実施した。その結果、単純同一期間比較では143MWhの減少となり、この数値は高崎研の省エネ年間削減目標値190MWh(19GWhの1%)の約75%に匹敵する。また、ISO14001の活動に関連して、従来紙媒体で資料配布していた課題募集申込書や実験計画書等について、共通ファイルを引用したパソコン画面上でのPaperless審査・検討方式に切り換え、紙資源節減を図った。

References

1) Y. Nakamura, S. Kurashima, W. Yokota, T. Nara, et al., JAEA-Review 2005-001 (TIARA Annual Report 2004), p361-363 (2005)

5-02 Operation of JAEA AVF Cyclotron System

T. Nara[a)], T. Agematsu[a)], I. Ishibori[a)], S. Kurashima[a)], K. Yoshida[a)], S. Okumura[a)], N. Miyawaki[a)], K. Kashiwagi[a)], Y. Yuri and W. Yokota[a)]
M. Fukuda[b)], K. Akaiwa[c)], To. Yoshida[c)], S. Ishiro[c)], Y. Arakawa[c)], Tu. Yoshida[c)], S. Kanou[c)], A. Ihara[c)] and K. Takano[c)]

[a)] Department of Advanced Radiation Technology, TARRI, JAEA,
[b)] Research Center for Nuclear Physics, Osaka University, [c)] Beam Operation Service, Co., Ltd.

Abstract

The JAEA AVF cyclotron system was operated for 3383 hours without a serious trouble in FY 2005. The percentages of operation time of the year used for experiments, joint-use, machine tuning, beam development, and machine study were 67%, 3%, 19%, 1%, and 10%, respectively. The regular overhaul was carried out for five weeks in summer, and the routine maintenance of power supplies for a week in fall. The technical development for higher stability of the cyclotron magnetic field and the flat-top acceleration were performed as well as beam development.

1. 運転状況

サイクロトロンでは平成17年度に計画されたイオンビーム提供を順調に遂行した。年間総運転時間は3383時間であった。ここ数年間は保守業務計画の効率化ならびに休祭日に保守整備を実施することにより運転時間を大幅に上昇させてきた。平成17年度では採択課題数が過去13年間の平均52件から80件と急増し、マシンタイムが細分化されて利用効率が低下することが予想されたため、マシンタイムの割当において運転条件変更回数を減らして実験利用以外に費やされる調整時間を削減することで運転時間を確保した。

平成17年度の運転内容はFig. 1に示すように共同利用を含むビーム提供が70%であった。また、イオン種別での利用割合はFig. 2に示す通りであった。

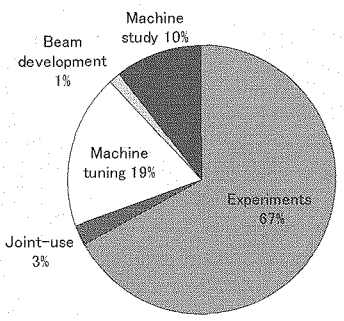


Fig. 1. Statistics of operation contents in FY2005

2. 整備状況

サイクロトロン本体系の定期整備は夏季の高崎量子応用研究所の最大消費電力低減のために、7月から8月にかけて実施した。サイクロトロンでは高い圧力の冷却水を循環するため漏水が起き易かった。このため、約80箇所に及ぶ流量計とフロースイッチをステンレス製の高耐圧仕様に変更することで冷却系の信頼性を高めた。また、平成16年度に製作した高安定軽イオン源入射系システムを同期間に既存のイオン源入射系に接続した。11月にはコイル電源の定期点検を実施した。サイクロトロンの制御用計算機システムでは、老朽化により故障が頻発したが、Windows NT 4.0で動作するPCの保守部品が入手できずメインテナンスが困難となった。そのため、PCを更新し、Windows Xpへの変更に伴うソフトウェアのバージョンアップならびに修正等の作業を3月の整備期間で実施した。

故障修理では加速電圧発生用RFアンプ真空管の寿命が、これまで定めていた定期交換の間隔より短くなったことが分かった。これは、近年の実験数の増加に伴って、当アンプの起動停止回数が増えたことが主な原因であると判断し、真空管のフィラメント電源の起動・停止の回数を少なくするように制御シーケンスを改造した。真空排気関係の整備では落雷による複数の停電によりECRイオン源用磁気浮上ターボポンプ（300リットル/sと2000リットル/s）の回転軸のベアリングが故障した。また、ビーム輸送部基幹ラインの磁気浮上ターボポンプの回転翼がサイクロトロン運転中に破損し、大気がビームダクト内に突入した。同様の故障は過去に2回あり、いずれもターボポンプを取り付けているビーム輸送ダクトまで損傷させたが、今回は幸いダクト等への影響は小さく、ターボポンプを予備品と交換し、散乱したアルミの回転翼破片を取り除いて翌日にはサイクロトロンの利用運転を再開した。このトラブルで基幹ライン以外のダクト内に散乱した細かな破片は、後の整備期間に回収した。

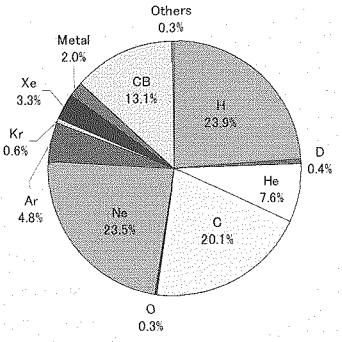


Fig. 2. Statistics of accelerated ion species in FY2005.

3. 技術開発

マイクロビーム形成などのビーム高品位化に向けて磁場の高安定化を進めている。この一環として、$\Delta I/I=\pm 1\times 10^{-6}$の電流安定度達成をめざしてメインコイルの出力電流のモニタを、従来のシャント抵抗から直流電流変換器(DCCT:Direct Current Current Transformer)に変更し、出力電流の精度向上を図った。

フラットトップ加速技術の開発では、Ne-260MeVビームを用い全加速半径において295回転にわたって全ターンセパレーションを初めて確認した。

新ビーム開発では、実験者から要望のあったH^+-34MeVおよび$^{40}Ar^{14+}$-530MeVビームを開発した。なお、$^{40}Ar^{14+}$ビームは、$^{20}Ne^{7+}$ビームと質量対電荷比が近接してサイクロトロンの分離能力限界に近いことから、両者が分離して引き出せることを実験的に確認した。

5-03 Operation of the electrostatic accelerators

K.Mizuhashi[a)], S.Uno[a)], K.Ohkoshi[a)], A.Chiba[a)], K.Yamada[a)], Y.Saitoh[a)], Y.Ishii[a)], T.Satoh[a)],T.Sakai[a)],W.Yokota[a)], T.Kitano[b)], T.Takayama[b)], T.Orimo[b)], S.Kanai[b)], A.Ohmae[b)],M.Kouka[b)] and M.Ishii[b)]

[a)]Department of Advanced Radiation Technology, TARRI, JAEA
[b)]Beam Operation Service, Co., Ltd

Abstract

Three electrostatic accelerators were almost operated smoothly for various experiments in FY 2005.The yearly operation time of each accelerator amounts to 1974, 2359.9, 1859.9 hour for the tandem, the single-ended and the ion implanter, respectively. Main trouble was a short circuit of a part of the ion source in the single-ended accelerator. This lets to the suspension of operation for fifteen days. New beam acceleration and improvement of each accelerator were carried out.

1. 静電加速器の運転状況

平成17年度のTIARA施設3台の静電加速器は順調に稼動し、計画されたイオン照射実験の内、ユーザー側の都合で中止したものを除き全てを終えた。17年度の年間運転時間はタンデム加速器、シングルエンド加速器、イオン注入装置について、それぞれ1974時間、2359.9時間、1859.9時間である。Fig.1に各加速器の月別運転時間を示す。4月、8月、12月は定期整備月にあたり、他の月と比較し運転時間は少ない。

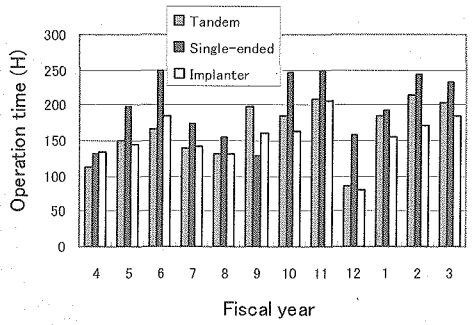


Fig.1 Monthly operation time in FY 2005

シングルエンド加速器では9月にイオン源のビーム引き出し部に故障が発生し、故障した部品が特注品であったことから製作に時間を要し、15日間の運転停止となった。この間に計画していた合計8件の実験は、運転計画を見直し、後日全てを実施した。静電加速器は稼動してから13～15年が経過し、この間に1週間以上に亘って加速器を停止させた故障は平成12年6月に発生したタンデム加速器の制御計算機のハードディスクの破損による約1ヶ月の停止と今回の15日間の停止の2回である。

静電加速器による本年度の共同利用（有料照射）件数はタンデム加速器が10件、イオン注入装置が21件の合計31件であった。この内、イオン注入装置の3件（3日分）は韓国からの利用で、国外からの共同利用はTIARAとして初めてであった。

また、本年度の特徴として、地震および落雷による加速器への影響が多く、7月中旬から8月下旬に掛けて落雷による停電が6回、大きな地震（震度5の宮城県沖地震、震度6の中越地震）が2回発生した。これらの停電でターボ分子ポンプ1台が故障、実験が数回中断された。また、こうした事象によって加速器施設の点検や停止してしまった施設の立上作業を余儀なくされた。

2. 加速器の整備状況

タンデム加速器では3台の負イオン源を有し、発生した負イオンを最大電圧80kVで加速器本体内に導入し加速している。この入射電圧の不安定化が進み印加できる電圧が年々低下している。特にHeの負イオンを生成するAlphatrossイオン源では30kV以下にまで低下した。メガテスターによる加速管の検査では特段の異常は見出せないが、ビームの発生に伴い不安定になることから加速管内部の汚損等が原因であると判断し、新品の加速管に交換した。その結果、最大電圧80kVで安定に運転が行える様になった。今後、取り外した加速管を再生し、順次他のイオン源の加速管も交換していく予定である。

シングルエンド加速器およびイオン注入装置では制御用計算機の操作機能の向上を図った。これによって、ターゲット室からの加速器操作が可能になる等、運転整備の作業性が改善された。

3. 技術開発

タンデム加速には負イオンが必要であり、電子親和力が小さいために負イオン化が困難なZn(0.09eV)についてはその値が大きな酸素(1.47eV)との化合物を用いてZnOとして約1μAを新たなビームとして生成した。この分子イオンをタンデム加速器へ入射、荷電変換に伴う解離によってZn単体イオンとして数百nAを得た。また、毎秒数万個程度のフラーレン(C_{60})の加速に成功し、加速電圧2.5MVでC_{60}^{+1}、C_{60}^{2+}、C_{60}^{3+}を検出した[1)]。

イオン注入装置ではSi^{1+}、Ge^{1+}、およびMINI-ECRイオン源でSi^{3+}を新たに加速した。ビーム電流量はSi^{1+}とGe^{1+}が約2μA、Si^{3+}は約3.6eμAである。この内、Si^{1+}の生成ではSiの質量数28がフィラメント支持物質の窒化ボロン(BN)より発生するN_2イオンと同じであることから分離出来ないため、セラミック用にフィラメント支持構造を変えることで安定な引き出しに成功した。

タンデム加速器ではペレットチェーンに一定の張りを持たせるためのスライド機構付チェーンモータ固定板を有するが、このスライド機能の改善を図るために同固定版を改造した。これにより、チェーンの動きが滑らかとなり、駆動中に発生する塵埃が抑制され、タンク内の汚損（煤化）が緩和された。また、本改造による電圧安定度の改善効果については評価中である。

References

1) 斎藤勇一他、第18回タンデム加速器及びその周辺技術の研究会報告集(2005)p47-49

5-04 Radiation Control in TIARA

Safety Section
Department of Administrative Services, TARRI, JAEA

Abstract

In order to confirm the radiation control in TIARA for FY 2005, individual monitoring for the workers and monitoring of radioactive gasses and radiation controlled areas have been carried out. The effective dose values of almost workers were below the detection limit (less than 0.1mSv). The maximum dose was 0.9mSv/y, which was based on the overhaul of the TIARA AVF cyclotron. A small amount of radioactive gasses was released sometimes during operation of the cyclotron through the stack of TIARA. Monitoring for external radiation and surface contamination was routinely carried out in/around the radiation controlled areas. Neither unusual value of dose equivalent rate nor surface contamination was detected.

1 個人線量の管理

(1) 放射線業務従事者の個人線量管理

2005 年度における放射線業務従事者の実効線量の分布を Table 1 に示す。ほとんどの放射線業務従事者の実効線量は 0.1mSv(検出下限値)未満であった。

最大実効線量は 0.9mSv であり、サイクロトロンの点検・保守に従事した作業者であった。

Table 1. Distributions of the effective dose of the radiation workers in FY 2005.

Items \ persons		Number of persons in each periods				Total
		1st quarter	2nd quarter	3rd quarter	4th quarter	
Distribution range of effective dose	HE < 0.1	555	606	571	600	707
	0.1 ≦ HE ≦ 1.0	2	4	5	4	12
	1.0 < HE ≦ 5.0	0	0	0	0	0
HE:Effective dose *1 (mSv)	5.0 < HE ≦ 15.0	0	0	0	0	0
	15.0 < HE	0	0	0	0	0
Number of persons under radiation control (A)		557	610	576	604	719
Exposure above 1mSv	Number of persons (B)	0	0	0	0	0
	(B)/(A)×100(%)	0	0	0	0	0
Mass effective dose (Person･mSv)		0.2	2.1	0.7	0.6	3.6
Mean dose (mSv)		0.00	0.00	0.00	0.00	0.01
Maximum dose (mSv)		0.1	0.7	0.2	0.2	0.9

*1 Not detected according to internal exposure.

(2) 一時立入者等の個人線量管理

管理区域への一時立入者の人数を Table 2 に示す。全ての一時立入者の実効線量は 0.1mSv 未満であった。

Table 2. Number of persons who temporary entered in the radiation controlled areas in FY 2005.

Periods	1st quarter	2nd quarter	3rd quarter	4th quarter	Total
Number of persons	491	520	319	412	1742

2 放出放射性物質の管理

2005 年度イオン照射研究施設のスタックから放出された、放射性物質の四半期ごとの最大放射能濃度と放出量を Table 3 に示す。

サイクロトロンの運転にともない ^{41}Ar が、ポジトロン放出核種を用いた植物体内移行実験にともない ^{11}C, ^{13}N が、フラーレンへのイオン注入実験にともない ^{133}Xe などの放射性ガスが少量放出された。放射性塵埃(^{65}Zn 等)は検出されなかった。

Table 3. Monitoring results of released gaseous radioactivity in FY 2005.

Nuclide	Items \ Periods	1st quarter	2nd quarter	3rd quarter	4th quarter	Total
^{41}Ar	Maximum concentration (Bq/cm^3)	$<1.4\times10^{-4}$	6.4×10^{-4}	$<1.4\times10^{-4}$	2.5×10^{-4}	6.4×10^{-4}
	Activity (Bq)	6.0×10^{7}	1.5×10^{9}	8.0×10^{7}	6.7×10^{8}	2.3×10^{9}
^{11}C	Maximum concentration (Bq/cm^3)	$<1.4\times10^{-4}$	$<1.4\times10^{-4}$	$<1.4\times10^{-4}$	$<1.4\times10^{-4}$	$<1.4\times10^{-4}$
	Activity (Bq)	3.1×10^{8}	3.4×10^{7}	3.6×10^{7}	2.4×10^{8}	6.2×10^{8}
^{13}N	Maximum concentration (Bq/cm^3)	$<1.4\times10^{-4}$	$<1.4\times10^{-4}$	$<1.4\times10^{-4}$	$<1.4\times10^{-4}$	$<1.4\times10^{-4}$
	Activity (Bq)	4.7×10^{6}	3.4×10^{8}	1.8×10^{8}	3.4×10^{6}	5.3×10^{8}
^{133}Xe	Maximum concentration (Bq/cm^3)	—	—	—	$<1.4\times10^{-4}$	$<1.4\times10^{-4}$
	Activity (Bq)	—	—	—	1.9×10^{7}	1.9×10^{7}
^{65}Zn	Maximum concentration (Bq/cm^3)	$<4.6\times10^{-10}$	$<4.7\times10^{-10}$	$<5.0\times10^{-10}$	$<5.4\times10^{-10}$	$<5.4\times10^{-10}$
	Activity (Bq)	0	0	0	0	0

3 線量当量率と表面密度の管理

放射性同位元素使用室等の管理区域内及び管理区域境界の線量当量率の測定及び、管理区域内の表面密度の測定を定期的に実施した。線量当量率と表面密度のどちらも異常な値は検出されなかった。

サイクロトロン棟の管理区域における線量当量率の代表的な例を Fig. 1 に示す。

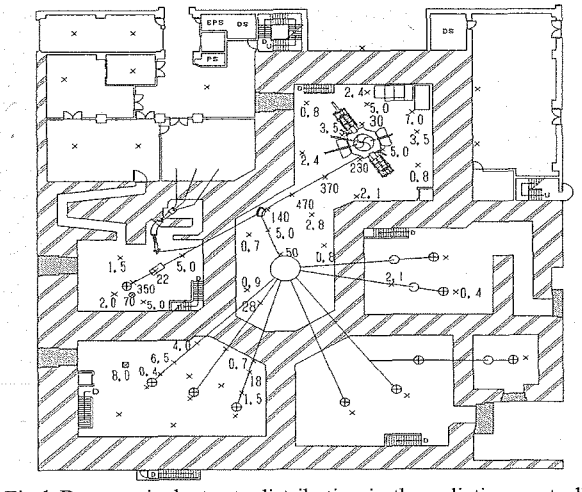


Fig.1 Dose equivalent rate distribution in the radiation controlled area in the cyclotron building.
Date measured : March 22 and 29, 2006
Measuring position : Indicated with × 1m above floor
Unit : μ Sv/h
(the dose rates less than 0.2 μ Sv/h are not indicated)

5-05 Radioactive Waste Management in TIARA

J.Yoshii and N.Higuchi

Department of Administrative Services, TARRI, JAEA

Abstract

The radioactive wastes generated in TIARA are managed by Utilities and Maintenance Section. The main radioactive wastes were the radioactive solid waste such as the rubber glove, paper, the cloth, the metal, and the glass generated by the research experiments and the maintenance of the cyclotron. Other radioactive wastes were the radioactive liquid waste such as inorganic waste fluids generated from the research experiment and the air-conditioning machine in radiation control area. These wastes were managed according to properties.

1. 放射性廃棄物管理

TIARA 第１種管理区域内で発生する固体及び液体の放射性廃棄物は工務課が管理する処理・保管設備において、廃棄物の性状に応じて安全に処理・保管されている。2005 年度の各四半期毎の発生量を以下の表に示す。

1.1 固体廃棄物

2005年度の各四半期毎に発生した性状別固体廃棄物の発生量をTable 1に示す。廃棄物は、可燃性（ゴム手袋等）、不燃圧縮性（金属片）及び不燃非圧縮性として汚染された部品類である。圧縮性廃棄物は主にサイクロトロンの保守により発生したものである。

1.2 液体廃棄物

2005年度の各四半期毎の液体廃棄物の発生量をTable 2に示す。殆どが無機性で、実験によるものや、第１種管理区域内に設置されている空調機から発生した凝縮水である。夏期（第２四半期）に発生した液体廃棄物の殆どは凝縮水によるものであり、これら無機廃液は蒸発処理を行って管理区域内で再利用される。また蒸発処理に伴い少量の濃縮液が発生する。

Table 1. Radioactive solid wastes generated in FY 2005.

Amounts / Items	Amounts of generation in each periods (m^3)					Number of packages /drum
	1st quarter	2nd quarter	3rd quarter	4th quarter	Total	
Category A*	0.54	0.48	0.84	1.14	3.00	
1)Combustible	0.48	0.40	0.62	0.34	1.84	11**
2)Incombustible	0.06	0.08	0.22	0.80	1.16	0
Compressible	0.06	0.08	0.22	0.14	0.50	3**
Filters	0	0	0	0.66	0.66	0
Category B*	0	0	0	0	0	0

* defined by dose at the outer surface of container : (A) ＜ 2 mSv/h ≦ (B)

** 200-liter drum

Table 2. Radioactive liquid waste generated in FY 2005.

Amounts / Items	Amounts of generation in each periods (m^3)					Number of packages /drum
	1st quarter	2nd quarter	3rd quarter	4th quarter	Total	
Category A*	11.24	17.71	7.40	7.12	43.47	
1)Inorganic	11.24	17.71	7.40	7.12	43.47	treatment
2)Organic	0	0	0	0	0	0
3)Sludge	0	0	0.10	0.10	0.20	2
Category B*	0	0	0	0	0	0

* defined by concentrations in $Bq/cm^3(\beta,\gamma)$: (A) ＜ 3.7×10 ≦ (B) ＜ 3.7×10^4

5-06 Utilization of the Electron Accelerator and Gamma-Ray Irradiation Facilities

T. Kanazawa [a)], H. Kaneko [a)], N. Haneda [a)], H. Hanaya [a)], R. Yamagata [a)], H. Seito [a)], S. Koyama [b)], T. Yamaguchi [b)], I. Kawashima [b)], N. Yagi [b)] and M. Takagi [b)]

[a)]Department of Advanced Radiation Technology, TARRI, JAEA,
[b)]Radiation Application Development Association, RADA

Abstract

An electron accelerator and three gamma ray irradiation facilities were operated without serious trouble for various experiments in FY 2005. The operation of No.2 accelerator was terminated at April 2005. The number of experimental subjects was 544 for the No.1 accelerator, 287 for the Cobalt No.1 facility, 630 for the Cobalt No.2 facility, and 339 for the Food irradiation facility.

１．１７年度の利用状況

１台の電子加速器及び３棟のガンマ線照射施設を、年間の運転計画に基づいて照射利用に供した。２号加速器は17年度から運転を停止した。

各施設の照射利用件数の集計は、電子加速器では照射希望日の２週間前の木曜日（木曜日又は金曜日が休日の場合は水曜日）正午まで、ガンマ線照射施設では照射希望日の前週木曜日正午までに照射施設管理課に提出された照射利用申込みに基づいて行った。

17年度の利用件数は電子加速器が５４４件、コバルト第１照射棟は２８７件、コバルト第２照射棟は６３０件、食品照射棟は３３９件であった。

電子加速器及びガンマ線照射施設の研究分野別の照射利用割合をFig.１に示す。利用形態別の照射利用割合をFig.２に示す。

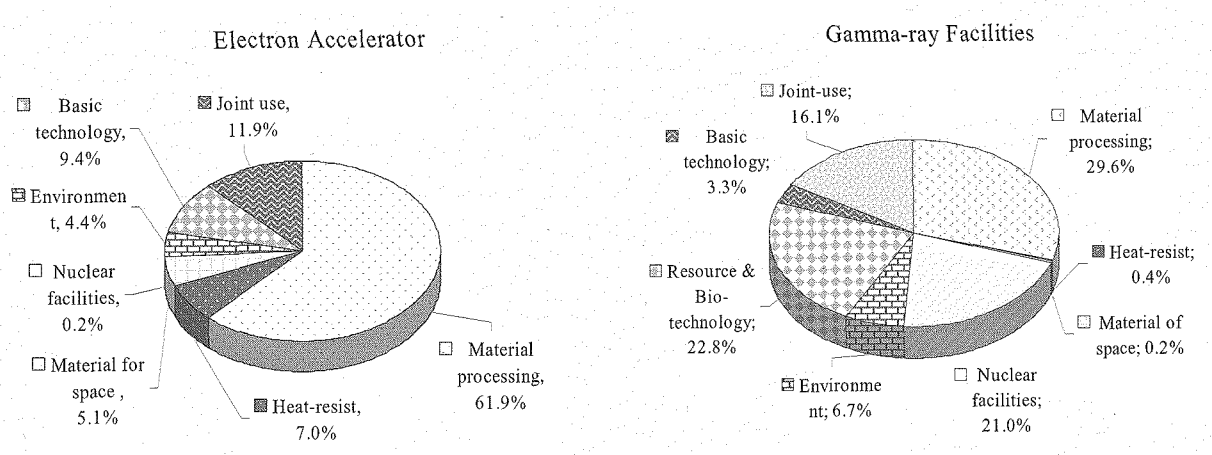


Fig.1 Distribution of research fields (FY 2005).

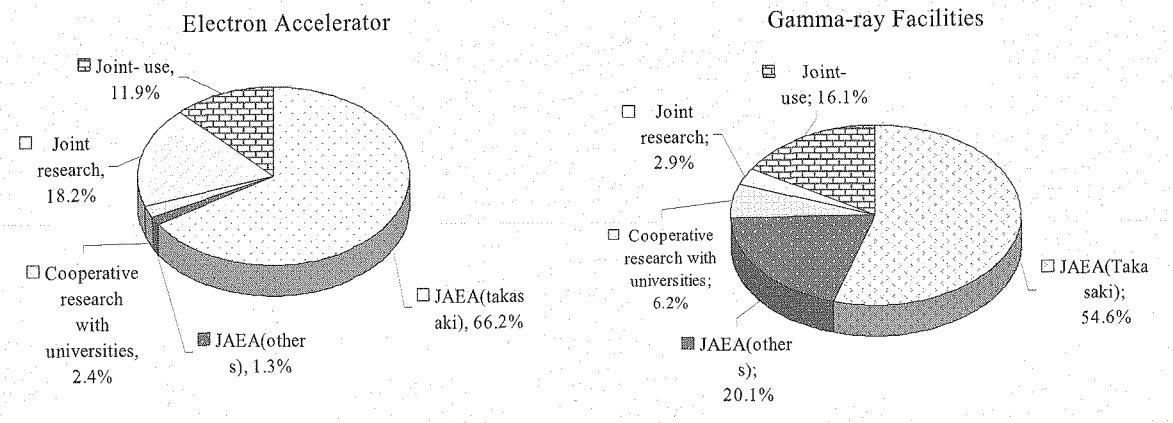


Fig.2 Distribution of cooperation type (FY 2005).

5-07 Operation of the Electron Accelerators

H. Kaneko [a)], H. Hanaya [a)], N. Haneda [a)], R. Yamagata [a)], H. Seito [a)], T. Kanazawa [a)],
T. Yamaguchi [b)], I. Kawashima [b)] and N. Yagi [b)]

Department of Advanced Radiation Technology, TARRI, JAEA [a)],
Radiation Application Development Association , RADA [b)]

Abstract

The No.1 accelerator has been smoothly on service since established in January 1986. The No.1 accelerator renewed both the high frequency inverter power supply in January 2000 and the accelerator control system in June 2001. The No.2 accelerator operation was terminated and the extended operation of the No.1 accelerator was started having one additional consignment operator at April 2005.

1．運転状況

平成 17 年度より、電子線利用を 1 号加速器に集約し、2 号加速器は平成 16 年度末をもって運転を休止した。平成 17 年度からの 1 号加速器集約運転に対応するため、運転委託員を 1 名増やし、運転時間を月・金は 9:00～17:30、火～木は 8:30～23:00 とし、必要運転時間を確保した。

Fig. 1 に平成 17 年度の垂直及び水平照射室の月別運転時間を示す。10 月には加速器の定期整備を行うため、例年この月の運転時間は少なくなっている。その他に受電設備の定期点検に伴う施設停止を 4 月下旬及び 10 月下旬に実施した。平成 17 年度の運転時間は、垂直照射室が 782.4 時間、水平照射室が 124.5 時間であった。

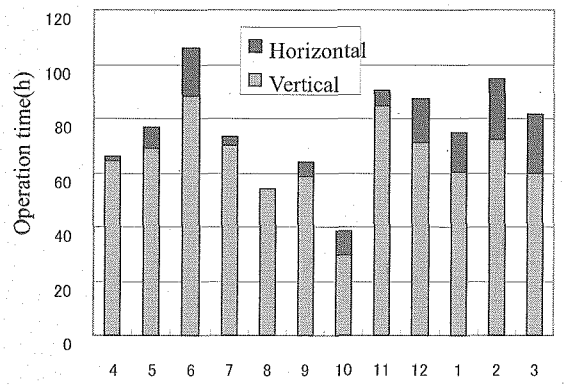
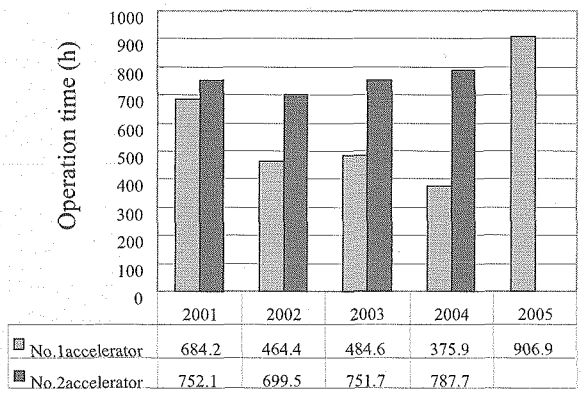


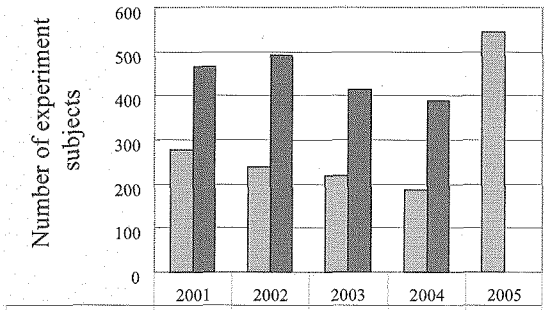
Fig.1 Monthly operation time in FY2005.



	2001	2002	2003	2004	2005
No.1accelerator	684.2	464.4	484.6	375.9	906.9
No.2accelerator	752.1	699.5	751.7	787.7	

Fig.2 Yearly operation time.

Fig. 2 に年度別の運転時間を、Fig. 3 に年度別の利用件数を示す。1 号加速器集約運転後の運転時間は 906.9 時間、利用件数は 544 件であった。



	2001	2002	2003	2004	2005
No.1accelerator	278	237	218	185	544
No.2accelerator	466	493	414	388	

Fig. 3. Yearly number of experiment subjects.

2．整備状況

1 号加速器は、昭和 56 年 1 月に設置されて以来 25 年が経過しているが、平成 12 年 1 月に高周波インバータ電源の更新、平成 13 年 6 月に制御系更新等の整備を実施して順調に稼働した。

平成 17 年度からの 1 号加速器集約運転に対応するため、新コンベアを設置して使用を開始した。新コンベアは 1 号加速器のビーム走査幅である 120cm 幅の試料台とし照射可能試料数の増大が行えるものである。

平成 17 年 10 月に 1 号加速器本体及びコンベア・照射室扉等付帯設備の定期点検を実施した。加速器本体の定期整備として、1 号加速器集約運転に対応するため、主に垂直側の窓箔、フィラメント、イオンポンプ等の交換を実施した。さらに、電子源 M-G モーターのオーバーホール及び M-G 起動方式を従来の瞬時起動よりインバータを組み込んでの徐起動方式に変更した。

平成 17 年 12 月に垂直照射室内 ITV カメラの交換、平成 18 年 2 月に垂直側ビームシャッター駆動用エアシリンダー及び近接スイッチの交換を実施した。

5-08 Operation of the Co-60 Gamma-Ray Irradiation Facilities

N. Haneda [a)], R. Yamagata [a)], H. Kaneko [a)], H. Hanaya [a)], H. Seito [a)], T. Kanazawa [a)], S.Koyama [b)], I. Kawashima [b)], N. Yagi [b)], M. Takagi [b)] and T. Yamaguchi [b)]

Department of Advanced Radiation Technology, TARRI, JAEA [a)],
Radiation Application Development Association , RADA [b)]

Abstract

The Co-60 gamma-ray irradiation facilities consist of three buildings and cover a wide dose-rate range from 0.04Gy/h to 20kGy/h with eight irradiation cells. All the facilities have been operated without serious trouble and served for the following various R&Ds of JAEA and outside users such as development of new materials, radiation resistance test, and radiation biotechnology.

1．運転状況

現在、高崎量子応用研究所には、コバルト第１照射棟（３照射室）、コバルト第２照射棟（３照射室）、食品照射棟（２照射室）の合計３棟のガンマ線照射施設がある。

17 年度の年間運転時間はコバルト第１照射棟が 23786 時間、コバルト第２照射棟が 6120 時間、食品照射棟が 7244 時間であった。Fig.1 に各コバルト照射施設の月別の運転時間を示す。

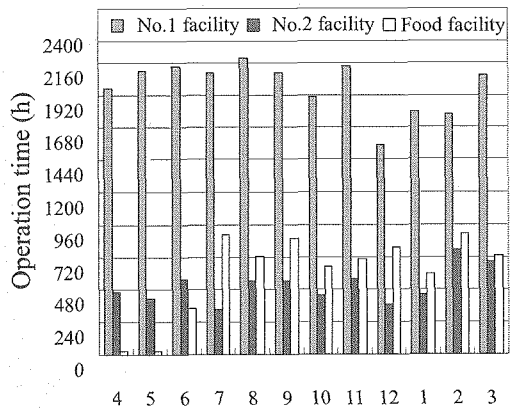


Fig.1 Monthly operation time in FY 2005.

Fig.2 に各ガンマ線照射施設の最近５年間の運転実績時間の推移を示す。

コバルト第１照射棟の運転時間は、19000～23700 時間であるが、これは平成 13 年度以降、原子力プラントの電線ケーブル類経年変化試験や大強度陽子加速器用材料の耐放射線性試験等の照射が開始され、３照射室とも長時間連続運転したためである。

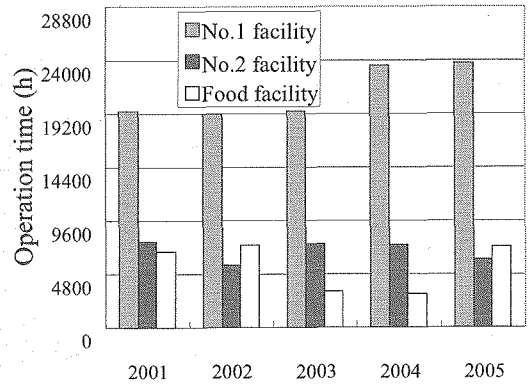


Fig.2 Annual operation time.

コバルト第２照射棟の場合は、第６照射室をスケジュール運用（一定時刻に線源を昇降）したために運転時間は 5000～7000 時間で推移しており、主に新機能性材料の開発試験や外部共同利用などの照射に利用された。

食品照射棟の運転時間は 3000～7000 時間であり、照射食品の検知技術法の開発や植物・バイオ研究関係の照射に利用されている。

照射利用件数は３照射施設合計で 1100～1300 件である。年度別の照射件数を Fig.3 に示す。

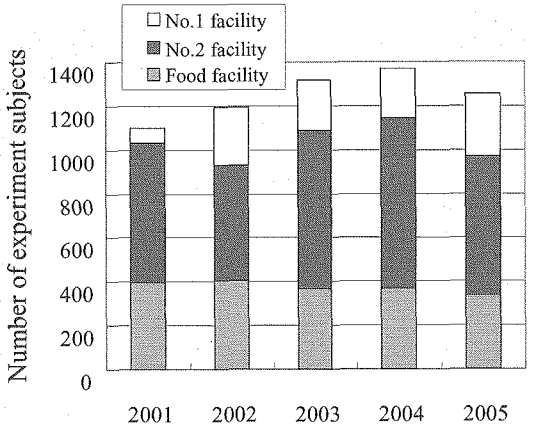


Fig.3 Yearly number of experiment subjects.

2．整備状況

照射施設の水抜き点検は、各照射施設を３年に１回の割合で実施し、その際に線源昇降・移動系を中心に点検した。また、各照射施設とも、主にインターロック関係の定期自主点検を年２回行った。

17 年度の稼働状況については、コバルト第１照射棟は全般に順調であったが、第３照射室線源昇降系のインバータ故障が１件発生した。

コバルト第２照射棟は、８月に水抜き点検を実施した後、特に異常も無く稼働していたが、10 月の計画停電後に第５，６照射室の昇降機構にトラブルが発生した。原因は、シーケンサに入出力信号を与える入出力信号カードの誤動作であることが解った。修理期間中のスケジュール照射は代替施設で行った。コバルト第２照射棟制御系は、昭和 63 年の更新以来 18 年間経過しており、シーケンサ更新などの老朽化対策が必要な段階である。

食品照射棟については、制御系の更新を 11 年度に行い、16 年度に水抜き定期点検を実施した。17 年度は順調な稼働状況であった。

Appendix

Appendix 1 List of Publication 205
A1- 1 Publications in Journal 205
A1- 2 Publications in Proceeding 221
Appendix 2 List of Related Patents 234
Appendix 3 List of Related Press-Release and TV Programs 237
Appendix 4 Type of Research Collaboration 238
Symbol used in the Appendix 240

This is a blank page.

Appendix 1. List of Publication

A1. 1 Publications in Journal

05J001 1-03 E SCS
N.J. Ekins-Daukes, H.S. Lee, T. Sasaki,
M. Yamaguchi, A. Khan, T. Takamoto, T. Agui,
K. Kamimura, M. Kaneiwa, M. Imaizumi,
T. Ohshima, T. Kamiya,
Carrier Removal in Lattice-Mismatched InGaP Solar Cells under 1-MeV Electron Irradiation,
Appl. Phys. Lett., Vol.85, No.13, (2004)2511-2513.

05J002 1-07 C T SCS 51004, 52002
高橋芳浩，芝田利彦，大西一功，平尾敏雄，
小野田忍，神谷富裕、
MOS 構造における重イオン照射誘起電流
電子情報通信学会論文誌, Vol. J89-C, No. 3,
(2006)104-112.

05J003 1-09 T I SCS 52004, 52041
T. Ohshima, T. Satoh, M. Oikawa, S. Onoda,
T. Hirao, and H. Itoh,
Charge Induced in 6H-SiC PN Diodes by Irradiation of Oxygen Ion Microbeams,
Mater. Sci. Forum in press.

05J004 1-09 I SCS 52004, 52041
A. Kinoshita, M. Iwami, K. Kobayashi, I. Nakano,
R. Tanaka, T. Kamiya, A. Ohi, T. Ohshima,
Y. Fukushima,
Radiation effect on pn-SiC diode as a detector,
Nucl. Instrum. Methods A 541 (2005) 213.

05J005 1-09 T I G SCS 52004, 52041
T. Ohshima, T. Satoh, M.Oikawa,T.Yamakawa,
S. Onoda, T. Wakasa, J. S. Laird, T. Hirao, T. Kamiya,
H. Itoh, A. Kinoshita, R. Tanaka, I. Nakano,
M. Iwami, Y. Fukushima,
Characterization of charge generated in silicon carbide n+p diodes using transient ion beam-induced current,
Nucl. Instrum. Methods A 541 (2005) 236.

05J006 1-09 E SCS 52004, 52041
G. Pensl, F. Ciobanu, T. Frank, D. Kirmse,
M. Krieger, S. Reshanov, F. Schmid, M. Weidner,
T. Ohshima, H. Itoh and W.J. Choyke,
Defect-engineering in SiC by ion implantation and electron irradiation,
Microelectron. Eng. 83 (2006) pp.146-149.

05J007 1-10 E SCS
H. Matsuura, S. Kagamihara, Y. Itoh, T. Ohshima,
H. Itoh,
Mechanisms of reduction in hole concentration in Al-doped 4H-SiC by electron irradiation,
Microelectron. Eng. 83(2006)17-19.

05J008 1-10 E SCS
H. Matsuura, S. Kagamihara, Y. Itoh, T. Ohshima,
H. Itoh,
Relationship between defects induced by irradiation and reduction of hole concentration in Al-doped 4H-SiC,
Physica B 376-377(2006)342-345.

05J009 1-10 E SCS
H. Matsuura, H. Iwata, S. Kagamihara, R. Ishihara,
M. Komeda, H. Imai, M. Kikuta, Y. Inoue,
T. Hisamatsu, S. Kawakita, T. Ohshima, H. Itoh,
Si substrate suitable for radiation-resistant space solar cells,
Jpn. J. Appl. Phys., 45(2006)2648-2655.

05J010 1-11 E SCS
T. Umeda, N. T. Son, J. Isoya, E. Janzen, T. Ohshima,
N. Morishita, H. Itoh, A. Gali, M. Bockstdete,

Identification of the carbon antisite-vacancy pair in *4H*-SiC,
Phys. Rev. Lett. 96, (2006)145501.

05J011 1-11 E SCS
N. T. Son, P. Carlsson, J. ul Hassan, E. Janzen,
T. Umeda, J. Isoya, A. Gali, M. Bockstedte,
N. Morishita, T. Ohshima, H. Itoh,
Divacancy in *4H*-SiC,
Phys. Rev. Lett. 96, (2006)055501.

05J012 1-11 E SCS
N. Mizuochi, S. Yamasaki, H. Takizawa,
N. Morishita, T. Ohshima, H. Itoh, T. Umeda,
J. Isoya,
Spin multiplicity and charge state of a silicon vacancy (T_{v2a}) in *4H*-SiC determined by pulsed ENDOR,
Phys. Rev., B 72, (2005) 235208.

05J013 1-11 E SCS
T. Umeda, Y. Ishitsuka, J. Isoya, N. T. Son, E. Janzen,
N. Morishita, T. Ohshima, H. Itoh, A. Gali,
EPR and theoretical studies of negatively charged carbon vacancy in *4H*-SiC,
Phys. Rev., B 71, (2005) 193202.

05J014 1-11 E SCS
T. Umeda, J. Isoya, N. Morishita, T. Ohshima,
T. Kamiya, A. Gali, P. Deak, N. T. Son, E. Janzen,
EPR and theoretical studies of positively-charged carbon vacancy in 4*H*-SiC,
Phys. Rev.,B 70, (2004)235212.

05J015 1-11 E SCS
T. Umeda, J. Isoya, N. Morishita, T. Ohshima,
T. Kamiya,
EPR identification of two types of carbon vacancy in *4H*-SiC,
Phys. Rev., B 69, (2004)121201(R).

05J016 1-11 E SCS
N. Mizuochi, S. Yamasaki, H. Takizawa,
N. Morishita, T. Ohshima, H. Itoh, J. Isoya,
EPR studies of the isolated negatively charged silicon vacancies in n-type *4H*- and 6H-SiC: Identification of C_{3v} symmetry and silicon sites,
Phys. Rev.,B 68, (2003)165206.

05J017 1-11 E SCS
N. Mizuochi, S. Yamasaki, H. Takizawa,
N. Morishita, T. Ohsima, H. Itoh, J. Isoya,
Continuous-wave and pulsed EPR study of negatively charged silicon vacancy with S = 3/2 and C_{3v} symmetry in *n*-type 4H-SiC,
Phys. Rev., B 66, (2002)235202.

05J018 1-13 I SCS 52007
H. Ofuchi, T. Nishiwaki, K. Takaba, K. Ogawa,
M. Tabuchi, Y. Takeda, A. Wakahara, A. Yoshida,
T. Ohshima and H. Itoh,
Fluorescence EXAFS study on local structures around Eu atoms implanted in $Al_xGa_{1-x}N$,
Physica B, Vol.376-377 (2006) 496-498.

05J019 1-13 I SCS 52007
A. Wakahara,
Impact of AlGaN on Luminescence Capability of Rare–Earth Ions in AlGaN,
Opt. Mater., Vol.28, Issues 6-7 (2006) 731-737.

05J020 1-13 I SCS 52007
V. Katchkanov, K. P. O'Donnell, S. Dalmasso,
R. W. Martin, A. Braud, Y. Nakanishi, A. Wakahara,
and A. Yoshida,
Photoluminescence Studies of Eu-implanted GaN Epilayers,
Phys. status solidi (b), Vol. 242, No.7 (2005) 1491-1496.

05J021 1-13 I SCS 52007
A.Wakahara, T.Fujiwara, H.Okada, A.Yoshida,

T.Ohshima, and H.Ithoh,
Energy-back-transfer process in rare-earth doped AlGaN,
Mater. Res. Soc. Symp. Proc., Vol. 866 (2005) V3.9.

05J022 1-14 TIS MAN 52011
I.Ioka, M.Futakawa, A.Naito, Y.Nanjyo, K.Kiuchi and T.Naoe,
Mechanical Characterization of Austenitic Stainless Steel Ion-irradiated under External Stress,
J. Nucl. Mater. 329-333(2004)1142-1146.

05J023 1-15 T IMO 52009
N. Okubo, E. Wakai, S. Matsukawa, K. Furuya, H. Tanigawa, T. Sawai, S. Jitsukawa, S. Ohnuki,
Tempering Treatment Effect on Mechanical Properties of F82H Steel Doped with Boron and Nitrogen,
Mater. Trans., 46, 8, (2005)193-195.

05J024 1-18 TIS IOM 52008
T. Taguchi, N. Igawa, S. Jitsukawa and K. Shimura,
Effect of He ions implantation on thermal diffusivities of SiC and SiC/SiC compoistes,
Nucl. Instum. Phys. Res., Sect. B, 242[1-2] (2006) 469-472.

05J025 1-20 TIS MAN 52012
木内清、井岡郁夫、田邊誠、南条吉保、小河浩晃、石島暖大、塚谷一郎、落合孝正、木﨑実、加藤佳明、小幡宏幸、藤村研、
高性能燃料被覆管材質の研究−平成 13ー17 年度（フェーズ 2）報告書−（共同研究）、
JAEA-Research 2006-023(2006).

05J026 1-24 S IOM 52034
M. Fukuzumi, Y. Chimi, N. Ishikawa, F. Ono, S. Kimatsu, A. Iwase,
Heavy ion induced magnetic phase transition of FeRh alloy,
Nucl. Instrum. Methods. B(2005) 269-273.

05J027 1-31 C RCO 51068
A. Hiroki, M. Asano, T. Yamaki, M. Yoshida,
Effect of γ -irradiation on latent tracks of polyethylene terephthalate(PET) film,
Chem. Phys. Lett., 406 (2005) 188-191.

05J028 2-05 E ECT
A. Jyo, J. Kugara, H. Trobradovic, and K. Yamabe, T. Sugo, M. Tamada, and T. Kume,
Fibrous Iminodiacetic Acid Chelating Cation Exchangers with a Rapid Adsorption Rate,
Ind. Eng. Chem. Res., Vol. 43, (2004)1599-1607.

05J029 2-07 E G RCO
N.Seko, A. Katakai, S. Hasegawa, M. Tamada, N. Kasai, H. Takeda, T. Sugo, K. Saito,
Aquaculture of uranium in seawater by fabric-adsorbent submerged system,
Nucl. Technol., 144 (2003) 274.

05J030 2-11 E ECT
A. Katakai, M. Tamada, H. Nagamoto, H. Miyagawa,
Preparation of Chelating Fiber by Repeated Use of Monomer Solution in Radiation-Induced Graft Polymerization,
J. Ion Exch, Vol.16 No.2 (2005)122-126.

05J031 2-12 E RCO
M. Takahashi,K. Tanaka, M. Tamada, T. Aoi,
Development of removal method for ferric and manganese ions with fibrous graft-absorbent,
Environ. Eng. Res., 41 (2004) 229.

05J032 2-13 E RCO
Y. Wada, H. Mitomo, K. Kasuya, N. Nagasawa, N. Seko, A. Katakai, M. Tamada,
Control of biodegradability of poly(3-hydroxybutyric acid) film with grafting acrylic acid and thermal remolding,
J Appl. Polym. Sci., 101, (2006) 3856.

05J033 **2-14** G E RCO
2-18 E RCO
L. Zhao, H. Mitomo, N. Nagasawa, F. Yoshii and T. Kume,
Radiation synthesis and characteristic of the hydrogels based on carboxymethylated chitin derivatives,
Carbohydr. Polym., 51(2003) 169-175.

05J034 **2-14** G E RCO
2-18 E RCO
L. Zhao, H. Mitomo, M. Zhai, F. Yoshii,
N. Nagasawa and T. Kume,
Synthesis of antibacterial PVA/CM-chitosan blend hydrogels with electron beam irradiation,
Carbohydr. Polym., 53(2003) 439-446.

05J035 **2-14** G E RCO
F. Yoshii, L. Zhao, R. A. Wach, N. Nagasawa,
H. Mitomo and T. Kume,
Hydrogels of polysaccharide derivatives crosslinked with irradiation at paste-like condition,
Nucl. Instum. Phys. Res., Sect. B, 208, (2003) 320-324.

05J036 **2-14** G E RCO
J. M. Wasikiewicz, N. Nagasawa, M. Tamada,
H. Mitomo and F. Yoshii,
Adsorption of metal ions by carboxymethylchitin and carboxymethylchitosan hydrogels,
Nucl. Instum. Phys. Res., Sect. B, 236(1-4), (2005) 617-623.

05J037 **2-15** G E RCO
H. Mitomo, A. Kaneda, T. M. Quynh, N. Nagasawa and F. Yoshii,
Improvement of heat stability of poly(L-lactic acid) by radiation-induced crosslinking,
Polymer, 46(3), (2005)4695-4703.

05J038 **2-15** G E RCO
N. Nagasawa, A. Kaneda, S. Kanazawa, T. Yagi, H. Mitomo, F. Yoshii and M. Tamada,
Application of poly(lactic acid) modified by radiation crosslinking,
Nucl. Instum. Phys. Res., Sect. B, 236(1-4), (2005) 611-616.

05J039 **2-16** G E RCO
K. Terao, N. Nagasawa, H. Nishida, K. Furusawa,
Y. Mori, T. Dobashi and F. Yoshii,
Regent-free crosslinking of aqueous gelatin: manufacture and characteristics of gelatin gels irradiated with gamma-ray and electron beam,
J. Biomater. Sci. Polym. Ed., 14, (2003)1197-1208.

05J040 **2-16** G E RCO
K. Terao, T. Karino, N. Nagasawa, F. Yoshii,
M. Kubo and T. Dobashi,
Gelatin microspheres crosslinked with gamma ray: preparation, sorption of proteins, and biodegradability,
J. Appl. Polym. Sci., 91, (2004)3083-3087.

05J041 **2-16** G RCO
K. Furusawa, K. Terao, N. Nagasawa, F. Yoshii,
K. Kubota and T. Dobashi,
Nanometer-sized gelatin particles prepared by means of gamma-ray irradiation,
Colloid Polym. Sci., 283(2), (2004)229-233.

05J042 **2-17** G RCO
2-18 G RCO
L. Q. Luan, N. Q. Hien, N. Nagasawa, T. Kume,
F. Yoshii and T. M. Nakanishi,
Study on the biological effect of radiation-degraded alginate on flower plants in tissue culture,
Biotech. Appl. Biochem., 38(2003) 283-288.

05J043 **2-17** G RCO
2-18 G RCO
L. Q. Luan, Vo. T. T. Ha, N. Nagasawa, T. Kume,
F. Yoshii and T. M. Nakanishi,

Biological effect of irradiated chitosan on plants *in vitro*,
Biotech. Appl. Biochem., 41(2005) 49-57.

05J044 2-17 G RCO
2-18 G RCO
L. Q. Luan, N. Nagasawa, M. Tamada and T. M. Nakanishi,
Enhancement of plant growth activity of irradiated chitosan by molecular weight fractionation,
Radioisotopes, 55(2006) 21-27.

05J045 2-18 G RCO
N. Q. Hien, N. Nagasawa, L. X. Tham, F. Yoshii, V. H. Dang, H. Mitomo, K. Makuuchi, T. Kume,
Growth-promotion of plants with depolymerized alginates by irradiation,
Radiat. Phys. Chem., 59 (2000) 97-101.

05J046 2-18 G RCO
N. Nagasawa, H. Mitomo, F. Yoshii and T. Kume,
Radiation-induced degradation of sodium alginate,
Polym. Degrad. Stab., 69 (2000) 279-285.

05J047 2-18 G RCO
L. X. Tham, N. Nagasawa, S. Matsuhashi, N. S. Ishioka, T. Ito and T. Kume,
Effect of radiation-degraded chitosan on plants stressed with vanadium,
Radiat. Phys.Chem., 61 (2001) 171-175.

05J048 2-18 G E RCO
T. Kume, N. Nagasawa, F. Yoshii,
Utilization of carbohydrates by radiation processing,
Radiat. Phys. Chem., 63 (2002) 625-627.

05J049 2-18 G E RCO
F. Yoshii, L. Zhao, R. A. Wach, N. Nagasawa, H. Mitomo and T. Kume,
Hydrogels of polysaccharide derivatives crosslinked with irradiation at paste-like condition,
Nucl. Instrum. Methods B, 208 (2003) 320-324.

05J050 2-21 E ECT
K. Hirota and T. Kojima
Decomposition behavior of PCDD/F isomers in incinerator gases under electron-beam irradiation
Bull. Chem. Soc. Jpn., 78, (2005)1685-1690.

05J051 2-21 E ECT
瀧上眞知子、新井英彦、広田耕一、田口光正、箱田照幸、小嶋拓治、
都市ごみ燃焼排煙に含まれるダイオキシン類分析のための迅速試料調製法、
環境化学, 14, (2004)13-23.

05J052 2-21 E ECT
箱田照幸、須永博美、瀧澤春喜、広田耕一、小嶋拓治,
ガス処理用 300 keV 電子ビーム照射場における吸収線量率分布、
Radioisotope, 53, (2004)59-69.

05J053 2-21 E ECT
K. Hirota, T. Hakoda, M. Taguchi, M. Takigami, H. Kim, and T. Kojima,
Application of electron beam for the reduction of PCDD/F emission from municipal solid waste incinerators,
Environ. Sci. Technol., 37, (2003)3164-3170.

05J054 2-22 E ECT
A.Shimada, T.Hakoda, T.Kojima,
Electron Beam Processing for Decomposition Treatment of Gaseous Formaldehyde after Sterilization,
J. Chem. Eng. Jpn., Vol.39, No.9,(2006) (in press).

05J055 2-23 G RCO
2-24 C RCO 51070
A.Kimura, M.Taguchi, T.Kojima, H.Hiratsuka and H.Namba

Decomposition of *p*-nonylphenols in water and elimination of their estrogen activities by ^{60}Co γ -ray irradiation,
Radiat. Phys. Chem., 75, (2006)61-69.

05J056 2-23 E RCO
2-24 C RCO 51070
M.Taguchi, Y.Zennyoji, M.Takigami, G.Baldacchino, A.Kimura, H.Hiratsuka, H.Namba, and T.Kojima,
Characteristics study on suspended fine particles in aqueous phenol solution formed by electron beam irradiations,
Radiat. Phys. Chem., 75, (2006)564-571.

05J057 2-23 G R RCO
A.Kimura, M.Taguchi, Y.Ohtani, Y. Shimada, H.Hiratsuka and T. Kojima,
Treatment of wastewater having estrogen activity by ionizing radiation,
Radiat. Phys. Chem., in press.

05J058 2-24 C RCO 51070
T.Miyazaki, Y.Katsumura, M.Lin, Y.Muroya, H.Kudo, M.Taguchi, M.Asano, M.Yoshida
Radiolysis of phenol in aqueous solution at elevated temperatures,
Radiat. Phys. Chem., 75, (2006)408-415.

05J059 3-01 G BMT
I. Narumi,
Unlocking radiation resistance mechanisms: still a long way to go,
Trends Microbiol. 11 (2003) 422.

05J060 3-01 G BMT
I. Narumi, K. Satoh, S. Cui, T. Funayama, S. Kitayama, H. Watanabe,
PprA: a novel protein from Deinococcus radiodurans that stimulates DNA ligation,
Mol. Microbiol. 54 (2004) 278.

05J061 3-01 G BMT
H. Sghaier, H. Mitomo, I. Narumi,
Genomic confession of Deinococcus radiodurans: it started out as a radiation resistant organism,
Viva Origino 33(2005) 243.

05J062 3-01 G BMT
E. Jolivet, F. Lecointe, G. Coste, K. Satoh, I. Narumi, A. Bailone, S. Sommer,
Limited concentration of RecA delays DNA double strand break repair in *Deinococcus radiodurans* R1,
Mol. Microbiol. 59 (2006) 338.

05J063 3-02 G BMT
H. Ohba, K. Satoh, T. Yanagisawa, I. Narumi,
The radiation responsive promoter of the *Deinococcus radiodurans pprA* gene,
Gene, 363, (2005) 133-141.

05J064 3-03 G BMT
M. Ukai, H. Nakamura, Y. Shimoyama,
An ESR Protocol based on relaxation phenomena in irradiated foods,
Spectrochim. Acta 63(4), (2006)879-882.

05J065 3-06 C BMT 51007
Y. Hase, K. H. Trung, T. Matsunaga and A. Tanaka,
A mutation in the uvi4 gene promotes progression of endo-reduplication and confers increased tolerance toward ultraviolet-B light,
Plant J. 46, (2006)317-326.

05J066 3-06 C BMT 51007
Y. Hase, S. Fujioka, S. Yoshida, G. Sun, M. Umeda and A. Tanaka,
Ectopic endoreduplication caused by sterol alteration results in serrated petals in Arabidopsis,
J. Exp. Bot., 56, (2005)1263-1268.

05J067 3-07 C BMT 51009
A. Urushibara, N. Shikazono, R. Watanabe, K. Fujii,

P. O'Neill, A. Yokoya,
DNA Damage Induced by the Direct Effect of He Ion Particles,
Radiat. Prot. Dosim. in press.

05J068 3-08 C BMT 51022
Y. Matuo, S. Nishijima, Y. Hase, A. Sakamoto,
A. Tanaka, K. Shimizu,
Specificity of mutations induced by carbon ions in budding yeast *Saccharomyces cerevisiae,*
Mutat.Res. in press.

05J069 3-09 C BMT 51010
Y. Yokota, N. Shikazono, A. Tanaka, Y. Hase,
T. Funayama, S. Wada, M. Inoue,
Comparative radiation tolerance based on the induction of DNA double-strand breaks in tobacco BY-2 cells and CHO-K1 cells irradiated with gamma rays,
Radiat. Res., 163. (2005)520-525.

05J070 3-12 C BMT 61009
K. Takata, Y. Saiki, K. Hirashima, T. Nakahara,
Plant regeneration in *Solanum integrifolium* microspores culture,
Bull. Fukuoka Agri. Res. Cent 25: (2006) 23-28.

05J071 3-18 C BMT 51018
N. Hata , K. Murakami, Y. Yoshida, M. Masuda,
A. Tanaka, N. Shikazono Y. Hase,
Mutagenesis in gynomonoecious spinach (*Spinacia oleracea* L.) plants and selection of low oxalate variants,
Sci. Rep. Fac. Agr. Okayama Univ. 95,(2006) 21-28.

05J072 3-18 C BMT 51018
N. Hata, K. Murakami, Y. Yoshida, M. Masuda,
Effect of photoperiod after bolting on the expression of gynomonoecy in *Spinacia oleracea* L.,
J. Japan. Hort. Sci. 75(1), (2006)141-147.

05J073 3-33 C BMT 51033
N. Hamada, T. Funayama, S. Wada, T. Sakashita,
T. Kakizaki, M. Ni, Y. Kobayashi,
LET-Dependent Survival of Irradiated Normal Human Fibroblasts and Their Descendents,
Radiat. Res. 166 (2006)24-30.

05J074 3-37 C BMT 51037
BB. Roy, A. Jinno-Oue, M. Shinagawa, A. Shimizu,
K. Tamura, N. Shimizu, A. Tanaka, and H. Hoshino,
Isolation of the feline alpha1,3-galactosyltransferase gene, expression in transfected human cells and its phylogenetic analysis,
J. Exp. Zool. B Mol. Dev. Evol. 306B, (2006) 59-69.

05J075 3-37 C BMT 51037
Y.Shimizu, M.Okoba, N.Yamazaki, Y.Goto, T.Miura,
M.Hayami, H.Hoshino and T.Haga,
Construction and in vitro characterization of a chimeric simian and human immunodeficiency virus with the RANTES gene,
Microbes Infect. 8, (2006)105-113.

05J076 3-37 C BMT 51037
M. N.Saha, A.Tanaka, A.Jinno-Oue, N.Shimizu,
K.Tamura, M.Shinagawa, J.Chiba and H. Hoshino,
Formation of vesicular stomatitis virus pseudotypes bearing surface proteins of hepatitis B virus,
J. Virol. 79, (2005) 12566-12574.

05J077 3-37 C BMT 51037
A. Jinno-Oue, N. Shimizu, Y. Soda, A. Tanaka,
T. Ohtsuki, D. Kurosaki, Y. Suzuki, and H. Hoshino,
The synthetic peptide derived from the NH2-terminal extracellular region of an orphan G protein-coupled receptor, GPR1, preferentially inhibits infection of X4 human immunodeficiency virus type 1,
J. Biol. Chem., 280, (2005)30924-30934.

05J078 3-37 C BMT 51037
K. Tamura, A. Oue, A. Tanaka, N. Shimizu,

H. Takagi, N. Kato, A. Morikawa and H.Hoshino,
Efficient formation of vesicular stomatitis virus pseudotypes bearing the native forms of hepatitis C virus envelope proteins detected after sonication,
Microbes Infect. 7,(2005) 29-40.

05J079 3-39 C RCO 61037
K. Shirai, T. Mizui, Y. Suzuki, Y. Kobayashi,
T. Nakano, T. Shirao,
Differential effects of x-irradiation on immature and mature hippocampal neurons in vitro,
Neurosci Lett. 399, (2006)57-60.

05J080 3-43 C BMT 51042
A. Takahashi, H. Matsumoto, Y. Furusawa,
K. Ohnishi, N. Ishioka, T. Ohnishi,
Apoptosis induced by high-LET radiations is not affected by cellular p53 gene status,
Int. J. Radiat. Biol., 81: (2005)581-586.

05J081 3-45 C BMT 51044
S. Sugimoto, K. Dazai, T. Sakashita, T. Funayama,
S. Wada, N. Hamada, T. Kakizakim Y. Kobayashi,
A. Higashitani,
Cell Cycle Arrest ad Apoptosis in *Caenorhabditis elegans* Germline Cells following Heavy-ion Microbeam Irradiation,
Int. J. Radiat. Biol. 82 (2006) 31-38.

05J082 3-49 C BMT 51048
E. Ling, K. Shirai, R. Kanekatsu, K. Kiguchi,
Y. Kobayashi, T. Funayama and H. Watanabe,
Contribution of circulating hemocytes to the regeneration of heavy ion beams ($^{12}C^{5+}$) irradiated hematopoietic organs in the silkworm, *Bombyx mori*, through the way of phagocytosis of injured cells after invation,
Dev. Comp. Immunol., 30, (2006)531-543.

05J083 3-49 C BMT 51048
K. Fukamoto, S. Shimura, K. Shirai, R. Kanekatsu,
K. Kiguchi, T. Sakashita, T. Funayama and Y. Kobayashi,
Effects of heavy-ion irradiation on the differentiation of epidermal cells in the silkworm, *Bombyx mori*,
J.Insect Biotechnol. Sericol.,in press

05J084 3-49 C BMT 51048
K. Fukamoto, K. Shirai, S. Sato, R. kanekatsu,
K. Kiguchi and Y. Kobayashi,
Process of in vitro cyst formation from the implanted larval integument in the sweet potato hornworm, Agrius convolvuli: A simple method for studing wound healing,
J.Insect Biotechnol. Sericol., in press.

05J085 3-50 C BMT 51049
J. Huang, Y. Arimatsu, K. Sadakane, Y. Endo and T. Furusawa,
Gene Expression and Localization of Trehalase during Embryonic Development of the Silkworm, *Bombyx mori*,
Inernational Journal of Wild Silkmoth & Silk 10, (2005)17-26

05J086 3-50 C BMT 51049
E. Kotani, Y. Hayashi, Y. Sugimura and T. Furusawa,
Identification of Novel Double-stranded RNA Produced in Midgut Epithelial Tissue of the Silkworm, *Bombyx mori*, during infection by a Cypovirus 1,
J.Insect Biotechnol. Sericol.,74, (2005)29-34

05J087 3-50 C BMT 51049
J. Huang, T. Furusawa, K. Sadakane, and
Y. Sugimura,
Purification and Properties of Two Types of Soluble Trehalases from Embryonic Larvae of the Silkworm, *Bombyx mori*,
J.Insect Biotechnol. Sericol.,75, (2006)1-8

05J088 3-50 C BMT 51049
Y. Arimatsu, T. Furuno, Y. Sugimura, M. Togoh, R. Ishihara, M. Tokizane, E. Kotani, Y. Hayashi, and T. Furusawa,
Purification and Properties of Double-stranded RNA-degrading Nuclease, dsRNase, from the Digestive Juice of the Silkworm, Bombyx mori,
J.Insect Biotechnol. Sericol., in press

05J089 3-55 C MT 51056
R. Suwa, N. T. Nguyen, H. Saneoka, R. Moghaieb, K. Fujita,
Effect of salinity stress on photosynthesis and vegetative sink in tobacco plants,
Soil. Sci. Plant nutr. 52(2), (2006) 243-250

05J090 3-56 C BMT 51057
Y. Ishimaru, M. Suzuki, T. Tsukamoto, K. Suzuki, M. Nakazono, T. Kobayashi,Y. Wada, S. Watanabe, S. Matsuhashi, M. Takahashi, H. Nakanishi, S. Mori. N. K. Nishizawa,
Rice plants take up iron as an Fe^{3+}-phytosiderophore and as Fe^{2+}.
Plant J. 45, (2006)335-346.

05J091 3-63 C BMT 51065
N. Kawachi, K. Sakamoto, S. Ishii, S. Fujimaki, N. Suzui, N. S. Ishioka, S. Matsuhashi,
Kinetic Analysis of Carbon-11-labeled Carbon Dioxide for Studying Photosynthesis in a Leaf Using Positron Emitting Tracer Imaging System,
IEEE Trans. Nucl. Sci., in press.

05J092 3-66 S BIT 52051
S. Harada, K. Ishii, T. Kamiya.
The detection of apoptosis by kinetic of Ca and Fe, using micro PIXE camera,
Radioisotopes, 55 (2006) 419-428.

05J093 3-66 S BIT 52051
S. Harada, K. Ishii, T. Kamiya,
Kinetics of cis-platinum after radiation, and targeting of cis-platinum, directed by radiation,
INNERVISION 21/7(2006) 61.

05J094 3-66 S BIT 52051
S. Harada, K. Ishii, H. Yamazaki, S. Matsuyama, K. Mizuma, K. Hotta, T. Izukawa, S. Anbe, M. Fukuda, T. Kamiya, S. Takuro, T. Satoh, and S. Oikawa,
The Targetchemotherapy directed by the radiation,
Int. J. PIXE 15,3-4(2005) 221-224.

05J095 3-66 S BIT 52051
S. Harada, K. Ishii, A. Tanaka, T. Satoh, S. Matsuyama, H. Yamazaki, T. Kamiya, T. Sakai, K. Arakawa, M. Saitoh, M.Oikawa and K. Sera,
Method for Determing the localization of Trace Elements Observed by the Micro PIXE camera,
Int. J. PIXE ,14 (2004)83-87

05J096 3-66 S BIT 52051
S. Harada, K. Ishii, S. Obara,
Determination of radiation Induced apoptosis by the kinetics of the trace-elements, and predicting the antitumor effect and prognosis of radiation therapy,
INNERVISION 17/7 (2004)27-28

05J097 3-66 S BIT 52051
S. Harada, S. Ehara, K. Ishii, A. Tanaka, T. Satoh, S. Matsuyama, H. Yamazaki, Y. Komori, T. Kamiya, T. Arakawa, M. Saitoh, M. Oikawa, and K. Sera,
The kinetics of Fe and Ca for the development of apoptosis,
Nucl. Instum. Phys. Res., Sect. B 210 (2003) 388 -394

05J098 4-03 C RCO 51005
Y. Maekawa, Y. Suzuki, K. Maeyama, N. Yonezawa, M. Yoshida,
Chemical Modification of the Internal Surfaces of Cylindrical Pores of Sub-micrometer Size in

Poly(ethylene terephthalate),
Langmuir 22 (2006) 2832.

05J099 4-04 E IOM
R. A. Wach, M. Sugimoto, M. Yoshikawa,
Development of Silicone Carbide Coating on Al_2O_3 Ceramics form Precursor Polymers by Radiation Curing,
Key Eng. Mater., 317-318 (2006)573-76.

05J100 4-05 O RCO 51072
A. Acharya, S. Seki, A. Saeki, Y. Koizumi, and S. Tagawa,
Study of Transport Properties in Fullerene-Doped Polysilane Films using Flash Photolysis Time-Resolved Microwave Technique,
Chem. Phys. Lett., 404 (2005) 356-360.

05J101 4-05 O RCO 51072
A. Acharya, Y. Koizumi, S. Seki, A. Saeki,
S. Tagawa, Y. Ie, and Y. Aso,
Effect of Substituents on Charge Carrier Dynamics in Thiophene Oligomers,
J. Photochem. Photobiol. A, 173 (2005) 161-168.

05J102 4-05 O RCO 51072
A. Saeki, S. Seki, Y. Koizumi, T. Sunagawa,
K. Ushida, and S. Tagawa
Increase of Mobility of Photogenerated Positive Charge Carriers in Polythiophene
J. Phys. Chem. B, 109 (2005) 10015-10019.

05J103 4-05 O RCO 51072
S. Seki, S. Kawachi, S. Tagawa, A. Egami,
K. Kurihara, M. Nakamura, and H. Itoh,
Etching Efficiency of Polymethacrylates for Monochromatic Low Energy Ion Beams,
J. Photopolym. Sci. Technol., 18 (2005) 255-256.

05J104 4-05 C RCO 51072
S. Tsukuda, S. Seki, M. Sugimoto, and S. Tagawa,
Formation of Nanowires Based on π -Conjugated Polymers by High-Energy Ion Beam Irradiation,
Jpn. J. Appl. Phys., 44 (2005) 5839-5842.

05J105 4-05 C RCO 51072
S. Seki, S. Tsukuda, S. Tagawa, and M. Sugimoto,
Correlation between Edge Roughness of Nanostructures and Backbone Configuration of Polymer Materials,
J. Photopolym. Sci. Technol., 18 (2005) 449-450.

05J106 4-05 O RCO 51072
S. Okuno, R. Arakawa, K. Okamoto, Y. Matsui,
S. Seki, T. Kozawa, S. Tagawa, and Y. Wada,
Requirements for Laser-Induced Desorption/Ionization on Submicrometer Structures,
Anal. Chem., 77 (2005) 5364-5369.

05J107 4-05 O RCO 51072
Y. Doi, A. Saeki, Y. Koizumi, S. Seki, K. Okamoto,
T. Kozawa, and S. Tagawa,
Nanopatterning of Polyfluorene Derivative Using Electron Beam Lithography,
J. Vac. Sci. Technol. B, 23 (2005) 2051-2055.

05J108 4-05 O RCO 51072
Y. Matsui, S. Seki, and S. Tagawa,
Fluoropolymer Outgassing in Focused Ion Beam Micromachining,
J. Photopolym. Sci. Technol., 18 (2005) 501-502.

05J109 4-05 O RCO 51072
A. Acharya, S. Seki, Y. Koizumi, A. Saeki, and S. Tagawa,
Photogeneration of Charge Carriers and Their Transport Properties in Poly[bis(*p*-*n*-butylphenyl)silane],
J. Phys. Chem. B, 109 (2005) 20174-20179.

05J110 4-05 C RCO 51072
S. Seki, S. Tsukuda, K. Maeda, S. Tagawa,

H. Shibata, M. Sugimoto, K. Jimbo, I. Hashitomi, and A. Koyama,
Effects of Backbone Configuration of Polysilanes on Nanoscale Structures Formed by Single-Particle Nanofabrication Technique,
Macromolecules, 38 (2005) 10164-10170.

05J111 4-05 O RCO 51072
S. Seki, A. Acharya, Y. Koizumi, A. Saeki, S. Tagawa, and K. Mochida,
Mobilities of Charge Carriers in Dendrite and Linear Oligogermanes by Flash Photolysis Time-Resolved Microwave Conductivity Technique,
Chem.Lett., 34 (2005) 1690-1691.

05J112 4-05 C RCO 51072
S. Tsukuda, S. Seki, M. Sugimoto, and S. Tagawa
Nanowires with Controlled Sizes Formed by Single Ion Track Reactions in Polymers,
Appl. Phys. Lett., 87 (2005) 233119.

05J113 4-05 O RCO 51072
A. Saeki, S. Seki, T. Sunagawa, K. Ushida, and S. Tagawa,
Charge Carrier Dynamics in Polythiophene Films Studied by In-Situ Measurement of Flash-Photolysis Time-Resolved Microwave Conductivity (FP-TRMC) and Transient Optical Spectroscopy (TOS),
Philos. Mag., 86 (2006) 1261-1276.

05J114 4-05 O RCO 51072
Y. Yamamoto, T. Fukushima, W. Jin, A. Kosaka, T. Hara, T. Nakamura, A. Saeki, S. Seki, S. Tagawa, and T. Aida,
Spinning of Hexa-peri-hexabenzocoronene Graphitic Nanotubes into a Macroscopic Fiber that Displays an Anisotropic Electrical Conduction,
Adv. Mater., 18 (2006) 1297-1300.

05J115 4-05 O RCO 51072
A. Acharya, S. Seki, A. Saeki, and S. Tagawa,
Photoconductivity in Fullerene Doped Polysilane Thin Films,
Synth. Met., 156 (2006) 293-297.

05J116 4-05 O RCO 51072
R. Yamagami, K. Kobayashi, A. Saeki, S. Seki, and S. Tagawa,
Photogenerated Hole Mobility in DNA Measured by Time-Resolved Microwave Conductivity,
J. Am. Chem. Soc., 128 (2006) 2213-2214.

05J117 4-05 O RCO 51072
S. Fratiloiu, F. C. Grozema, Y. Koizumi, S. Seki, A. Saeki, S. Tagawa, A. P. H. J. Schenning, and L. D. A. Siebbeles,
Electronic Structure and Optical Properties of Charged Oligofluorenes Studied by VIS/NIR Spectroscopy and Time-Dependent Density Functional Theory,
J. Phys. Chem. B, 110 (2006) 5984-5993.

05J118 4-05 O RCO 51072
A. Sharma, M. Katiyar, Deepak, S. Seki, and S. Tagawa,
Room Temperature Ultra Violet Emission at 357 nm from Polysilane based OLEDs,
Appl. Phys. Lett., 88 (2006) 143511.

05J119 4-05 O RCO 51072
M. Abe, M. Hattori, A. Takegami, A. Masuyama, T. Hayashi, S. Seki, and S. Tagawa,
Experimental Probe for Hyperconjugative Resonance Contribution in Stabilizing the Singlet State of 2,2-Dialkoxy-1,3-diyls: Regioselective 1,2-Oxygen Migration,
J. Am. Chem Soc., 128 (2006) 8008-8014

05J120 4-05 O RCO 51072
K. Okamoto, S. Seki, and S. Tagawa,

Formation of Trimer and Dimer Radical Cations of Methyl Substituted Benzenes in γ -irradiated Low Temperature Matrices,
J. Phys. Chem. A, 110 (2006) 8073-8080.

05J121 4-05 O RCO 51072
Y. Koizumi, S. Seki, S. Tsukuda, S. Sakamoto, and S. Tagawa,
Self-Condensed Nanoparticles of Oligofluorenes with Water-soluble Side Chains,
J. Am. Chem Soc., 128 (2006) 9036-9037.

05J122 4-05 O RCO 51072
A. Saeki, S. Seki, and S. Tagawa,
Electrodeless Measurement of Charge Carrier Mobility in Pentacene by Microwave and Optical Spectroscopy Techniques,
J. Appl. Phys., in press

05J123 4-05 O RCO 51072
K. Enomoto, J. A. LaVerne, S. Seki, and S. Tagawa,
Formation and Decay of the Triplet Excited State of Pyridine,
J. Phys. Chem. A, 110 (2006) in press.

05J124 4-05 C RCO 51072
S. Seki, S. Tsukuda, M. Sugimoto, and S. Tagawa,
Cross-Linked Silicon Based Polymer Nanowire Formation by High Energy Charged Particles,
Surf. Coat. Technol., in press

05J125 4-05 C RCO 51072
S. Tsukuda, S. Seki, M. Sugimoto, and S. Tagawa,
Effect of Ion Beam Energy and Polymer Weight on the Thickness of Nanowires Produced by Ion Bombardment of Polystyrene Thin Films,
Surf. Coat. Technol., in press

05J126 4-05 CT RCO 51072
S. Tagawa, S. Tsukuda, S. Seki, M. Sugimoto,
T. Sato, M. Oikawa, and T. Sakai,
Ion Beam Induced Nano-Space Reactions and Nanowire Formation in Polymers by High Energy Sub-μ m Heavy Ion Beams,
Surf. Coat. Technol. in press

05J127 4-06 I IOM 52025
粕壁善隆、王建軍、山村力、藤野豊、山本春也、吉川正人、
イオン注入法によるチタン薄膜の窒化機構、
2006年・まてりあ, 45 (2006) 23-31.

05J128 4-08 I IOM 52026
S. Nagata, S. Yamamoto, K. Tokunaga, B. Tsuchiya, K. Toh, K. Shikama,
Hydrogen up-take in noble gas implanted W,
Nucl. Instum. Phys. Res., Sect. B. 242 (2006) 553—556.

05J129 4-08 I IOM 52026
A. Inouye, K. Takano, S. Yamamoto, M. Yoshikawa, S. Nagata,
Gasochromic Property of Oriented Tungsten Oxide Thin Films,
Trans. Mater. Res. Soc. Jpn., 31(1) (2006)227-230.

05J130 4-09 S MAN 52028
K. Takahiro, A. Terai, K. Kawatsura, H. Naramoto, S. Yamamoto, B. Tsuchiya, S. Nagata, F. Nishiyama,
Rutherford Backscattering Spectrometry of Electrically Charged Targets: Elegant Technique for Measuring Charge-State Distribution of Backscattered Ions,
Jpn. J. Appl. Phys. 45 (2006) 1823-1825.

05J131 4-09 I IOM 52037
Z. Q. Chen, M. Maekawa, A. Kawasuso, S. Sakai and H. Naramoto,
Annealing process of ion-implantation-induced defects in ZnO: Chemical effect of the ion species,
J. Appl. Phys. 99 (2006) 093507-1～093507-5.

05J132 **4-09** T I IOM 52027
4-10 T I IOM MAN 52027
K. Narumi, S. Sakai, H. Naramoto and K. Takanashi,
Characterization of C_{60} Films Polymerized by Ion Irradiation,
Fullerenes, Nanotubes and Carbon Nanostructures 14 (2006) 429-434.

05J133 **4-09** I S MAN 52028
K. Takahiro, A. Terai, S. Oizumi, K. Kawatsura, S. Yamamoto and H. Naramoto,
Amorphization of Carbon Materials Studied by X-ray Photoelectron Spectroscopy,
Nucl. Instrum. Methods B242 (2006) 445-447.

05J134 **4-09** T IOM 52030
H. Tanimoto, K. Yamada, H. Mizubayashi, S. Sakai, K. Narumi and H. Naramoto,
Elasticity Study of the Irradiation-induced Polymerization and Decomposition of C_{60} Solid,
Mater. Sci. & Eng. A (2006), in press

05J135 **4-09** O IOM 52030
V. Lavrentiev, H. Abe, H. Naramoto, S. Sakai and K. Narumi,
Polymeric Chains in C_{60} and Co Mixture,
Chem. Phys. Lett., 424 (2006) 101–104.

05J136 **4-09** I S IOM 52030
V. Lavrentiev, H. Naramoto, K. Narumi, S. Sakai and P. Avramov,
Planar doping of crystalline fullerene with cobalt,
Chem. Phys. Lett., 423 (2006) 366–370.

05J137 **4-09** O IOM 52030
X.D. Zhu, F. Ding, H. Naramoto and K. Narumi,
AFM Investigation on Surface Evolution of Amorphous Carbon during Ion-beam-assisted Deposition,
Appl. Surf. Sci., (2006), in prass.

05J138 **4-13** T IOM 52029
Y. Mokuno, A. Chayahara, Y. Soda, Y. Horino, N. Fujimori,
Synthesizing single-crystal diamond by repetition of high rate homoepitaxial growth by microwave plasma CVD,
Diam. Relat. Mater., 14, (2005)1743.

05J139 **4-14** O IOM
S. Kitazawa, S. Yamamoto, M. Asano, Y. Saitoh and S. Ishiyama,
Radiation-induced luminescence from sol-gel anatase TiO_2 by 10 keV O^+ irradiation,
Nucl. Instum. Phys. Res., Sect. B., 232, (2005) 94 -97.

05J140 **4-14** O IOM
S. Kitazawa, S. Yamamoto, M. Asano, Y. Saitoh, S. Ishiyama,
Radiation-induced luminescence from TiO_2 by 10, 20 and 30 keV oxygen ion irradiations,
Nucl. Instum. Phys. Res., Sect. B., accepted.

05J141 **4-16** S MAN 52028
K. Takahiro, A. Terai, K. Kawatsura, H. Naramoto, S. Yamamoto, B. Tsuchiya, S. Nagata, F. Nishiyama,
Rutherford Backscattering Spectrometry of Electrically Charged Targets:Elegant Technique for Measuring Charge-State Distribution of Backscattered Ions,
Jpn. J. Appl. Phys. 45 (2006) 1823-1825.

05J142 **4-17** I IOM 52036
H. Abe, R. Morimoto, F. Satoh, H. Azuma, and H. Uchida,
Effects of Surface Modification by Ion Irradiation on Electrochemical Hydriding Rate of Pd,
J. Alloy and Compounds 404-406 (2005) 288-292.

05J143 **4-19** I S IOM 52021
S. Yamamoto, S. Nagata, A. Takeyama,

M. Yoshikawa,
Blister Formation in Rutile TiO_2 (100) Thin Films by Helium Ion Implantation,
Trans. Mater. Res. Soc. Jpn., 30[3] (2005)789-792.

05J144 4-19 S IOM 52021
K. Takano, S. Yamamoto, M. Yoshikawa, A. Inouye, A. Sugiyama,
High Sensitive Gasochromic Hydrogen Sensors using Tungsten Oxide Thin Films,
Trans. Mater. Res. Soc. Jpn., 31[1] (2006)227-230.

05J145 4-19 S IOM 52021
A. Inouye, K. Takano, S. Yamamoto, M. Yoshikawa, S. Nagata,
Gasochromic Property of Oriented Tungsten Oxide Thin Films,
Trans. Mater. Res. Soc. Jpn., 31[1] (2006)223-226.

05J146 4-19 S I IOM 52021
S. Yamamoto, S. Nagata, A. Takayama, M. Yoshikawa,
Blister formation in rutile TiO_2(100) films by helium irradiation,
Nucl. Instum. Phys. Res., Sect. B 249 (2006)374–376.

05J147 4-23 O NRI
S. Watanabe, N. S. Ishioka, T. Sekine, H. Kudo, H. Shimomura, H. Muramatsu, T. Kume,
Conversion of endohedral ^{133}Xe-fullerene to endohedral ^{133}Xe-fullerenol to be used for nuclear medicine,
J. Radioanal. Nucl. Chem. 266 (2005) 499–502.

05J148 4-23 O NRI
S. Watanabe, T. Katabuchi, N. S. Ishioka, S. Matsuhashi, H. Muramatsu,
Production of Endohedral ^{133}Xe-Higher Fullerenes by Ion Implantation,
J. Radioanal. Nucl. Chem., in press.

05J149 4-24 C NRI 51066
K. Ochiai, M. Nakao, J. Hori, S. Sato, M. Yamauchi, N.S. Ishioka and T. Nishitani,
Measurements of deuteron-induced activation cross sections for IFMIF accelerator structural materials in the energy range of 22-40 MeV,
Fusion Eng. Des., 81, Issues 8-14, (2006)1459-1464.

05J150 4-24 C NRI 51066
M. Nakao, J. Hori, K. Ochiai, N. Kubota, S. Sato, M. Yamauchi, N.S. Ishioka and T. Nishitani,
Measurements of deuteron-induced activation cross-sections for IFMIF accelerator structural materials,
Nucl. Instrum. Methods .,A562, Issue 2, (2006)785-788.

05J151 4-27 S ACT 52046
T. Satoh, T. Sakai, M. Oikawa,
Correction of X-ray detection yield in micro-PIXE analysis according to sample thickness variation measured by STIM,
Nucl. Instrum. Methods., B249 (2006) 234.

05J152 4-29 S STA 52048
T Nagamine, T Kusakabe, H Takada, K Nakazato, T Sakai, M Oikawa, T Satoh, K Arakawa,
Interferonbeta-induced changes in metallothionein expression and subcellular distribution of zinc in HepG2 cells,
Cytokine, 2006.in press

05J153 4-29 S STA 52048
中里 享美, 鈴木 慶二, 長嶺 竹明, 中嶋 克行, 酒井 卓郎、
長期経口投与によるカドミウムのマウス肝・腎への蓄積 :—大気マイクロ PIXE による組織内カドミウムの測定—、
Biomedical Research on Trace Elements, Vol. 16, (2005) 364-366.

05J154 4-30 S STA 52050
K. Endo, T. Yamamoto, Y. Shibata, K. Tsuboi,
A. Matsumura, H. Kumada, K. Yamamoto, T. Sakai,
T. Satoh, M. Oikawa, Y. Ohara, K. Ishii,
Demonstration of Inter- and Intracellular Distribution of Boron and Gadolinium Using Micro Particle Induced X-ray Emission (micro-PIXE),
Oncol. Res. 16 (2006)57-65.

05J155 4-32 S ACT 52053
K.Ishii, H.Yamazaki, S.Matsuyama, W. Galster,
T.Satoh, and M.Budnar,
Contribution of Atomic Bremsstrahlung in PIXE spectra and screening effect in atomic bremsstrahlung,
X-ray Spectrom., 34 (2005) 363-365.

05J156 4-32 S ACT 52053
K. Ishii, S. Matsuyama, H. Yamazaki, Y. Watanabe,
T. Yamaguchi, G. Momose, T. Amartaivan, A. Suzuki,
Y. Kikuchi and W.Galster,
Micron-CT using PIXE with Micro-beams,
Int. J. PIXE 15 (3&4), (2005)111-124.

05J157 4-32 S ACT 52053
T.Yamaguchi, K. Ishii, H. Yamazaki, S. Matsuyama,
Y. Watanabe, S. Abe, M. Inomata, A. Ishizaki,
R. Oyama and Y. Kawamura,
Development of an image reconstruction method for Micron-CT using PIXET,
Int. J. PIXE Vol.15, Nos. 3&4, (2005)195-202.

05J158 4-32 S ACT 52053
S.Matsuyama, K.Ishii, H.Yamazaki, Y.Kikuchi,
Ts.Amartaivan, S.Abe, K.Inomata, Y.Watanabe,
A.Ishizaki, R.Oyama, Y.Kawamura, A.Suzuki,
G.Momose, T.Yamaguchi and H. Imaseki,
Microbeam analysis of single aerosol particles at Tohoku University,
Int. J. PIXE Vol.15, Nos.3&4, (2005) 257-262.

05J159 4-32 S ACT 52053
H.Yamazaki, K.Ishii, Y.Takahashi, S.Matsuyama,
Y.Kikuchi, Ts. Amartaivan, T.Yamaguchi, G.Momose,
S.Abe, K.Inomata, Y.Watanabe, A.Ishizaki,
Identification of Qxidation States of Trace-Level Arsenic in Environmental Water Samples Using PIXE,
Int. J. PIXE Vol.15, Nos.3&4, (2005)241-247

05J160 4-40 C RSH 51075
Y. Kanda, Y., Oki, S. Yokoyama, K. Sato,
H. Noguchi, S. Tanaka and T. Iida,
Measurement of radiolytic yield of nitric acid in air,
Rad. Phys. Chem., 74 (5), (2005)338-340

05J161 4-40 C RSH 51075
S. Yokoyama, K. Sato, H. Noguchi, Su. Tanaka,
T. Iida, S. Furuichi, Y. Kanda, Y. Oki and T. Kaneto,
Characterization of Radionuclides Formed by High-Energy Neutron Irradiation,
Radia. Protect. Dosim., 116 (1-4), (2005)401–405

05J162 4-41 C MAN 51076
T. Sanami , M. Baba, M. Hagiwara, T. Hiroishi,
M. Hosokawa, N. Hirabayashi, T. Oishi,
H. Nakashima and S. Tanaka,
Measurement of differential cross sections for evaluation of radiation dose of ten's of MeV neutrons,
J. Nucl. Sci. Technol., Supplement-4(2004)502-504.

05J163 4-42 C RSH 51077
T. Sato, D. Satoh, A. Endo, Y. Yamaguchi.
Development of dose monitoring system applicable to various radiations with wide energy ranges.
J. Nucl. Sci. Technol., 42, (2005)768-778.

05J164 4-42 C RSH 51077
K. Oda, Y. Imasaka, T. Yamauchi, Y. Nakane,
A. Endo, H. Tawara, Y. Yamaguchi,
Radiator design for detecting high-energy neutrons

with a nuclear track detector,
Radiat. Meas., 40, (2005)570-574.

05J165 4-42 C RSH 51077
D. Satoh, T. Sato, A. Endo, Y. Yamaguchi, M. Takada,
K. Ishibashi,
Measurement of response functions of a liquid
organic scintillator for neutrons up to 800 MeV,
J. Nucl. Sci. Technol., 43, (2006)714-719.

05J166 4-51 C ACT
S. Okumura, S. Kurashima, N. Miyawaki,
K. Yoshida, and M. Fukuda,
Time-of-flight system with a movable ion detector
for absolute measurement of cyclotron beam energy,
Rev. Sci. Instrum. 76, (2005)113106.

05J167 3-14 C BMT 51014
M. Okamura et al.,
Advances of Mutagenesis in Flowers and their
Industrialization, In J. Teixeira da Silva (ed.) Floric.
Ornam. Plant Biotechnol.Vol. I, Global Science
Books (2006) 619

A 1. 2 Publications in Proceedings

05C001 1-01 I C T E SCS 51006, 52006
S. Kawakita, M. Imaizumi, K. Kibe, S. Yoda,
T. Ohshima, H. Itoh, M. Yamaguchi,
Analysis of Proton Induced Defects in Cu(In,Ga)Se2 Thin-Film Solar Cells,
Mater. Res. Soc. Proc. Vol. 865, March-April 2005 (San Francisco) 161.

05C002 1-01 I C T E SCS 51006, 52006
S. Kawakita, M. Imaizumi, K. Kibe, S. Yoda,
T. Ohshima, H. Itoh,
Anomalous Degradation of Cu(In,Ga)Se2 Thin-Film Solar Cells with High Fluence Protons,
Proc. of 20th European Photovoltaic Solar Energy Conf., June 2005 (Barcelona) p.480.

05C003 1-01 C I T SCS 51006, 52006
1-02 C I T SCS 51005, 52005
H. Miyamoto, T. Ohshima M. Imaizumi, H. Itoh,
K. Kibe, K. Kawano,
Recovery of Short Circuit Current of 3J Solar Cells by Current Injection at Low Temperature,
Proc. of 4th World Conf. on Photovoltaic Energy Conversion, May 2006 (Waikoloa), in press.

05C004 1-01 I C T E SCS 51006, 52006
1-02 C T I E SCS 51005, 52005
C. Morioka, M. Imaizumi, T. Ohshima, H. Itoh,
K. Kibe,
Study on Optimum Structure of AlInGaP Top Cell for Triple-Junction Space Solar Cell,
Proc. of 4th World Conf. on Photovoltaic Energy Conversion, May 2006 (Waikoloa) in press.

05C005 1-01 I C T SCS 51006, 52006
K. Shimazaki, M. Imaizumi, T. Ohshima, H. Itoh,
K. Kibe,
Analysis of Radiation Response and Recovery Characteristics of Amorphous Silicon Solar Cells,
Proc. of 4th World Conf. on Photovoltaic Energy Conversion, May 2006 (Waikoloa) in press.

05C006 1-02 C I SCS 51005, 52005
T. Ohshima, H. Miyamoto, M. Imaizumi, C. Morioka,
S. Kawakita, K. Shimazaki, K. Kibe, K. Kawano and H. Itoh,
Current Injection Effects on the Electrical Performance of 3J Solar Cells Irradiated with Low and High Energy Protons,
Proc. of 4th World Conf. on Photovoltaic Energy Conversion, May 2006 (Waikoloa) in press.

05C007 1-03 E SCS
N.J. Ekins-Daukes, H.S. Lee, T. Sasaki,
M. Yamaguchi, A. Khan, T.Takamoto, T. Agui,
K. Kamimura, M.Kaneiwa, M. Imaizumi,
T. Ohshima, T. Kamiya,
Carrier Removal and Defect Generation in Lattice-Mismatched InGaP under 1MeV Electron Irradiation,
Proc. 19th European Photovoltaic Solar Energy Conference and Exhibition, June 2004 (Paris) 3640.

05C008 1-03 E SCS
N.J. Ekins-Daukes, K. Arafune, H.S. Lee, T. Sasaki,
M. Yamaguchi, A. Khan, T.Takamoto, T. Agui,
K. Kamimura, M.Kaneiwa, M. Imaizumi,
T. Ohshima, H. Itoh,
Native and Radiation Induced Defects in Lattice Mismatched InGaAs and InGaP,
Proc. 31st IEEE Photovoltaic Specialists Conference, January 2005 (Lake Buena Vista) 683.

05C009 1-04 C SCS 51003
A. Makihara, M. Midorikawa, T. Yamaguchi, Y. Iide,
T. Yokose, Y. Tsuchiya, T. Arimitsu, H. Asai,
H. Shindou, S. Kuboyama, and S. Matsuda,
Hardness-by-Design Approach for 0.15 μm

FullyDepleted CMOS/SOI Digital Logic Devices with Enhanced SEU/SET Immunity,
The IEEE Nuclear and Space Radiation Effects Conference(NSREC 2005).

05C010 1-04 C SCS 51003
H. Shindou, S. Kuboyama, T. Hirao, and S. Matsuda, Local and pseudo SELs observed in digital LSIsand their implication to SEL test method,
The IEEE Nuclear and Space Radiation Effects Conference(NSREC 2005).

05C011 1-04 C SCS 51003
N. Ikeda, S. Kuboyama, S. Matsuda, T. Handa, Analysis of Angular Dependence of Proton-Induced Multiple-Bit Upsets in a Synchronous SRAM,
The IEEE Nuclear and Space Radiation Effects Conference(NSREC 2005).

05C012 1-04 C SCS 51003
H.Shindou, S.Kuboyama, N.Ikeda, S. Matsuda., T.Hirao,
Bulk Damage Caused by Single Protons in SDRAMs,
The IEEE Nuclear and Space Radiation Effects Conference(NSREC 2003).

05C013 1-04 C SCS 51003
S. Kuboyama, H.Shindo S. Matsuda, T.Hirao, Consistency of Bulk Damage Factor and NIEL for Electrons, Protons, and Heavy Ions in Si CCDs,
The IEEE Nuclear and Space Radiation Effects Conference(NSREC 2002).

05C014 1-05 T SCS 51002
S. Onoda, T. Hirao, H. Itoh, T. Okamoto, Evaluation of Transient Current Induced by High Energy Charged Particles in Si Pin Photodiode –substituted,
Proceeding of The School of Engineering of Tokai University, in press.

05C015 1-07 C T SCS 51004, 52002
長澤賢治，中嶋康人，府金賢，高橋芳浩、大西一功、
MOSFET の作製プロセスの評価 ーSOIFET の試作ー、
日本大学理工学部学術講演会予稿集, M-2, (2005) 1146-1147.

05C016 1-07 C T SCS 51004, 52002
大木隆広，川鍋龍，高橋芳浩，大西一功、
SOI 構造におけるシングルイベント過渡電流の解析、
日本大学理工学部学術講演会予稿集, M-3, (2005) 1148-1149.

05C017 1-07 C T SCS 51004, 52002
高橋芳浩，大木隆広，長澤賢治，中嶋康人，川鍋龍，大西一功，平尾敏雄，小野田忍，三島健太，河野勝泰，伊藤久義、
酸化膜を介した重イオン照射誘起電流、
第 53 回応用物理学関係連合講演会講演予稿集, 22a-V-11, (2006)816.

05C018 1-11 E SCS
T. Umeda, N.T. Son, J. Isoya, N. Morishita, T. Ohshima, H. Itoh, E. Janzen,
Electron paramagnetic resonance of the SI5 center in *4H*-SiC,
Proceedings of International Conference on Silicon Carbide and Related Materials (ICSCRM2005), (Sep. 17-23, 2005, Pittsburgh, USA); Materials Science Forum (2006) in press.

05C019 1-11 E SCS
N.T. Son, T. Umeda, J. Isoya, A. Gali, M. Bockstedte, B. Magunsson, A. Ellison, N. Morishita, T. Ohshima, H. Itoh, E. Janzen,
Divacancy model for P6/P7 centers in 4H- and 6H-SiC,
Proceedings of International Conference on Silicon Carbide and Related Materials (ICSCRM2005), (Sep.

17-23, 2005, Pittsburgh, USA). Materials Science Forum (2006) in press.

05C020 1-11 E SCS
M. Bockstedte, A. Gali, T. Umeda, N.T. Son, J. Isoya, E. Jazen,
Signature of the negative carbon vacancy-antisite complex,
Proceedings of International Conference on Silicon Carbide and Related Materials (ICSCRM2005), (Sep. 17-23, 2005, Pittsburgh, USA). Materials Science Forum (2006) in press.

05C021 1-11 E SCS
A. Gali, M. Bockstdete, N.T. Son, T. Umeda, J. Isoya, E. Janzen,
Divacancy and its identification : Theory,
Proceedings of International Conference on Silicon Carbide and Related Materials (ICSCRM2005), (Sep. 17-23, 2005, Pittsburgh, USA). Materials Science Forum (2006) in press.

05C022 1-11 E SCS
N. T. Son, T. Umeda, J. Isoya, A. Gali,
M. Bockstedte, B. Magnusson, A. Ellison,
N. Morishita, T. Ohshima, H. Itoh, E. Janzen,
Identification of divacancies in *4H*-SiC,
Proceedings of the 23rd International Conference on Defects in Semiconductors (ICDS-23) (July 24-29, 2005, Awaji-island, Japan), Physica B 376-377, (2006)334-337.

05C023 1-11 E SCS
T. Umeda, Y. Ishitsuka, J. Isoya, N. Morishita,
T. Ohshima, T. Kamiya,
EPR and pulsed ENDOR study of EI6 and related defects in *4H*-SiC,
Proceedings of the 10th International Conference on Silicon Carbide and Related Materials (ICSCRM2003) (Oct. 5-10, 2003, Lyon, France), Materials Science Forum 457-460, (2004) 465-468.

05C024 1-12 T SCS 52035
J. Isoya, M. Katagiri, T. Umeda, N.T. Son, A. Henry, E. Janzen, T. Ohshima, N. Morishita, H. Itoh,
Shallow phosphorous donors in 3C-, 4H-, and 6H-SiC,
Proceedings of International Conference on Silicon Carbide and Related Materials (ICSCRM2005), (Sep. 17-23, 2005, Pittsburgh, USA); Materials Science Forum (2006) in press.

05C025 1-13 I SCS 52007
A. Yoshida, Y. Nakanishi, A. Wakahara
Visible light-emission increased in rare-earth-doped GaN and related nitride alloy semiconductors
ISSC2005 (Fourth ISSS Int. Conf. on Smart Materials, Structures and Systems) July 28-30, 2005 (Bangalore, India) SC-12

05C026 1-13 I SCS 52007
T. Nishiwaki, H. Ofuchi, K. Takaba, K. Ogawa, M.Tabuchi, Y. Takeda, Y. Nakanishi, A. Wakahara, A.Yoshida,
Fluorescence EXAFS study on local structures around Eu atoms implanted in $Al_xGa_{1-x}N$,
The 23rd International Conference on Defects in Semiconductors July 24 - 29, 2005 (Awaji Island) TuP.117

05C027 1-13 I SCS 52007
A.Wakahara
Impact of AlGaN on Luminescene Capability of Rare - Earth Ionns in AlGaN,
E-MRS May 30 - June 3 , 2005 (Strasbourg, France) C-III.01

05C028 1-13 I SCS 52007
A. Wakahara, T.Fujiwara, H.Okada, A.Yoshida, T. Ohshima, and H.Ithoh,
Energy-back-transfer process in rare-earth doped AlGaN,
MRS Spring meeting March 28-April 1, 2005 (San

Francisco) V3.9, Abstract book, p.513

05C029 1-16 S IOM 52033
飛田 徹、鬼沢 邦雄、板倉 充洋、蕪木 英雄、鈴木 雅秀、岩瀬彰宏、
Fe-Cu 合金における電子線照射効果の反応速度論によるモデル計算、
日本原子力学会「2005 年春の年会」, 2005 (東海大学) p.621.

05C030 1-26 C MAN 51078
X.-M. Marechal, T. Bizen, Y. Asano, H.Kitamura,
65 MEV Neutron Irradiation of ND-FE-B Permanent Magnets,
European Particle Accelerators EPAC2006
Edinburgh, Scotland U.K. (2006)

05C031 1-27 G RCO
1-28 G RCO
T. Nakamoto, A. Idesaki, N. Morishita, H. Itoh,
T. Kamiya, N. Kimura, Y. Makida, T. Ogitsu,
H. Ohhata, A. Yamamoto,
Mechanical Properties of Organic Materials Used in Superconducting Magnets Irradiated by Gamma Rays at Liquid Nitrogen Temperature,
Cryogenic Engineering Conference & International Cryogenic Materials Conference 2005, 29 Aug. - 2 Sep. 2005, Keystone, U.S.A., Advances in Cryogenic Engineering, Vol. 52, (2006) 225-232.

05C032 1-27 G RCO
1-28 G RCO
A. Idesaki, N. Morishita, H. Itoh, T. Kamiya,
T. Nakamoto, N. Kimura, Y. Makida, T. Ogitsu,
H. Ohhata, A. Yamamoto,
"Evolved Gases from Organic Materials Used in the Superconducting Magnets Irradiated by Gamma Rays at Liquid Nitrogen Temperature",
Cryogenic Engineering Conference & International Cryogenic Materials Conference 2005, 29 Aug. - 2 Sep. 2005, Keystone, U.S.A., Advances in Cryogenic Enegineering, Vol. 52, (2006)330-334.

05C033 1-30 G ACT
槙田康博、飯田真久、大畠洋克、岡村崇弘、荻津透、木村誠宏、田中賢一、中本建志、山本明、出崎亮、森下憲雄、
J-PARC ニュートリノビームライン用超伝導電磁石システム（12）－耐放射線性を有する自動弁・安全弁の開発、
第 73 回 2005 年度秋季低温工学・超伝導学会

05C034 2-05 E ECT
A. Jyo, K. Okada, M. Tamada, T. Kume, T. Sugo, and M. Tazaki,
Bifunctional Cation Exchange Fibers Having Phosphonic Acid and Sulfonic Acid Groups,
Environmental Science Research Vol. 59, Chemistry for the Protection of Environment 4, Springer Inc., New York, (2005) 49-62.

05C035 2-07 G RCO
清水 隆夫, 玉田 正男,
モール状捕集材を用いた海水ウラン捕集の実規模システムの検討、
海洋開発論文集, 20 (2004) 617.

05C036 2-17 G RCO
2-18 G RCO
N. Q. Hien, L. Hai, L. Q. Luan, T. T. Hanh,
N. Nagasawa, F. Yoshii, K. Makuuchi and T. Kume,
Radiation degradation of alginate and some results of biological effect of degraded alginate on plants.,
Proceeding of Takasaki Workshop on Bilateral Cooperations, Radiation Processing of Natural Polymers, JAERI-Conf 2000-003, (2000)94-100.

05C037 2-17 G RCO
2-18 G RCO
L. Q. Luan, V. T. T. Ha, L. Hai, N. Q. Hien,
N. Nagasawa, F. Yoshii and T. Kume,
Effect of radiation-degraded chitosan on growth

promotion of flower plant in tissue culture.,
Proceeding of Takasaki Symposium on Radiation Processing of Natural Polymers in Asia. JAERI-Conf 2002-003, (2002) 144-154.

05C038 2-18 G RCO
N. Nagasawa, F. Yoshii, H. Mitomo and T. Kume
Radiation degradation of alginate and chitosan
Proc. of Takasaki Workshop on Bilateral Cooperations, Radiation Processing of Natural Polymers, JAERI-Conf 2000-003, (2000)107-119.

05C039 2-18 G RCO
N. Nagasawa, P. T. L. Ha, S. Watanabe, T. Ito, H. Mitomo, H. Takeshita, F. Yoshii and T. Kume
Suppression of Zn stress on barley by irradiated chitosan,
Proc. of Takasaki Symposium on Radiation Processing of Natural Polymers. JAERI-Conf 2001-005, (2001) 27-34.

05C040 2-18 G RCO
N. D. Lam, T. B. Diep, T. M. Quynh, N. M. Hung, N. Nagasawa and T. Kume
Biopolymer molecular weight control by radiation treatment for functional property improvement
Proc. of Takasaki Symposium on Radiation Processing of Natural Polymers in Asia. JAERI-Conf 2002-003, (2002)117-130.

05C041 2-21 E ECT
K. Hirota, T. Hakoda, M. Taguchi, M. Takigami, and T. Kojima,
Electron-beam treatment of PCDD/Fs in the flue gas from a municipal solid waste incinerator
Proceedings of RadTech Asia 03 Yokohama, Japan (2003)123-126.

05C042 2-21 E ECT
S. Hashimoto, K. Hirota, T. Hakoda, and M. Taguchi
Electron beam decomposition of organic pollutants in gases
Proceeding of the 23rd KAIF-JAIF Seminar on Nuclear Industry, Seoul, Korea (2001) 251-263.

05C043 3-03 G BMT
M. Ukai, H. Kameya, H. Nakamura, and Y. Shimoyama,
An ESR study of free radicals in irradiated cereals,
IMRP2006 (International Meeting on Radiation Processing), 26 FEB 2006-01 MAR 2006, Kuala Lumpur, Malaysia.in press.

05C044 3-15 C BMT 51015
長井純一，遠嶋太志，大江正和，安庭誠，田中淳，
変異誘発によるサトウキビ「Ni17」の毛群除去優良系統の開発 (1)幼苗検定による毛群除去個体の初期選抜
九州農業研究発表会　専門部会発表要旨集
2005 年　8 月　p43

05C045 3-15 C BMT 51015
長井純一，遠嶋太志，大江正和，安庭誠，田中淳，
変異誘発に適したサトウキビ「Ni17」の培養系開発 (1)不定胚誘導に適した培養部位の検討
九州農業研究発表会　専門部会発表要旨集
2005 年　8 月　p44

05C046 3-15 C BMT 51015
長井純一，遠嶋太志，大江正和，安庭誠，田中淳，
変異誘発に適したサトウキビ「Ni17」の培養系開発(2)不定胚からの効率的な再分化条件の検討
九州農業研究発表会　専門部会発表要旨集
2005 年　8 月　p45

05C047 3-15 C BMT 51015
長井純一，遠嶋太志，大江正和，安庭誠，田中淳，
変異誘発に適したサトウキビ「Ni17」の培養系

開発(3)再分化シュートの発根に及ぼすオーキシンの効果
九州農業研究発表会　専門部会発表要旨集
2005年　8月　p46.

05C048　3-15　C　BMT　51015
遠嶋太志，白尾吏，上野敬一郎，大江正和，
安庭誠，長谷純宏、田中淳，
サトウキビの有用変異体作出に適するイオンビーム線量
九州農業研究発表会　専門部会発表要旨集
2006年　8月　p15

05C049　3-20　C　BMT　51020
T.Sato,
Breeding of Chrysanthemum.
Annual of Akita prefecture Agricultural experiment station (2005)　in press .

05C050　3-23　C　BMT　61017
Y. Kawashima, T. Matsumoto, Y. Hase, Y. Yokota.
Effects of Ion Beam Irradiation on spore germination, mycelial growth and fruit body formation of Pleurotus ostreatus,
Transaction of 57th Kanto Branch of The Japanese Forest Society, October 2005p.349-350.

05C051　3-33　C　BMT　51033
N. Hamada, M. Ni, T. Funayama, T. Sakashita,
T. Kakizaki, S. Wada, Y. Yokota and Y. Kobayashi,
Bystander Killing in Normal Human Fibroblasts by Heavy-Ion Microbeams,
Extended Abstracts of the 7th International Workshop: Miceobeam Probes of Cellular Radiation Response (Mar 15-17, 2006, Columbia Univ., NY, USA) Radiat. Res. in press

05C052　3-34　C　ACT　51034
K. Harada,T. Nonaka,N. Hamada,T. Funayama,
H. Sakurai,S. Wada, T. Sakashita, M. Hasegawa,
Y. Kobayashi, T. Nakano
Analysis of bystander effect using high-LET heavy-ion microbeam,
The Second International Symposium on Biomedical Research Using Accelerator Technology November 2005(Maebashi) p.61.

05C053　3-39　C　RCO　61037
K. Shirai, T. Mizui, Y. Suzuki, N. Hamada,
T. Funayama, T. Sakashita, S. Wada, Y. Kobayashi,
T. Nakano, T. Shirao,
Response of Developing Neurons to X-rays in Cultured Hippocampal Neurons
The Second International Symposium on Biomedical Research Using Accelerator Technology,November 2005 (Maebashi) p.74.

05C054　3-39　C　RCO　61037
Y. Yoshida, K. Shirai, Y. Suzuki, A. Takeuchi,
N. Hamada, T. Funayama, S. Wada, T. Sakashita,
Y. Kobayashi, S. Ozawa, T. Nakano,
Effects of X-ray and Heavy Ion Irradiation on the Postnatal Cerebellum in Organotypic Slice Cultures
The Second International Symposium on Biomedical Research Using Accelerator Technology, November 2005 (Maebashi) p.73.

05C055　3-39　C　RCO　61037
H. Kiyohara, Y. Ishizaki, H. Katoh, Y. Suzuki,
N. Hamada, T. Hunayama, S. Wada, T. Sakashita,
Y. Kobayashi,
Effects of Irradiation with Heavy Ion Beam on the Expression of ICAM-1 and TGF-b1 on HUVEC
The Second International Symposium on Biomedical Research Using Accelerator Technology, November 2005 (Maebashi) p.60.

05C056　3-39　C　RCO　61037
吉田由香里，鈴木義行，浜田信行，白井克幸，
野田真永，Wael S. Al-Jahdari，舟山知夫，坂下哲哉，和田成一，小林泰彦，小澤瀞司，中野隆史，
小脳培養切片におけるX線と炭素線の生物学的

効果の比較
第45回日本医学放射線学会生物部会学術大会,
2006年, 7月 (弘前) p.42.

05C057 3-43 C BMI 51042
H. Matsumoto, T. Ohnishi,
Radiation-induced advantageous bystander effect and adaptive response through NO radical generations.
Proc. of Int. Symposium on Low-dose radiation exposure and bio-defense system. Ed. S. Tanaka, K. Fujikawa, Y. Oghiso. (Sept. 28-30, 2005, Rokkasho, Japan) (2006) p.23-26.

05C058 3-46 C BIM 51045
明尾潔 、舟山知夫、浜田信行、
小林泰彦、明尾庸子、坪田一男
イオンビーム照射後のヒト培養網膜血管内皮細胞のグルタチオンペルオキシダーゼ発現
第110回日本眼科学会総会 2006. 4.14, 大阪

05C059 3-46 C BIM 51045
明尾潔、舟山知夫、浜田信行、小林泰彦、
明尾庸子、坪田一男
イオンビーム照射後の培養網膜色素上皮と網膜血管内皮のグルタチオンペルオキシダーゼ
第17回眼科ストレス研究会 2006.4.13 大阪

05C060 3-47 C BMT 51046
鈴木敬子、和田成一、山田直明、佐野忠士、
金子惠実、今岡豊、柿崎竹彦、夏堀雅宏、
小林泰彦、伊藤伸彦
異なる線質の細胞照射により生じるイヌ株化腫瘍細胞における放射線感受性の比較
第140回 日本獣医学会学術集会 講演要旨集、
2005年（鹿児島）p.182

05C061 3-47 C BMT 51046
金子惠実、和田成一、大村俊江、今岡豊、
佐野忠士、夏堀雅宏、伊藤伸彦
獣医学領域における陽子線治療のための基礎的研究
第138回 日本獣医学会学術集会 講演要旨集、
2004年（北海道）p.154

05C062 3-50 C BMT 51041
有松祐治,古澤壽治,鈴木英子,野島久美恵,
長岡俊治,永松愛子,鈴木ひろみ,島津徹,
石岡憲昭：
カイコ胚発育期の遺伝子発現に及ぼす重粒子線の影響
日本宇宙生物科学会第19回大会、東京大学・駒場キャンパス・数理科学研究科大講堂室、プログラム・予稿集 p43、2005年9月29日・30日

05C063 3-50 C BMT 51041
有松祐治, 古澤壽治, 鈴木英子, 長岡俊治,
野島久美恵, 永松愛子, 石岡憲昭：
カイコ個体での形質および遺伝子発現による重粒子線影響解析
日本放射線影響学会第48回大会・第1回アジア放射線研究会議、広島国際会議場、講演要旨集 p139、2005年11月15日-17日

05C064 3-50 C BMT 51041
Y. Arimatsu, T. Fursawa, E. Suzuki, S. Nagaoka,
K. Nojima, A. Nagamatsu, N. Ishioka :
Detection of influence in morphology formation and gene expression in larvae of the silkworm, Bombyx mori, induced by heavy ion irradiation to diapause eggs.
The 1st Asian Congress of Radiation Research, Proceedings pp.144-145、(Nov. 16- 17, Hiroshima) 2005

05C065 3-57 C BMT 51058
本田修三、関本均、松木良祐、加藤翔太、
米山香織、落合由記子、米山弘一、竹内安智、
松橋信平、河地有木、藤巻秀、阪本浩一、
鈴井伸郎、石井里美、石岡典子、渡辺智、
荒川和夫、久米民和
^{13}Nを用いたホスト植物根吸収窒素の根寄生植物による収奪の可視化と収奪率の定量解析

2005年度日本土壌肥料学会関東支部大会講演要旨集、ｐ８．2005年11月（前橋）

05C066 3-63 C BMT 51065
N. Kawachi, K. Sakamoto, S. Ishii, S. Fujimaki, N. Suzui, N. S. Ishioka and S Matushashi,
Quantitative Measurement of Photosynthetic Rate Constant within Leaf Using Carbon-11-Labeled Carbon Dioxide and Positron Emitting Tracer Imaging System,
IEEE Nuclear Science Symposium Conference Record, 2005, J03(35), 2908-2913

05C067 3-64 C BMT 51067
4-25 C NIR 51067
T. Katabuchi, S. Watanabe, N. S. Ishioka, Y. Iida, H. Hanaoka, S. Matsuhashi and K.Endo,
Production of ^{67}Cu at JAEA-Takasaki for Nuclear Medical Application
Proc. of The Second International Symposium on Biomedical Research Using Accelerator Technology, November 10-11, 2005, Maebashi, Japan. p.80.

05C068 3-65 S BMT 52018
K. Okada, H. Kimura, H. Kuwano
The evaluation of intracellular elements in hepatocellular carcinoma and hepatocyte cell line by PIXE: influence of hypoxic conditions
The 2nd Int. Symp. on Biomedical Research Using Accelerator Technology November 2005 (Gunma) p.69.

05C069 3-65 S BMT 52018
H. Kimura, A Faried, K. Okada, S. Ma, M. Sohda, M. Nakajima, T. Miyazaki, H. Kato, T. Asao, H. Kuwano
The sensitivity evaluation of Cisplatin in esophageal cancer cell lines
The 2nd Int. Symp. on Biomedical Research Using Accelerator Technology November 2005 (Gunma) p.37.

05C070 3-66 S BIT 52051
S. Harada, S. Ehara, K. Ishii, A. Tanaka, T. Satoh, S. Matsuyama, H. Yamazaki, Y. Komori, T. Kamiya, T. Arakawa, M. Saitoh, M. Oikawa, and K. sera.
Innovation of the Target preparation of the micro PIXE Camera for the floating cells.
Proceeding of the 10th International Conference on Particle-Induced X-ray Emission and its Analytical Applications (CDR publication)

05C071 3-66 S BIT 52051
S. Harada, S. Ehara, K. Ishii, A. Tanaka, T. Satoh, S. Matsuyama, H. Yamazaki, Y. Komori, T. Kamiya, T. Arakawa, M. Saitoh, M. Oikawa, and K. sera.
The alteration of the cis-platinum (Platinum analogues for cancer therapy) by the low dose irradiation studied in human leukemia, A preliminary study.
Proceeding of the 10th International Conference on Particle-Induced X-ray Emission and its Analytical Applications (CDR publication)

05C072 4-01 C RCO 41058
Y. Yoshida, M. Taguchi, J. Yang, S. Seki, T. Kozawa, S. Tagawa, H. Shibata, M. Taguchi, H. Nanba, and T. Kojima,
Heavy ion beam pulse radiolysis for absorption spectroscopy
Proc. of Radiat. Chem. workshop, October 2003 (Hakone) p.102.

05C073 4-02 C RCO 51073
S. Nakagawa, M. Taguchi and T. Kojima,
LET effect on irradiation of hydroxymaleimide in 2-propanol (1)
Proceeding of 86th Spring Meeting of Chemical Society of Japan, March 2006 (Chiba) 4E4-02.

05C074 4-04 E IOM
Presentation - R.A. Wach, M. Sugimoto, N.D. Lam, M. Yoshikawa,

Development of SiC coatings on Al_2O_3 ceramics from precursor polymers by radiation curing, *The 8th SPSJ International Polymer Conference (IPC 2005) Emerging Horizons in Polymer Science and Technology,* 26–29 July 2005, Fukuoka, Japan.

05C075 4-04 E IOM
Poster - M. Sugimoto, R.A. Wach, M. Yoshikawa, K. Ikenoya, K. Onuki, M. Nomura, S. Nakao, Development of silicone carbide coating from Si-based polymers by EB curing, *6th Pacific Rim Conference on Ceramic and Glass Technology,* 11-16 September 2005, Maui Hawaii, USA.

05C076 4-04 E IOM
Presentation - R.A. Wach, M. Sugimoto, M. Yoshikawa, M. Nomura, S. Nakao, Polycarbosilane derived SiC ceramics for gas separation membranes, *The 8th Polymers for Advanced Technologies International Symposium*, 13-16 September 2005 Budapest, Hungary.

05C077 4-04 E IOM
Presentation - R.A. Wach, M. Sugimoto, M. Yoshikawa, M. Nomura, S. Nakao, Polycarbosilane derived SiC ceramics for gas separation membranes, *Workshop on Polymeric Biomaterials, Center of Excellence - Application of Laser Techniques and Biomaterials in Medicine*, 26-28 September 2005, Lodz, Poland.

05C078 4-04 E IOM
Poster - M. Sugimoto, R.A. Wach, N. Lam, M. Yoshikawa, Development of SiC micro tube from polycarbosilane by EB irradiation, *The 30th International Conference & Exposition on Advanced Ceramics & Composites,* 22-27 January 2006, Cocoa Beach, FL, USA.

05C079 4-04 E IOM
Presentation - R.A. Wach, M. Sugimoto, M. Nomura, S. Nakao, M. Yoshikawa, Production of polymer derived SiC coatings by irradiation for gas separation membranes, *The 30th International Conference & Exposition on Advanced Ceramics & Composites*, 22-27 January 2006, Cocoa Beach, FL, USA.

05C080 4-15 S 52024
杉山僚、小田知弘、阿部智之、楠勲
表面活性化手法による光学素子接合技術の開発
第 7 回光量子科学研究シンポジウム論文集、京都（2006）提出済

05C081 4-17 I IOM 52036
R. Morimoto, H. Uchida and H. Abe,
Effects of Ion Irradiation on Electrochemical Hydrogen Absorption Rate of Pd,
International Hydrogen Energy Congress & Exhibition, Istanbul (Turkey), July 2005, in press.

05C082 4-22 C NRI 51065
N. S. Ishioka, S. Watanabe, S. Fujimaki, K. Sakamoto and S. Matsuhashi
Extension of the Irradiation System at TIARA for Production of Radioisotopes to Be Used in Plant Physiology
Proc. of the Internat. conf. on Cyclotrons and Their Applications, October 2004 (Tokyo, Japan) p.45-47.

05C083 4-24 C NRI 51066
中尾誠，堀順一，落合謙太郎，久保田直義，佐藤聡，山内通則，石岡典子，西谷健夫
IFMIF 加速器構成材料の重陽子入射による放射化断面積の測定
FAPIG No. 172, (2006)3～7

05C084 4-25 C BMT 51067
Y.Iida, H.Hanaoka, N.Oriuchi, T.Higuchi, M.Miyakubo and K.Endo
Preclinical Evaluation of Radiolabeled Anti-CD20 Monoclonal Antibody, NuB_2, for Cancer Therapy.
Proc. of EANM'05 - Annual Congress of the European Assocation of Nuclear Medicine, October 15 - 19, 2005, Istanbul, Turkey, S206.

05C085 4-28 S ACT 52017
M. Hasegawa, H. Sakurai, M. Shioya, A. Takeuchi, T. Tamamoto, T. Sakai, M. Oikawa, M. Fukuda, T. Satoh, K. Arakawa, and T. Nakano,
In Vivo Analysis of Cell Death by An In-Air Micro-Particle-Induced X-ray Emission (Micro-PIXE)
21st Century COE Program, The Second International Symposium on Biomedical Research Using Accelerator Technology, November 2005 (Maebashi) p71.

05C086 4-28 S ACT 52017
長谷川正俊，桜井英幸，中野隆史，塩谷真里子，竹内あい子，玉本哲郎，浅川勇雄，酒井卓郎，及川将一，荒川和夫，
大気マイクロ PIXE による細胞死の解析
日本放射線腫瘍学会第 18 回学術大会報文集，2005 年 11 月（川越）p.162

05C087 4-29 S STA 52048
長嶺竹明
インターフェロンによる肝臓内メタロチオネイン誘導とその臨床的意義について
メタロチオネイン 2005（前橋）2005.9.2-3.p27-28

05C088 4-29 S STA 52048
草壁孝彦、長嶺竹明、高田久嗣、中里享美、鈴木慶二、中嶋克行、酒井卓郎、荒川和夫
精巣組織中のカドミウム分布について～大気マイクロ PIXE 測定法ならびにメタロチオネイン発現からのアプローチ
環境ホルモン学会 第８回研究発表会（東京）2005.9.27-29,p56

05C089 4-29 S STA 52048
草壁孝彦、長嶺竹明、高田久嗣、中里享美、塙亜希子、小島佐江子、鈴木慶二、中嶋克行、酒井卓郎、荒川和夫
精巣組織中のカドミウム分布について大気マイクロ PIXE 測定法ならびにメタロチオネイン発現からのアプローチ
メタロチオネイン２００５（前橋）2005.9.2-3.p48.

05C090 4-29 S STA 52048
T. Kusakabe , H. Takada, K. Nakazato , K Suzuki, K. Nakajima, K. Arakawa,T. Nagamine ,
Study on the cadmium distribution in the rat testis using in air micro-Particle Induced X-ray Emission (PIXE) and metallothionein expression
Gunma University Graduate School of Medicine, The 21st Century COE Program The Second International Symposium on Biomedical Research Using Accelerator Technology,Maebashi Japan,2005.11.10-11.p34-36

05C091 4-29 S STA 52048
中里享美、鈴木慶二、長嶺竹明、中嶋克行、酒井卓郎
長期経口投与によるカドミウムのマウス肝・腎への蓄積－大気マイクロ PIXE による組織内カドミウムの測定
メタロチオネイン２００５（前橋）2005.9.2-3.p47

05C092 4-29 S STA 52048
中里 享美, 鈴木 慶二, 長嶺 竹明, 中嶋 克行, 酒井 卓郎
長期経口投与によるカドミウムのマウス肝・腎への蓄積：-大気マイクロ PIXE による組織内カドミウムの測定-
第 16 回日本微量元素学会（京都）p160

05C093 4-30 S STA 52050
K. Endo, K. Nakai, T. Yamamoto, Y. Shibata,
A. Matsumura ,H. Kumada, K. Yamamoto,T. Sakai,
T. Sato, M. Oikawa, Y. Obara, K. Ishii
Analysis of Intracellular Distribution of Boron and Gadolinium in 9L Sarcoma Cells Using a Single-Ended Accelerator (Micro PIXE)
第６４回日本脳神経外科学会総会（２００５年１０月７日：パシフィコ横浜）

05C094 4-34 S ACT 52045 応用物理
T. Harada, N. Uchiya, M. Murai, H. Nishikawa,
T. Sakai, T. Sato, Y, Ishii, M. Fukuda,
Micro-machining of Polymers on Silicon by Proton Microbeam Irradiation
The Japan Society of Applied Physics, The 77th Autumn Meeting, September 2005 p.629.

05C095 4-34 S ACT 52045
N. Uchiya, T. Harada, H. Nishikawa, J. Haga,
T. Sakai, T. Sato, Y. Ishii, T. Kamiya,
Micro-machining of Resist on Silicon by Proton Beam Writing
Institute of Engineers on Electrical Discharge in Japan, November 2005 p.90.

05C096 4-34 S ACT 52045
N. Uchiya, T. Harada, H. Nishikawa, J. Haga,
T. Sakai, T. Sato, Y. Ishii, T. Kamiya,
Micro-machining of Resist on Silicon by Proton Beam Writing
The Japan Society of Applied Physics, The 53rd Spring Meeting, March 2006 p.770.

05C097 4-35 S IOM 52039 応用物理
H. Aiba, T. Nakamura, Y. Ohki, M. Murai,
H. Nishikawa, M. Oikawa, T. Sato, K. Arakawa
Microscopic structural change of silica glass induced by ion microbeam irradiation
Extended Abstracts (The 53rd Spring Meeting, 2006); The Japan Society of Applied Physics and Related Societies, March 2006 (Tokyo) p.962

05C098 4-36 T ACT 52054
斎藤勇一、千葉敦也、鳴海一雅
「TIARA 3MV タンデム加速器によるフラーレン加速」
第１８回タンデム加速器とその周辺技術の研究会報告集、p47.

05C099 4-41 C MAN 51076
M. Hagiwara, T. Sanami, M. Baba, T. Oishi,
N. Hirabayashi, M. Takada, H. Nakashima and
S. Tanaka,
Measurement of differential cross sections of secondary heavy particles induced by tens of MeV particles,
Proceeding of the international conference on Nuclear Data for Science and Technology, 769 (2005) 1031-1034.

05C100 4-41 C MAN 51076
M. Hagiwara, T. Sanami, T. Oishi, M. Baba and
M. Takada,
Measurements of double differential cross sections of secondary heavy charged particles induced by 70 MeV protons for microdosimetry study,
Journal of Radiation Protection Bulletins, a special issue (2005) 53-56.

05C101 4-41 C MAN 51076
M. Hagiwara, T. Sanami, M. Hosokawa, M. Baba
and M. Takada,
Development of a Bragg Curve Spectrometer (BCS) for Fragment Spectroscopy from Neutron and Proton Induced Reactions,
KEK proceedings 2002-12 Radiation Detector and Their Uses (Sep. 2002) 70.

05C102 4-41 C MAN 51076
Mamoru Baba,
Experimental Studies on Particle and Radionuclide

Production Cross Sections for Tens of MeV Nuetrons and Protons,
Proceeding of the international conference on Nuclear Data for Science and Technology, 769 (2005) 884-889.

05C103 4-41 C MAN 51076
M. Baba,
Differential cross-sections of complex particle emission reactions,
Proceedings of Internasional Workshop on Perspectives on Nuclear Data for the Next Decade (in press).

05C104 4-41 C MAN 51076
T. Oishi, M. Hagiwara, M. Baba, T. Sanami and T. Takada,
Application of The Digital Waveform Analysis to Bragg Curve Spectrometer,
KEK proceedings 2004-14 Radiation Detector and Their Uses (Nov. 2004) 166.

05C105 4-41 C MAN 51076
M. Hagiwara, T. Sanami, T. Oishi, M. Baba,
M. Takada, H. Nakashima, S. Tanaka,
Measurement of double differential cross sections for fragment-production induced by tens of MeV particles,
Proceedings of the 2003 Symposium on Nuclear Data, 2004-005 (2004) 115-120.

05C106 4-41 C MAN 51076
M. Hagiwara, T. Sanami, T. Oishi, M. Baba,
M. Takada,
Measurements of double differential heavy particles production cross sections for 70 MeV protons,
Proceedings of the 2004 Symposium on Nuclear Data, 2005-003 (2005) 152-157.

05C107 4-42 C RSH 51077
D. Satoh, T. Sato, A. Endo, Y. Yamaguchi, M. Takada, K. Ishibashi.
Study on response function of organic liquid scintillator for high-energy neutrons.
Proceedings of International Conference on Nuclear Data for Science and Technology, AIP Conference Proceedings, 769, 1680-1683 (2005).

05C108 4-42 C RSH 51077
D. Satoh, T. Sato, A. Endo, N. Matsufuji, S. Sato, M. Takada, K. Ishibashi.
Study of light output and response function of liquid organic scintillator for high-energy neutron spectrometry.
2005 IEEE Nuclear Science Symposium Conference Record, 1288-1290 (2005).

05C109 4-45 C ACT 51074
W. Yokota, Y. Ohara, K. Arakawa
Microbeam system for heavy ions from cyclotron to irradiate living cells
Proc. of 36th ICFA Advanced Beam Dynamics Workshop (NANOBEAM 2005), October 2005 (Kyoto) p.11

05C110 4-49 I ACT
K. Yamada, K. Ohkoshi, Y. Saitoh, K. Mizuhashi, W. Yokota, T. Orimo, A. Ohmae
Production of Fullerene(C_{60}) Ion with Freeman Ion Source
Proceedings of the 42nd Annual Meeting on Radioisotope and Radiation Research

05C111 4-51 C ACT
S. Okumura, S. Kurashima, N. Miyawaki, K. Yoshida, H. Kashiwagi, M. Fukuda, T. Nara, T. Agematsu, I. Ishibori, Y. Nakamura, W. Yokota, Magnetic Field Stabilization at the JAERI AVF Cyclotron
Proceedings of the 2nd Annual Meeting of Particle Accelerator Society of Japan and the 30th Linear Accelerator Meeting in Japan, Tosu, Japan

(2005).p.745.

05C112 4-51 C ACT

S. Kurashima, N. Miyawaki, S. Okumura, I. Ishibori,
K. Yoshida, H. Kashiwagi, M. Fukuda, T. Nara,
T. Agematsu and Y. Nakamura,
Single-Turn Extraction Technique in the JAERI AVF Cyclotron
Proceedings of the 2nd Annual Meeting of Particle Accelerator Society of Japan and the 30th Linear Accelerator Meeting in Japan, Tosu, Japan (2005) p.717.

Appendix 2
List of Related Patents

05PAT001　1-31
吉田、八巻、浅野、森田（原子力機構）
「ナノ構造制御高分子イオン交換膜の製造方法」、
特開 2005－78849 号

05PAT002　1-31
吉田、八巻、浅野、森田（原子力機構）
「Process for producing nano-space controlled polymer ion-exchange membranes」、
公開 US-2005-0049320-A1

05PAT003　2-01
玉田、瀬古（原子力機構）
「エマルショングラフト重合法とその生成物」、
特願 2004-167017 号

05PAT004　2-06
岡田、瀬古、玉田（原子力機構）
「強酸性領域で使用可能なキレート吸着材」
特願 2006-005784 号

05PAT005　2-10
竹田（倉敷繊維加工）、玉田（原子力機構）
「水中の陽イオンを高速かつ高効率で除去する材料と、この材料を用いた廃水の２次処理」
特願 2004-169481 号

05PAT006　2-11
玉田、片貝、瀬古（原子力機構）、永本（三井金属鉱業）、
「重金属捕集イオン交換繊維の製造方法」、
特願 2004-12877 号

05PAT007　2-11
玉田、片貝、瀬古（原子力機構）、永本（三井金属鉱業）、
「グラフト重合装置」、
特願 2004-59224 号

05PAT008　2-12
田中、安斉（アンザイ）、瀬古、玉田、吉井（原子力機構）高橋、武井
「水中金属成分の吸着装置および回収装置」、
特開 2005-238093 号

05PAT009　2-14
吉井、久米、長澤（原子力機構）、三友（群大）
「橋かけ生分解性材料の製造方法」、
特許 3759067 号

05PAT010　2-14
吉井、長澤、八木（原子力機構）、三友（群大）
「キチン及びキトサン誘導体ハイドロゲルによる浄化剤」、
特開 2004-358292 号

05PAT011　2-15
吉井、久米、長澤（原子力機構）、三友（群大）
「橋かけ生分解性材料の製造方法」、
特許 3759067 号

05PAT012　2-15
長澤、八木、吉井（原子力機構）、金澤、川野、中谷（住電ＦＰ）、三友（群大）
「生分解性熱収縮材および該生分解性熱収縮材の製造方法」
特開 2005-125674 号

05PAT013　2-15
長澤、八木、吉井（原子力機構）、金澤、中谷（住電ＦＰ）
「生分解性材料および生分解性材料の製造方法」
特開 2005-126599 号

05PAT014　2-15
長澤、八木、吉井（原子力機構）、金澤、川野、中谷（住電ＦＰ）
「生分解性を有する耐熱性架橋物およびその製造方法」
特開 2005-126603 号

05PAT015　2-15
長澤、八木、吉井（原子力機構）、金澤（住電ＦＰ）「生分解性を有する耐熱性架橋物および該耐熱性架橋物の製造方法」
特開 2005-126605 号

05PAT016　2-15
長澤、八木、吉井（原子力機構）、金澤（住電ＦＰ）「ポリ乳酸製透明材料の製造方法およびポリ乳酸製透明材料」
特願 2004-123461 号

05PAT017　2-15
長澤、八木、吉井（原子力機構）
「生分解性ポリエステルの高効率橋かけ方法」
特開 2005-350503 号

05PAT018　2-16
長澤、吉井（原子力機構）、土橋、寺尾（群大）
「ゼラチンからなる耐熱性成形体の製造方法および、ゼラチンからなる耐熱性成形体」
特開 2004-339395 号

05PAT019　2-16
土橋、古澤（群大）、長澤、八木、玉田（原子力機構）
「デオキシリボ核酸を安定に含むゲル組成物の製造方法及び該方法により得られたゲル組成物」、
特願 2006-171015 号

05PAT020　2-16
土橋、窪田、古澤（群馬大学工学部）、長澤、八木、玉田（原子力機構）：
「タンパク質からなる粒子状成形体の製造方法及び、該方法により得られたタンパク質からなる粒子成形体」、
特願 2006-171016 号

05PAT021　2-17
吉井、久米、長澤（原子力機構）、三友（群大）
「橋かけ生分解性材料の製造方法」、
特許 3759067 号

05PAT022　2-17
吉井、長澤、久米（原子力機構）、ルアン（VAEC）
「放射線処理多糖類を利用した植物組織培養方法」
特開 2004-049164 号

05PAT023　2-18
幕内、吉井、長澤、久米（原子力機構）
「植物成長促進剤」、
特許 3617912 号

05PAT024　2-18
吉井、久米、長澤（原子力機構）、三友（群大）
「橋かけ生分解性材料の製造方法」、
特許 3759067 号

05PAT025　2-18
吉井、長澤、八木（原子力機構）、三友（群大）
「キチン及びキトサン誘導体ハイドロゲルによる浄化剤」、
特開 2004-358292 号

05PAT026　2-19
宇田川、八木、池田（原子力機構）
「四フッ化エチレン樹脂多耐孔質体の製造方法」、
特開 20004-142106 号、

05PAT027　2-19
八木、宇田川、池田（原子力機構）
「放射線改質四フッ化エチレン樹脂粉末及びその成形体の製造方法」、
特開 20004-149650 号

05PAT028　2-20
片貝，玉田（原子力機構），角田，梅村（群馬大学）
「有機ポリマー製モノリスキャピラリーカラム及びその製造法」、
特願 2005-66929 号

05PAT029　2-21
小嶋、広田（原子力機構）、 谷口、鈴木、石原、阿部 (大成建設(株))
「ダイオキシン類汚染無害化装置」
特願平 16-359382 号

05PAT030　2-21
小嶋、広田（原子力機構）、三野、飯阪、大田、寺本(日立造船(株) 50%)
「排ガス処理装置及び排ガス処理方法」
特願平 17-121355 号

05PAT031　2-22
田久保、岩崎、木下、大宮（岩崎電気）、小嶋、箱田、島田（原子力機構）　：
「ホルムアルデヒド含有ガスの浄化方法及びホルムアルデヒド含有ガスの浄化装置」、
特願 2005-143441 号

05PAT032　3-01
佐藤、和田、鳴海、菊地、舟山、小林(原子力機構)
「DNA 鎖切断の効率的検出法」、
特開 2004-239639 号

05PAT033　3-03
鵜飼（北海道教育大）
「放射線照射食品の検査方法」、
特願 2005-61622 号

05PAT034　3-06
長谷、田中、K H Trung（原子力機構）
「紫外線抵抗性植物」
特願 2006-56858 号

05PAT035　3-37
星野、田中、Saha Manujendra Narayan（群馬大学）
「B 型肝炎ウイルスの感染性の測定方法。」
特願 2005-263575 号

05PAT036　4-04
杉本、ラドスラフバフ、 吉川（原子力機構）
「ケイ素系混合高分子材料による炭化ケイ素(SiC)薄膜の合成法.」
特願 2005-266711 号
h17.9.14 (Synthesis process of SiC thin film using Si-Based polymer blend, M. Sugimoto, R.A. Wach, M. Yoshikawa, Patent application 2005-266711, Sep. 14 2005).

05PAT037　4-05
杉本, 吉川（原子力機構）, 関, 佃, 田川,
「イオンビーム照射によるセラミックナノワイヤーの製造法」
特願 2005-269602 号

05PAT038　4-05
A. Sharma, M. Katiyar, D. Gupta, S. Seki, and S. Tagawa
"An improved organic light emitting diode, an improved organic light emitting diode for tunig the white emission and a process for fabrication thereof" Indian Patent Application No. 1532/DEL/2005.

05PAT039　4-05
松井, 村杉, 関, 田川, 原, 吉本護, 竹内, 青田, 小山, 古滝, 砂川, 矢口, 並木
「単結晶基板表面に形成されるステップ構造のピン止め方法、及びピン止めされたステップ構造を有する単結晶基板」
特願 2005-378335 号

05PAT040　4-42
佐藤, 佐藤, 遠藤,山口 (原子力機構)
「高エネルギー中性子, 光子及びミューオンに対する高感度線量測定方法」
特願平 17-091744 号.

05PAT041　4-46
島田, 及川, 加藤, 佐藤, 堀内, 遊佐, 岸, 中野（群馬大学）, 佐藤, 酒井, 上松, 福田, 荒川（原子力機構）
「荷電粒子線の照準位置決定装置及びその使用方法」,
特願 2006-4794 号

05PAT042　4-50
吉田、田島（原子力機構）横山（信越化学工業）：
「径方向駆動によるミラー磁場可変法」、
特開：2006-49020 号

Appendix 3
List of Related Press-Release and TV Programs

05NP001　3-01
毎日新聞他１０紙、
平成１８年1月２４日、
原子力機構
「傷ついたＤＮＡを直す遺伝子を発見し、産業利用に成功」

05NP002　3-55
中国新聞
平成 17 年 10 月 29 日
広島大学
「研究テーマ　ジャズで表現」

05NP003　3-59,　4-22
朝日新聞、日本経済新聞、東京新聞、読売新聞（群馬版）他多数
平成１８年3月１５日
原子力機構、秋田県立大学：
「イネに吸収されたカドミウムの動きを初めて観測／植物ポジトロンイメージング技術で生きたまま画像化を可能に」

05TV001　3-01
ＮＨＫ教育、
平成１８年２月４日１８時、
原子力機構
「サイエンス ZERO、―極限環境生物の不思議に迫る―」

*The lists are made based on the report from authers.

Appendix 4 Type of Research Collaboration

Section of this Report	Type of Research Collaboration[*1]				Irradiation Facilities[*2]						Section of this Report	Type of Research Collaboration[*1]				Irradiation Facilities[*2]					
	Joint Res,	Coop. Res, Univ.	Joint Res, Proj.	JAEA	TIARA				Co	E.B		Joint Res,	Coop. Res, Univ.	Joint Res Proj.	JAEA	TIARA				Co	E.B
1-01	●				C	T	I			E	2-21				●						E
1-02	●			●	C		I	S		E	2-22	●									E
1-03		●								E	2-23				●					G	E
1-04	●				C						2-24				●	C				G	E
1-05		●		●	C																
1-06				●	C	T					3-01				●					G	
1-07		●			C	T					3-02		●							G	
1-08		●				T	I				3-03		●							G	
1-09				●		T			G	E	3-04				●					G	
1-10		●								E	3-05	●									E
1-11		●								E	3-06				●	C					
1-12		●				T					3-07				●	C					
1-13		●					I			E	3-08		●			C					
1-14				●		T	I	S			3-09		●			C					
1-15			●			T	I	S			3-10	●				C					
1-16		●						S			3-11				●	C					
1-17	●					T					3-12	●				C					
1-18			●			T	I	S			3-13	●				C					
1-19				●		T	I	S			3-14	●				C					
1-20				●		T	I	S			3-15	●				C					
1-21		●				T	I				3-16	●				C					
1-22				●		T	I	S			3-17		●			C					
1-23				●				S			3-18		●			C					
1-24		●						S			3-19		●			C					
1-25				●					G		3-20	●				C					
1-26	●				C						3-21	●				C					
1-27		●							G		3-22	●				C					
1-28				●					G		3-23	●				C					
1-29				●					G		3-24	●				C					
1-30		●							G		3-25		●			C					
1-31				●	C						3-26	●				C					
											3-27	●				C					
2-01				●						E	3-28		●			C					
2-02				●						E	3-29	●				C					
2-03				●					G	E	3-30	●				C					
2-04	●									E	3-31			●	●	C	T				
2-05	●									E	3-32			●		C					
2-06				●						E	3-33			●		C					
2-07	●								G	E	3-34			●		C					
2-08	●									E	3-35			●		C					
2-09	●									E	3-36			●		C					
2-10	●									E	3-37			●		C					
2-11	●									E	3-38			●		C	T				
2-12	●									E	3-39			●		C					
2-13				●						E	3-40				●	C					
2-14	●								G	E	3-41				●	C					
2-15	●								G	E	3-42	●				C					
2-16	●								G	E	3-43		●			C					
2-17	●								G		3-44		●			C					
2-18	●								G	E	3-45		●			C					
2-19	●								G		3-46		●			C					
2-20	●								G		3-47		●			C					

Section of this Report	Type of Research Collaboration[*1]				Irradiation Facilities[*2]						Section of this Report	Type of Research Collaboration[*1]				Irradiation Facilities[*2]					
	Joint Res,	Coop. Res, Univ.	Joint Res, Proj.	JAEA	TIARA				Co	E.B		Joint Res,	Coop. Res, Univ.	Joint Res, Proj.	JAEA	TIARA				Co	E.B
3-48	●				C						4-21				●			I	S		
3-49		●			C						4-22				●	C					
3-50		●			C						4-23				●(OL)						
3-51		●			C						4-24				●	C					
3-52		●			C						4-25			●		C					
3-53			●		C						4-26		●					I	S		
3-54			●		C						4-27			●					S		
3-55			●		C						4-28			●					S		
3-56			●		C						4-29			●					S		
3-57			●		C						4-30			●					S		
3-58				●	C						4-31			●					S		
3-59		●			C						4-32			●					S		
3-60	●				C						4-33			●					S		
3-61		●			C						4-34		●				T		S		
3-62		●			C						4-35		●				T		S		
3-63				●	C						4-36			●			T				
3-64			●		C						4-37			●			T		S		
3-65			●					S			4-38			●			T				
3-66			●					S			4-39			●			T	I			
3-67			●					S			4-40			●		C					
											4-41			●		C					
4-01		●			C						4-42			●		C					
4-02	●				C						4-43				●(OL)	C					E
4-03				●	C						4-44				●						E
4-04				●						E	4-45				●	C					
4-05		●			C	T					4-46				●	C					
4-06		●					I				4-47				●				S		
4-07		●					I	S			4-48				●(OL)						
4-08		●					I	S			4-49				●(M.S)		T	I	S		
4-09			●			T	I	S			4-50				●(OL)						
4-10				●		T	I	S			4-51				●(M.S)	C					
4-11		●					I				4-52				●(M.S)		T	I	S		
4-12				●			I														
4-13	●					T					5-01					C	T	I	S		
4-14				●(OL)							5-02					C					
4-15				●				S			5-03						T	I	S		
4-16		●					I	S			5-04					C	T	I	S		
4-17		●				T	I				5-05					C					
4-18				●			I	S			5-06									G	E
4-19				●			I	S			5-07										E
4-20				●			I	S			5-08									G	

Type of Research Collaboration

[*1]Joint Res.: Joint research with private company or governmental institution

Coop. Res. Univ.: Cooperative research with a university or universities

Joint Res. Proj. : The Joint Research Project #

#For administration of these programs, we appreciate the cooperation of

Research Center for Nuclear Science and Technology, The University of Tokyo.

O.L, off line

M.S, Machine study

Utilization of Irradiation Facilities

[*2]C; AVF Cyclotron System

T; Tandem Electrostatic Accelerator

I; Ion implanter

S; Single-ended Electrostatic Accelerator

G; Co-60 Gamma-Ray Irradiation Facilities

E; Electron Accelerator

Symbol used in the Appendix

Written example

05	J	173	4-42	C	RSH	51077
①	②	③	④-⑤	⑥	⑦	⑧

① Abbreviation of A.D. year

② J : Publications in Journal
C : Publications as Proceeding
NP : Press-Release
TV : TV Programs
PA : Patent

③ Reference number

④ The number of research field
1 Space,nuclear and energy engineering
2 Environmental conservation and resource security
3 Bioyechnology and medical application
4 Advanced materials, analysis and novel technology

⑤ The number of papers

⑥ Irradiation Facilities
C AVF Cyclotron System
T Tandem Electrostatic Accelerator
I Ion implanter
S Single-ended Electrostatic Accelerator
G Co-60 Gamma-Ray Irradiation Facilities
E Electron Accelerator
O Off-line
MS Machine study

⑦ Research fields
SCS : Semiconductors for Space
BNT : Biotechnology and Medical Application
RCO : Radiation Chemistry / Organic Materials
IOM : Inorganic Materials
MAN: Material Analysis
NRI : Nuclear Science and Radioisotope Production
ECT : Environmental Consevation Technology
RSH : Radiation Shielding for Accelerator
ACT : Accelerator Technology / TIARA Facilities
STA : Status of TIARA / TIARA General

⑧ Reseach Program Number of TIARA

国際単位系（SI）

表１．SI 基本単位

基本量	SI 基本単位	
	名称	記号
長さ	メートル	m
質量	キログラム	kg
時間	秒	s
電流	アンペア	A
熱力学温度	ケルビン	K
物質量	モル	mol
光度	カンデラ	cd

表２．基本単位を用いて表されるSI組立単位の例

組立量	SI 基本単位	
	名称	記号
面積	平方メートル	m^2
体積	立法メートル	m^3
速さ，速度	メートル毎秒	m/s
加速度	メートル毎秒毎秒	m/s^2
波数	毎メートル	m^{-1}
密度（質量密度）	キログラム毎立法メートル	kg/m^3
質量体積（比体積）	立法メートル毎キログラム	m^3/kg
電流密度	アンペア毎平方メートル	A/m^2
磁界の強さ	アンペア毎メートル	A/m
（物質量の）濃度	モル毎立方メートル	mol/m^3
輝度	カンデラ毎平方メートル	cd/m^2
屈折率	（数の）1	1

表５．SI 接頭語

乗数	接頭語	記号	乗数	接頭語	記号
10^{24}	ヨタ	Y	10^{-1}	デシ	d
10^{21}	ゼタ	Z	10^{-2}	センチ	c
10^{18}	エクサ	E	10^{-3}	ミリ	m
10^{15}	ペタ	P	10^{-6}	マイクロ	μ
10^{12}	テラ	T	10^{-9}	ナノ	n
10^{9}	ギガ	G	10^{-12}	ピコ	p
10^{6}	メガ	M	10^{-15}	フェムト	f
10^{3}	キロ	k	10^{-18}	アト	a
10^{2}	ヘクト	h	10^{-21}	ゼプト	z
10^{1}	デカ	da	10^{-24}	ヨクト	y

表３．固有の名称とその独自の記号で表されるSI組立単位

組立量	SI 組立単位			
	名称	記号	他のSI単位による表し方	SI基本単位による表し方
平面角	ラジアン(a)	rad		$m \cdot m^{-1}=1$(b)
立体角	ステラジアン(a)	sr(c)		$m^2 \cdot m^{-2}=1$(b)
周波数	ヘルツ	Hz		s^{-1}
力	ニュートン	N		$m \cdot kg \cdot s^{-2}$
圧力，応力	パスカル	Pa	N/m^2	$m^{-1} \cdot kg \cdot s^{-2}$
エネルギー，仕事，熱量	ジュール	J	N・m	$m^2 \cdot kg \cdot s^{-2}$
工率，放射束	ワット	W	J/s	$m^2 \cdot kg \cdot s^{-3}$
電荷，電気量	クーロン	C		s・A
電位差（電圧），起電力	ボルト	V	W/A	$m^2 \cdot kg \cdot s^{-3} \cdot A^{-1}$
静電容量	ファラド	F	C/V	$m^{-2} \cdot kg^{-1} \cdot s^4 \cdot A^2$
電気抵抗	オーム	Ω	V/A	$m^2 \cdot kg \cdot s^{-3} \cdot A^{-2}$
コンダクタンス	ジーメンス	S	A/V	$m^{-2} \cdot kg^{-1} \cdot s^3 \cdot A^2$
磁束	ウエーバ	Wb	V・s	$m^2 \cdot kg \cdot s^{-2} \cdot A^{-1}$
磁束密度	テスラ	T	Wb/m^2	$kg \cdot s^{-2} \cdot A^{-1}$
インダクタンス	ヘンリー	H	Wb/A	$m^2 \cdot kg \cdot s^{-2} \cdot A^{-2}$
セルシウス温度	セルシウス度(d)	℃		K
光束	ルーメン	lm	cd・sr(c)	$m^2 \cdot m^{-2} \cdot cd=cd$
照度	ルクス	lx	lm/m^2	$m^2 \cdot m^{-4} \cdot cd=m^{-2} \cdot cd$
（放射性核種の）放射能	ベクレル	Bq		s^{-1}
吸収線量，質量エネルギー分与，カーマ	グレイ	Gy	J/kg	$m^2 \cdot s^{-2}$
線量当量，周辺線量当量，方向性線量当量，個人線量当量，組織線量当	シーベルト	Sv	J/kg	$m^2 \cdot s^{-2}$

(a)ラジアン及びステラジアンの使用は、同じ次元であっても異なった性質をもった量を区別するときの組立単位の表し方として利点がある。組立単位を形作るときのいくつかの用例は表４に示されている。
(b)実際には、使用する時には記号rad及びsrが用いられるが、習慣として組立単位としての記号“１”は明示されない。
(c)測光学では、ステラジアンの名称と記号srを単位の表し方の中にそのまま維持している。
(d)この単位は、例としてミリセルシウス度m℃のようにSI接頭語を伴って用いても良い。

表４．単位の中に固有の名称とその独自の記号を含むSI組立単位の例

組立量	SI 組立単位		
	名称	記号	SI 基本単位による表し方
粘度	パスカル秒	Pa・s	$m^{-1} \cdot kg \cdot s^{-1}$
力のモーメント	ニュートンメートル	N・m	$m^2 \cdot kg \cdot s^{-2}$
表面張力	ニュートン毎メートル	N/m	$kg \cdot s^{-2}$
角速度	ラジアン毎秒	rad/s	$m \cdot m^{-1} \cdot s^{-1}=s^{-1}$
角加速度	ラジアン毎平方秒	rad/s^2	$m \cdot m^{-1} \cdot s^{-2}=s^{-2}$
熱流密度，放射照度	ワット毎平方メートル	W/m^2	$kg \cdot s^{-3}$
熱容量，エントロピー	ジュール毎ケルビン	J/K	$m^2 \cdot kg \cdot s^{-2} \cdot K^{-1}$
質量熱容量（比熱容量），質量エントロピー	ジュール毎キログラム毎ケルビン	J/(kg・K)	$m^2 \cdot s^{-2} \cdot K^{-1}$
質量エネルギー（比エネルギー）	ジュール毎キログラム	J/kg	$m^2 \cdot s^{-2} \cdot K^{-1}$
熱伝導率	ワット毎メートル毎ケルビン	W/(m・K)	$m \cdot kg \cdot s^{-3} \cdot K^{-1}$
体積エネルギー	ジュール毎立方メートル	J/m^3	$m^{-1} \cdot kg \cdot s^{-2}$
電界の強さ	ボルト毎メートル	V/m	$m \cdot kg \cdot s^{-3} \cdot A^{-1}$
体積電荷	クーロン毎立方メートル	C/m^3	$m^{-3} \cdot s \cdot A$
電気変位	クーロン毎平方メートル	C/m^2	$m^{-2} \cdot s \cdot A$
誘電率	ファラド毎メートル	F/m	$m^{-3} \cdot kg^{-1} \cdot s^4 \cdot A^2$
透磁率	ヘンリー毎メートル	H/m	$m \cdot kg \cdot s^{-2} \cdot A^{-2}$
モルエネルギー	ジュール毎モル	J/mol	$m^2 \cdot kg \cdot s^{-2} \cdot mol^{-1}$
モルエントロピー，モル熱容量	ジュール毎モル毎ケルビン	J/(mol・K)	$m^2 \cdot kg \cdot s^{-2} \cdot K^{-1} \cdot mol^{-1}$
照射線量（X線及びγ線）	クーロン毎キログラム	C/kg	$kg^{-1} \cdot s \cdot A$
吸収線量率	グレイ毎秒	Gy/s	$m^2 \cdot s^{-3}$
放射強度	ワット毎ステラジアン	W/sr	$m^4 \cdot m^{-2} \cdot kg \cdot s^{-3}=m^2 \cdot kg \cdot s^{-3}$
放射輝度	ワット毎平方メートル毎ステラジアン	$W/(m^2 \cdot sr)$	$m^2 \cdot m^{-2} \cdot kg \cdot s^{-3}=kg \cdot s^{-3}$

表６．国際単位系と併用されるが国際単位系に属さない単位

名称	記号	SI 単位による値
分	min	1 min=60s
時	h	1h =60 min=3600 s
日	d	1 d=24 h=86400 s
度	°	1° =(π/180) rad
分	’	1’ =(1/60)° =(π/10800) rad
秒	”	1” =(1/60)’ =(π/648000) rad
リットル	l、L	$1l=1\ dm^3=10^{-3}m^3$
トン	t	$1t=10^3$ kg
ネーパ	Np	1Np=1
ベル	B	1B=(1/2)ln10(Np)

表７．国際単位系と併用されこれに属さない単位でSI単位で表される数値が実験的に得られるもの

名称	記号	SI 単位であらわされる数値
電子ボルト	eV	$1eV=1.60217733(49)\times10^{-19}J$
統一原子質量単位	u	$1u=1.6605402(10)\times10^{-27}kg$
天文単位	ua	$1ua=1.49597870691(30)\times10^{11}m$

表８．国際単位系に属さないが国際単位系と併用されるその他の単位

名称	記号	SI 単位であらわされる数値
海里		1海里=1852m
ノット		1ノット=1海里毎時=(1852/3600)m/s
アール	a	$1a=1\ dam^2=10^2m^2$
ヘクタール	ha	$1ha=1\ hm^2=10^4m^2$
バール	bar	$1bar=0.1MPa=100kPa=1000hPa=10^5Pa$
オングストローム	Å	$1Å=0.1nm=10^{-10}m$
バーン	b	$1b=100fm^2=10^{-28}m^2$

表９．固有の名称を含むCGS組立単位

名称	記号	SI 単位であらわされる数値
エルグ	erg	$1\ erg=10^{-7}$ J
ダイン	dyn	$1\ dyn=10^{-5}N$
ポアズ	P	$1\ P=1\ dyn \cdot s/cm^2=0.1Pa \cdot s$
ストークス	St	$1\ St=1cm^2/s=10^{-4}m^2/s$
ガウス	G	1 G ^10^-4T
エルステッド	Oe	1 Oe ^(1000/4π)A/m
マクスウェル	Mx	1 Mx ^10^-8Wb
スチルブ	sb	$1\ sb=1cd/cm^2=10^4cd/m^2$
ホト	ph	$1\ ph=10^4lx$
ガル	Gal	$1\ Gal=1cm/s^2=10^{-2}m/s^2$

表10．国際単位に属さないその他の単位の例

名称	記号	SI 単位であらわされる数値
キュリー	Ci	$1\ Ci=3.7\times10^{10}Bq$
レントゲン	R	$1\ R=2.58\times10^{-4}C/kg$
ラド	rad	$1\ rad=1cGy=10^{-2}Gy$
レム	rem	$1\ rem=1\ cSv=10^{-2}Sv$
X線単位		$1X\ unit=1.002\times10^{-4}nm$
ガンマ	γ	$1\gamma=1\ nT=10^{-9}T$
ジャンスキー	Jy	$1\ Jy=10^{-26}W \cdot m^{-2} \cdot Hz^{-1}$
フェルミ		$1\ fermi=1\ fm=10^{-15}m$
メートル系カラット		$1\ metric\ carat=200\ mg=2\times10^{-4}kg$
トル	Torr	$1\ Torr=(101\ 325/760)\ Pa$
標準大気圧	atm	$1\ atm=101\ 325\ Pa$
カロリー	cal	
ミクロン	μ	$1\ \mu=1\mu m=10^{-6}m$

（第７版，1998年改訂）